CRANFIELD INSTITUTE OF TECHNOLOGY

SILSOE COLLEGE

PhD THESIS

Roland Hiederer

MONITORING RANGELAND VEGETATION IN THE SAHEL BY LANDSAT MSS AND NOAA AVHRR

SUPERVISORS:
DR. J.C. TAYLOR
DR. G. D'SOUZA

July 1991

ABSTRACT

Quantities of herbaceous vegetation of Sahelian rangelands in Niger and Mali were compared to vegetation indices (VI) derived from Landsat MSS and NOAA AVHRR LAC images. Field data was collected in 1985, 1988 and 1989 in Niger and an appropriate sampling scheme for the study area was developed. Herbaceous vegetation could be estimated to within ± 150 kgha^{-1} at an 80% confidence level up to 1300 kgha^{-1}.

Establishing site positions was found to be a primary obstacle when selecting suitable sampling areas. Suggested is the use of Landsat MSS image hard-copies in combination with a global positioning system.

Landsat MSS and NOAA AVHRR LAC data were available for dates corresponding to field surveys of 1985 and 1988. While Landsat MSS scenes were geometrically corrected to maps, NOAA AVHRR images were registered to Landsat MSS with a simulated resolution of 1.1 km. Data from both satellites were radiometrically corrected and standardized to atmospheric conditions to the image with the highest relative scene contrast for each study area. These reference images were identified on the basis of bare soil spectral reflectance values and a binary decision tree.

Five methods of resampling image data to represent field sites were applied. The image data sampling methods were found to have a significant influence on spectral reflectance values attributed to a site and, consequently, on the relationship between ground and satellite VIs. Ratio, normalized difference and perpendicular VIs (RVI, NDVI and PVI) were computed for each step of pre-processing procedures. For Landsat MSS VIs were also derived from average spectral reflectance values of bands 3 and 4 to simulate NOAA AVHRR channel 2. VIs were compared for the same sensor, between sensors and related to field data by using linear and logarithmic regression analyses.

RVIs and NDVIs achieved very similar results, while PVIs showed a more variable relationship to ground data. Overall, VIs from simulated NOAA AVHRR channel 2 values were found to be not superior to those derived from just band 4.

NOAA AVHRR VIs could be related to Landsat MSS ratio VIs by a single regression line for 1985 and 1988 growing seasons for Niger and Mali survey sites. For the inter-calibration a simulation of the NOAA AVHRR pixel size was found to be better suited than the high resolution Landsat MSS data.

LIST OF CONTENTS

Page

1. INTRODUCTION

1.1 Enigma of Sahelian Rangeland Vegetation 1.1

1.2 Monitoring Rangeland Vegetation by Satellite 1.2

1.3 Project Objectives 1.5

2. BACKGROUND AND LITERATURE SURVEY

2.1 Study Area 2.1
2.1.1 Location of Study Area 2.2
2.1.2 Climate 2.3
2.1.3 Geography 2.4
2.1.4 Soils 2.5
2.1.5 Vegetation 2.7
2.1.2 Rangeland Productivity in the Sahel 2.10

2.2 Estimation of Vegetation Properties from Remotely Sensed Data 2.12
2.2.1 Interaction of Solar Radiation with Vegetation and Soil 2.13
2.2.2 Vegetation Indices 2.17
2.2.3 Phytomass Estimation of Rangeland Vegetation 2.21

2.3 Satellites and Sensors 2.29
2.3.1 Television Infra-Red Observation Satellite 2.30
2.3.2 Landsat-4 and Landsat-5 ..... 2.34
2.3.3 Comparison of Sensors Products 2.37

2.4 Rangeland Monitoring by Satellite Data 2.38
2.4.1 Choice of Sensor for Rangeland Management 2.38
2.4.2 Rangeland Monitoring with AVHRR 2.40

3. FIELD WORK

3.1 Introduction to Ground Data Acquisition 3.3
3.1.1 Purpose of Field Visits 3.3
3.1.2 Selection of Study Area 3.6
3.1.3 Period of Field Survey 3.7

3.1.4 Selection of Sample Sites 3.8
3.1.5 Positioning of Sample Sites 3.9
3.1.6 Layout of Sampling Method 3.10
3.1.7 Site Parameters 3.12
3.1.8 Determination of Dry Matter Production 3.14
3.1.9 Correlations and Accuracy Assessment 3.17

3.2 Peripheral Field Surveys 3.19
3.2.1 CIPEA Field Survey of 1985 in Niger 3.19
3.2.2 ITE/Silsoe Field Survey of 1985 in Niger 3.26
3.2.3 CAZS Field Survey of 1988 in Mali 3.29

3.3 Field Visit of 1988 ..... 3.40
3.3.1 Compendium on Field Work Procedures 3.41
3.3.2 Performance of WILE 35 Moisture Meter 3.44
3.3.3 Compendium on Site Parameter Data 3.46
3.3.4 Feasibility of Using WILE 35 Moisture Meter 3.52
3.3.5 Accuracy Assessment of Herbaceous Dry Matter Estimates 3.54

3.4 ITE/Silsoe Field Visit of 1989 ..... 3.56
3.4.1 Compendium on Field Work Procedures 3.56
3.4.2 Performance of Air-drying Samples 3.62
3.4.3 Compendium on Site Parameter Data 3.64
3.4.4 Feasibility of Air-drying Samples 3.75
3.4.5 Accuracy Assessment of Herbaceous Dry Matter Estimates 3.75

3.5 Integration of Field Survey Results 3.81
3.5.1 Discussion of Field Work Procedures 3.81
3.5.2 Discussion of Site Parameter Data 3.85
3.5.3 Conclusions and Implications for Future Field Surveys 3.94

4. IMAGE PROCESSING

4.1 Available Satellite Data 4.2

4.2 Data Format Transformation 4.3

4.3 Cloud Masking 4.4

4.4 Geometric Correction 4.6

4.5 Radiometric Correction 4.11
4.5.1 Conversion of Landsat MSS DNs to Spectral Reflectance 4.11
4.5.2 Conversion of NOAA AVHRR DNs to Spectral Albedo 4.23

4.6 Atmospheric Correction 4.37

4.7 Discussion of Pre-processing Procedures 4.48
4.7.1 Available Satellite Data 4.48
4.7.2 Data Transformation 4.49
4.7.3 Cloud Masking 4.49
4.7.4 Geometric Correction 4.50
4.7.5 Radiometric Correction 4.51
4.7.6 Atmospheric Correction 4.52

4.8 Conclusions and Implications of Pre-Processing 4.53

5. Relationship Between Ground and Satellite Data

5.1 Transect Positions 5.1
5.1.1 CIPEA Survey 5.2
5.1.2 CAZS Survey 5.4
5.1.3 ITE/Silsoe Surveys 5.5

5.2 Image Data Sampling Methods 5.5
5.2.1 Image Data Sampling Methods for Landsat MSS 5.6
5.2.2 Image Data Sampling Methods for NOAA AVHRR 5.9

5.3 Landsat MSS and NOAA AVHRR Data Comparison 5.10
5.3.1 Spatial Correspondence Between Satellite Data 5.10
5.3.2 Radiometric Correspondence Between Satellite Data 5.23

5.4 Relationships Between Ground Data and VIs 5.30
5.4.1 CIPEA Survey 5.31
5.4.2 1985 ITE/Silsoe Survey 5.35
5.4.3 CAZS Survey 5.40
5.4.4 1988 ITE/Silsoe Survey 5.45

5.5 Integration of Field Survey Data 5.51
5.5.1 Field Survey Data and Landsat MSS VIs 5.51
5.5.2 Field Survey Data and NOAA AVHRR VIs 5.55
5.5.3 Estimating NOAA AVHRR VIs from Landsat MSS VIs 5.62

5.6 Discussion of Ground to Satellite Data Relationships 5.67
5.6.1 Field Survey Sampling Layout 5.68
5.6.2 Transect Positions 5.69
5.6.3 Image Data Sampling Method 5.70
5.6.4 Landsat MSS vs. NOAA AVHRR Wavebands 5.71
5.6.5 Performance of VIs 5.72
5.6.6 Simulation of NOAA AVHRR VIs by Landsat MSS VIs 5.73

5.7 Conclusions for Relating Satellite to Ground Data 5.73

6. Conclusions and Implications

6.1 Calibration of NOAA AVHRR LAC VIs to Herbaceous Vegetation 6.2

6.2 Structure of Operational Rangeland Monitoring System 6.3

6.3 Areas for Additional Research 6.5

APPENDIX I: Concepts of Data Analysis

APPENDIX I: Concepts of Data Analysis

A1. CONCEPT OF ESTIMATING GROUND DATA VALIDITY

A1.1 Confidence Limits of Rangeland Estimates A.1

A1.2 Required Sample Size for Desired Confidence Limit A.4

A1.3 Duration for Sampling Period A.4

A2. STATISTICAL CONCEPT OF REGRESSION ANALYSIS

A2.1 Assumptions for Hypothesis Testing with Linear Regression A.6

A2.2 Procedure for Hypothesis Testing A.8

A3. GEOMERIC CORRECTION

A3.1 Sources of Deviations of Images from Map Projections A.10
A3.2 Image Referencing A.11
A3.3 Estimation of Geometric Errors A.13
A3.4 General Approach to Orbital Models A.19
A3.5 General Approach to Polynomial Correction A.22
A3.6 Resampling A.23

A4. RADIOMETRIC CORRECTIONS A.25

A4.1 Sensor Response Characteristic A.25
A4.1.1 In-scene Differences in Detector Sensitivity A.25
A4.1.2 Temporal Changes in Sensor Sensitivity A.26
A4.1.3 Digitization Errors A.26

A4.2 Scene Illumination A.27
A4.2.1 Solar Elevation A.27
A4.2.2 Solar Distance Adjustment A.29

A4.3 Viewing Geometry A.30

A4.4 Conversion of DNs to Spectral Reflectance A.32
A4.1.1 Conversion of Landsat MSS DNs to Spectral Radiance A.32
A4.1.2 Conversion of Landsat MSS Spectral Radiance to Spectral Reflectance A.33
A4.1.3 Conversion of NOAA AVHRR DNs to Spectral Albedo A.34

A5. ATMOSPHERIC CORRECTION

A5.1 Forms of Atmospheric Scattering and Absorption A.36

A5.2 Influence of Atmospheric Conditions on VIs A.37

A5.3 Atmospheric Modell A.38

A5.4 Atmospheric Correction Techniques A.42
A5.4.1 Image Processing Side Products A.42
A5.4.2 Empirical Methods A.44
A5.4.3 Atmospheric Correction Based on Physical Models A.45
A5.4.4 Analysis of Multi-temporal Sequences A.47

Appendix II: Tables A.49

Appendix III: Figures A.119

Bibliography A.125

LIST OF TABLES

Page

Table 2.1: Technical Specifications of NOAA AVHRR 2.33

Table 2.2: Technical Specifications of Landsat-4 and -5 MSS and TM 2.36

Table 3.1: Summary of Field Survey Characteristics 3.2

Table 3.2: Field Methods for Dry Matter Determination 3.14

Table 3.3: Specification of WILE 35 Moisture Meter 3.16

Table 3.4: Average Rangeland Production Values for 1985 ITE/Silsoe Field Survey 3.27

Table 3.5: Dominant Plant Species Encountered During CAZS Field Survey 3.30

Table 3.6: Development of Herbaceous Fresh Production, Dry Matter, Moisture Content and Cover During the 1988 Growing Season in Mali 3.32

Table 3.7: Dominant Plant Species Found in 1988 ..... 3.41

Table 3.8: Estimated Site Parameters for Transects of 1988 Field Survey to Niger (Transect Averages) 3.47

Table 3.9: Summary of Measurements and Estimates of 1989 ITE/Silsoe Survey in Niger 3.66

Table 3.10: Significance Test on Average Rangeland Production of Soil Colour Classes 3.73

Table 3.11: Summary of Recommended Field Survey Sampling Scheme 3.98

Table 4.1: Threshold and Saturation Radiance Values for Landsat-5 Multispectral Scanner (after 9 November 1984) 4.14

Table 4.2: Slope and Intercept Parameters for Converting Landsat MSS DNs to Spectral Radiance 4.15

Table 4.3: Nominal and Actual Bandwidths for Landsat MSS Spectral Bands 4.17

Table 4.4: Linear Coefficients for Direct Conversion of Landsat MSS DNs into Exoatmospheric Spectral Reflectances, Including Correction for Earth-Sun Constellation 4.21

Table 4.5: Spectral Parameters and Calibration Coefficients for NOAA-9 AVHRR 4.32

Table 4.6: Thekaekara and Neckel and Labs Solar Irradiances and Equivalent Bandwidths for Channels 1 and 2 of NOAA-9 AVHRR 4.32

Table 4.7: Coefficients for Linear Conversion of NOAA-9 AVHRR DNS to Percentage Spectral Albedo Based on Neckel & Labs 4.33

Table 4.8: Decision Table for Selecting Clear NOAA AVHRR Image for 1985 ITE/Silsoe Survey 4.43

Table 4.9: Dates of Reference Images for Relative Atmospheric Correction of NOAA AVHRR Data 4.44

Table 4.10: Linear Relationships Between NOAA AVHRR Images to Standard Image for Growing Season 4.45

Table 4.11: Relationship Between Band 2 and 4 Spectral Reflectance for Landsat MSS 50 m and 1.1 km Resolution Images 4.46

Table 4.12: Comparison of Linear Relationships Between NOAA AVHRR Channel 1 and 2 Spectral Albedos and Landsat MSS 1.1 km Bands 1, 2, 3 and 4 for Unvegetated Soil and Rock Surfaces 4.47

Table 5.1: Map and Image Co-ordinates of 1985 CIPEA Field Survey Sites 5.3

Table 5.2: Map and Image Co-ordinates of 1988 CAZS Field Survey Sites 5.4

Table 5.3: Map and Image Co-ordinates of 1985 and 1988 ITE/Silsoe Field Survey Sites 5.6

Table 5.4: Relationships Between Image Data Sampling Methods for Landsat MSS Data for 1985 CIPEA Survey 5.12

Table 5.5: Relationships Between NOAA AVHRR Data from Different Image Sampling Methods for 1985 CIPEA Survey 5.14

Table 5.6: Relationships Between Landsat MSS Data from Different Image Sampling Methods for 1985 ITE/Silsoe Survey 5.15

Table 5.7: Relationships Between NOAA AVHRR Data from Different Image Sampling Methods for 1985 ITE/Silsoe Survey 5.16

Table 5.8: Relationships Between Landsat MSS Spectral Reflectances Obtained from Five Different Image Sampling Methods for 1988 CAZS Field Survey and Map Positions 5.18

Table 5.9: Relationships Between NOAA AVHRR Spectral Albedos Obtained from Different Image Sampling Methods for 1988 CAZS Field Survey 5.19

Table 5.10: Relationships Between Landsat MSS Spectral Reflectances Obtained from Five Different Image Sampling Methods for 1988 ITE/Silsoe Field Survey and Image Positions 5.21

Table 5.11: Relationships Between NOAA AVHRR Spectral Albedos Obtained from Different Image Sampling Methods for 1988 ITE/Silsoe Field Survey 5.22

Table 5.12: Relationship Between NOAA AVHRR and Landsat MSS DNs for 31 August 1985 Images 5.24

Table 5.13: Relationship Between NOAA AVHRR and Landsat MSS Vegetation Indices from DNs for 31 August 1985 Images 5.31

Table 5.14: Summary of Results of Vegetation Index Calibration of CIPEA Field Survey 5.34

Table 5.15: Summary of Results of Vegetation Index Calibration of 1985 ITE/Silsoe Field Survey ... 5.37

Table 5.16: Summary of Results of Vegetation Index Calibration of CAZS Field Survey 5.43

Table 5.17: Summary of Results of Vegetation Index Calibration of 1988 ITE/Silsoe Field Survey ... 5.49

Table 5.18: Coefficients of Correlation from Linear and Logarithmic Regressions Between Herbaceous Vegetation Estimates and Landsat MSS VIs Derived from Atmospherically Standardized Data 5.54

Table 5.19: Coefficients of Correlation from Linear and Logarithmic Regressions Between Herbaceous Vegetation Estimates and NOAA AVHRR VIs Derived from DNs 5.57

Table 5.20: Coefficients of Correlation from Linear and Logarithmic Regressions Between Herbaceous Vegetation Estimates and NOAA AVHRR VIs Derived from Radiometrically Corrected Spectral Albedos 5.60

Table 5.21: Coefficients of Correlation from Linear and Logarithmic Regressions Between Herbaceous Vegetation Estimates and NOAA AVHRR VIs Derived from Atmospherically Standardized Spectral Albedos 5.62

Table 5.22: Coefficients of Correlation from Linear and Logarithmic Regressions Between Landsat MSS and NOAA AVHRR VIs Derived from Atmospherically Standardized Image Data 5.64

Tables Appendix II

Table A.1: Map Coordinates of 1985 CIPEA Sampling Sites in Niger A.49

Table A.2: Average Rangeland Production and Cover Values for 1985 CIPEA Survey A.50

Table A.3: Map Coordinates of 1985 and 1988 ITE/Silsoe Sampling Sites in Niger A.51

Table A.4: Position of CAZS Sampling Sites A.51

Table A.5: Standard Deviation, Coefficient of Variation and Standard Error of Mean for Herbaceous Rangland Vegetation Qunatities of CAZS Field Survey A.52

Table A.6: Average Rangeland Production Values for 1988 CAZS Survey A.54

Table A.7: Average Herbaceous Cover and Trees and Shrubs Counts for 1988 CAZS Survey A.55

Table A.8: Estimated Herbaceous Production Levels for Transects of 1988 Field Survey A.56

Table A.9: Results of In-Field WILE 35 Moisture Meter Readings During 1988 ITE/Silsoe Field Survey A.58

Table A.10: Results of Laboratory WILE 35 Moisture Meter Readings During 1988 ITE/Silsoe Field Survey of Air-dired Samples A.58

Table A.11: Calibration of WILE 35 to Moisture Content (Non-linear regression) A.59

Table A.12: Estimated Herbaceous Cover and Moisture Content of 1988 ITE/Silsoe Field Visit to Niger A.60

Table A.13: Variations in Dry Matter Production for Samples of 1985 and 1988 ITE/Silsoe Field Survey in Niger A.62

Table A.14: Relation Between Dry Matter Production and Class Width for 1985 and 1988 ITE/Silsoe Field Surveys A.62

Table A.15: Image and GPS Co-ordinates of 1988/89 ITE/Silsoe Sample Sites (Starting Points) A.63

Table A.16: Relationship Between Fresh Weight and Oven-dried M.C. for Individual Sites of Both Sampling Periods of 1989 CASTE/ITE/Silsoe Field Survey A.64

Table A.17: Results of 1989 CASTE/ITE/Silsoe Field Survey (Averages from all Sites) A.65

Table A.18: Standard Deviation, Coefficient of Variation and Standard Error of the Mean for Herbaceous Rangeland Vegetation of 1989 CASTE/ITE/Silsoe Field Survey A.66

Table A.19: Classes of Soil Colour and Average Rangeland Production for 1989 CASTE/ITE/Silsoe Field Survey A.67

Table A.20: Landsat MSS and NOAA AVHRR LAC Data Used for Geometric Correction and Image to Ground Data Correlation A.68

Table A.21: Ratio Between Bright and Dark Soil Surfaces for NOAA AVHRR Images for CIPEA, 1985 ITE/Silsoe, CAZS and 1988 ITE/Silsoe Field Surveys A.70

Table A.22: Relationships Between Landsat MSS Spectral Reflectances Obtained from Five Different Image Sampling Methods for 1985 CIPEA Survey for Shifted Image and Without Site No. 2 ..... A.72

Table A.23: Relationships Between Landsat MSS Spectral Reflectances Obtained from Five Different Image Sampling Methods for 1988 CAZS Field Survey for GPS Transect Positions A.73

Table A.24: Relationships Between Landsat MSS Spectral Reflectances Obtained from Five Different Image Sampling Methods for 1988 ITE/Silsoe Field Survey for Shifted Image and Without Site No. 2 ..... A.73

Table A.25: Relationships Between Landsat MSS Spectral Reflectances and NOAA AVHRR Spectral Albedos for 1985 CIPEA Field Survey Sites (3 by 3 Averages) A.74

Table A.26: Relationships Between Landsat MSS Spectral Reflectances (31.08.85) and NOAA AVHRR Spectral Albedos (31.08.85) Obtained from Five Different Image Sampling Methods for 1985 CIPEA Field Survey Sites A.75

Table A.27: Relationships Between Landsat MSS Spectral Reflectances (31.08.85) and NOAA AVHRR Spectral Albedos (31.08.85) Obtained from Five Different Image Sampling Methods for 1985 CIPEA Field Survey Sites for Shifted Image and Without Site No. 2 ..... A.77

Table A.28: Relationships Between Landsat MSS Spectral Reflectances (31.08.85) and NOAA AVHRR Spectral Albedos for 1985 ITE/Silsoe Field Survey Sites (3 by 3 Averages) A.78

Table A.29: Relationships Between Landsat MSS (31.08.85) Spectral Reflectances and NOAA AVHRR (31.08.85) Spectral Albedos Obtained from Five Different Image Sampling Methods for 1985 ITE/Silsoe Field Survey Sites (3 by 3 Averages) A.79

Table A.30: Relationships Between Landsat MSS Spectral Reflectances and NOAA AVHRR Spectral Albedos for 1988 CAZS Field Survey Sites (3 by 3 Averages) A.80

Table A.31: Relationships Between Landsat MSS (30.08.88) Spectral Reflectances and NOAA AVHRR (20.08.88) Spectral Albedos Obtained from Five Different Image Sampling Methods for 1988 CAZS Field Survey Sites, Map Positions A.82

Table A.32: Relationships Between Landsat MSS (30.08.88) Spectral Reflectances and NOAA AVHRR (06.09.88) Spectral Albedos Obtained from Five Different Image Sampling Methods for 1988 CAZS Field Survey Sites, Image Positions A.83

Table A.33: Relationships Between Landsat MSS Spectral Reflectances and NOAA AVHRR Spectral Albedos for 1988 ITE/Silsoe Field Survey Sites (3 by 3 Averages) A.85

Table A.34: Relationships Between Landsat MSS (08.09.88) Spectral Reflectances and NOAA AVHRR (20.08.88) Spectral Albedos Obtained from Five Different Image Sampling Methods for 1988 ITE/Silsoe Field Survey Sites A.86

Table A.35: Relationships Between Landsat MSS (08.09.88) Spectral Reflectances and NOAA AVHRR (06.09.88) Spectral Albedos Obtained from Five Different Image Sampling Methods for 1988 ITE/Silsoe Field Survey Sites A.88

Table A.36: Results of Regression Analysis Between CIPEA Ground Data and Landsat MSS VIs for Sites Positioned by Aerial Photographs on Images A.90

Table A.37: Results of Regression Analysis Between CIPEA Ground Data and NOAA AVHRR VIs for Sites Positioned by Aircraft Instrument (Central Sampling) A.91

Table A.38: Results of Regression Analysis Between CIPEA Ground Data and NOAA AVHRR VIs for Sites Positioned by Aerial Photographs on Images (Central Sampling) A.92

Table A.39: Results of Regression Analysis Between CIPEA Ground Data and Maximum Value VIs of NOAA AVHRR for Sites Positioned by Aerial Photographs on Images A.93

Table A.40: Results of Regression Analysis Between Landsat MSS and NOAA AVHRR VIs for CIPEA Field Survey Site, Positioned by Image Identification A.93

Table A.41: Results of Regression Analysis Between 1985 ITE/Silsoe Ground Data and Landsat MSS VIs for Sites Positioned by Image Identification A.94

Table A.42: Results of Regression Analysis Between 1985 ITE/Silsoe Ground Data and NOAA AVHRR VIs for Sites Positioned by Image Identification (Central Value) A.95

Table A.43: Results of Regression Analysis Between 1985 ITE/Silsoe Ground Data and NOAA AVHRR VIs for Sites Positioned by Image Identification (3 by 3 Image Data Sampling) A.96

Table A.44: Results of Regression Analysis Between 1985 ITE/Silsoe Ground Data and NOAA AVHRR VIs for Sites Positioned by Image Identification (Transect Image Data Sampling) A.96

Table A.45: Results of Regression Analysis Between 1985 ITE/Silsoe Ground Data and NOAA AVHRR Maximum Value VIs for Sites Positioned by Image Identification (Transect Image Data Sampling) A.97

Table A.46: Results of Regression Analysis Between Landsat MSS and NOAA AVHRR VIs for 1985 ITE/Silsoe Field Survey Site, Positioned by Image Identification A.97

Table A.47: Results of Regression Analysis Between CAZS Field Survey Data from 5th and 6th Sampling Period and Landsat MSS NDVI for Sites Positioned by GPS A.98

Table A.48: Results of Regression Analysis Between CAZS Field Survey Data from 5th Sampling Period and Landsat MSS NDVI for Sites Positioned by Map Identification A.99

Table A.49: Results of Regression Analysis Between CAZS Field Survey Data from 6th Sampling Period and Landsat MSS NDVI for Sites Positioned by Map Identification A.100

Table A.50: Results of Regression Analysis Between CAZS Field Survey Data and NOAA AVHRR NDVI for Sites Positioned by GPS (Central Image Data Sampling) A.101

Table A.51: Results of Regression Analysis Between CAZS Field Survey Data and NOAA AVHRR NDVI for Sites Positioned by Map Identification (Central Image Data Sampling) A.102

Table A.52: Results of Regression Analysis Between CAZS Field Survey Data and NOAA AVHRR NDVI for Sites Positioned by Map Identification (3 by 3 Pixel Image Data Sampling) A.103

Table A.53: Results of Regression Analysis Between CAZS Field Survey Data and NOAA AVHRR Maximum Value VIs for Sites Positioned by Map Identification A.104

Table A.54: Results of Regression Analysis Between CAZS Field Survey Data and NOAA AVHRR Moving Average VIs for Sites Positioned by Map Identification (Central Data Image Sampling) A.104

Table A.55: Results of Regression Analysis Between Landsat MSS and NOAA AVHRR VIs for CAZS Field Survey Site, Positioned by Image Identification A.105

Table A.56: Results of Regression Analysis Between 1988 ITE/Silsoe Field Survey Data and Landsat MSS VIs for Sites Positioned by Image Identification A.106

Table A.57: Results of Regression Analysis Between 1988 ITE/Silsoe Field Survey Data and Landsat MSS VIs for Sites Positioned by Image Identification, Excluding Sites No. 6, 7 and 8 ..... A.107

Table A.58: Results of Regression Analysis Between 1988 ITE/Silsoe Field Survey Data and NOAA AVHRR VIs for Sites Positioned by Image Identification A.108

Table A.59: Results of Regression Analysis Between 1988 ITE/Silsoe Field Survey Data and NOAA AVHRR Maximum Value VIs for Sites Positioned by Image Identification A.108

Table A.60: Results of Regression Analysis Between 1988 ITE/Silsoe Field Survey Data and NOAA AVHRR VIs for Sites Positioned by Image Identification, Excluding Sites No. 6, 7 and 8 ..... A.109

Table A.61: Results of Regression Analysis Between Landsat MSS and NOAA AVHRR VIs for 1988 ITE/Silsoe Field Survey Site, Positioned by Image Identification A.109

Table A.62: Results of Regression Analysis Between Combined CIPEA and 1985 ITE/Silsoe Ground Data for Landsat MSS VIs for Sites Positioned by Image Identification A.110

Table A.63: Results of Regression Analysis Between Combined CIPEA and 1985 ITE/Silsoe Ground Data for NOAA AVHRR for Sites Positioned by Image Identification A.111

Table A.64: Results of Regression Analysis Between Combined CIPEA and 1985 ITE/Silsoe Ground Data for NOAA AVHRR Maximum Value VIs for Sites Positioned by Image Identification A.111

Table A.65: Cloud Cover Over Field Survey Samples of 1985 ITE/Silsoe Field Survey Single Band Threshold and Local Variation Methods A.112

Table A.66: Cloud Cover Over Field Survey Samples of 1985 CIPEA Field Survey Single Band Threshold and Local Variation Methods A.113

Table A.67: Cloud Cover Over Field Survey Samples of CAZS and 1988 ITE/Silsoe/CASTE Field Survey Single Band Threshold and Local Variation Methods ... A.114

Table A.68: Correction Factors of Variations in Solar Illumination Conditions for Landsat MSS A.115

Table A.69: Correction Factors of Variations in Solar Illumination Conditions for NOAA AVHRR LAC Data A.116

Table A.70: Linear Coefficients for Direct Conversion of NOAA AVHRR DNs into Exoatmospheric Spectral Albedo, Including Correction for Earth-Sun Constellation A.117

Table A.71: Ratio Between Bright and Dark Soil Surfaces for NOAA AVHRR Images for CIPEA, 1985 ITE/Silsoe, CAZS and 1988 ITE/Silsoe Field Surveys A.118

LIST OF FIGURES

Page

Figure 2.1: Map of Africa with Position of Sahel 2.2

Figure 2.2: Mean Annual Rainfall over Study Area 2.4

Figure 2.3: Distribution of Soils over Study Area 2.6

Figure 2.4: Distribution of Major Vegetation Zones over Study Area 2.8

Figure 2.5: Reflectance of Vegetation and Soil in the RED and NIR 2.14

Figure 2.6: Soil Reflectance Curves 2.16

Figure 2.7: Lines of Equal Green Response for Ratio and Orthogonal VIs 2.26

Figure 2.8: Temporal and Spatial Scales at the Arid Rangelands With the Capabilities of Landsat MSS and NOAA AVHRR 2.39

Figure 3.1: Study Areas of Mali and Niger Field Surveys ... 3.7

Figure 3.2: Layout of Field Survey Sampling Methods 3.3

Figure 3.3: Arrangement of Sampling Sites of 1985 CIPEA Field Survey in Niger 3.0

Figure 3.4: Development of Herbaceous Vegetation Dry Matter Quantities and Cover during 1985 CIPEA Field Survey 3.1

Figure 3.5: Duration of Field Survey Mission (for 10% Observed Significance Level, CIPEA Survey) 3.2

Figure 3.6: Herbaceous Dry Matter Production vs. Cover for 1985 CIPEA Field Survey in Niger (Transect Averages) 3.3

Figure 3.7: Relationship Between Herbaceous Dry Matter Quantities and Confidence Level for Standard Errors of the Mean of ± 125, ± 150 and ± 200 $kgha^{-1}$ (1985 CIPEA Sites, 2nd Mission) 3.4

Figure 3.8: Required Number of Samples to Achieve Standard Error of the Mean of ± 150 $kgha^{-1}$ Herbaceous Dry Matter at 60, 70 and 80% Confidence Levels (1985 CIPEA Sites) 3.25

Figure 3.9: Arrangement of Sampling Sites of 1985 ITE/Silsoe Field Survey 3.26

Figure 3.10: Relationship Between Herbaceous Dry Matter Quantities and Confidence Level for Standard Errors of the Mean of ± 125, ± 150 and ± 200 $kgha^{-1}$ (1985 ITE/Silsoe Sites) 3.28

Figure 3.11: Required Number of Samples to Achieve Standard Error of the Mean of ± 150 $kgha^{-1}$ Herbaceous Dry Matter at 60, 70 and 80% Confidence Levels (1985 ITE/Silsoe Sites) 3.28

Figure 3.12: Arrangement of Sampling Sites of 1988 CAZS Field Survey in Mali 3.29

Figure 3.13: Development of Air-dried Moisture Content During CAZS Field Survey (Transect Averages) 3.31

Figure 3.14: Development of Herbaceous Dry Matter, Moisture Content and Cover During 1988 Growing Season in Mali 3.32

Figure 3.15: Slope Coefficients of Regression Between Herbaceous Dry Matter and Moisture Content and Cover for 1988 Field Survey in Mali 3.33

Figure 3.16: Relationship Between Herbaceous Dry Matter Quantities and Confidence Level for Standard Errors of the Mean of ± 125, ± 150 and ± 200 $kgha^{-1}$ (1988 CAZS Sites, 5th Mission) 3.35

Figure 3.17: Relationship Between Herbaceous Dry Matter Quantities and Confidence Level for Standard Errors of the Mean of ± 125, ± 150 and ± 200 $kgha^{-1}$ (1988 CAZS Sites, 6th Mission) 3.35

Figure 3.18: Relationship Between Herbaceous Dry Matter Quantities and Confidence Level for Standard Errors of the Mean of ± 125, ± 150 and ± 200 $kgha^{-1}$ (1988 CAZS Sites, 7th Mission) 3.36

Figure 3.19: Required Number of Samples per Site to Achieve a Standard Error of ± 150 $kgha^{-1}$ at 60, 70 and 80% Confidence Level (1988 CAZS Sites, 5th Mission) 3.37

Figure 3.20: Required Number of Samples per Site to Achieve a Standard Error of ± 150 $kgha^{-1}$ at 60, 70 and 80% Confidence Level (1988 CAZS Sites, 6th Mission) 3.37

Figure 3.21: Required Number of Samples per Site to Achieve a Standard Error of ± 150 kgha^{-1} at 60, 70 and 85% Confidence Level (1988 CAZS Sites, 7th Mission) 3.38

Figure 3.22: Duration of Field Survey Mission (for 10% observed significance level, CAZS Survey, 5th Mission) 3.39

Figure 3.23: Duration of Field Survey Mission (for 10% observed significance level, CAZS Survey, 6th Mission) 3.39

Figure 3.24: Duration of Field Survey Mission (for 10% observed significance level, CAZS Survey, 7th Mission) 3.40

Figure 3.25: Arrangement of Sampling Sites of 1988 ITE/Silsoe Field Survey 3.42

Figure 3.26: Relationship between WILE 35 Instrument Readings and Oven-dried Moisture Content 3.46

Figure 3.27: Area of Low Phytomass Level 3.48

Figure 3.28: Area of High Phytomass Level 3.48

Figure 3.29: Herbaceous Dry Matter Quantity vs. Average Cover, Moisture Content and Number of Bushes and Trees for 1988 Field Survey in Niger (Transect Averages) 3.50

Figure 3.30: Slope Coefficients of Regression between Herbaceous Dry Matter and Moisture Content and Cover for 1988 Field Survey in Niger 3.51

Figure 3.31: Relationship Between Duration of Storage and Air-dried M.C. (1988 ITE/Silsoe Survey) 3.53

Figure 3.32: Relationship Between Herbaceous Dry Matter Quantities and Confidence Level for Standard Errors of the Mean of ± 125, ± 150 and ± 200 kgha^{-1} (1988 ITE/Silsoe Sites) 3.55

Figure 3.33: Required Number of Samples to Achieve Standard Error of the Mean of ± 150 kgha^{-1} Herbaceous Dry Matter at 60, 70 and 80% Confidence Levels (1988 ITE/Silsoe Sites) 3.55

Figure 3.34: Arrangement of Sampling Sites of 1989 ITE/Silsoe Field Survey in Niger 3.57

Figure 3.35: Development of Air-dried M.C. With Duration of Storage 3.63

Figure 3.36: Average Vegetation Moisture Content for Sites of Both Sampling Periods 3.64

Figure 3.37: Development of Cover and Height of Herbaceous Vegetation over Sampling Period 3.67

Figure 3.38: Relationship between Rangeland Production and M.C. of Herbaceous Vegetation 3.69

Figure 3.39: Relationship between Rangeland Production and Herbaceous Vegetation Ground Cover 3.70

Figure 3.40: Rangeland Production vs. Average Height of Herbaceous Vegetation 3.71

Figure 3.41: Rangeland Production vs. Bush and Tree Count 3.72

Figure 3.42: Rangeland Production vs. Soil Colour Classes 3.74

Figure 3.43: Relationship Between Herbaceous Dry Matter Quantities and Confidence Level for Standard Errors of the Mean of ± 125, ± 150 and ± 200 $kgha^{-1}$ (1st Mission of 1989 ITE/Silsoe Sites) 3.76

Figure 3.44: Relationship Between Herbaceous Dry Matter Quantities and Confidence Level for Standard Errors of the Mean of ± 125, ± 150 and ± 200 $kgha^{-1}$ (2nd Mission of 1989 ITE/Silsoe Sites) 3.77

Figure 3.45: Required Number of Samples to Achieve Standard Error of the Mean of ± 150 $kgha^{-1}$ Herbaceous Dry Matter at 60, 70 and 80% Confidence Levels (1989 ITE/Silsoe Sites, 1st Mission) 3.78

Figure 3.46: Required Number of Samples to Achieve Standard Error of the Mean of ± 150 $kgha^{-1}$ Herbaceous Dry Matter at 60, 70 and 80% Confidence Levels (1989 ITE/Silsoe Sites, 2nd Mission) 3.78

Figure 3.47: Duration of Field Survey Mission (for 10% observed significance level, ITE/Silsoe/CASTE Survey, 1st to 2nd Mission) 3.80

Figure 3.48: Comparison of Herbaceous Dry Matter Quantities of 1985, 1988 and 1989 ITE/Silsoe Field Surveys in Niger 3.86

Figure 3.49: Comparison of Herbaceous Vegetation Moisture Content of 1988 CAZS and 1988 and 1989 ITE/Silsoe Field Surveys 3.88

Figure 3.50: Comparison of Herbaceous Vegetation Ground Cover of 1985 CIPEA, 1988 CAZS and 1988 and 1989 ITE/Silsoe Field Surveys 3.90

Figure 3.51: Comparison of Herbaceous Vegetation Dry Matter Quantity per Percent Ground Cover of 1985 CIPEA, 1988 CAZS and 1988 and 1989 ITE/Silsoe Field Surveys 3.91

Figure 3.52: Development of Percentage Cover per 1000 kg of Rangeland Vegetation 3.92

Figure 4.1: Temporal Distribution of Landsat MSS and NOAA AVHRR Satellite Data for CAZS, CIPEA and ITE/Silsoe Field Survey Areas 4.3

Figure 4.2: Method of Geometric Correction of Landsat MSS and NOAA AVHRR Images 4.7

Figure 4.3: Geometrically Corrected Landsat MSS (31.08.85, 50 Resampling, NN) 512 x 512 Extract over ITE/Silsoe Study Area (Band 2: Blue, Band 4: Red) 4.10

Figure 4.4: Geometrically Corrected NOAA AVHRR (31.08.85, 1.1km Resolution, NN) Extract over ITE/Silsoe Study Area (Channel 1: Blue, Channel 2: Red) 4.10

Figure 4.5: Method of Radiometrically Correcting Landsat MSS DN to Values of Apparent Spectral Reflectance 4.12

Figure 4.6: Raw Digital Numbers for Landsat MSS Bands 2 and 4 from 31 August 1985 (191/49), 30 August 1988 (192/49) and 8 September 1988 (191/49) 4.18

Figure 4.7: Exoatmospheric Spectral Reflectance for Landsat MSS Bands 2 and 4 from 31 August 1985 (191/49), 30 August 1988 (192/49) and 8 September 1988 (191/49) 4.19

Figure 4.8: Normalized Vegetation Indices from Digital Numbers and Exoatmospheric Spectral Reflectances for Landsat MSS Bands 2 and 4 from 31 August 1985 (191/49), 30 August 1988 (192/49) and 8 September 1988 (191/49) 4.19

Figure 4.9: Average Decompression Functions for Landsat MSS Bands from 31 August 1985 ..... 4.21

Figure 4.10: Comparison of Average Spectral Reflectances of Landsat MSS Bands 2 and 4 for Bare Soil Values for Images from 31 August 1985, 30 August 1988 and 8 September 1988 ..... 4.22

Figure 4.11: Comparison of Average Spectral Reflectances of Landsat MSS Band 4 for Bare Soil Values of Identical Image Positions for Images from 31 August 1985 and 8 September 1988 ..... 4.23

Figure 4.12: Method of Radiometrically Correcting NOAA AVHRR DNs to Values of Apparent Spectral Albedo 4.24

Figure 4.13: Relationship Between Solar Zenith Angle and Channel 2 Spectral Albedo Values for Bare Soil over CIPEA, 1985 ITE/Silsoe, CAZS and 1988 ITE/Silsoe Field Surveys 4.27

Figure 4.14: Relationship Between Solar Zenith Angle and NDVI Values for Bare Soil over CIPEA, 1985 ITE/Silsoe, CAZS and 1988 ITE/Silsoe Field Surveys 4.28

Figure 4.15: Relationship Between View Angle and NDVI for NOAA AVHRR Images of 1985 ..... 4.29

Figure 4.16: Relationship Between View Angle and NDVI for NOAA AVHRR Images of 1988, First Half of Growing Season 4.30

Figure 4.17: Relationship Between View Angle and NDVI for NOAA AVHRR Images of 1988, Second Half of Growing Season 4.30

Figure 4.18: Raw Digital Numbers for NOAA AVHRR Channel 1 for CIPEA, 1985 ITE/Silsoe, CAZS and 1988 ITE/Silsoe Surveys 4.34

Figure 4.19: Raw Digital Numbers for NOAA AVHRR Channel 2 for CIPEA, 1985 ITE/Silsoe, CAZS and 1988 ITE/Silsoe Surveys 4.35

Figure 4.20: Exoatmospheric Spectral Albedo for NOAA AVHRR Channel 1 for CIPEA, 1985 ITE/Silsoe, CAZS and 1988 ITE/Silsoe Surveys 4.35

Figure 4.21: Exoatmospheric Spectral Albedo for NOAA AVHRR Channel 2 for CIPEA, 1985 ITE/Silsoe, CAZS and 1988 ITE/Silsoe Surveys 4.36

Figure 4.22: Normalized Vegetation Indices for NOAA AVHRR Based on Digital Numbers From Channel 1 and 2 for CIPEA, 1985 ITE/Silsoe, CAZS and 1988 ITE/Silsoe Surveys 4.36

Figure 4.23: Normalized Vegetation Indices for NOAA AVHRR Based on Spectral Albedo From Channel 1 and 2 for CIPEA, 1985 ITE/Silsoe, CAZS and 1988 ITE/Silsoe Surveys 4.37

Figure 4.24: Graphical Representation of Definition Components of Apparent Spectral Radiance 4.38

Figure 4.25: Procedure of Identifying Reference Image for Atmospheric Standardization for NOAA AVHRR Images of the 1988 ITE/Silsoe Field Survey ... 4.42

Figure 5.1: Schematic description of Transect Sampling Method for 1.1 km Resolution Landsat MSS and NOAA AVHRR Images 5.9

Figure 5.2: Development of Coefficients of Determination from Linear Regression Between Transect Sampling and a Single Pixel for Channels 1 and 2 over 1985 CIPEA Field Survey Sites 5.15

Figure 5.3: Development of Coefficients of Determination from Linear Regression Between Transect Sampling and a Single Pixel for Channels 1 and 2 over 1985 ITE/Silsoe Field Survey Sites 5.17

Figure 5.4: Development of Coefficients of Determination from Linear Regression Between Transect and a Single Pixel Image Sampling Methods for Channels 1 and 2 over 1988 CAZS Field Survey Sites 5.20

Figure 5.5: Development of Coefficients of Determination from Linear Regression Between Transect and a Single Pixel Image Sampling Methods for Channels 1 and 2 over 1988 ITE/Silsoe Field Survey Sites 5.23

Figure 5.6: Radiometric Affinity Between Spectral Albedos of NOAA AVHRR Channels 1 and 2 and Spectral Reflectances of Landsat MSS Bands 2 and 4 for 8 CIPEA Field Survey Sites (3 by 3 Average Image Sampling Method) 5.26

Figure 5.7: Radiometric Affinity Between Spectral Albedos of NOAA AVHRR Channels 1 and 2 and Spectral Reflectances of Landsat MSS Bands 2 and 4 for 1985 ITE/Silsoe Field Survey Sites (3 by 3 Average Image Sampling Method) 5.27

Figure 5.8: Radiometric Affinity Between Spectral Albedos of NOAA AVHRR Channels 1 and 2 and Spectral Reflectances of Landsat MSS Bands 2 and 4 for 1988 CAZS Field Survey Sites (3 by 3 Average Image Sampling Method) 5.28

Figure 5.9: Radiometric Affinity Between Spectral Albedos of NOAA AVHRR Channels 1 and 2 and Spectral Reflectances of Landsat MSS Bands 2 and 4 for 1988 ITE/Silsoe Field Survey Sites (3 by 3 Average Image Sampling Method) 5.30

Figure 5.10: Relationship Between Estimates of Herbaceous Vegetation of CIPEA Field Survey Sites and NDVIs from Landsat MSS and NOAA AVHRR for Sites Positioned by Aerial Photographs on Images (Central Sampling) 5.34

Figure 5.11: Relationship Between Estimates of Herbaceous Vegetation of 1985 ITE/Silsoe Field Survey Sites and NDVIs from Landsat MSS and NOAA AVHRR (Central Sampling) 5.38

Figure 5.12: Image Representation of Landsat MSS NDVI (50 m Resampling, NN) from 31 August 1985 ..... 5.39

Figure 5.13: Image Representation of NOAA AVHRR NDVI (1.1 km, NN) from 31 August 1985 ..... 5.39

Figure 5.14: Relationship Between Estimates of Herbaceous Vegetation of CAZS Field Survey Sites and NDVIs from Landsat MSS and NOAA AVHRR (Central Sampling) 5.44u

Figure 5.15: Development of NOAA AVHRR Average NDVIs Throughout 1988 Growing Season for CAZS Sample Sites 5.44

Figure 5.16: Relationship Between Estimates of Herbaceous Vegetation of 1988 ITE/Silsoe Field Survey Sites and NDVIs from Landsat MSS and NOAA AVHRR from 6 September 1988 (Central Sampling) 5.50

Figure 5.17: Relationship Between Estimates of Herbaceous Vegetation of 1988 ITE/Silsoe Field Survey Sites and NDVIs from Landsat MSS and NOAA AVHRR from 5 October 1988 (Central Sampling) 5.50

Figure 5.18: Comparison of Landsat MSS NDVIs Derived from 50 m Resolution Atmospherically Standardized Data for All Field Survey Sites 5.52

Figure 5.19: Comparison of Landsat MSS NDVIs Derived from 1.1 km Resolution Atmospherically Standardized Data for All Field Survey Sites 5.53

Figure 5.20: Comparison of NOAA AVHRR NDVIs Derived from DNs and Atmospherically Standardized Data for CAZS and 1988 ITE/Silsoe Field Survey Sites 5.55

Figure 5.21: Relationship Between Herbaceous Vegetation Estimates of CIPEA, CAZS and ITE/Silsoe Field Surveys and NOAA AVHRR NDVIs Derived from DNs 5.56

Figure 5.22: Relationship Between Herbaceous Vegetation Estimates of CIPEA, CAZS and ITE/Silsoe Field Surveys and NOAA AVHRR NDVIs Derived from Radiometrically Corrected Spectral Albedos ... 5.58

Figure 5.23: Relationship Between Herbaceous Vegetation Estimates of CIPEA, CAZS and ITE/Silsoe Field Surveys and NOAA AVHRR NDVIs Derived from Atmospherically Standardized 5.61

Figure 5.24: Relationship Between Landsat MSS NDVIs of 50 m Resampled Image Data and NOAA AVHRR NDVIs Derived from Atmospherically Standardized for All Field Surveys 5.65

Figure 5.25: Relationship Between Landsat MSS NDVIs of 1.1 km Resolution Image Data and NOAA AVHRR NDVIs Derived from Atmospherically Standardized for All Field Surveys 5.65

Figure 5.26: Relationship Between Landsat MSS NDVIs of 1.1 km Resolution Image Data and NOAA AVHRR PVIs Derived from Atmospherically Standardized for All Field Surveys 5.67

FIGURES APPENDIX I

Figure A.1: Assumption About Data Characteristics for Regression Analysis A.7

Figure A.2: Orbital Model for Geometric Image Referencing A.14

FIGURES APPENDIX III

Figure A.1: Relationship Between Fresh Sample Weight and Oven-Dried Moisture Content for 1988 ITE/Silsoe Survey A.119

Figure A.2: Relationship Between View Angle and NOAA AVHRR Channel 1 Sensor Response of 1985 ..... A.120

Figure A.3: Relationship Between View Angle and NOAA AVHRR Channel 2 Sensor Response of 1985 ..... A.120

Figure A.4: Relationship Between View Angle and NOAA AVHRR RVI of 1985 ..... A.121

Figure A.5: Relationship Between View Angle and NOAA AVHRR Channel 1 Sensor Response of 1988, First Half of Growing Season A.121

Figure A.6: Relationship Between View Angle and NOAA AVHRR Channel 1 Sensor Response of 1988, Second Half of Growing Season A.122

Figure A.7: Relationship Between View Angle and NOAA AVHRR Channel 2 Sensor Response of 1988, First Half of Growing Season A.122

Figure A.8: Relationship Between View Angle and NOAA AVHRR Channel 2 Sensor Response of 1988, Second Half of Growing Season A.123

Figure A.9: Relationship Between View Angle and RVI for NOAA AVHRR Images of 1988, First Half of Growing Season A.123

Figure A.10: Relationship Between View Angle and RVI for NOAA AVHRR Images of 1988, Second Half of Growing Season A.124

ABBREVIATIONS

ATN	Advanced TIROS-N
AVHRR	Advanced Very High Resolution Radiometer
CASTE	Cambridge Agromet Sharan Tandem Expedition
CAZS	Centre for Arid Zone Studies, Bangor
CCT	Computer Compatible Tape
CIPEA	Centre International Pour l'Elevage en Afrique
C.V.	Coefficient of Variation
DN	Digital number
EM	Electromagnetic
ERIM	Environmental Research Institute of Michigan
ERTS	Experimental Earth Resource Technology Satellite
FAO	United Nations Food and Agricultural Organization
FCCAD	Foreign Crop Condition Assessment Division
FOV	Field of View
GAC	Global Area Coverage
GCP	Ground Control Point
GLAI	Green Leaf Area Index
GPS	Global Positioning System
GVI	Global Vegetation Index
HIRS/2	High Resolution Infrared Radiation Sounder 2
HRPT	High Resolution Direct Readout
IFOV	Instantaneous Field Of View
ILCA	International Livestock Commission for Africa
IR	Infra Red
ITE	Institute of Terrestrial Ecology, Monks Wood
ITOS	Improved TIROS Operation System
LAC	AVHRR Large Area Coverage
m.c.	Moisture Content (%)
MOS	Marine Observation Satellite
MSS	Landsat Multispectral Scanner
MSU	Microwave Sounding Unit
MT	Magnetic Tape
MVC	Maximum Value Composite
NERC	Natural Environmental Research Counsel
NOAA	US National Oceanographic and Atmospheric Administration
NDVI	Normalized Difference Vegetation Index
NIR	Near infrared portion of electromagnetic spectrum (0.78 - 1.5 μm)
PAR	Photosynthetically Active Radiation
PC	Personal Computer
PVI	Perpendicular Vegetation Index
RED	Red portion of electromagnetic spectrum
RVI	Ratio Vegetation Index
SBI	Soil Brightness Index
SLI	Soil Line Index
SSU	Stratospheric Sounding Unit
TDRSS	Tracking and Data Relay Satellite System
TIROS	Television Infrared Observation Satellite
TOVS	TIROS Operational Vertical Sounder
TM	Landsat Thematic Mapper
VHRR	Very High Resolution Radiometer
VI	Vegetation Index

UNITS

(a) SI Units:

m	meter
kg	kilogramme
s	second

(b) British and other Units:

a	annum
°C	degree Celcius
µ	micron, 10^{-6}
g	gramme
h	hour
ha	hectar
l	litres
mb	mega byte
mHz	mega Hertz
min.	minutes
mio.	million, 10^{6}
mrad	mili rad
sr	steridian
V	volt
W	watt

(c) Statistical Units:

n	number of samples
r	Pearson's correlation coefficient
r^2	coefficient of determination
σ	population standard deviation
s	sample standard deviation
t	Student's t value
$\bar{x}$	sample mean
µ	population mean

VARIABLES IN EQUATIONS

(a) Geometric, Radiometric and Atmospheric Equations

A	sample area (m^2)
$a_{im}(l)$	slope coefficient relating surface spectral reflectance to apparent spectral reflectance of non-standardized image (unitless)
$a_{ref}(l)$	slope coefficient relating surface spectral reflectance to apparent spectral reflectance of reference image (unitless)
$a_s(l)$	fraction of reflected radiation backscattered by the atmosphere to the surface (unitless)
a(i)	slope coefficient for spectral radiance conversion of DNs ($Wm^{-2}\Omega_i^{-1}sr^{-1}DN^{-1}$)
a(*l*,i)	slope calibration coefficient for linear spectral radiance conversion of DNs as supplied by NOAA ($Wm^{-2}\mu m^{-1}sr^{-1}count^{-1}$)
$a_{1..6}$	polynomial coefficients (reference $unit^{-1}$)
b_a	coefficient for optical thickness of aerosol scattering
$b_{im}(l)$	off-set constant relating surface spectral reflectance to apparent spectral reflectance of non-standardized image (unitless)
$b_{ref}(l)$	off-set constant relating surface spectral reflectance to apparent spectral reflectance of reference image (unitless)
b_s	intercept of soil line with y-axis
b_t	coefficient for optical thickness of molecular scattering
b(i)	off-set constant for spectral radiance conversion of DNs ($Wm^{-2}\Omega_i^{-1}sr^{-1}$)
b(*l*i)	off-set calibration coefficient for linear spectral radiance conversion of DNs ($Wm^{-2}\mu m^{-1}sr^{-1}$)
$b_{1..6}$	polynomial coefficients (reference $unit^{-1}$)
c_a	constant for band a, summarizes variation in illumination conditions (unitless)
c_b	constant for band b, summarizes variation in illumination conditions (unitless)
c_{cal}	correction factor for solar illumination conditions (unitless)
c_{cos}	correction factor for solar azimuth angle (unitless)
CHl_{deg}	changes in instrument sensitivity in NOAA AVHRR channel 1
CH_{2deg}	changes in instrument sensitivity in NOAA AVHRR channel 2
c_{sd}	correction factor for variation in the solar irradiance (unitless) due to differing Sun-Earth distance over time
d	Julian date of year
d_{ax}	ground distance in across-track direction (m)

d_{nax}	displacement of nth scan line element from nominal position (m)
DN_c	digital count corrected for solar zenith angle (count)
DN_i	digital count on CCT for channel i (count)
DN_{maxi}	maximum digital count in band i (count)
DN_{nir}	digital count in the NIR band (count)
DN_{red}	digital count in the red band (count)
DN_u	digital count uncorrected for solar zenith angle (DN)
d_s	sidereal day, 86164.09 s
d(i)	off-set calibration constant for linear spectral albedo conversion (%)
D(i)	reflectance constant for off-set calibration constant of linear spectral radiance conversion (% $count^{-1}$)
e	Euler's value, 2.718...
$E_A(\lambda)$	absorbed energy at wavelength λ
$E_G(\lambda)$	global surface spectral irradiance on target at the bottom of the atmosphere ($Wm^{-2}\mu m^{-1}$)
$E_I(\lambda)$	incident spectral solar radiance at wavelength λ ($Wm^{-2}\mu m^{-1}$)
e_o	eccentricy of the Earth orbit, 0.0167
$E_R(\lambda)$	reflected spectral radiance at wavelength λ ($Wm^{-2}\mu m^{-1}$)
$E_S(\lambda)$	reflected spectral radiance at wavelength λ from surface directly to sensor ($Wm^{-2}\mu m^{-1}$)
$E_T(\lambda)$	transmitted spectral radiance at wavelength λ ($Wm^{-2}\mu m^{-1}$)
E(i)	spectral solar irradiance on the top of the atmosphere per unit projected area for band i ($Wm^{-2}\mu m^{-1}$)
$E(i)_T$	spectral solar irradiance at the top of the atmosphere for wavelength λ, based on Thekaekara ($Wm^{-2}\mu m^{-1}$)
$E(\lambda)$	spectral solar irradiance at the top of the atmosphere for wavelength λ ($Wm^{-2}\mu m^{-1}$)
$E(\lambda,i)$	spectral solar irradiance at the top of the atmosphere for central wavelength λ in band i ($Wm^{-2}\mu m^{-1}$)
$E(\lambda i,d)$	spectral solar irradiance at Julian date d ($Wm^{-2}\mu m^{-1}$)
g_c	earth gravitational constant ($3.98601*10^{14}$ m^3s^{-2}
g(i)	slope calibration coefficient for linear spectral albedo conversion (% $count^{-1}$)
G(i)	reflectance coefficient for slope calibration coefficient of linear spectral radiance conversion (% $count^{-1}$)
h	actual orbital altitude of platform above earth surface (m)
H	nominal orbital altitude of platform above earth surface (m)
i	spectral channel
L	Location accuracy (pixels)
$L_a(\lambda)$	atmospheric radiance ($Wm^{-2}\mu m^{-1}sr^{-1}$)
$L_b(\lambda)$	background radiance ($Wm^{-2}\mu m^{-1}sr^{-1}$)
l_{Elong}	longitude at equator crossing (deg)
$L_e(\lambda)$	environmental radiance from surrounding area

	of pixel of interest ($Wm^{-2}\mu m^{-1}sr^{-1}$)
l_{lat}	latitude of central pixel (deg)
$l_{latgeocentric}$	geocentic latitude (deg)
$l_{latgeographic}$	geographic latitude (deg)
l_{long}	longitude (deg)
L_{maxi}	sensor saturation spectral band radiance level for band i ($Wm^{-2}\Omega_i{}^{-1}sr^{-1}$)
$L_{max\lambda i}$	sensor saturation spectral radiance level for band i ($Wm^{-2}\mu m^{-1}sr^{-1}$)
L_{mini}	sensor threshold spectral band radiance level for band i ($Wm^{-2}\Omega_i{}^{-1}sr^{-1}$)
$L_{min\lambda i}$	sensor threshold spectral radiance level for band i ($Wm^{-2}\mu m^{-1}sr^{-1}$)
L_n	line number in image (unitless)
$L_p(\lambda)$	Rayleigh plus aerosol path radiance ($Wm^{-2}\mu m^{-1}sr^{-1}$)
$L_s(\lambda)$	surface leaving spectral radiance ($Wm^{-2}\mu m^{-1}sr^{-1}$)
L(i)	incident spectral band radiance in channel i ($Wm^{-2}\Omega_i{}^{-1}sr^{-1}$)
$L(i,\Omega_i)$	spectral band radiance in band i
$L(\lambda)$	spectral radiance at top of atmosphere ($Wm^{-2}\mu m^{-1}sr^{-1}$)
$L(\lambda,i)$	spectral radiance at top of atmosphere for central wavelength λ of band i ($Wm^{-2}\mu m^{-1}sr^{-1}$)
$L(\lambda,\phi)$	spectral radiance at viewing angle ø ($Wm^{-2}\mu m^{-1}sr^{-1}$)
m_s	slope of soil line
M_x	position in geometric reference data in x-direction (reference data unit)
M_y	position in geometric reference data in y-direction (reference data unit)
M.R.	moisture meter reading
NIR_{soil}	sensor response of soil in the NIR
NIR_{veg}	sensor response of vegetation in the NIR
n_x	number of pixel element in scan line
N_x	number of elements per scan line
n(a)	additive noise component in band a
n(b)	additive noise component in band b
O	off-nadir point on earth surface
P_n	nominal pixel size at nadir (m)
P_{al}	pixel size in along track direction (m)
P_{ax}	pixel size in across track direction (m)
PVI_{cos}	PVI with cosine correction for solar elevation applied (unitless)
P_x	pixel position along scan line
$R_{a/b}$	ratio of band a over band b
r_e	equatorial earth radius (6378160 m)
r_{lat}	earth radius at latitude l_{lat} (m)
r_p	polar earth radius (6356775 m)
R_{soil}	reflectance of soil in red (%)
R_{veg}	reflectance of Vegetation in red (%)
S	sub-satellite point on earth surface
s_o	distance between satellite and off-nadir point (m)
S_{lat}	latitude od sub-satellite point S (deg)
SLN	solar noon, time at which the sun crosses the

	meridian
S_{long}	latitude of sub-satellite point S (deg)
s(a)	spectral sensor response in band a
s(b)	spectral sensor response in band b
S(i)	equivalent solar band radiance in channel i ($Wm^{-2}\Omega_i{}^{-1}sr^{-1}$)
S(*l*,i)	equivalent solar radiance for central wavelength *l* in channel i ($Wm^{-2}\mu m^{-1}sr^{-1}$)
t	time between data acquisition and crossing of ascending node (s)
T	orbital period (s)
t_f	time between data acquisition of first line and crossing of ascending node (s)
t_l	time required to scan one line (s)
T_h	time of data acquisition in hour
T_m	time of data acquisition in minutes
X	column position in input data (unitless)
Y	row position in output data (unitless)
Ya	ground size of image along-track (m)
a(*l*i)	equivalent spectral albedo in channel i, as supplied by NOAA (%)
$a(li)_N$	equivalent spectral albedo in channel i, based on Neckel and Labs (%)
h	local hour angle (deg)
l	wavelength (μm)
O_e	earth oblateness (0.00108263) (unitless)
$p_a(l)$	atmospheric reflectance at wavelength *l* (unitless)
$p_a(l,\varepsilon)$	aerosol reflectance at wavelength *l* and scattering angle ε (unitless)
p_e	orbit precession (rad s^{-1})
$p_e(l)$	environmental reflectance of surfaces surrounding pixel of interest (unitless)
$p_{im}(l)$	apparent reflectance of earth-atmosphere system for non-standardized image (unitless)
$p_r(l,\varepsilon)$	molecular reflectance at wavelength *l* and scattering angle ε (unitless)
$p_{ref}(l)$	apparent reflectance of earth-atmosphere system for reference image (unitless)
$p_s(l)$	spectral reflectance of Lamberttion surface at surface level (unitless)
p(*l*)	spectral reflectance of Lambertian surface (%)
p(*l*,i)	spectral reflectance of Lambertian surface for central wavelength *l* in band i (%)
p(*l*,d,Θ)	spectral reflectance of Lambertian surface, corrected for solar distance and zenith (%)
$t_{dif}(l)$	diffuse transmission of atmosphere from surface to satellite (dimensionless)
$t_{dir}(l)$	direct transmission of atmosphere from surface to satellite (dimensionless)
t(*l*)	transmission of atmosphere from surface to satellite (dimensionless)
V_e	angular velocity of earth ($7.29246*10^{-5}$ rad s^{-1})
V_n	angular velocity of earth relative to satellite orbit plane (rad s^{-1})
V_s	angular velocity of satellite (rad s^{-1})

α_o	angle between sun vector and the perpendicular to the surface (=Θ_s for flat surface) (deg)
α_s	solar altitude (deg)
α_x	standard solar zenith angle (deg)
α_z	solar zenith angle at time of data acquisition (deg)
α_{zs}	standard solar zenith angle (deg)
$\alpha(i)$	slope coefficient for converting Landsat MSS DNs to apparent spectral reflectance (DN^{-1})
$\alpha(i)_N$	slope coefficient for converting NOAA AVHRR DNs to spectral albedo based on Neckel and Labs (% DN^{-1})
$ß_{ax}$	geocentric arc between nadir and pixel position in across-track direction (rad)
$ß_{ES}$	arc between ascending node E and sub-satellite point S (rad)
$ß_i$	geocentric step size for inverse image referencing (rad)
$ß_{IFOV}$	geocentric arc for IFOV (rad)
$ß_{lat}$	latitude of observed point (rad)
$ß_{long}$	longitude of observed point (rad)
$ß_{max}$	arc between nadir point and first pixel (rad)
$ß_{OE}$	arc between equator crossing and point of observation (rad)
$ß_{Olong}$	arc between observed and nadir point (rad)
$ß_r$	earth rotational contribution per scan line to longitute position of pixel (rad)
$ß_s$	arc including IFOV in along-track direction (rad)
$ß(i)$	off-set constant for converting Landsat MSS DNs to apparent spectral reflectance (DN^{-1})
$ß(i)_N$	off-set constant for converting NOAA AVHRR DNs to spectral albedo based on Neckel and Labs (% DN^{-1})
δ_s	solar declination (deg)
ε	backscattering angle (rad)
Θ_{rel}	relative azimuth angle (deg)
Θ_s	solar azimuth (deg)
$ø$	sensor viewing angle (rad)
$ø_i$	sensor scan step angle (rad)
$ø_{IFOV}$	instantaneous field of view angle (rad)
$ø_{max}$	maximum sensor scan angle (rad)
$ø_o$	latitude of place of observation (deg)
$ø_v(n_x)$	actual viewing angle at nth scan line element (deg)
$\tau(\lambda)$	optical thickness of atmosphere (m)
$\tau_a(\lambda)$	aerosol optical thickness (m)
$\tau_g(\lambda)$	gaseous optical thickness (m)
$\tau_r(\lambda)$	Raleigh optical thickness (m)
Φ	orbital inclination (deg)
Φ_l	crossing angle of orbital path with latitude at latitude l_{lat} (deg)
Φ_O	arc between equator and the line between the points of the eqautor crossing and observqtions (rad)
Φ_S	sensor skew angle (rad)
Ω_i	bandwidth in spectral band i (µm)

(b) Statistical Equations

C.V.	coefficient of variation (%)
$d\bar{x}$	Difference between means
e	admissible error
M_{res}	standard error of y-estimate
n_1	number of samples from survey
n_2	number of samples from hypothetical survey
r_{pop}	coefficient of determination for population
r_{samp}	coefficient of determination for samples
rms	root means square error
$\hat{s}$	best estimate of standard deviation
s_B	standard deviation with Bessel's correction factor
sd_1	standard deviation from survey
sd_2	standard deviation from hypothetical survey
s_{dd}	standard difference
s_{x1}	standard deviation of sample ($kgha^{-1}$)
t_{80}	t-value for 80% confidence level
w_c	width of class ($kgha^{-1}$), e.g. ± 100 $kgha^{-1}$ (two-sided t)
$\bar{x}_1$	average rangeland production from samples ($kgha^{-1}$)
$\bar{x}_2$	average sample mean of hypothetical survey ($kgha^{-1}$)
x_i	independent value of sample
x_0	fixed value of independent variable
$\hat{y}_0$	predicted value for dependent variable
y_i	observed value
μ_1	rangeland production at site ($kgha^{-1}$)

1. INTRODUCTION

The Sahel is an ecological region south of the Sahara desert. It is defined by the mean annual precipitation, which ranges from 200 to 400 mm (Le Houerou, 1980; White, 1983). For 5500 km it stretches as a belt from the Atlantic Ocean to the Red Sea. For this study an area in Niger was chosen, where the Sahel and its bordering Sudanian ecological zone to the South and the Sahara Desert to the North can be found.
The principal source of livelihood of the people in the Sahel is pastoralism. Food supply and economic prosperity depend on the production of land, which is useful for grazing. These areas are summarized by the term rangelands (Tueller, 1987). In the Sahel rangeland vegetation yields may reach an overall average of 1200 to 1500 $kgha^{-1}$ of above ground total dry matter (Le Houerou & Hoite, 1977; Bille, 1977). An additional 80 to 300 $kgha^{-1}$ dry matter may be composed of woody leaves, twigs and fruits (Le Houerou, 1980).

1.1 Enigma of Sahelian Rangeland Vegetation

The amount of vegetation available for grazing varies considerably for different regions and years. As a consequence, a frequent shortage in grazing material is inherent to the area. Maps identifying phytomass quantities would enable government agencies to inform herdsmen to shift stock from areas with low phytomass levels to areas with more grazing material.
In order to mitigate the results of extreme climatic conditions on larger scales, a prediction as to the extent of possible consequences of low precipitation and constant monitoring are required. Governments of the areas concerned could begin to take action to reduce the number of animals before the shortage in grazing material becomes acute. Additionally, the planning of a relief program and the amount of food called for

could start well in advance. Monitoring of rangelands would allow the identification of long-term changes in vegetation productivity and areas of desertification.

1.2 Monitoring Rangeland Vegetation by Satellite

In order to be usefull for administrative decisions estimates of rangeland vegetation have to be comparable between several growing seasons. A precondition is a reference based on absolute instead of relative values. Therefore, predictions for the rangeland productivity should be based on quantitative measurements rather than qualitative impressions. The latter can be given by experienced persons without the aid of modern technology. For a quantitative estimate of rangeland vegetation production a number of methods could be employed:

(a) Modelling

Of major influence on phytomass production in the Sahel is rainfall, followed by soil fertility (Tucker *et al*, 1985). Further sources of variability in production are species diversity, dry matter accumulation and decomposition and topographic influences. Vegetation growth is mainly restricted to the rainy season, while decomposition, animal grazing and consumption by invertebrates proceed during the whole year. As a consequence, rangeland canopies contain a complex mixture of living and dead plant materials, which varies spatially and over time and which is difficult to model (Huete & Jackson, 1987).

(b) Ground Data Collection

A monitoring system solely based on the collection of ground data is faced by a number of difficulties introduced by the conditions found in the Sahel. The short period of the rainy season very much restricts the available time for any field work aimed at measuring green phytomass. Moreover, large areas have to be covered, but population density and accessibility of

many areas are low. The number of staff needed for data collection and the cost connected with the measurements prohibit rangeland productivity assessments by sampling ground data alone.

(c) **Satellite Remote Sensing**

Estimates of the amount and distribution of phytomass and rainfall can be obtained by satellite remote sensing. It is considered a suitable and relatively low cost tool for the task, since

- large areas can be covered in a continuous process;
- repeated coverage can be provided;
- data can be available in near real time;
- it is comparatively inexpensive;
- the requirements for technical staff are low.

(After: Tueller, 1987)

Vegetation indices (VIs) calculated from the red (0.6 to 0.78 µm, RED) and the photographic or near infra-red (0.78 to 1.5 µm, NIR) portions of the electromagnetic (EM) spectrum have been used to estimate vegetation characteristics. Among these characteristics were phytomass (Maxwell, 1976a), plant cover (Richardson & Wiegand, 1977) and leaf area (Tucker, 1979). Most VIs were developed for agricultural crops, which give a uniform appearance and a dense cover.

The application of VIs for estimating rangeland vegetation has been more problematic (Huete & Jackson, 1987). One of the main obstacles in estimating phytomass over rangeland can be attributed to the influence of the soil background on the overall reflectance of an area. At a vegetation cover below 25 to 35%, reflected EM energy from the soil is the principal component contributing to the overall spectral response. Further sources of variations in VIs for estimating green phytomass originate from dry and decomposed plant material (Huete *et al*, 1985).

For areas with low vegetation densities, the most promising VIs

are the normalized difference vegetation index (NDVI) and the orthogonal VIs (Huete *et al*, 1985). The NDVI can be computed from multi spectral data alone without any prior knowledge of the phytomass within the scene. It is provided as a standard product from the US National Oceanographic and Atmospheric Administration (NOAA) in the form of the global vegetation index (GVI). Although useful for estimating phytomass in areas of low vegetation densities, the NDVI is dependent on the reflectance of the underlying substrata. Over rangelands the main influence results from soils and, to a lesser degree, from litter. This dependence on the background limits the use of the NDVI in areas with varying background reflections.

For two wavebands an orthogonal VI, the perpendicular vegetation index (PVI), was developed as the perpendicular distance to a soil line to indicate plant development (Richardson & Wiegand, 1977).

An advantage of the PVI over the NDVI is the reduced influence of linear background variations by the regression (Elvidge & Lyon, 1985). Contrary to the NDVI, some ground information in the form of soil reflectance values have to be known in order to establish the soil line.

Another obstacle for the use of satellite data for rangeland monitoring is the trade-off between spatial resolution, the frequency of coverage and the amount of data to be processed. Most of the work of estimating rangeland vegetation was based on Landsat Multispectral Scanner (MSS) data (Maxwell, 1976; McGraw & Tueller, 1983; Ringrose & Matheson, 1987). The images were mainly used for land inventory and assessment. For monitoring the rapid changes in vegetation, the usefulness of Landsat data is limited by its 16 to 18 days frequency of coverage. NOAA satellites provide daily coverage at the expense of a lower spatial resolution. The data does not permit land inventory, but this is not the main requirement for rangeland management (Tueller, 1987). The reduction of spatial resolution and spectral data make it more suitable for the routine use with operational systems running on personal computers (PCs). AVHRR images have been used to monitor spatial and temporal changes at regional scales (Tucker *et al*, 1984). For a quantitative estimate of phytomass, VIs have to be related to

ground measurements. The spatial resolution of AVHRR large area coverage (LAC) imagery of 1.1 km instantaneous field of view (IFOV) renders more difficult the procedure of sampling ground data. Taking measurements over large areas are time consuming, while sampling of smaller areas may not represent the reflectance at pixel size and the locations are more difficult to identify on the image.
Part of the problem can be overcome by employing satellite data with a higher spatial resolution like Landsat MSS or Thematic Mapper (TM) data as an intermediate step for the calibration of NOAA AVHRR data. These images can be geometrically corrected via a platform orbit model or ground control points (GCP) to a map projection. The AVHRR LAC image can then be corrected by matching it to the higher resolution image (Taylor *et al*, 1986).

1.3 Project Objectives

The aim of this project is to determine the possibilities and requirements of assessing and monitoring above ground phytomass in the Sahel for an operational rangeland monitoring system, based on NOAA AVHRR data. For this purpose satellite VIs are to be calibrated to estimates of herbaceous vegetation by the statistical method of regression analysis.
The investigation can be divided into four steps:

(a) Identification of a relationship between above ground phytomass and Landsat MSS data at the end of the growing season, when maximum phytomass is present. Determination of correlation between NDVI and PVI and phytomass over the study area.

(b) Establishment of the quantitative relationship between the NDVI and PVI from NOAA AVHRR to phytomass. Evaluation of employing simulated AVHRR data from Landsat MSS for the calibration of NOAA AVHRR.

(c) Assessment of the stability of the relationship between the NDVI and the PVI and phytomass over the period of vegetation development. Confirmation of NDVI or PVI as suitable phytomass indicators.

(d) Statement on data and processing requirements for an operational system for monitoring rangeland productivity in the Sahel from NOAA AVHRR data.

2. BACKGROUND AND LITERATURE SURVEY

In this chapter basic information on the foundations of the project are presented. It is directed at demonstrating that quantitative monitoring of rangeland vegetation in the Sahel could be possible by satellite remote sensing and the work done so far is briefly introduced. During the first part of this chapter geographic, geologic and bio-climatic conditions characteristic for the region of the study area are described. Their relevance to the project manifests itself for example in the choice of the sensor, the period of data acquisition or the adequate representation of phytomass by satellite data.
The second part of the chapter concentrates on the feasibility of estimating phytomass by satellite remote sensing for semi-arid areas. The limitations of the approach encountered in investigations similar to this project and conclusions which can be drawn from them are presented.
The section is followed by a description of Landsat MSS and NOAA AVHRR platform and sensor specifications. The properties are further evaluated with respect to the suitability of the data derived from the satellite sensors for the investigation.

2.1 Study Area

Rangeland production depends on a number of factors of which the main elements are:

- climate
- nature of soil
- botanical composition and vegetation structure
- type and intensity of management
  e.g. grazing pattern and stocking rates

- fire
- wildlife

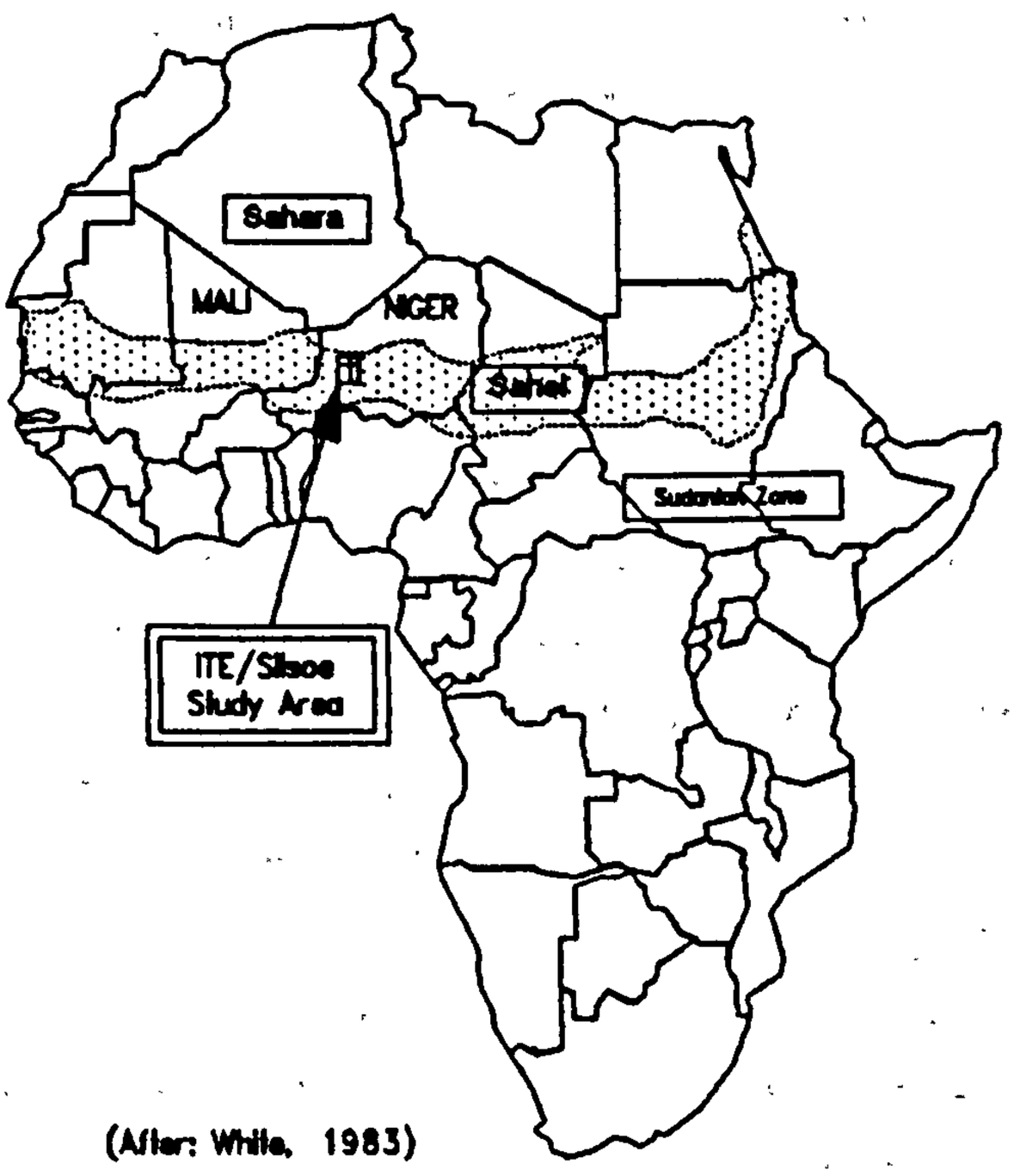
(After: Le Houerou & Hoite, 1977)

These factors are related to, and dependent upon, each other in various ways.
The dependency of vegetation productivity on climatic and pedological factors and the influence of soil on the reflectance of an area demands a brief coverage of these factors.

2.1.1 Location of Study Area

The location of the study area was chosen to cover part of the Sahel completely from the northern to its southern extent (see Figure 2.1). The pixel size of 1.1 km of NOAA Advanced Very High Resolution Radiometer (AVHRR) Local Area Coverage (LAC) data corresponds to a ground cover of approximately 560 by 560 km for a 512 by 512 image, thus allowing the coverage required.

Figure 2.1: Map of Africa with Position of Sahel



(After: White, 1983)

The position of the sample sites in Niger was determined by previous work in that country undertaken by Silsoe College. They were further determined by the TAMSAT meteorological stations, established jointly between the Department of Meteorology of Reading University and the Agrhymet Centre in Niamey, Niger. In addition, the study area included test sites of the International Livestock Commission for Africa (ILCA or Centre Internationale pour l'Elevage en Afrique, CIPEA) to provide an independent data set for testing earlier assumptions.

The area for ground sampling was restricted to a region covered by a Landsat MSS image. The locations of the sample sites ranged between 5.65° to 5.90° E and 15.25° to 15.75° N. The sites were spread over an area of 35 by 60 km. Their location can be divided into two groups:

(a) Sites at the Ibeceten State Ranch
(approx. 5.9° E and 15.3° N)

(b) Sites along the road between Ibeceten and Tchin Tabaraden
(approx. along 5.75° E)

The final decision for the location of sample sites was made in the field, based on their accessibility and possibility of identifying the sites either on image hard-copies or a map.

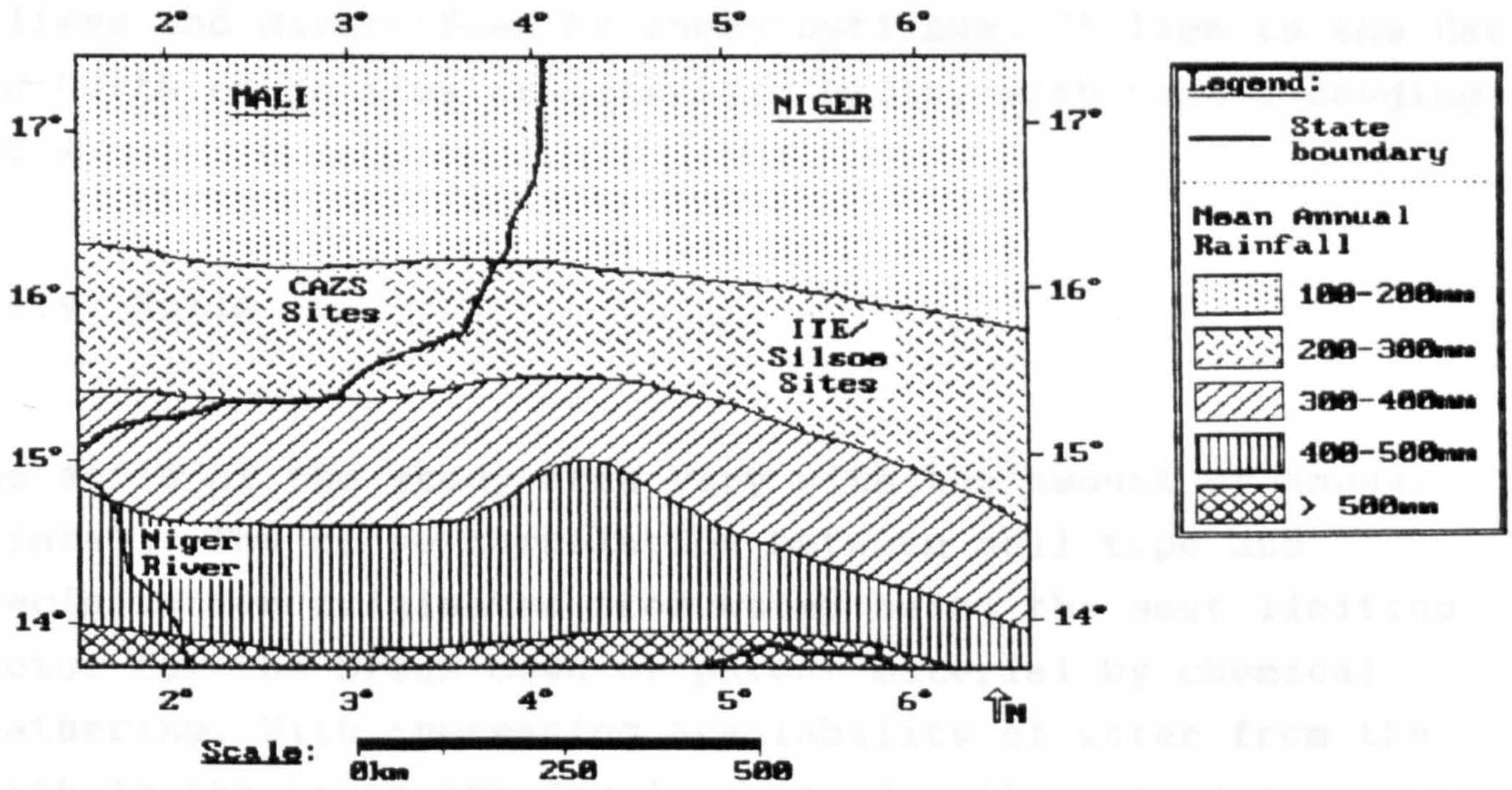
2.1.2 Climate

The Sahel forms a belt of approximately 400 to 500 km width, which covers an area of 2.5 mio. km². It is defined by a mean annual precipitation of either 150 to 400 mm (White, 1983) or 200 to 400 mm (Le Houreou, 1980). The gradient of precipitation runs from north to south with an increase in precipitation of approximately 1 $mmkm^{-1}$ (White, 1983).

Rainfall occurs mainly over a period of 1.5 months (July to August) in the north and 3.5 months (June to September) in the south of the zone. The period is defined by the time when rainfall is equal to or greater than 50% of the potential

evaporation (Tucker, 1985) or 35% of the potential evaporation (Le Houerou & Popov, 1981). Rains may occur from June to the end of September. Rainfall outside the rainy season is exceptional. The number of rain days (more than 0.1 mm rainfall) increases from 20 days in the north to 60 days per year in the south. With a decrease in mean annual precipitation the coefficient of variation for the rainfall increases. It is 25% in the south and 40% in the north (White, 1983).

Figure 2.2: Mean Annual Rainfall over Study Area



The average maximum temperature of 40° C is reached between April and May, the lowest average minimum temperature of 15° C occurs during December and January (White, 1983).

2.1.3 Geography

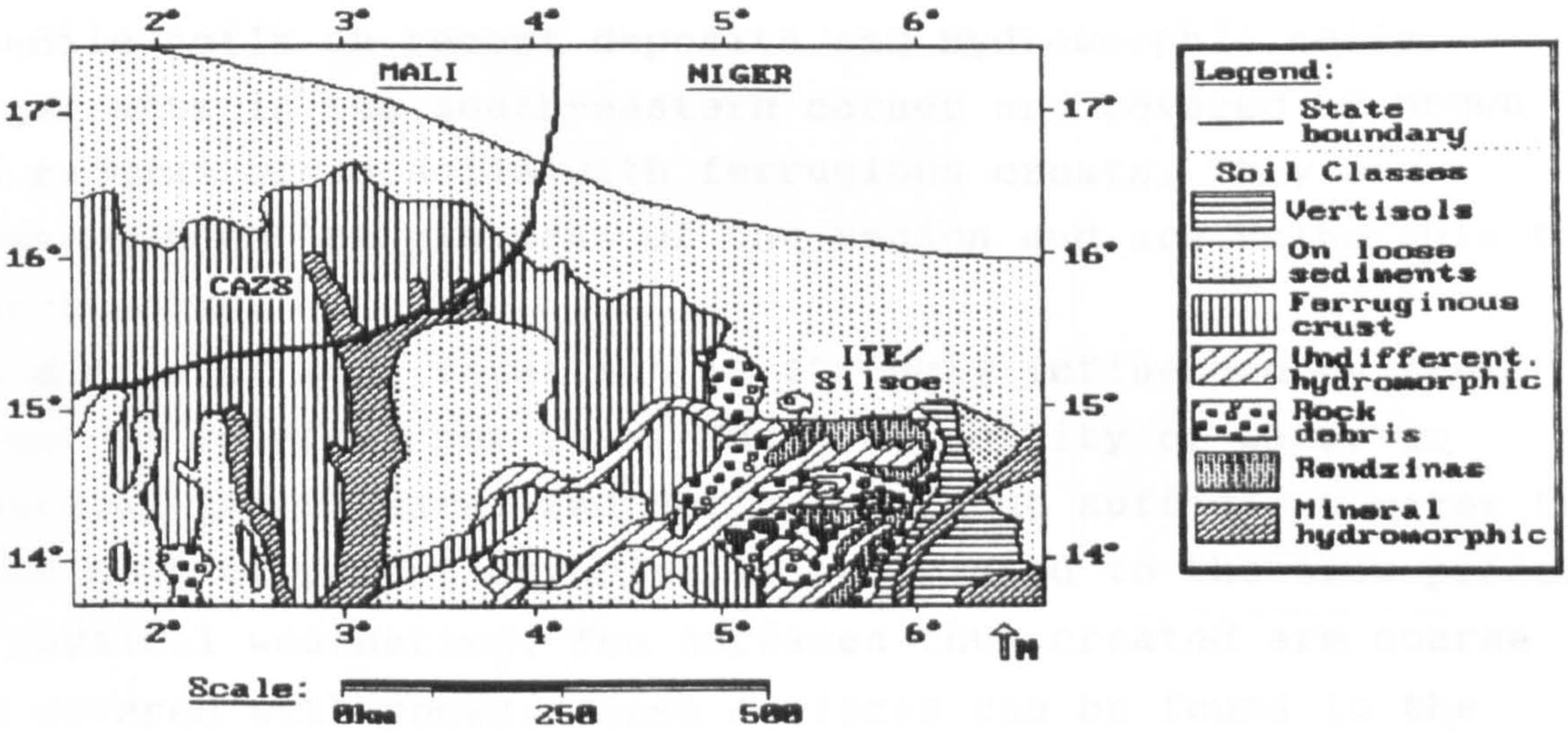
The central part of the NOAA AVHRR images cover the flat or gently undulating terrain of the Azaouk. The plain is approximately 350 to 400 m in elevation and partly dissected by fossil valleys (dallols). To the North the Azaouk is bordered by the Talak desert region. The North-Eastern part of the image contains the lower parts of the Aïr Massif. It is a mountainous

area, rugged and with steep slopes. The average annual rainfall is higher than over the surrounding areas due to the increase in elevation up to some 2000 m. The 512 x 512 extracts from NOAA AVHRR, however, only cover the foot slopes of the Aïr Massif.
South of the Azaouk lies the monoclinal plateau of the Ader-Doutchi. It is a rocky limestone area, rising some 100 m from the plains.
The study area itself, which lies south of the 16° meridian, is situated in a plain of low relief. It is dissected by fossil valleys and diversified by rocky outlines. It lies to the East and North of an area of lateritic hills, with tops exceeding 650 m.

2.1.4 Soils

The soils of the study area vary with the amount of annual rainfall. The close correlation between soil type and precipitation originates from water being the most limiting factor for the break-down of parent material by chemical weathering. With increasing availability of water from the North to the South the development of soil progresses.
The distribution of soils across the study area and the terminology used is based on the classification adopted for the soil maps of Africa (d'Hoore, 1964). A visual presentation of the distribution of soils in West Niger is given in Figure 2.3.

Figure 2.3: Distribution of Soils over Study Area



In the northern part of the image desert detrius with rock and rock debris dominates the ground. A coarse residual material is formed mainly by physical weathering. Since the minerals are not leached out by the rain the soil reaction is neutral to calcareous.

The central part of the study area is covered by sub-desert soils with rock. They are transitional soils between the almost undeveloped desert detrius and the well developed brown soils of the semi-arid regions. The sub-desert soils are low in organic matter and sometimes develop a hardened surface. The nutrient potential is high, but biological activity is low and pastures on these soils are poor due to the soluble salt content.

In areas receiving more than 250 mm of rain annually brown and reddish brown soils become dominant. In the southern parts of the study area they are formed from loose sediments. The soils contain appreciable amounts of clay minerals and darken with an increase in organic matter content. They are suited for grazing and have a good structure and permeability in the natural state. The original soil may be covered with sandy sheets, which derive from continental deposits or were distributed by wind action during the drier periods of the Pleistocene.

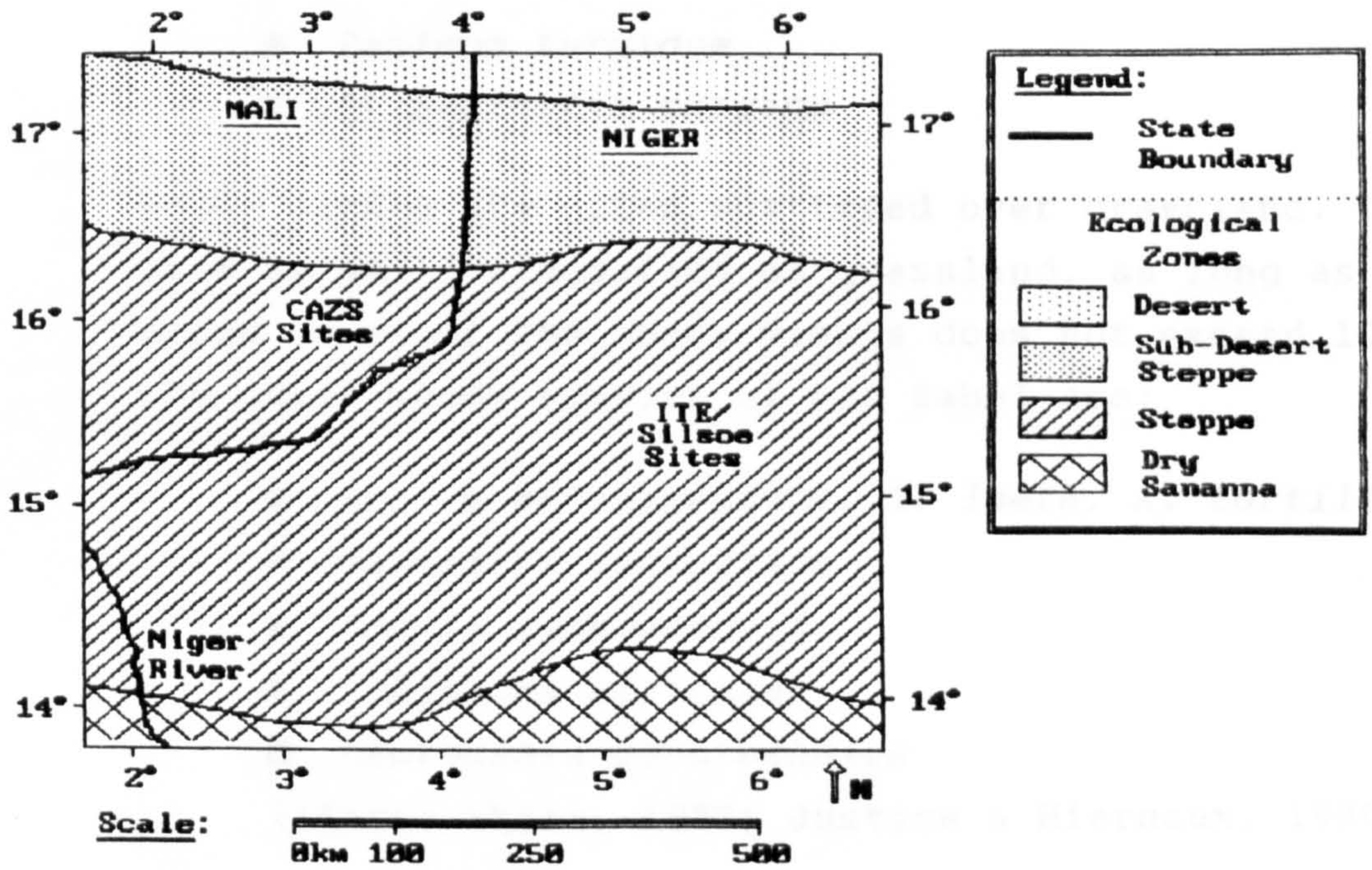
At the southern part of the scene the composition of soils becomes more complicated. Along the water courses there are juvenile soils on recent deposits and hydromorphic soils. Larger arts in the south-eastern corner are covered by brown and reddish brown soils with ferrugious crusts. They are widespread on the plateaus of the region and are vulnerable to over-grazing.

The degree of soil formation is strongly influenced by the amount of rainfall per year. The availability of water is essential for chemical weathering. Without sufficient water the break down of parent material is restricted to the slow process of physical weathering. The surfaces thus created are coarse and covered with rocks. These surfaces can be found in the northern region of the study area. In the southern region, where higher rainfall occurs, the development of soils is further advanced and top and sub-soils can be found. Due to the sparsity of vegetation across the study area soils generally form the major contribution to the overall scene reflectance.

2.1.5 Vegetation

The close correspondence between soils and vegetation boundaries found for other regions of Africa can also be observed in the Sahel (Milne, 1935; White, 1983). There are a great many classification models typifying rangelands (Cole, 1986). For remote sensing projects using AVHRR LAC data a codification according to physiognomy for the primary and secondary level seemed to be appropriate. In particular, number and height of trees constitute an important source of modifying satellite VIs (see following Chapter). The primary class would be determined by the horizontal spacing between plants. The secondary discriminant would be plant height with thresholds at 2 m and 8 m (Cole, 1986). A description of the main classes found over the study area is given below and presented in Figure 2.4.

Figure 2.4: Distribution of Major Vegetation Zones over Study Area



(a) **Grassland** (Savanna Grassland by Cole, 1986)

On deep sandy soils and particularly in the northern Sahel with annual rainfall of 400 mm or less grassland is the prevalent vegetation type. Grassland is land covered with grasses and other herbs, with the former being the physiognomically dominant plant.

The most frequent grass species are:

- *Aristida mutabilis, A. stipoides*
- *Cenchrus biflorus*
- *Schoenefeldia gracilis*
- *Tragus berteronionus, T. racemosus*
- *Tribulus terrestis*

(After: White, 1983; Justice & Hiernaux, 1986)

Only in the drier north of the Sahel are the following grass species found:

- *Panicum turgidum*
- *Stipagrostis pungens*

Woody plants are often scattered over grassland. The area is still classified as grassland, as long as the crown cover of the woody plants does not exceed 10%. The chief woody species of the Sahel are:

- *Acacia ehrenbergiana, A. laeta, A. tortillis*
- *Balanites aegyptiaca*
- *Boscia senegalensis*
- *Comiphora africana*
- *Leptodenia pyrotechnica*

(After: White, 1983; Justice & Hiernaux, 1986)

In the northern Sahel grasslands the woody plants do not exceed a height of 5 m and are frequently found to be 2 m to 3 m. The main woody species over most areas in Niger is *Acacia ehrenbergiana* (Justice & Hiernaux, 1986).

(b) **Wooded Grassland** (Savanna Parkland by Cole, 1986)
Further to the south, where annual rainfall of 250 to 500 mm occurs, the most widespread cover type on sandy soils is wooded grassland, also called savanna. Wooded grassland is defined by a crown cover of the wooded species, which ranges between 10 and 40%. The cover class is thus situated between grassland and woodland. The sward of wooded grassland principally consists of:

- *Aristida stipoides*
- *Cenchrus biflorus*
- *Schoenefeldia gracilis*
- *Tragus racemosus*

With increasing amounts of rainfall the portion of broad-leaved trees increased, too (Ahn, 1970). The chief wooded species are:

- *Acacia laeta, A. tortilis*
- *Balanites aegyptiaca*
- *Boscia senegalensis*
- *Commiphora africana*
- *Leptodenia pyrotechnica*
- *Maeru crassifolia*

Euphorbia balsamifera and *Leptodinia pyrotechnica* were found to be absent on more sandy soils (Justice & Hiernaux, 1986). The trees are 4 m to 8 m tall, increasing from north to south.

(c) **Bushland** (Low Tree and Shrub Savanna/Thicket and Scrub by Cole, 1986)

In areas without deep sandy soils and where the surface is covered with weathered rock bushland dominates. In regions with 250 to 500 mm annual rainfall bushes may be more than 3 m tall. The surface cover of bushes is mainly less than 40% and classified as open bushland. The dominant bush species are:

- *Acacia mellifera*
- *Boscia senegalensis*
- *Commiphora africana*
- *Dichrostachus cenera*

The grass and tree species over open bushland correspond to the species found in wooded grassland.

2.1.2 Rangeland Productivity in the Sahel

The most important single factor limiting rangeland vegetation growth in the Sahel is the average amount of rainfall per year. When correlating rangeland productivity with climatic conditions the annual precipitation can serve as an integrated factor, since it is strongly related to other climatic components like

- rain variability,
- number of rain days,

- length of rainy season and
- potential evapotranspiration.

The rainy season determines the duration of the growing period, which lasts from July to September. The peak of the growing period occurs between the end of August and the beginning of September (LeHouerou & Hoite, 1977).

With water being the most limiting factor for plant growth in the Sahel the amount of grasses and forbes for animal consumption can be directly related to the amount of rainfall per year. Forage productivity of a region can be estimated by its rain use efficiency. For the Sahel the rain use efficiency, defined as units of phytomass per area per unit precipitation per year, has been estimated to be 2.5 $kgha^{-1}mm^{-1}a^{-1}$ of above ground phytomass and 1.0 $kgha^{-1}mm^{-1}a^{-1}$ of consumable dry matter (LeHouerou & Hoite, 1977). Generally, the rain use efficiency ranges from 0.5 $kgha^{-1}mm^{-1}a^{-1}$ for a depleted subdecent ecosystem to 3.0 to 6.0 $kgha^{-1}mm^{-1}a^{-1}$ for arid and semi-arid grazing lands (Le Houerou, 1984; Wagenaar & De Ridder, 1986). Rangeland vegetation reached between 1200 and 1500 $kgha^{-1}$ of above ground total dry matter for grazing and browsing. Not included are leaves, twigs and fruits (Le Houerou & Hoite, 1977).

However, not all the vegetation potentially suitable for animal consumption can be utilized. This portion of consumable forage of the total amount of grasses and forbes has been found to be 70% of above ground phytomass during the rainy season and 30% during the dry season (Le Houerou & Hoite, 1977).

For a more detailed investigation the amount of annual precipitation becomes an insufficient indicator for growth conditions. The reliability of rainfall, its distribution, hydrological site conditions like percolation and run-off characteristics and vegetation type and comparison have to be taken into consideration (Tucker *et al*, 1985).

Vegetation type and species composition within a rangeland community depend farther on the seed stock produced in previous years, annual precipitation in those years and the grazing history of the region (Justice & Hiernaux, 1986). For example, heavy stocking in one year may lead to a lower than expected rangeland productivity in the following year. The imbalance

prevents the mainly annual grass species from developing sufficient seed to allow adequate regrowth.
The strong relationships between vegetation growth, hydrological and morphological site conditions in the Sahel become obvious within a common dune-like terrain. There, vegetation growth is a repeated pattern of vegetation stripes running along the depressions, called brousse tigree. The density of vegetation in the depressions is higher than in the open bushland and can reach impermeability. It may then be classified as thicket. The intervening dunes are covered with grass, but are sometimes virtually devoid of vegetation. In most cases the vegetation changes of the brousse tigree are not due to gross soil differences (White, 1983). More likely the cause is a greater availability of moisture in depresssions.

2.2 Estimation of Vegetation Properties from Remotely Sensed Data

In satellite remote sensing an area is represented as a composition of discrete points (pixels). The value attached to each individual pixel comprises the record EM energy intercepted by a sensor, which originates from the exitance radiance of a section of the area on the surface, the instantaneous field of view (IFOV). The exitance radiance of this section is the integral of the exitance radiance of the different surface cover types and conditions present in that section. As a consequence, individual pixel values stand for a mixture of surface covers. An understanding of the interaction between incident EM energy and various surface cover types allows the extraction of information on properties of single cover types in the mixed signal intercepted.
For the Sahel the main surface cover types are vegetation and soil. Therefore, the characteristics of reflected solar radiation from these two cover types are presented in the first section of this chapter. It is followed by a discussion about various methods on extracting vegetation properties from multi spectral satellite images. After having established the

requirements, the two satellite sensors found most suitable to meet the objectives of this project, Landsat MSS and NOAA AVHRR, are compared.

2.2.1 Interaction of Solar Radiation with Vegetation and Soil

EM energy from the sun incident on any given earth surface feature will be reflected, absorbed or transmitted by the feature. The relationship between these energy interactions is expressed in an energy balance equation:

$$E_I(\lambda) = E_R(\lambda) + E_A(\lambda) + E_T(\lambda) \quad (Wm^{-2}\mu m^{-1}) \qquad (2.1)$$

(After: Lillesand & Kiefer, 1987)

The equation states that the proportion of incident energy reflected, adsorbed or transmitted by an object depends on the wavelength. It also varies with type and condition of the object. These distinct particularities of the fate of incident EM energy for different earth surface features allow their discrimination by multi spectral remote sensors.
The source of EM energy detected by remote sensors at wavelengths below 5 µm originates of reflected EM radiation from the sun. To quantify the reflectance characteristics of the earth surface features the portion of the incident energy at a given wavelength which is reflected, the spectral reflectance $p(\lambda)$, may be measured. It is defined by the following equation:

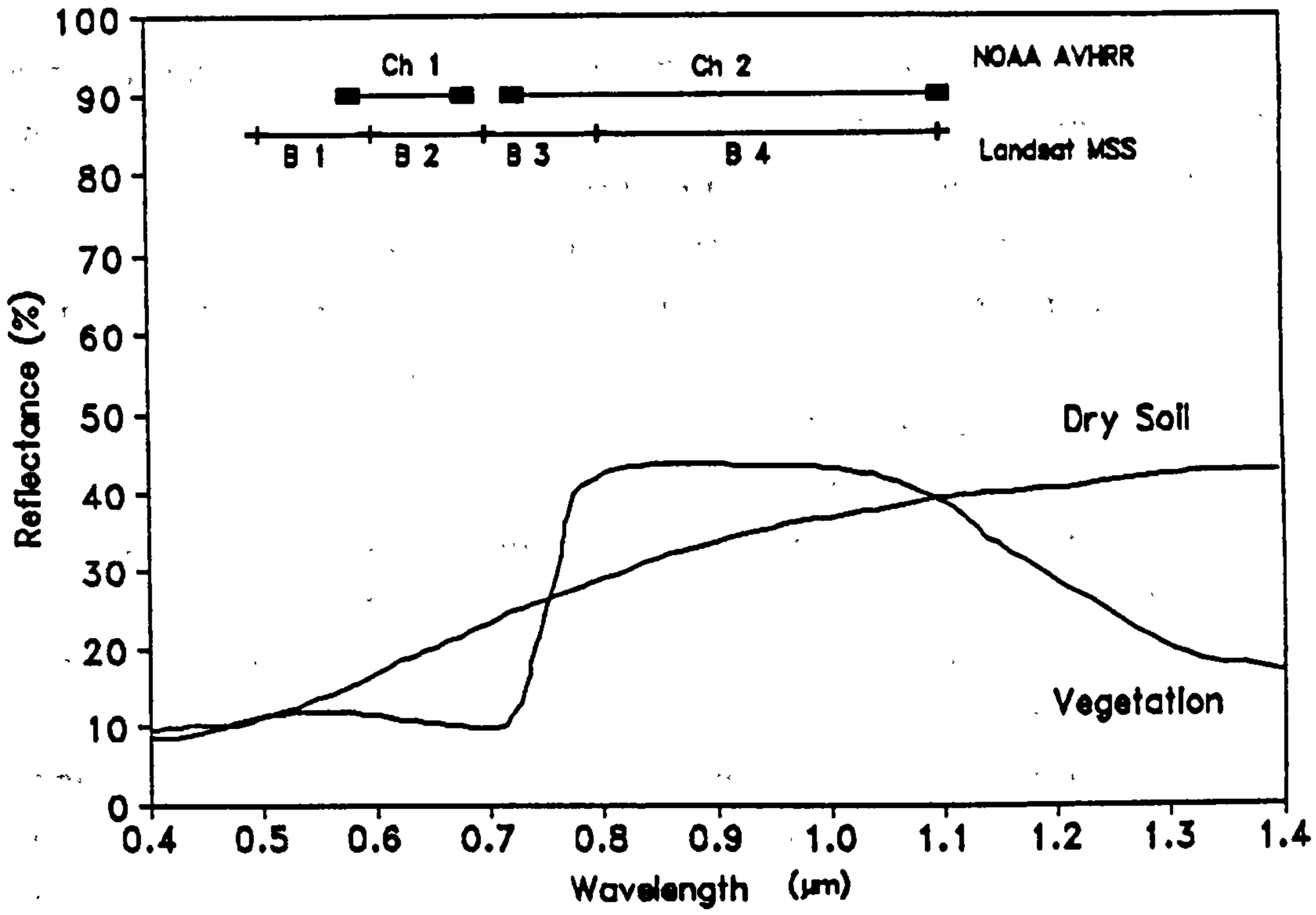
$$p(\lambda) = \frac{E_R(\lambda)}{E_I(\lambda)} \times 100 \ (\%) \qquad (2.2)$$

(After: Lillesand & Kiefer, 1987)

Landsat MSS and NOAA AVHRR bands 1 and 2 are sensitive to the visible part (0.38 to 0.72 µm) and the NIR part (0.72 to 1.3 µm) of the EM spectrum. In these wavebands atmospheric effects like emittance or absorption of EM energy by oxygen (O_2), carbon dioxide (CO_2) or water (H_2O) molecules are minimal.
In the atmospheric windows of the visible and NIR vegetation

and soil have characteristic and distinguishable pattern of reflectance. The spectral reflectance of vegetation typically has a high absorption and low reflectance and transmittance in the visible part of the EM spectrum. The relationship is presented graphically in Figure 2.5.

Figure 2.5: Reflectance of Vegetation and Soil in the RED and NIR



(After: Tucker, 1979)

The process of photosynthesis is based on solar radiation between 0.4 and 0.7 µm wavelength. This part of the EM spectrum is referred to as the photosynthetically active radiation (PAR). It accounts for approximately 50% of the total solar radiation (Daughtry, 1988). Adsorption of radiant energy from the sun by vegetation is highest in the blue (0.4 to 0.5 µm) and red (0.6 to 0.7 µm) bands. It arises from pigment activity, particularly from chlorophyll a, chlorophyll b and carotinoids (Smith, 1983). The pigments are highly transparent to infra-red radiation and do not account for the reflectance in the NIR. Reflectance of vegetation in the visible is typically less than 10% (Harris, 1987).

The amount of incident NIR radiation reflected by green

vegetation is approximately 50%. It is caused by the scattering effect in the spongy mesophyll portion of the leaves. The amount of scattering is assumed to be proportional to the cellular density and based on refrective index differences of the cell-wall air-space (Bauer, 1978). In growing leaves the number of air spaces increases, so diffused energy passes more frequently from cells with a high refractive index to the intercellular air with a low refractive index (Harris, 1987).
The high transmittance of green vegetation in the NIR part allows energy to reach underlying surfaces. From these surfaces, which may be another leaf, senescent vegetation or bare soil, part of the incident energy is reflected and contributes to the overall reflectance of an area. Consequently, the relationship between leaf area and PAR is typically non-linear.
The photosynthetic activity of pigments is indirectly correlated with primary production of plants. Leaf reflectance of incident NIR energy increases from emergency to maturity, while it simultaneously decreases in the red waveband. In young and active plants with high growth rates the difference in reflectance between the red and the NIR is expressed most, leading to the high contrast between the two wavebands and the low correlation. From maturity to senescence the relations are inverse.
Senescent vegetation is characterized by a low contrast between the visible and the NIR wavebands (Satterwhite & Henley, 1982). The decrease in moisture content changes the pigmentation and the structure of the spongy mesophyll and palisade parenchym. Reflectance increases in the visible, particularly in the red part. Chlorophyll pigments are modified and carotinoids become the dominant pigments. Reflectance in the NIR decreases, because scattering of energy decreases with the diminished number of cell-wall air-spaces in the plant tissue. However, changes in reflectance due to a decreasing moisture content only become substantial at less than 75% turgidity (Aaronson & Davis, 1980) and the decreased reflectance in the NIR is not a sensitive indicator for initial stages of drought (Jackson *et al*, 1983).
Contrary to green vegetation soil has an approximately linear

increase in reflectance from visible to the NIR wavelengths. In its reflectance pattern it is very similar to senescent vegetation. Generalizing the factors influencing that pattern they may be described as follows:

(a) An increase in soil moisture will lower the reflectance.

(b) An increase in particle size with an increase in surface roughness will decrease reflectance.

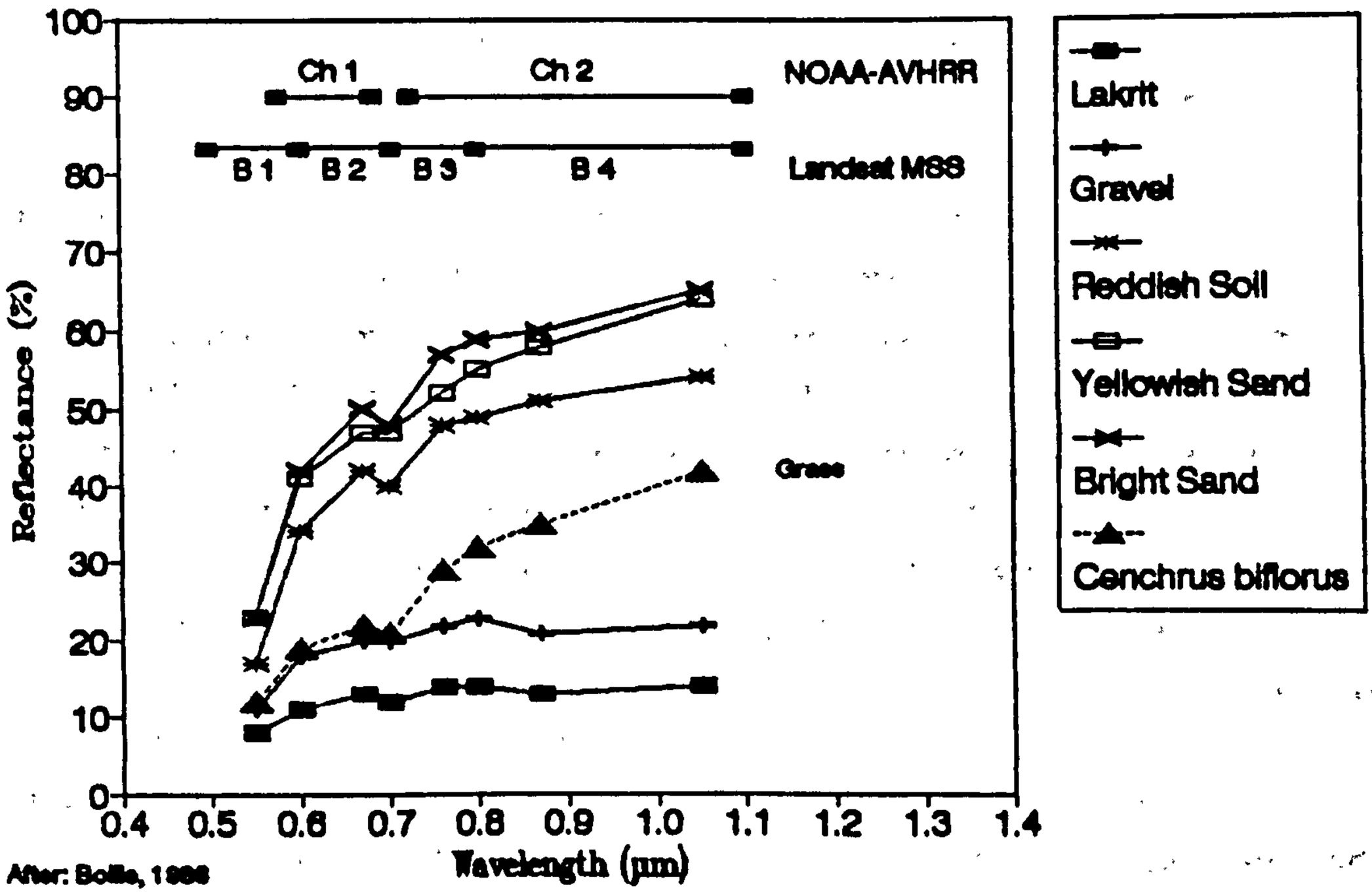
(c) An increase in organic matter will decrease reflectance.

(d) An increase in iron oxide will cause a decrease in reflectance.

(After: Harris, 1987)

The reflectance pattern of soils in the study area of this project is given in Figure 2.6.

Figure 2.6: Soil Reflectance Curves



Relatively flat reflectance curves come from dark toned surfaces, like shaded soils or coarse surfaces. Fine textured soils have intermediate slopes of reflectance in the red and

NIR wavebands. Highly reflective are saline soils with salt precipitates or salt crusts (Henley & Satterwhite, 1987).
The presence of vegetation causes a displacement away from the line of soil reflectance, with lower reflectance in the red and higher in the NIR. The displacement has been correlated to the GLAI and can be used to estimate phytomass.

2.2.2 Vegetation Indices

The characteristic reflectance pattern of vegetation and soil in the visible and NIR part of the EM spectrum has formed the theoretical basis for transformations of spectral data to estimate parameters of green vegetation (Elvidge & Lyon, 1985). The transformation results in a single number, the VI. This number may be the reflective count of a single band or the a combination of reflective counts of several bands (Aaronson & Davis, 1979).
Generally, sensors on spacecrafts are not sensitive to spectral reflectance at wavelengths of chlorophyll absorption in the blue. The scattering of reflected energy from earth surface features by the atmosphere negatively affects the contrast of the data and consequently its usefulness.
Using the green portion of the spectrum either on its own or as part of a ratio of wavebands has given low correlations to vegetation characteristics like GLAI and wet and dry phytomass (Tucker, 1979). This can be explained by the high correlation between bands in the visible part of the spectrum and a lower correlation between greenness and photosynthetic activity.
The correlation between the RED and the NIR wavebands for green vegetation ranges from -0.2 to -0.01. For soils and senescent vegetation there is a high positive correlation between the two wavebands (Satterwhite & Henley, 1982).
Mathematically VIs are designed to increase the contrast between data from the red and NIR wavebands for vegetation and to reduce the influence of data variations from other surface features. Desirable properties of a VI are a high sensitivity towards vegetation, insensitivity towards soil background changes and minimum influence of varying atmospheric conditions

on the radiance recorded by the sensor (Jackson *et al*, 1983). The most widely used VIs for two bands and their merits are briefly mentioned below.

(a) Single Band VIs

i. RED (0.6 - 0.7 µm)

The red portion of the EM spectrum covers the section of minimum reflectance for living vegetation (0.67 - 0.69 µm) within the visible range. It constitutes a very good single waveband to discriminate between living and dead or dormant vegetation. Soil and green vegetation can be discriminated in the red waveband, but the success depends on uniform background conditions. It has a high correlation to crop cover and height.

ii. NIR (0.8 - 1.3 µm)

Over the wavelengths covered by the NIR waveband reflectance for living vegetation reaches its maximum. With reflectance of green vegetation being higher than that of most soils in this portion of the EM spectrum, the waveband constitutes a useful indicator of vegetation. Useful for quantitative analysis is the high correlation between the sensor response and the LAI (Aaronson & Davis, 1979).

(b) Ratio VIs

Multi band VIs tend to give more stable results under varying conditions and thus provide better capability for season to season comparison of vegetation quantity and condition. In many cases the amount of "noise" is reduced by multi band VIs, for example changes in atmospheric conditions from images taken at different times of the year, attenuation effects due to clouds and haze, topography, shadow, soil and dead vegetation (Pearson & Miller, 1973).

i. *Ratio Vegetation Index* (RVI)

The RVI is defined as:

$$RVI = \frac{NIR}{RED} \quad \text{(unitless)} \tag{2.3}$$

The simple ratio between the NIR and red wavebands of a sensor discriminates vegetation from other surface cover types by exploiting the negative relationship, which exists between these two with increasing quantities of vegetation. The RVI reduces topographical effects and variations in scene illumination.

ii. *Normalized Difference Vegetation Index* (NDVI)

The NDVI is defined as:

$$NDVI = \frac{NIR - RED}{NIR + RED} \quad \text{(unitless)} \tag{2.4}$$

The NDVI was developed after the RVI (Ashley & Rea, 1975). The range of values is restricted to lie between -1 and +1 and is usually not scaled. The normalization of the sensor response in the two wavebands reduces the influences of sun angle and haze on the VI and enables the comparison of multi temporal images.

The calculation of the NDVI requires no previous knowledge of the vegetation on the ground. It is available as a regular product from NOAA in the form of the GVI. It is a standard NOAA product derived from images of seven continuous days of global area coverage (GAC) data resampled to a resolution of about 20 km and projected into a polar stereographic format (Holben, 1986).

(c) **Orthogonal VI**

Reflectances of bare soils in the red and NIR reveal the same pattern of variation along a line in the 2-dimensional space of the reflectance in these wavebands. An average soil reflectance pattern can be estimated by a linear regression. The result of the regression in the cluster of soil reflectance points has been named the soil line (Richardson & Wiegand, 1977).

It is worth pointing out that the soil line represents a best fit and that individual soils show variations in slope of the relation between soil reflectance values in the red and NIR waveband.
The presence of vegetation causes a displacement of two-band reflectance values away from the soil line. The perpendicular distance of these points to the soil line is positively correlated to the quantity of vegetation in the scene. This distance of a vegetation candidate signature point to the soil background line has been described as the perpendicular vegetation index (PVI) (Richardson & Wiegand, 1977):

$$PVI = \left[(R_{soil}-R_{veg})^2+(NIR_{soil}-NIR_{veg})^2\right]^{1/2} \qquad (2.5)$$

The PVI is based on the four-dimensional green VI, which was developed for Landsat MSS data. It is analoguous to the green VI in a two-dimensional space for red and NIR wavebands. Similarly, the soil brightness index (SBI) computed from four Landsat MSS bands was simplified to the soil line index (SLI) for two wavebands (Wiegand & Richardson, 1982).

There are a number of other VIs, such as the transformed VI, the Ashburn VI (Tucker, 1979) or the Green VI (Kauth & Thomas, 1976). These are less widely used for estimating phytomass and do not offer any significant advantage over the afore mentioned VIs. In addition, only two-dimensional VIs were considered, because the calibration would be based on NOAA AVHRR channels 1 and 2. Therefore, their application has not been regarded as being relevant for this project. They were subsequently omitted from the investigation.
Generally, VIs are poor measurements for both phytomass and leaf area index when one or more of the following conditions is present:

i. The leaf area index exceeds the value of three.

ii. Part of the area covered by the sensor IFOV is bare ground.

iii. Dead material is present in the canopy with an unknown amount.

iv. The solar elevation is high and the distribution of leaf angles is unknown.

(After: Sellers, 1985)

When applying VIs to rangeland vegetation it has to be remembered that most VIs are originally derived from data with a single variable, a specific vegetation property, which was to be estimated. Additionally, the calibration of the index values and the establishment of their feasibility were often applied to homogeneous cover types of agricultural crops. The problems encountered when using VIs for monitoring rangeland vegetation are discussed in the following section.

2.2.3 Phytomass Estimation of Rangeland Vegetation

The main object for monitoring rangelands by multi spectral satellite remote sensing systems is to estimate of the quantity of photosynthetically active phytomass for consumption by domestic animals throughout the season. It has been shown under Chapter 2.2.2 that the quantity of phytomass can be estimated by computing VIs from data of satellite sensors. The composition of rangeland, however, differs quite considerably from an agricultural cropping environment, on which VIs were critically based on. The reflected energy from rangeland surfaces represents a composition of the reflectance characteristics of soil, vegetation, litter and standing dead vegetation. The assemblage of these components is called a canopy (Colwell, 1974). With satellite data the spectral response of each pixel represents the area weighted average of the reflectance characteristics of all components of the canopy in the measured wavelength region (Siegal & Goetz, 1977).

Having a more heterogeneous canopy the spectral response from rangelands is more an amalgamation of information than from agricultural crops.
The differences between agricultural crop and rangeland vegetation conditions are mainly due to environmental influences, which are attributable to:

- temporal and spatial variations in phytomass,
- species composition and plant communities,
- dry matter accumulation and decomposition,
- soil associations and
- topographic characteristics.

The requirements to be met by a VI to be useful for rangeland monitoring may be summarized as follows:

i. an indication of vegetation for the great variety of species;

ii. sensitive to differences in groups of species;

iii. unaffected by variation of soil background, shadow, standing dead vegetation and vegetation litter and

iv. as little as possible affected by atmospheric radiance conditions.

(After: Tueller, 1987)

For monitoring rangeland production VIs have to give reliable estimates of phytomass for low ground cover (< 30%) and low phytomass levels (< 1500 $kgha^{-1}$). The influence of background variations on the estimates should be negligible.
In order to establish the usefulness of applying a VI to rangeland conditions the obstacles in fulfilling the above mentioned requirements are to be identified.

(a) **Period of Growth**

The period of vegetation growth in the Sahel is generally determined by the season of rainfall. Decomposition, grazing and consumption by invertebrates is less restricted to a certain period. Subsequently,

the composition of rangeland cover is highly complex and difficult to model (Huete & Jackson, 1987).
The quantitative estimation of vegetation properties is based on the presence of photosynthetically active plant tissue (see Chapter 2.2.1). With progressing senescence of vegetation it becomes more and more spectrally similar to soil. Depending on the sensor wavebands senescent vegetation can even become virtually indistinguishable from soil. The consequence for rangeland monitoring over the Sahel is an emphasis on timing for data acquisition. In order to be able to estimate the maximum amount of phytomass satellite data should be obtained at the end of the growing season while vegetation is still active (also see Chapter 3).

(b) **Vegetation Density**

The reflectances of soil-vegetation surfaces varies directly with the percentage of vegetation and the soil in the sensors IFOV and the reflectance contrast between the vegetation and soil (Satterwhite & Henley, 1982). As a threshold of 25 to 35% of vegetation cover, soil is the principal component contributing to the overall spectral response (Tueller, 1987).

(c) **Soil Background**

The contribution of the soil background to the overall amount of energy reflected from a canopy does not only vary with vegetation density but it is also subject to the reflectance of the soil itself. Grassland with a 37% vegetation cover on a light soil was found to have a canopy reflectance of 9.0% in the red (650 µm) spectral region, whereas the reflectance for the canopy dropped to 3.2% over a dark soil background (Colwell, 1974). The sandy soils of the Sahel are highly reflective, especially when dry (<5% moisture content), with a steady increase in reflectance with wavelength. The spectral separation of sparse vegetation, particularly on high reflective soils, has been found difficult (Griffiths & Collins, 1981). In those cases the reflectance of vegetation in the NIR is not sufficiently

higher to allow a separation of vegetation from these soils.

A sparse density of vegetation and a high reflectance from dry soils results in imagery that mostly reveals variation in soil type and not changes in land cover composition or distribution of vegetation (Griffiths & Collins, 1981). For rangeland vegetation in Arizona with canopy covers less than 20% it has been shown that vegetation classes could be accurately mapped only when associated with homogeneous soil and landform units (Bently, 1976 in: Griffiths & Collin, 1981).

(d) **Vegetation Geometry**

Satellite measurements of vegetated areas are also influenced by structural and optical differences of a plant canopy of all the species present in the FOV. Destructive ground measurements for green phytomass like clipping of vegetation usually do not account for these variations. The total green phytomass for an erectophile canopy may be identical to that of a planophile canopy, but the VIs for the two plant canopies will be substantially different (Tucker *et al*, 1983).

(e) **Species Distribution**

The estimation of phytomass of rangelands, when compared to results of VIs from agricultural crops, is further complicated by the spatial variation in landscape cover. Broad changes in vegetation densities occur more gradually than for crops with definite field sizes. On the other hand the plant community is composed of a variety of species with a spatially changing distribution. A calibration of VIs for phytomass estimates will have to be based on a typical community rather than a single species. This inevitably restricts the VI calibration to a specific area.

(f) **Others**

Up to almost half of the radiance from rangeland communities can be attributed to factors other than soil and vegetation (Tueller & Wilson, 1987). Slope, aspect,

> physiognomy, shadow and soil moisture account for that influence. Their individual contribution, however, is difficult to quantify due to problems in ground sampling.

The conclusions which may be drawn when comparing rangeland conditions with the requirements for a successful application of VI is that VIs may be poor estimators of rangeland phytomass (Sellers, 1985).

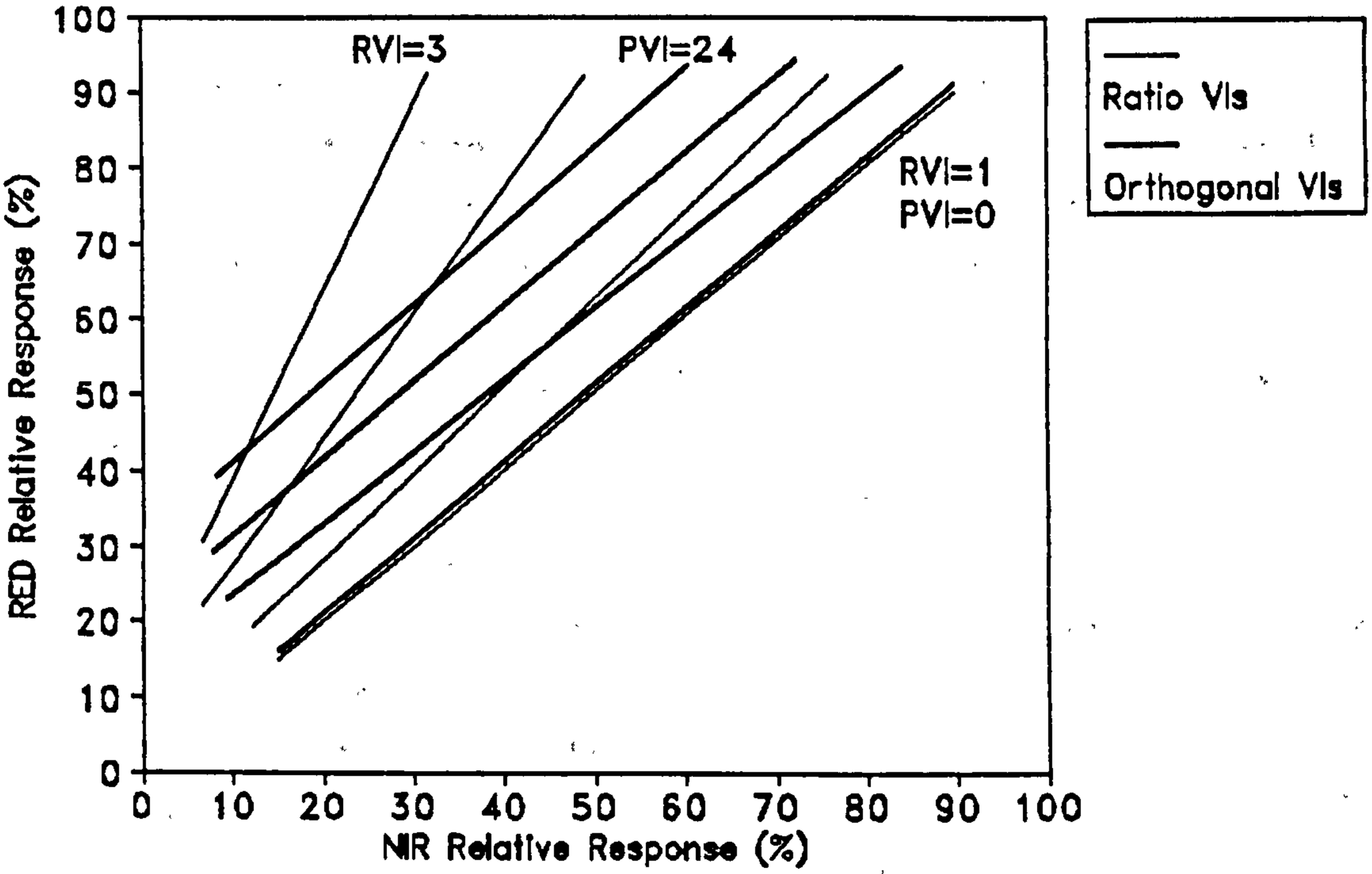
Ratio VIs assume lines of equal green vegetation to be linear and to converge at the origin. Graphically speaking, for spectral ratios the lines of equal green response radiate from the origin at different slopes (see Figure 2.7. Therefore, they are considerably affected by differences in the slope coefficients. Changes in atmospheric conditions cause a shift of these isolines. Subsequently, ratio values decrease with increasing atmospheric turbidity (Huete & Jackson, 1988).

The advantage of the PVI over ratio VIs is that it incorporates soil reflectance and reduces the influence of the soil background reflectance on the VI (Elvidge & Lyon, 1985). It seems to be suitable for the application in areas of sparse vegetation and varying backgrounds.

The PVI assumes lines of equal green response for a constant vegetation cover to be linear and parallel to the soil line (see Figure 2.7). However, the canopy isolines were found to be not parallel to the bare soil line. In addition, an increase in atmospheric turbidity decreases the canopy isoline towards the soil line, thus decreasing corresponding PVI values (Huete & Jackson, 1988).

The RVI, NDVI and PVI seem to be suited for quantitative rangeland estimations. The most widely used VI for rangeland is the NDVI. Apart from its advantages of being more sensitive to low phytomass levels it is computed by NOAA as a routine product for AVHRR GAC data (see Chapter 2.3.1). The PVI with its reduced impact of soil background variation on the overall reflectance signature appears to be worth considering alongside the NDVI. These two VIs are presented as to their merits and disadvantages in more detail below. For a brief introduction of these and other common VIs see Chapter 2.2.2.

Figure 2.7: Lines of Equal Green Response for Ratio and Orthogonal VIs



(After: Major *et al*, 1988)

(a) Ratio Vegetation Index (RVI)

The simple band ratio seems to be related best with percentage green vegetation. A high correlation ($r > 0.9$) between the RVI and phytomass, both living and dead has been found for grass under laboratory conditions (Pearson & Miller, 1973). On the other hand, the RVI is an unreliable indicator for vegetation quantities at vegetation covers below 30% (Jackson *et al*, 1983). This is mainly due to the influence of the spectral characteristic of the underlying soil on the RVI. Low reflecting soils result in high VI values (Elvidge & Lyon, 1984), while highly reflecting soils decrease the values of the RVI (Colwell, 1974; Huete, 1987).

The RVI was further found to be largely dependent on atmospheric and satellite orbit characteristics. This very much limits the use of the RVI for multi temporal sets of data (Joint Research Centre, 1989).

(b) **Normalized Difference Vegetation Index (NDVI)**

For areas of low phytomass the NDVI has been found advantageous over other ratio VIs (Satterwhite & Henley, 1987). The NDVI showed increased sensitivity to green phytomass at levels of less than 2000 $kgha^{-1}$ when compared to other ratio VIs (Huete & Jackson, 1987). Using ground cover instead of quantity, the NDVI has been found effective for estimating vegetation below 30% cover (Tucker, 1977; Ripple, 1985).

Quantitative estimates of vegetation vary with the soil background reflectance. High reflecting soils like dry sands decrease response compared to low reflecting soils, like wet clays. The extent of the variability depends on the amount of vegetation present. It is less expressed at low (< 2000 $kgha^{-1}$) and at high (> 6000 $kgha^{-1}$) phytomass levels (Huete *et al*, 1985; Lamprey & De Leeuwen, 1988). In that respect the NDVI differs from the RVI, since there the effect of the soil background reflectance on the VI is more expressed at low phytomass levels. However, the results achieved with the NDVI were found to be site specific, year specific and sensitive to the presence of senescent vegetation (Huete & Jackson, 1987). In areas with sparse vegetation and varying soils places of vegetation may be confused with bare soil (Taylor *et al*, 1986).

The influence itself can be attributed to the downward scatter flux from green plants reflected back upwards by the underlying soil (Huete *et al*, 1985).

For vegetation over dark soils the slope of equal green response for the NDVI, or any other ratio VI, is reduced. This results in an intercept greater than zero and, as a consequence, higher values for the NDVI for darker soil backgrounds (Major *et al*, 1988).

The impact of senescent vegetation on the NDVI is a reduction in values and a consequent underestimate of the amount of dry matter present (Sellers, 1985). The influence of senescent vegetation can be attributed to

- a reduction in intensity of radiant flux by shade of green phytomass by senescent grass, particularly at emergence and
- the erectophile canopies of many grass species, which cause reflected energy not to be scattered upwards.

Grey litter, standing or on the ground, has been found to be of little influence on the index value. (Gallo & Daughtry, 1987; Kimes *et al*, 1984; Kimes, 1985).
The NDVI can be a useful and reliable indicator for the amount of vegetation over heterogeneous areas, which are more likely to be encountered with the larger FOV of NOAA AVHRR than with Landsat images, if similar soil brightness and spectral conditions throughout the scene can be assumed (Ormsby *et al*, 1987).
With the sensitivity of the NDVI for low phytomass levels and a reduced influence of soil background variations for a sparse vegetation cover over light soils, the NDVI appears to be suitable for a calibration to phytomass levels of the Sahel rangeland.

(c) **Perpendicular Vegetation Index (PVI)**
The PVI has been found suitable for phytomass estimations at low levels of vegetation cover (<30%) (Huete & Jackson, 1987). As with the NDVI it has been found to be affected by the soil background reflectance, although information on the soil background reflectance is supposedly taken into account. The reaction, however, is just the opposite to the previous: Darker soils have no effect on PVI (Elvidge & Lyon, 1985), but red soils and higher reflective soils increase the response (Huete & Jackson, 1987). Because of the influence of the soil background on the PVI, it has also been found sensitive to soil moisture conditions (Jackson *et al*, 1983). The effect of soil brightness on the PVI decreases with decreasing vegetation covers and densities (Huete *et al*, 1985). As with the other VIs the presence of yellow standing grass within green phytomass reduces the

greenness signal of the VI by 20% to 30%.
The assumption of a single soil line may not coincide with the actual conditions met at a site. Significant differences between soil lines in both slope and intercept were found for a semi-arid area in Australia (Williamson, 1988). The use of a mean soil line may, therefore, obscure phytomass estimates.
In areas with low vegetation the PVI was found to over-estimate vegetation on dark backgrounds and to under-estimate it on light coloured soils (Huete *et al*, 1985). It also seems to be less sensitive to sparse vegetation than the NDVI (Jackson *et al*, 1983).
But not only the soil line is liable to ground conditions but so is the PVI. The underlying assumption for the PVI is that different levels of vegetation run as parallel lines to the soil line. Thus, the PVI should be independent of variations in the soil background reflectance. However, although the PVI removes soil brightness effects for bare soil, it is affected by soil background variations at low quantities of vegetation (< 2000 $kgha^{-1}$). As a consequence, the amount of vegetation is underestimated over soils with a low reflectance at high phytomass levels (Major *et al*, 1988).
Furthermore, the PVI and other orthogonal VIs are not independent of background variations other than soil. The influence of litter on phytomass estimates were found to be well expressed by increased index values (Huete & Jackson, 1987).

2.3 Satellites and Sensors

As stated in the review on previous work on rangeland monitoring by satellite data (Chapter 2.2) the main data sources are NOAA AVHRR and Landsat MSS and, to a much lesser degree, TM and SPOT. In order to compare these two sensors with respect to their usefulness for this project (see Chapter 2.4),

the respective technical specifications are presented in this chapter.

2.3.1 Television Infra-Red Observation Satellite

The Television Infrared Observation Satellite (TIROS) was launched on 1 April 1960. It gave the name to a whole program of weather satellites that followed. Individual satellites were named NOAA-n, with n being numbers for successive launches. NOAA satellites operate in a near-polar sun-synchronous orbit. The orbital altitude varies between 833 and 870 km and the inclination between 98.7° and 98.9°. The repeat cycle of 12 hours provides daily coverage of the illuminated side of the Earth. The non-integer number of 14.1 orbits per day results in coverage of a different sub-orbital track on a daily basis. However, the local solar time of the satellite passage remains essentially constant for any latitude (Kidwell, 1988).
The TIROS-N NOAA family represents the third generation of the program and was introduced in 1978 with the launch of TIROS-N. It was followed by NOAA-6 and ended with the launch of NOAA-7 on 23 June 1981. The later satellite contributed most of the data for this investigation. The succeeding series was named Advanced TIROS-N (ATN). The modifications introduced gave enhanced data and expended observation application. The first satellite, NOAA-8, was launched 28 March 1983. It was followed by NOAA-9 and -10.
TIROS satellites have been the main source for meteorological and environmental data required to support both the operational and experimental portion of the World Weather Watch Program. For this task, the platforms are equipped with a variety of instruments:

(a) Advanced Very High Resolution Radiometer (AVHRR) Data

i. HRPT - High Resolution Direct Readout (1.1 km resolution)

ii. LAC - Local Area Coverage
(High resolution recorded readout, 1.1 km resolution)

iii. GAC - Global Area Coverage
(Reduced resolution recorded, 3.3 by 5 km resolution)

(b) TIROS Operational Vertical Sounder (TOVS)
It includes

i. MSU - Microwave Sounding Unit

ii. SSU - Stratospheric Sounding Unit

iii. HIRS/2 - High Resolution Infrared Radiation Sounder 2

(After: Kidwell, 1988; Schnapf, 1985)

GAC data, which is always recorded, originates from subsampling of high resolution pixel values. A single GAC pixel is composed of the average of four pixels along a scan line. The fifth pixels on the line is disregarded. The data reduction in along-track direction is achieved by sampling every third line only (Lamprey & De Leeuwe, 1987).
Of major interest to this project was the implementation of the cross-track scanning AVHRR from TIROS-N onward. It succeeded the Very High Resolution Radiometer (VHRR), which was implemented onboard the Improved TIROS Operation System (ITOS) family. The last satellite equipped with the VHRR was NOAA-5. Compared to the VHRR the AVHRR gives an increased amount of radiometric information by featuring four channels instead of two. The AVHRR is also sensible in the thermal IR portion of the EM spectrum in addition to its day-and-night imagery in the visible and IR wavebands. The four-channel AVHRR can be found onboard TIROS-N, NOAA-6, -8 and -10. A five-channel AVHRR, the AVHRR/2, was implemented on NOAA-7 and -9 satellites. The additional channel collects data in the thermal IR (11.2 to 12.5 μm). Subsequent satellites will be equipped either with the AVHRR/1 or /2.
The data format of all satellites has been provided with five

channels. For AVHRR/1 data Channel 5 consists of a repeated Channel 4 signal. The first four channels of the AVHRR instrument are essentially identical on all the satellites that succeeded TIROS-N. The latter differs in the bandwidth of Channel 1 of the AVHRR, which ranged from 0.55 to 0.9 µm. The change has been introduced to give better quantitative detection of vegetation. The sensitivity of 0.58 to 0.68 µm for Channel 1 of AVHRR onboard the following satellites corresponds better to the maximum absorption of the incident EM energy by photosynthetically active plant tissue and does not overlap with Channel 2.

Data is both transmitted continually (direct readout mode) and recorded by five digital tape recorders onboard for latter transmission. The capacity of the recorders provides

- 110 min. (one full orbit) of GAC data.
- 10 min. of HRPT data, which is called LAC data when recorded

The visible Channel 1 and the NIR Channel 2 from GAC data are combined to produce an NDVI as a standard product, the global vegetation index (GVI). The GVI provided by NOAA associates low DNs with highly active phytomass, where the difference between the channels is greatest (Koffler & Callicott, 1985).

The following table summarizes platform and sensor specifications. For a comparison to the specification of NOAA AVHRR sensors Table 2.1 may be used.

Table 2.1: Technical Specifications of NOAA AVHRR

Launch:	
TIROS-N Series	
NOAA-6 :	27 June 1979 (4 channels)
NOAA-7 :	23 June 1981 (5 channels) (operational in 1985)
Advanced TIROS-N (ATN)	
NOAA-8 :	28 March 1983 (4 channels)
NOAA-9 :	12 December 1984 (5 channels) (operational in 1985)
NOAA-10:	17 September 1986 (4 channels)
NOAA-11:	24 September 1988 (5 channels)
Orbital parameters:	
Orbit:	near polar sun synchronous
Equatorial crossing: (local sun time)	14:30 ascending node (North-bound) 2:30 descending node (South-bound) NOAA-7 and NOAA-9
Altitude:	833 to 870 km
Coverage:	90° N to 90° S
Inclination:	98.7° - 98.9°
Period:	101.6 - 102.4 min., 14.1 orbits/day
Repeat cycle:	12 h per satellite
Orbit repeat period:	8 to 9 days (caused by non-integer value of orbits/days)
Sensors:	
Scan principle:	oscillating mirror
Scan angle:	± 55.3846°
Swath width:	2700 km (plane tangent to Earth)
IFOV:	1.39 to 1.51 mrad
Ground resolution:	1.1 km at nadir 2.4 km max off-nadir along track 6.9 km max off-nadir cross track
Image size:	2048 pixels across 1000 scan lines = 3 orbital minutes
Quantisation:	10 bit

AVHRR spectral specifications:

Waveband	Bandwidth	IFOV
Channel 1	0.58 to 0.68 µm	1.39 mrad
Channel 2	0.725 to 1.10 µm	1.41 mrad
Channel 3	3.55 to 3.93 µm	1.51 mrad
Channel 4	10.30 to 11.30 µm	1.41 mrad
Channel 5 *	11.50 to 12.50 µm	1.30 mrad

*AVHRR/1: Channel 5 constitutes repeated channel 4 signal

Note: The digitizing rate of 39.936 samples per second corresponds to an angle of 0.95 mrad for the scanner rotation. With an average IFOV of 1.4 mrad the number of samples per IFOV amounts to 1.362.

(After: Brush, 1988; Kidwell, 1988; Townshend & Tucker, 1981)

Interference between operational satellites on the same orbit was reduced by delaying the local time of overpass by 0.5 h $year^{-1}$ with a subsequent drift in satellite zenith angles and illumination conditions (Holben & Kaufman, 1989). Beside the choice of the channels, the NOAA AVHRR data differs from other satellites like Landsat or SPOT in a much larger IFOV, field of view (FOV) and shorter repeat cycle. As a consequence, atmospheric and geometric correction procedures, the latter based on orbital models instead of GCP, are common for AVHRR images than for higher resolution data.

2.3.2 Landsat-4 and Landsat-5

The Landsat programme was initiated in 1967 as the Experimental Earth Resource Technology Satellite (ERTS). It was intended to evaluate the feasibility of images collected from unmanned space platforms for providing information about practical Earth resource management applications. The first satellite of the program, ERTS-1, was launched on 23 July 1972. In 1975 the program was renamed to Landsat.
The second generation consists of so far two spacecrafts, Landsat-4 and Landsat-5. The second generation spacecrafts were equipped with the Thematic Mapper (TM), which was not available on the predecessors. The Return-bean Vidicon and on-board storage facilities were omitted. The capability for real-time global data read-out by a tracking and data relay satellite system (TDRSS) was also introduced.
Complete coverage of the earth surface is provided once every 16 days. The equator is crossed at 9:45 local time. The time was selected to take advantage of early morning skies that are generally clearer than later in the day.
The payload of the second generation Landsat systems consists of two sensors, the Multi Spectral Scanner (MSS) and the TM.

(a) **Multispectral Scanner (MSS)**

The MSS system is a line scanning device using an oscillating mirror. The Earth surface is scanned from west to east during one oscillation of the mirror. The retrace cycle is used to calibrate the detectors. The

movement of the satellite to the south during scanning results in lines that are not exactly at right angle to the orbital path. The west drift during scanning is compensated for by the off-set of lines, which gives the images the form of a parallelogram.
At each scan mirror oscillation 6 lines are imaged onto the detector arrays for each of the 4 wavebands. The IFOV of each detector element is equivalent to an 82 m square projected onto the ground (Landsat-4 and -5). This corresponds essentially with the 79 m IFOV of the previous MSS system. The radiometric resolution is 6 bit for all bands. During subsequent ground-based processing the data is scaled to 7 bit for Bands 1 to 3, while Band 7 normally remains unchanged.
The MSS optics and scanning mechanism on Landsat-4 and -5 were modified for the lower altitude of the satellites. The spectral bands were kept identical but renumbered. Bands 4 to 7 on previous systems correspond to Bands 1 to 4 on Landsat 4 and 5 MSS. For computer compatible tapes (CCTs) the representation of Band 4 was changed from 6 to 7 bit (Price, 1988). The modifications thus allow direct comparisons to earlier images. A summary of Landsat MSS technical specifications is provided in Table 2.2.

(b) **Thematic Mapper (TM)**

Like the MSS the TM uses an oscillating mirror for reflecting intercepted radiation towards the detector arrays. Contrary to the MSS both the oscillations are used for imaging the surface. In order to avoid a crossing of imaged lines induced by the forward motion of the spacecraft, a pair of scan line correcting mirrors are driven at the scan rate to alter the imaged areas into parallel strips.
The TM device records radiant energy in 7 spectral wavebands. The spectral wavebands are different from the MSS wavebands. They have been chosen to improve the spectral separation of major earth surface features. The IFOV gives a 30 m ground resolution in Bands 1 to 5 and 7. The resolution in Band 7 is 120 m. The visible

spectrum is covered by bands 1 to 3, the NIR by Bands 4, 5 and 7 while Bands 5 and 6 detect radiant energy in the far infra-red spectrum.
Each scan line projects the energy onto a detector array of 16 elements per band. The radiometric data of all bands is digitized to a 8 bit precision and is not decompressed by ground processing.

Table 2.2: Technical Specifications of Landsat-4 and -5 MSS and TM

Launch:		
Landsat-4:	16 July 1982 (TM not operational)	
Landsat-5:	1 March 1984	
Orbital parameters:		
Orbit:	near polar sun synchronous	
Equatorial crossing:	9:45 local sun time	
Altitude:	705 km	
Coverage:	81° N to 81° S	
Inclination:	98.2°	
Period:	98.94 min. 14 9/16 orbits per day	
Orbit repeat period:	16 days	
Sensors:		
Scan principle:	oscillating mirror	
	MSS	TM
Scan angle:	± 7.46°	± 7.70°
Swath width:	185 km 185 km	185 km East - West 170 km North - South
IFOV:	0.118 mrad	0.043 mrad VIS & NIR 0.17 mrad thermal IR
Ground resolution:	82 m	30 m 120 m Band 6
Image size:	3240 x 2430	
Quantisation:	7 bit	8 bit
MSS and TM spectral specifications:		
Band 1	0.50 - 0.60 µm	0.45 - 0.52 µm
Band 2	0.60 - 0.70 µm	0.52 - 0.60 µm
Band 3	0.70 - 0.80 µm	0.63 - 0.69 µm
Band 4	0.80 - 1.10 µm	0.76 - 0.90 µm
Band 5		1.55 - 1.75 µm
Band 6		10.40 -12.50 µm
Band 7		2.08 - 2.35 µm

(After: Lillesand & Kiefer, 1987; Robinson, 1985; Sabins, 1985)

2.3.3 Comparison of Sensors Products

Although similar in respect to orbital parameters, data derived from NOAA AVHRR differs considerably from Landsat MSS and TM data and other high resolution satellite sensors. Four principal aspects of differences can be identified (Hayes, 1985):

(a) **Radiometric Resolution**

AVHRR data is recorded and transmitted as 10-bit data in all channels. Landsat MSS data is recorded as 6-bit data and rescaled to 7 bit for bands 1, 2 and 3. Landsat TM data is recorded and distributed in an 8 bit resolution in all bands.

(b) **Field of View**

With a nominal ground resolution of 1.1 km, 1 pixel from AVHRR covers much the same area as 200 Landsat MSS and 1345 TM pixels. While Landsat images contain data from an area of 185 km x 185 km, AVHRR covers approximately 2700 km across the line of flight. The image size along track is typically 1100 km, but can be up to 4000 km (Hastings *et al*, 1988).

(c) **Spectral Resolution**

The visible and the NIR portion of the spectrum of EM energy is measured in four wavebands with Landsat MSS compared to 2 wavebands with NOAA-AVHRR. There is a certain amount of correspondence between Landsat MSS Bands 2 and 4 and NOAA-AVHRR Channels 1 and 2, with a wider bandwidth in the NIR Channel of the latter. The saturation threshold of AVHRR sensors is significantly higher than that of MSS sensors.

(d) **Frequency of Coverage**

The NOAA-AVHRR platforms provide daily coverage, thus making it useful for monitoring rapid processes in the Earth's atmosphere and on its surface. Landsat platforms provide repeated coverage every 16 days.

Despite these large differences between Landsat MSS and NOAA AVHRR in technical respects, the informational content of the data has been found to be similar. A comparison of NOAA AVHRR channels 1 and 2 to Landsat MSS bands 5, 6 and 7 yielded coefficients of correlation of 0.86 for vegetated surfaces (Wiegand & Richardson, 1982).

NDVI values computed from the two sensors have been compared over the Imperial Valley, California, the Nile Delta, Egypt and southern Italy (Townshed & Tucker, 1981; Townshend & Tucker, 1984). The coefficients of correlation obtained between MSS and AVHRR NDVIs range from 0.69 to 0.73. In a study over Scotland a similar comparison yielded a coefficient of correlation of 0.96 (Hayes & Cracknell, 1984). For an 80 km transect in South Africa the correlation coefficient between MSS and AVHRR NDVI varied between 0.77 and 0.88 (Hayes & Cracknell, 1985). The differences tend to decrease with an increase in spatial reflectance uniformity. Therefore, a substitution of AVHRR for MSS data is likely to be more successful for rangeland areas than the technical differences suggest.

2.4 Rangeland Monitoring by Satellite Data

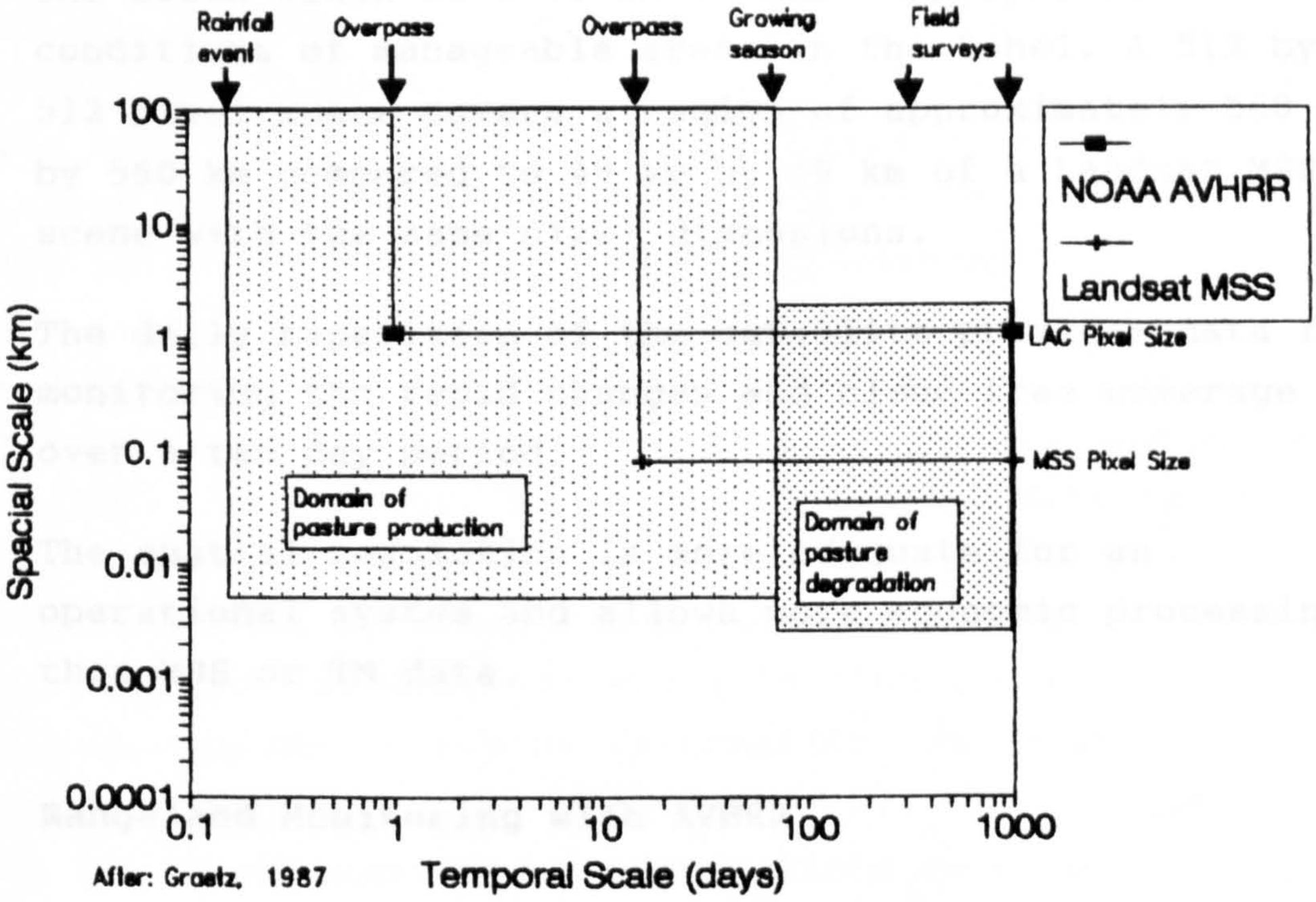
The suitability of Landsat MSS and NOAA AVHRR data for an operational rangeland monitoring system will be discusses in this chapter. The conclusion of NOAA AVHRR as being an appropriate data source for deriving phytomass estimates for the Sahel is followed by a compendium on previous work of utilizing NOAA AVHRR data for investigations over semi-arid rangelands.

2.4.1 Choice of Sensor for Rangeland Management

For the estimation of vegetation production and degradation of rangelands Landsat MSS, Landsat TM and NOAA AVHRR data are suited for different tasks. Landsat MSS and TM data differ in their number of spectral bands, the choice and width of these

bands and their spatial resolution. With TM a land inventory would be possible due to its higher resolution. Landsat MSS data has been widely used for rangelands. Their main limitation is the frequency of coverage. A return period of 16 days cannot monitor the rapid change of vegetation development during the rainy season, since cloud free conditions may not always be present. To adequately estimate the temporally dynamic nature of the photosynthetically active phytomass data collection at intervals of 5 to 13 days is required (Tucker *et al*, 1983).

Figure 2.8: Temporal and Spatial Scales at the Arid Rangelands With the Capabilities of Landsat MSS and NOAA AVHRR



As presented in Figure 2.8 a direct calibration of ground data with satellite data is possible for Landsat MSS but not for NOAA AVHRR data. The reason is the area needed for sampling phytomass for the calibration of VIs. It may be calculated by the following equation:

$$A = [P * (1 + 2 * L)]^2 \ (m^2) \qquad (2.6)$$

(After: Townshend & Tucker, 1981)

For AVHRR LAC data with a pixel size P of 1.1 km and a location accuracy L of one pixel, the sampling area A would be 3.3 km². Thus the calibration of AVHRR LAC data requires either specially designed ground sampling schemes or a multi-stage system comprising Landsat images to intercalibrate these data (Graetz, 1987). The degradation of the landscape is best sampled by Landsat MSS, whereas phytomass production would be adequately captured by NOAA AVHRR.

The reasons for the suitability of NOAA AVHRR data for estimating and monitoring rangeland vegetation for seasonal changes on a regional and continental scale are:

- The swath width of 2700 km is more appropriate to conditions of manageable areas in the Sahel. A 512 by 512 pixel scene covers a region of approximately 560 km by 560 km compared to 49 km by 49 km of a Landsat MSS scene with the same pixel dimensions.

- The daily repetition of the satellite provides data for monitoring the rapid changes and cloud free coverage over a ten day period.

- The spatial resolution is more adequate for an operational system and allows more economic processing than MSS or TM data.

2.4.2 Rangeland Monitoring with AVHRR

Spectral similarities between Landsat MSS Bands 2 and 4 and NOAA AVHRR Channels 1 and 2 suggest similar procedures as with Landsat MSS data could be applied to NOAA AVHRR and comparable results achieved with the latter (Norwine & Gregor, 1983). Investigations into the feasibility of NOAA AVHRR data for monitoring vegetation have been started at the beginning of the 1980s (Townshed & Tucker, 1981). The general usefulness of AVHRR data for estimating phytomass over sparsely vegetated areas and the feasibility for monitoring vegetation production has also been demonstrated (Schneider *et al*, 1985; Tucker *et al*, 1983).

On a global scale NOAA AVHRR-GAC data and the GVI has been applied for monitoring vegetation activity (Justice *et al*, 1985) and found to be useful as an indicator for detecting drought conditions (Choudhury & Tucker, 1987).
Temporal changes of vegetation productivity have been monitored on a continental scale (Tucker *et al*, 1985) and on regional scales, for example rangeland in Mali (Hiernaux & Justice, 1986) and grassland in Niger (Justice & Hiernaux, 1986). Most of the investigations were qualitative interpretations of GVI images like the monitoring of vegetation changes over several years in Sudan (Hielkema *et al*, 1986). Although the results suggested a close relation between the GVI respectively the NDVI to the phytomass of green vegetation and seemed to allow the prediction of annual primary production, a quantitative analysis and regression is desirable. There is also a need for calibrating the sensor response for changes in sensitivity and allowing inter-satellite comparisons (Townshend & Justice, 1986).

For more general uses of NOAA AVHRR data for land surface investigations it may be referred to a literature survey by Hayes (1985). Details of the use of NOAA AVHRR data for land cover studies are presented. The paper also contains a description of VIs for Channels 1 and 2. A special edition of the International Journal of Remote Sensing (Justice, 1986) constitutes another source of information on activities in monitoring rangelands with NOAA AVHRR.
Most of the above mentioned investigations were research studies. A combination of data from NOAA and Landsat satellites for a routine operation has been used in the locust plague control program of the United Nations Food and Agricultural Organization (FAO) (Tucker *et al*, 1985; Hussey, 1987). NOAA data were used to monitor temperature and moisture content of air, ground and standing crop, the primary factors that influence growth and movement of locust. NOAA images are examined in detail with Landsat images of areas with presumed rainfall. Areas of emergent vegetation can then be identified and examined.
Experiments of the FAO in connection with the locust project have shown that the spatial resolution of Landsat MSS images

exceeds the requirements by a factor of 35. This confirms the feasibility of utilizing NOAA AVHRR LAC data monitoring rangeland vegetation in the Sahel.

3. FIELD WORK

Field and image data constitute the main sources of information to obtain near real time maps of rangeland vegetation quantities. Other sources, like soil maps or rainfall distribution, are of secondary importance. Because of the significance of data from field surveys a large portion of the project was allocated to designing a field sampling procedure adapted to Sahelian rangeland conditions and assess its applicability.

The period of ground data acquisition stretched over five years, with data being collected for three years (1985, 1988 and 1989) and three different areas in Mali and Niger. The data originated from three different sources:

- Institute of Terrestrial Ecology, Monks Wood (ITE) and Silsoe College Field Visits in Niger (1985, 1988 and 1989)
- Centre International Pour l'Elevage en Afrique (CIPEA) Ground Survey (1985) in Niger
- Centre for Arid Zone Studies at the University College of North Wales, Bangor (CAZS) field visits in Mali (1988)

Detailed procedures of collecting herbaceous vegetation in the Sahel could not be reviewed since they have not been published in the literature. Only through personal communication was it possible to obtain some information on sampling techniques (Brown, 1988; Wylie, 1989). As a consequence, the design of a sampling method had to constitute an iterating process, using results from previous surveys to propose a new and more appropriate sampling method. None of the surveys presented a simple repetition of any other, but differed significantly in one or more respects.

The 1985 ITE/Silsoe and CIPEA surveys and the Mali survey from 1988 are only covered briefly. There was no active involvement

of the author in these surveys and so they were considered as being literature.
A descriptive summary of the five field surveys investigated is given in Table 3.1. The sampling schemes differed in a number of ways as well as the constrains imposed by manpower and logistical considerations.

Table 3.1: Summary of Field Survey Characteristics

	CIPEA 1985	ITE/Silsoe 1985	CAZS 1988	ITE/Silsoe 1988	ITE/Silsoe/ CASTE 1989
Team Size	?	4	2	4	8
Transport	?	1 vehicle	1 vehicle	1 vehicle	2 vehicles
Survey Area	5.5°-8.0° E 14.5°-17.0° N	5.5°-6.0° E 15.0°-15.5° N	2.5°-3.5° E 15.5°-16.0° N	5.5°-6.0° E 15.0°-16.0° N	5.5°-6.0° E 15.0°-16.0°
Survey Periods	3 periods 03.08-10.08 26.08-03.09 16.09.26.09	1 period 28.08-03.09	7 periods 05.07-11.07 17.07-23.07 01.08-06.08 14.08-18.08 28.08-02.09 11.09-16.09 24.09-29.09	1 period 24.09-02.10	2 periods 23.08-28.08 08.09-13.09
Site Positioning	Aircraft navigation	Landsat MSS hard-copies	GPS, 1:200000 maps	Landsat MSS hard-copies	GPS, Landsat hard-copies
Sampling Layout	2 parallel 2km transects 500m distance	Single 1km transect	Single 1km transect	Single 500m transect	Single 1km transect
Sample Points	10 measured 40-50 estim.	10 measured	10 measured	5 measured	20 measured
Point Distance	random	100m fixed	random	100m fixed	50m fixed
Sample Area	1st: 0.5m² 2nd: 0.1m²	0.25m²	1m²	0.25m²	1m²
Site Parameters	?	Trees/bushes ± 50m 0.25/2/8m	Trees/bushes ± 25m 0.25/2/8m	Trees/bushes ± 50m 0.25/2/8m	Trees/bushes ± 50m <2/2-4/>4m
Sample Point Parameters	Herbaceous fresh weight Cover ?	Herbaceous fresh weight Cover Trees/bushes Soil texture	Herbaceous fresh weight Cover Height Trees/bushes	Herbaceous fresh weight Cover Trees/bushes Soil texture	Herbaceous fresh weight Cover Height Trees/bushes Soil texture Soil colour
Drying Method	Oven	Oven	Air & Oven	Air & Moist. Meter	Air & Oven

? Procedure unknown

3.1 Introduction to Ground Data Acquisition

For monitoring vegetation a VI derived from satellite data can provide a relative value for comparing areas of different quantities of vegetation. However, it is not possible to derive a productivity estimate of an area from satellite data alone. For that purpose the VI has to be calibrated to the corresponding amount of phytomass on the ground. In order to be useful for monitoring vegetation the relation between VI and phytomass level is required to be stable over time and the area of interest. Therefore, measurements over a number of growing periods and regions were required.
During this project rangeland production was then expressed as an estimate of dry matter weight of herbaceous vegetation per area. A regression analysis of the relationship allowed to expand production estimates over the whole image.

3.1.1 Purpose of Field Visits

The field visits in 1985, 1988 and 1989 were aimed at providing the necessary data for relating Sahel rangeland phytomass levels to VIs derived from satellite images.
The objectives of the field visits to Mali and Niger were as follows:

(a) Phytomass measurements (grass and herbs) were to be taken at the end of the growing season to establish the maximum amount of vegetation.

(b) The temporal stability of the VI calibration was to be assessed by repeated measurements over the study area.

(c) The spatial stability of the VI calibration was to be investigated by acquiring herbaceous vegetation quantities from different regions.

ITE/Silsoe field surveys were designed on the experience gained from previous ones. However, information from these were not always availble in time to determine proedures for following

surveys. Further more, individual field surveys had additional aspects for investigations.

(a) **CIPEA Survey**

- The survey was intended to cover a larger area (approx. 400 km by 300 km) than all other surveys.
- Multi-temporal sampling missions (three times) during the second half of the growing season were carried out.
- The sampling layout was designed for a direct correlation between ground and NOAA AVHRR VIs. Calibrated VI images were to form part of an early warning system to identify forage shortages and areas susceptible to over-grazing.

(b) **ITE/Silsoe Survey of 1985**

- Estimate herbaceous vegetation once at the end of the growing season to establish the maximum amount.
- Define study area for further surveys.
- The field data sampling scheme was designed to inter-calibrate NOAA AVHRR LAC data by Landsat MSS.

(c) **CAZS Survey**

- Herbaceous vegetation over the whole growing season was to be monitored.
- Instead of producing regional phytomass estimates the calibration was aimed at a local scale, which resulted in a relatively close spacing of sample sites (appprox. 20 km by 10 km). The study area was also restricted to allow rapid access to sites.
- Originally, ground data was intended to be correlated to data obtained from the high resolution Marine Observation Satellite (MOS-1). A

direct correlation of ground data to NOAA AVHRR VIs was not envisaged.

(d) **ITE/Silsoe Survey of 1988**

- The temporal stability of the VI calibrations from 1985 was to be asssessed.
- The sampling scheme was modified to allow an increase in the number of sample sites visited.
- Alternative methods of establishing vegetation m.c. should be investigated and a suitable method tested in the field.

The analysis of the spatial variability of the relationship between the levels of grass and VIs was not the purpose of the survey. It would be unrealistic to assume that temporal and spatial variations could be separated from another by a single repetition, since expanding the results over a larger area requires independent additional data from that section. For the 1988 growing season there was no possibility of achieving that target with the resources available.

(e) **ITE/Silsoe Survey of 1989**

- The temporal stability of VI calibrations should be assessed once more.
- The number of sample sites should be increased beyond the 10 sites of 1988.
- The use of a GPS for site positioning should be investigated.
- Information on soil background colour was to be collected.

Compared to 1988 the 1989 field survey was more ambitious. An increased number of samples was to be taken, more parameters established and a larger area covered. During previous surveys, one of the limiting

factors for visiting a larger number of sites found was the lack of man-power. With the support of the CASTE team it was considered possible to achieve the objectives mentioned above.

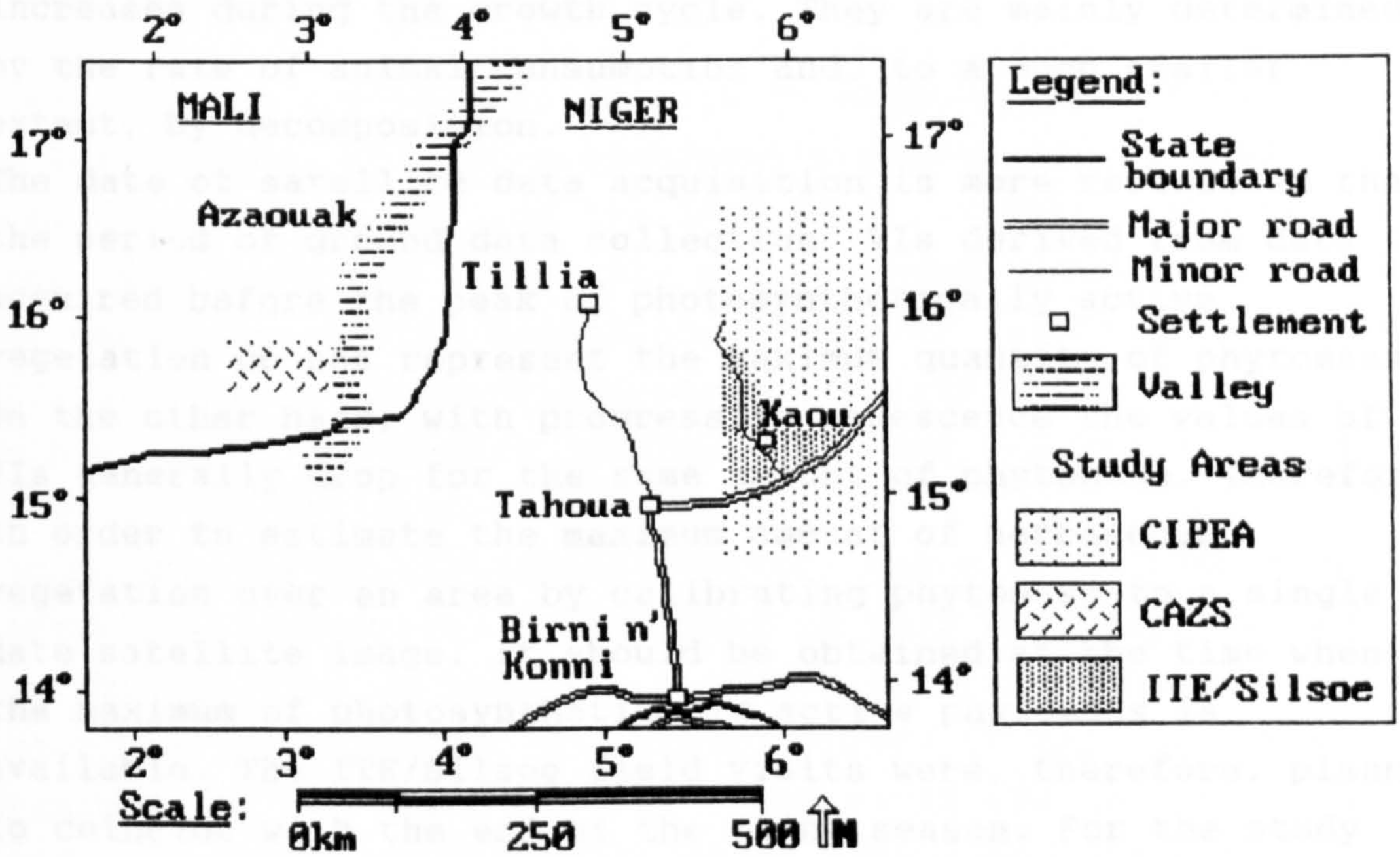
3.1.2 Selection of Study Area

The area for ground data collection should comply with the following conditions:

- Exemplary for Sahel rangeland;
- Accessible by roads;
- Include previous surveys;
- Covered by a high resolution satellite (Landsat MSS).

The main study area for this project was determined by the 1985 ITE/Silsoe field survey. It was located between approximately 5.5° to 6.0° East and 15.0° to 15.5° North. The CIPEA survey covered a much larger area with sites between 5.5° to 8.0° East and 14.5° to 17.0° North. Ground data from Mali were collected in an area between 2.5° to 3.5° East and 15.5° to 16.0° North. The relative position of study areas of the various field surveys is given in Figure 3.1.

Figure 3.1: Study Areas of Mali and Niger Field Surveys



3.1.3 Period of Field Survey

The establishment of a regression between quantities of herbaceous vegetation on the ground and VIs from satellite data relies on the number of points available and on their spread over different rangeland production levels. The number of measurement points depends on the time available for sampling and local growth conditions. The ground information collected over a period of time is related to satellite data, which originates from a single date, the time of the satellite over-pass. The more rapid the changes in vegetation development, the greater the discrepancy between VI and phytomass estimate when collected at different dates.

Performing a ground survey before the maximum amount of phytomass has been reached may result in an error in calibrating the VI caused by the difference in the time of data acquisition rather than the ineffectiveness of the VI. In that respect, the date of the ground data collection should coincide with the peak of growth or shortly after. Changes in the vegetation quantity of the herbaceous layer after maximum

growth has been reached occur at a much slower rate than increases during the growth cycle. They are mainly determined by the rate of animal consumption and, to a much smaller extent, by decomposition.
The date of satellite data acquisition is more restricted than the period of ground data collection. VIs derived from data acquired before the peak of photosynthetically active vegetation do not represent the maximum quantity of phytomass. On the other hand, with progressing senescence the values of VIs generally drop for the same amount of phytomass. Therefore, in order to estimate the maximum amount of herbaceous vegetation over an area by calibrating phytomass to a single date satellite image, it should be obtained at the time when the maximum of photosynthetically active phytomass is available. The ITE/Silsoe field visits were, therefore, planned to coincide with the end of the rainy season. For the study area this normally corresponds to the beginning of September (see Table 3.1). CAZS and CIPEA surveys approached the problem by sampling several times throughout the growing season.

3.1.4 Selection of Sample Sites

For an extension of calibrated VIs over more than the sample sites ground data had to be collected for a variety of phytomass levels. Ideally, sample sites themselves have to comply with a number of conditions to be suitable for the purpose of the project. These conditions are:

- Accessible by survey team;
- Uniformity of vegetation.
- Cover a range of production levels;
- Identification of sample sites;

Accessibility, uniformity and the range of vegetation quantities for a growing period were all established in the field by inspection.

3.1.5 Positioning of Sample Sites

Positioning a specific point is a formidable task in many parts of West Africa. This is predominantly caused by the almost featureless landscape and the lack of up-to-date large scale maps. New roads are frequently not included and smaller tracks may have been shifted depending on weather conditions. Provided accurate maps at appropriate scales are available and 20 to 25 points can be identified both on image and map, a one-pixel rms error may be achieved.

For many parts of the Sahel, however, there are a number of factors preventing the achievement of this accuracy. Generally, the availability of accurate maps for correcting Landsat MSS images is very limited. Locational errors on maps can reach a magnitude of 300 m for natural features (Hiederer & Maidoukia, 1988). In addition, the surfaces of some areas are too homogeneous to identify a sufficient number of points at an adequate spread across the image. Particularly the correction of NOAA AVHRR data is affected by difficulties of identifying GCPs.

Even when enough points can be identified, the positional accuracy provided by the image processor is based solely on these points, on which the calculated transformation is based on in the first place. With an unreliable map this accuracy is likely to be unrealistic and the positional error exceeds the value provided by the image processing software, because the accuracy assessment has to be based on the reference data, the GCPs, themselves. Therefore, a widely representative value of the positional error could not be provided in the course of this project, in that the error in the reference data was unknown.

Possible ways of achieving the aim were identified:

(a) **In-field Identification on Image Hard-copies**
A high resolution image, which has been reliably corrected to a map projection, may be used as a substitute for maps. For ITE/Silsoe surveys hard-copies of an image were employed to identify sample sites directly as to their pixel position. The images were

corrected to comply with a map projection and reproduced to the scale of a map of the area (1:200000). Map positions of sites could then be transferred to pixel positions on the hard-copies. The required accuracy for site positions is 100 m, preferably 50 m (for Landsat MSS data).

(b) **Global Positioning System (GPS)**

The use of a satellite positioning system (CAZS and 1989 ITE/Silsoe surveys) greatly simplifies the procedure of positioning sites. Sample sites can be identified on the image by a transformation of map to image position. Once sites are located and positioned subsequent surveys would only have to identify those same sites.

(c) **Aircraft Navigation and Aerial Photographs**

Aerial photographs with approximate transect positions recorded by the aircraft instruments were used by CIPEA. With the aid of geometrically corrected high resolution images, sites can then be located more accurately.

While the 1985 and 1988 ITE/Silsoe Surveys used maps and image hard-copies to identify sample site positions, all other surveys relied on a GPS or aircraft instrument readings.

3.1.6 Layout of Sampling Method

The general layout of the sampling scheme was determined by the geometric properties of the satellite data and the conditions over the study site. As has been mentioned in Chapter 2, the size of the area for calibrating satellite derived VIs to ground data depends on the pixel size and the achievable accuracy of locating the sites. For a location accuracy of one pixel the required size of the sample area would be some 250 m x 250 m (0.065 km^2) for Landsat MSS and 3.3 km x 3.3 km (10.9 km^2) for NOAA AVHRR LAC data.

A sampling scheme aimed at taking measurements for an individual pixel was considered unsuitable. Measurements would have to be taken over an area with sample points spread across

it. The proportion between demands on time for locating sample points and the usefulness of the measurement would be too unfavourable.

(a) **Restrictions for Sampling Method**

A randomization of sites over the study area can be considered impractical. Only a small number of sites (10 to 12) can be examined by a team of three to four observers and it is essential to cover a range of vegetation quantities. Site accessibility and suitability of pre-determined sites is also unknown. For similar reasons sampling according to a stratified sampling scheme is difficult to implement. The only feasible method would be to pre-determine broad areas by a reconnaissance survey and satellite images from a previous wet season and to make a final decision during the field survey (Taylor *et al*, 1986; Wylie *et al*, 1988a).

(b) **Sampling Layout**

For both satellite data sets, Landsat MSS and NOAA AVHRR LAC, phytomass production figures of pixel size areas can only be acquired by extrapolating results from point measurements and are, therefore, estimates. The position and number of these points should accommodate for the variation in vegetation density on the one hand and ease of identification on the other.

Climatic conditions and the time required for data collection very much limit the layout of the sampling method. Sampling at grid points, for example, would require observers to walk for several kilometres, which would be unreasonable in many cases. Other methods, like parallel transects or spirals were investigated but found unsuitable (Wylie, 1989).

All field surveys presented in this chapter employed transects as the basic sampling scheme. Thus, a number of adjoining pixels could be covered and the identification of successive sample points was a comparatively simple task. The length of each transect varied between 500 m for 1988 Niger sites and 2 km for

CIPEA sites (see Table 3.1). Rangeland production attributed to a site was usually obtained by using the average of all measurements along a transect.
A graphical presentation of the sampling layouts used is provided in Figure 3.2.

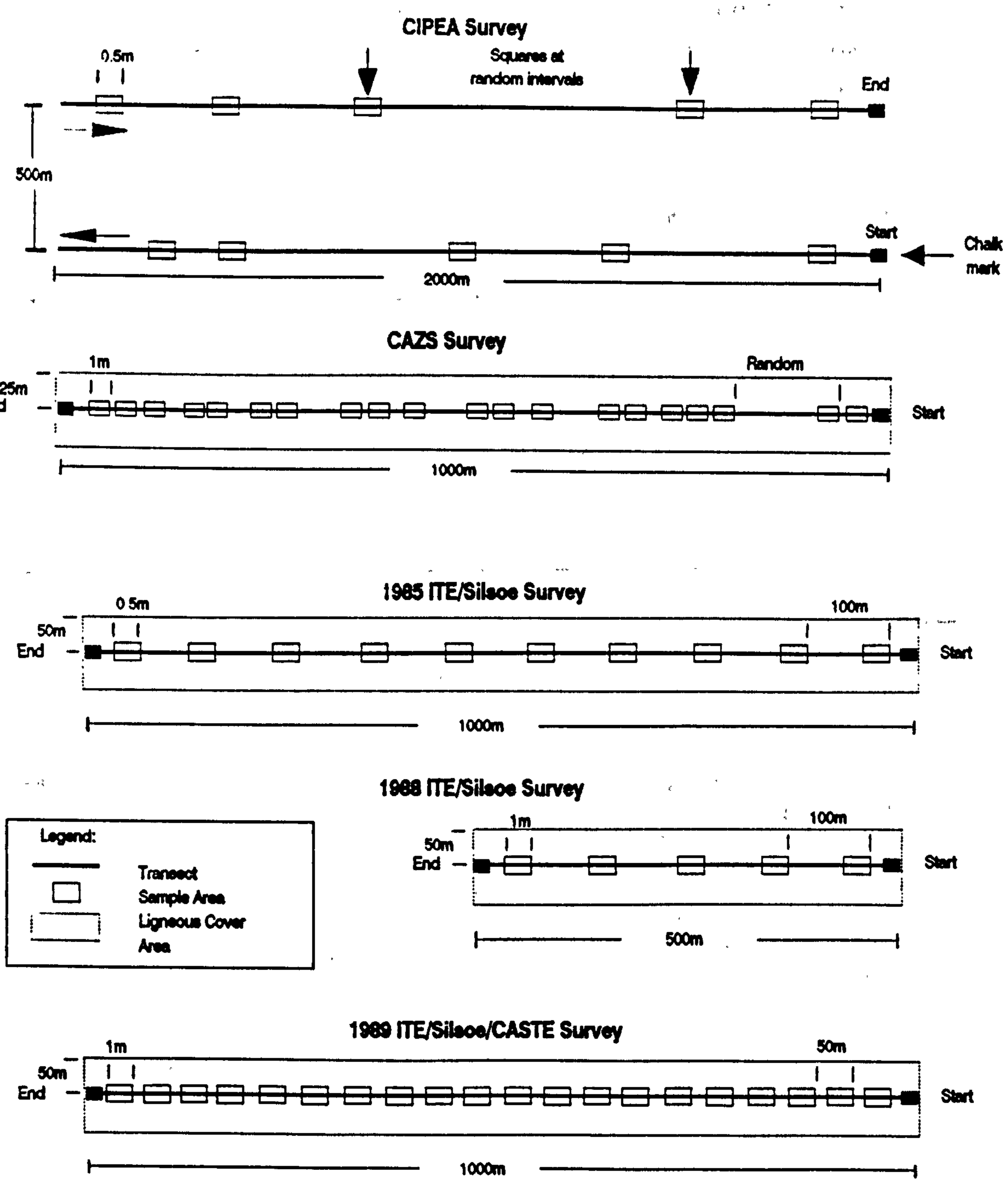
3.1.7 Site Parameters

The objective of all field surveys was to establish herbaceous dry matter yields. Additional information on site characteristics, which may influence the satellite sensor response and VI calibration, could also be collected. The site parameters in question are:

- Dry Matter Weight of Herbaceous Vegetation
- Herbaceous Vegetation Cover
- Herbaceous Vegetation Height
- Soil Texture
- Soil Colour
- Number of Bushes and Trees

The site parameters assessed for individual surveys are provided in Table 3.1. Again a trade-off between accuracy and time required decides on whether to measure or estimate site characteristics.
Shadow by vertical protrusions as an influence factor on VIs was excluded from all surveys, since no method for a rapid estimation of this property could be established.
Distances between sample sites along a transect were established by pacing or a vehicle (CIPEA survey only).

Figure 3.2: Layout of Field Survey Sampling Methods



3.1.8 Determination of Dry Matter Production

The use of the standard method for determining vegetation dry matter content requires the collection of vegetation from all sample points and subsequent oven-drying. The samples may become infested by mould, which could lead to losses in material in form of gas produced by the mould during decomposition of the samples. Also, not only may the number of samples and subsequent storing be problematic, but facilities for drying them may be hundreds of kilometres away. Also, access to these facilities cannot generally be assumed. The most likely methods, which were considered suitable for Sahelian rangelands, and their merits are summarized in Table 3.2.

Table 3.2: Field Methods for Dry Matter Determination

Instrument	Method	Advantage	Disadvantage
Portable Oven	air temp. of 105° C, 24 h	exact result independent of material	mains required storing of samples time consuming instrument cost
Air and sun	drying in the sun	cheap storing limited simple operation	inaccurate stop during the day accurate scale req.
IR Moist. Meter	water absor-ption of EM at 1.45 µm	non-destructive instant result light instrument no storing	material dependent requires calibration increasing error with decreasing m.c. cost
Distilla-tion	evaporation of water in hot oil	simple equip. no electricity inexpensive should not fail	storing of samples time consuming requires a fire
Moisture Meter	electrical capacitance and resistor	light simple operation instant results no storing	material dependent requires calibration increasing error with increasing m.c.

The decision for ITE/Silsoe surveys for a method was based on the following assumptions:

(a) The use of a portable oven would have been unpractical for the survey. It is too heavy to transport and power from mains is not always available.

(b) Air drying of samples with solar energy can be considered possible under the climatic conditions of the Sahel. Advantages of air-drying samples as compared to other methods of establishing vegetation moisture contents are a reduction in equipment (only plastic and paper bags), a simplification of procedure (no in-field measurements), in-field estimates of rangeland production levels are obtained and it is relatively rapid in the field.
Using a moisture meter for assessing vegetation m.c.s was dismissed following the experience of 1988 and a combination of oven-drying and air-drying was introduced in 1989. The method of air-drying samples was rejected in 1988, following the advice given at Silsoe College. However, it has been used successfully in Mali and Niger (Brown, 1988; De Wispelaere & De Fabregues, 1988). Samples of herbaceous vegetation could be dried to a constant moisture content with a standard error of the mean of less than 0.5% at a 95% confidence level. Oven-drying sub-samples would still be necessary, since the equilibrium moisture content depends on the stage of vegetation development and weather conditions at the time of sampling and, therefore, varies for a specific day for different growing seasons.

(c) The Infra-Red Moisture Meter was a new instrument and its ruggedness under field conditions unproven. Similar to satellite remote sensing the error in estimated moisture content increases with progressing senescence of vegetation. Since samples should be taken rather late in the rainy season, the state of the vegetation would have been unfavourable.

(d) Although comparatively simple, the distillation method was considered too time consuming. It also requires an

open fire for a considerable amount of time and constant attention during evaporation.

(e) A moisture meter provides instant estimates and storing samples is dispensable. The error of estimated moisture content decreases with progressing senescence, which makes it more suited than the IR Moisture Meter for rangeland vegetation at the end of the growing period. But there are also a number of disadvantages. Since at least two or three readings have to be taken from each sample point, the time spent in the field is prolonged. Readings differ with plant material and the instrument has to be calibrated for local conditions.
For the 1988 ITE/Silsoe survey the use of a moisture meter for estimating the moisture content of samples was the most promising method. The instrument available for the study was a WILE 35 Moisture Meter from KONE OY, Finland. Details on technical specifications are given in Table 3.3.

Table 3.3: Specification of WILE 35 Moisture Meter

Specification	WILE 35
Readings	analog dial
Range	10.0 to 60.0 % moisture content
Power	9 V battery
Dimension	182 x 120 80 mm
Weight	1.2 kg
Accessory	Extension cylinder with position for measuring grass
Manufacturer	KONE OY, Farmcomp, Fonseenintie 6, SF-00370 Helsinki

A summary of the methods applied for establishing the vegetation m.c. during the field surveys is presented in Figure 3.1. Not investigated was a double sampling technique for obtaining dry matter of herbaceous rangeland vegetation, as employed during the CIPEA survey. For each site above ground vegetation was clipped off at 10 sample points. Samples were stored in bags for subsequent drying. The majority of data (40 points for the first and 50 for the second and third visit), however, were acquired from visual estimates by observers. The procedure requires an additional and independent survey to

verify results of estimates. For ITE/Silsoe surveys the time available in the field was insufficient to allow a double sampling technique.
The criteria for selecting a method for the 1988 and 1989 ITE/Silsoe investigations are presented in more detail when discussing individual surveys.

3.1.9 Correlations and Accuracy Assessment

Concepts for the statistical analysis are presented in Chapters A1 and A2 in Appendix I. Four main areas of data analysis can be identified:

(a) **Reliability of Mean Herbaceous Dry Matter Estimates**
Sahelian rangeland vegetation displays a high variation in distribution and quantity not only from year to year, but also on very small scales. It originates from the growth pattern of grass and constitutes a function of the size of the area clipped of for measurements. Herbs and grasses grow in clusters which, at low and medium densities, are separated by stretches of bare ground. If the point for sampling happens to be at such a cluster, the measurement is entirely unrepresentative of the area.
Wherever possible and applicable the confidence at which the average dry matter quantity of herbaceous vegetation could be estimated was assessed. Three standard errors of the mean were distinguished: ± 125, ± 150 and ± 200 $kgha^{-1}$. A pilot study based on the 1988 data sets revealed that smaller values than ± 125 $kgha^{-1}$ could only be estimated at confidence levels below 60%. Larger values than ± 200 $kgha^{-1}$ for the standard error would result in four classes of herbaceous vegetation quantities for a calibrated satellite image for average growing seasons. This was considered as being of little use.

(b) **Required Number of Samples per Site**
As a consequence of the close relationship between

herbaceous dry matter quantity and variability in the distribution of vegetation, the required sample size for a specified confidence level is subject to the production level. In areas with higher productivity or in years with average or above average rainfall the sample number has to be larger than in areas with sparse vegetation or in years of below average rainfall to achieve the same error of the mean in absolute units. For rangeland vegetation an accuracy of estimating herbaceous dry matter quantities to a confidence level of 80% was suggested (Mueggler, 1976) and applied. Under Sahelian conditions, this would either require a wide step size for VI calibration classes or a large number of samples. Therefore, confidence levels of 70 and 60% were included for estimating the necessary sample size. The standard error of the mean was fixed to ± 150 $kgha^{-1}$. A corresponding class width would yield 6 to 7 classes under average conditions, which was considered a reasonable compromise between detail and legibility of a calibrated map.

(c) **Duration of a Single Sampling Mission**

Ground data collection for satellite image calibration cannot accurately match with the time of satellite data acquisition. It only takes about 30 sec. for a Landsat scanner to cover the 185 km of a scene. In comparison, collecting data for 16 sites took six days and eight observers in 1989.

With an increasing temporal difference between date of image and ground data acquisition the correlation between the two deteriorates. It was, therefore, necessary to estimate the possible duration of a ground data sampling period, before changes in vegetation development would influence the calibration.

The duration of a single sampling mission was defined as the number of days, when the probability of the change in mean vegetation quantity from the date of data acquisition is 10% or less.

(d) **Relationship Between Site Parameters**

Interdependencies between herbaceous vegetation and other site parameters should be investigated, because of their influence on satellite data. In particular soil background information can alter VI values, but also vegetation m.c. and shadow. These site characteristics were estimated by assessing herbaceous ground cover, number of trees and bushes and a soil definition.

In order to reduce the amount of data processing and concentrate on the correlation of herbaceous dry matter quantities to satellite VIs, the analysis of interdependences should be restricted to 2-dimensional comparisons with dry matter as one variant.

3.2 Peripheral Field Surveys

This section briefly presents field surveys, which were not undertaken by the author, but procedures applied and conclusions drawn were taken into account to define the 1988 and 1989 field surveys in Niger. For detailed descriptions of the 1985 CIPEA and ITE/Silsoe and the 1988 Mali field data it may be referred to corresponding survey reports (Wagenaar & deRidder, 1986; Taylor *et al*, 1986; Brown, 1988).
However, an accuracy assessment as introduced in the previous section was not carried out and is, therefore, included in the following paragraphs. In addition, ground data collected from these surveys was used to calibrate satellite VIs (see Chapter 5).

3.2.1 CIPEA Field Survey of 1985 in Niger

The field survey conducted by the Centre International Pour l'Elevage en Afrique (CIPEA) of 1985 in Niger was carried out completely independently of this project. Methods and data were kindly made available by Mr. D. Bourn from CIPEA.
Overall, the CIPEA survey was conducted within a much larger

frame of financial and technical support. Methods and procedures applied cannot be directly compared to ITE/Silsoe surveys. Nevertheless, the analysis of the data can provide recommendations for ground sampling and can be employed to calibrate satellite VIs.

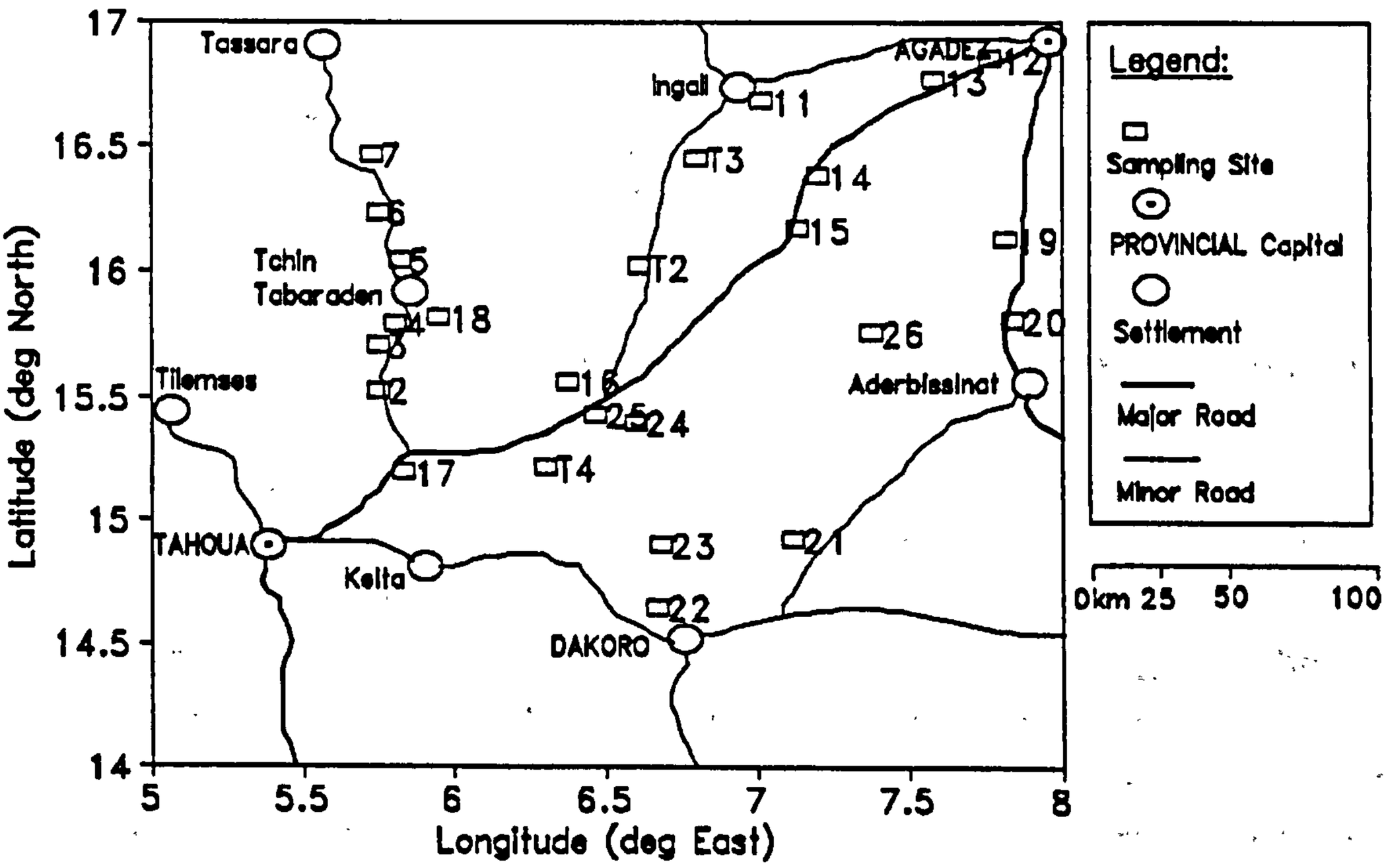
Overall, the CIPEA survey was conducted within a much larger frame of financial and technical support. Methods and procedures applied cannot be directly compared to ITE/Silsoe surveys.

(a) **Sample Sites**

25 sites were established for ground data collection.

- Most sites were selected along roads between Tahoua and Tassara, Tahoua and Agadez and Agadez and Aderbissinat. A graphical demonstration of the relative distribution of sites across the study area is given in Figure 3.3. Absolute site positions in terms of latitude and
- longitude are given in Table A.1 in Appendix II.

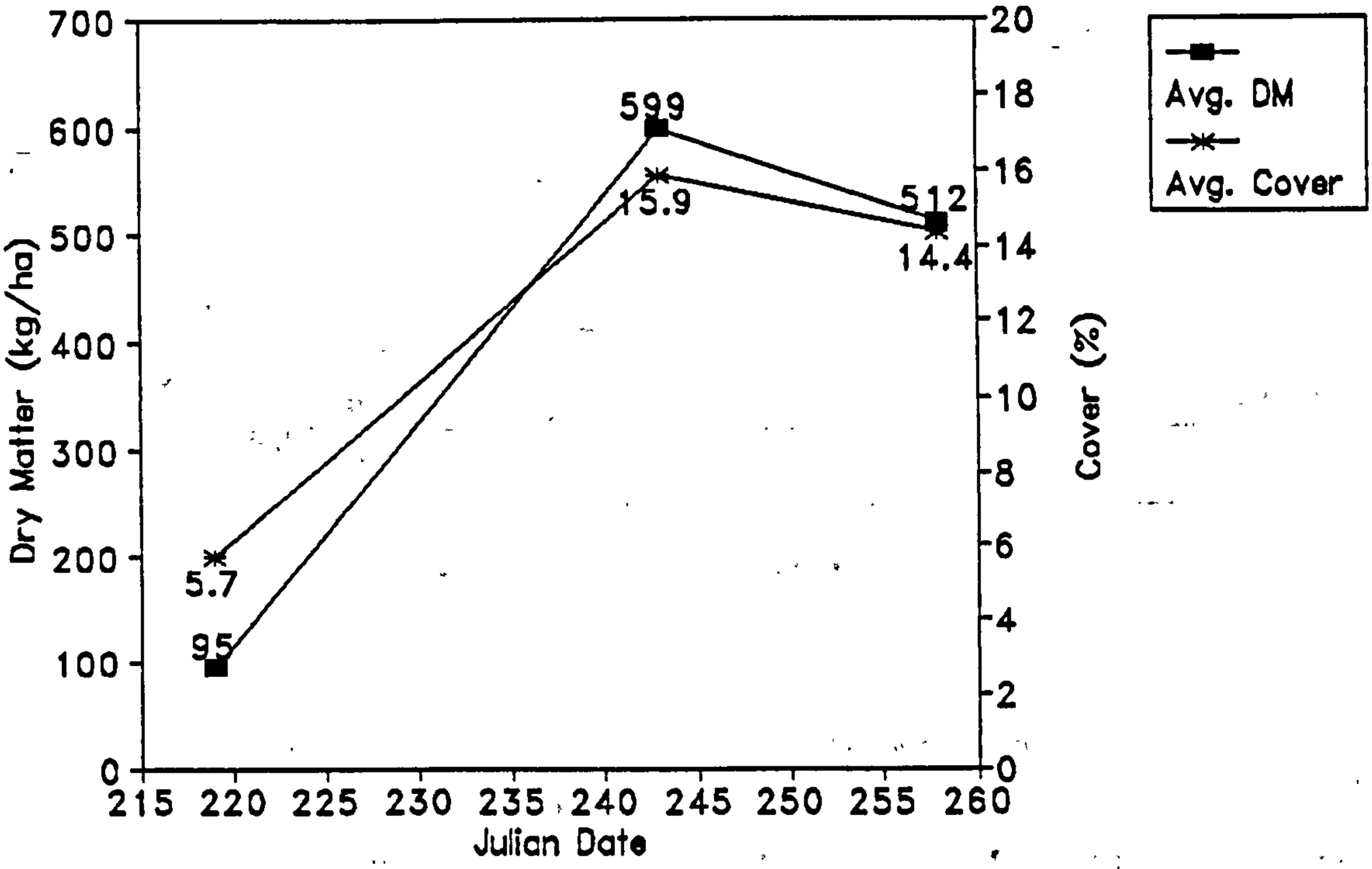
Figure 3.3: Arrangement of Sampling Sites of 1985 CIPEA Field Survey in Niger



(b) **Results of Site Parameters**

Average values of dry matter of herbaceous vegetation and percentage cover for each mission are graphically presented in Figure 3.4. Results from individual sites are given in Table A.2 in Appendix II.

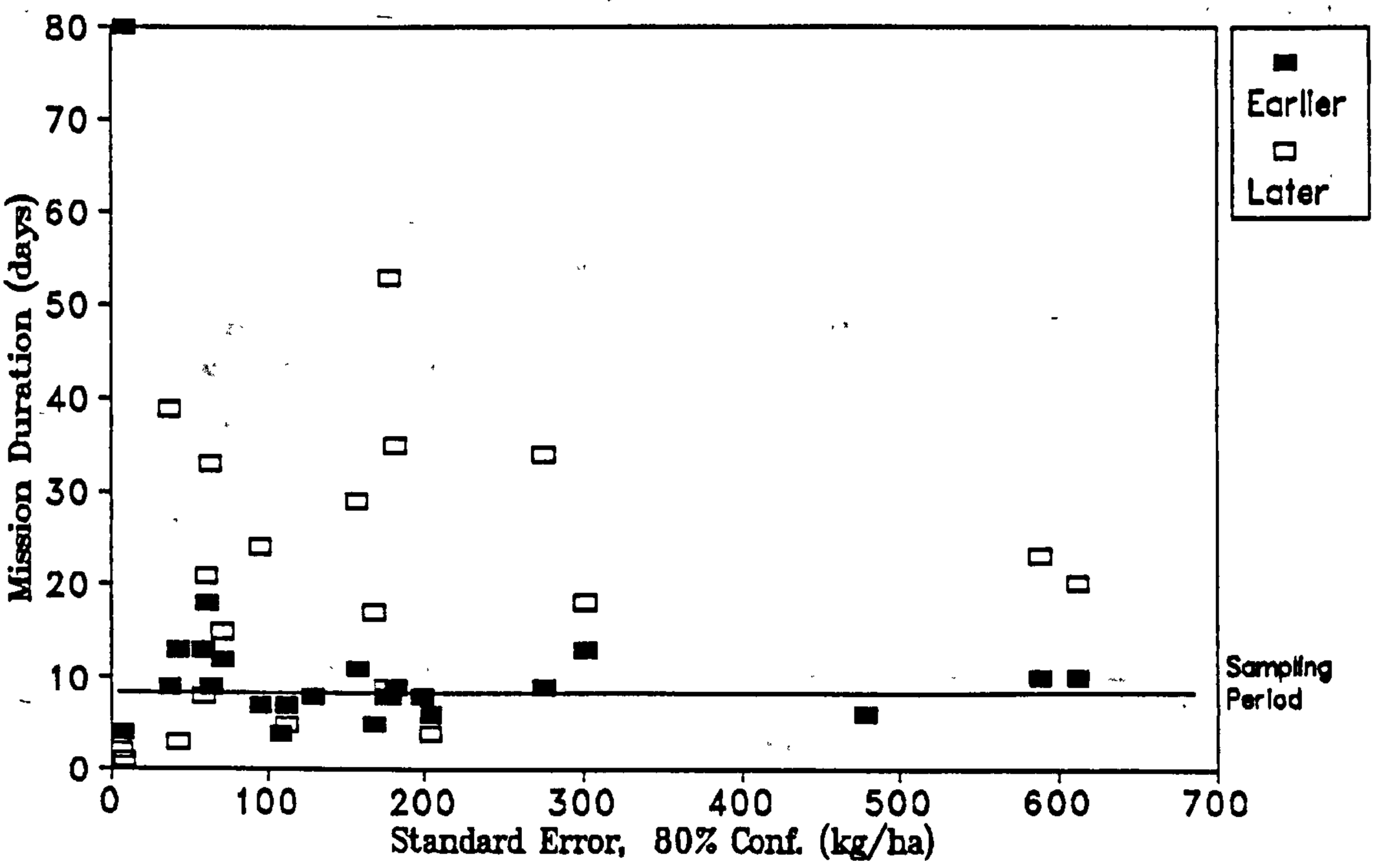
Figure 3.4: Development of Herbaceous Vegetation Dry Matter Quantities and Cover during 1985 CIPEA Field Survey



The highest average amount of herbaceous vegetation from all sites (599 $kgha^{-1}$) was found during the second mission, which was conducted between 26 August and 3 September. Most of the vegetation of that year grew within only three weeks in August. The drop in quantity from beginning to the end of September is within the range of the variation of dry matter estimates.
The findings suggest that sampling for a single date of satellite data in 1985 should not have occurred before the end of August, if it is intended to cover the peak of herbaceous vegetation quantity of a growing period. The duration of a single sampling mission is restricted by the number of days, when the probability of the

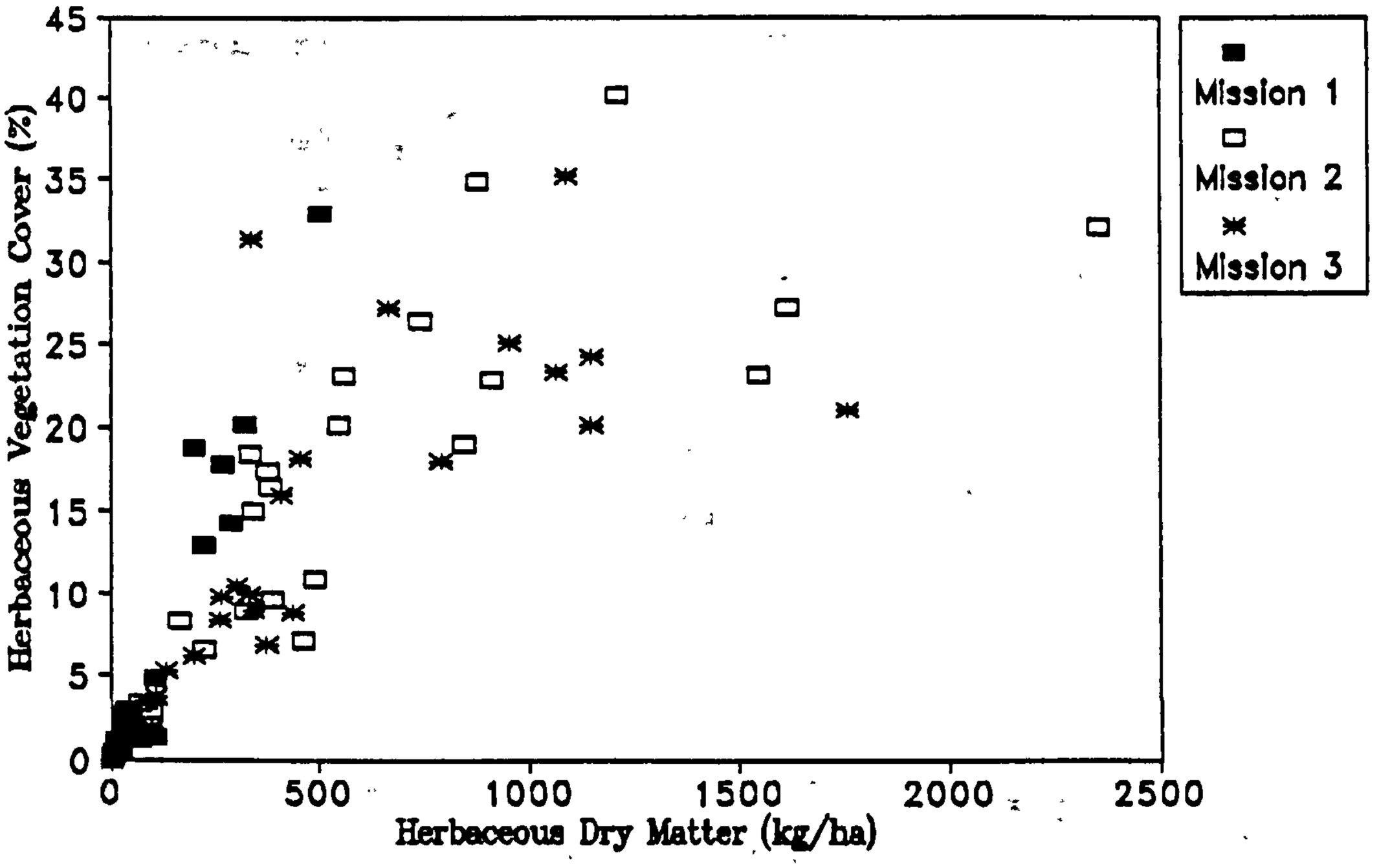
change in mean vegetation quantity from the date of data acquisition is 10% or less (see Figure 3.5).

Figure 3.5: Duration of Field Survey Mission (for 10% Observed Significance Level, CIPEA Survey)



It can be concluded that a single mission within the CIPEA study area should have been restricted to six to eight days until the end of August. Sampling at a later date was less critical, because changes in vegetation quantities occurred over a longer period.
During all three missions a strong non-linear relationship between herbaceous dry matter quantities and cover was observed (see Figure 3.6).

Figure 3.6: Herbaceous Dry Matter Production vs. Cover for 1985 CIPEA Field Survey in Niger (Transect Averages)

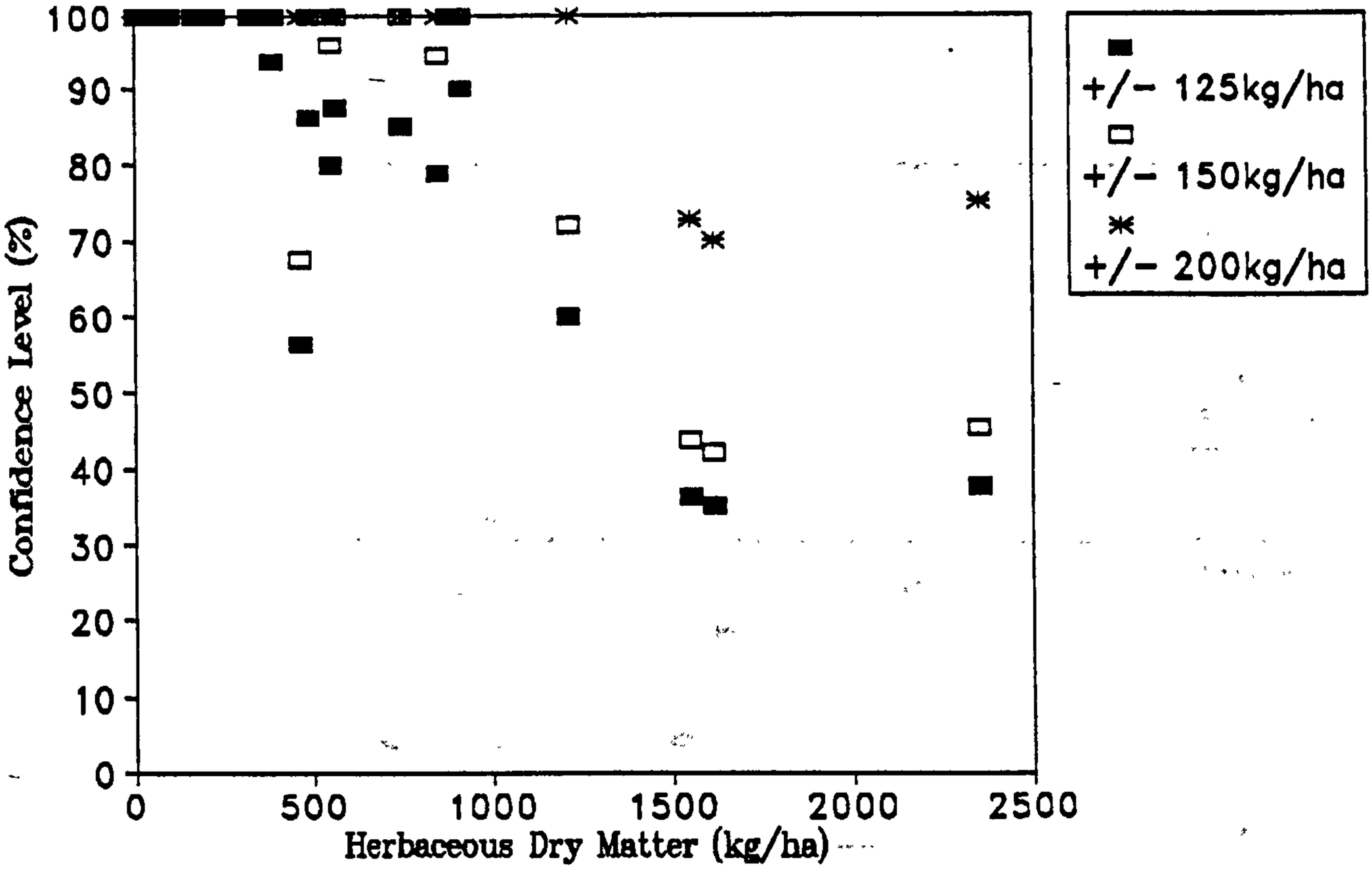


For the first mission herbaceous vegetation ground cover increased linearly with quantity up to the maximum amount found. During the second and third mission cover became insensitive to increases in vegetation above dry matter quantities of approximately 600 $kgha^{-1}$. This corresponded to the average amount of vegetation found, but it could also constitute an environmental constant typical for the area. Further field survey results are needed to decide on the issue.

(c) Accuracy Assessment of Herbaceous Dry Matter Estimates

Three classes for the standard error of the mean were investigated (± 125, ± 150 and ± 200 $kgha^{-1}$). A confidence level of 80% was suggested for rangeland vegetation (Mueggler, 1976). The statistical methods applied to estimate the validity of the ground data are provided in Chapter A1 of Appendix I. At this stage, only the results of the analysis are presented.
A graphical presentation of the relationship is given in Figure 3.7.

Figure 3.7: Relationship Between Herbaceous Dry Matter Quantities and Confidence Level for Standard Errors of the Mean of ± 125, ± 150 and ± 200 $kgha^{-1}$ (1985 CIPEA Sites, 2nd Mission)



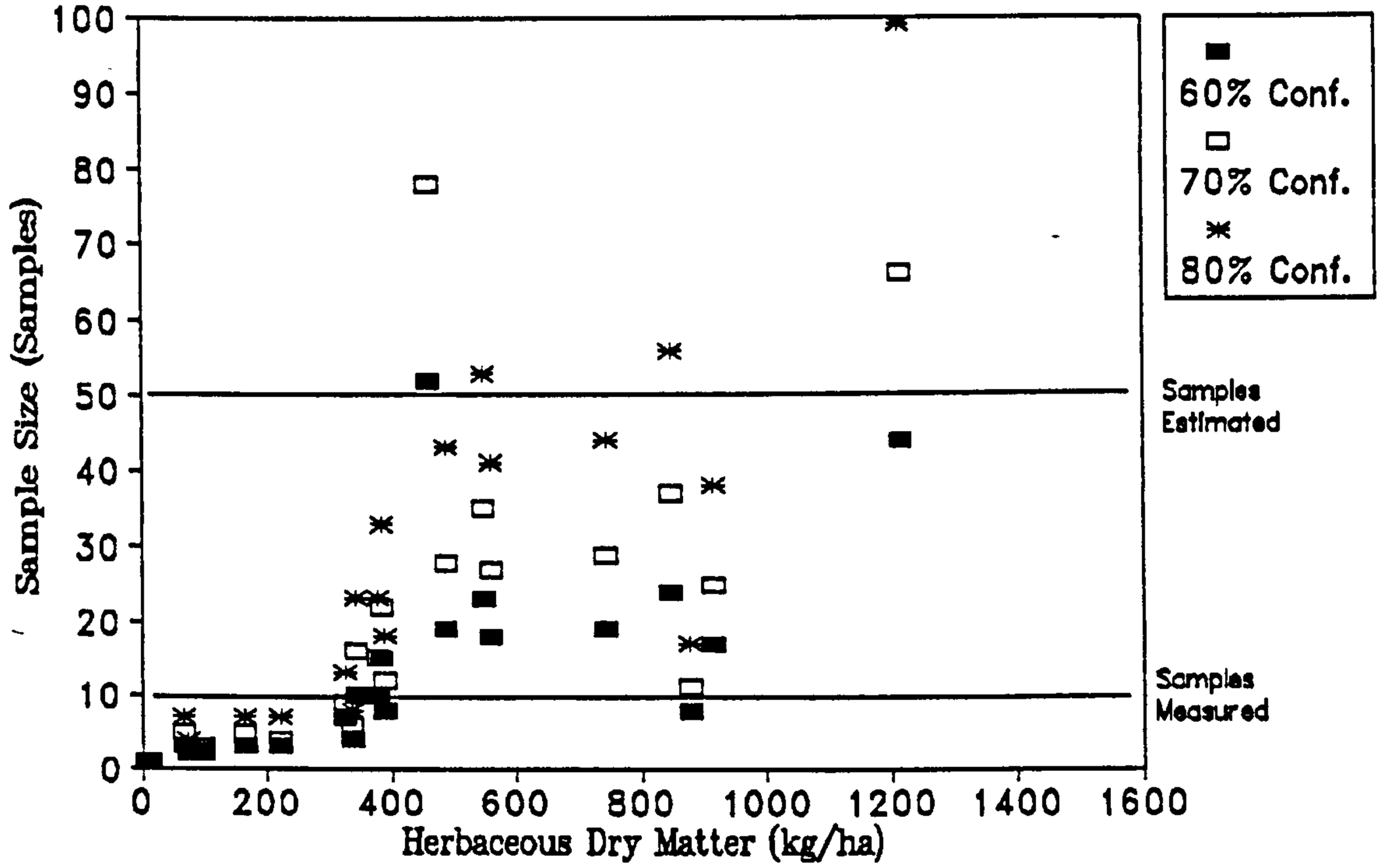
The population mean can be estimated up to approximately 900 $kgha^{-1}$ at an 80% confidence level and a 150 $kgha^{-1}$ standard error. For estimating the average of higher vegetation quantities either the confidence level would be reduced or the standard error would have to be increased.

Relationships for the first mission were not investigated, because it was considered as having been conducted too early for estimating total herbaceous rangeland vegetation quantities of a growing season. For the third mission values of the standard deviation were not reported. An attempt of using standard deviations from the second mission did not yield any interpretable results and was not further pursued.

The number of samples per site was assessed for three confidence levels (60%, 70% and 80%). Based on the conclusions of the achievable range and accuracy of estimating the mean population vegetation quantity (see

previous paragraph) the confidence level of 95% was excluded. The findings are presented in Figure 3.8.

Figure 3.8: Required Number of Samples to Achieve Standard Error of the Mean of ± 150 $kgha^{-1}$ Herbaceous Dry Matter at 60, 70 and 80% Confidence Levels (1985 CIPEA Sites)



The graph reveals a strong increase in the number of samples required for vegetation quantities above approximately 600 $kgha^{-1}$. With 10 samples the population average could not be estimated, not even at a 60% confidence level, over the whole range of vegetation quantities encountered to within ± 150 $kgha^{-1}$. The actual range may be less than the one presented here. It is worth remembering at this stage that 80% of herbaceous vegetation samples were obtained by estimating quantities. This introduces a further element of variation, which was not included when computing standard deviations for sites. Without this information the reliability of mean vegetation quantities are likely to be over-estimated, while the number of samples required to achieve a desired confidence level is under-estimated.

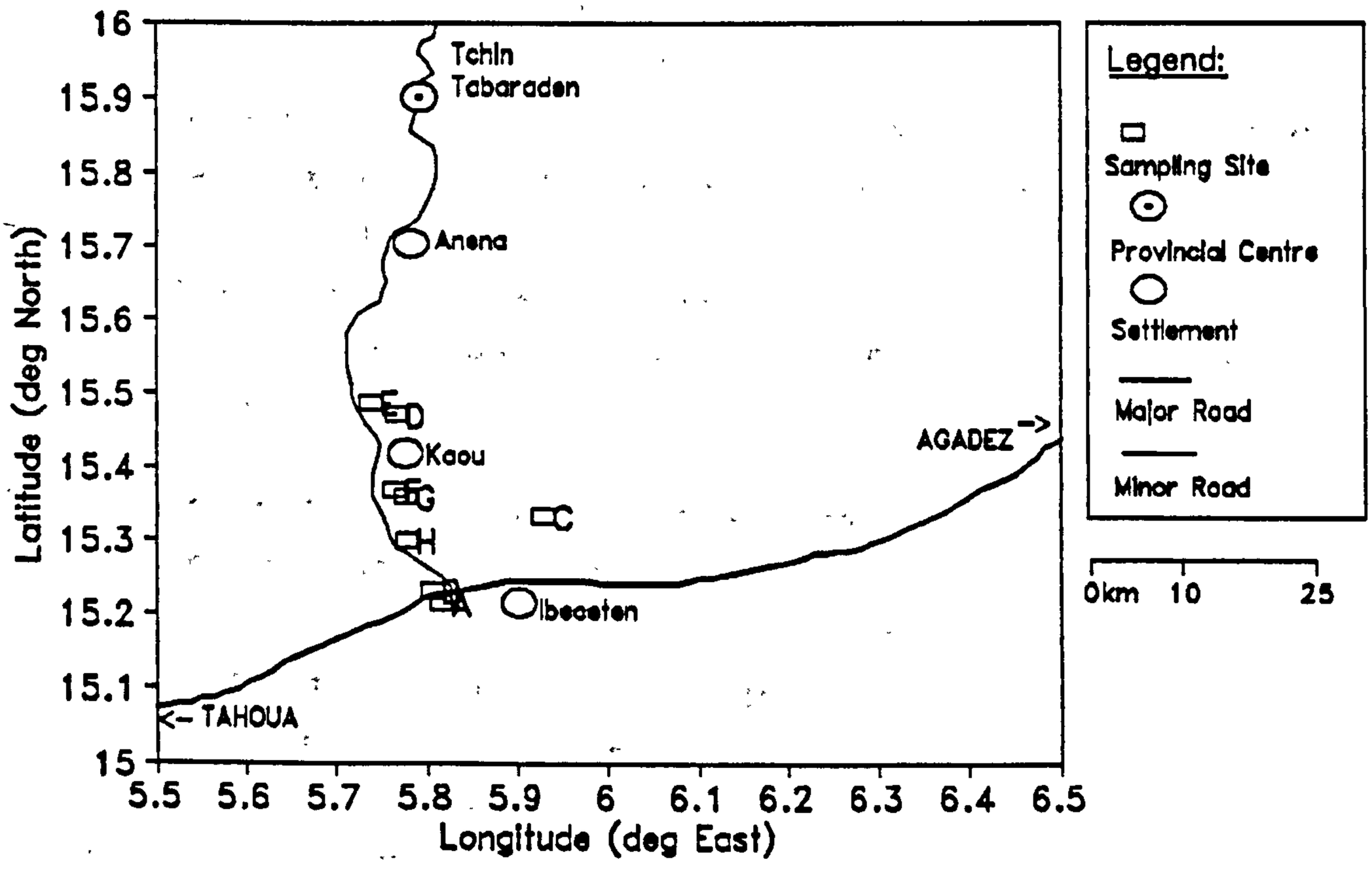
3.2.2 ITE/Silsoe Field Survey of 1985 in Niger

A first step to relating multi-spectral satellite data to the amount of rangeland vegetation for areas belonging to the Sahel ecological region in the Republic of Niger was taken by Silsoe College in 1985.

(a) **Sample Sites**

The position of sample sites is indicated in Figure 3.9 and more accurately in Table A.3 in Appendix II.

Figure 3.9: Arrangement of Sampling Sites of 1985 ITE/Silsoe Field Survey



(b) **Results of Site Parameters**

From the eight investigated sites of the survey three were without any vegetation. The production levels from the remaining sites ranged between 38 $kgha^{-1}$ and 1452 $kgha^{-1}$. The results of dry matter production for the transects are summarized in Table 3.4.

Table 3.4: Average Rangeland Production Values for 1985 ITE/Silsoe Field Survey

Site No.	Dry Matter of Samples (g 0.25m^{-2}) 1	2	3	4	5	6	7	8	9	10	Dry Matter kgha^{-1}
A	43.8	28.3	33.9	27.9	29.6	45.8	39.7	54.6	22.8	*	1452
B	19.6	-	13.1	29.6	12.8	17.8	10.2	20.3	10.2	17.5	604
C	-	6.3	-	3.7	16.4	26.7	9.9	3.1	18.1	*	374
D	-	3.1	2.9	3.4	-	-	-	-	-	-	38
H	-	-	-	18.5	12.1	6.8	-	39.2	*	*	383

* No data collected.
\- Points of bare ground.
Note: Sites E, F and G were situated in areas of bare soil.

Dry matter levels found in 1985 stayed below average productivity levels of the Sahel (1200 to 1500 kgha^{-1}). Since a range of phytomass levels was to be examined, an average from the sites is not representative for the overall production level, but a rough estimate can still be drawn from the survey results.

Additional information on the 1985 survey was not available.

(c) **Accuracy Assessment of Herbaceous Dry Matter Estimates**

The relationship between the amount of vegetation assessed at a site and the confidence level of estimating the range of the population mean for the three classes (± 125, ± 150 and ± 200 kgha^{-1}) is graphically presented in Figure 3.10.

Only five ground measurements were available for drawing conclusions with respect to a generalized verdict on the accuracy of ground survey data. A non-linear regression indicated that herbaceous vegetation could be estimated to within ± 150 kgha^{-1} at an 80% confidence level up to approximately 500 kgha^{-1}.

By interpreting the ground information as a pilot study, the number of samples required to estimate the average herbaceous vegetation amount for a desired reliability was evaluated. The relationship was investigated for a 60, 70 and 80% confidence levels (see Figure 3.11).

Figure 3.10: Relationship Between Herbaceous Dry Matter Quantities and Confidence Level for Standard Errors of the Mean of ± 125, ± 150 and ± 200 $kgha^{-1}$ (1985 ITE/Silsoe Sites)

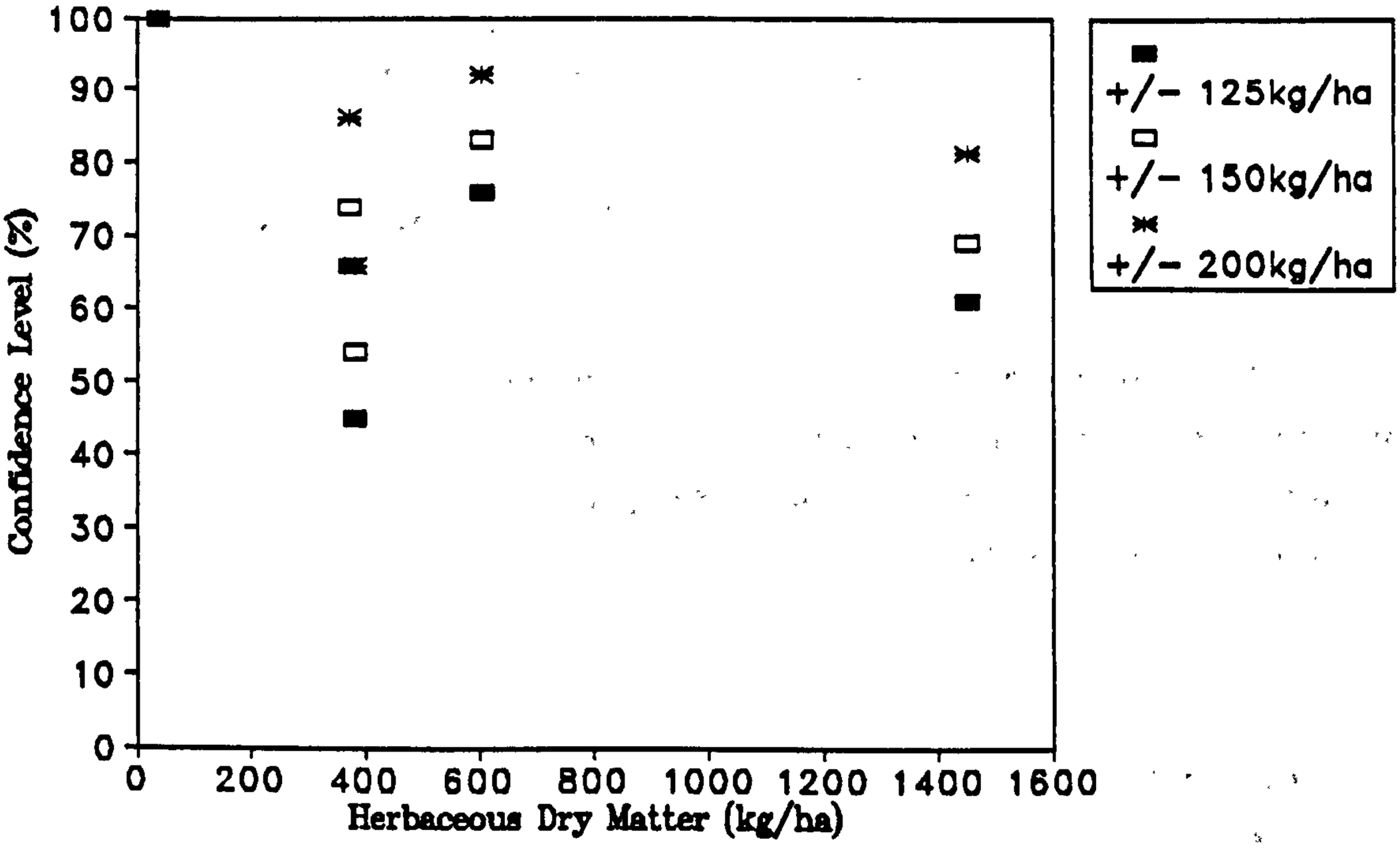
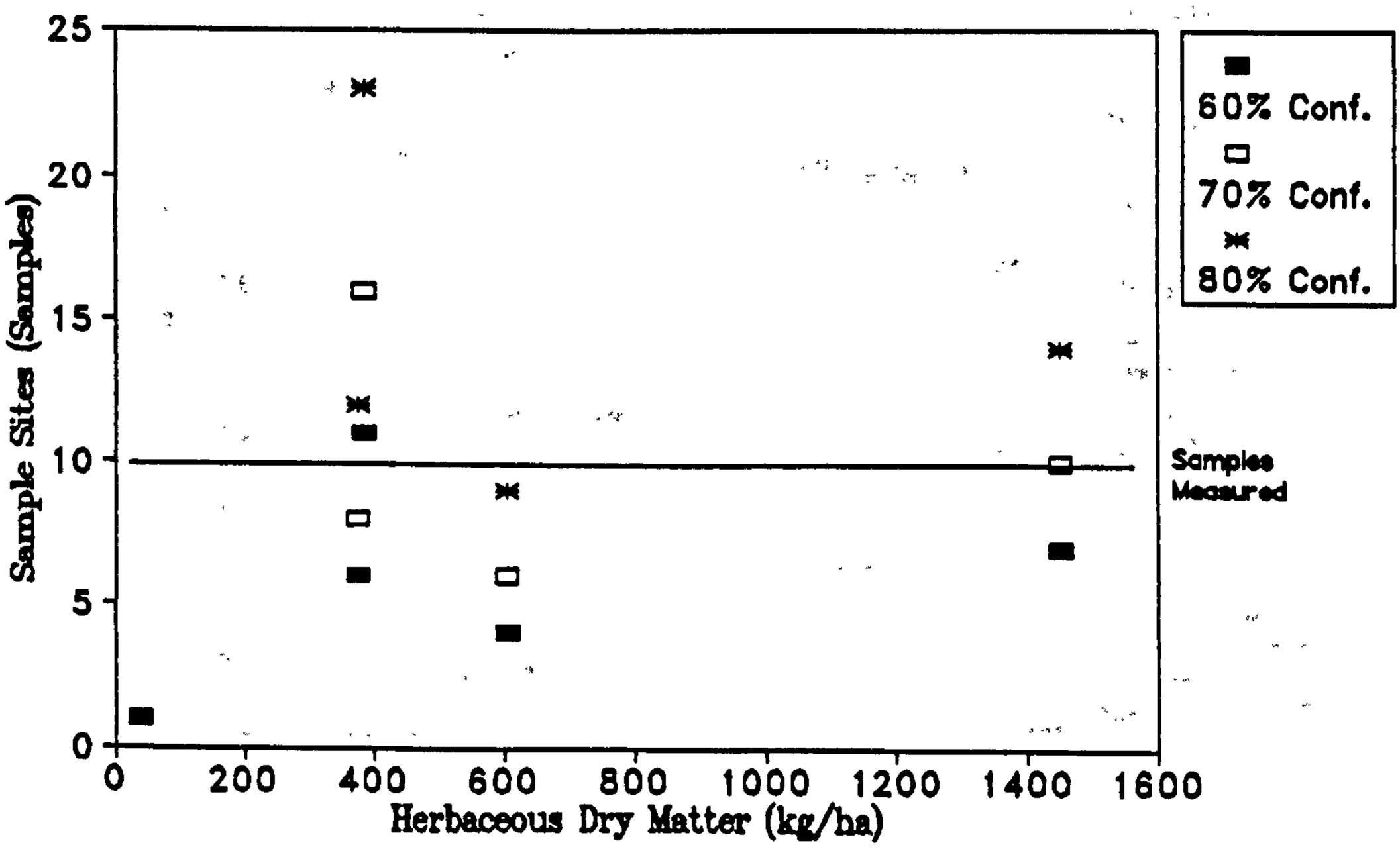


Figure 3.11: Required Number of Samples to Achieve Standard Error of the Mean of ± 150 $kgha^{-1}$ Herbaceous Dry Matter at 60, 70 and 80% Confidence Levels (1985 ITE/Silsoe Sites)



The variation in the data does not allow a confident formation of the number of samples needed to estimate herbaceous dry matter quantities to within ± 150 $kgha^{-1}$. For 10 samples the vegetation limit seems to be between 500 and 700 $kgha^{-1}$ average herbaceous dry matter.

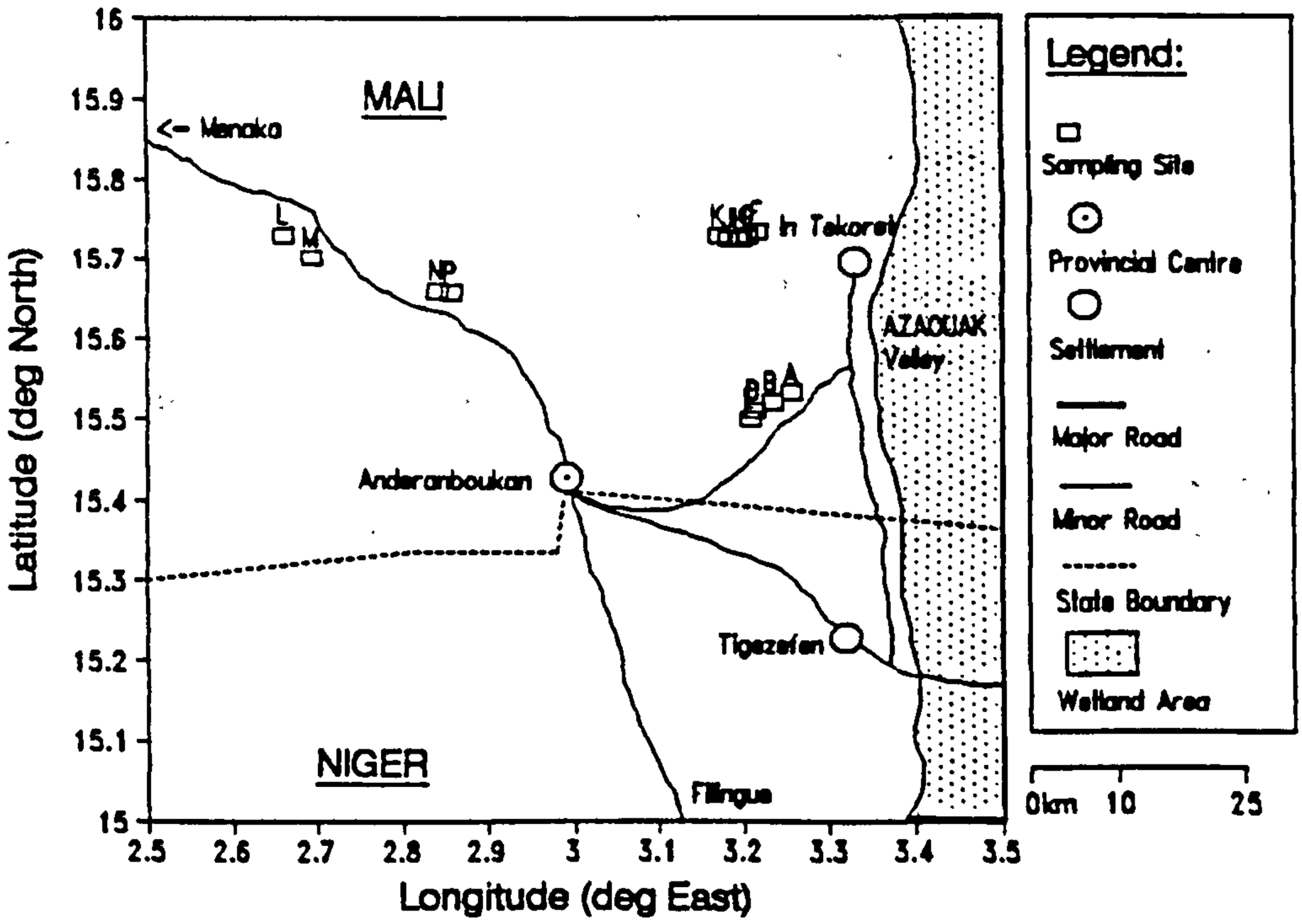
3.2.3 CAZS Field Survey of 1988 in Mali

Estimates on rangeland production levels during the 1988 growing season were collected by Mr. R. Brown for a project co-operation between ITE, Bangor, the Centre for Arid Zone Studies (CAZS) at the University College of North Wales, Bangor and ACORD, Mali.

(a) **Sample Sites**

The arrangement of sample sites across the study area is presented in Figure 3.12. Map co-ordinates of these sites can be found in Table A.4 in Appendix II.

Figure 3.12: Arrangement of Sampling Sites of 1988 CAZS Field Survey in Mali



With about 400 mm mean annual precipitation is similar to the ITE/Silsoe study area in Niger. The main soil class of the area has been defined as "undifferentiated brown soil", as compared to "brown soils on loose sediments" for the Niger study area. The dominant species of the herbaceous and ligneous layer are presented in Table 3.5.

Table 3.5: Dominant Plant Species Encountered During CAZS Field Survey

Herbaceous Species	Ligneous Species
Aristida adscensionis *Bracharia xantholeuca* *Cenchrus biflorus* *Tragus racemosus* *Panicum turgidum*	*Acacia ehrenbergiana* *A. radiana, A. senegal* *Balinites aegyptiaca* *Boscia senegalensis* *Calotropis procera* *Comiphora africana* *Maeru crassifolia*

(After: Brown, 1988)

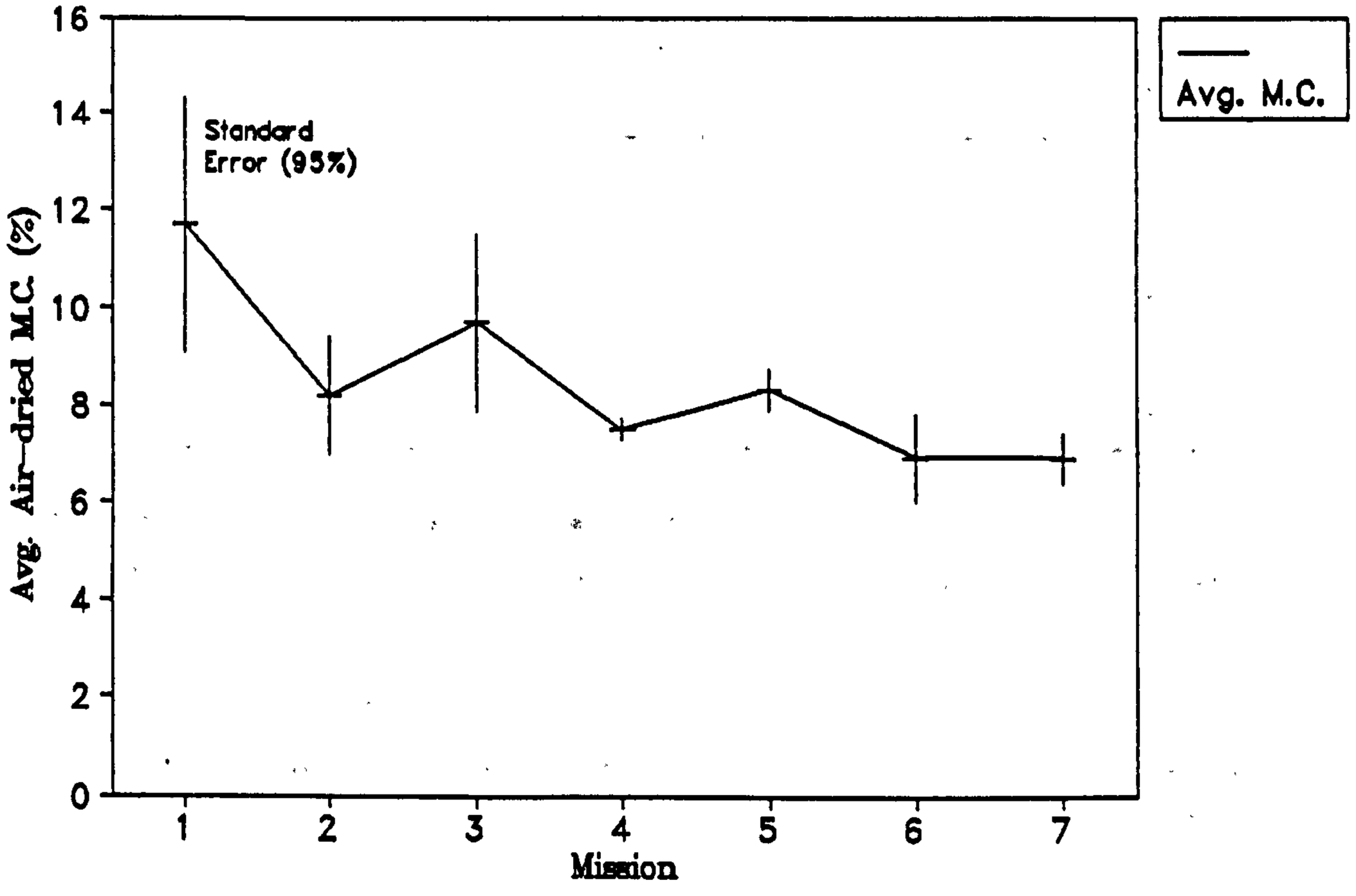
Soil types and plant species are typical for Sahelian grassland as defined in Chapter 2. Results from the survey could thus be used to estimate the spatial validity of satellite VI calibrations.

(b) Development of Air-Dried Moisture Content

The vegetation moisture content was established by taking sub-samples along the transect. These samples were air-dried and the moisture content was later determined by oven-drying the samples.

The average air-dried moisture content of herbaceous vegetation during the seven missions is graphically presented in Figure 3.13.

Figure 3.13: Development of Air-dried Moisture Content During CAZS Field Survey (Transect Averages)



It reveals a clear trend for a decrease in moisture over the growing season. Because all samples were oven-dried after mission 7 was completed, the trend could be attributed to the development state of the vegetation at the time of sampling. The average moisture content of the airdried samples stabilized at the end of the sampling period to being 6.9% with an error of ± 0.5% at a 95%. confidence level.

Based on this outcome, an average moisture content for samples of the transect was established. It was applied to all measurements of samples along the transect to obtain dry matter production levels.

Average herbaceous vegetation quantities thus established are given in Table A.6 in Appendix II. An indication of the development of all the site parameters collected is given in Table 3.6.

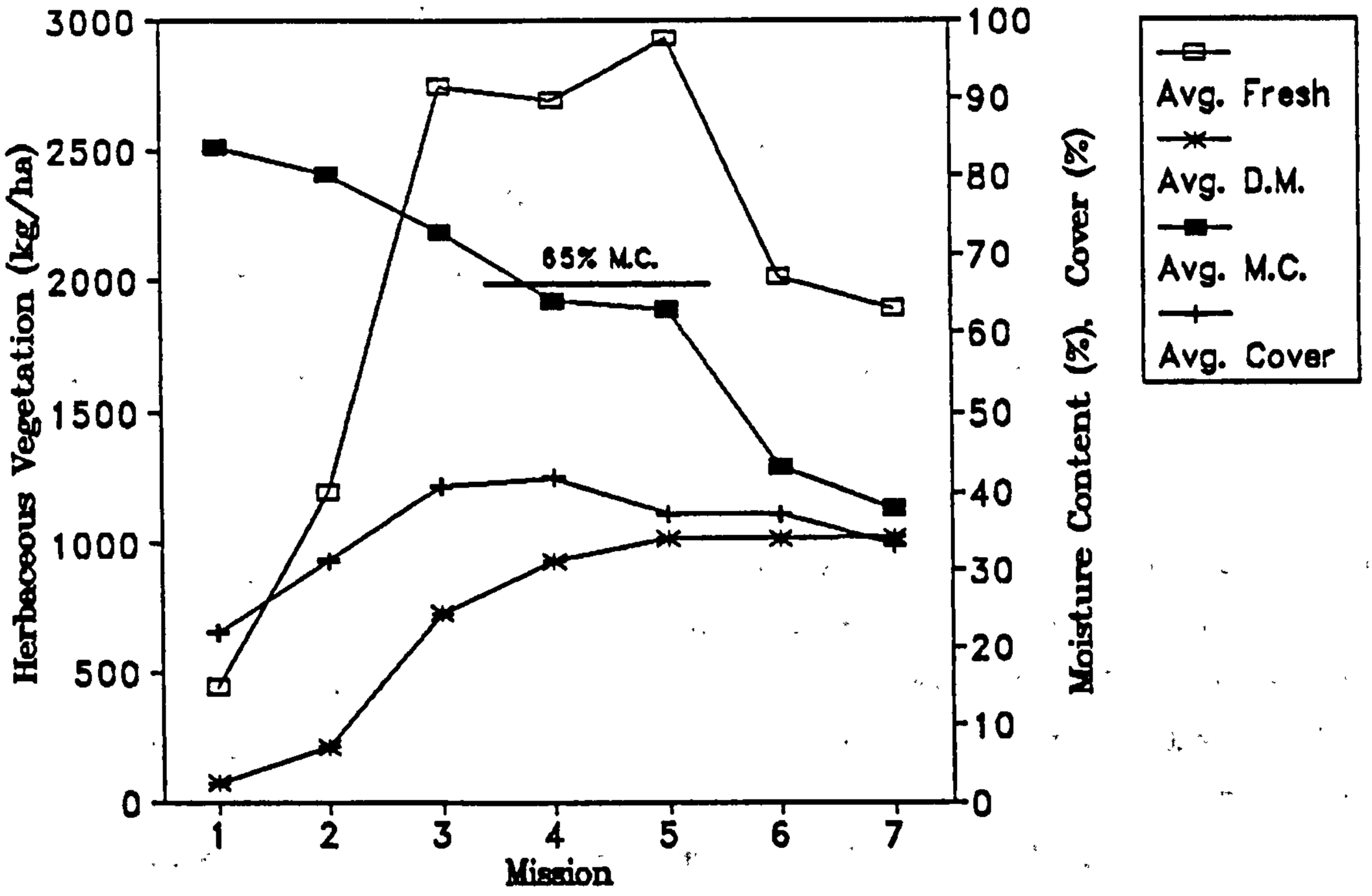
Table 3.6: Development of Herbaceous Fresh Production, Dry Matter, Moisture Content and Cover During the 1988 Growing Season in Mali

Mission No.	Fresh Matter ($kgha^{-1}$)	Dry Matter ($kgha^{-1}$)	Moisture Content (%)	Cover (%)
1	447.7	71.6	83.6	21.8
2	1201.0	216.5	80.2	31.1
3	2744.4	728.6	72.8	40.7
4	2690.5	934.5	64.0	41.8
5	2929.8	1021.1	62.9	37.1
6	2012.5	1022.1	43.3	37.1
7	1896.1	1029.4	38.0	33.2

(c) Results of Site Parameters

The temporal development of herbaceous dry matter, cover and moisture content is graphically displayed in Figure 3.14.

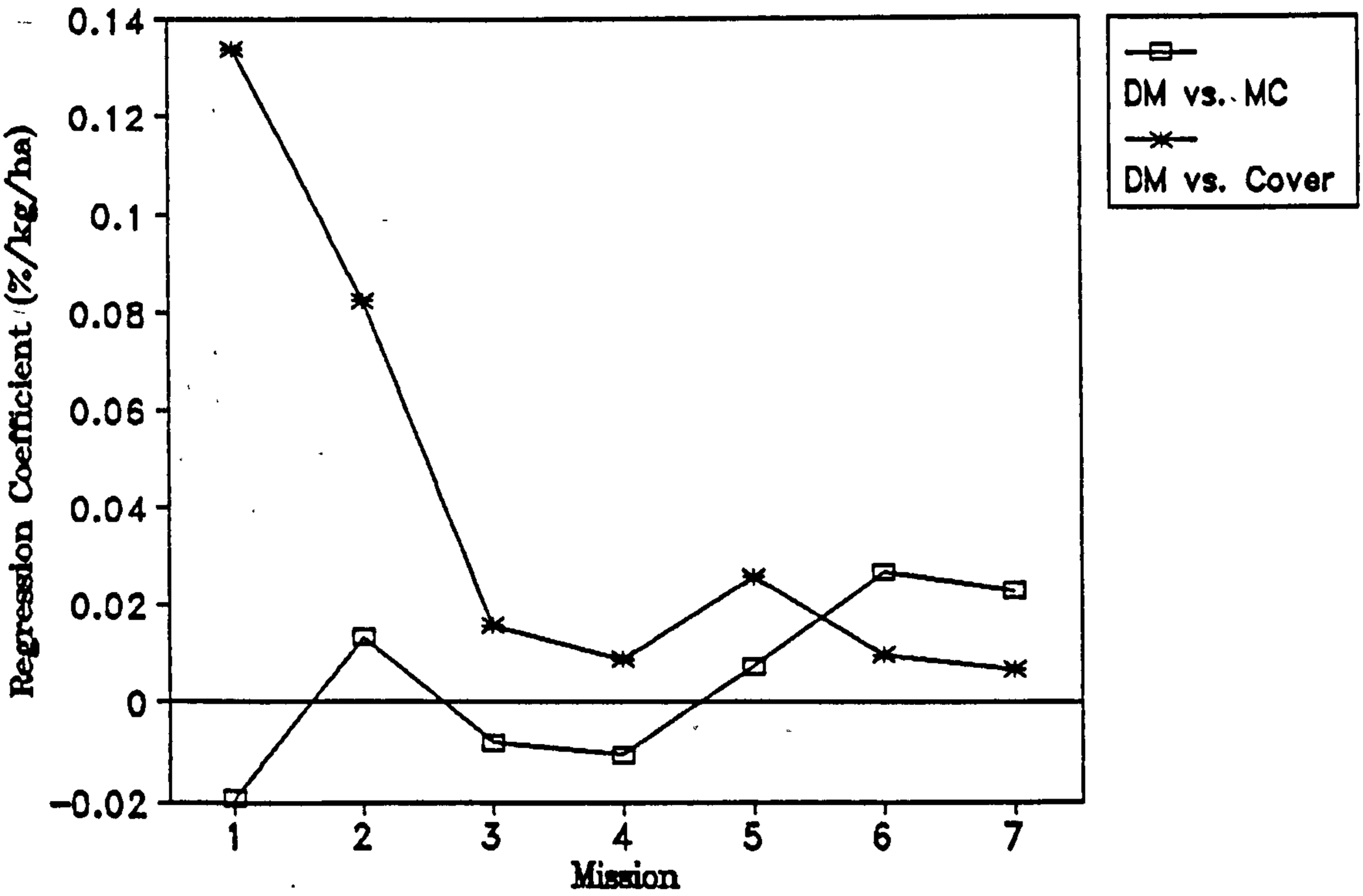
Figure 3.14: Development of Herbaceous Dry Matter, Moisture Content and Cover During 1988 Growing Season in Mali



Between July and September rangeland production increased almost continuously. On average there was no significant increase in the amount of vegetation after

mid August and it remained almost constant until the end of September.
The increase in herbaceous dry matter was accompanied by a decrease in average moisture content. It dropped from more than 80% in July to less than 40% at the end of September. The relationship between vegetation moisture content and dry matter production was found to change over time (see Figure 3.15).

Figure 3.15: Slope Coefficients of Regression Between Herbaceous Dry Matter and Moisture Content and Cover for 1988 Field Survey in Mali



Following the trend over the growing season it was found that it shifted from being negative (decrease of moisture content with increasing amounts of vegetation) at the beginning of July to being positive after mid-August. A linear regression through the points gave a coefficient of determination (r^2) of 0.55.
The development of herbaceous ground cover did not correspond to its dry matter production. After an initial increase to an average value of about 40% in mid-August, it decreased to about 33% at the end of September (see Figure 3.14, Tables 3.6 and A.6 in

Appendix II). This trend is still without a satisfactory interpretation.
As it was the case with the relationship between herbaceous dry matter and moisture content the association between vegetation quantity and cover changed over time (see Figure 3.15). Opposite to m.c. the trend was negative and a linear regression provided a r^2 value of 0.66. At this stage, however, the origin of the trend is speculative: It could be a function of time and a decreasing moisture content or of increasing vegetation quantities. Since information from individual sampling points was not available, the cause could not be established.
Trees and shrubs were almost exclusively of a height of less than 2 m, less than 10% were larger. With 139 shrubs and trees per hectare Site A could be classified as open bushland rather than grassland. The relatively large portion of ligneous vegetation on that site may influence the calibration of VIs for that site.
A relationship between the number of trees and shrubs and herbaceous dry matter and cover at individual sites was not observed, neither was a trend over the growing period.

(d) **Accuracy Assessment of Herbaceous Dry Matter Estimates**
Presented are only the results from the last three missions, since their dates of ground data acquisition corresponds the period of ITE/Silsoe surveys. A graphical presentation of the relationships between amount of vegetation and achievable accuracy is given in Figures 3.16 to 3.18.

Figure 3.16: Relationship Between Herbaceous Dry Matter Quantities and Confidence Level for Standard Errors of the Mean of ± 125, ± 150 and ± 200 $kgha^{-1}$ (1988 CAZS Sites, 5th Mission)

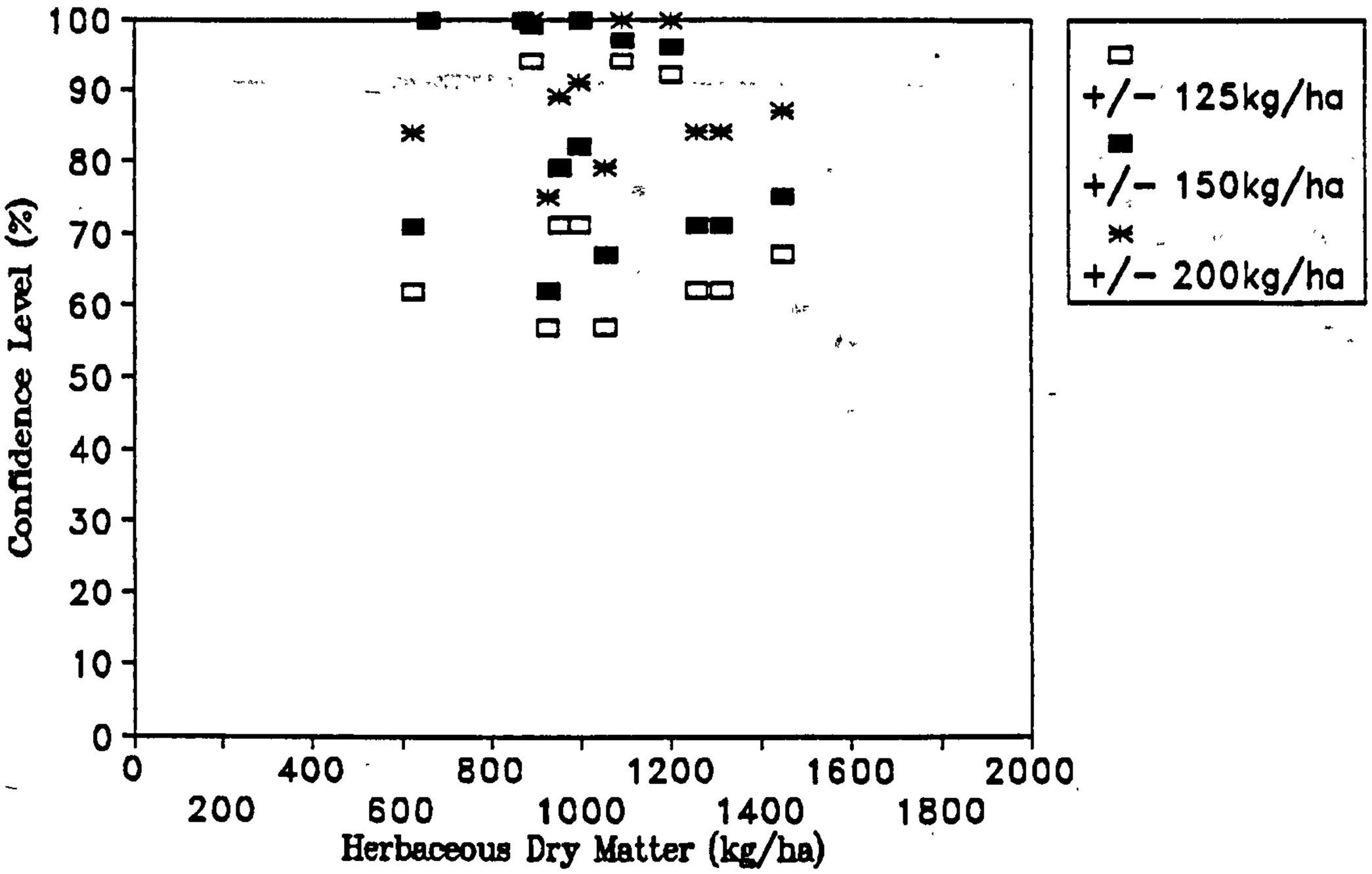


Figure 3.17: Relationship Between Herbaceous Dry Matter Quantities and Confidence Level for Standard Errors of the Mean of ± 125, ± 150 and ± 200 $kgha^{-1}$ (1988 CAZS Sites, 6th Mission)

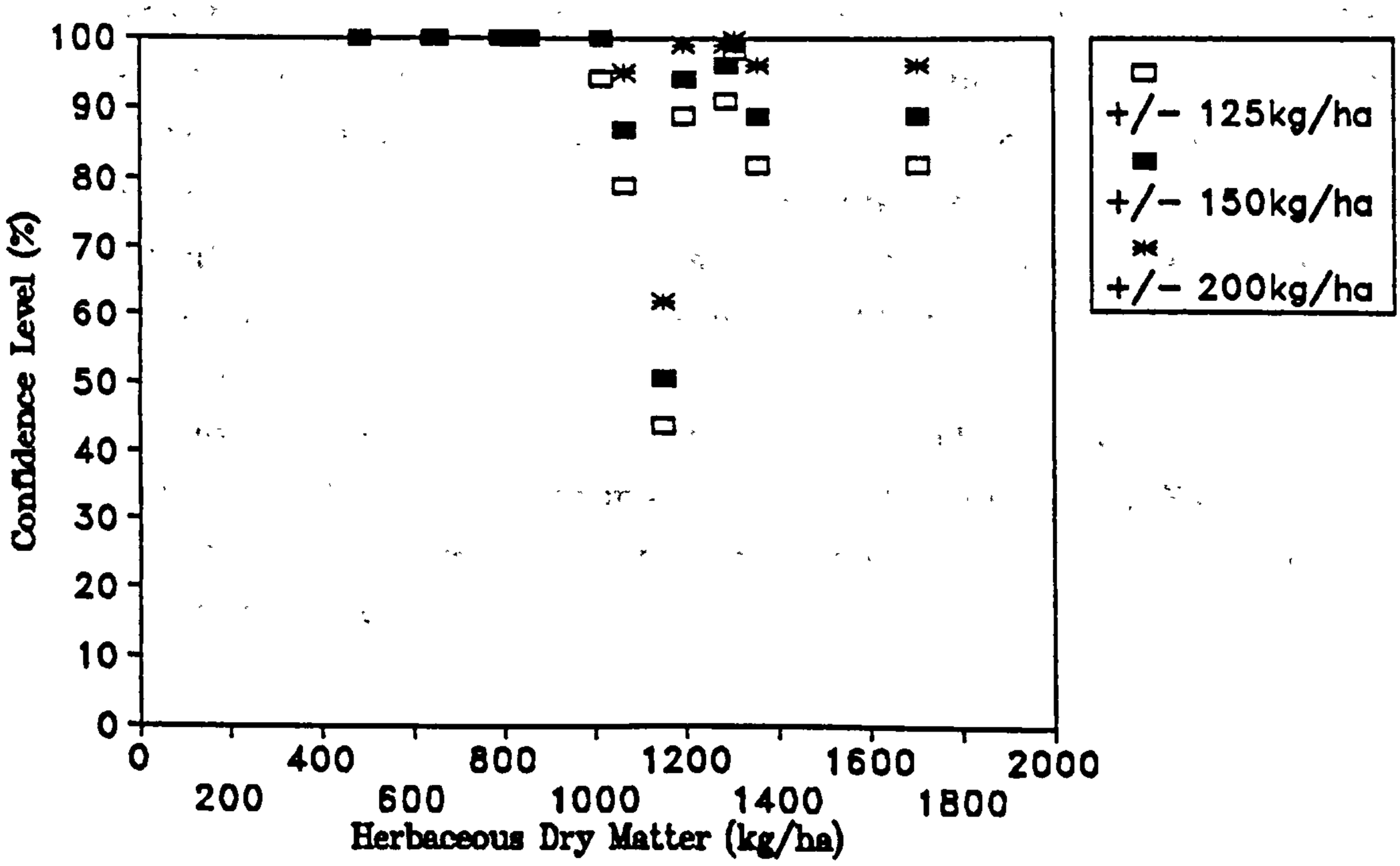
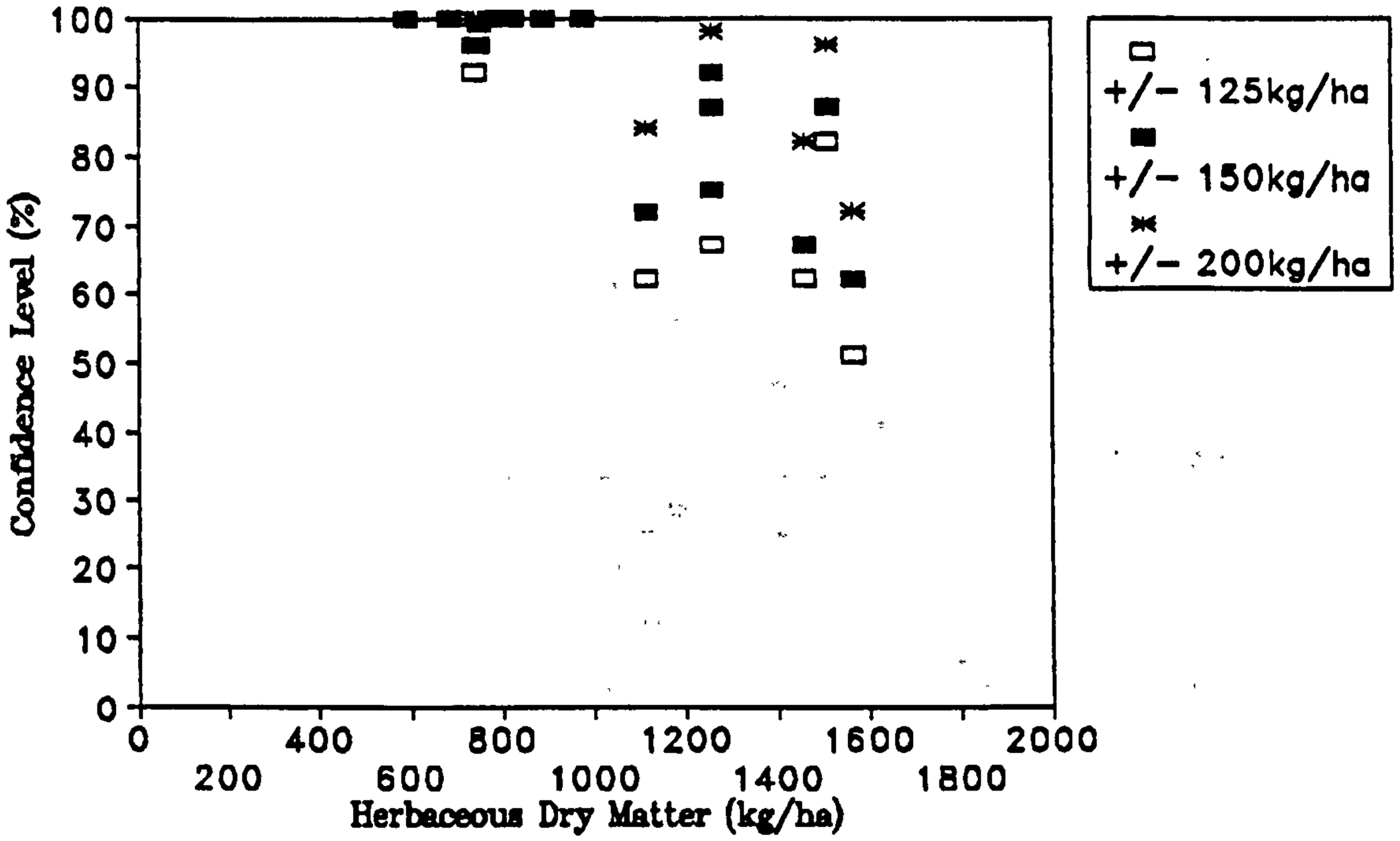


Figure 3.18: Relationship Between Herbaceous Dry Matter Quantities and Confidence Level for Standard Errors of the Mean of ± 125, ± 150 and ± 200 kgha^{-1} (1988 CAZS Sites, 7th Mission)



The number of samples required to estimate the standard error of the mean to ± 150 kgha^{-1} was computed for three confidence levels (60, 70 and 80%). The results are graphically displayed in Figures 3.19 to 3.21. Sample sizes for Missions 1 to 4 are not included, but their standard deviation was established. Lower values for standard deviations as a consequence of lower vegetation quantities require less samples to obtain the same absolute error of the mean and they could be safely excluded.

Although the variation at individual sites is considerable when comparing the three missions the limits of estimating the true rangeland production are very similar.

Figure 3.19: Required Number of Samples per Site to Achieve a Standard Error of ± 150 kgha^{-1} at 60, 70 and 80% Confidence Level (1988 CAZS Sites, 5th Mission)

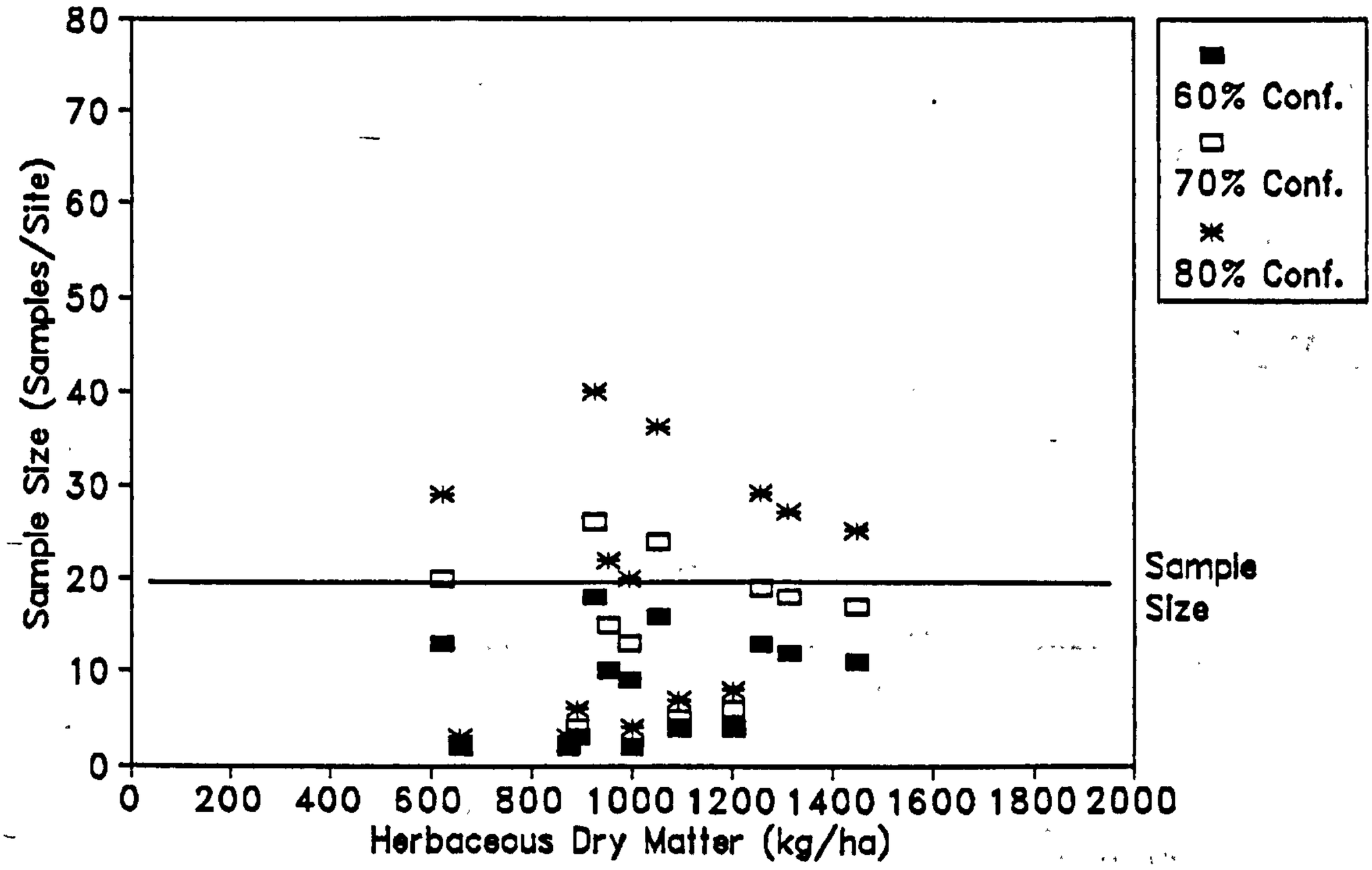


Figure 3.20: Required Number of Samples per Site to Achieve a Standard Error of ± 150 kgha^{-1} at 60, 70 and 80% Confidence Level (1988 CAZS Sites, 6th Mission)

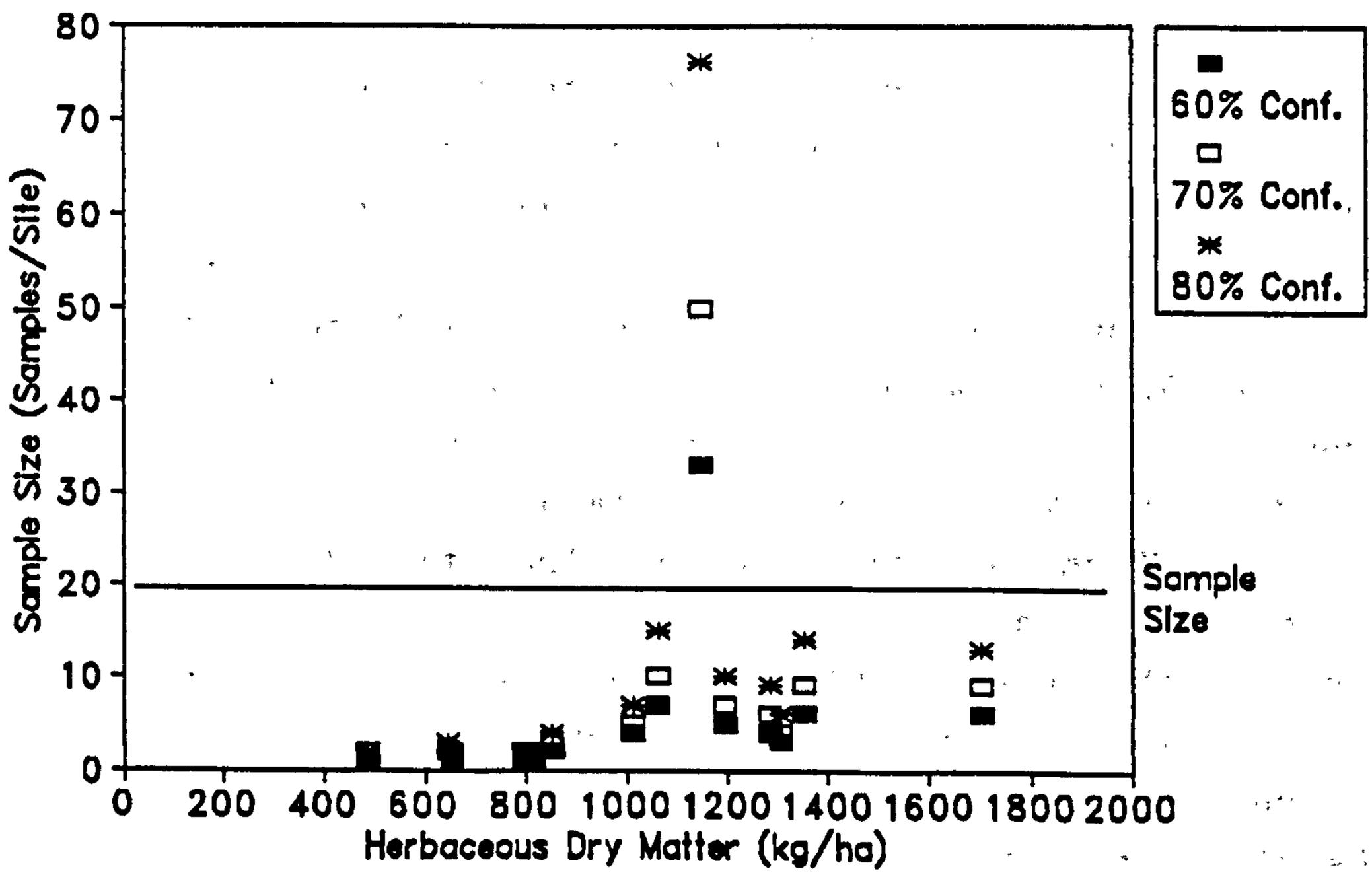
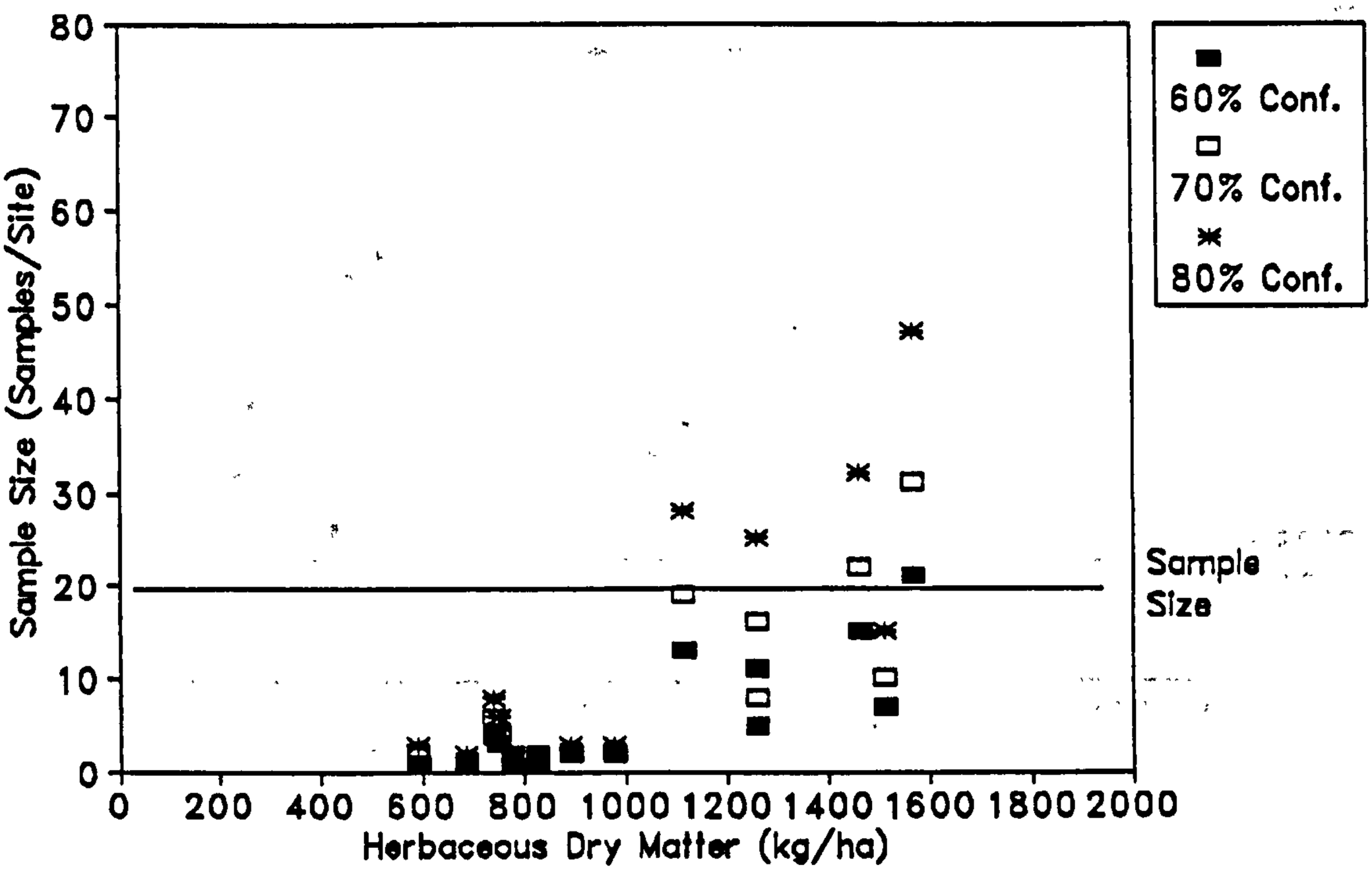


Figure 3.21: Required Number of Samples per Site to Achieve a Standard Error of ± 150 kgha^{-1} at 60, 70 and 85% Confidence Level (1988 CAZS Sites, 7th Mission)



With 20 sample points between 1350 and 1450 kgha^{-1} can be estimated within a range of ± 150 kgha^{-1} at a 80% confidence level or better. These values, however, can only provide a guidance on the number of samples per site. Due to the uneven distribution of vegetation in the Sahel larger errors at lower production levels are common.

For Missions 5 to 7 the duration in days, until the amount of herbaceous vegetation becomes significantly different from the one assessed during the survey, was estimated. Since the standard deviation was not constant over time but strongly dependent on the amount of vegetation present, an iterating process for determining survey durations was employed. The standard deviation for the end of the suggested survey period was interpolated backward, to the previous mission, and forward, to the following mission. It was then related to the number of days found as the maximum length of the field survey and re-assessed (see Figures 3.22 to 3.24).

Figure 3.22: Duration of Field Survey Mission (for 10% observed significance level, CAZS Survey, 5th Mission)

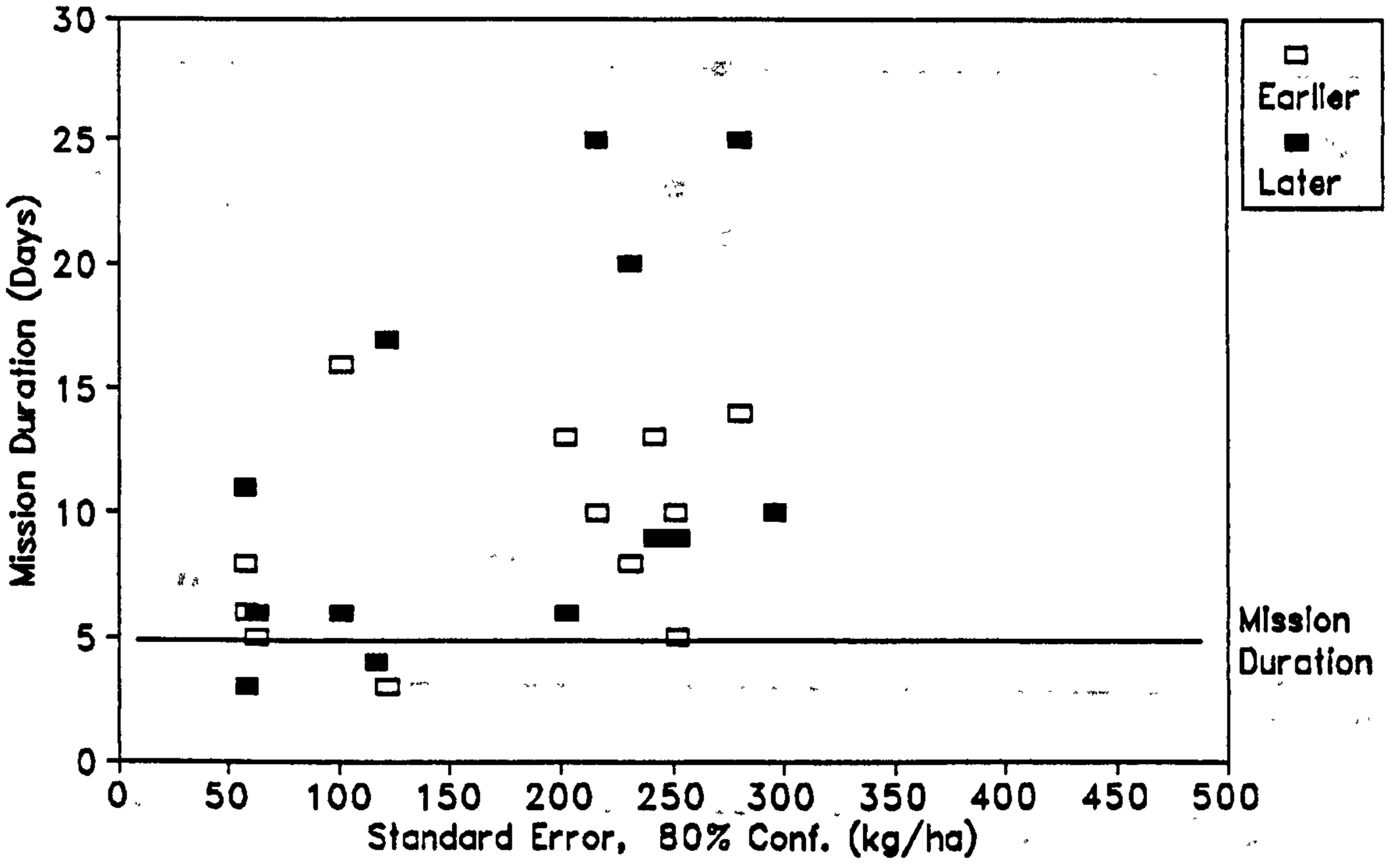


Figure 3.23: Duration of Field Survey Mission (for 10% observed significance level, CAZS Survey, 6th Mission)

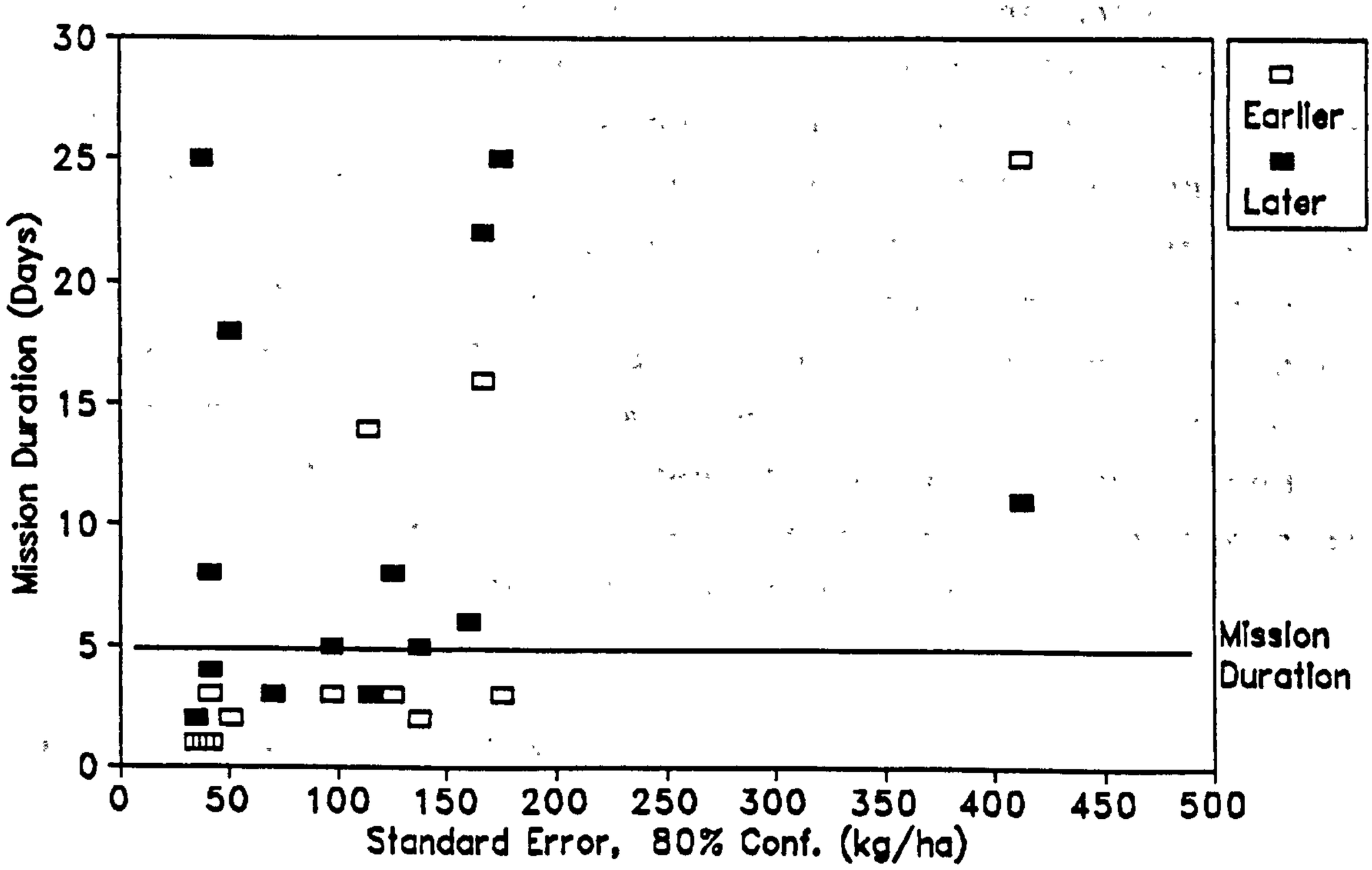
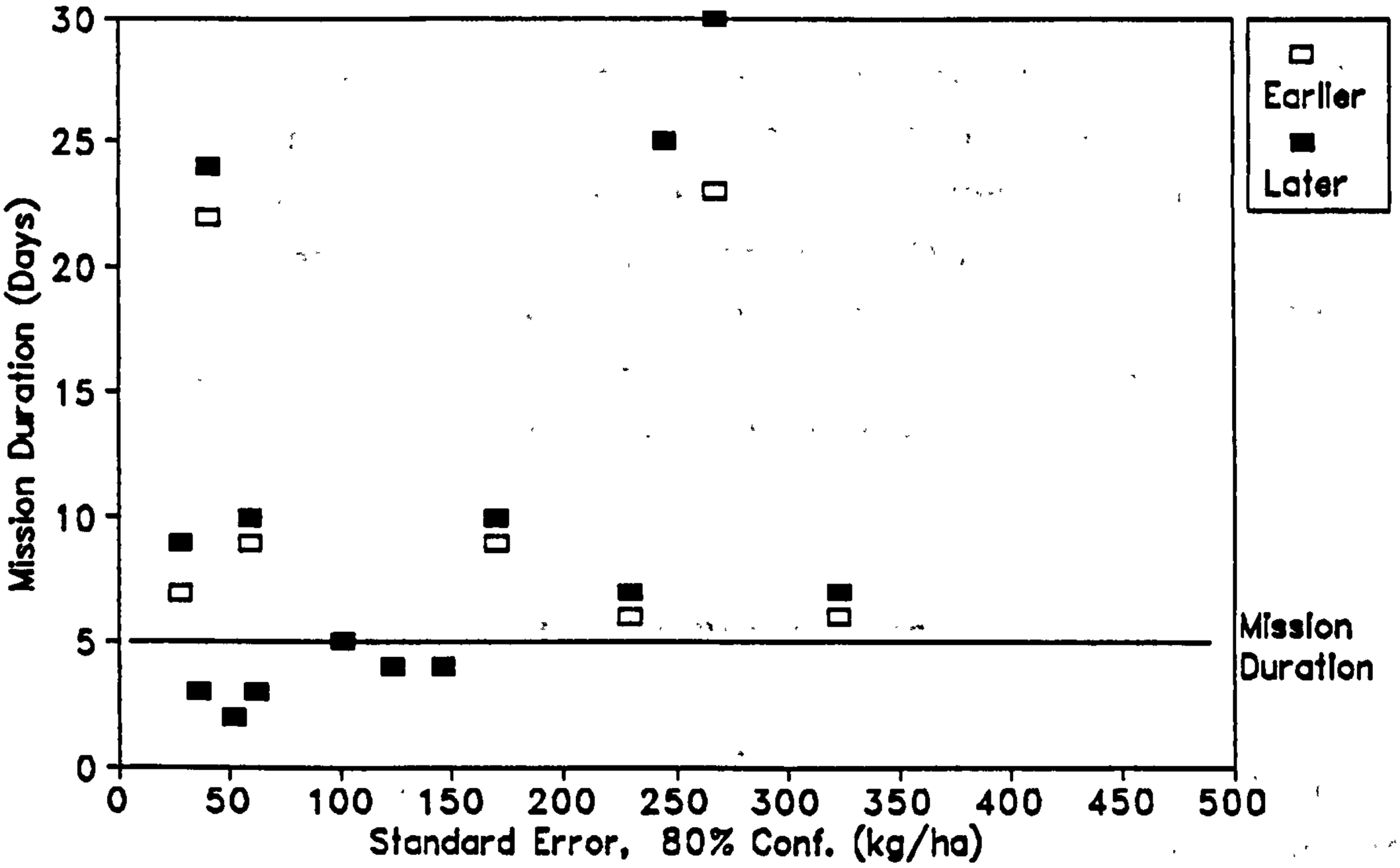


Figure 3.24: Duration of Field Survey Mission (for 10% observed significance level, CAZS Survey, 7th Mission)



The length of the proposed mission duration in days is plotted against the standard error of the data at a site. Thus, it was possible to indicate the level at which a significant change occurs. During Mission 6, for example, in the majority of cases significant changes occurred after two to five days, but the standard error at an 80% confidence level was below 50 $kgha^{-1}$. Since a class interval of 300 $kgha^{-1}$ for calibrating VI maps was proposed, longer periods than two to five days would still be acceptable. It can, therefore, be concluded that a duration of one week for a sampling mission could be advocated on the basis of these findings.

3.3 Field Visit of 1988

The field visit to the Republic of Niger in 1988 was organized by the Institute of Terrestrial Ecology (ITE), Bangor and Cranfield IT, Silsoe Campus. The purpose of the 1988 survey was

aimed at evaluating the temporal stability of the relationship between rangeland phytomass levels and VIs values derived from Landsat MSS and NOAA AVHRR data established on the basis of field work from 1985.
At the time of planning the field survey many details of the previous surveys were unknown and only became available at a later stage. For example, the variation of vegetation along transects was not at hand and, consequently, the required number of samples for a desired confidence level for estimating rangeland vegetation could not be assessed. For that reason, only small modifications to the 1985 survey method were proposed.

3.3.1 Compendium on Field Work Procedures

The specific methods applied during the field survey had to be defined in the field and results of the sampling procedures are presented in this chapter.

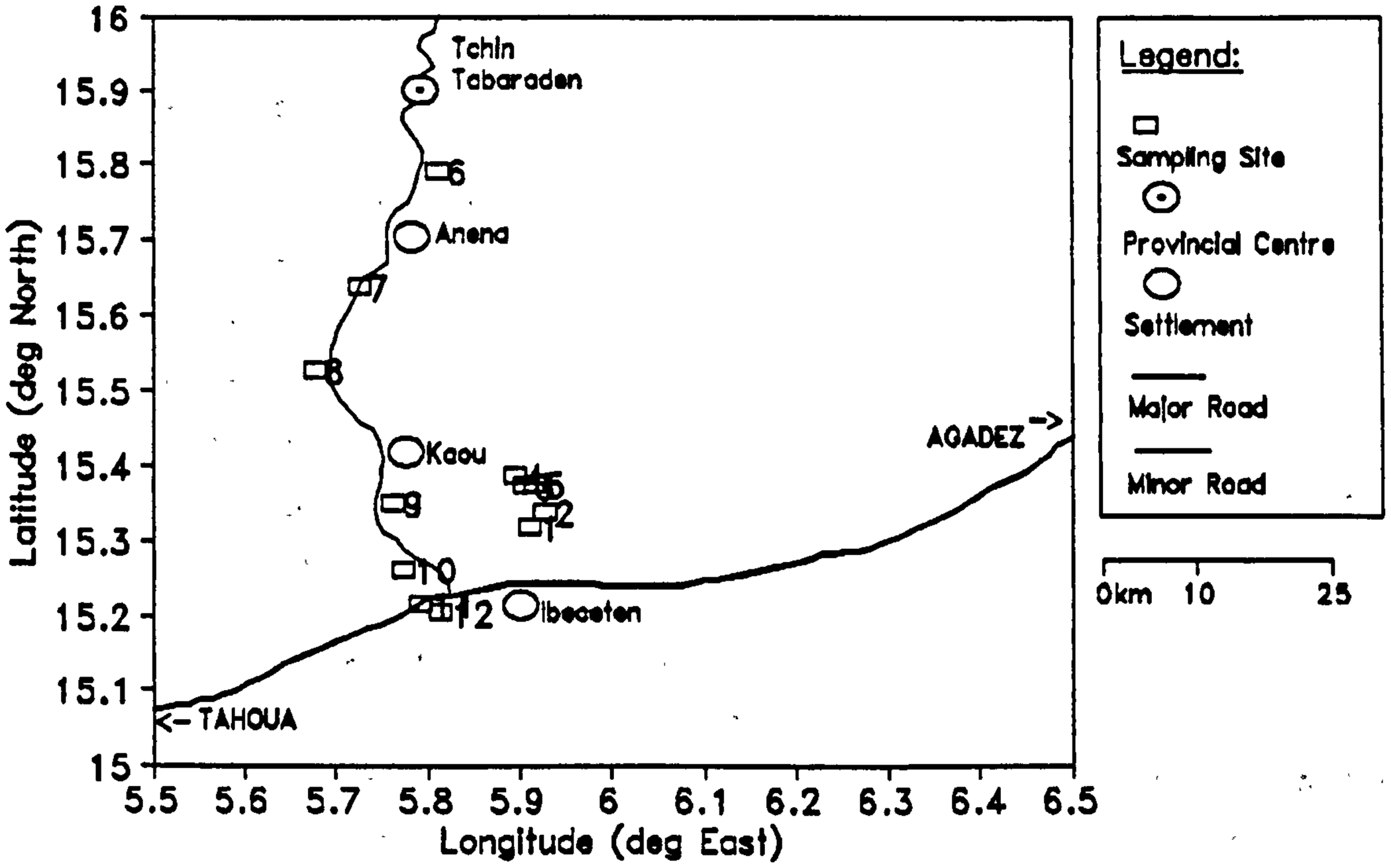
(a) Study Area

It was recommended to revisit 1985 sites to investigate the temporal stability of the calibration and to keep the spatial component constant. An increase of the study area was considered as being outside the scope of the project.
The distribution of sampling sites across the study area is given in Figure 3.25. The main herbaceous and ligneous species found are presented in Table 3.7:

Table 3.7: Dominant Plant Species Found in 1988

Herbaceous species:	Shrub and tree species:
Aristida mutabilis	*Acacia ehrenbergiana*
Cenchrus biflorus	*Acacia senegal*
Echinocloa colonum	*Balanites aegyptiaca*
Schoenfeldia gracilis	*Comophora africana*
Tragus racemosus	*Calotropis procera*

Figure 3.25: Arrangement of Sampling Sites of 1988 ITE/Silsoe Field Survey



The most common herbaceous species were *Cenchrus biflorus* and *Schoenfeldia gracilis* with the first being dominant. The main shrubs and trees were *Acacia senegal* and *Calotropis procera*. The grass species found in 1985 was almost exclusively *Cenchrus biflorus*. The emergence of a variety of herbaceous species in 1988 was unexpected and can be attributed to the above average precipitation of the rainy season. The influence of different species compositions on the relation between herbaceous phytomass and VIs was assumed to be of secondary importance. Therefore, the distribution of plant species within the study area was not assessed with respect to individual species contribution.

(b) **Period of Field Survey**

Based on rainfall data provided by Mr. A. Maidoukia from the Direction de la Meteorologie Nationale, Niamey it was concluded that under most conditions there would be additional development of vegetation in September. As a consequence, in order to estimate the maximum amount of

rangeland vegetation from a single-period survey it should be carried out at a later stage than the 1985 ITE/Silsoe investigation. No other guide-lines for a more specific period for the end of the growing season could be found.

(c) **Layout of Sampling Method**

In order to increase the number of sites visited it was then recommended to shorten the length of individual transects from 1 km to 500 m. However, with the variation of vegetation distribution unknown at this stage, no quantitative foundation could be provided for the modification of the sampling scheme.

(d) **Selection of Sample Sites**

Data on the distribution of precipitation in July and August became available before the field survey started (correspondence with Mr. A. Maidoukia, Direction de la Meteorologie Nationale, Niamey). Due to above average precipitation of the 1988 rainy season and the exceptionally low one in 1985 a largely different distribution of growth could be expected when compared to 1985. Therefore, a prior classification of a 1985 image was considered as being of little use for identifying new sites. A further consideration was the limited amount of time available (about 8 days in the field). As a consequence, a major restriction for collecting data was accessibility of the sampling sites and the identification of their map or image position. This could best be determined in the field. Uniformity of vegetation and level of phytomass were also assessed in the field by visually comparing areas.

(e) **Site Parameters**

Site parameters assessed would be the same as in 1985, but a change in establishing herbaceous dry matter seemed to be indispensable. It was, therefore, recommended to investigate the use of a moisture meter for assessing the dry matter weight of samples.

(f) Positioning of Sample Sites

Sample sites were identified on geometrically corrected Landsat MSS hard-copies and maps of 1:200000 scale in the field. The position of the 1985 and 1988 sample sites as co-ordinates of a map projection are summarized in Table A.3 in Appendix II (also see Figure 3.25). Sites not re-visited in 1988 (Sites D, E and F) were later re-located by transferring the image position marked on a slide to image co-ordinates on the processing system and then to map co-ordinates.

3.3.2 Performance of WILE 35 Moisture Meter

The WILE 35 Moisture Meter was not designed to provide moisture content readings for rangeland vegetation and some impediments of using it for that purpose were identified.

(a) In-field Handling and Operation

The Wile 35 Moisture Meter was found to be small, solid and light. It was easy to use and did not fail to operate throughout the survey.

A minimum amount of vegetation was required to fill the cylinder and build up sufficient pressure on the sample in order to take measurements. In some cases, like along the whole of Transect 9, the amount of vegetation found was insufficient for more than one reading or even a single one. At these points no readings were taken and the vegetation was stored for oven-drying.

Another important obstacle was the size of the sample measured. Samples for instrument readings should have the same distribution of vegetation as found over the sample point, but this is not easily achieved.

Dicotyledone species frequently had a much higher moisture content than grass species at the same place. The moisture content of the vegetation found at several points was too diverse to yield similar readings for repeated measurements. Only by increasing the number of measurements and taking the average of the readings was it possible to obtain estimates of the moisture content.

Because of the dependence of the instrument readings on the material measured, the instrument had to be calibrated for the conditions of the Sahel grassland. The calibration of the estimated moisture content given by the instrument was based on oven-dried dry matter weights of the samples.

(b) Relating Instrument Readings to Moisture Content

For the calibration of instrument readings from the WILE 35 Moisture Meter two sets of data were put to use:

i. *In-Field Readings*
At each sampling point the moisture content readings of fresh material was assessed (see Table A.9, Addendum II).

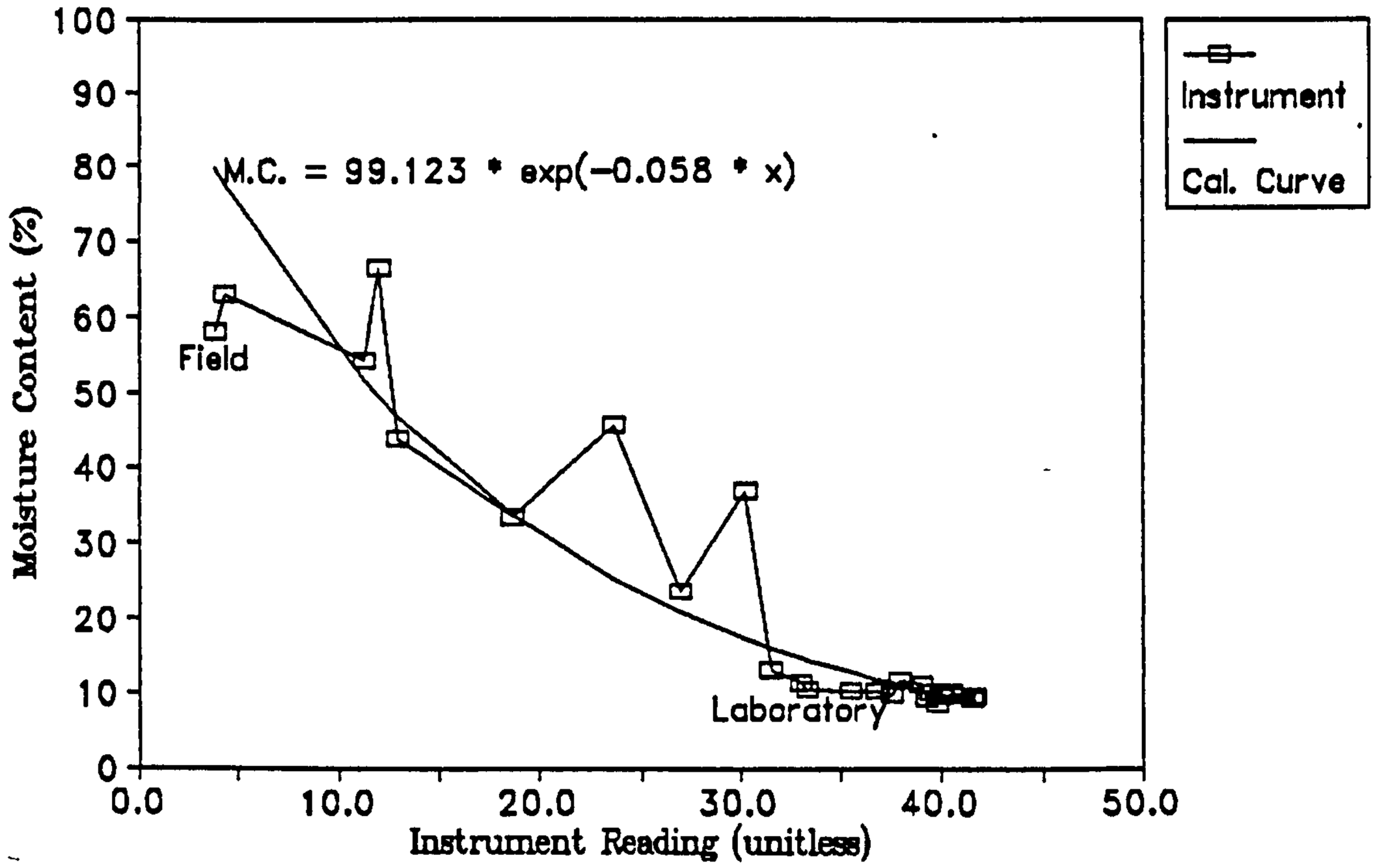
ii. *Laboratory Readings*
Readings of air-dried samples were obtained in the laboratory just before oven-drying (see Table A.10, Appendix II).

These 26 measurements were then related to the moisture content obtained from the oven-dried samples. A cross-section of samples was stored for oven-drying and calibrating the moisture meter. Results from drying samples are summarized under Section 3.3.6.
The non-linear relation found between the moisture content m.c. and instrument readings M.R. was expressed by the following equation:

$$m.c. = 99.123 * e^{(-0.058 * M.R.)} \quad (\%) \qquad (3.1)$$

Individual results from the calibration are summarized in Table A.11 in Appendix II. The relation between instrument readings and vegetation moisture content is graphically represented in Figure 3.26.

Figure 3.26: Relationship between WILE 35 Instrument Readings and Oven-dried Moisture Content



(c) **Estimation of Rangeland Production**

The calibration was applied to all sample points to obtain estimates of the vegetation dry matter weight over the sample area of 0.25 m². Estimates for the calibration of satellite sensor response to rangeland grass levels were derived by averaging the results from each transect and using one hectare as the base for the production level of an area.

The estimated dry matter weight of individual samples and phytomass production levels for the sites are summarized in Table A.12 in Appendix II.

3.3.3 Compendium on Site Parameter Data

The quantitative results of individual site parameters are presented in this chapter. Soil characteristics were excluded from the investigation. The definition of classes was very vague and dependent on the observer.

(a) Dry Matter Quantities of Herbaceous Rangeland Vegetation

Table 3.8 contains average values for each transect with the moisture content based on the calibration derived from the Wile 35 moisture meter (see previous section).

Table 3.8: Estimated Site Parameters for Transects of 1988 Field Survey to Niger (Transect Averages)

Transect No.	Herbaceous Dry Matter (kg ha^{-1})	M.C. of Sample (%)	Herbaceous Cover * (%)	Ligneous Cover ** < 2m No./ha	2m-8m No./ha	Total No./ha
1/88	1305	55.0	63.3	4.4	4.4	8.8
2/88	1280	36.2	59.0	5.2	3.4	8.6
3/88	1400	32.0	30.0	0.8	2.2	3.0
4/88	2002	33.9	40.0	1.4	1.7	3.0
5/88	1634	25.9	28.0	1.6	2.3	3.9
6/88	2728	57.7	46.0	1.9	1.8	3.8
7/88	1290	39.9	10.0	4.2	2.8	7.0
8/88	1135	32.1	1.0	2.8	2.7	5.5
9/88	296	38.4	2.8	3.0	1.8	4.8
10/88	2677	70.1	36.0	1.5	0.7	2.2
11/88	2075	37.3	48.0	6.5	6.2	12.6
12/88	1426	36.5	46.0	6.8	5.0	11.8

* Estimated over 4 m^2
** Ligneous Cover Class "<25 cm":
- only two entries, combined with class "0.25-2m"
Ligneous Cover Class ">8 m":
- no entries, class omitted

The smallest amount of rangeland production found along the 12 transects was over an area with clay and laterite gravel (Site 9). The production level measured at this site was less than 300 $kgha^{-1}$. There, grass and herb species grew as single plants, spatially completely separated from each other (see Figure 3.27).

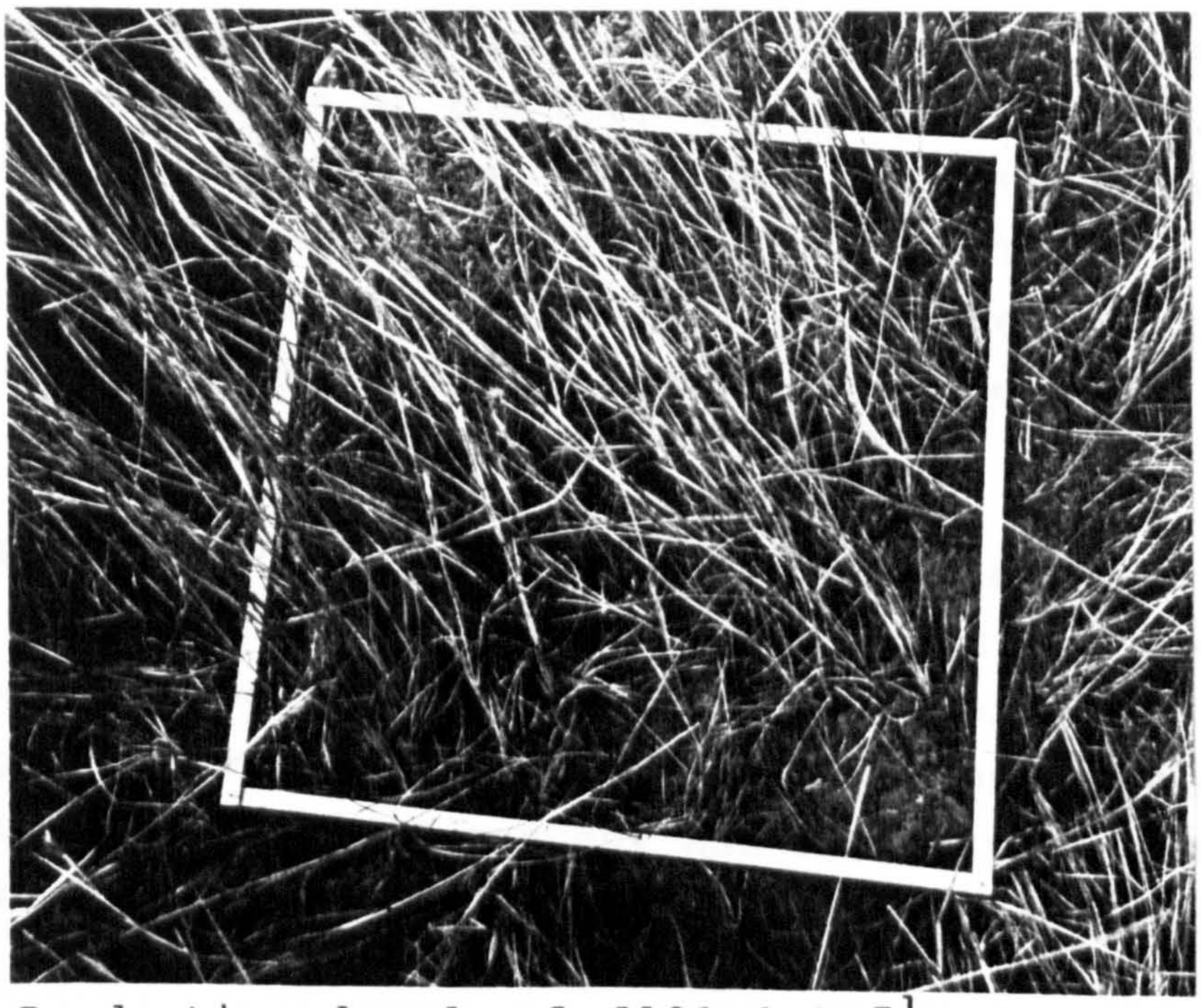
The highest amount of rangeland production was 2728 $kgha^{-1}$ (Site 6). Grasses and herbs were found to be dense, with multiple layers of leaves (see Figure 3.28).

Figure 3.27: Area of Low Phytomass Level



Production level of 296 $kgha^{-1}$ on clay with laterite gravel (Site No. 9, Point No. 3). The area defined within the metal square was 0.25 m^2. Vegetation within the square was clipped off and weighed to establish the herbaceous production level at the sample point.

Figure 3.28: Area of High Phytomass Level



Production level of 2180 $kgha^{-1}$ on sandy soil (Site No. 4, Point No. 2). The area covered within the metal square corresponds to 0.25 m^2. Dense stand of grass with height of approximately 60 cm.

(b) **Herbaceous Ground Cover**

Herbaceous cover was estimated by eye over an area of 4 m^2 at each sampling point. This was always performed by the same member of the team to avoid any divergences introduced by changing observers.

The average herbaceous cover along transects is given in Table 3.8. It varied between 1% and 63.3% with an average of 34.3% for all sites.

(c) **Number of Bushes and Tress**

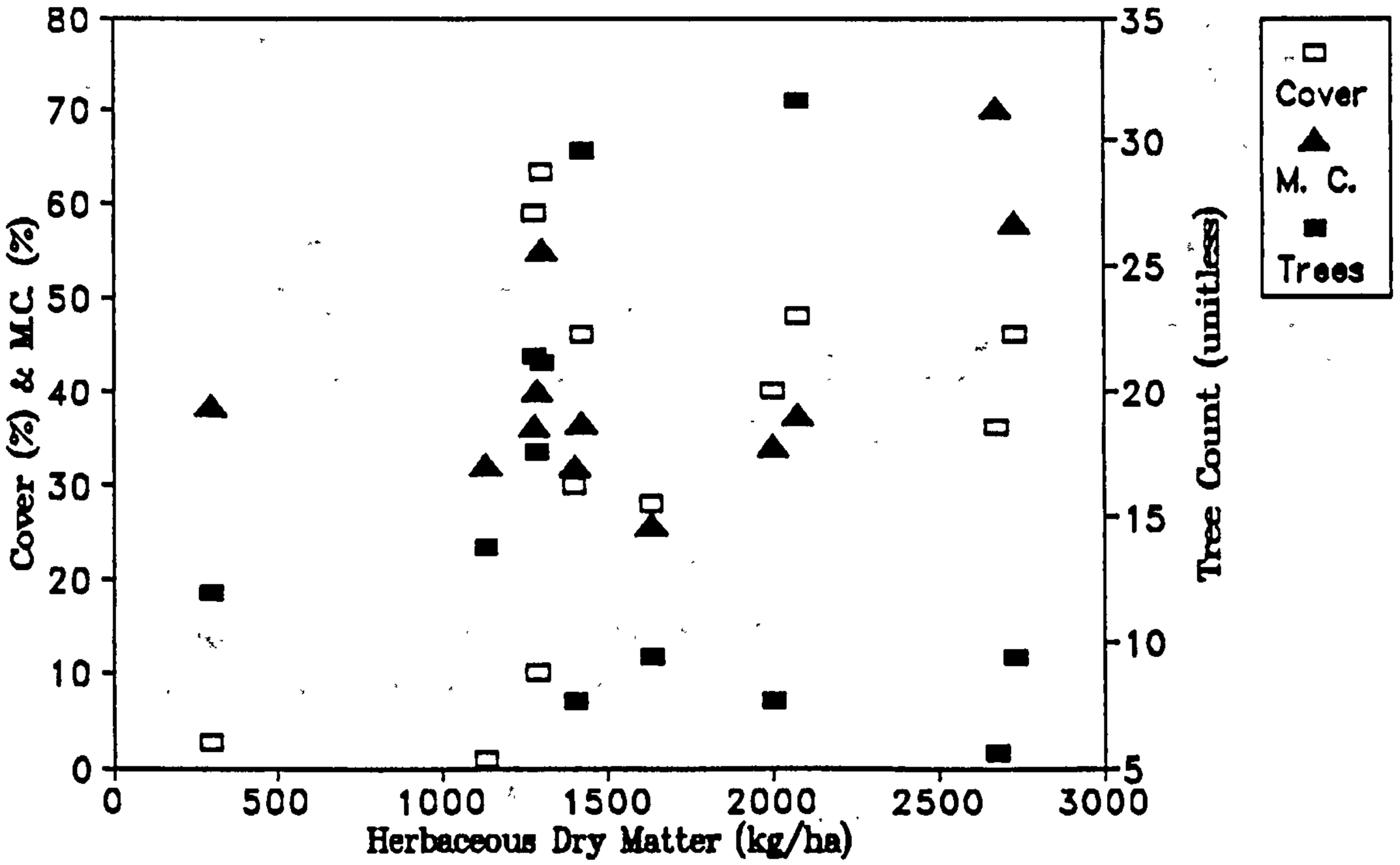
The first class with ligneous vegetation of less than 25 cm contained only two entries and was merged with class 2 (shrubs between 0.25 m and 2 m). The fourth class, trees higher than 8 m, contained no entries and was thus omitted. The remaining two classes and the corresponding entries are given in Table 3.8.

As stated in Chapter 2.2 estimates of rangeland production levels by satellite remote sensing are influenced by various plant properties and ground features. Due to the limited amount of time and facilities available in the field, information on only the more important parameters were obtained. At each sample point estimates of the sample moisture content, the herbaceous cover and the number of bushes and trees over the sites were established for all transects (see Table 3.8). Possible consequences of the parameters obtained on the calibration of VIs to rangeland production levels are discussed below.

(a) **Herbaceous Dry Matter vs. Moisture Content**

The average vegetation moisture content for transects ranged between 25.9% and 70.1% (see Table 3.8). A graphical representation of the relationship between herbaceous moisture content and dry matter production is given in Figure 3.29.

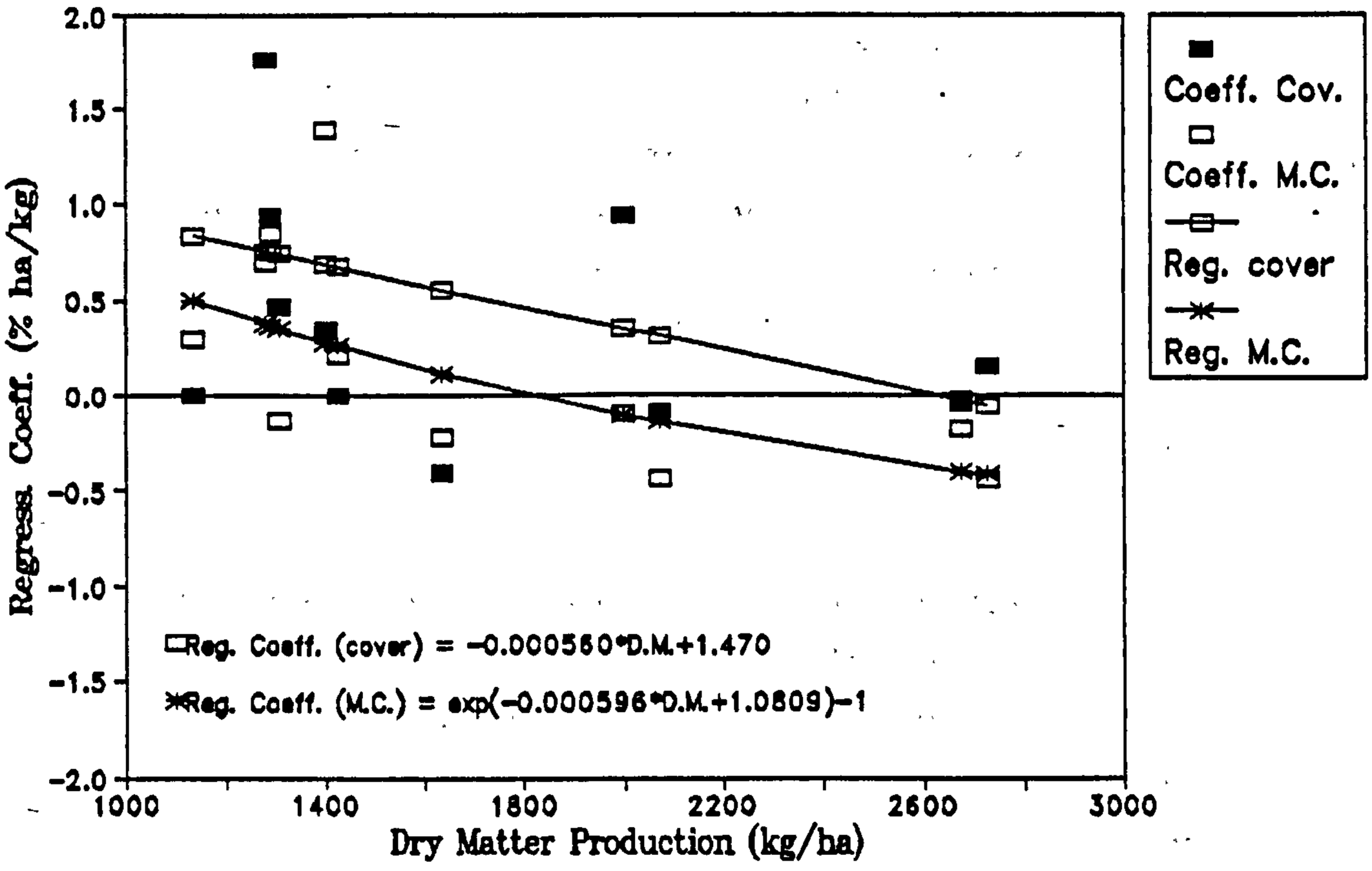
Figure 3.29: Herbaceous Dry Matter Quantity vs. Average Cover, Moisture Content and Number of Bushes and Trees for 1988 Field Survey in Niger (Transect Averages)



Although a strong positive correlation between herbaceous dry matter production and moisture content has been found when comparing results between sites, the relationship within sites is more complex. Figure 3.30 contains the slope coefficients of regressions between moisture content and dry matter production for individual sites.

The regression through these slope coefficients can be interpreted as an approximation of the first derivative of the relationship between the two parameters. A strong dependency of the regression slope coefficient and dry matter production has been found (r^2 of 0.71). With increasing quantities of vegetation the relationship shifts from being positive to negative. This is of some immediate importance for the calibration of VIs. The contrast or difference between VIs from areas of high and low vegetation quantities will be reduced, which is counteracting a consistent calibration.

Figure 3.30: Slope Coefficients of Regression between Herbaceous Dry Matter and Moisture Content and Cover for 1988 Field Survey in Niger



(b) **Herbaceous Dry Matter vs. Cover**

Average values for herbaceous ground cover for each site are given in Table 3.8 and the graphical illustration in Figure 3.29. The graphical representation indicates that there was no increase in cover at dry matter quantities above approximately 1500 $kgha^{-1}$. At that level herbaceous cover ranged between 40% and 50%. Hence, variations in the soil background can be expected to affect the EM energy reflected from areas with dry matter production of more than 2000 $kgha^{-1}$.

Figure 3.29 also indicates an inconsistency in cover estimates. A 1% cover for 1135 $kgha^{-1}$ and 10% for 1290 $kgha^{-1}$ are rather implausible. At almost the same level of dry matter production, 1280 and 1305 $kgha^{-1}$, the highest cover values were found (59.0% and 63.3% respectively).

First and second order regressions did not indicate any highly significant relationship between cover and dry matter production. A more consistent affiliation can be

found when employing regression coefficients between the two parameters obtained from individual sample points. The result is given in Figure 3.30. As could have been expected, it demonstrates that with increasing amounts of rangeland vegetation the relationship between herbaceous dry matter and cover weakens until it ceases to exist at quantities above approximately 2700 $kgha^{-1}$. At this level average cover was reported to be still below 50% (see Table 3.8). This implies that the recorded cover estimates were progressively unreliable indicators for vegetation quantities with increases of the latter.

(c) **Herbaceous Dry Matter vs. Number of Bushes and Tress**

Figure 3.29 displays graphically the association between herbaceous vegetation quantities and the number of bushes and trees. A prevalent relationship between the number of bushes and trees and any of the other factors measured or estimated could not be found.

As far as the calibration of VIs is concerned the distribution of bushes and trees is random over grassland areas and their influence cannot be accounted for.

3.3.4 Feasibility of Using WILE 35 Moisture Meter

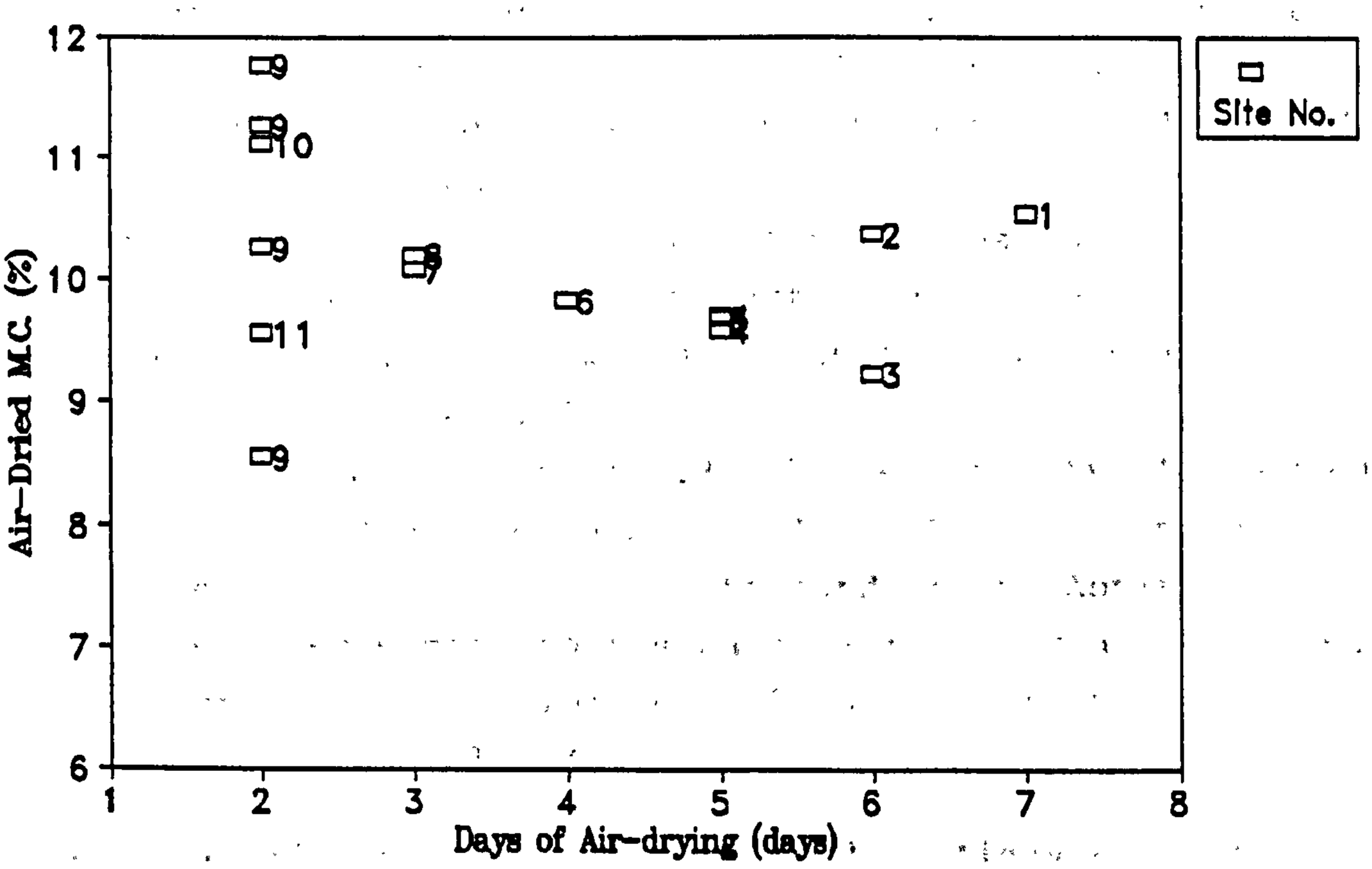
The use of the WILE 35 moisture meter seemed to be an improvement over the oven-drying method as far as the ease of acquiring rangeland production estimates are concerned. A more detailed evaluation of the instrument requires a larger number of points for the calibration. Alas, the seeds from *Cenchrus biflorus* in its mature state were found to oppose being squeezed into the cylinder of the instrument by hand.
With eight readings taken from fresh samples for a calibration against moisture content, the number of points and their distribution in the two-dimensional space for the calibration was insufficient. From established calibration curves it was clear that instrument reading and moisture content were related by an exponential function. Using those eight points a linear

regression gave a higher, but not significantly different, coefficient of determination (r^2) than exponential regressions (z-test, 95% confidence level).

An alternative to the use of any dedicated instrument for estimating the sample dry matter weight would be air-drying of samples. The values of moisture contents for air dried samples presented in Table A.10 in Appendix II indicate that a constant moisture content can be achieved. The findings are even more encouraging, since the samples were not arranged for uniform drying.

An approximate range of the number of days required to achieve an equilibrium air dried m.c. was obtained by plotting the m.c. of the samples, which were oven-dried, against the duration of storage. A graphical presentation of the result is given in Figure 3.31.

Figure 3.31: Relationship Between Duration of Storage and Air-dried M.C. (1988 ITE/Silsoe Survey)



The average m.c. of approximately 10% seems to be high when compared to results from Mali (see Chapter 3.2.3). But, as stated above, the samples were not arranged for even drying and

an unknown component of variation was likely to be introduced by the method of handling and storing the samples.

3.3.5 Accuracy Assessment of Herbaceous Dry Matter Estimates

Of main interest for calibrating satellite VI to herbaceous rangeland vegetation is the reliability of the ground data and, for future surveys, the number of samples required to achieve a desired accuracy. An additional aspect is the possible duration of a sampling mission before adverse effects on the VI calibration can be expected. The following paragraphs concentrate on these three points.

(a) **Validity of Ground Data**

For all data sets a strong dependence of the variation in vegetation growth on the overall production level has been observed. For example, for the 1988 ITE/Silsoe data a coefficient of determination of 0.90 and a t-value of 3.71 was computed for the relationship between dry matter and standard deviation, which suggested a highly significant association.

A graphical representation of relationships between confidence levels and dry matter quantities at fixed values of the class width for an image calibration is given in Figure 3.32.

As indicated by Figure 3.32 the reliability of the mean of the 1988 ground data is below 60% for the majority of sites for a ± 150 $kgha^{-1}$ standard error. Applying a linear regression to the data, a ± 200 $kgha^{-1}$ standard error provides a limit of 650 $kgha^{-1}$ for an 80% confidence level (r^2 of 0.66).

(b) **Required Sample Size for Desired Confidence Limit**

The necessary number of samples to achieve a standard error of the mean of ± 150 $kgha^{-1}$ at three different confidence levels (60, 70 and 80%) is graphically displayed in Figure 3.33.

Figure 3.32: Relationship Between Herbaceous Dry Matter Quantities and Confidence Level for Standard Errors of the Mean of ± 125, ± 150 and ± 200 kgha^{-1} (1988 ITE/Silsoe Sites)

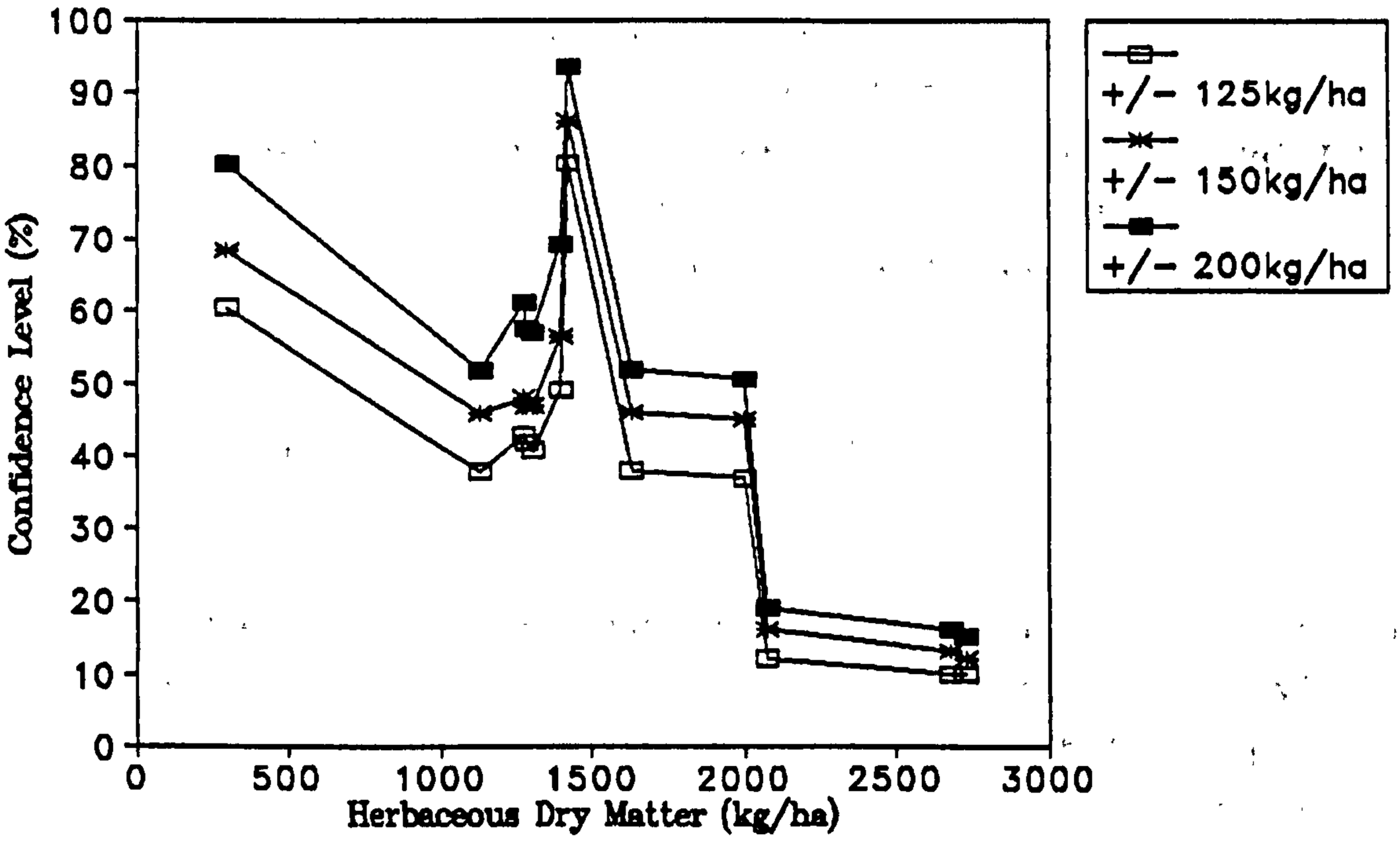
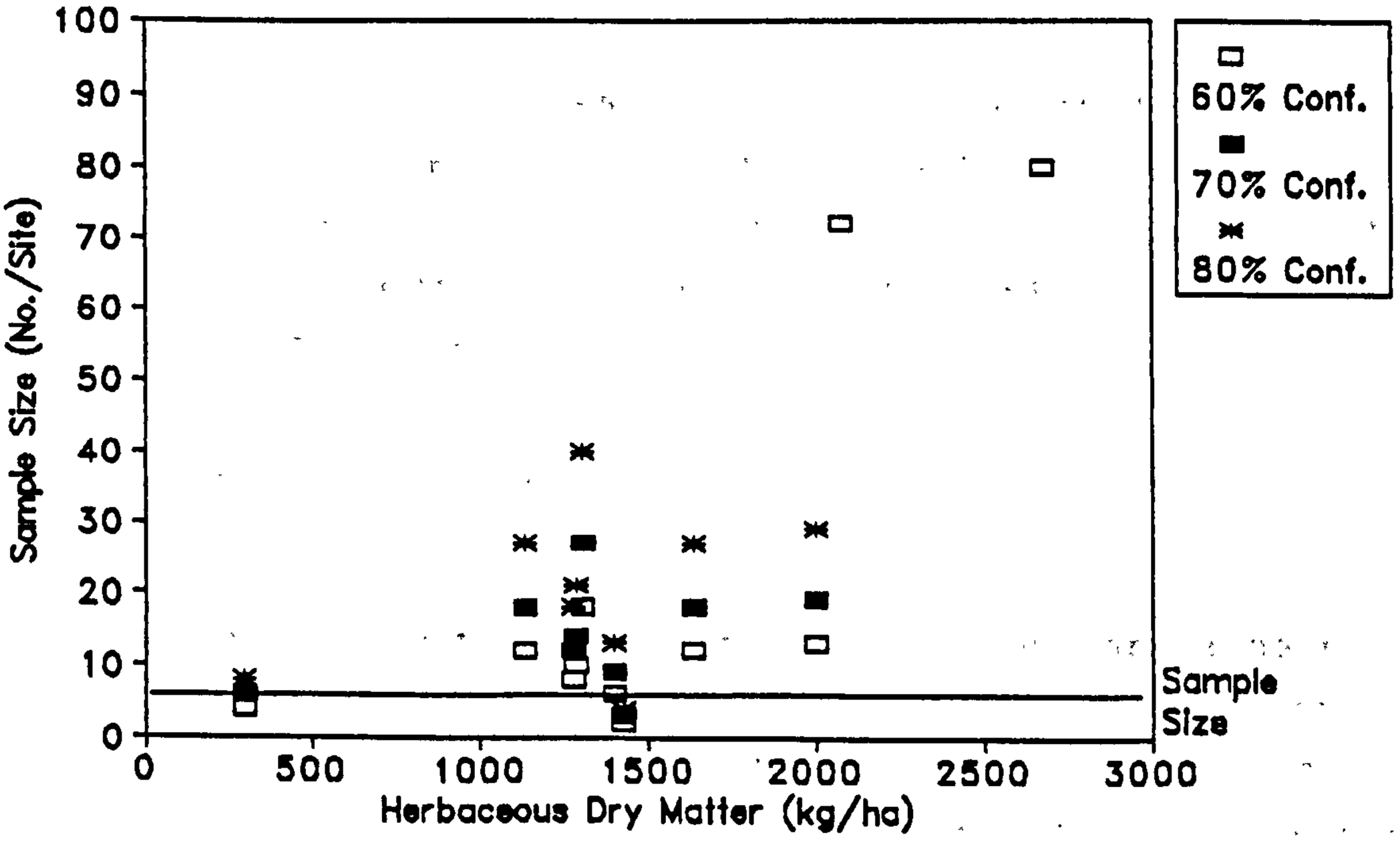


Figure 3.33: Required Number of Samples to Achieve Standard Error of the Mean of ± 150 kgha^{-1} Herbaceous Dry Matter at 60, 70 and 80% Confidence Levels (1988 ITE/Silsoe Sites)



Clearly indicated is the trend that in order to maintain the same level of confidence for a productivity class the number of ground data required grows exponentially for higher quantities. With 20 samples per site dry matter quantities up to the average amount of herbaceous rangeland vegetation could be estimated at the above mentioned accuracy requirements or better. Estimating herbaceous dry matter of more than 1500 $kgha^{-1}$ would necessitate a sample size of 40 and above.

3.4 ITE/Silsoe Field Visit of 1989

As it was the case in 1985 and 1988, ground data collection in 1989 was arranged by the Institute of Terrestrial Ecology; Monks Wood (ITE) and Silsoe College, Silsoe with the support of the Direction de la Meteorologie Nationale, Niamey and the Agrhymet Centre, Niamey. In order to increase the number of transects observed, the sampling team was reinforced by members of the Cambridge Agromet Saharan Tandem Expedition (CASTE). Sampling procedures applied were based on experience from previous field visits and the results of the statistical analysis of the data collected (see previous section and Hiederer & Maidoukia, 1988).
Analysis of the 1985 and 1988 ground data indicated a need for additional information to broaden the base for generalizing results from VI calibrations. Furthermore, the influence of the soil background information on VIs was to be evaluated and appropriate data collected.

3.4.1 Compendium on Field Work Procedures

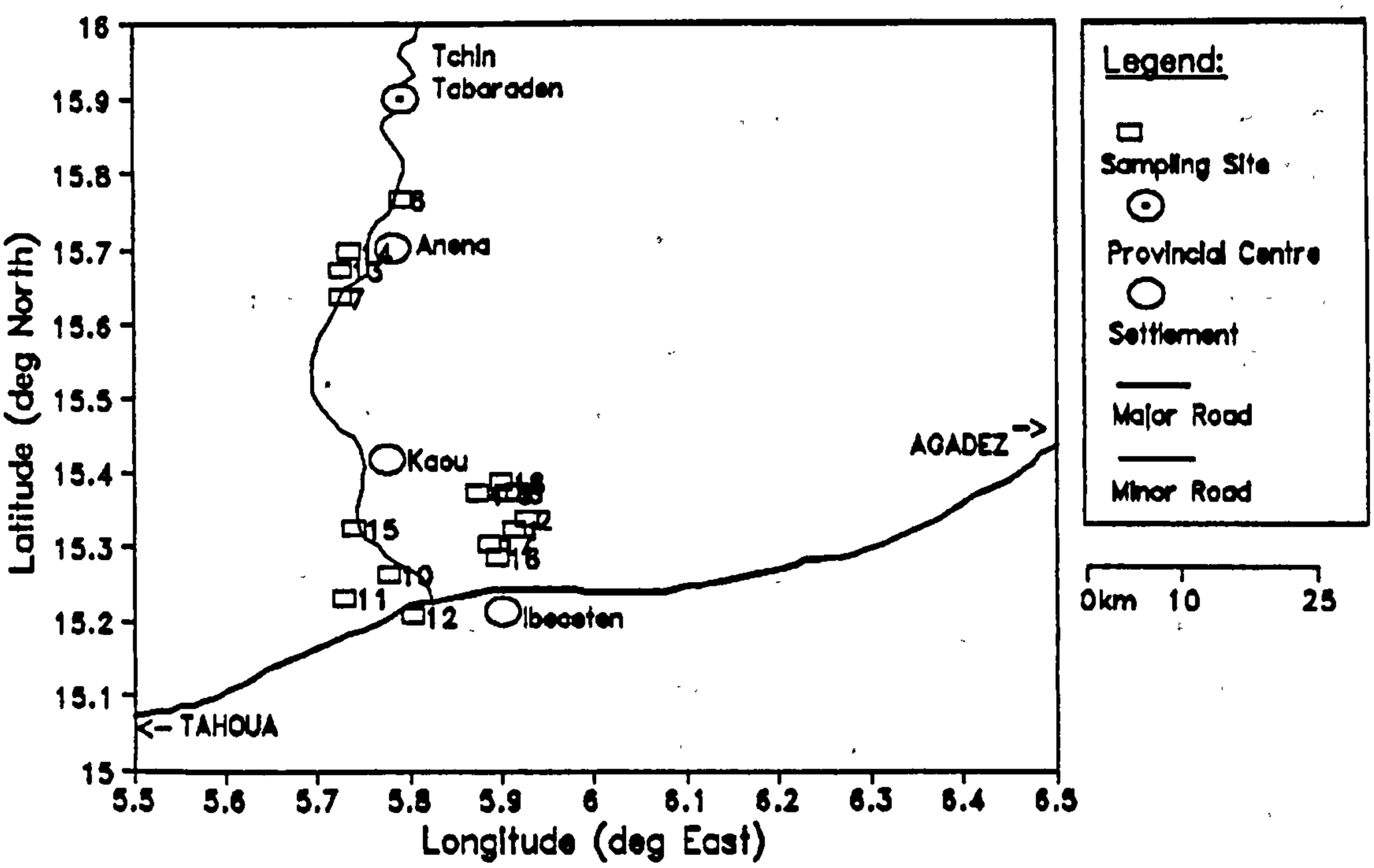
An inherent dilemma with field work is that too many aspects of it are unpredictable. The 1989 field survey was no exeption to the rule. Conditions impeding the survey from being carried out as planned ranged from strikes of airline personnel to flooded sites as a consequence of heavy rains. Therefore, a number of

adaptations to changing conditions had to be implemented in the field.

(a) **Study Area**

The study area was identical to previous ITE/Silsoe surveys in Niger. The distribution of 1989 sampling sites is graphically presented in Figure 3.34.
New sites were established mainly along the road between Ibecetene and Tchin-Tabaraden.

Figure 3.34: Arrangement of Sampling Sites of 1989 ITE/Silsoe Field Survey in Niger



(b) **Period of Ground Survey**

In order to reduce the risk of sampling for a certain date, which may yield inadequate satellite data due to cloud cover, two sample periods were intended. The dates were set to coincide with Landsat MSS over-passes over the study area (25 August and 11 September).
Ground data collection itself was carried out three days before and after the satellite over-pass. A shorter sampling period would not have been feasible, since previous sites could not have been re-visited and new ones identified. As stated before, a longer sampling

period to increase the number of sites would have inflated the discrepancy between phytomass at the time of sampling and at the time of the satellite over-pass.

(c) **Layout of Sampling Method**

Previous surveys were treated as pilot tests for evaluating the required number of samples in order to achieve a specific accuracy in estimating the production level of a site (Hiederer & Maidoukia, 1988). Differences to the 1988 sampling scheme were:

i. The length of the transect was increased to 1 km. This was suggested to include vegetation changes, which occur within the pixel size of NOAA AVHRR LAC data. Longer transects would have been desirable for a direct correlation between ground and AVHRR data. However, since AVHRR images could be registered to Landsat MSS to within 0.5 pixels and with time being a limiting factor, 1 km transects were considered an acceptable compromise.

ii. The number of sample points per transect was increased to 20. Experience suggested that 20 would be the maximum number of sampling points for a transect feasible under local conditions. It should then be possible to estimate the rangeland production level of an area to within ± 150 $kgha^{-1}$ at a 70% confidence level up to 1500 $kgha^{-1}$ or at an 80% confidence level up to 1200 $kgha^{-1}$.
The spacing between sampling points was still fixed, but reduced to 50 m. Assuming that the distribution of vegetation does not follow a pattern, randomized distances between sampling points were unnecessary.

iii. The size of the area over which herbaceous phytomass was measured was enlarged to a square of 1 m^2. This would reduce the micro-variation in vegetation quantities found at a sampling point. These variation consist of bare spots in areas of high vegetation or a vigorous plant in an area of

sparse vegetation growth. In 1988 such non-representative spots repeatedly coincided with sampling points. By increasing the size of the sampling square to 1 m^2 the accuracy was likely to improve to 80% for a range of ± 150 $kgha^{-1}$ of the mean rangeland production.

(d) Site Parameters Assessed

Site condition parameters assessed for the square were fresh weight of herbaceous vegetation, ground cover, average vegetation height and soil texture and background colour, using a Munsell Soil Color Chart.

i. *Fresh Weight of Herbaceous Vegetation*
At each sampling point the amount of phytomass in terms of fresh weight was established by clipping off the herbaceous vegetation directly above the ground over an area of 1 m x 1 m.

ii. *Ground Cover and Average Height*
Ground cover and average height of herbaceous vegetation were both estimated by eye to the nearest 5% or 10 cm respectively. Using this method, it was likely to introduce an error in determining vegetation cover, but faster than any other method involving measurements. It was considered preferable to select one person in each group to estimate vegetation cover and average height. This would avoid variations introduced to the estimates by different observers and yield a more constant relationship between recorded and actual values.

iii. *Soil Texture and Colour*
Soil texture was determined in relation to a soil texture triangle. Recording soil colour according to the Munsell Colour Chart (Munsell, 1954) was a new parameter suggested for the 1989 field survey. Soil colour is recorded in intensity, hue and chroma. The image processing system was capable of transforming satellite data displayed in red, green

and blue into values of intensity, hue and saturation. This would allow to establish a correlation between soil colour and satellite data (Escadafal *et al*, 1989). Experience from previous field surveys and an interpretation of Landsat MSS images also suggested that a relationship between soil type and vegetation quantities could be expected. Herbaceous vegetation was found mainly on yellow sandy loams. The grey clays and soils with ferrugeous crusts or gravel, which appeared dark red, could only support small amounts of vegetation (< 500 $kgha^{-1}$). Given the influence of the soil background on VIs, ground to image data calibrations could be adjusted according to soil colour, thus improving rangeland vegetation estimates.

v. *Tree and Bush Cover*

A tree and bush count was performed for the whole transect. Ligneous vegetation was recorded according to height in four classes:

Class A	Class B	Class C	Class D
< 2 m	2 - 4 m	4 - 6 m	> 6 m

Trees and bushes would be counted continuously within a range of 50 m either side of the transect.

(e) Positioning of Sample Sites

A GPS (Magnavox MX 1502 Satellite Surveyor) was employed to determine sample site positions. The system had been used successfully for ground data collection in Mali (Brown, 1989). The MX 1502 uses signals from TRANSIT satellite passes and processes the data in real time. The accuracy of the fix increases with the number of satellite passes. Three to four passes are required to establish three positional dimensions of a site, which corresponds to five to six hours. Utilizing data from several satellite passes a point positioning accuracy of ± 5 m rms on a geodetic basis can be achieved.

Finding the 1989 transects relied very much on the ability of survey team members from previous visits to re-locate the sites. This method worked successfully in most cases. There were, however, two problems:

i. Some of the sites on the Ibecetene ranch could not be found, even with the aid of image hard-copies or maps (Sites 2/88, 3/88 and 4/88). In these cases, the sites were re-defined and their positions was determined with the GPS.

ii. Two sites along the road to Tchin-Tabaraden could be found, but their position on the image was unreliable (Sites 6 and 7). The position of these sites were determined by the GPS.

The 1989 field survey confirmed the experience of previous visits that a GPS would greatly enhance the potential and practicability of ground data collection. First, sites could be freely chosen with respect to their suitability as sample areas for the project rather than the prospect of identifying their position on images or maps. Secondly, the time required for establishing site positions is shortened and the achievable accuracy increased.
However, the GPS developed a fault on the keyboard and could not be used to determine some of 1988 sites positions. For these sites the position had to be based on image identification.
Hard-copies of high-resolution satellite images still have a rôle in the field survey. They can be used to verify the results from the GPS and to act as a back-up means for positioning sites in case of a malfunctioning GPS. They also provide valuable information about the distance of a transect to spectrally different areas and sites selected accordingly.
Site co-ordinates according to image identification and instrument position for sites of the 1988 and 1989 surveys are given in Table A.15 in Appendix II. As a result of a malfunction of the system, positions of only

six sites from 1988 could be compared. Differences of site locations between using the GPS and maps or image hard-copies varied between 444 m (Site 10) and 7105 m (Site 11). The location of Sites 6 and 7 on maps in 1988 was clearly wrong. The road between Kaou and Tchin-Tabaraden was marked incorrectly on the map. The error was found by over-laying a geometrically corrected Landsat MSS satellite image, where the road was identifiable, onto the map. The image was corrected to the map, but without using map control points along the road. With all other features in place, only the road was found to be drawn approximately 2 km to the east from its actual position (see Table A.15, Appendix II). The distance of 7 km between GPS and map/image location for Site 11 could only be explained by the difficulties encountered with the GPS unit. The site could be positively identified on the image. In this case, the GPS location was definitely inaccurate.

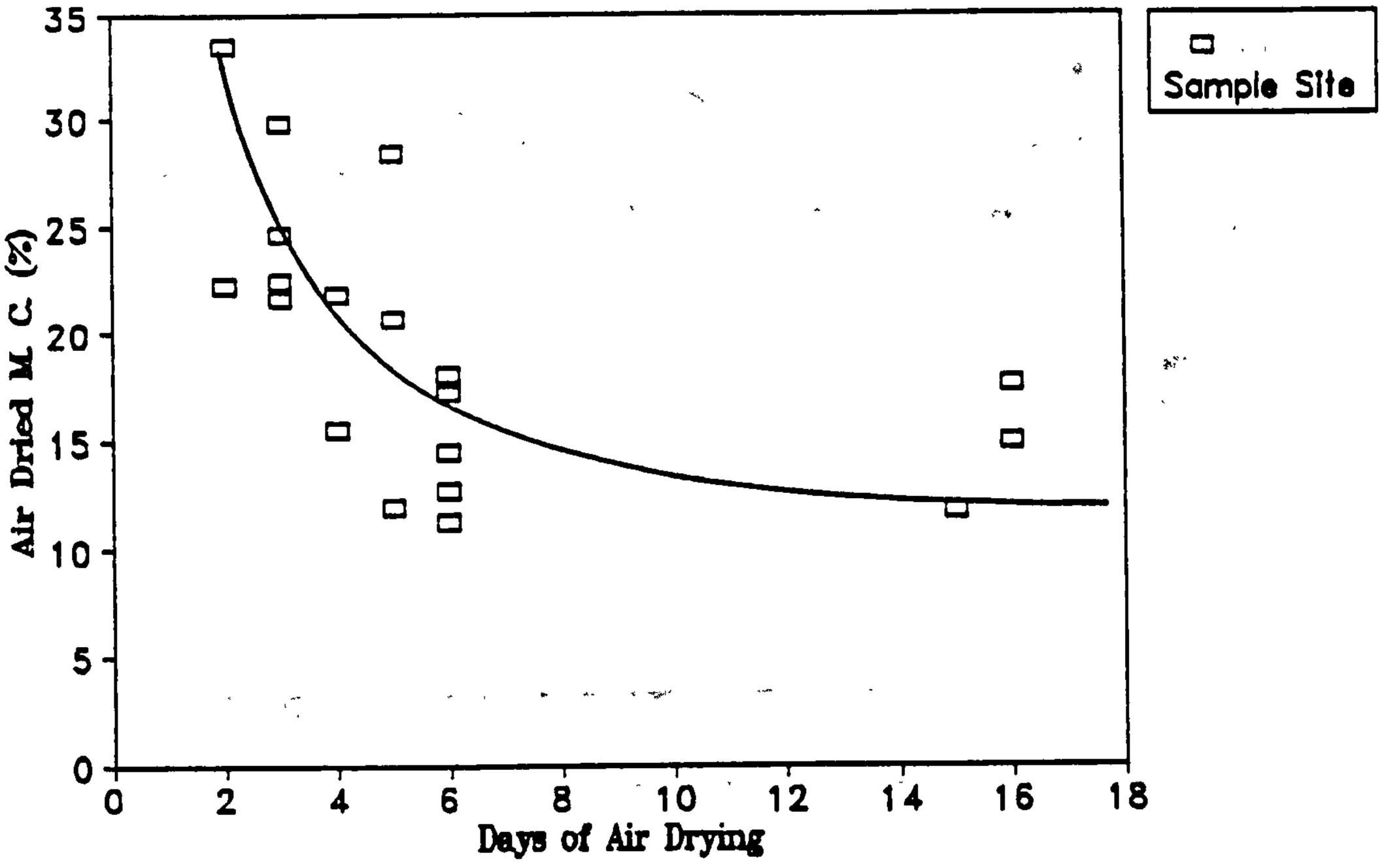
3.4.2 Performance of Air-drying Samples

Establishing the vegetation m.c. was a primary task of the field survey design, because of central concern was the identification of rangeland production estimates, which were representative for the whole site investigated. Results from air-drying samples were explored as to the suitability of the method for obtaining production estimates and storage requirements. For most of the other site parameters assessed the average sufficiently characterizes site properties.

(a) Air-drying Samples

Samples were air-dried and stored for a period ranging from one to 16 days. The relationship between the time of drying and storing samples and the m.c. obtained is graphically presented in Figure 3.35.

Figure 3.35: Development of Air-dried M.C. With Duration of Storage

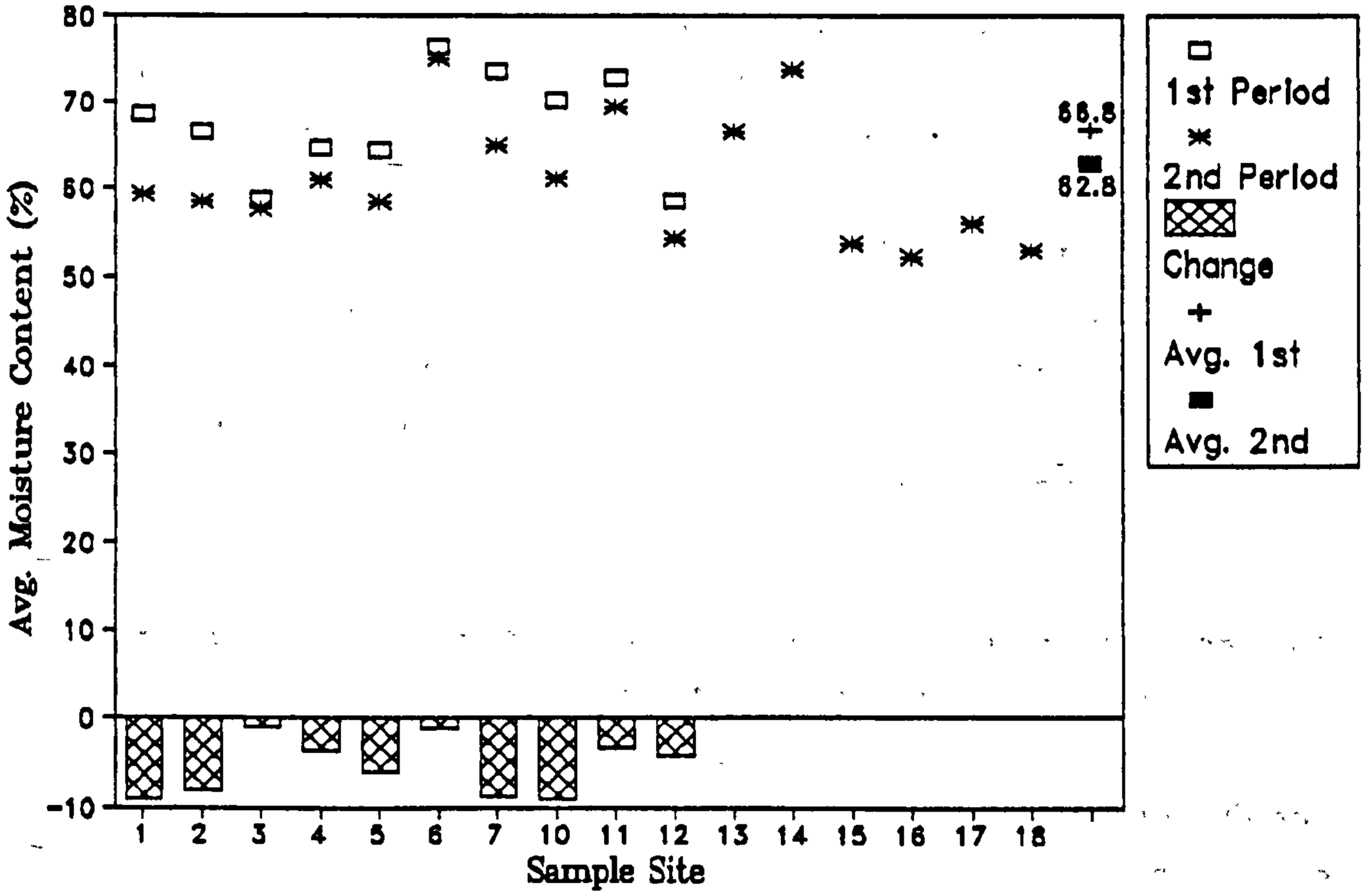


The points within the graph represent the average air-dried m.c. for a site. A strong logarithmic relationship was found between the duration of storage and the resulting m.c. An equilibrium for the air-dried samples was reached after about seven days of storage with a m.c. of approximately 12%.

(b) **Oven-Drying**

As mention above oven-drying must still be considered a necessity in order to verify and adjust the results from air-drying. The results of these measurements are given in Table 3.9. A graphical representation is given in Figure 3.36.

Figure 3.36: Average Vegetation Moisture Content for Sites of Both Sampling Periods



For re-visited, sites m.c. were generally higher for the first period than for the second. The average m.c. for all samples of the first period was 66.8% as compared to 62.8% for the second period. There was also a strong linear relationship between m.c. from the first to the second mission (r^2 of 0.71).

This relationship could be put to use to adjust vegetation m.c. to a specific date, like the day of the satellite overpass. As a consequence, the reference data should be more representative of herbaceous vegetation quantities present at a site, when calibrating satellite data to ground data collected over a period of time.

3.4.3 Compendium on Site Parameter Data

Numeric results of the data collected will be presented in this chapter. First, each criterion was treated as a separate item, independent from other site characteristics. Relationships between parameters were investigated thereafter.

In contrast to the determination of dry matter quantities the other parameters established were not measured but estimated by the observers. This method was more rapid and could be more easily applied than measuring these criteria. Yet, subjective observations contain an element of variation, which is not a property of the parameter investigated.
A constant over- or under-estimation would not influence the strength of the assumed connection. However, variations introduced by changing observers would reduce the correlation between parameters and increase variation. Reflecting on these potential pitfalls is essential when interpreting results from the investigation.

(a) **Dry Matter Quantities of Herbaceous Rangeland Vegetation**

A summary of the results from the two field missions of 1989 is given in Table 3.9.
The figures presented constitute average values from measurements and estimates of individual sites. Since measurements of vegetation m.c. were based on a subset of samples taken, the estimates for average herbaceous vegetation quantities were based on the average m.c. established for a site.
With the exeption of Sites No. 3 and 6 rangeland vegetation quantities increased in the two weeks between the first and the second period. The decrease encountered at Site 3 was not significant (50% probability of the two means being not different). On the other hand, for Site 6 the probability of a difference as large as the one observed was only 10%. A possible explanation for the decrease there could be that grazing has occurred in the meantime. This assumption is supported by the only slight decrease in m.c. (from 76.2 to 75.0%), which might have been caused by re-growth counteracting against a stronger decrease by senescence.

Table 3.9: Summary of Measurements and Estimates of 1989 ITE/Silsoe Survey in Niger

Site No.	Cover (%)	Height (cm)	Munsell Soil Colour	Oven M.C. (%)	Rangel. Prod. (kg/ha)	Std. Deviat. (kg/ha)	Bushes & Trees (No/ha)
		First Sampling Period					
1	17.6	23.5	10/76	68.5	768	558	11.4 4.2
2	16.7	24.7	10/76	66.5	880	818	5.4 6.7
3	10.5	17.5	75/68	58.8	667	344	1.9 1.5
4	19.1	26.9	10/78	64.7	1036	981	12.5 9.9
5	9.3	15.7	10/76	64.3	687	400	3.3 0.0
6	8.7	22.0	75/66	76.2	757	504	13.3 4.3
7	10.0	21.5	10/76	73.6	565	302	10.5 6.7
10	6.0	17.5	10/76	70.2	522	116	3.9 0.9
11	7.5	13.0	10/84	72.8	415	199	16.1 25.5
12	5.7	20.0	75/64	58.5	642	230	2.7 1.5
		Second Sampling Period					
1	10.0	19.4	75/66	59.4	999	497	11.4 4.2
2	7.5	36.9	75/66	58.5	1300	457	5.4 6.7
3	5.6	20.0	75/66	57.7	558	299	1.9 6.7
4	10.1	27.5	10/76	61.0	1239	1280	12.5 9.9
5	9.2	19.2	75/66	58.4	750	384	3.3 0.0
6	2.6	17.8	75/76	75.0	386	481	13.3 7.7
7	7.5	25.3	10/76	64.8	666	333	10.5 6.7
10	9.3	20.8	10/76	61.1	799	201	3.9 0.9
11	12.0	17.3	10/74	69.5	689	396	16.1 25.5
12	7.3	33.0	10/76	54.2	736	252	2.7 1.5
13	5.8	17.5	75/76	66.5	649	767	5.8 3.0
14	6.3	30.3	10/76	73.6	603	484	14.8 19.0
15	6.7	19.4	75/78	53.7	554	220	8.2 0.2
16	6.5	29.5	10/76	52.2	895	239	76.1 1.5
17	4.3	28.5	10/78	56.0	996	656	15.4 0.7
18	8.9	24.2	10/66	53.0	1051	399	3.4 1.0

Munsell: 75/76 is 7.5YR/7/6
Cover : Herbaceous cover estimated over 1 m².
Height : Average height of herbaceous cover over 1 m².
Bushes : Number of ligneous species ≤ 2 m high over 1 ha.
Trees : Number of ligneous species > 2 m high over 1 ha.

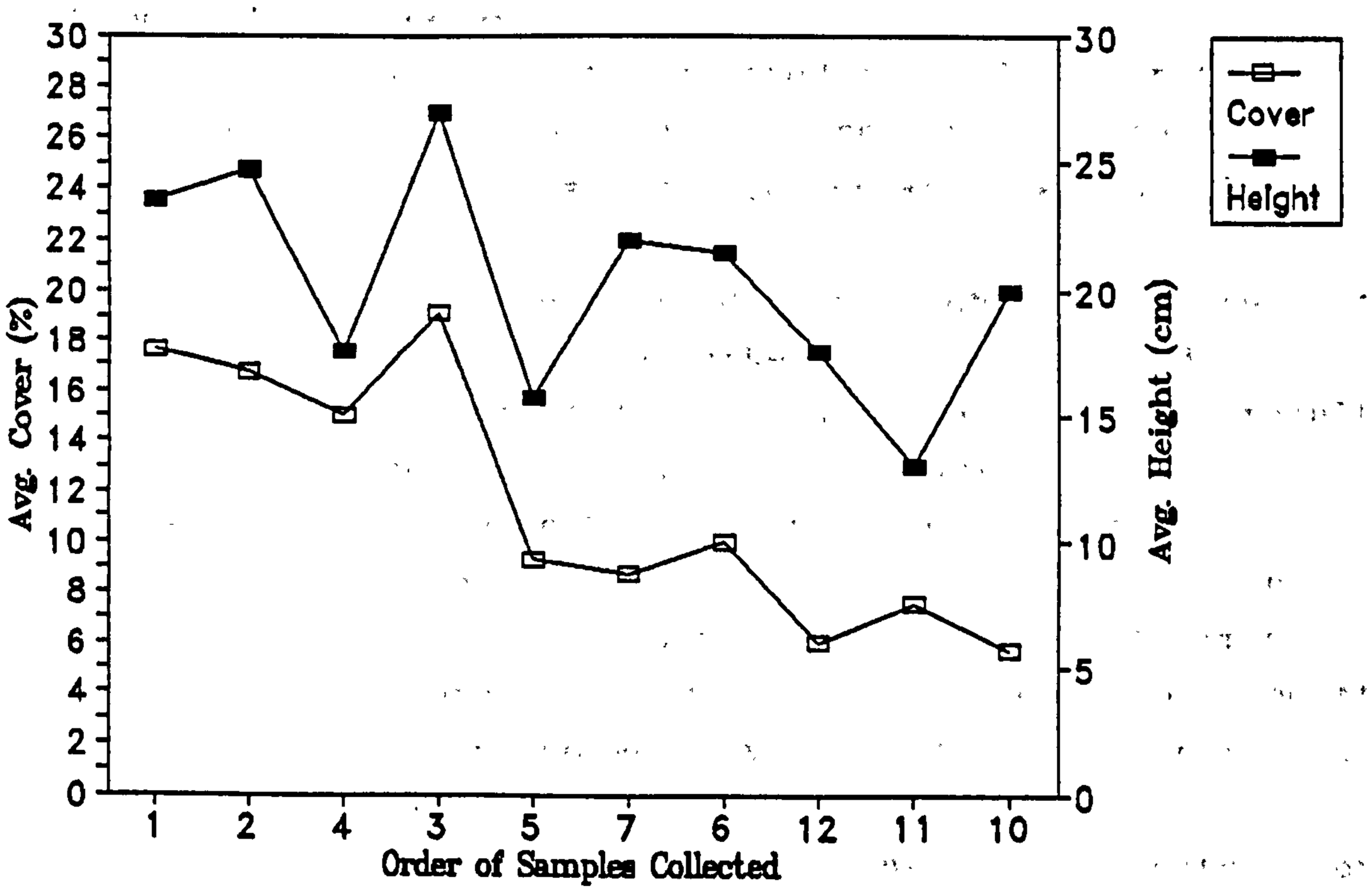
(b) Herbaceous Ground Cover and Average Height

Table 3.9 contains average values of herbaceous ground cover and height for each site. From the first to the second season average cover fell from 11.6% to 8.1%. Average vegetation height increased from 20.2 cm to 23.7 cm.

The increase in height over time could have been expected, since vegetation quantities generally built up. The marked decrease in cover for two third of the

sites, however, was not envisaged.
The decrease in vegetation cover stands in contrast to the increase in rangeland vegetation over the sampling period. One explanation would be a reduced cover as a consequence of a drying vegetation and folding leaves. Also, the judgement of observers may have adjusted to conditions. Herbaceous vegetation cover and height were, therefore, compared with the order in which they were assessed. The results are given in Figure 3.37.

Figure 3.37: Development of Cover and Height of Herbaceous Vegetation over Sampling Period



For all parameters a decrease with progressing sampling can be observed. This might have been a chance trend, but could also indicate a change in the judgement of observers. Comparing the relationship of cover with rangeland production with other survey results should provide more information on the subject (see next section).

(c) **Number of Bushes and Trees**

In Table 3.9 the tree count is given in form of two groups, ligneous plants with 2 m height or less and

bushes and trees higher than 2 m. The division was based on experience and a portion of what was grouped into "bushes" were actually small trees. For the purpose of the investigation this is of no importance. A two-class tree count was just used to reduce the data presented. Only those trees and bushes with photosynthetically active leaves were counted, dead ones were not included. Albeit, there was a gradual change between dead plants and those with vigorous growth. So again, there was room for subjective interpretations as to what was worth counting and what not.

(d) **Munsell Soil Colour**

Soil colour assessment was based on finding for the soil colour at a sampling point a corresponding tone in the reference table. This could be accomplished rapidly and easily.

Soil colours were found to differ slightly from one period to the other. The darker tones attributed to sites during the second period were most likely a result of an increased soil m.c. Thunder storms occurred during the night of 9 September and the sites visited after that date had been dry during the previous visit. In addition to rainfall, heavy dew was present at times early in the morning. Thus, the soil colours observed at a site in the morning may have been different from those in the afternoon.

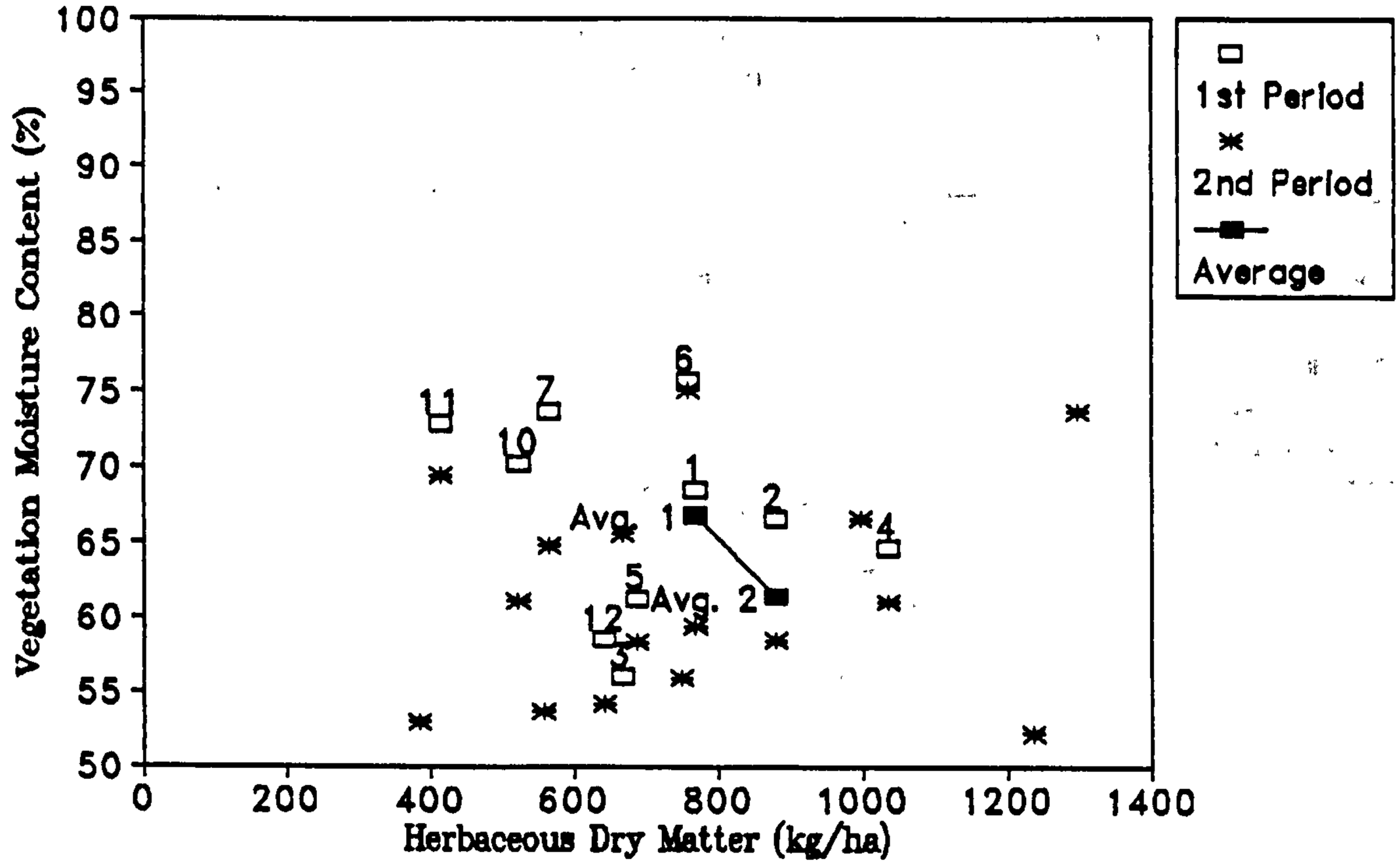
The soil surface was not uniform, neither in texture nor in colour. In many places brighter sand particles were blown over darker patches of loam and clay. The surface appeared variegated with homogeneous areas of only a few centimetres wide. A satellite sensor would proportionally integrate the spectral response from these and larger areas. This is not possible for ground observations utilizing a colour chart. Therefore, a dominant and a sub-dominant soil colour was noted for heterogeneous sites. In Table 3.9 only the dominant soil colour is given, which mainly represented the sandy portion.

The additional information sampled was intended to support investigations into the influence of environmental site conditions on VIs derived from satellite data. The relationships between herbaceous dry matter quantity and vegetation cover, height, tree count and soil colour are discussed in the second part of this chapter. As for all other surveys, multi-variable approach was omitted, since it would be of no relevance to a straight forward correlation of satellite VIs to values of rangeland production.

(a) **Herbaceous Dry Matter vs. Moisture Content**

The result of using average rangeland production estimates from all samples collected at a site and relating them to the vegetation m.c. is displayed in Figure 3.38.

Figure 3.38: Relationship between Rangeland Production and M.C. of Herbaceous Vegetation



It reveals a definite trend of decreasing m.c. with increasing quantities of vegetation. The trend was more expressed for the second period than for the first, but not significantly different.

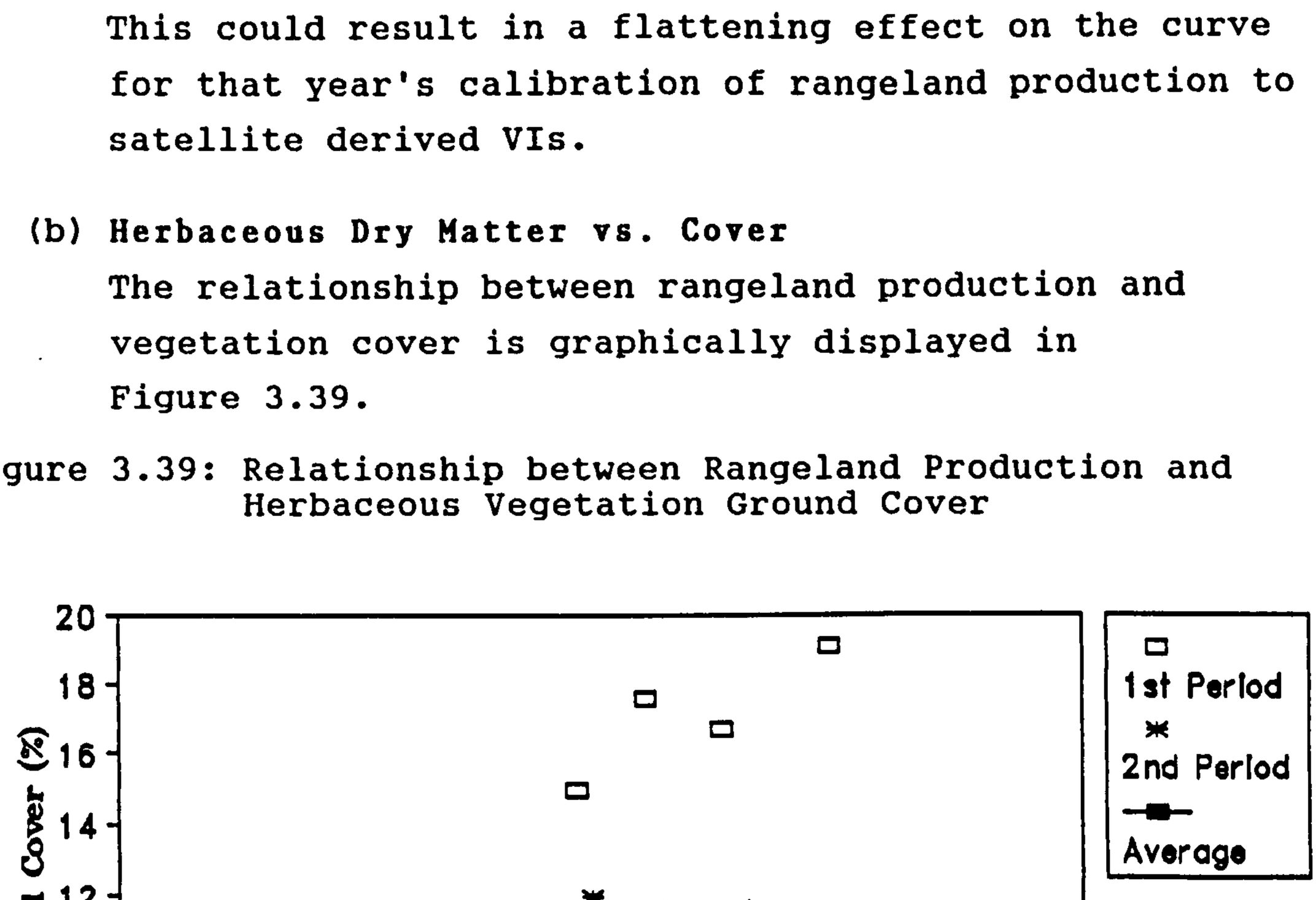
The relationship between herbaceous vegetation m.c. and

the corresponding rangeland production level is of importance, since it reflects the tendency of plant material to photosynthesize. For m.c. of 70% or more, there is probably little or no influence detectable by satellite derived VIs. At lower levels, VIs become increasingly sensitive to the m.c. of plant tissues. High but dry quantities of vegetation can subsequently be confused with lower but photosynthetically active vegetation. As can be seen in Figure 3.38, a large portion of sites had an average m.c. of 65% or less. This could result in a flattening effect on the curve for that year's calibration of rangeland production to satellite derived VIs.

(b) **Herbaceous Dry Matter vs. Cover**

The relationship between rangeland production and vegetation cover is graphically displayed in Figure 3.39.

Figure 3.39: Relationship between Rangeland Production and Herbaceous Vegetation Ground Cover



There is a distinct difference between the first and the second period. The almost continuous increase over the

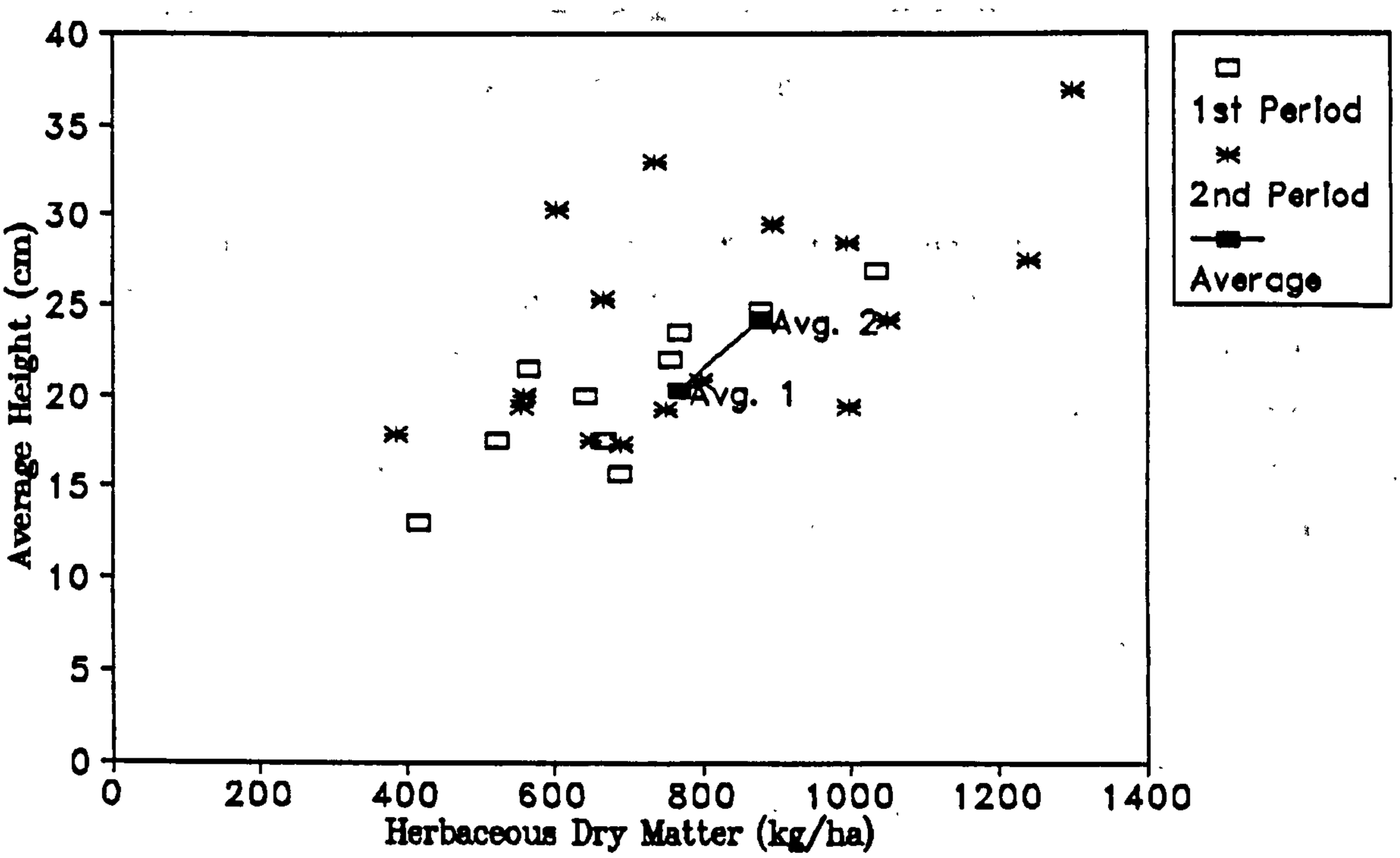
first period changed to a logarithmic relationship for the second one with no increase beyond approximately 800 $kgha^{-1}$.

(c) Herbaceous Dry Matter vs. Average Height of Herbaceous Vegetation

The relationship between rangeland vegetation levels and average height of herbaceous vegetation over 1 m^2 is presented in Figure 3.40.

The trend for the first and second period are not significantly different. There is only a larger variation for the second period.

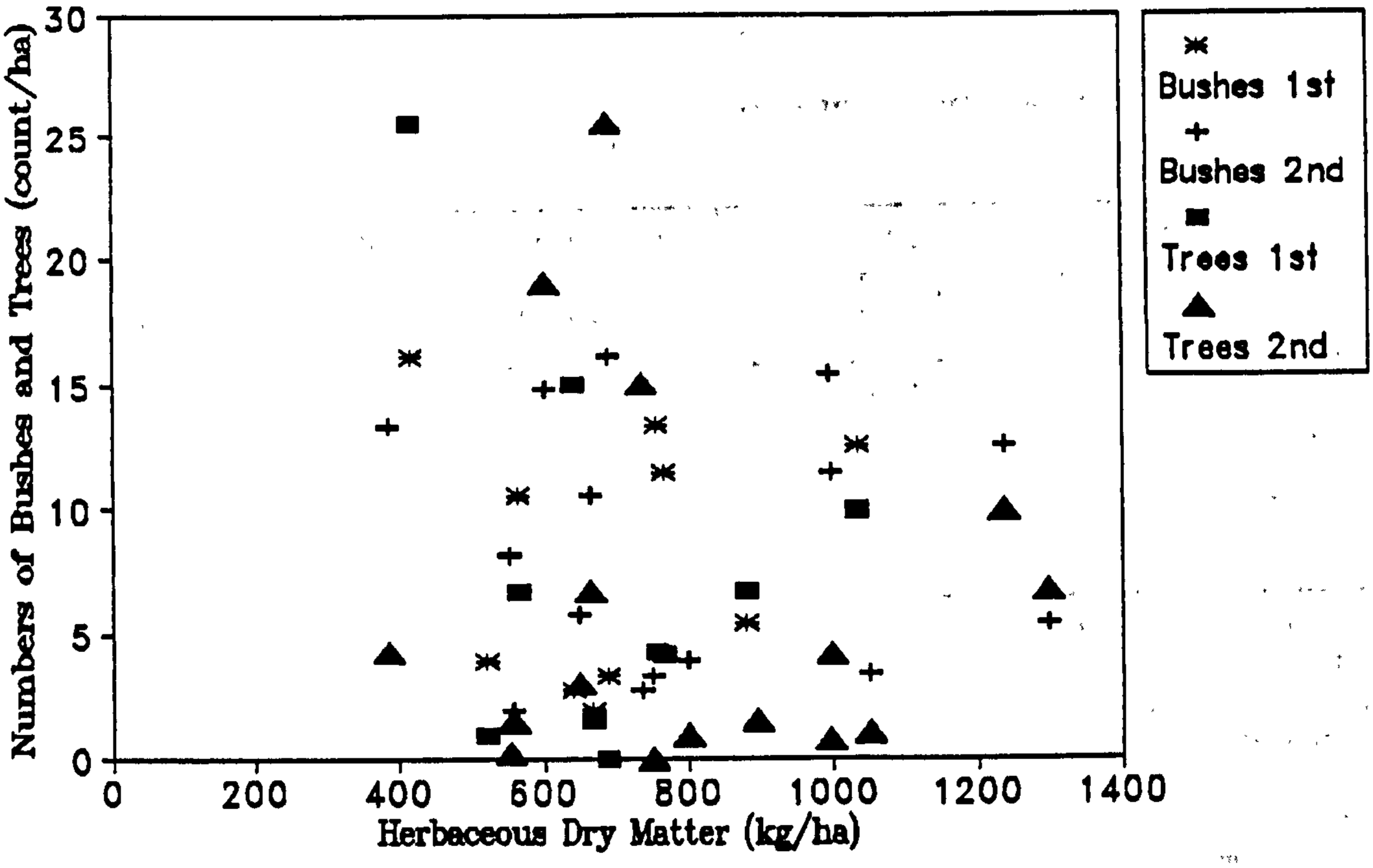
Figure 3.40: Rangeland Production vs. Average Height of Herbaceous Vegetation



(d) Herbaceous Dry Matter vs. Number of Bushes and Tress

Figure 3.41 indicates the dispersion of bushes and trees in dependence of rangeland production quantities. As has been mentioned before, the original four classes of ligneous vegetation have been condensed into two classes, separated at a threshold of 2 m height. No correlation between the number of bushes and trees and rangeland production has been found.

Figure 3.41: Rangeland Production vs. Bush and Tree Count



(e) Herbaceous Dry Matter vs. Munsell Soil Colour

The soil colour found at a sample point has been determined in order to investigate, if an adjustment of satellite data for variations in VIs caused by changing soil back ground information was possible and necessary. Provided it is possible to identify soil colour from satellite images and a relationship between rangeland production and soil colour can be established, then maps of production potentials could be developed. This would allow to mark areas with relatively higher growth capabilities independent of the seasonal variations.

Because no information on any possible connection between soil colour and productivity was available, the first step taken was to compute the average rangeland production level for each soil colour identified. This was done for all values available, integrating the first and second survey. In a second step, all classes with less than five entries were excluded. This was carried out to reduce the number of soil colour classes and the effect of outliers, which may occur as a consequence of a small entry number. Soil classes were then sorted

according to the related rangeland production. Three broad groups depending on a value of 6, 7 and 8 were immediately obvious (see Table 3.10).

Table 3.10: Significance Test on Average Rangeland Production of Soil Colour Classes

Soil Colour Group	Avg. Herb. Dry Matter ($kgha^{-1}$)	Std. Dev. ($kgha^{-1}$)	Conf. Interv. ($kgha^{-1}$)	Probability of diff. mean Groups (%)
1	932	650	784 - 1080	
2	824	546	699 - 949	1, 2 27.4
3	723	427	658 - 788	2, 3 12.2
4	625	653	455 - 795	3, 4 20.5
5	488	283	334 - 642	4, 5 46.4

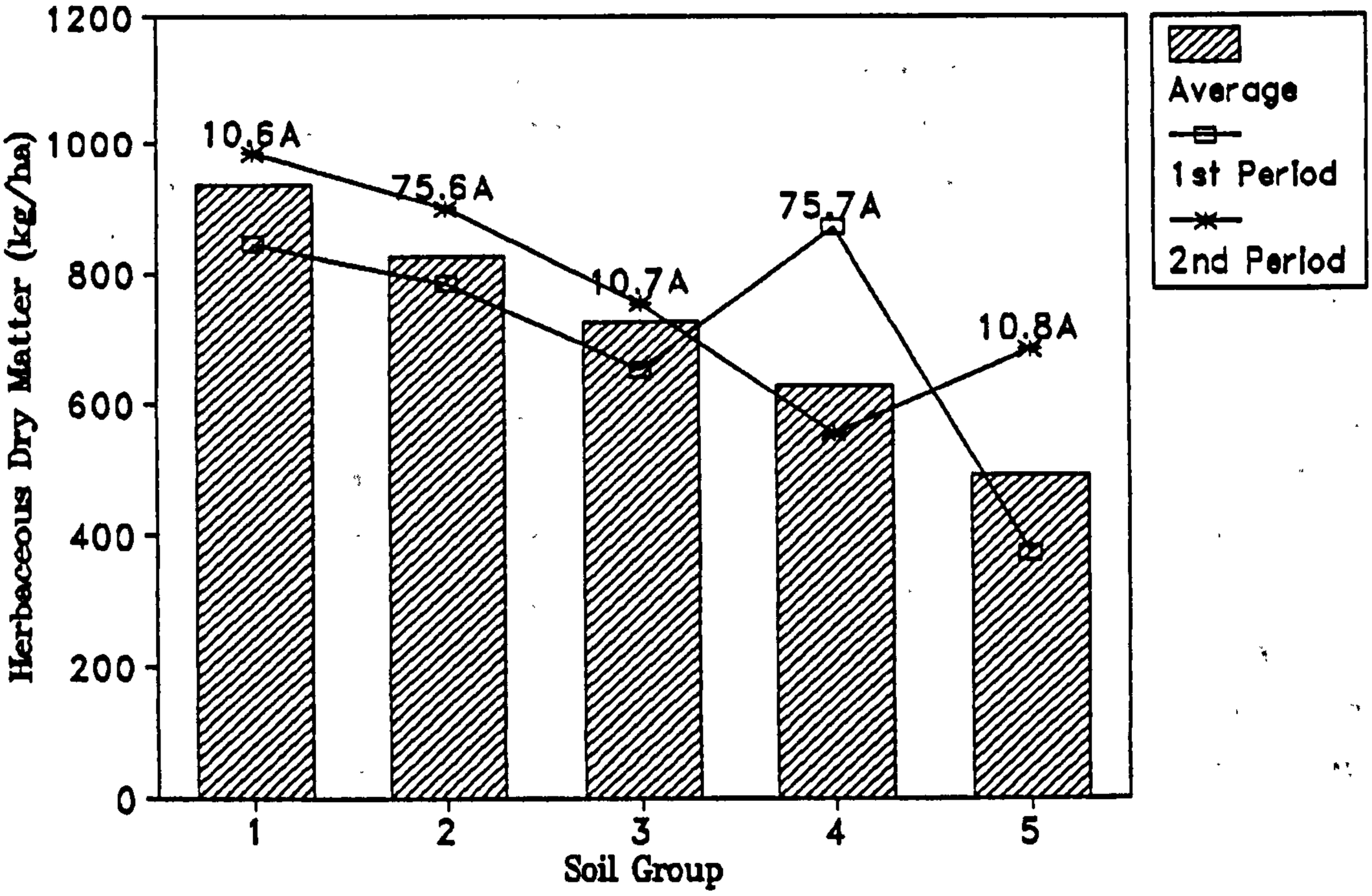
Soil Colour Group:
1 10 YR/6.A
2 7.5YR/6.A
3 10 YR/7.A
4 7.5YR/7.A
5 10 YR/8.A

Conf. Interval: at 95% confidence level

Probability: likeliness of observed diff. ±1.96 std.err. with no diff. between population means

A further division into five groups depending on hue values of 10YR and 7.5YR could be accomplished. Thereupon, the method was applied separately to values from the two sampling periods. Apart from soil group 7.5YR 7/X, with X being any value found for chroma, the same trend could be observed for both periods.
The whole procedure, using data from both individual periods and the combined data, was then repeated, this time including all soil colours identified. A graphical representation of the results for the five groups is given in Figure 3.42.

Figure 3.42: Rangeland Production vs. Soil Colour Classes



Chroma seems to be of very little importance and classes were not based on it. The only values found for hue were 10YR and 7.5YR. They form the sub-dominant criteria for group allocation.

Establishing confidence intervals for the estimated range of the average herbaceous dry matter quantities of each soil class reveals that rangeland production overlaps for all classes. A test on significance between independent sample means confirmed impediments in separating rangeland production according to soil colour. Table 3.10 contains the results of a t-test on class independence.

In none of the cases are the differences between groups significant. However, since the general relationship was observable for both sampling periods, further investigations into a more defined correlation are suggested. This would require to repeat sampling for a different growing season and area.

3.4.4 Feasibility of Air-drying Samples

Air-drying samples with subsequent oven-drying of a subset represents a realistic option for establishing rangeland production levels. The method requires refinements, but the applicability of the concept itself has been confirmed.
The unexpectedly high average air-dried m.c. of 12.9% may be explained by weather conditions at the time of sampling and the method of storing the samples. In 1989 heavy thunderstorms and high levels of humidity occurred throughout the period of the survey. In addition, the samples were kept in paper bags to allow continuous drying and to avoid decomposition by mould. However, the storage equipment consisted of a metal box and fresh samples were kept collectively. Thus, with the box being closed most of the day while travelling between sites and new, moist material added to dried one, the equilibrium remained at a comparatively high level.
For future surveys it is recommended to store samples from different dates separately and to transfer dried samples to plastic bags. It should then be possible to reach an equilibrium within a week.
Due to the nature of collecting and treating vegetation samples for air-drying, the m.c. measured were unsuitable for establishing rangeland production levels. But the results strongly support the possibility of using air-drying of herbaceous vegetation for establishing rangeland production levels. Furthermore, the investigation revealed a dependency of the equilibrium m.c. on environmental characteristics of the growing season. It also demonstrated the need for oven-drying a cross-section of the samples taken.

3.4.5 Accuracy Assessment of Herbaceous Dry Matter Estimates

The average rangeland production level of all samples from a site represents an estimate of the average vegetation quantity at a site, which corresponds to the population mean. The population mean itself is not known, but a range can be specified, which contains it with a certain reliability. The

ranges within which the population mean is likely to be found and the number of samples required to reduce these ranges to a preset width and confidence level will be discussed in this chapter.

(a) **Validity of Ground Data**

For the first sampling mission a strong exponential relationship between herbaceous dry matter quantity and its standard deviation was observed. The second survey, only two weeks later, did not display a clearly defined trend. This sets it apart from all previous survey results and is without explanation. These differences in variation largely influence the validity of the ground data and the two missions will have to be treated separately.

The likely confidence level, which could be achieved for a certain amount of herbaceous dry matter, is graphically presented in Figure 3.43 for the first mission and Figure 3.44 for the second.

Figure 3.43: Relationship Between Herbaceous Dry Matter Quantities and Confidence Level for Standard Errors of the Mean of ± 125, ± 150 and ± 200 $kgha^{-1}$ (1st Mission of 1989 ITE/Silsoe Sites)

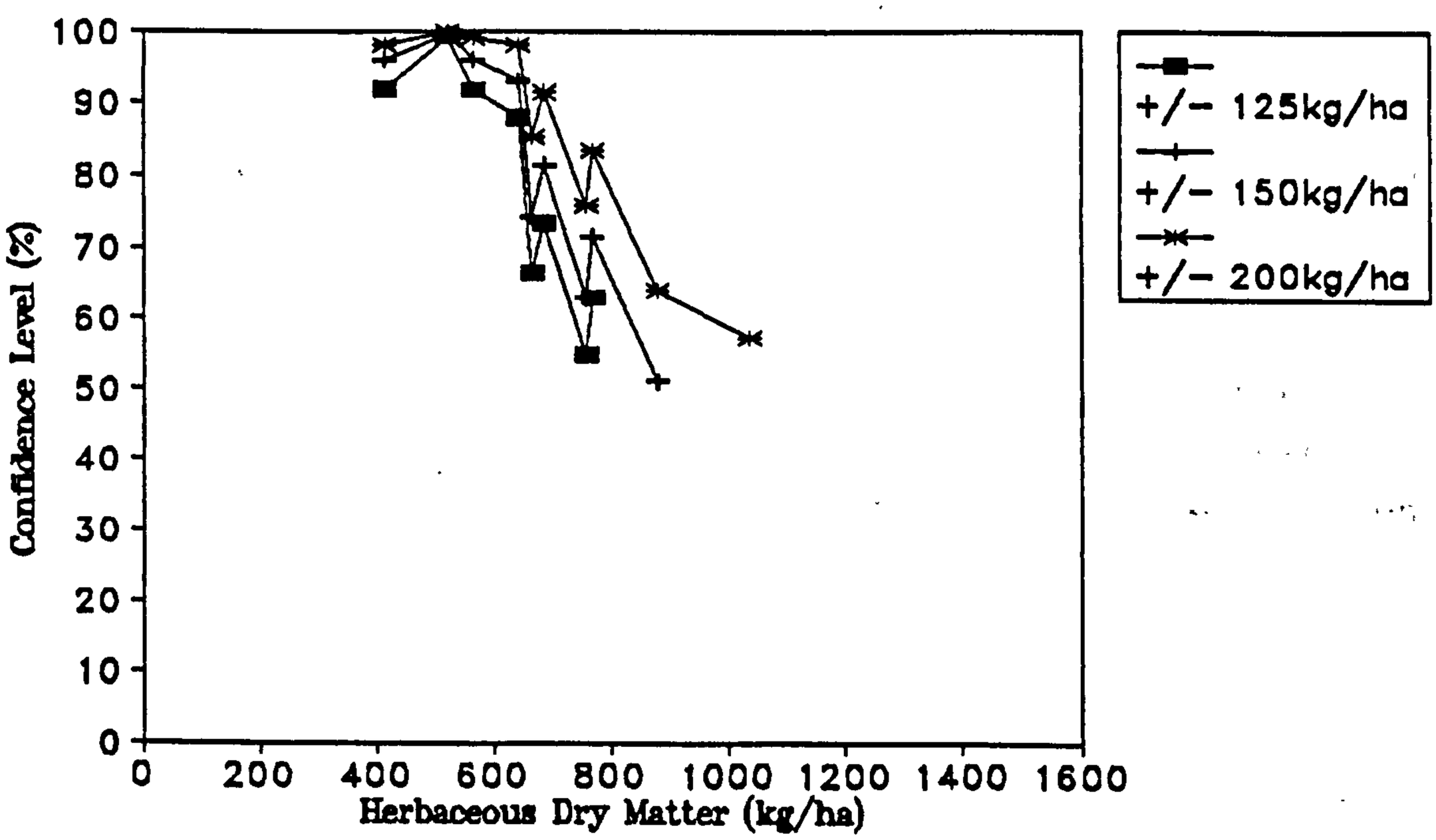
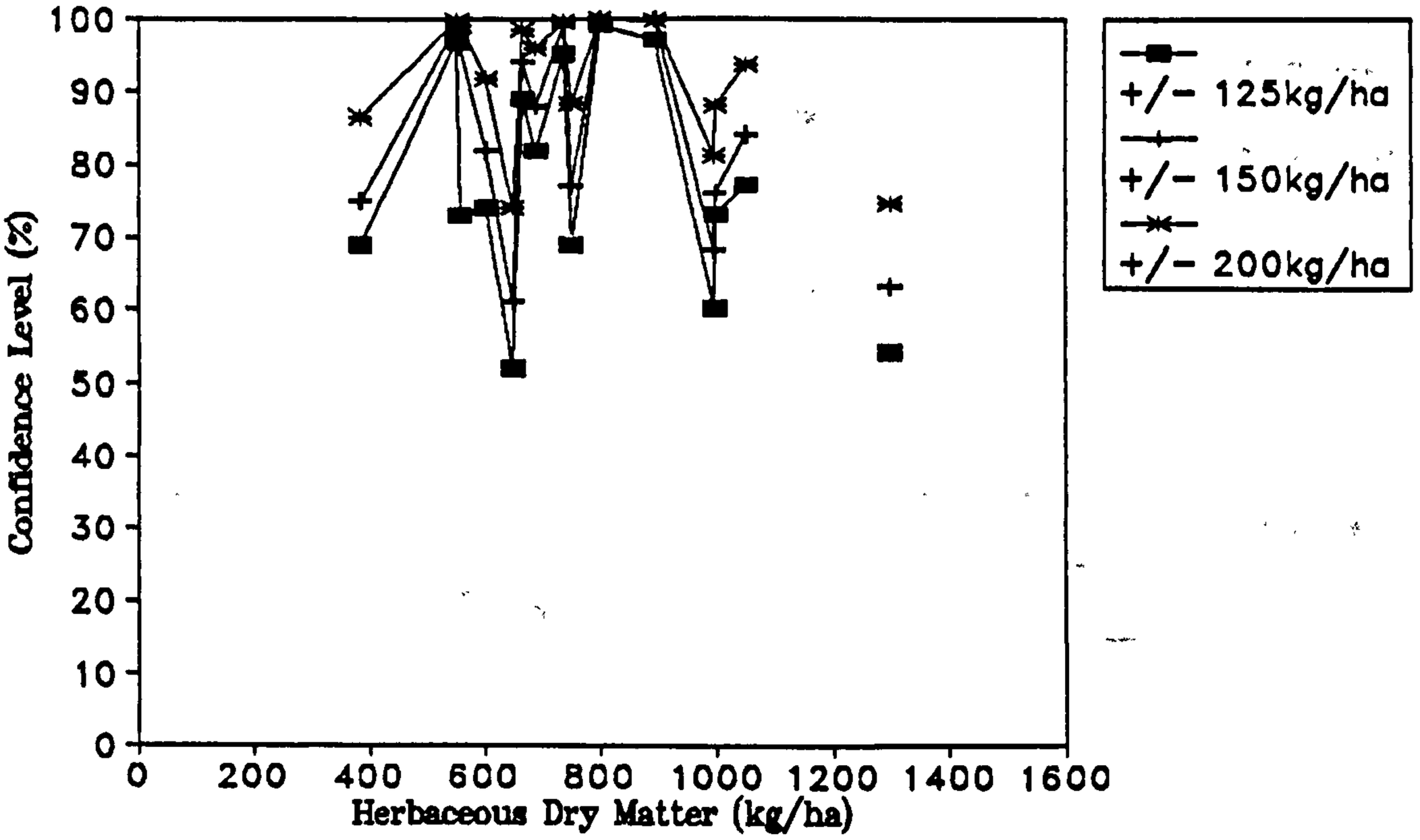


Figure 3.44: Relationship Between Herbaceous Dry Matter Quantities and Confidence Level for Standard Errors of the Mean of ± 125, ± 150 and ± 200 kgha^{-1} (2nd Mission of 1989 ITE/Silsoe Sites)



For the first period (Figure 3.43) an 80% confidence for the ± 150 kgha^{-1} class would cover a range up to approximately 600 kgha^{-1}. Beyond that value, the confidence decreases almost steadily.
Relations for the second period are not as straight forward. This is caused by a drop at 600 kgha^{-1}. Without it the class could be stretched to approximately 1000 kgha^{-1} at an 80% confidence (see Figure 3.44).

(b) Required Sample Size for Desired Confidence Limit

The number of samples necessary to achieve a desired accuracy is given in Figure 3.45 for the first mission and in Figure 3.46 for the second.

Figure 3.45: Required Number of Samples to Achieve Standard Error of the Mean of ± 150 $kgha^{-1}$ Herbaceous Dry Matter at 60, 70 and 80% Confidence Levels (1989 ITE/Silsoe Sites, 1st Mission)

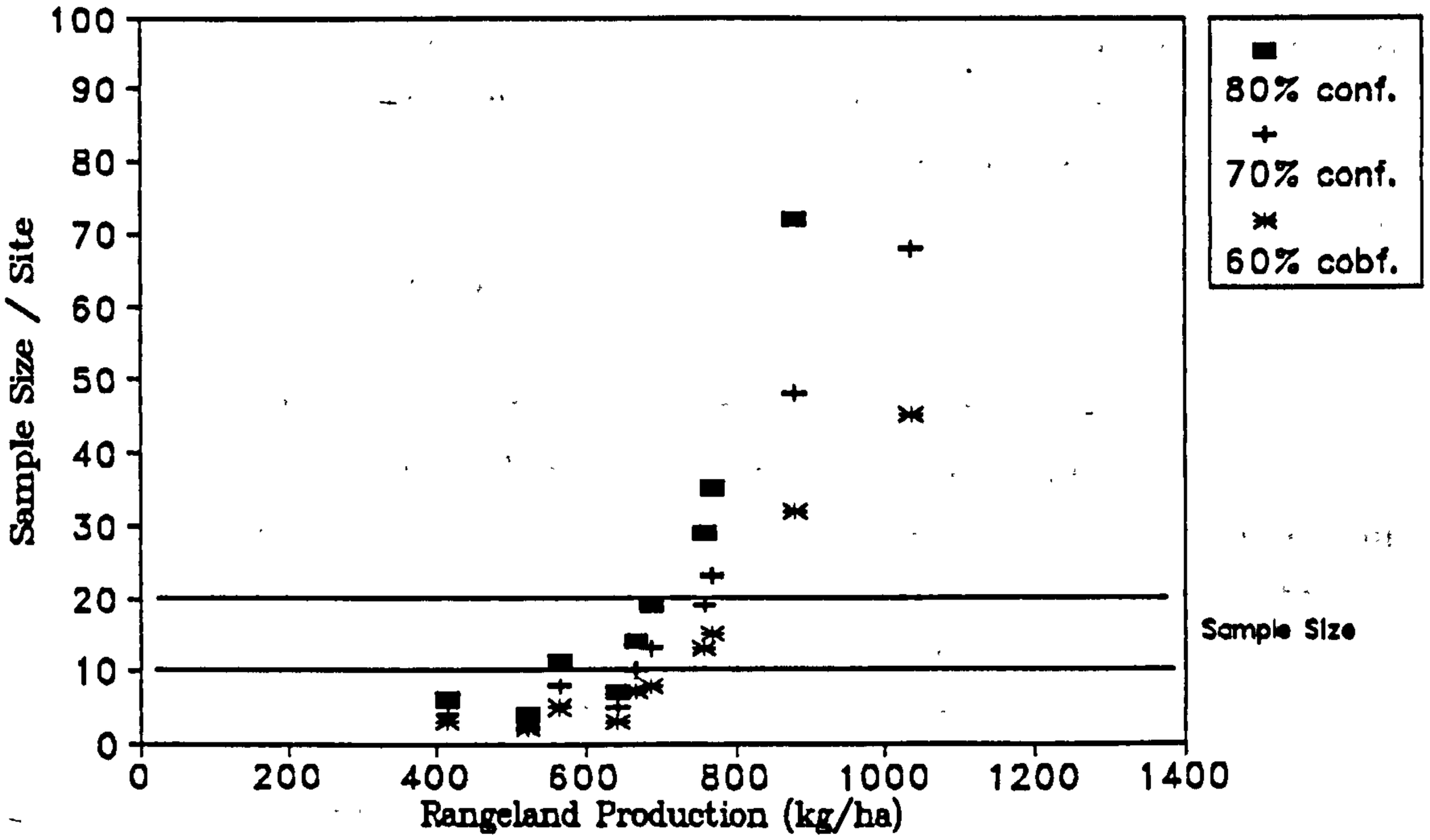
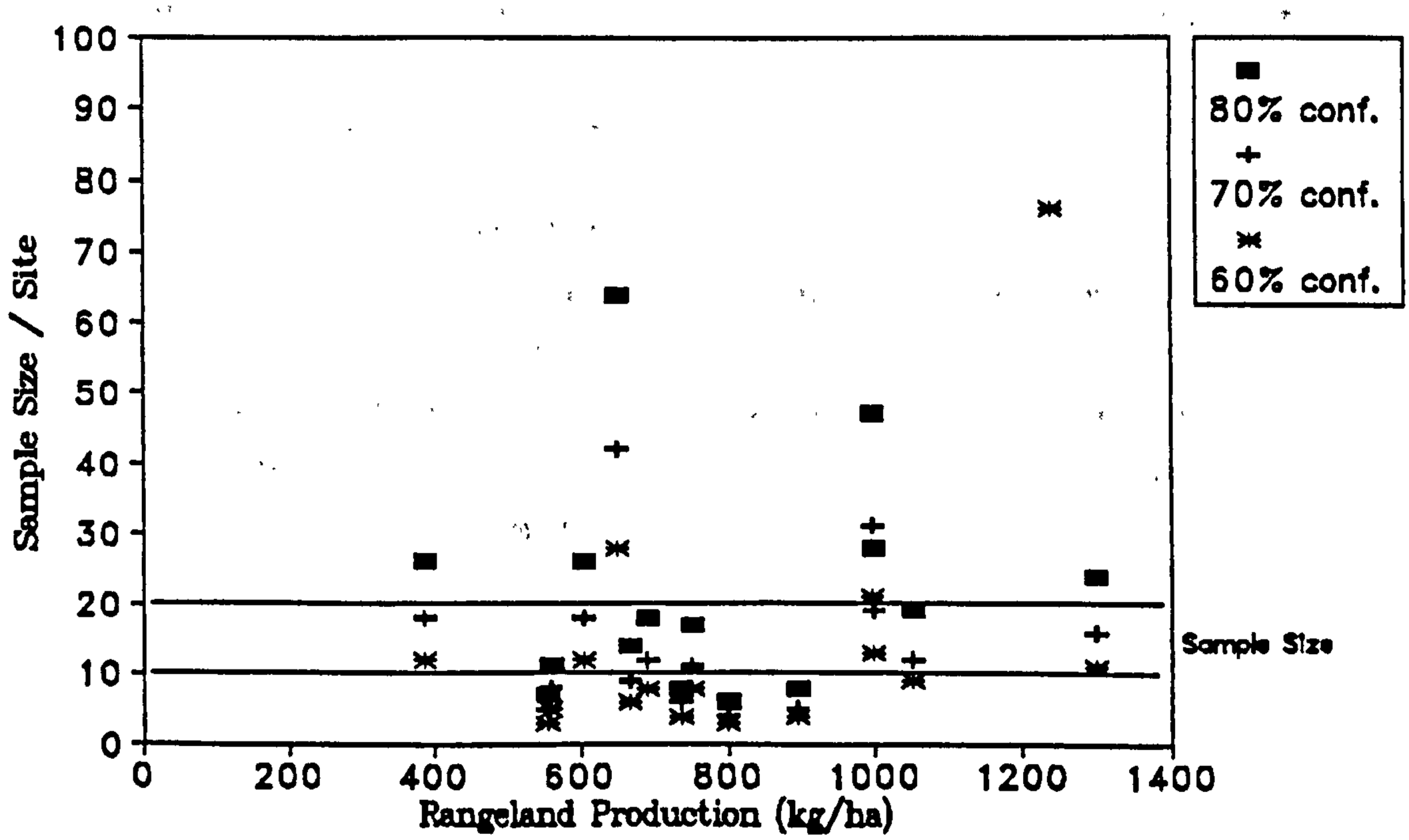


Figure 3.46: Required Number of Samples to Achieve Standard Error of the Mean of ± 150 $kgha^{-1}$ Herbaceous Dry Matter at 60, 70 and 80% Confidence Levels (1989 ITE/Silsoe Sites, 2nd Mission)



The field work compendium confirmed that the maximum number of samples per transect, which could be handled in the field, was about 20. This would allow to estimate rangeland production at an 80% confidence level up to approximately 700 $kgha^{-1}$ herbaceous dry matter quantity. The graphs show that for any higher degree of accuracy, either in confidence or in production class width, the number of samples required inflates beyond attainable sizes.

Assessing the required sample size for the second mission is much less straight forward due to the increase in variation of measurements. Applying a non-linear regression to the data, herbaceous dry matter quantities could be estimated to approximately 1000 $kgha^{-1}$ at an 80% confidence level.

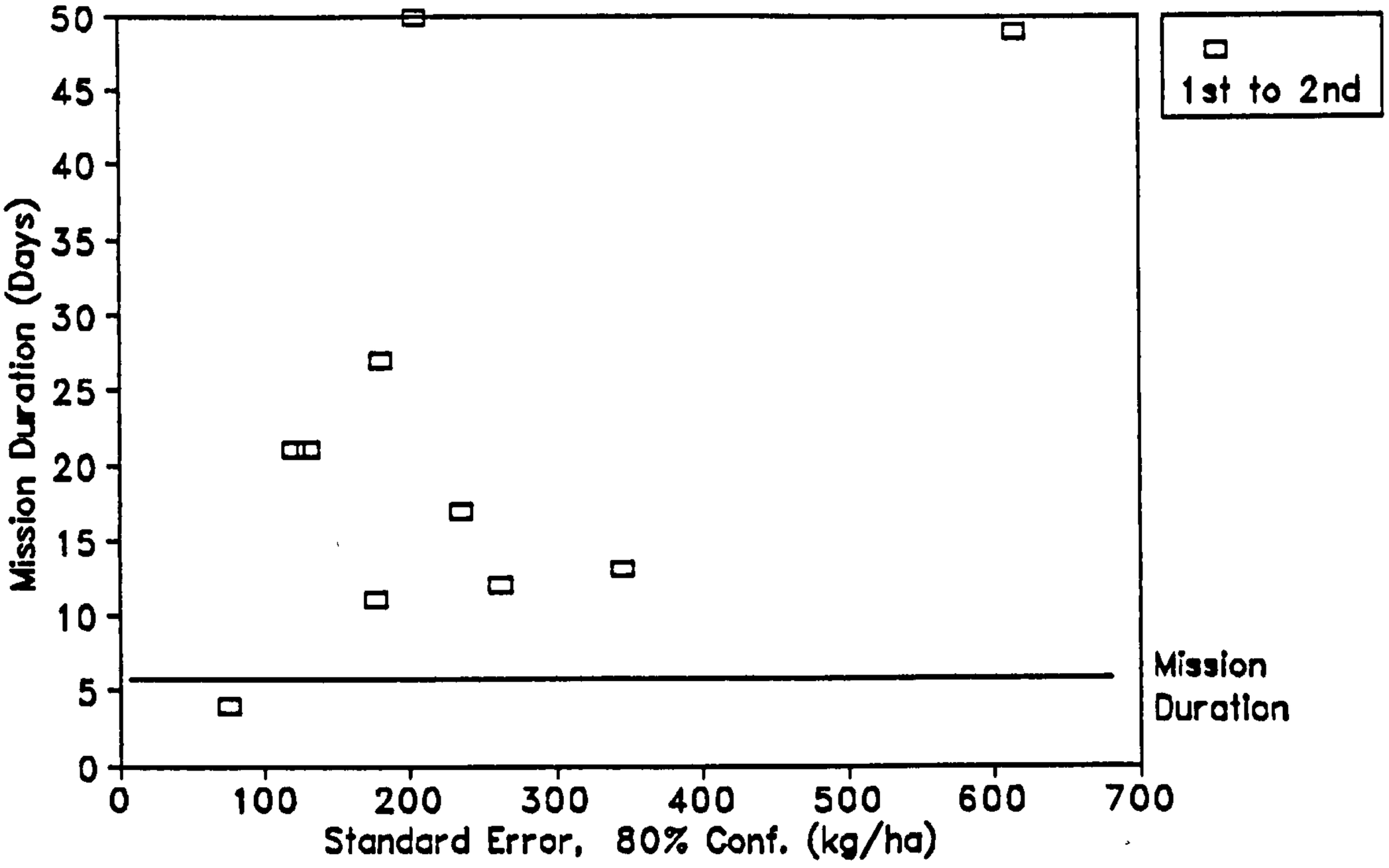
(c) Duration for Sampling Period

The number of days, when the probability that the estimated difference between averages of herbaceous dry matter quantities fell below 20%, ranged between five (Site 10) and 53 (Site 5). A graphical representation of possible mission durations is given in Figure 3.47. These findings can only provide an approximation for the length of the sampling period. Impediments for more accurate estimates were:

i. *Variation of Site Vegetation*

The variation in rangeland vegetation over an area represented by a satellite pixel was not known. It was estimated by the samples standard deviation. Therefore, the length of the sampling period might be over-estimated.

Figure 3.47: Duration of Field Survey Mission (for 10% observed significance level, ITE/Silsoe/CASTE Survey, 1st to 2nd Mission)



ii. *Vegetation Development*

The growth pattern of rangeland vegetation was assumed to be linear. Actual growth, however, occurs in steps and does not represent a continuous increase. Vital portions of the observed advance from the first to the second sampling period may have taken place in less than the 16 days, which lay between the two periods. The permissible extent of the sampling period would then be over-estimated.

iii. *Sample Size*

The computation of the confidence range for the mean was based on a sample size taken during the 1989 survey. In the majority of cases the actual number of samples taken was less than the proposed 20. Consequently, the confidence range is likely to be wider than with 20 samples and the estimated duration of a sampling period too long.

Sensor properties, like spatial resolution and sensor sensitivity, also influence the temporal limits for sampling periods. However, an investigation into demands induced by sensor properties was outside the potential of the survey.

It could be concluded that sampling over a period of six to eight days should not critically degrade the relationship between rangeland vegetation quantities and satellite VIs.

3.5 Integration of Field Survey Results

The growing seasons of 1985, 1988 and 1989 were all very different from each other. While 1985 was one of the driest years of the decade, 1988 was probably the wettest. The rains of 1989 were unusually late in some areas. In order to identify a widely applicable field survey procedure and common trends in herbaceous vegetation characteristics, results from all five field surveys are combined and discussed in this chapter. The findings are summarized in the last section of this chapter and recommended procedure for future field surveys are presented.

3.5.1 Discussion of Field Work Procedures

(a) Selection of Study Areas

A wide range of herbaceous vegetation densities could be collected within the ITE/Silsoe study area and there was no need to identify sites outside the study area. On the other hand, results from sites on the Ibecetene State Ranch cannot be directly compared to those from outside its boundaries. Grazing on the ranch is controlled by fencing off areas and the grazing density is kept low. This results in a markedly higher amount of herbaceous vegetation on the ranch and possibly a different species composition. However, an evaluation of the effect of different grazing activities on calibrating VIs was

outside the scope of this project.
Conditions within the CIPEA and CAZS study area could be assumed to be comparable to those of the ITE/Silsoe region. Only soils were markedly different for CAZS sites (see Chapter 2), but the effect of this could not be established.

(b) **Period of Field Survey**

A comparison to CAZS data suggests that the time of the 1988 ITE/Silsoe survey may have been too late in the season. For many sites the average moisture content fell below 65% despite the rains within two weeks before the survey and the prospect of additional growth.
Because of the delay in the onset of the 1989 rainy season significant increases in growth and the emergence of new, fresh vegetation could be observed for the second half of September. This was a likely cause for the relatively high variation in rangeland production for the first sampling period, which was very different from the second.

(c) **Selection of Sample Sites**

All three ITE/Silsoe field surveys confirmed that it is advantageous to determine individual sites in the field. Then, site accessibility, vegetation uniformity and likely vegetation quantity could be best established. Pre-determination of sites according to a rigid sampling scheme would be unsuitable for a small survey team.

(d) **Positioning of Sample Sites**

The method of using Landsat MSS hard-copies did support the establishment of site positions. In some cases higher resolution images than Landsat MSS provides might have been advantageous. North of Kaou, towards Tchin-Tabaraden, there were no features, which could be identified on the image and ground and identifying site locations had to be based on maps. Even though all team members were experienced in reading images and maps there were disputes and uncertainties about many site locations.

Relying on maps for site identifications can be misleading. The road between Kaou and Tchin-Tabaraden was used to determine site positions along it. But the road was drawn on the map about 2 km to 3 km from its actual position. This was only discovered later when processing the images.
The use of a GPS was found to vastly improve the identification of site positions. Selecting a site can be done on the basis of its suitability for estimating rangeland vegetation rather than chances of determining its position on a map or image hard-copy.
Image hard-copies remain being of importance in identifying homogeneous areas and avoiding spectrally divers regions. They are also valuable in case of technical problems with the system, as experienced.
Generally, it was found that without the capability of locating sample sites at an accuracy of the pixel size of the satellite sensors used, the number of sites can hardly be increased.

(e) Layout of Sampling Method

The layout of the sampling scheme was designed to accommodate for the need of a larger number of ground measurements on the one hand and the restricted number of survey team members and field days available on the other. Identified as the most restricting factor preventing an increase in the number of sample sites was the time required to determine site positions, rather than for example the transect length. Up to two hours were spent in finding suitable sites identifiable on image hard-copies or the map. In comparison, the time required for collecting the samples varied between 45 and 90 min. Consequently, the sampling layout cannot be separates from the method applied for site positioning.
Based on the analysis of variation of herbaceous vegetation the length was extended to 1 km in 1989, which was found to represent an acceptable compromise between including the variation in rangeland vegetation for an AVHRR pixel and practical consideration of walking long distances.

The procedure of the 1988 ITE/Silsoe survey of using only five points did not provide a meaningful estimate of the variation of vegetation densities along the transect. Collecting 20 samples per site was about the maximum number possible and estimates of rangeland production could be improved from 60% to 80% confidence levels for CAZS and the 1989 ITE/Silsoe/CASTE surveys. Any increase in the number of sample sites would require to adopt a smaller area than 1 m x 1 m for measurements.

(f) Acquisition of Site Parameters

i. *Herbaceous Vegetation Samples*

Herbaceous vegetation should have been clipped off over a larger area than 0.25 m². Most of the grass species found grew in form of clumps. By including or excluding such a point of growth the amount of grass found varied between no vegetation and up to 94.3 g of dry matter for 0.25 m².

The 1989 survey verified that 1 m² represented the maximum size of herbaceous vegetation, which could be clipped off by hand in the time available to assess a single site.

ii. *Herbaceous Cover*

Cover could not be directly compared between different surveys and in 1989 not even for the same survey. The error of estimating herbaceous cover could not be established. An additional investigation would have been required, which was outside the possibilities of the project.

Estimating the average vegetation cover and height over just the sampling point (1 m²) was found less demanding for inexperienced observers than estimating average herbaceous vegetation cover over an area of 4 m². A grid over the sample point may have aided estimating cover at lower quantities.

iii. *Soil Background Information*

Assessing soil texture according to a soil texture triangle was straight forward. Sites were located

almost exclusively over loamy sands and sandy loams.
Determining soil colour of a sample site according to a Munsell Colour Chart was found to be both easy and rapid. Differences in soil colour between the two missions were attributed to variations in soil m.c.
A relationship between soil colour and rangeland production has been found, but at a low level of confidence. In order to arrive at a more conclusive result, further work is required.

iv. *Bush and Tree Count*

One observer for counting bushes and trees was found to be sufficient in 1985 and 1988, but not for 1989. Members of the CASTE team found it difficult to count bushes and trees and three team members were required for counting bushes and trees. It was then suggested to reduce the distance for ligneous cover to ± 25 m either side of the transect.
Shrubs smaller than 80 cm could hardly be seen, because of the height of the herbaceous vegetation. The vast majority of bushes and trees were between 2 and 4 m. Trees larger than 8 m were not found. The original four classes could be merged into three with a 2 m class widths.

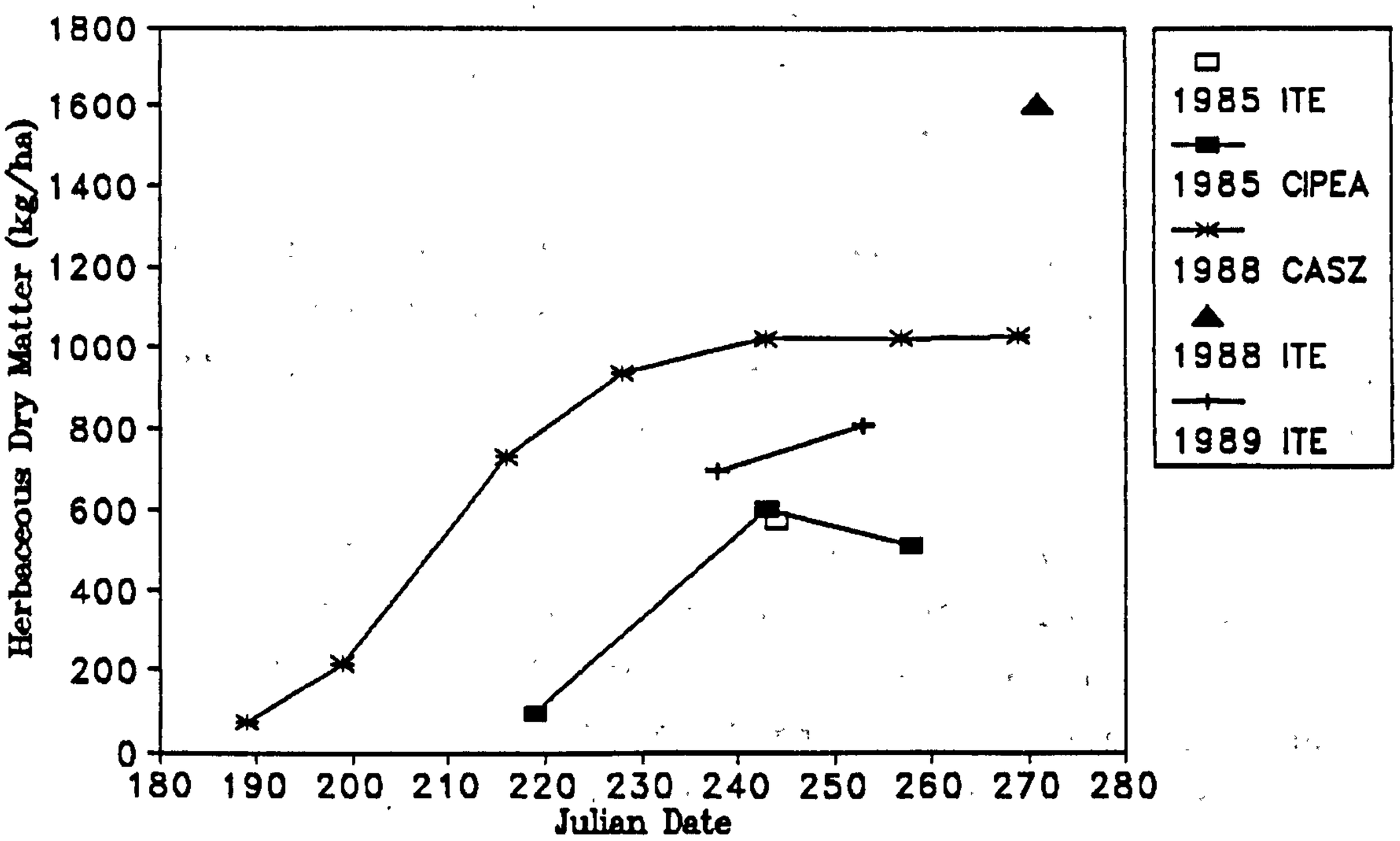
3.5.2 Discussion of Site Parameter Data

In this chapter the feasibility of the applied procedure for sampling rangeland vegetation in the Sahel is being investigated. The methodology is discussed under the aspect of forming a basis for future field operations.

(a) **Rangeland Production Levels**

A comparison of average herbaceous vegetation quantities from 1985, 1988 and 1989 for corresponding sites is graphically presented in Figure 3.48.

Figure 3.48: Comparison of Herbaceous Dry Matter Quantities of 1985, 1988 and 1989 ITE/Silsoe Field Surveys in Niger



The average amount of herbaceous vegetation was plotted against the date of its acquisition. It is worth noting, however, that none of the sampling procedures was based on a random sampling scheme. Hence, average overall production levels are not directly comparable.

With an average of 568 $kgha^{-1}$ herbaceous dry matter (vegetated sites only) for the 1985 ITE/Silsoe and 599 $kgha^{-1}$ for CIPEA sites of the second sampling period, rangeland production corresponded well for the two surveys.

For Mali, the average dry matter production at the end of the monitoring period was 1021 $kgha^{-1}$. This is substantially lower than the quantities found in Niger, where the average herbaceous production of all transects was 1604 $kgha^{-1}$.

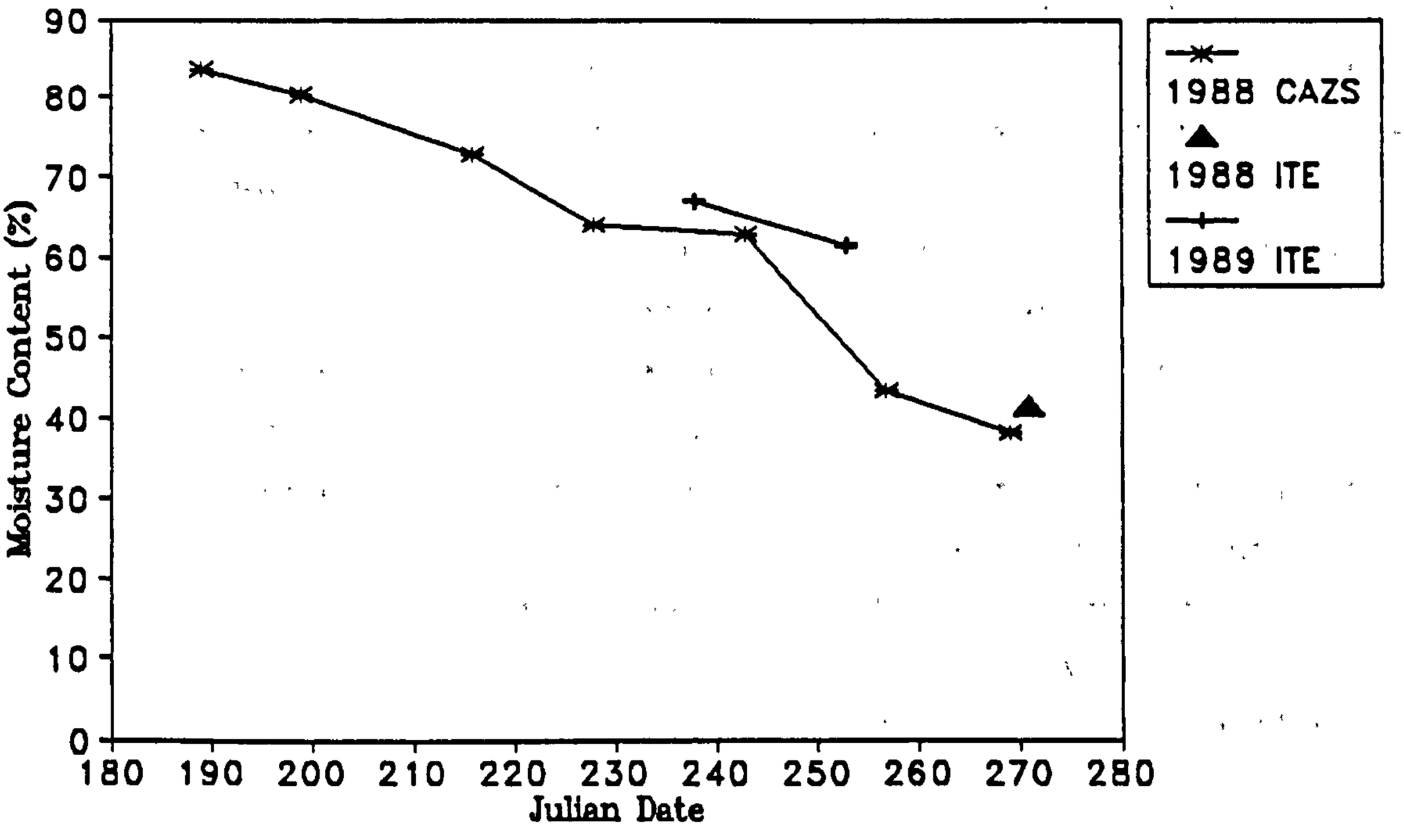
There was a noteworthy bias towards higher production levels for the Niger sites, caused by the location of sites within the Ibecetene State Ranch. There, grazing densities are controlled and rangeland vegetation quantities were found to be significantly higher than

outside the ranch boundaries. When excluding sites on the ranch an average dry matter production of 694 $kgha^{-1}$ was estimated.
For the 1989 ITE/Silsoe field survey dry matter quantities averaged 640 $kgha^{-1}$ for the first and 812 $kgha^{-1}$ for the second mission for sites visited twice.
The figures indicate that vegetation quantities were approximately twice as high in 1988 compared to 1985. Furthermore, they suggests that rangeland production of the 1989 growing season (700 $kgha^{-1}$) was in between 1985 and 1988.
In contrast to previous surveys stands a significant growth for the second mission in 1989, which could not be observed in 1985 and 1988. An explanation may be the late arrival of substantial rainfall across the study area with the consequence of shifting the general growing pattern backwards.

(b) Vegetation Moisture Content

The m.c. of herbaceous vegetation was only available for 1988 and 1989 surveys. A comparison between average herbaceous vegetation m.c. of each mission from the 1988 CAZS and ITE/Silsoe and the 1989 survey is graphically displayed in Figure 3.49. For Mission 7 of the Mali survey the average from all sites was 43.3% and for ITE/Silsoe 41.5%. An analysis based on the moisture content of individual sites of a transect, as carried out for Niger, was not possible for the Mali sites, since only the average moisture content for a transect was available. In 1989 the average m.c. of herbaceous vegetation for the first sampling mission was 67.4% and 62.0% for the second mission for the sites visited twice. These findings suggest that analogous conditions to September 1989 existed in 1988 one month earlier, at the beginning of August. They also indicate that the m.c. of herbaceous vegetation after the peak of the growing season can be expected to influence VIs and, consequently, calibrations between ground and satellite data.

Figure 3.49: Comparison of Herbaceous Vegetation Moisture Content of 1988 CAZS and 1988 and 1989 ITE/Silsoe Field Surveys



All surveys indicate that VI values from satellite data acquired during latter stages of a growing period are lower than those obtained earlier on in the season for the same amount of vegetation due to the smoothing effect of senescence on vegetation profiles.
In addition, for Mali and Niger sites of 1988 the moisture content was found to depend on the quantity of rangeland vegetation present. The direction of the relationship depended on the scale of observations: Within sites it was positive while it was negative for the whole study area. However, the relationship was not stable over time and also changed from being positive at the beginning of the season to becoming increasingly negative towards the end. For ITE/Silsoe site a non-linear regression revealed that about 50% of the variation in the data could be attributed to changes in the vegetation moisture content. The observed relationship between DM and m.c. will render more difficult the detection of vegetation with less than approximately 30% ground cover. As a consequence, the

accuracy of the calibration of VIs to rangeland production can be expected to be affected unfavourably. In 1989 no such relationship was found, neither for individual sites nor for site averages. This does not mean that a relationship has been ruled out, only that it could not be confirmed. The cause may be found in the distribution of precipitation during the 1989 growing season. Rainfall in September over some areas stimulated additional growth and increased the diversity of fresh vegetation across the range of dry matter quantities. The discrepancy of inter-site and intra-site relationship between vegetation moisture content and dry matter production clearly reveals that a relationship between two parameters may be much more complex and inconsistent at disparate scales. This may be of more significance when employing a satellite with a higher resolution than NOAA AVHRR or Landsat MSS over rangelands.

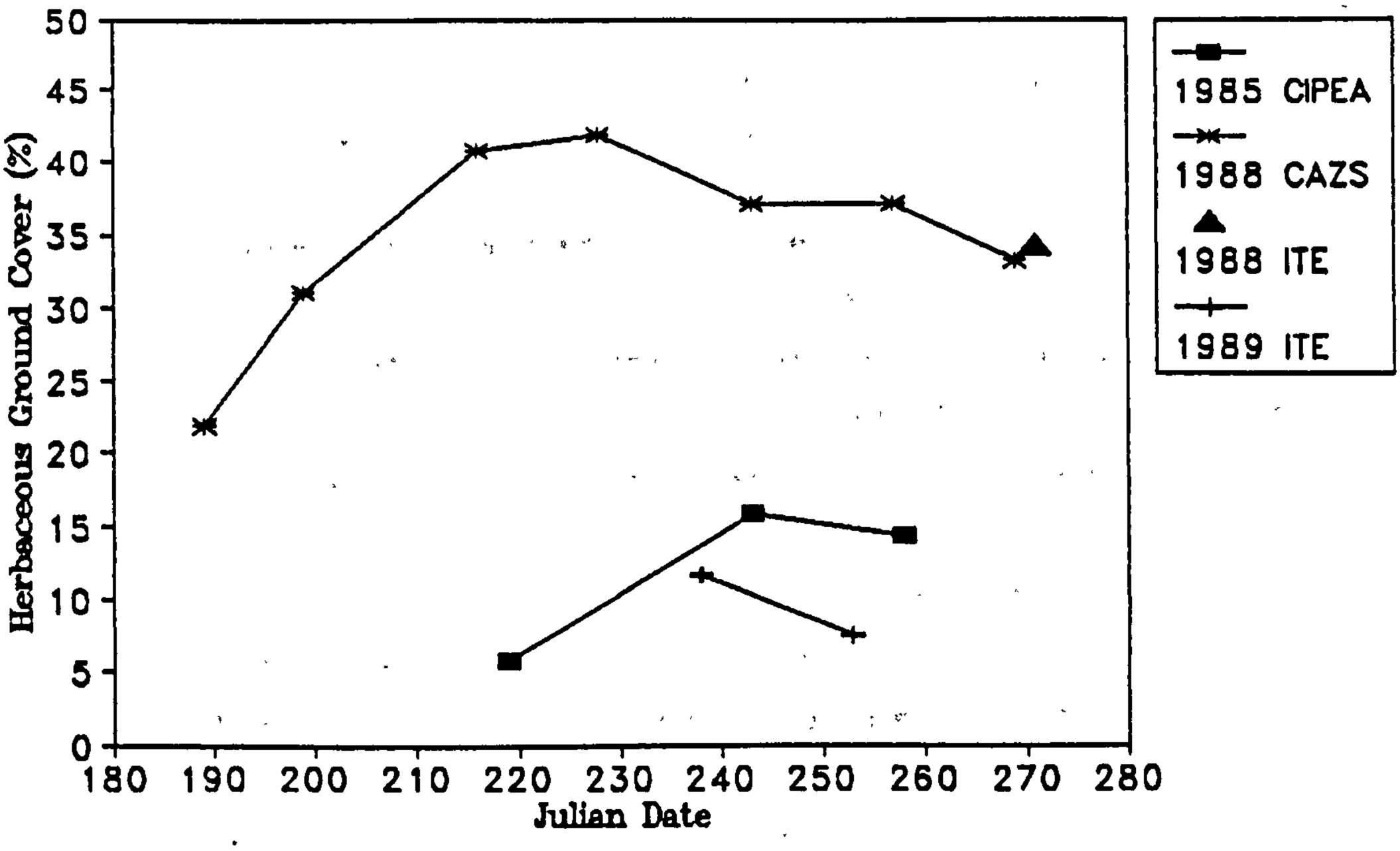
(c) Herbaceous Vegetation Cover and Height

For 1985 herbaceous cover is only available for CIPEA sites. The average of all sites was 16.9% for the second sampling period, which was conducted at a time comparable to the ITE/Silsoe survey. More than twice as much cover was reported from the 1988 surveys. The average for Mission 7 in Mali was 37.1% and 34.2% for ITE/Silsoe sites. Average cover of the 1989 season (11.6% for 1st mission, 7.5% for 2nd mission) ranged below all surveys.

The development of cover over time is graphically represented in Figure 3.50.

These findings suggest that cover data collected from the same growing season may be comparable, but that the transfer of values from one year to another may be problematic.

Figure 3.50: Comparison of Herbaceous Vegetation Ground Cover of 1985 CIPEA, 1988 CAZS and 1988 and 1989 ITE/Silsoe Field Surveys



(d) Ligneous Cover

The number of bushes and trees counted during the 1988 ITE/Silsoe survey were comparable to those established in 1989 for the second mission and identical sites. On average between 3 and 13 bushes and trees were found per ha. Trees mainly covered less than an area of a 4 m diameter, consequently, ligneous vegetation covered less than 0.4 to 1.6% of the area as seen by a satellite. Although this accounts for a very small contribution to the over-all cover, the effect on the VI may be unproportionally higher due to the dissimilar development pattern in photosynthetic activity between herbaceous and ligneous vegetation. Ligneous vegetation usually remains photosynthetically active after the rains have subsided and herbaceous vegetation matured (Defourny, 1989). This may be of particular significance at the very beginning and the end of the wet season. Also, the spatial distribution of bushes and trees is not even. Growth is concentrated in areas with a higher soil moisture content, like river valleys and

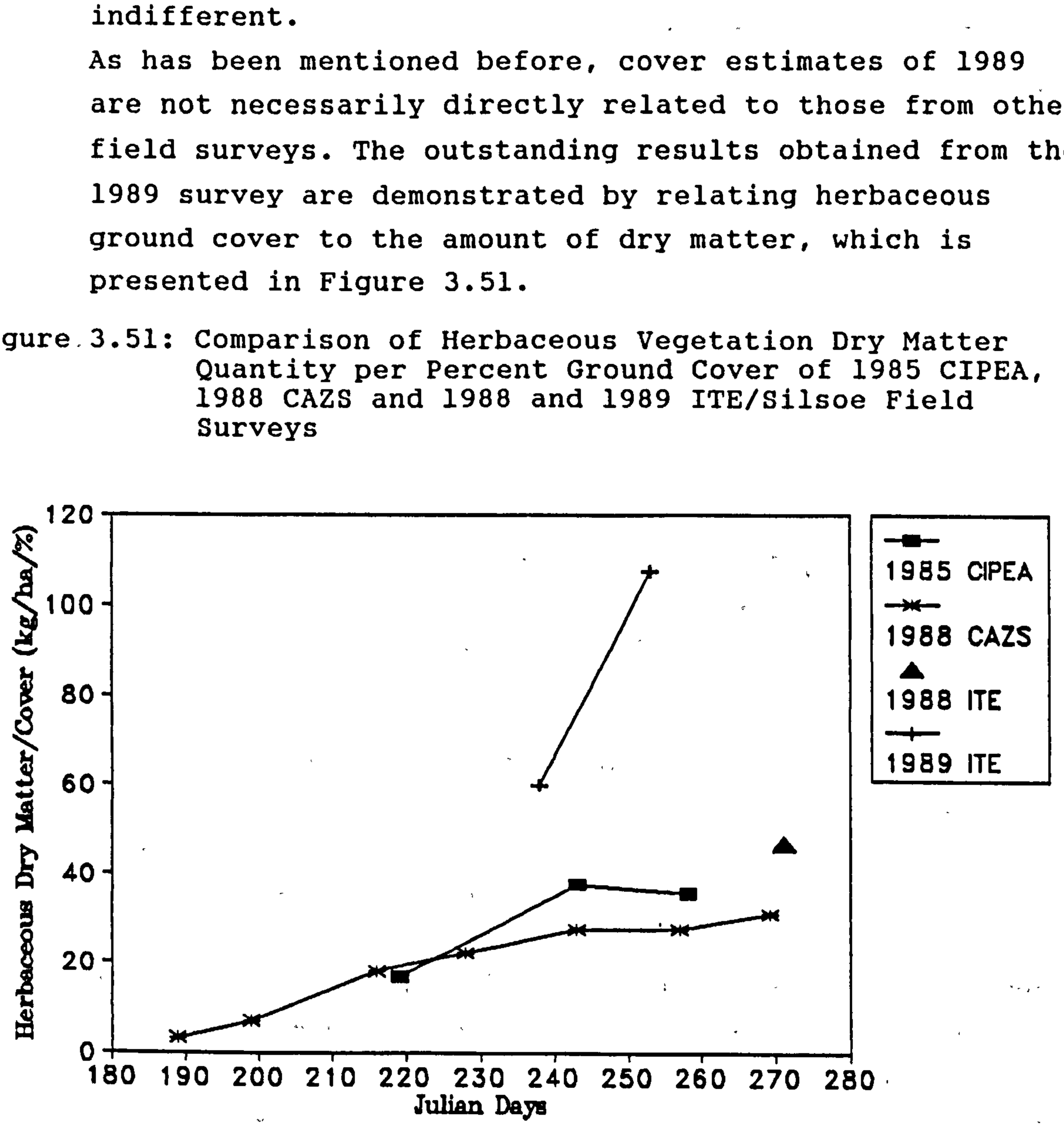
depressions, which were not included in the survey. On an image these areas of dense ligneous vegetation can be distinguished from grassland by their higher reflectances in the NIR portion of the EM spectrum. This results in high VI values and over-estimates for the amount of herbaceous vegetation.

(e) Herbaceous Dry Matter vs. Cover

Quantities of herbaceous rangeland vegetation were closely related to cover in areas of sparse vegetation growth or below approximately 1000 $kgha^{-1}$ dry matter. At higher amounts of vegetation the relationship became indifferent.

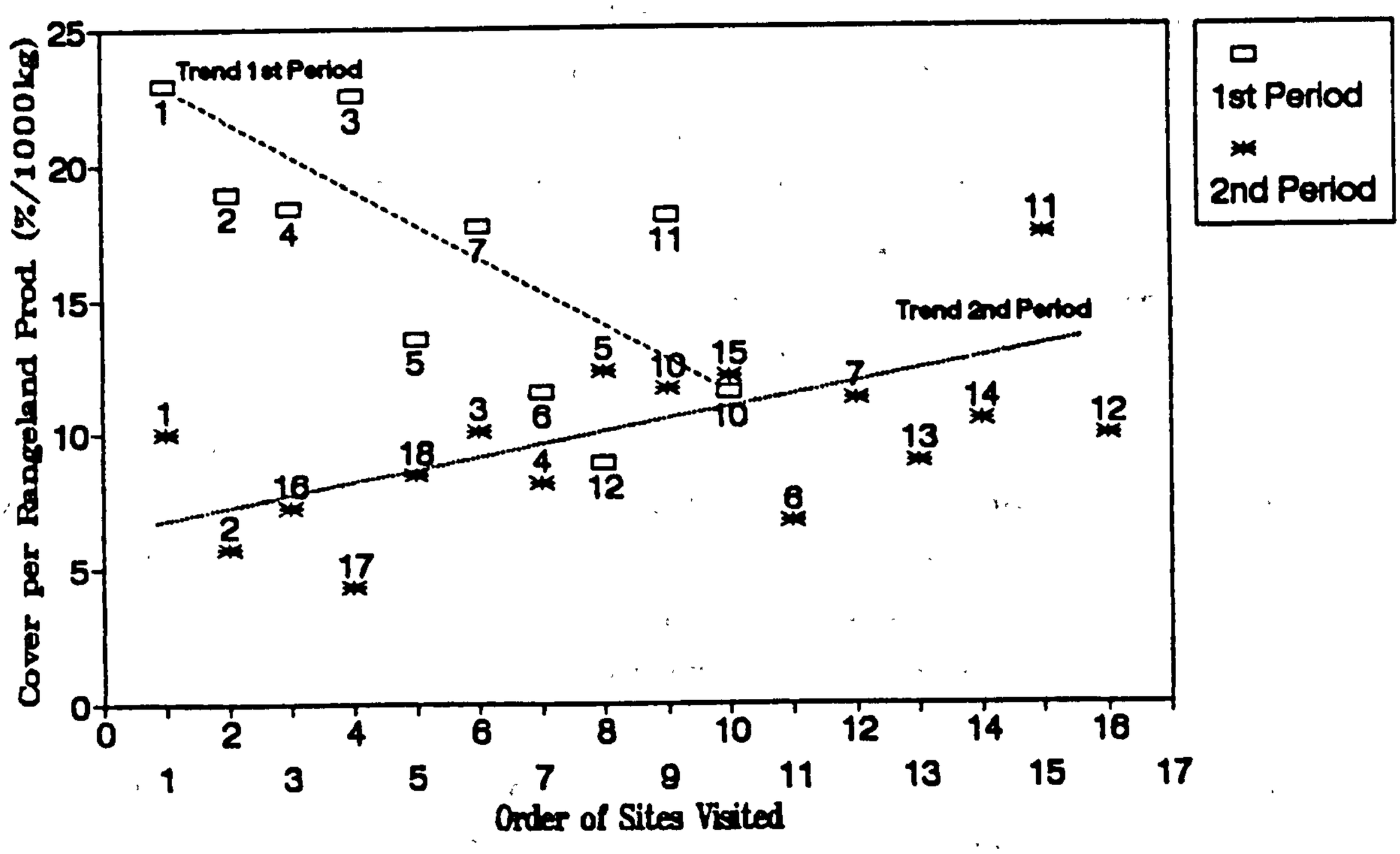
As has been mentioned before, cover estimates of 1989 are not necessarily directly related to those from other field surveys. The outstanding results obtained from the 1989 survey are demonstrated by relating herbaceous ground cover to the amount of dry matter, which is presented in Figure 3.51.

Figure 3.51: Comparison of Herbaceous Vegetation Dry Matter Quantity per Percent Ground Cover of 1985 CIPEA, 1988 CAZS and 1988 and 1989 ITE/Silsoe Field Surveys



It reveals that, although the growing seasons of 1985 and 1988 were very different, the amount of vegetation produced per percent cover are comparable between the various surveys. Results from the 1989 survey deviate from the trend indicated by other surveys. Therefore, the development of cover over time independent of the spread of rangeland production was investigated. The result is presented in Figure 3.52.

Figure 3.52: Development of Percentage Cover per 1000 kg of Rangeland Vegetation



For sites with comparable quantities of vegetation (Sites 1, 2, 3, 4, 5, 6 and 12) a steady decrease in cover per phytomass can be observed. This development is repeated from Site 7 to Site 10 at an almost identical rate.

These results suggest a change in judgment by observers as to the amount of cover present over the span of the first period. The trend could not be found for the second one. The steady increase of cover with rangeland vegetation quantities presented in Figure 3.52 could then be explained as being a product of the order, in

which vegetation quantities were collected, because the higher quantities were observed first.
The gradual increase of cover with quantities of rangeland vegetation may or may not have been actually present in the field. In any case, cover estimates from the first sampling period are to be treated with caution. Yet, without objective measurements the cause of the trend is not free from speculation.

(f) **Herbaceous Dry Matter vs. Number of Bushes and Tress**

For grassland a positive relationship between herbaceous dry matter production and ligneous vegetation could have been expected. Trees and bushes tend to grow in areas of higher soil moisture content and there the growth of herbaceous species should also be encouraged, as long as there are wide spaces in between (Savanna grassland). None of the three surveys with a count of ligneous vegetation gave any indication of a relationship to herbaceous dry matter quantities assessed at a site.

(g) **Accuracy Assessment**

A comparison of the accuracy of estimating the average herbaceous dry matter quantity between the various surveys was hampered by the differences in sampling vegetation. In particular the confidence level is dependent upon the number of samples collected per site. The number of samples required to estimate the average amount of rangeland vegetation (1500 $kgha^{-1}$) at an 80% confidence level was approximately 40 for both surveys of 1985. For Mali sites in 1988 a number of 20 samples would have been sufficient to achieve that level with the exemption of mission 5. There, 40 samples were needed. A similar number is suggested by findings from the 1988 ITE/Silsoe survey. With a number of 20 samples per site the amount of herbaceous vegetation could be estimated up to at least four fifth of the sample mean for all surveys. It is worth noting that the average dry matter quantity from a survey is not representative for the whole study area, since it was intended to sample over a range of vegetation quantities of a growing

period, while the distribution of quantities within the study area was not considered.

The comparison of data from the four field survey expeditions generally confirmed the prominent differences between the 1985 and 1988 growing seasons and similarities of data from the same season, but different area (Niger and Mali).
Summarizing the results of comparing the main characteristics of the five surveys investigated it can be stated that the dynamic and inconsistent nature of Sahelian rangeland vegetation was pronounced. The term *temporal stability* in association with the calibration of remotely sensed data demands a generous interpretation.

3.5.3 Conclusions and Implications for Future Field Surveys

From the results obtained from individual sites of a specific survey and from comparisons between surveys the following conclusion can be drawn:

(a) **Realisation of Survey Objectives**

- *Acquisition or Rangeland Vegetation Estimates*
  All five surveys provided estimates of the maximum amount of herbaceous rangeland vegetation of a growing season and area.

- *Estimation of Temporal Stability of VI Calibration*
  Assessing the temporal stability of VI calibrations relied on the ITE/Silsoe surveys, since only there samples were acquired over several seasons within the same study area. However, in 1988 it was not possible to find a range of production levels that would overlap with the 1985 levels. The consequence is that the regression between phytomass levels and satellite sensor response established in 1985 cannot be directly compared to the 1988 regression. There is still a need to investigate the temporal stability of vegetation developments over the study area.

- *Estimation of Spatial Stability of VI Calibration*
  The spatial variability could only be established for single years, but not successive seasons. Thus, it cannot be stated with certainty, to what degree and spatial extent results from this project can be transferred to other regions in the Sahel and additional investigations over different regions of the Sahel are required.

(b) **Field Survey Design**

- *Peak of Growing Period*
  The maximum amount of DM could be expected in mid-September for the study area with a probable variation of 2 weeks.

- *Mission Duration*
  A survey mission should be completed within six to eight days.

- *Transect Length*
  A 1 km transect has been found preferable to 500 m and 2 km ones.

- *Positioning of Sample Sites*
  The use of a lightweight, portable GPS can be considered essential for collecting ground data in the Sahel, when time is a limiting factor for the survey. Maps have been proven unreliable and the use of high resolution images depends on a pre-selection of sites in order to keep number and size of hard-copies within manageable limits.

- *Sample Size per Transect*
  A minimum sample size of 20 points per transect is needed to estimate rangeland production to within ± 150 $kgha^{-1}$ standard error of the mean up to 1500 $kgha^{-1}$ herbaceous dry matter quantity of a season at an 80% confidence level. The actual limit depends on the season and the time of sampling.

- *Measurement Area*
  An area of 1 m² was found better suited to local variations than 0.25 m².

- *Determination of M.C.*
  Air-drying of samples was found to be preferable to using a moisture meter. A m.c. of 7% ± 0.5% can be expected. The equilibrium m.c. will have to be verified by oven-drying sub-samples.

- *Herbaceous Cover*
  A reliable and rapid method of estimating herbaceous vegetation cover still has to be identified, which could be used successfully by less experienced survey team members.

- *Bush and Tree Count*
  A limit of 25 m either side of the transect was found advantageous over a 50 m distance for less experienced users. A grouping of bushes and trees according to three classes with 2 m intervals could be applied.

(c) Site Parameters

- *Intra-Seasonal Stability of VI Calibration*
  A single date calibration may not be applicable to the whole growing season. The continuing process of senescing and emerging vegetation can be expected to affect VIs derived from satellite data.

- *Cover*
  An appreciable amount of soil background information (> 50%) is present in satellite data even at relatively high levels of vegetation (> 2000 $kgha^{-1}$).

- *Herbaceous DM vs. M.C.*
  There is a strong relationship between vegetation quantity and moisture content. At the end of the growing season the relation is generally positive at the scale of a whole transect. The moisture

content drops significantly below 60% particularly for sparse vegetation during September. As a consequence, low vegetation quantities may be difficult to distinguish from soil by satellite sensors from imagery acquired even before September.

- *Herbaceous DM vs. Cover*
  The contribution of the soil background information is very variable and unpredictable at levels of more than approximately 800 $kgha^{-1}$.

- *DM vs. Munsell Soil Colour*
  A relationship between quantities of herbaceous vegetation and soil colour may exist, but could not be verified for more than three classes.

(d) **Recommendations for Future Field Survey**

A summary of recommendations based on the five field surveys is provided in Table 3.11. Additional aspects to be considered for field surveys are:

- *Study Area*
  For an assessment of the spatial validity of a VI calibration at least two study areas are required, where ground data are collected using the same sampling scheme.

- *Selection of Sample Sites*
  For new sampling sites a pre-selection could be applied by using satellite VI images. Landsat MSS data is available from four years (1984, 1985, 1988 and 1989). By comparing VI images areas of homogeneous growth and their distribution may be evaluated. The final decision remains with the field observation team.

- *Herbaceous Dry Matter Estimates*
  The survey should investigate possibilities of implementing a combination of measurements and estimates, similar to the CIPEA survey.

- ***Herbaceous Ground Cover Estimates***
  It is proposed to supply a guide-line to survey teams by providing photographs for a range of ground cover values, similar to estimating vegetation quantities.

Table 3.11: Summary of Recommended Field Survey Sampling Scheme

Field Survey	Established from Survey	Recommended Sampling Layout
1984 Field Visit ITE/Silsoe	Study Area	Niger, 5.5°E 15.5°N
1985 Field Visit ITE/Silsoe	Sampling Period	Twice in September
	Site Criteria	Stratify area: ■ homogeneous soil ■ uniform vegetation
1985 Field Visit CIPEA	Site Selection	Fulfil site criteria Accessibility Representative range Identifiable position
1988 Field Visit ITE/Silsoe	Sampling Layout Sample Size Sample Area	Transect, 1km length 20 samples/transect 1m x 1m square fixed intervals
1988 Field Visit CAZS	Site Characteristics	■ Herbac. Vegetation - dominant species - fresh weight - cover - height ■ Soil - texture triangle - Munsell colour ■ Ligneous Vegetation - dominant species - number ± 25m
1989 Field Visit ITE/Silsoe/CASTE	Drying Method	Air-drying for 5 days oven-drying samples
	Accuracy	± 150 $kgha^{-1}$ at 80% confidence level

4. IMAGE PROCESSING

This chapter focuses on the steps of data processing required to produce calibrated maps of herbaceous rangeland vegetation in the Sahel at the end of the growing season.
Before utilizing the recorded response of satellite sensors to incident EM energy reflected from the earth surface for the purpose of comparing different sensors or for calibrating it to ground features, a common reference basis has to be established. The methods applied for transforming Landsat MSS and NOAA AVHRR data to comparable units were largely determined by the amount of supplementary information, for example visibility for an atmospheric correction. In addition, the need to minimize user interaction was recognized, considering the constrains for operational rangeland monitoring systems in the Sahel.
Furthermore, the techniques employed for data adjustments are closely linked to the equipment available. For this project the standard software accessible was insufficient to handle or analyse 10 bit NOAA AVHRR data. Only the initial image screening for clouds and coverage and geometric corrections were performed on the image processing system. All subsequent analysis was carried out on PCs. Where not explicitly stated the routines and programmes applied were developed by the author.
In the first part of this chapter the developments and results of the pre-processing techniques applied for this project are presented. For each step one method, which was considered the most suitable and applicable, was selected on the basis of results presented in the literature. Details on principals, terminology, units, physical and mathematical concepts of pre-processing procedures are provided in Chapters A3 to A5 of Appendix I.
The second part contains conclusions about the data conversion methods applied for Landsat MSS and NOAA AVHRR data.

4.1 Available Satellite Data

For each of the three study areas (CIPEA, CAZS and ITE/Silsoe) satellite data from both Landsat MSS and NOAA AVHRR were available. A list of images available is given in Table A.20 in Appendix II.

(a) **Landsat MSS**

For three field surveys (ITE/Silsoe 1985, CAZS and ITE/Silsoe 1988) one Landsat MSS image acquired in the second half of the growing season was to hand. For CIPEA sites only a portion (eight sites) were covered by Landsat MSS data at the time of the field survey.

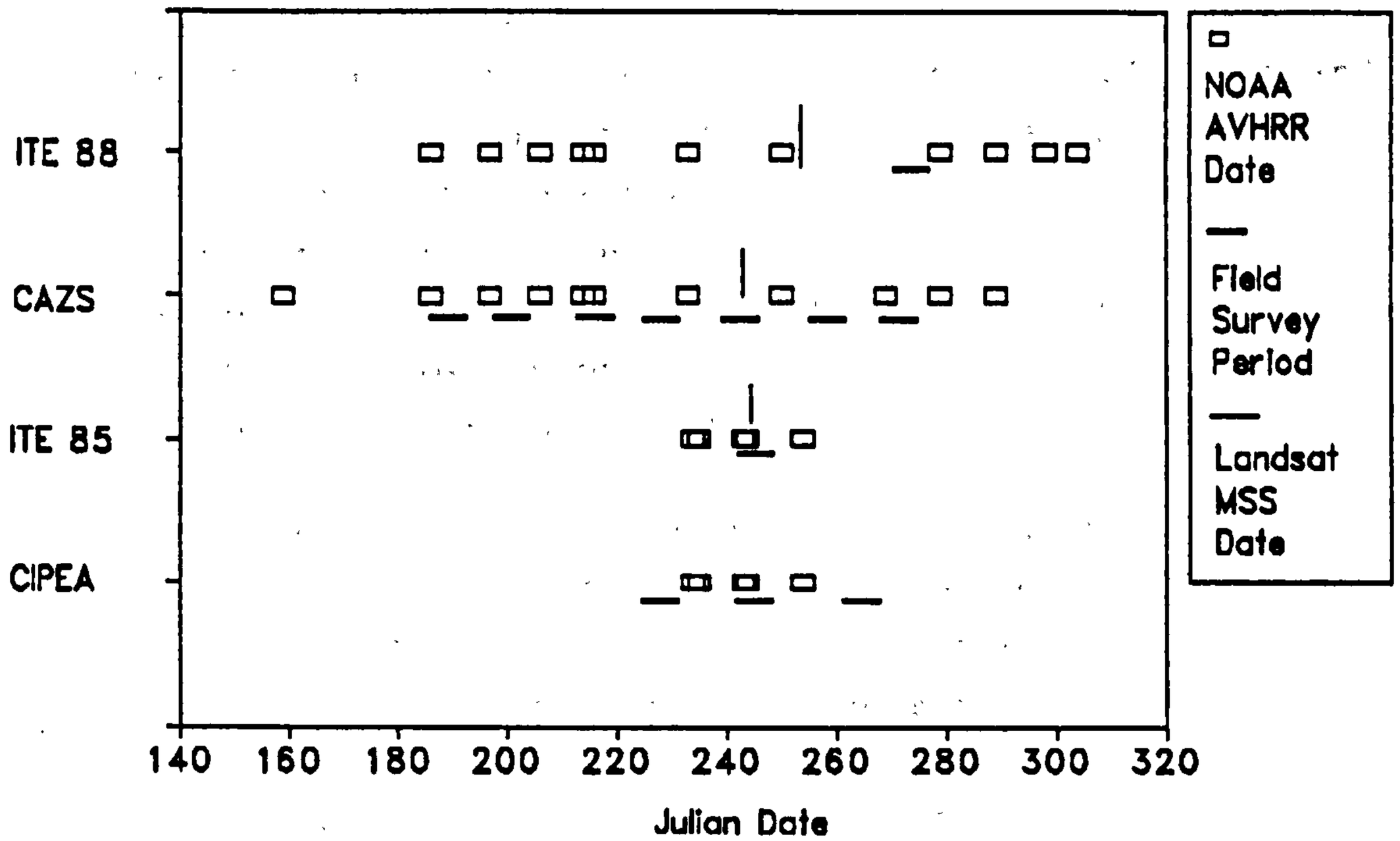
(b) **NOAA AVHRR**

For 1985 five out of 14 NOAA AVHRR images were found suitable for correlating ground to satellite data. The images were acquired within three weeks and only one 10-day composite could be produced. The 1988 growing season was also covered by 14 NOAA AVHRR images. Yet, the temporal spacing does not allow the creation of any MVCs.

In many cases, however, images had to be rejected, because of cloud cover or ground surveys sites were situated too far off-centre (see Table A.20, Appendix II). A ± 20° limit of the scan angle, which would support reducing off-nadir viewing effects (Holben, 1986) could not be applied. For 1985 that would have resulted in three images for the whole growing season of the 12 images obtained. Instead, all images were considered where the study areas were within 600 pixels from the nadir, which corresponds to a scan angle of approximately 35°. At this distance from the nadir VIs were found to be influenced by the viewing geometry (see Chapter A4, Appendix I).

A graphical presentation of the distribution of satellite data used for the project is given in Figure 4.1.

Figure 4.1: Temporal Distribution of Landsat MSS and NOAA AVHRR Satellite Data for CAZS, CIPEA and ITE/Silsoe Field Survey Areas



4.2 Data Format Transformation

For reading and storing Landsat MSS data a standard utility was available on the host computer. For NOAA AVHRR tapes a data transformation routine had to be developed for the project. Since non-standard procedures had to be used in order to process 10 bit data, the methods developed are presented.

(a) Landsat MSS Data Transformation

On board the Landsat platform the representation of the analog MSS sensor response to incident EM radiation was represented by 6 bits and later distributed as 7 bit data (see Chapter 2). When comparing Landsat MSS and NOAA AVHRR data it may be worth mentioning at this point that although 8 bit data is processed, the radiometric resolution of MSS is 7 bit at the most. This may produce

a false impression of radiometric sensitivity of Landsat MSS data.

(b) **NOAA AVHRR Data Transformation**

Because no routine for reading the file format was available a programme was written by Mr. M.J. Stuttard, which allowed unpacking the data. It was later modified by the author to obtain data at the full 10 bit radiometric resolution.

The images used were acquired by the afternoon pass of NOAA-9. Because the orbital path is north-bound images had to be rotated by 180 degrees.

As a consequence of inadequacies of the image processing system to operate on 10 bit data an alternative method of analysing satellite data had to be developed. The only data adjustment procedure carried out on the image processing system were geometric corrections. Then, all necessary information was transferred to personal computer systems (PCs).

As a result of the data transfer from an image processing to a sole data analysis system visual representations of the whole study area were not available.

4.3 Cloud Masking

The procedure employed for cloud masking was based on a reflectance threshold in a visible waveband (Robinon, 1985). A similar method is used in an operational system of the Foreign Crop Condition Assessment Division (FCCAD) of the U.S. Department of Agriculture's Foreign Agricultural Services for NOAA AVHRR data (Phillipson & Teng, 1988). Temperature threshold within channels 4 and 5 (Tucker *et al*, 1982; Saull, 1985) were not considered, because it was intended to reduce the amount of data required and to apply comparable methods to both NOAA AVHRR and Landsat MSS images.

For each image a threshold value for cloud masking in the red waveband (band 2 for Landsat MSS and channel 1 for NOAA AVHRR) was established. The threshold value was based on radiometer

measurements on the ground of surfaces of bare soil (Taylor *et al*, 1986; Bolle, 1988) and image inspection. The highest values of spectral reflectances at ground level found were approximately 20% (only site averages were available). On images the highest values observed were for desert sands in forward scatter direction, which corresponded to 30% spectral albedo at the top of the atmosphere. Apparent spectral albedo from clouds was typically 30% or more. At this stage no atmospheric correction was applied, because most of the interaction between incident EM and atmospheric particles occurs below the altitude of cloud tops. The threshold value was then set to 30% apparent spectral albedo for NOAA AVHRR channel 1 spectral albedos. For Landsat MSS images haze and clouds could be clearly distinguished from surface features at apparent spectral reflectances of 25% or more in band 2. Therefore, the threshold value was set at 25% for Landsat MSS images.

Sub-pixel sized cloud cannot be detected reliably by this method. For these the use of a local variation indicator was suggested (Gutman *et al*, 1987; Kaufman, 1987; Singh & Saull, 1988). Hence, for each sample site the C.V. of the sensor response over 3 by 3 pixels at 1.1 km resolution was established. The presence of sub-pixel clouds could then be detected by an increased local variation.

For Landsat MSS the C.V. was based on pixel values found along a transect. The image sampling width was restricted to one pixel either side of a transect.

Tables A.65 to A.67 in Appendix II provide a graphical presentation of the number of samples left for correlating ground to image data after cloud screening.

For both 1985 field surveys cloud cover considerably affected data from NOAA AVHRR. In particular images acquired at the 22 and 30 August had most of the sampling areas under total or partial cloud cover. For 1985 ITE/Silsoe sites the threshold in the red waveband coincided well with the local variation in that waveband. This cannot generally be said for CIPEA sites. Site 2, for example, was cloud free at all dates but displayed a strong local variation. Investigating the site on a Landsat MSS image revealed the site to be situated in an area of very

diverse surface cover types (sand dunes and river).
For 1988 images cloud cover seemed to have been much less problematic than for 1985. More images were available so those widely covered by clouds could be rejected. Only the image acquired at 24 July for CAZS and 20 August for ITE/Silsoe/CASTE sites indicated cloud cover over some sites.
The use of local variation for identifying partial or sub-pixel size cloud cover was hampered by the temporal spacing of satellite data. Within a rapidly changing region, like the Sahel during the growing season, a two-weekly interval of data acquisition does not allow to distinguish variations caused by sub-pixel clouds or surface conditions.

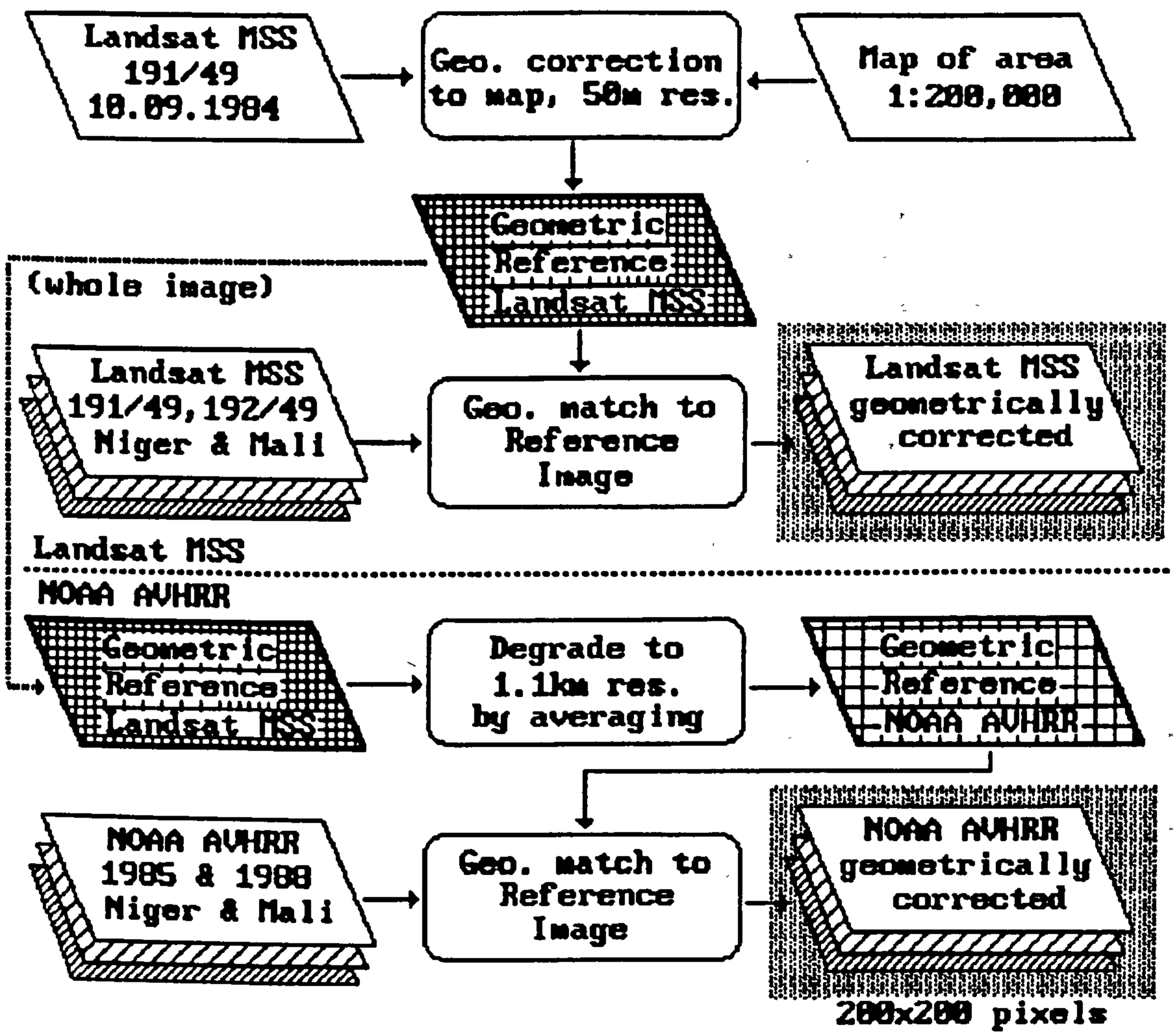
4.4 Geometric Correction

The method employed for transferring image pixel positions to a map projection was solely based on GCPs (for further details see Chapter A3, Appendix I). The basis for obtaining geometrically corrected Landsat MSS and NOAA AVHRR scenes, which would be correlated to ground survey data, was founded on a set of processed Landsat MSS reference images. A graphical description of the methods applied is given in Figure 4.2.

(a) **Geometric Correction of Landsat MSS Data**

For each of the three study areas Landsat MSS images were available. Maps of the study areas were at hand at a scale of 1:200000. The accuracy of establishing co-ordinates on the maps available was assumed to be 0.5 mm. This corresponds to 100 m for features on the ground. A higher accuracy of identifying map co-ordinates was considered as being unlikely, since some maps were only available as photocopies. Landsat MSS images were registered to maps with an rms error of less than 1 pixel position for Niger sites and less than three for Mali. The larger error in the latter originated from greater obstacles of identifying GCPs (unfamiliarity with the area and images with very low contrast).

Figure 4.2: Method of Geometric Correction of Landsat MSS and NOAA AVHRR Images



The images were resampled to 50 m resolution using a 1st order polynomial and nearest neighbour resampling technique (see Chapter A3, Appendix I).
In order to reduce variations between multi-temporal data caused by differences in the geometric representation, for each of the three study areas only one Landsat MSS image was directly related to maps. All other images were matched to those three references. This was necessary because features north of approximately 15° N were found to be very difficult to identify on maps and vice versa. The soils within the ITE/Silsoe study area were relatively uniform and the identifiable dark lateritic rock around Kaou was frequently under cloud (see Chapter 2.1). It was,

therefore, assumed that image-to-image matching would result in greater correspondence between scenes than individual image-to-map matching. Another advantage of this method is that it can be carried out in a fraction of the time.

(b) **Geometric Correction of NOAA AVHRR Data**

In order to investigate differences between Landsat MSS and NOAA AVHRR images both data sets should be co-registered as closely as possible. It was found that identifying suitable GCPs was even more difficult for NOAA AVHRR data than for Landsat MSS. For that reason the geometric correction of all NOAA AVHRR images was achieved by matching scenes to a reference derived from Landsat MSS reference images. A comparable spatial resolution of one LAC pixel at nadir was obtained by computing the average DN over 22 rows and 22 columns in the reference data and assigning the value to the central pixel position of that square. The new simulated NOAA AVHRR reference would thus possess the same geometric properties as the Landsat MSS reference. This would not be the case when resampling Landsat MSS scenes to 1.1 km. There, a difference of up to 0.5 pixels could be expected, which would have to be added to the error from matching NOAA AVHRR images to the reference.
Using image-to-image matching a second order polynomial was established, where a rms error of 0.5 or better was considered adequate. A nearest neighbour algorithm was applied for resampling the data.
A Landsat MSS image corresponds to a NOAA AVHRR LAC image of approximately 200 x 200 pixels. However, sites of the 1985 CIPEA field survey required a slightly larger size and images of 250 x 250 pixels were used. The transform equation was established over the area of the Landsat MSS reference image and then extended to correct the larger image. Extending the transformation equation beyond the domain over which it was defined included the chance of having a greater geometric error in the outside area. On the other hand, the increase in image size was only 12.5% on all sides of the image and

due to a lack of maps and images, there was no alternative.

A graphical illustration of a Landsat MSS geometrically corrected image (50 m resampling, NN) from 31 August 1985 and a NOAA AVHRR image from the same date is provided in Figures 4.3 and 4.4.

Relying on maps for geometrical corrections of images does have its pitfalls, however. In mainly featureless areas a crossing between a road and a river bed or some other seemingly distinct feature related to a road may be used to identify a GCP on a Landsat MSS image or sample sites in the field. During field surveys it was found that the position of roads marked on maps is not reliable (see Chapter 3.4). If only few GCPs or several similar points exist, an error is introduced to the transform equation, which cannot be identified by comparing rms errors. Under those conditions geometric correction procedures based on orbital models can provide more stable results.

(c) Investigation into Orbital Model Correction

A geometric correction procedure for operational applications of daily satellite images would best be accomplished by employing an orbital model for automatic processing. An algorithm for combining a nominal orbital model with GCPs was developed, based on Ho and Asem (1986) and Tozawa (1983). A general introduction to the approach is given in Chapter A3 of the Appendix. Only then was it discovered that a very similar approach was taken by a software development team at the University of Copenhagen. The algorithm was already implemented as a programme and to be released in September 1990 as part of the image processing package CHIPS, developed under the same EC initiative as this project at the University of Copenhagen. There was no need to re-invent the wheel and further work on the implementation of the orbital model was abandoned. Unfortunately, the programme did not arrive in time for an evaluation of its positional accuracy with respect to the method used.

Figure 4.3: Geometrically Corrected Landsat MSS (31.08.85, 50 Resampling, NN) 512 x 512 Extract over ITE/Silsoe Study Area (Band 2: Blue, Band 4: Red)

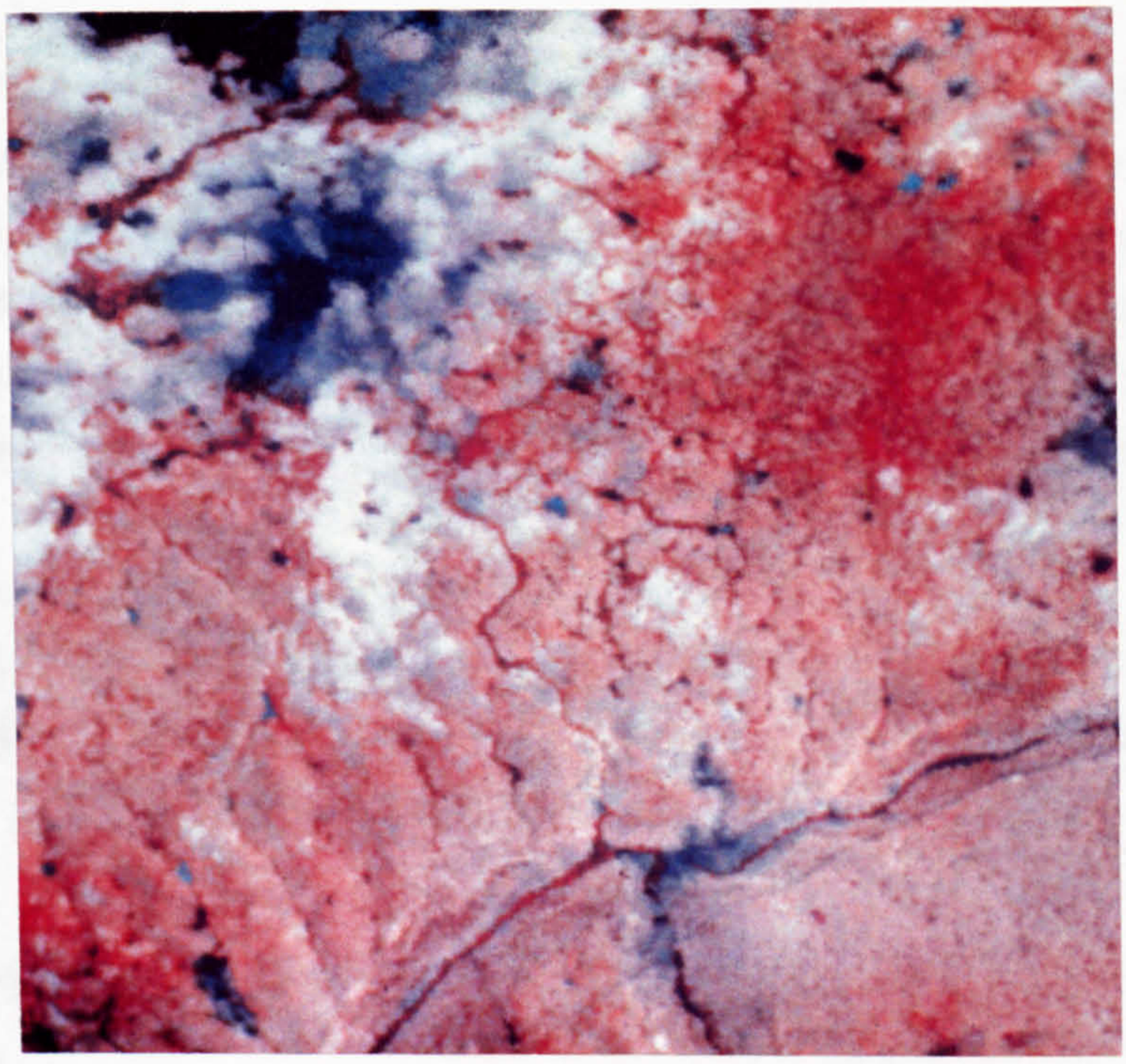


Figure 4.4: Geometrically Corrected NOAA AVHRR (31.08.85, 1.1km Resolution, NN) Extract over ITE/Silsoe Study Area (Channel 1: Blue, Channel 2: Red)



4.5 Radiometric Correction

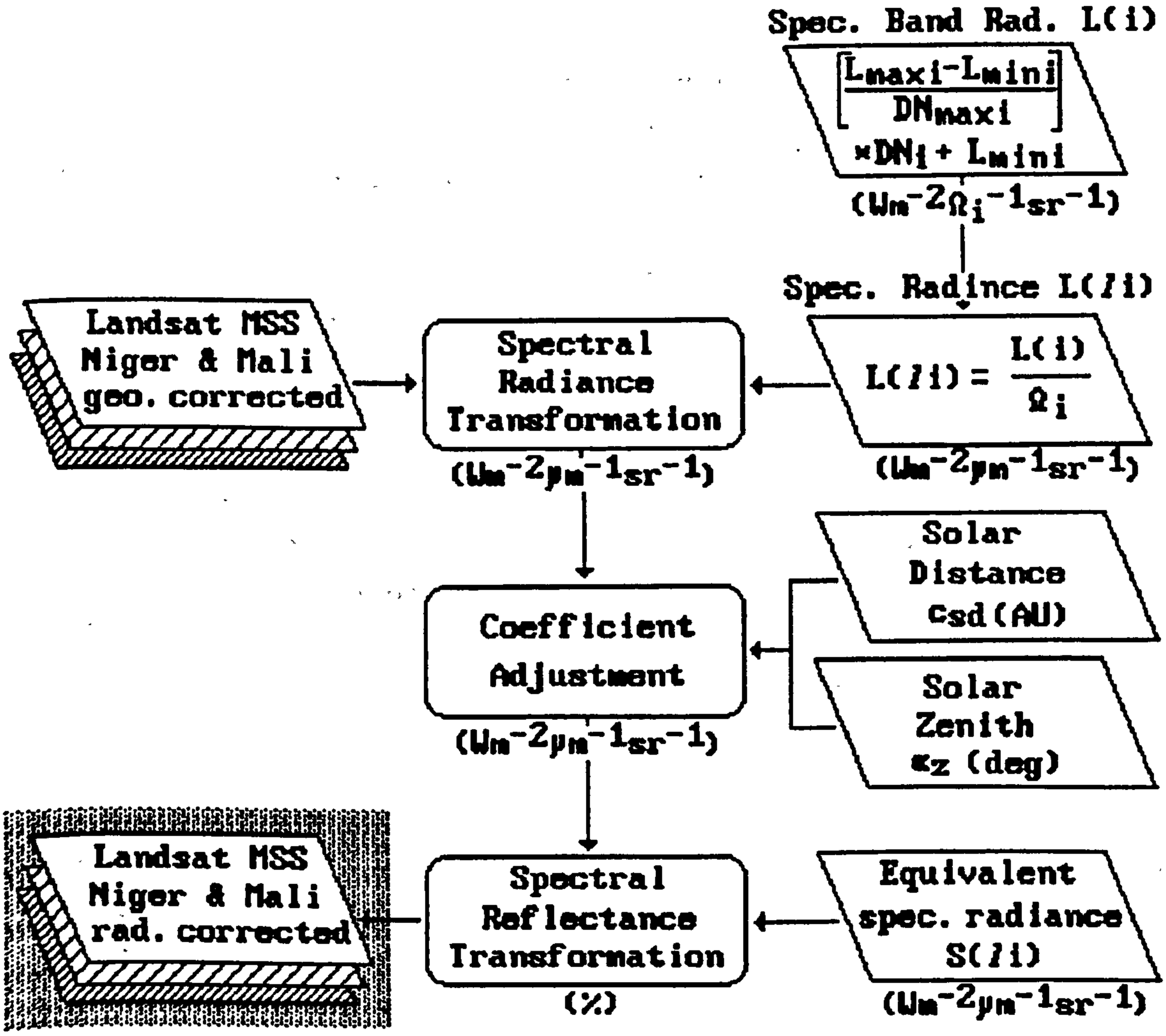
The interger values (DNs) transmitted by the satellites and recorded at receiving station represent unitless and relative values. They are only comparable to data obtained from other dates or sensors, if identical external conditions exist for imaging a particular surface. In the course of this project raw DNs were recalculated to values of spectral reflectance, because this unit allows a more immediate comparison of satellite responses than uncorrected DNs.
The steps applied to satellite data during the investigation are presented in the following paragraphs. The fundamental concepts are presented in Chapter A4 of Appendix I.

4.5.1 Conversion of Landsat MSS DNs to Spectral Reflectance

Prior to presenting the details of the radiometric corrections implemented some assumptions about the method of calibrating the MSS instrument onboard the Landsat satellite have to be stated.
Before launch the electrical output of the MSS instrument was calibrated to a reference scale, as were the internal calibration units (for further details see: Markham & Barker, 1987). Simplifying the procedure the calibration process can be described as linearly relating DNs to spectral radiance values of the reference instrument. The referencing process for the MSS instrument is directly relevant to parameters and units for the radiometric correction. It was not possible to clarify completely, which reference units were used when calibrating the instrument output. For this project it was assumed from the literature (Markham & Barker, 1987) that it was based on the nominal band width Q_i. It constitutes the difference between the upper and lower limits of the sensor response function for a spectral band. For MSS bands 1 to 3 there is little difference between the nominal bandwidth and those based on relative spectral response characteristic of the sensor (Q_{ai}). Only for Band 4 (and Channel 2 for AVHRR) the actual bandwidth

is only approximately 75% of the nominal value (Price, 1987; Price, 1988).
The significance of the assumption is that instead of the actual bandwidth Ω_{ai}, which considers the sensor response function, the nominal bandwidth Ω_i should be applied to obtain spectral radiance values from DNs.
A graphical illustration of the stages of radiometrically correcting Landsat MSS data is provided in Figure 4.5.

Figure 4.5: Method of Radiometrically Correcting Landsat MSS DN to Values of Apparent Spectral Reflectance



(a) Sensor Response Characteristics

Differences between the six array elements of the Landsat MSS sensor were not corrected for. Commonly employed de-striping methods (see Chapter A4, Appendix I) constitute an averaging operation of element

responses to incident EM energy. During this project the relationship between quantities of rangeland vegetation and satellite VIs would be based on the average spectral reflectance over the whole sample site, thus reducing the need to compensate for differences in array element characteristics.

Changes in sensor sensitivity are accounted for by updating coefficients based on internal calibration sources.

(b) Scene Illumination

i. *Solar Distance*

A correction factor for variations in the solar distance was calculated for each data set of 1985 and 1988. The correction factors c_{sd} for the 31 August 1985 (1985 ITE/Silsoe), 30 August 1988 (CAZS) and for 8 September 1988 (1988 ITE/Silsoe) are given in Table A.68 in Appendix II. Details of the computations are given in Chapter A4 in Appendix I.

ii. *Solar Elevation*

Solar irradiation was standardized to a solar zenith angle of 39°. For the three dates of calibrating ground to image data the corresponding correction factors are given in Table A.68 in Appendix II.

A programme was developed for calculating solar distances and zenith angles. The algorithm was based on the equation stated in Chapter A4, Appendix I.

The variation of the solar zenith angle across the area covered by Landsat MSS was determined to establish, if the assumption of a single angle for the whole scene could be applied. For the 31.08.85 image, the solar zenith angle at the top left corner was computed as being 31.94° and 32.00° deg for the bottom right corner. The correction factor c_{cos} would change by less than 0.06% from the image centre to the corners. This variation was considered as being not significant and

the solar zenith angle was assumed to be constant across the whole of a Landsat MSS scene.

(c) **Viewing Geometry**

Findings for simulated and actual satellite data suggest that a correction for off-nadir viewing is not required for scan angles below approximately 20° (see Chapter A4, Appendix I). Consequently, no attempts for view angle corrections were made.

(d) **Conversion of DNs to Spectral Radiance**

Originally, Landsat MSS spectral radiance threshold and saturation parameters for a linear transformation of DNs to spectral radiances were documented as in-band values (Robinove, 1982; Nelson, 1985). This can be mathematically expressed by

$$L(i) = \frac{L_{maxi} - L_{mini}}{DN_{maxi}} * DNi + L_{mini} \quad (Wm^{-2}\Omega_i^{-1}sr^{-1}) \qquad (4.1)$$

(After: Nelson, 1985)

The parameters for Landsat-5 MSS required to convert DNs into values of spectral radiance are summarized in Table 4.1.

Table 4.1: Threshold and Saturation Radiance Values for Landsat-5 Multispectral Scanner (after 9 November 1984)

Band i No.	Waveband nominal (μm)	Bandwidth nominal Q_i (μm)	Threshold Radiance L_{minli} ($Wm^{-2}\mu m^{-1}sr^{-1}$)	Saturation Radiance L_{maxli} ($Wm^{-2}\mu m^{-1}sr^{-1}$)	Maximum Digital Count DN_{maxi}
1	0.5-0.6	0.1	0.4 (0.3)	24.0 (26.8)	127
2	0.6-0.7	0.1	0.3 (0.3)	17.0 (17.9)	127
3	0.7-0.8	0.1	0.5 (0.5)	15.0 (14.8)	127
4	0.8-1.1	0.3	0.2 (0.3)	12.7 (12.3)	127

After: Royer *et al*, 1988; in (): Markham & Barker, 1987

As indicated in Table 4.1, there is a certain amount of variation in the literature as to which values to use for threshold and saturation spectral radiances.

Conveniently spectral band radiance L(i) is converted to

the spectral radiance L(*l*,i), which is independent of the bandwidth Ω_i (Robinove, 1982; Nelson, 1985; Markham & Barker, 1987; Price, 1987; Royer *et al*, 1988). The conversion is achieved by normalizing spectral band radiance L(i) by the nominal bandwidth Ω_i (see Chapter A4, Appendix I). The use of the nominal bandwidth takes account of the bandwidth of the reference instrument, not the sensor response function.

During this project the in-band threshold and saturation spectral radiance values of Markham & Barker (1987) were converted to spectral radiance values by applying the nominal spectral bandwidth as given by Price (1987). Similar values are available from Royer *et al* (1988). For a nominal band width the coefficients used are given in Table 4.1. The maximum DN was assumed to be 255 grey levels. Slope (a(*l*i)) and intercept (b(*l*i)) parameters for a linear conversion of DNs to spectral radiances were computed as follows:

$$a(li) = \frac{L_{maxi} - L_{mini}}{DN_{maxi} * \Omega_i} \quad (Wm^{-2}\mu m^{-1}sr^{-1}) \qquad (4.2)$$

and

$$b(li) = \frac{L_{mini}}{\Omega_i} \quad (Wm^{-2}\mu m^{-1}sr^{-1}) \qquad (4.3)$$

The parameters used for this project are given in Table 4.2.

Table 4.2: Slope and Intercept Parameters for Converting Landsat MSS DNs to Spectral Radiance

Band i No.	Threshold Radiance L_{mini} ($Wm^{-2}sr^{-1}$)	Saturation Radiance L_{maxi}	Slope Coefficient a(*l*i) ($Wm^{-2}\mu m^{-1}sr^{-1}$)	Intercept Constant b(*l*i)	Maximum Digital Count DN_{maxi} (count)
1	0.3	26.8	1.039	3.0	255
2	0.3	17.9	0.690	3.0	255
3	0.5	14.8	0.561	5.0	255
4	0.9	36.9	0.471	3.0	255

After: Markham & Barker, 1987

The use of slope and intercept parameters instead of threshold and saturation values for converting DNs to spectral radiances is more economic in terms of time required for computation. Only one multiplication and one addition is needed per pixel.

(d) **Conversion of Spectral Radiance to Reflectance**

The spectral radiance L(*l*,i) is related to the spectral reflectance *p*(*l*,i) for band i at the top of the atmosphere by

$$p(l,i) = \frac{\pi}{E(l,i)} * L(l,i) \text{ (unitless)} \qquad (4.4)$$

The solar spectral irradiance E(*l*,i) is derived from the solar spectral band irradiance E(i), which is weighted by the spectral response function of the waveband (see Chapter A4, Appendix I). In order to obtain the bandwidth-independent solar spectral irradiance E(*l*,i) the solar spectral band irradiance is divided by the wavelength Q_{ai}, which is determined by the spectral response function.

For comparisons with NOAA AVHRR data, instead of the spectral solar irradiance E(*l*,i) the solar spectral irradiance at nominal incidence, the equivalent spectral radiance S(*l*,i), is used (Price, 1988):

$$p(l,i) = \frac{L(l,i)}{S(l,i)} \text{ (unitless)} \qquad (4.5)$$

Values for the equivalent spectral irradiance S(*l*,i) for the four Landsat MSS wavebands are provided in Table 4.3. Similar values for the actual bandwidth Q_{ai} are also provided by Suits *et al* (1988). The equivalent solar spectral radiance S(*l*,i) in Table 4.3 was given by Price (1987). The values for Markham & Barker (1987) were calculated from the solar spectral irradiance E(*l*,i) and the equivalent bandwidth of the spectral response function Q_{ai}.

Table 4.3: Nominal and Actual Bandwidths for Landsat MSS Spectral Bands

Band i No.	Waveband centre actual (µm)	Bandwidth actual Ω_{ai} (µm)	Solar Spectral Band Irradiance E(i) (Wm^{-2})	Equivalent Spec. Radiance S(*l*,i) ($Wm^{-2}\mu m^{-1}sr^{-1}$)
1	0.54	0.106 (0.116)	194.5 (214.9)	584 (589)
2	0.65	0.089 (0.099)	142.0 (157.6)	508 (508)
3	0.76	0.103 (0.116)	130.1 (145.7)	402 (400)
4	0.93	0.221 (0.275)	190.9 (239.4)	275 (278)

After: Price, 1987 (equivalent rectangular method)
() Markham & Barker, 1987 (quadratic moment method)

All correction and conversion factors presented can be integrated in one single linear transformation equation to convert Landsat MSS DNs to exoatmospheric (apparent) spectral reflectances $p(l,i)$. It can be expressed as

$$p(l,i) = \alpha(i) * DN_i + ß(i) \quad \text{(unitless)} \tag{4.6}$$

where

$$\alpha(i) = \frac{c_{cos} * \Omega_{ai} * \pi}{c_{sd} * \Omega_i * E(i)} * \left[\frac{L_{maxi} - L_{mini}}{DN_{maxi}} \right] \quad (DN^{-1}) \tag{4.7}$$

and

$$ß(i) = \frac{c_{cos} * \Omega_{ai} * \pi * L_{mini}}{c_{sd} * \Omega_i * E(i)} \quad \text{(unitless)} \tag{4.8}$$

As can be seen from these equations the stage at which correction factors are applied is of consequence on the result of the conversion. If a transformation of DNs to spectral radiance or reflectance is intended, correction factors, be it for changes in solar elevation or distance, should be included after the conversion. If they are applied to DNs before a transformation, the intercept value is not corrected for. Slope and intercept parameters of data conversions from DNs to physical units are specific for a site and date of image acquisition. The advantages of assessing criteria for data conversions prior to a step-by-step implementation for whole scenes are savings in computing time and space for storing intermediate files.

The consequences of the data transformation from raw DNs to spectral reflectances were investigated by comparing data from bands 2 and 4. Areas of bare soil, which were assumed to be non-changing surfaces, were identified on 50 m and 1.1 km resolution images. A graphical presentation of the changes for individual bands and the NDVI from bands 2 and 4 are given in Figures 4.6 to 4.8.

After adjusting for scene illumination conditions it became apparent that the pre-processing applied to the data before it was received was significantly different for all three images. As mentioned above Landsat MSS data is processed before distribution. Bands 1, 2 and 3 are transmitted in compressed 6 bits. They are then decompressed non-linearly to 7 bit. Band 4, however, is linearly stretched to 7 bits.

Figure 4.6: Raw Digital Numbers for Landsat MSS Bands 2 and 4 from 31 August 1985 (191/49), 30 August 1988 (192/49) and 8 September 1988 (191/49)

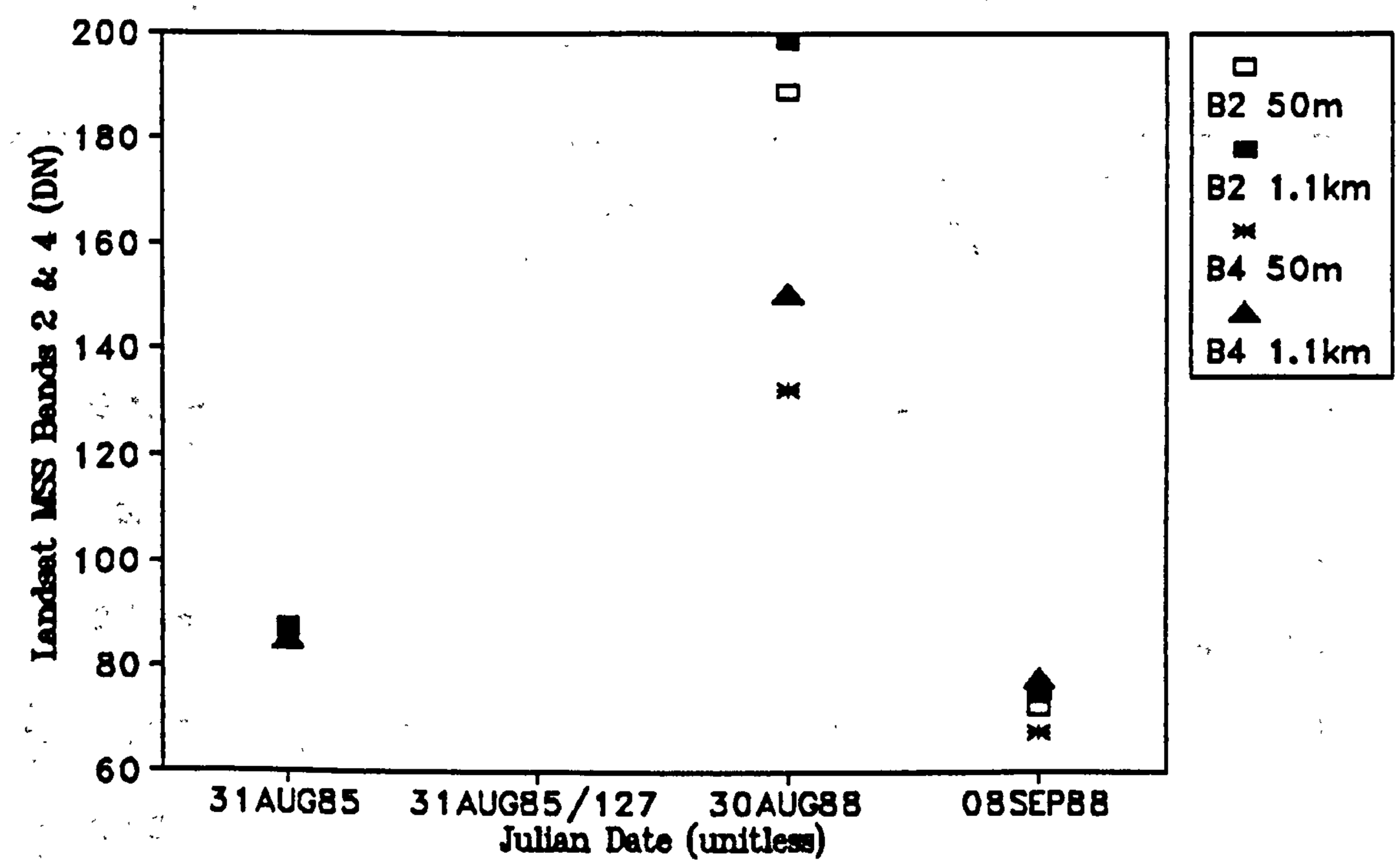


Figure 4.7: Exoatmospheric Spectral Reflectance for Landsat MSS Bands 2 and 4 from 31 August 1985 (191/49), 30 August 1988 (192/49) and 8 September 1988 (191/49)

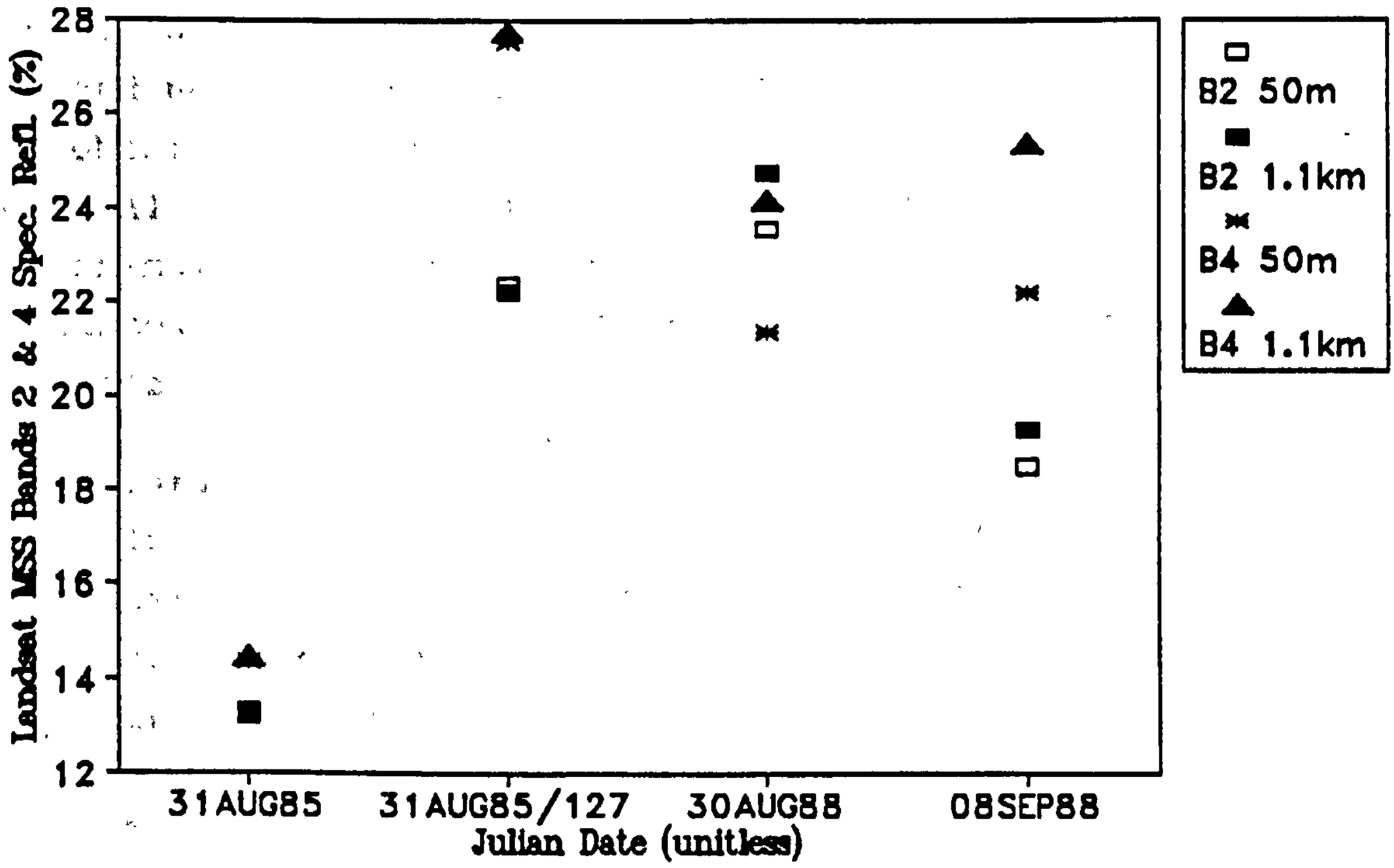
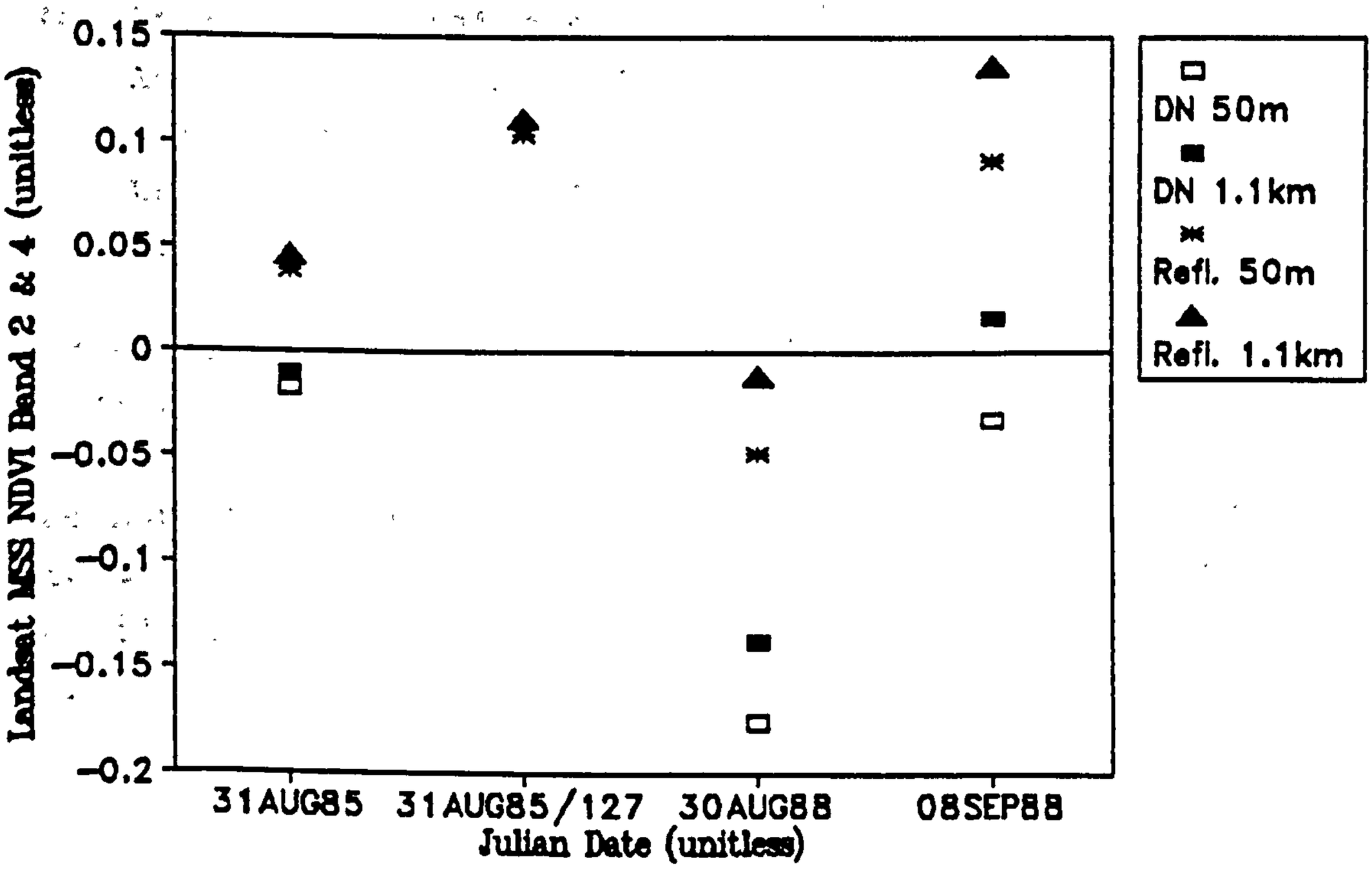


Figure 4.8: Normalized Vegetation Indices from Digital Numbers and Exoatmospheric Spectral Reflectances for Landsat MSS Bands 2 and 4 from 31 August 1985 (191/49), 30 August 1988 (192/49) and 8 September 1988 (191/49)



Information on decompression and stretching data is recorded in the file header information of the original tapes in form of look-up tables for all detector elements of all four bands. This was only available for the image acquired at 31 August 1985 and not for 1988. For the latter dates sequential files were obtained, which did not contain the decompression look-up table. Although all sensor responses were recorded as 8 bit DNs the maximum DN required to convert DNs to spectral radiances was unknown. Three different maximum DNs had to be employed to homogenize spectral reflectances.

(a) Data from 31 August 1985 (ITE/Silsoe Survey)

The radiometric look-up table was available. The maximum DNs used for the spectral radiance conversion were based on the average maximum DN of all detector elements for one band. A graphical presentation of the average data expansion functions is given in Figure 4.9 (also see Table 4.4).

(b) Data from 30 August 1988 (CAZS Survey)

Decompression information was not available for this image. Data inspection suggested that the maximum DN was 255 for all bands (see Table 4.4)).

(c) Data from 8 September 1988 (ITE/Silsoe Survey)

As it was the case with the previously mentioned image data from this scene was pre-processed before delivery. DNs found during image inspection suggested a maximum DN of 127 (see Table 4.4).

These newly established values for maximum DNs were used to determine coefficients and constants of a linear transformation of DNs to exoatmospheric spectral reflectances. The corresponding values for each date and band are provided in Table 4.4. The parameters are also corrected for variations in solar illumination conditions.

Figure 4.9: Average Decompression Functions for Landsat MSS Bands from 31 August 1985

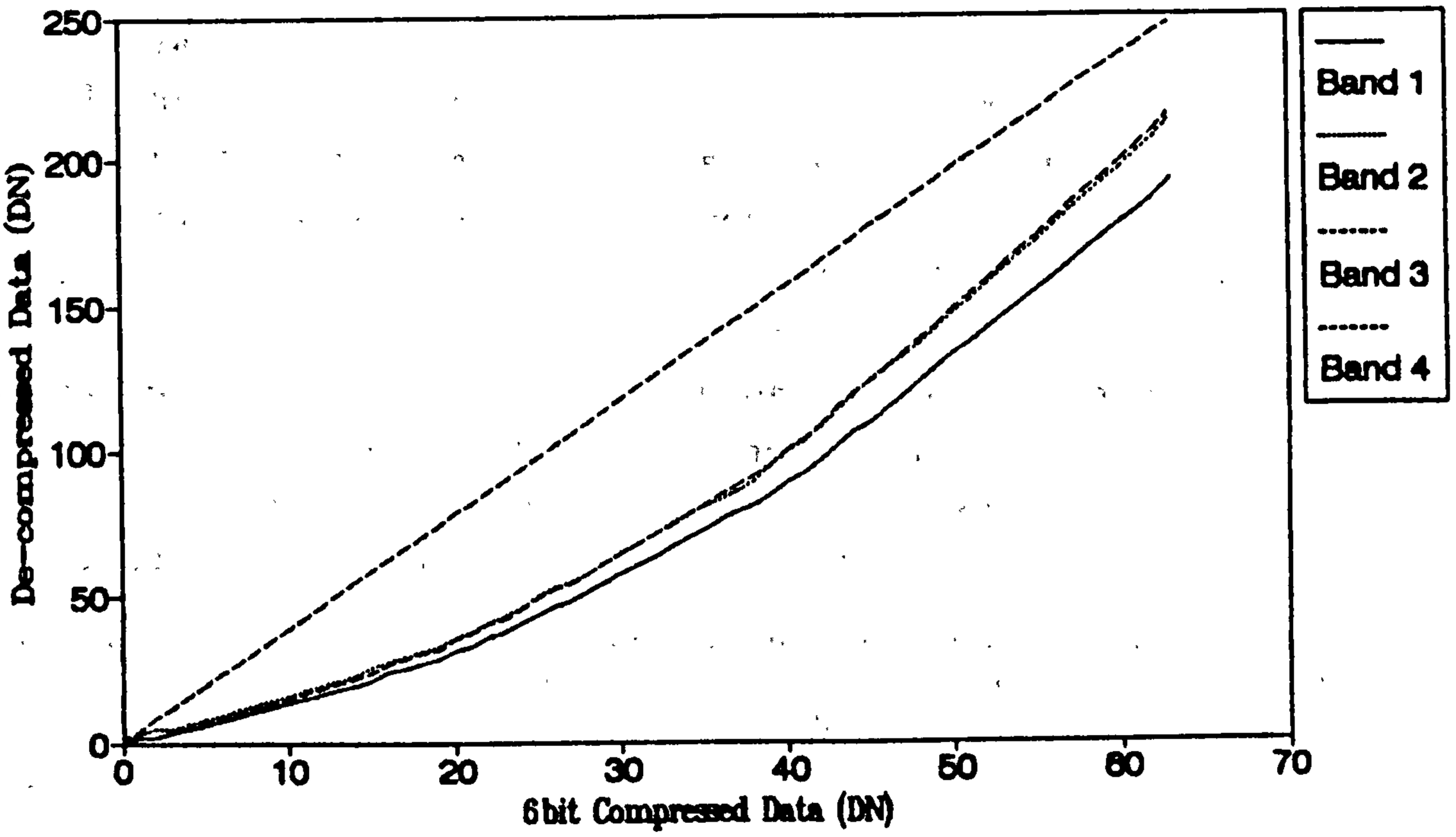
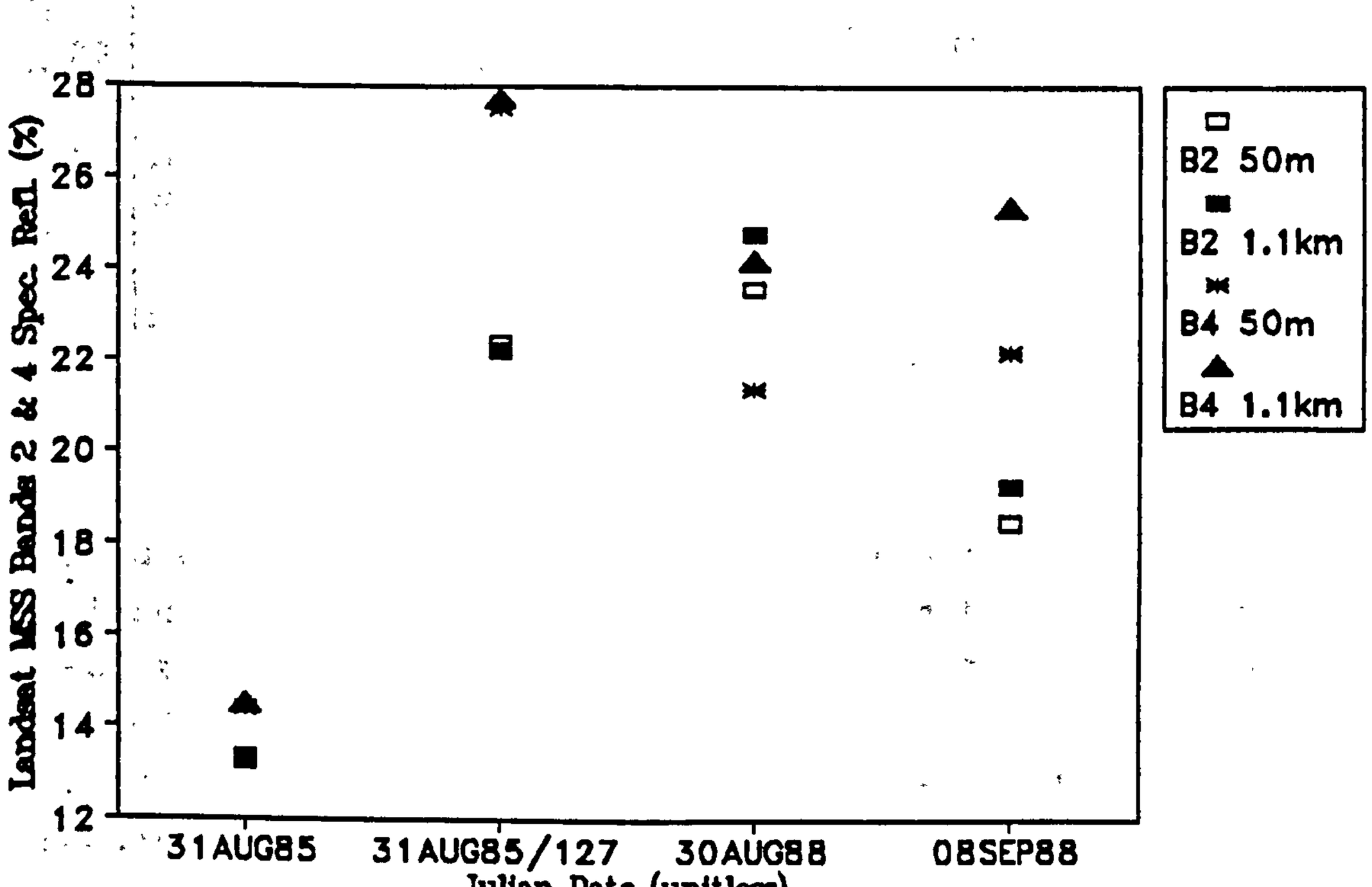


Table 4.4: Linear Coefficients for Direct Conversion of Landsat MSS DNs into Exoatmospheric Spectral Reflectances, Including Correction for Earth-Sun Constellation

Date	Waveband i No.	Slope Coefficient $\alpha(i)$ (% DN^{-1})	Intercept Constant $\beta(i)$ (%)	Maximum DN DN_{maxi} (DN)
31.AUG.85	1	0.2121	0.4622	193
	2	0.1465	0.5315	213
	3	0.1484	1.1190	216
	4	0.1590	0.9818	247
30.AUG.88	1	0.1598	0.4612	255
	2	0.1220	0.5304	255
	3	0.1252	1.1167	255
	4	0.1537	0.9797	255
08.SEP.88	1	0.3266	0.4696	127
	2	0.2495	0.5400	127
	3	0.2560	1.1369	127
	4	0.3142	0.9975	127

After conversion, exoatmospheric spectral reflectances for bare soil were extracted from each image. These would be used to establish soil lines and derive parameters for atmospheric standardization. Since two different areas (Landsat MSS 192/49 for Mali and 191/49 for Niger) were to be examined it was not possible to select identical sites. Therefore, approximately 40% of image samples were taken over bright sands, 40% over dark lateritic surfaces and 20% over clay. Between 12 (Mali 1.1 km resolution image) and 45 (Niger 50 m resolution image from 31 August 1985) sites were investigated. Average values of DNs and spectral reflectances for bands 2 and 4 were then compared. A graphical illustration of these averages for the three images used is given in Figure 4.10.

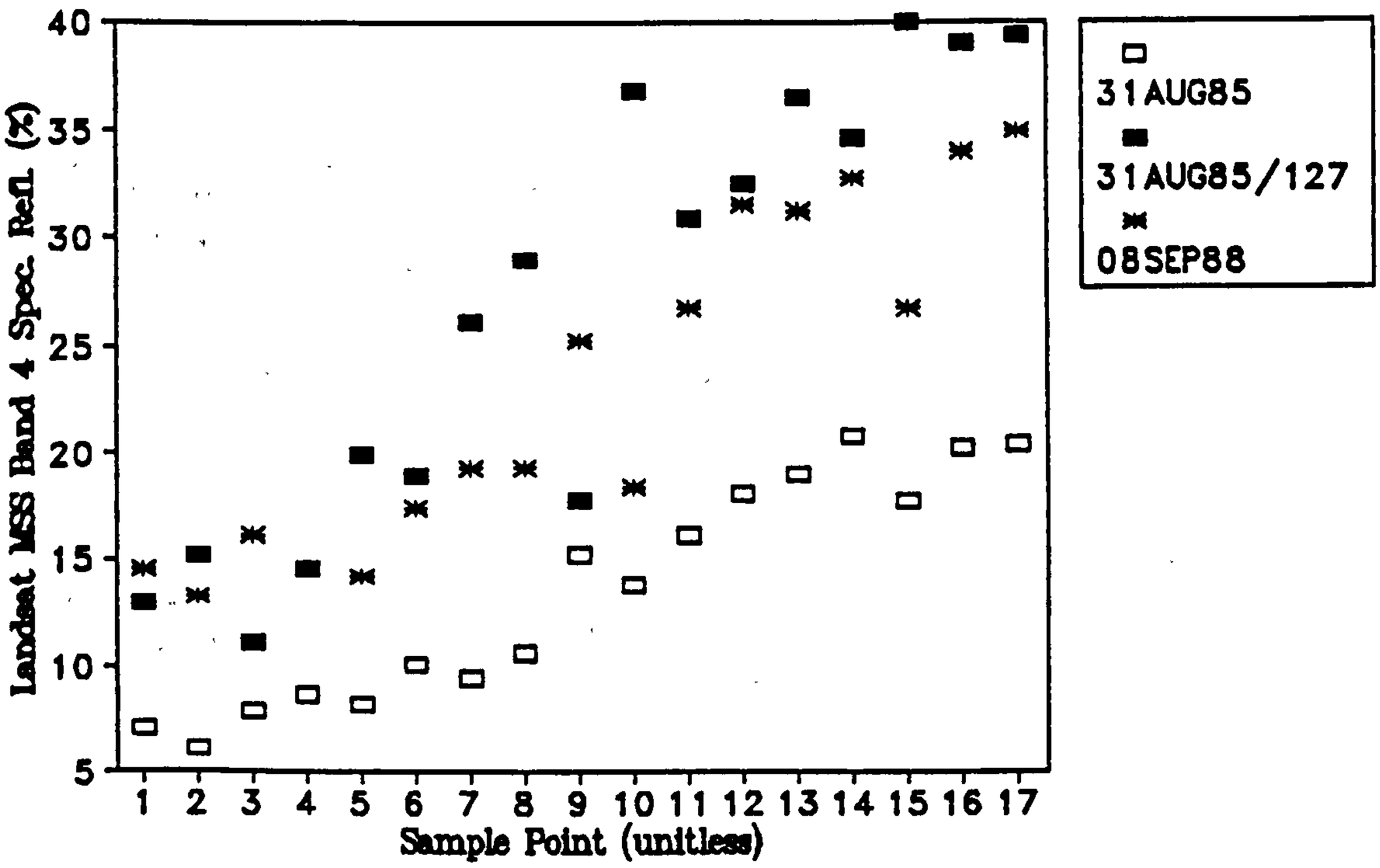
Figure 4.10: Comparison of Average Spectral Reflectances of Landsat MSS Bands 2 and 4 for Bare Soil Values for Images from 31 August 1985, 30 August 1988 and 8 September 1988



The findings presented indicated that spectral reflectances of bare soils over CAZS and 1988 ITE/Silsoe sites were comparable. Values from the 1985 image were then calibrated assuming a maximum DN of 127. The resulting spectral reflectances are displayed as "31AUG85/127". These values seem to correspond more closely with averages from 1988 than those obtained on the

basis of the tape header information. The discrepancy was investigated further by selecting pixels over bare soil at identical positions within the 1985 and 1988 images for ITE/Silsoe surveys. The result is graphically displayed in Figure 4.11.

Figure 4.11: Comparison of Average Spectral Reflectances of Landsat MSS Band 4 for Bare Soil Values of Identical Image Positions for Images from 31 August 1985 and 8 September 1988



The findings suggest that by using a maximum DN of 127 for the 1985 image instead of the information from the radiometric look-up table a closer relationship to spectral reflectance values of the 1988 image can be obtained. Without additional information it could not be confidently established which correction would be the most appropriate to use.

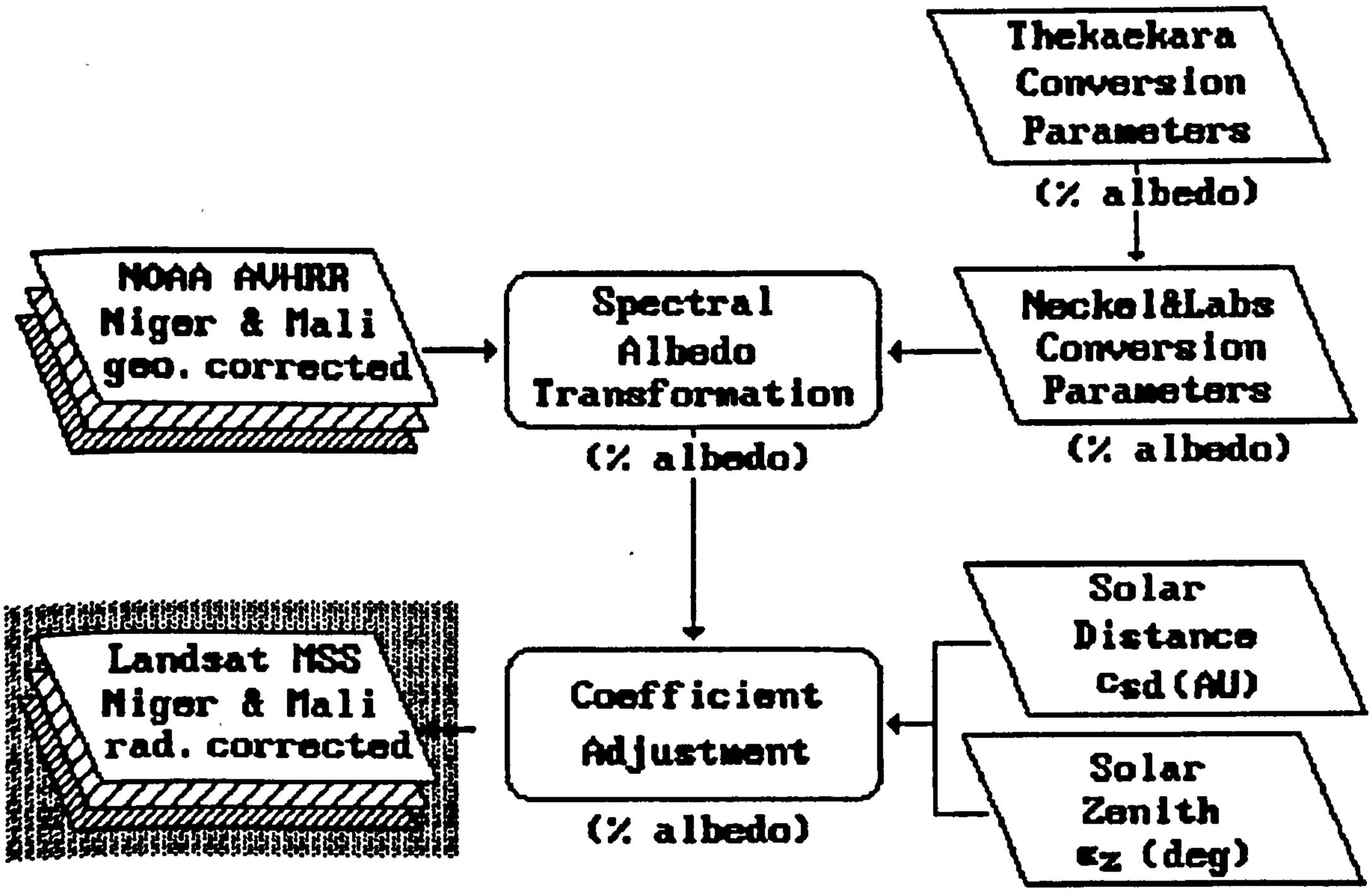
4.5.2 Conversion of NOAA AVHRR DNs to Spectral Albedo

The steps applied for radiometrically correcting NOAA AVHRR data mainly correspond to those for Landsat MSS images. However, due to differences in the sensor design between the two systems the radiometric correction of NOAA AVHRR data has

to be treated separately.

An illustration summarizing the methods applied to radiometrically correct NOAA AVHRR data is provided in Figure 4.12

Figure 4.12: Method of Radiometrically Correcting NOAA AVHRR DNs to Values of Apparent Spectral Albedo



(a) **Sensor Response Characteristics**

Temporal changes in sensor sensitivities have to be corrected for with NOAA AVHRR data, since the instrument does not provide on-board calibration other than deep space viewing (see Chapter A4, Appendix I). The linear decrease in detector sensitivity reported by Holben *et al* (1990) allows simple correction factors to be applied for monthly intervals. For a given number of months after launch the relative decrease in sensor sensitivity can be found according to

$$Ch1_{deg} = -0.42 * (\text{months after launch}) + 95.30 \quad (4.9)$$

$$Ch2_{deg} = -0.22 * (\text{months after launch}) + 86.63 \quad (4.10)$$

(Holben *et al*, 1990)

Correction factors for the 1985 and 1988 images are given in Table A.69 in Appendix II.

The effectiveness of correcting for a degradation in sensor sensitivity could be estimated by comparing DNs with spectral albedo values from unvegetated areas over the four field surveys. The corresponding values are graphically presented in Figures 4.19 and 4.21 later in this section. Julian days of the year instead of days after launch were related to spectral albedos in order to allow a direct graphical comparison. The use of the NIR channel is suggested, because it is less affected by atmospheric conditions. No significant discrepancy between 1985 and 1988 was observed for Niger sites. However, there seemed to be a trend towards reduced values within the 1988 growing season. This could also be observed when comparing channel 1 spectral albedo values.

The influence of temporal changes of instrument sensitivity on ratio VIs were estimated by relating Julian Day and NDVI from bare soil. A graphical presentation is provided in Figures 4.22 and 4.23 later in this section. The variation of NDVI values between years was less than the variation found for the 1988 ITE/Silsoe survey. It was, therefore, concluded that the sensor degradation correction employed sufficiently compensated for changes in the detector sensitivity. On the other hand Figures 4.22 and 4.23 indicate a tendency for increasing NDVI values with progressing growing period. This might be attributed to variations in scene illumination conditions, as will be discussed in the following paragraph.

(b) **Scene Illumination Conditions**

Due to the wide scan angle of the AVHRR instrument illumination conditions vary greatly across an image. Consequently, adjustments of these variations should be implemented on a pixel-by-pixel basis. For this project only small sub-scenes were investigated (200 x 200 pixels). The sizes of the sub-scenes were determined by

Landsat MSS images, which were employed to geometrically correct NOAA AVHRR data.

i. *Solar Distance*

Variations in the solar distance from the nominal value were computed for images, which were not rejected by the cloud screening procedure. The correction factors c_{sd} for 1985 and 1988 images are given in Table A.69 in Appendix II.

ii. *Solar Elevation*

The solar elevation for NOAA AVHRR image cannot be assumed constant across the scene. The 1985 CIPEA and ITE/Silsoe study areas were covered by the same image, although individual sample sites were some 300 km apart. The distance between CAZS and ITE/Silsoe sites in 1988 was even larger (see Chapter 2). In order to account for the corresponding changes in solar elevation each area was treated separately. Within the area the solar elevation could the be considered constant (see previous section on Landsat MSS). As with Landsat MSS data solar irradiation was standardized to a solar zenith angle of 39°.

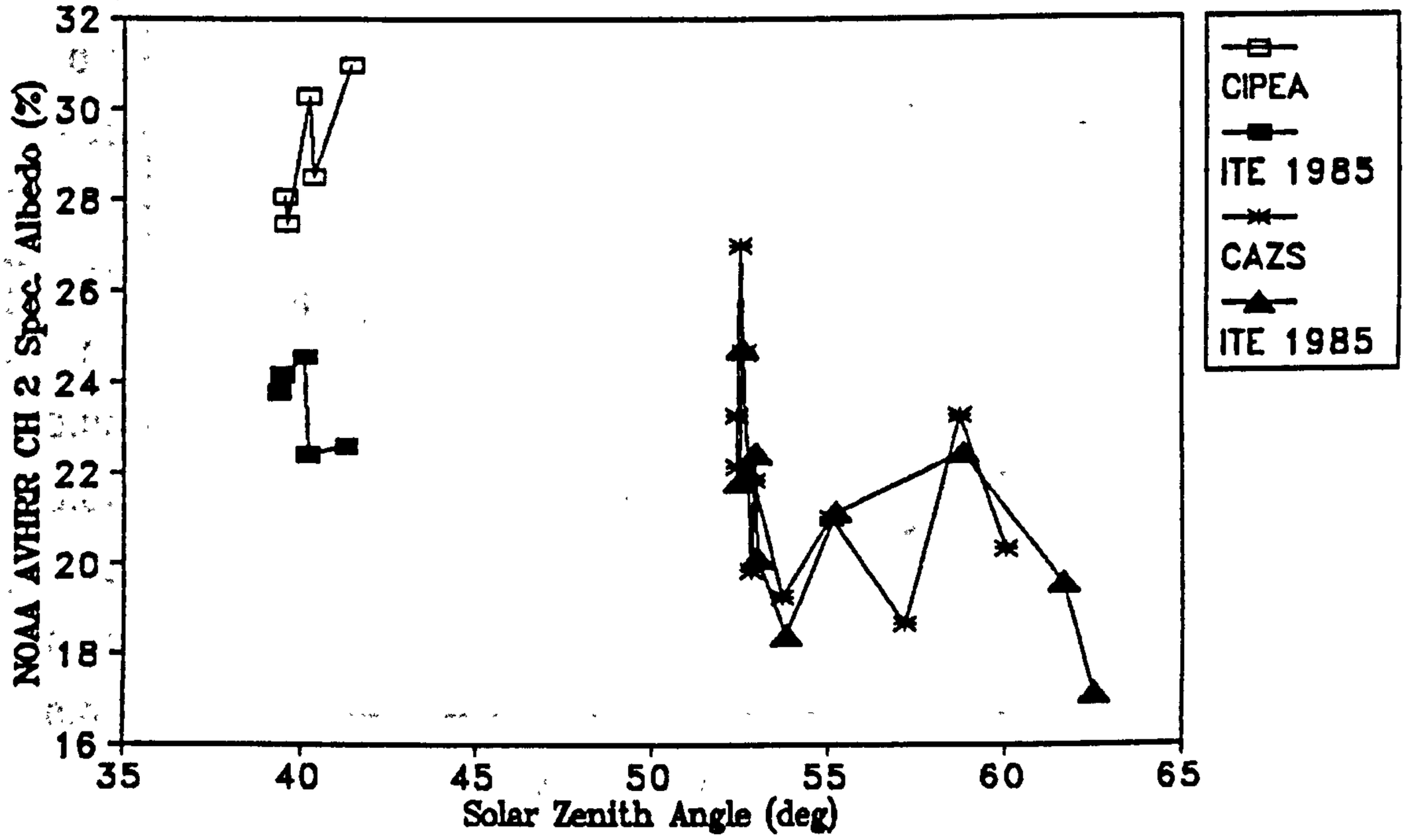
Table A.69 in Appendix II contains solar zenith angles and correction factors for the two years of observation and three areas of field surveys.

For 1985 the standard solar zenith angle of 39° was close to the range of actual angles at the time of image acquisition. As a result of the NOAA-9 platform drift of approximately 0.5 h per year towards later equatorial crossing times, the solar zenith angle increased significantly from 1985 to 1988. Since Sahelian rangelands are only partially covered by vegetation some effects of the low solar elevation angles on VIs, which are not accounted for by the cosine correction, can be expected.

The influence of scene illumination conditions on single channel spectral albedos and ratio VIs were evaluated by

relating averages from bare soil pixels to the solar zenith angle at the time of data acquisition. The association between solar zenith angle and channel 2 spectral albedo is presented in Figure 4.13.

Figure 4.13: Relationship Between Solar Zenith Angle and Channel 2 Spectral Albedo Values for Bare Soil over CIPEA, 1985 ITE/Silsoe, CAZS and 1988 ITE/Silsoe Field Surveys

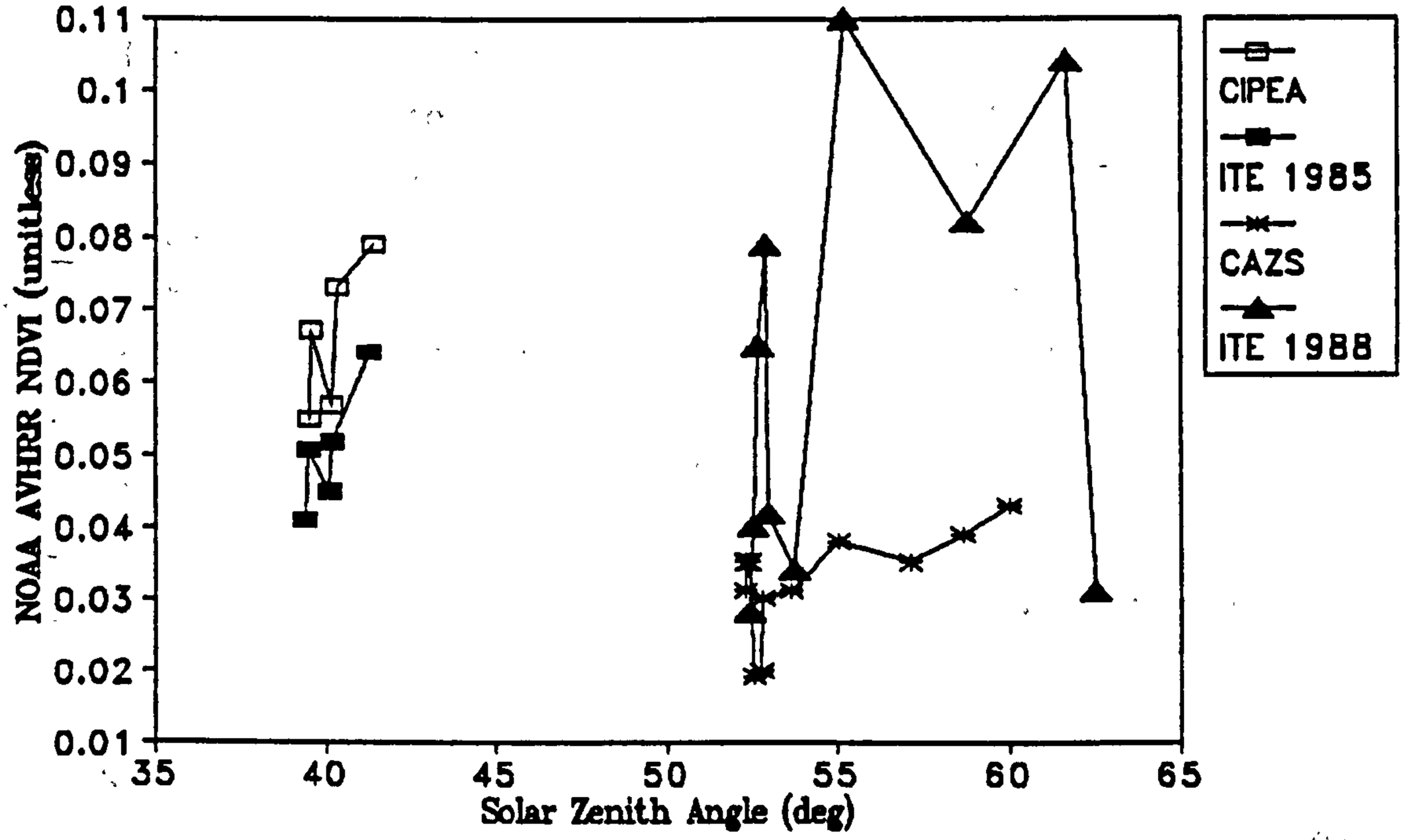


A coefficient of determination (r^2) of 0.47 was established for a logarithmic relationship between Julian day and channel 1 spectral albedo over the 1988 ITE/Silsoe study area (r^2 of 0.64 for Julian date vs. channel 2 spectral albedo). The trend was less clearly expressed over the CAZS study area.

This supports assumptions and results of other investigations presented in Chapter A4 in Appendix I that a cosine correction cannot compensate fully for variations in illumination conditions. Assessing the causes of the observed relationship, like non-Lambertian surface characteristics, increased areas of shadow or changes in leaf orientation with senescing vegetation, were considered as being outside the scope of this project.

The effect of changing illumination conditions on ratio VIs were assessed by relating solar zenith angles to NDVI values. The results are graphically presented in Figure 4.14.

Figure 4.14: Relationship Between Solar Zenith Angle and NDVI Values for Bare Soil over CIPEA, 1985 ITE/Silsoe, CAZS and 1988 ITE/Silsoe Field Surveys



Since the source of the changes were not altogether understood no attempts for any corrections were made at this level.

(c) Viewing Geometry

The original method of reducing scan angle effects on VIs was to limit the area of extracts to ± 20° from the nadir (see Chapter A4, Appendix I). A rigourous implementation of the intention would have resulted in but a few images for the growing seasons. For example, for the 1985 growing season only five of the 12 delivered images were readable and at least partially cloud free. In addition, no separate data was available covering CIPEA or CAZS sites in 1988. Hence, these areas were frequently further off-nadir than ITE/Silsoe sites (see Table A.20, Appendix II). The limit for taking

extracts was set to ± 600 pixels from the nadir. This corresponds to a scan angle of approximately 35°. A variation in VIs values with increasing distance from the nadir can, therefore, be expected.

The effect of off-nadir viewing on the sensor response to reflected EM energy in channels 1 and 2 was evaluated by subdividing each image into strips of 200 pixels in across-track and 600 pixels in along-track direction (after cloud screening). Averages and standard deviations from each of the strips were calculated. From these average values mean RVIs and NDVIs for each strip were obtained. Single channel apparent spectral albedos and VIs were then related to their distance from the nadir. The results are graphically presented in Figures 4.15 to 4.17. The effect of the view angle on single channels and the RVI are given in Figures A.4, A.9 and A.10 in Appendix III.

Figure 4.15: Relationship Between View Angle and NDVI for NOAA AVHRR Images of 1985

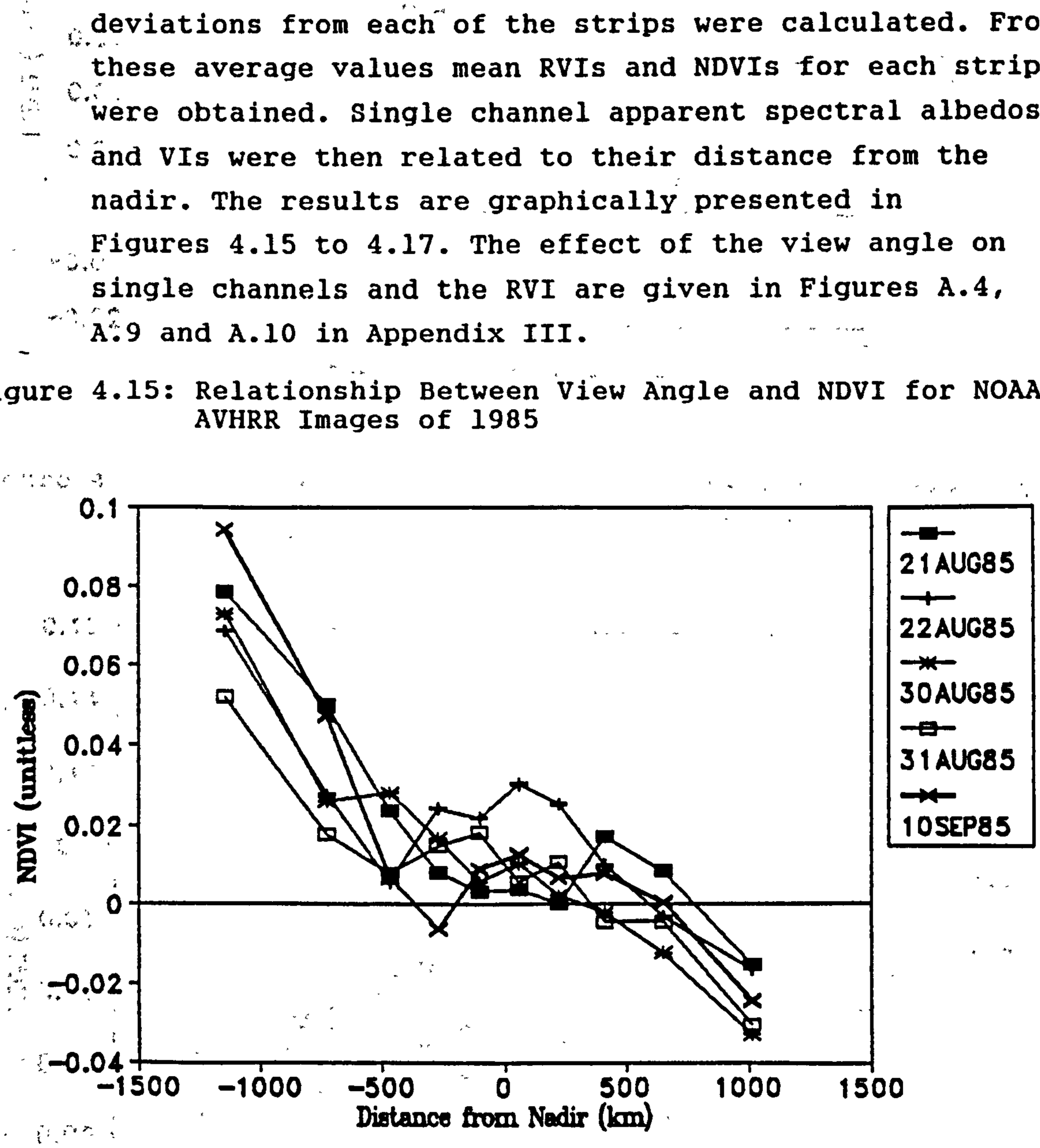


Figure 4.16: Relationship Between View Angle and NDVI for NOAA AVHRR Images of 1988, First Half of Growing Season

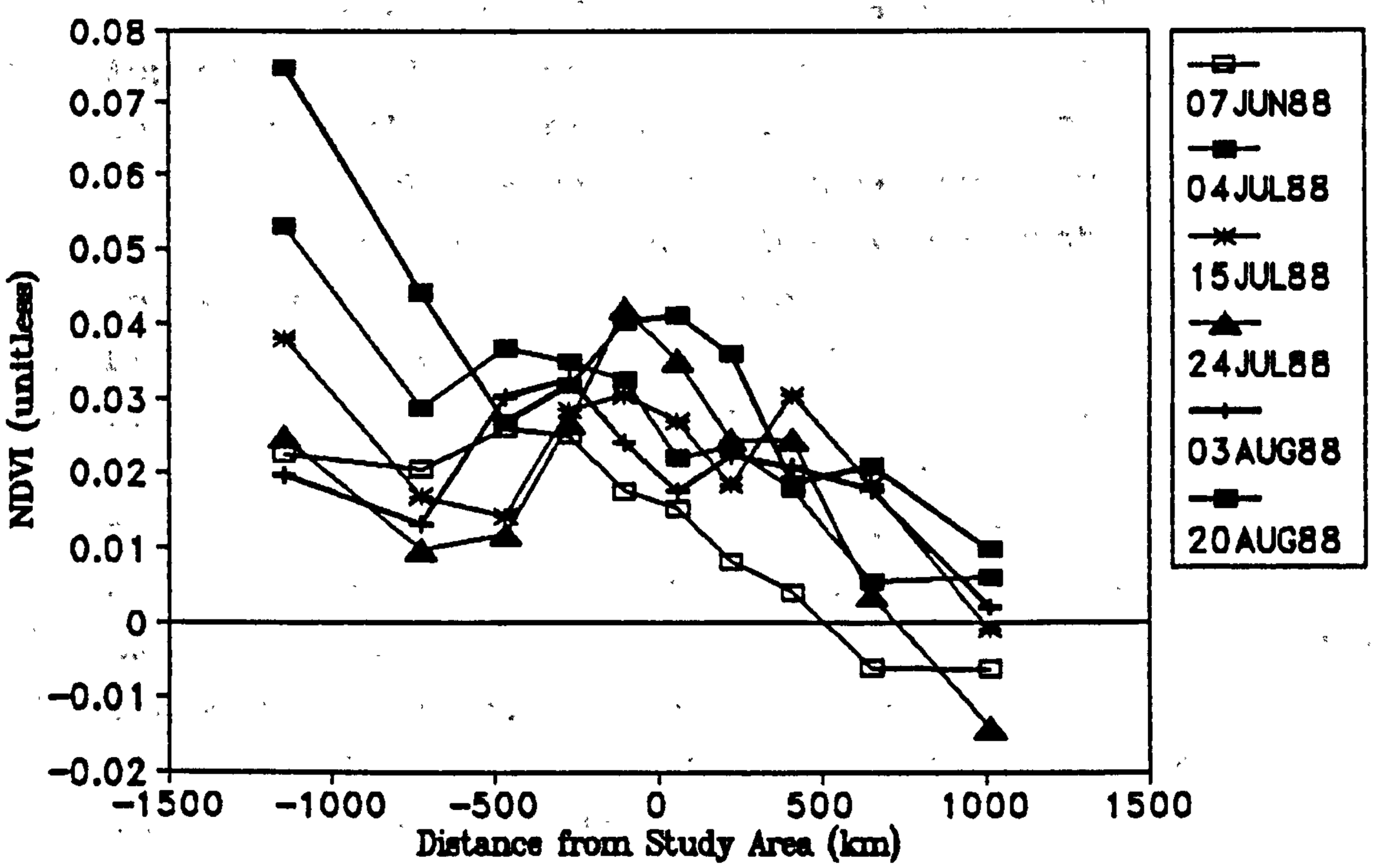
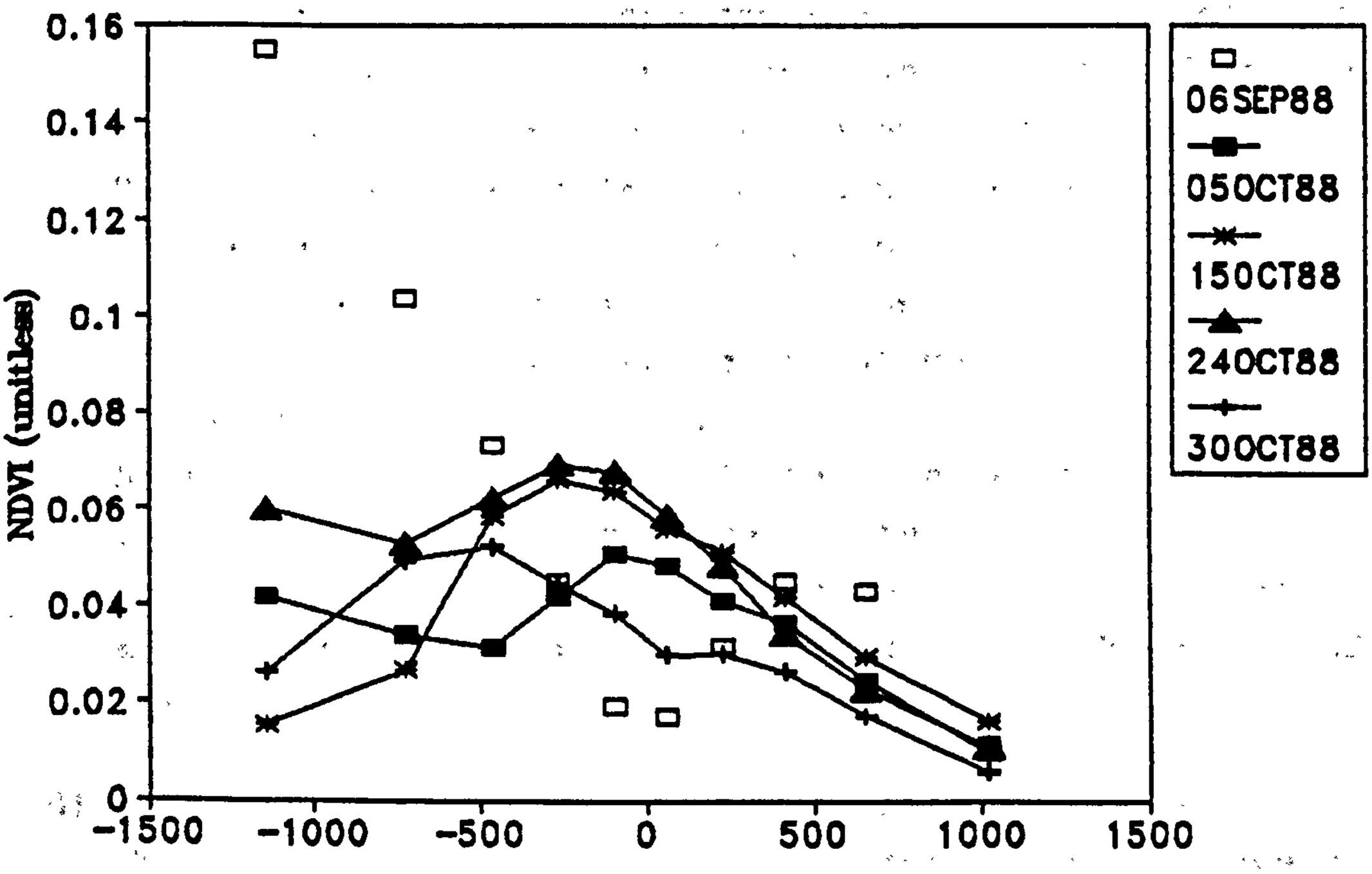


Figure 4.17: Relationship Between View Angle and NDVI for NOAA AVHRR Images of 1988, Second Half of Growing Season



For partially vegetated surfaces lowest values of reflected EM energy in channels 1 and 2 could be expected near the nadir of the image (see Chapter A4.3, Appendix I). The highest NDVI values were presumed to be found in a slight forward scattering direction with decreasing NDVI values with increasing view angles. These predictions were not clearly observable for all images assessed. At this stage only the relationship between NDVI and scan angle will be discussed, because single bands are of less importance and the RVI displayed a very similar performance.

During the 1985 and 1988 growing seasons the NDVI decreased distinctively from the forward (West) to the backward (East) scattering direction for all end of July and August images. Before and after this period the relationship approaches the expected form of an arc (Holben & Fraser, 1984).

In 1988 there was generally more vegetation in the Sahel than in 1985, which was one of the driest seasons of the decade. Hence, increases in rangeland vegetation quantities alone are unlikely to be the cause for temporal changes between forward and backward scatter directions. Plausible sources are changes in atmospheric constituents, like an increased humidity in mid-season and a dependency on the solar azimuth angle.

From the data available it was not possible to identify and separate the various conditions, which induce changes in ratio VI values as a function of the sensor scan angle. A corresponding investigation was outside the scope of this project.

Nonetheless, the results of the dependency of ratio VIs on the sensor scan angle are in line with recommendations for restricting data to a scan angle of ± 20° from the nadir (Duggin *et al*, 1982; Tucker *et al*, 1983).

(d) Conversion of NOAA AVHRR DNs to Spectral Albedo

For NOAA AVHRR data coefficients for a direct conversion of DNs to values of percentage equivalent spectral

albedo are documented (Kidwell, 1988; Planet, 1988). It can be expressed as:

$$a(l,i) = g(i) * DN_i + d(i) \quad (\% \text{ albedo}) \qquad (4.11)$$

The calibration coefficients for calculating spectral reflectance and equivalent spectral albedo are stated in Table 4.5.

Table 4.5: Spectral Parameters and Calibration Coefficients for NOAA-9 AVHRR

Channel i No.	Waveband nominal (µm)	Bandwidth nominal Ω_i (µm)	Slope Albedo g(i) (% DN^{-1})	Intercept Albedo d(i) (%)	Maximum Digital Count (DN_{maxi})
Ch 1	0.58 -0.68	0.100	0.1063	-3.846	1023
Ch 2	0.725-1.10	0.375	0.1075	-3.877	1023
After: Planet, 1988					

Parameters provided by NOAA AVHRR are based on Thekaekara's values for the solar spectral irradiance, while those for Landsat MSS are based on Neckel and Labs (Kidwell, 1988; Price, 1987). A comparison of spectral solar irradiance values for channels 1 and 2 between the two methods is given in Table 4.6.

Table 4.6: Thekaekara and Neckel and Labs Solar Irradiances and Equivalent Bandwidths for Channels 1 and 2 of NOAA-9 AVHRR

Channel i No.	Waveband centre actual (µm)	Bandwidth actual Ω_{ai} (µm)	Solar Spectral Band Irradiance E(i) (Wm^{-2})	Equivalent Spec. Radiance S(*li*) ($Wm^{-2}\mu m^{-1}sr^{-1}$)
	Thekaekara			
1	0.635	0.117	181.5	493.8
2	0.833	0.239	245.5	327.0
	Neckel & Labs			
1	0.636	0.117	191.3	520.5
2	0.833	0.239	251.8	335.4
After: Planet, 1988				

The equivalent solar spectral radiance S(*l*,i) for channel i can be obtained from the solar spectral band irradiance E(i) by

$$S(l,i) = \frac{E(i)}{\Omega_{ai} * \pi} \text{ (unitless)} \qquad (4.12)$$

The solar spectral band irradiance E(i) is normalized by the equivalent width Ω_{ai} of the spectral response function, because it was established on its basis. Spectral albedo values based on Neckel & Labs can then be obtained according to

$$a(li)_N = \frac{L(l,i)*\Omega_{ai}*\pi*100}{E(i)_T*c_{cal}} = \alpha(i)_N*DN_i+ß(i)_N \qquad (4.13)$$

The equation demonstrates that the parameters $\alpha(i)_N$ and $ß(i)_N$ for the linear conversion of NOAA AVHRR DNs into values of spectral albedo $a(li)_N$, which conform to solar spectral band irradiance estimates from Neckel & Labs, can be obtained from the documented values by dividing channel 1 parameters by 1.054 and those for channel 2 by 1.025. Since spectral reflectance is associated with Landsat MSS and spectral albedo with NOAA AVHRR radiometrically corrected data the distinction in terminology has been maintained in this thesis. Table 4.7 presents slope and intercept parameters documented and those suggested for this project.

Table 4.7: Coefficients for Linear Conversion of NOAA-9 AVHRR DNS to Percentage Spectral Albedo Based on Neckel & Labs

Channel No.	Thekaekara Slope Coefficient (% DN^{-1})	Thekaekara Intercept Constant (%)	Neckel & Labs Slope Coefficient (% DN^{-1})	Neckel & Labs Intercept Constant (%)
1	0.1063	-3.846	0.1009	-3.649
2	0.1075	-3.877	0.1049	-3.782

Instead of using single step implementations for sensor degradation, variations in scene illumination conditions, solar irradiance modification and

exoatmospheric spectral albedo transformation coefficients and constants for a linear conversion of original DNs directly into spectral albedo were established. For each image, channel and survey these parameters are summarized in Table A.70 in Appendix II. A graphical comparison between DNs, spectral albedos and NDVIs based on the two units are provided in Figures 4.18 to 4.23.

Figure 4.18: Raw Digital Numbers for NOAA AVHRR Channel 1 for CIPEA, 1985 ITE/Silsoe, CAZS and 1988 ITE/Silsoe Surveys

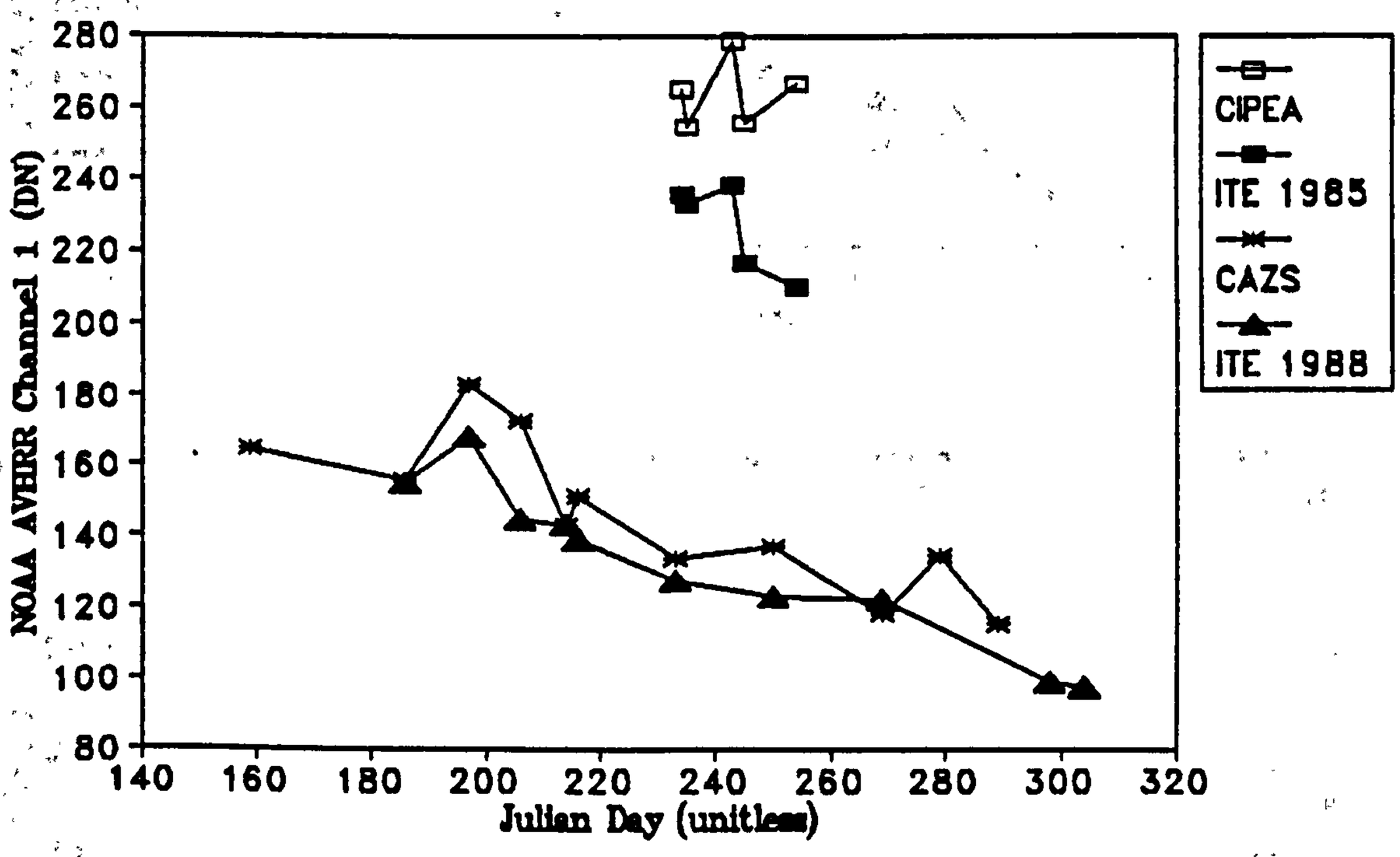


Figure 4.19: Raw Digital Numbers for NOAA AVHRR Channel 2 for CIPEA, 1985 ITE/Silsoe, CAZS and 1988 ITE/Silsoe Surveys

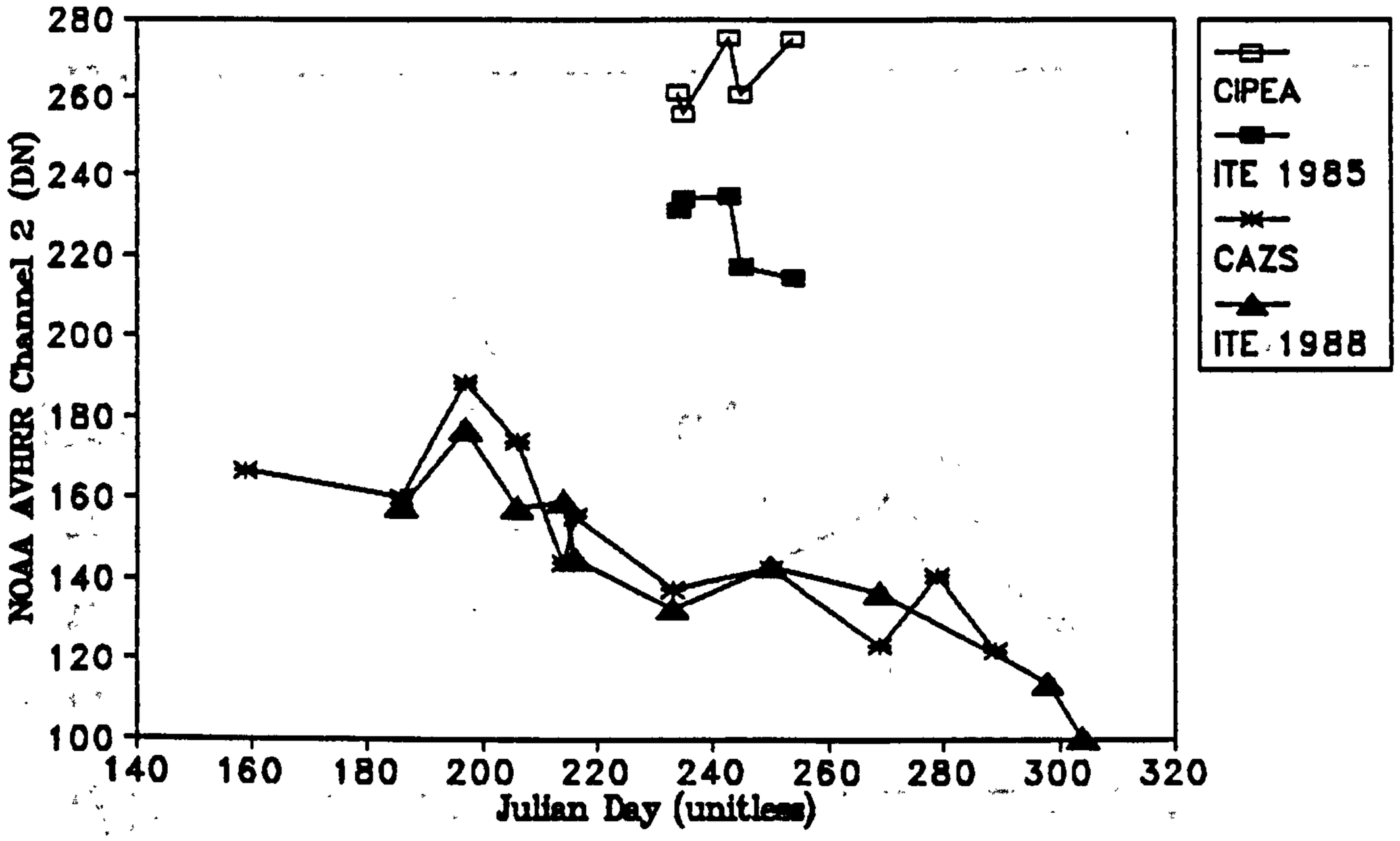


Figure 4.20: Exoatmospheric Spectral Albedo for NOAA AVHRR Channel 1 for CIPEA, 1985 ITE/Silsoe, CAZS and 1988 ITE/Silsoe Surveys

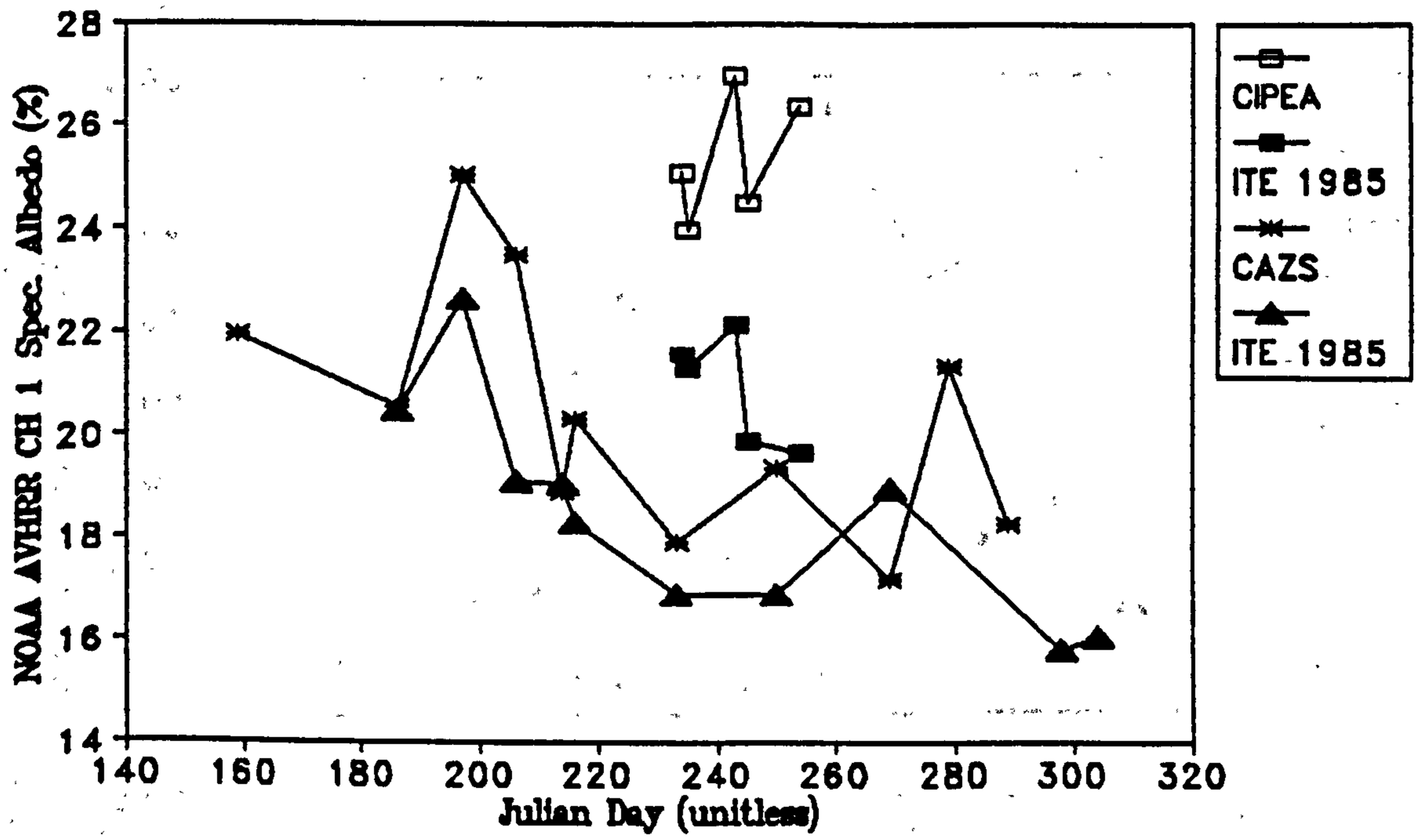


Figure 4.21: Exoatmospheric Spectral Albedo for NOAA AVHRR Channel 2 for CIPEA, 1985 ITE/Silsoe, CAZS and 1988 ITE/Silsoe Surveys

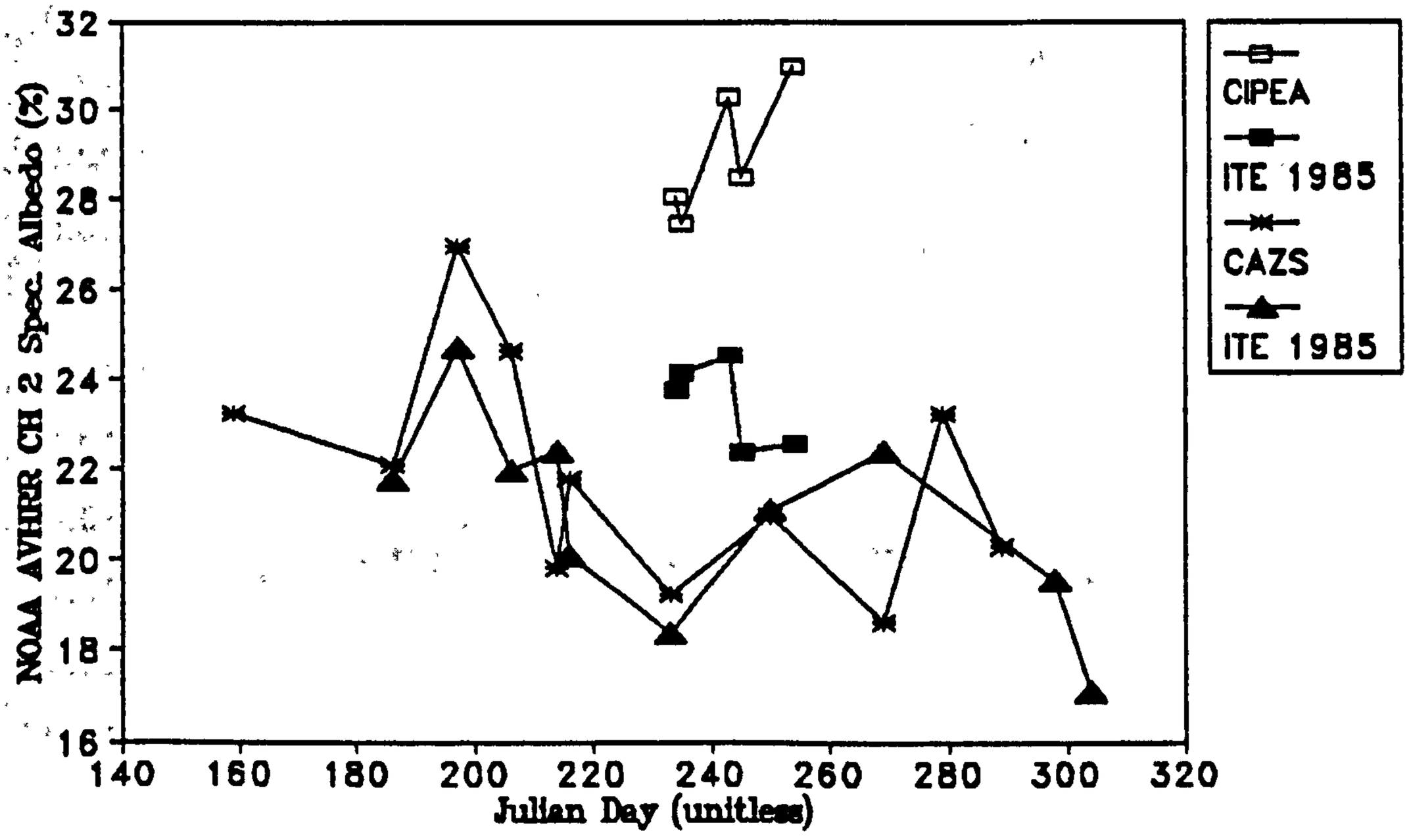


Figure 4.22: Normalized Vegetation Indices for NOAA AVHRR Based on Digital Numbers From Channel 1 and 2 for CIPEA, 1985 ITE/Silsoe, CAZS and 1988 ITE/Silsoe Surveys

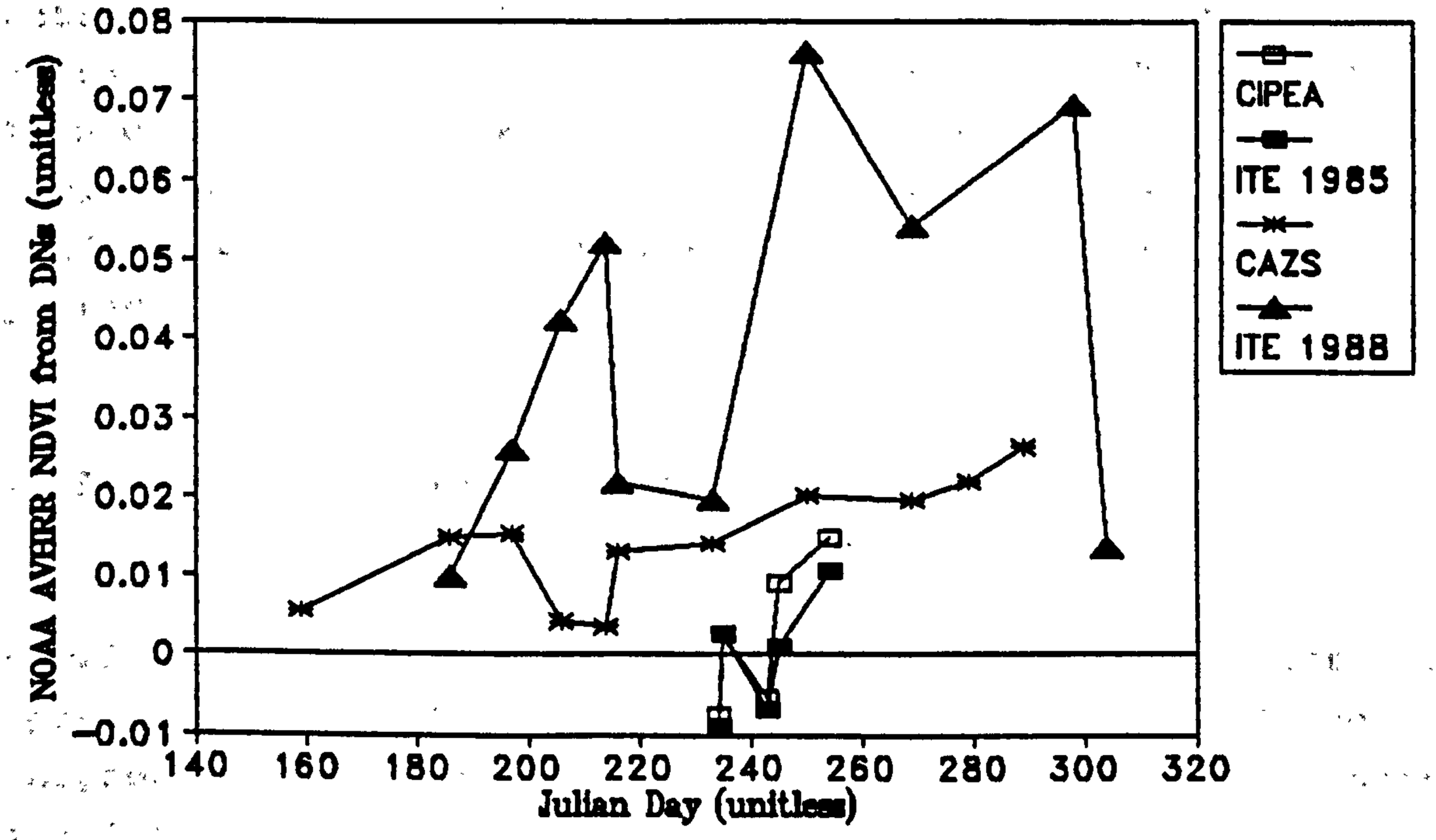
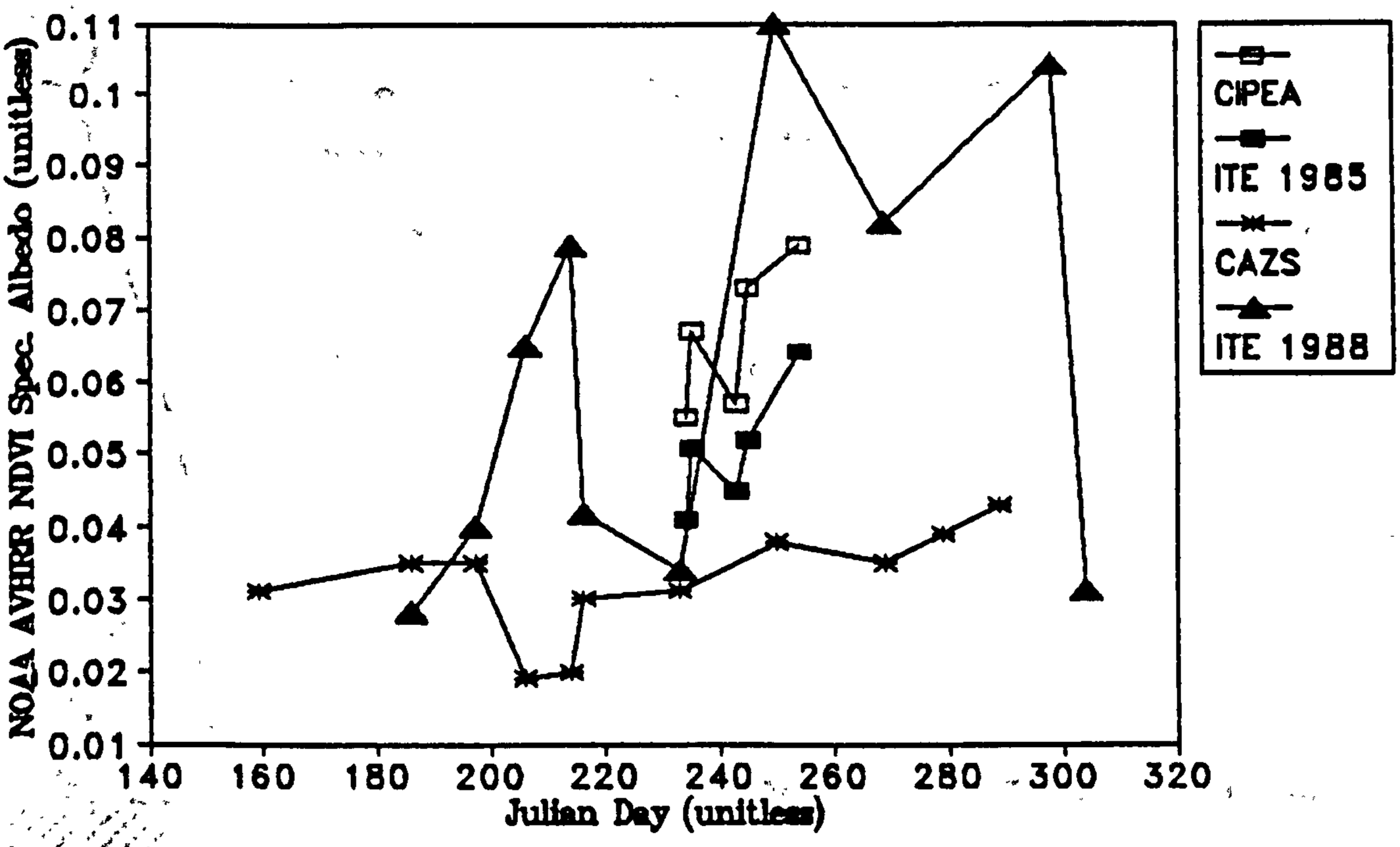


Figure 4.23: Normalized Vegetation Indices for NOAA AVHRR Based on Spectral Albedo From Channel 1 and 2 for CIPEA, 1985 ITE/Silsoe, CAZS and 1988 ITE/Silsoe Surveys

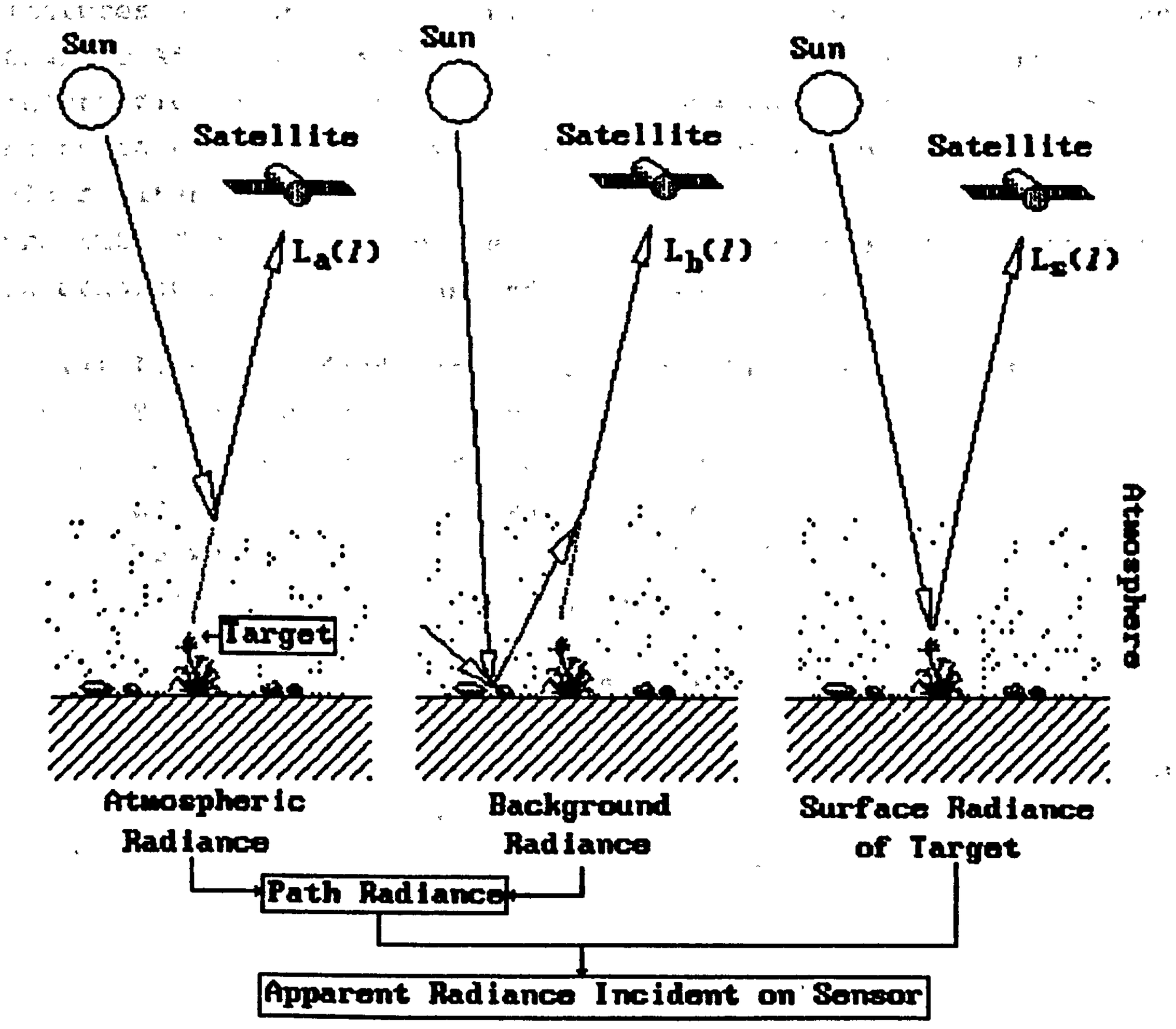


Before implementing correction factors for variations in scene illumination conditions it may be worth while to check the need for it. When calculating ratios, like the RVI or NDVI, from spectral reflectances the cosine correction factor cancels algebraically. Its implementation is superfluous. Yet, for the PVI an effect of a cosine correction for changes in illumination conditions is inevitable due to its definition and an influence of changing illumination conditions can be expected.

4.6 Atmospheric Correction

The reflected solar energy detected by a space borne sensor has to pass twice through some distance, the path length, of the atmosphere. A graphical illustration of the interaction between solar irradiance and the atmosphere is presented in Figure 4.24.

Figure 4.24: Graphical Representation of Definition Components of Apparent Spectral Radiance



(After: Deschamps *et al*, 1983)

An introduction to units, atmospheric models and correction methods is provided in Chapter A5 in Appendix II.

The principal mechanisms of atmospheric effects on satellite data are molecular scattering, aerosol scattering and absorption and gaseous absorption (Fraser & Kaufman, 1985; Saunders, 1990). While molecular scattering can be calculated from remote sensing applications (Robinson, 1985), scattering and absorption by aerosols are the main sources of variations in atmospheric conditions both spatially and with time. Compensating for the influence of aerosols on the signal requires knowledge or assumptions about environmental conditions of the study area. This can be, for example,

additional ancillary information to be implemented in an atmospheric radiative transfer model or the presence of features with known or assumed reflectance characteristics (see Chapter A5, Appendix I). For the study area no additional information on atmospheric constituents were available. Also, no surface cover types with known reflectance properties, like clear water, dense forest areas or shadowed valleys, were present. The method employed constitutes a relative adjustment in atmospheric conditions and is presented below.

(a) **Image Standardization for Atmospheric Adjustment**

Since conditions prevented the implementation of an absolute atmospheric correction procedure, a relative adjustment strategy was developed. Thus, relationships between ground and satellite VIs should become comparable among the standardized image data.

i. *Assumptions of an Atmospheric Model*

The influence of changes in atmospheric conditions on the surface leaving signal can be simplified and expressed in form of a linear transfer equation (Caselles & Garcia, 1989; see Chapter A5, Appendix I)):

$$p(l) = a(l) * p_s(l) + b(l) \text{ (unitless)} \qquad (4.14)$$

It should be noted that, strictly speaking, the constants $a(l)$ and $b(l)$ also depend on the surface reflectance $p_s(l)$ (Dave, 1981). Furthermore, it may be worth mentioning at this stage that reflectance interaction between vegetation canopy, sensor view angle, solar zenith angle and atmospheric conditions is not expressed in the equation, because canopies on the earth surface are non-isotropic diffuse reflectors (Colwell, 1974; Kimes, 1985). The relationship presents only a simple model of atmospheric influences.

ii. *Relative Adjustments for Atmospheric Variatons*

Under the assumption of scanning a Lambertian surface where the target and the average of the

surrounding pixel have the same, or negligible different, reflectance the apparent reflectance $p_{ref}(l)$ of the earth-atmosphere system for the reference image can be written as:

$$p_{ref}(l) = a_{ref}(l) * p_s(l) + b_{ref}(l) \quad (4.15)$$

and for any other image:

$$p_{im}(l) = a_{im}(l) * p_s(l) + b_{im}(l) \quad (4.16)$$

The linear coefficients a_{ref} and a_{im} summarize the influence of atmospheric constituents on the surface reflectance $p_s(l)$ (Teillet, 1986; Caselles & Garcia, 1989). The constants b_{ref} and b_{im} represents the atmospheric path reflectance $p_a(l)$. Over surfaces with a stable reflectance over time the relationship between the reference and any other image thus becomes:

$$p_{im}(l) = \frac{a_{im}(l)}{a_{ref}(l)} * p_{ref}(l) - \frac{a_{im}(l)*b_{ref}(l)}{a_{ref}(l)} + b_{im}(l) \text{ (unitless)} \quad (4.17)$$

Subsequently, the magnitude of the parameters $a_{im}(l)$ and $b_{im}(l)$ can be assessed relative to a standard size.

(b) Non-changing Surface Cover for Sahel

Within the study area, and across the Sahel, surface cover types with non-changing reflectances are present in form of bare soil and rock. Even in years of exceptionally high vegetation growth, like in 1988, some areas remained without vegetation cover. Should values for bare soil reflectances become available at a later stage then the relationship between herbaceous rangeland quantities and VIs could be easily adjusted by determining the difference between ground measurements and their corresponding values in the reference image. Adjusting any other images would be dispensable.

(c) Selection of Reference Pixels

In order to investigate changes in atmospheric conditions all aformentioned pre-processing steps should be applied to the data prior to atmospheric adjustments. In each channel and image a number of dark and bright pixels over bare soil or rock should be identified. Ideally, the same area on the surface is examined at each image. However, the distribution of clouds prohibits complying with this demand.

(d) Identification of Reference Image

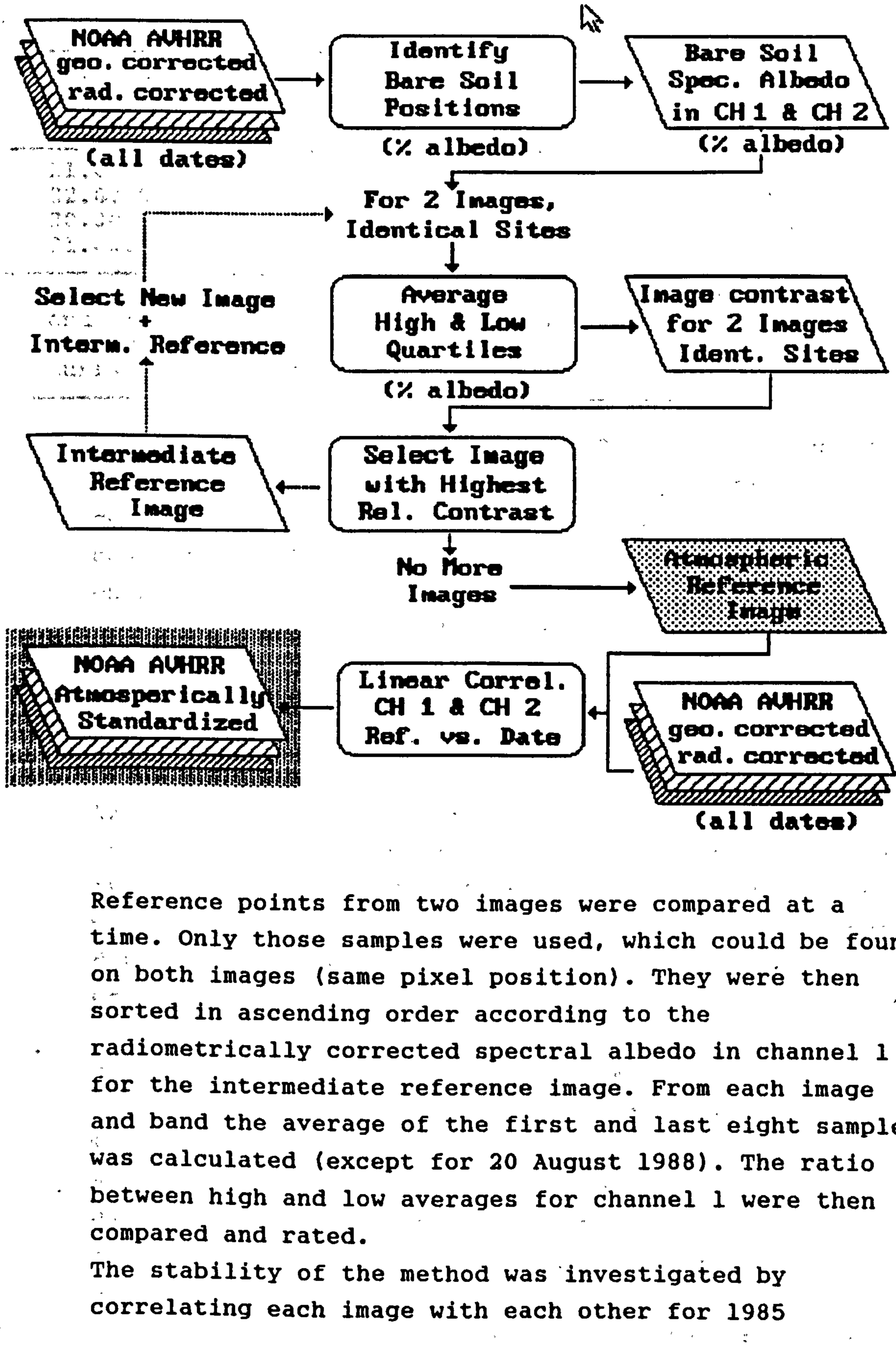
The method of standardizing atmospheric conditions to conditions from a reference image depends mainly on the ability to identify surface features with constant spectral reflectance characteristics. For the study area the main source of impeding this condition would be vegetation growth. Variations in soil moisture content have been excluded in the investigation, because of a lack in information of assessing it.

The development of significant vegetation over a site was estimated by a simple adaptation of the PVI. Image soil samples with distance of more than twice the average distance from the soil line were disregarded. This rarely occurred for the 1985 and 1988 ITE/Silsoe images. The test was, therefore, not applied to images for the 1988 CAZS survey.

During this project a minimum of 30 bare soil and rock samples was collected per image and channel. In most cases this allowed the selection of 15 to 20 samples with identical positions on two images. Only in case of one image (20 August 1988, ITE/Silsoe sites) did cloud cover prevent a direct comparison with any other image, since no more than five (four for the reference image) corresponding samples could be found.

The binary procedure of identifying the image with the least atmospheric influence on the surface leaving signal is graphically demonstrated in Figure 4.25.

Figure 4.25: Procedure of Identifying Reference Image for Atmospheric Standardization for NOAA AVHRR Images of the 1988 ITE/Silsoe Field Survey



Reference points from two images were compared at a time. Only those samples were used, which could be found on both images (same pixel position). They were then sorted in ascending order according to the radiometrically corrected spectral albedo in channel 1 for the intermediate reference image. From each image and band the average of the first and last eight samples was calculated (except for 20 August 1988). The ratio between high and low averages for channel 1 were then compared and rated.

The stability of the method was investigated by correlating each image with each other for 1985

ITE/Silsoe sites. The results obtained from 1985 ITE/Silsoe sites are presented in Table 4.8.

Table 4.8: Decision Table for Selecting Clear NOAA AVHRR Image for 1985 ITE/Silsoe Survey

Reference Image	Image for Comparison Ratio of Relative Scene Contrast * 22.08.85	30.08.85	31.08.85	10.09.85
21.08.85	1.014	1.170	0.965	1.176
22.08.85		1.081	0.952	1.055
30.08.85			0.865	0.903
31.08.85				1.086

* Ratio between relative scene contrast in reference image and image for comparison. Scene contrast was determined by average spectral albedo in channel 1 for 8 brightest soil surfaces over 8 darkest soil surfaces.

The image acquired on 31 August 1985 produced constantly higher ratio values for relative scene contrast when compared to other images than any other. All five images could be rated with respect to scene contrast in channel 1 without any inconclusiveness. The stability of the method was confirmed by results obtained from images of the other surveys. Only in one case (3 August and 5 October 1988 for ITE/Silsoe survey) did the definition of bright and dark areas shift the relationship from the reference image towards the image under investigation. As a consequence of the stability of relative ratings, not all images for one survey had to be compared to each other. In order to identify the clearest image it was possible to start with the first date as the reference date and to change the reference to whatever date produced a higher relative contrast than the comparison image.

However, the procedure does not permit a simply absolute comparison of channel 1 or 2 relative scene contrasts. The average spectral albedos for bright and dark soil surfaces, and subsequently the relative scene contrasts, depend on the pixels extracted. Thus, a comparison is only credibly, if identical image positions are compared.

Table A.71 in Appendix II provides the ratios between

bright and dark soil targets for each reference image of the four surveys and the other images on the basis of identical positions of the bare soil pixel values.

A comparison of the two reference images for the ITE/Silsoe study area (31 August 1985 and 3 August 1988) resulted in the 3 August 1988 to be the higher contrast image for channel 1. Comparing the less atmospherically affected channel 2 would have given a different result.

Landsat MSS images were not included in the selection procedure to allow a transfer of the method to areas for which only NOAA AVHRR data is available.

Table 4.9 summarizes the images, which were established as the reference data set for a relative atmospheric correction of NOAA AVHRR data.

Table 4.9: Dates of Reference Images for Relative Atmospheric Correction of NOAA AVHRR Data

Survey	Reference Image for Atmospheric Standardization
CIPEA	31 August 1985
1985 ITE/Silsoe	31 August 1985
CAZS	03 August 1988
1988 ITE/Silsoe	03 August 1988

(e) Standardization to Clear Image

The standardisation of atmospheric conditions comprised a linear transfer of red and NIR apparent spectral reflectances and albedos of an image to those of the standard image. This was carried out for each of the three field survey regions (CAZS, CIPEA, ITE/Silsoe) separately.

i. *Standardization of NOAA AVHRR Images*

The parameters of the linear transformation are summarized in Table 4.10.

Table 4.10: Linear Relationships Between NOAA AVHRR Images to Standard Image for Growing Season

Date	Channel 1			Channel 2		
	Coeff. $p(2)^{-1}$ (%CH2^{-1})	Const. $p(2)$ (%CH2)	Coeff. Determ. r^2	Coeff. $p(2)^{-1}$ (%CH2^{-1})	Const. $p(2)$ (%CH2)	Coeff. Determ. r^2
	CIPEA 1985					
21.08.85	1.028	-1.735	0.88	1.010	-0.479	0.87
22.08.85	1.083	-2.889	0.82	1.012	-0.803	0.71
30.08.85	0.638	6.666	0.62	0.566	11.000	0.64
10.09.85	1.155	-6.790	0.82	1.058	-5.187	0.84
	ITE/Silsoe 1985					
21.08.85	0.926	-0.093	0.96	0.942	-0.004	0.97
22.08.85	0.891	0.723	0.94	0.854	1.755	0.96
30.08.85	1.154	-5.593	0.93	1.121	-5.082	0.96
10.09.85	1.200	-3.959	0.93	1.133	-3.649	0.95
	CAZS 1988					
15.10.88	1.085	-0.717	0.97	0.979	0.445	0.98
05.10.88	1.113	-4.993	0.74	1.132	-6.128	0.87
25.09.88	1.701	-9.221	0.76	1.520	-6.731	0.84
06.09.88	1.542	-9.031	0.89	1.467	-8.456	0.91
20.08.88	0.996	0.989	0.84	1.004	0.687	0.91
01.08.88	1.218	-2.990	0.95	1.214	-3.069	0.97
24.07.88	1.969	-25.958	0.86	1.657	-19.962	0.92
15.07.88	1.379	-13.746	0.87	1.330	-13.380	0.90
04.07.88	1.503	-10.033	0.94	1.510	-10.848	0.97
06.07.88	1.677	-15.703	0.96	2.419	-33.823	0.95
	ITE/Silsoe 1988					
30.10.88	2.478	-21.39	0.90	2.466	-20.94	0.90
24.10.88	1.389	-4.40	0.88	1.284	-4.46	0.91
05.10.88	1.994	-19.89	0.83	1.848	-20.25	0.89
06.09.88	2.683	-26.46	0.91	1.939	-18.88	0.79
20.08.88	0.923	1.11	0.90	1.194	-5.12	0.93
01.08.88	1.402	-8.43	0.94	1.352	-8.52	0.90
24.07.88	1.083	-2.30	0.92	1.095	-2.26	0.96
15.07.88	1.465	-14.67	0.79	1.465	-14.31	0.88
04.07.88	1.202	-6.13	0.81	1.305	-6.68	0.90
31.08.85	0.847	1.44	0.89	0.876	1.95	0.94

ii. *Standardization of Landsat MSS Images*

Landsat MSS was adjusted to NOAA AVHRR by correlating 1.1 km resolution data from bands 2 and 4 to channels 1 and 2. Landsat MSS resampled at 50 m was transformed according to the same parameters. This was considered applicable, since

the 1.1 km resolution MSS image represents a 50 m image with a local low filter applied to it. All other external and sensor conditions were identical. The validity of the assumption was investigated by linearly correlating bands 2 to 4 for both images and comparing coefficients and constants of the correlation. The results for the three Landsat MSS images used for correlating ground to image data are given in Table 4.11.

Table 4.11: Relationship Between Band 2 and 4 Spectral Reflectance for Landsat MSS 50 m and 1.1 km Resolution Images

Date	Resolution (m)	Slope $p(2)^{-1}$ ($\%^{-1}$)	Intercept $p(2)$ (%)	Coeff. of Determination r^2 (unitless)
31.08.85	1100	1.256	-2.140	0.94
	50	1.285	-2.742	0.98
30.08.88	1100	0.993	-0.581	0.98
	50	0.967	-1.434	0.96
08.09.88	1100	1.232	0.954	0.94
	50	1.171	0.137	0.91

Slope and intercept were found to be not significantly different for 50 m and 1.1 km resolution images. This means that for a spectral reflectance in band 2 at 50 m resolution the same corresponding spectral reflectance in band 4 in both the 50 m and the 1.1 km image can be expected. So far, this assumption is only valid for unvegetated areas of bare soil and rock.
The scatter along the line is also comparable between the two resolutions. The presence of vegetation within the IFOV, which could be expected to occur more likely over the 1.1 km resolution image than in the 50 m one, would have increased the distance from the line for these pixels and thus the scatter. It was, therefore, concluded that it is feasible to select pixels at NOAA AVHRR LAC resolution, which can be considered presenting spectral reflectances from unvegetated areas.

Previous investigations for vegetated surfaces exhibited a closer relationship between NOAA AVHRR channel 2 and the average response of Landsat MSS bands 3 and 4 (Taylor *et al*, 1986; D'Souza & Hiederer, 1989). A linear regression analysis between NOAA AVHRR and Landsat MSS 1.1 km resolution for identical image positions was, therefore, carried out for various waveband combinations. The results are summarized in Table 4.12.

Table 4.12: Comparison of Linear Relationships Between NOAA AVHRR Channel 1 and 2 Spectral Albedos and Landsat MSS 1.1 km Bands 1, 2, 3 and 4 for Unvegetated Soil and Rock Surfaces

Date	Landsat MSS	NOAA AVHRR Channel 1			NOAA AVHRR Channel 2		
		Coeff. $p(1)^{-1}$ (%$^{-1}$)	Const. $p(1)$ (%)	Coeff. Determ. r^2	Coeff. $p(1)^{-1}$ (%$^{-1}$)	Const. $p(1)$ (%)	Coeff. Determ. r^2
	Band						
31.08.85	1	1.672	-3.522	0.92			
	2	1.369	0.186	0.97	1.661	-1.364	0.96
	3	1.145	-0.311	0.96	1.400	-2.169	0.96
	4				1.355	0.930	0.96
	3,4				1.378	-0.618	0.96
30.08.88	1	0.455	12.701	0.62			
	2	0.488	10.740	0.88	0.444	14.898	0.74
	3	0.475	10.790	0.83	0.446	14.596	0.74
	4				0.457	14.847	0.75
	3,4				0.452	14.706	0.75
08.09.88	1	2.621	-5.453	0.94			
	2	1.945	-0.440	0.94	2.481	-2.316	0.96
	3	1.481	-1.556	0.91	1.906	-3.922	0.94
	4				1.772	-1.081	0.93
	3,4				0.839	-2.478	0.94
3,4: Average apparent spectral reflectance of bands 3 and 4.							

Channel 1 of NOAA AVHRR appears to be correlated foremost to Landsat MSS band 2. For these two wavebands the radiometric properties are congruent. As for channel 2 no preference could be attributed to either band 3, 4 or the average of both. These findings are in agreement with the general development of soil and rock

reflectance behaviour in the visible and NIR portion of the EM spectrum. The continual increase in reflectance results in high positive correlations between any two wavebands in this portion of the EM spectrum (see Chapter 2).

Nevertheless, apparent spectral reflectances of bands 3 and 4 were standardized to channel 2 apparent spectral albedos of the reference images to allow an assessment of waveband similarities for vegetated areas, where visible and NIR wavebands are not positively correlated.

4.7 Discussion of Pre-processing Procedures

The pre-processing procedures applied were governed by the need to minimize spatial, temporal and radiometric variations and differences between satellite data. Their implementation was mainly determined by the amount of data to be processed and the equipment available. An influence of the procedures applied on VIs, like the radiometric correction function, was demonstrated. The conclusions drawn and implications for interpretating the results are given below.

4.7.1 Available Satellite Data

For the ITE/Silsoe survey of 1985 a suitable NOAA AVHRR and Landsat MSS image acquired at the same day and overlapping with the sampling period was available (31 August 1985). For 1988 surveys acceptable NOAA AVHRR and Landsat MSS images were acquired up to four weeks apart (ITE/Silsoe study area).
It can be concluded that although the number of images in 1985 was small, more valid deductions about the potential of satellite VIs for estimating rangeland vegetation quantities can be obtained from correlating Landsat MSS to ground and NOAA AVHRR data than for 1988. Within four weeks ground conditions can be expected to change significantly, as demonstrated in Chapter 3.

The advantages of reducing scene variations offered by MVCs could not be investigated due to the temporal spacing of satellite data. As a consequence, other methods of minimizing cloud cover or changes in atmospheric conditions had to be explored.
For a single date field survey a closer temporal spacing of NOAA AVHRR images to the sampling period is recommended. As demonstrated by CIPEA and CAZS multi-temporal sampling surveys the amount of herbaceous vegetation found at the end of the growing season does not necessarily constitute the maximum quantity of the year. Subsequently, MVC integrated over the whole growing period cannot be correlated to the appropriate ground data if only one survey at the end of the season is used to estimate herbaceous rangeland vegetation quantities. For those cases the maximum amount of vegetation during the growing season should be available.

4.7.2 Data Transformation

Reading NOAA AVHRR tapes presented unforeseen difficulties with the image processing system and NOAA 10 bit data. This was found to be one of the major obstacles for the data analysis and VI calibration. Apart from geometric corrections, alternative methods for analysing satellite data had to be designed. For any operational rangeland monitoring system tape format and input routine of the processing unit would have to conform.

4.7.3 Cloud Masking

Total cloud cover of pixels could be successfully identified by setting a spectral reflectance threshold in the red waveband. A visual inspection of images revealed that haze could not be reliably detected by the method.
By employing local variation partial cloud cover over a site could be identified by a steep increase in variation at a site for a single image. On the other hand, a lower than average

variation, which would indicate the presence of sub-pixel clouds or strong haze, could not be reliably employed. A more frequent temporal sequence of images than 14 days would be required.

4.7.4 Geometric Correction

Using Landsat MSS as an intermediate step for matching NOAA AVHRR data to a map projection was found a feasible method, providing a high degree of accuracy (< 1 pixel average positional rms error). On the other hand, a number of disadvantages of the method were also encountered. Fitting a polynomial function to a set of GCPs does not necessarily correct for the distortions within the image. The rms error only represents the average deviation from GCPs and not as such the geometric discrepancy between images. Thus, the achievable accuracy of the method very much depends on the quality of the maps, which was found to be lacking. In addition, the large number of GCPs required for accurate image referencing (20 to 25 GCPs) constitutes a tedious and time consuming process. For an operational system a geometric correction procedure, based on an orbital model would be better suited (Forrest, 1981; Friedman *et al*, 1983). The advantage of employing a satellite model orbit for image referencing instead of GCPs is the use of a simpler, shorter and, therefore, faster programme. The introduction of errors by a user is reduced, because less interaction occurs. The process can be highly automated and is, consequently, more applicable for vegetation monitoring with NOAA AVHRR than a GCPs based referencing method.

The method suggested comprises a hybrid procedure between an orbital model and the use of GCPs. After pre-correction of images according to a model an intermediate image would be matched manually to a reference image for easier identifications of GCPs. A modified transform equation is thus established, incorporating model and GCP parameters. Provided suitable sites can be established over the monitoring area an automated process could be used to identify a set of GCPs.

4.7.5 Radiometric Correction

It could be demonstrated that changes in illumination conditions and instrument properties can modify ratio VIs. Remaining variations of the recorded instrument response over non-changing ground surfaces were assessed.

(a) Sensor Response Characteristics
Without adjusting for the sensor degradation for NOAA AVHRR ratio VIs would decrease with time. Empirically determined correction factors (Holben & Kaufman, 1989) effectively compensated for the decrease in instrument sensitivity.

(b) Scene Illumination
Annual oscillations of the solar distance were accounted for. Changes in illumination conditions could not be fully eliminated by using a cosine correction based on the solar zenith angle. A reduction in apparent spectral albedo towards the end of growing season was observed. This was attributed to an increase in shadowed areas from vertical protrusion. Other than normalizing images to a set level of spectral albedo no method for neutralizing this trend was considered applicable.

(c) Viewing Geometry
The dependency of ratio VIs on the sensor scan angle was analysed over the study area for NOAA AVHRR data. The inconsistent variation in the forward scattering direction could not be reliably attributed to a single factor. It was considered most likely that the relative solar azimuth angle to the scan line was of major importance. A dominance of photosynthetically active vegetation over bare soil and senescent vegetation could also contribute to the pattern due to different preferences in scattering directions. Since data located outside the central 20° either side from the nadir was incorporated a modification of VIs due to view angel effects can be expected. For an operational system a restriction in the viewing angle should be observed.

(d) Landsat MSS

The maximum DN for determining radiometric transformation parameters had to be estimated by assessing image data, since the decompression method of the receiving station was unknown. As a consequence, the agreement between different Landsat MSS images was found to be less than for NOAA AVHRR data. In addition, the parameters published in the literature were found to vary between sources. A standardization to a reference image could correct for the variations. For a transformation of quantitative comparisons between the two sensors the processing steps applied before distribution are needed.

(e) NOAA AVHRR

The radiometric correction of NOAA AVHRR DN to apparent spectral albedo included a conversions of the transformation parameters from being based on solar irradiances from Thekaekara to those from Neckel and Labs. The modification is recommended in order to achieve a closer correlation between NOAA AVHRR and Landsat MSS data.

4.7.6 Atmospheric Correction

From the range of methods for reducing the influence of variable atmospheric conditions on the surface leaving signal presented in Chapter A4, Appendix I only one was considered applicable to the conditions of the survey. It was assumed that the reflectance of bare soils and rocks was constant over time and that areas the size of the sensor IFOV could be identified on images. The validity of the assumptions, as far as this project is concerned, was demonstrated for three study areas. Reference images could be determined by using identical image positions for a binary decision process. The criterion of the relative scene contrast provided largely unambiguous results. Landsat MSS data was adjusted to NOAA AVHRR via 1.1 km resolution images. Close relationships were found between MSS 1.1 km and NOAA AVHRR wavebands. Averaging bands 3 and 4, on

the other hand, did not improve the relationship between sensor wavebands for bare soil and rock surfaces.
The radiometric standardisation of images was also considered applicable in reducing other variations between images, like effects of illumination conditions and viewing geometry.

4.8 Conclusions and Implications of Pre-Processing

Identified as major impediments in pre-processing Landsat MSS and NOAA AVHRR data were technical problems with the image processing system and a lack of accessible information. While the former could be overcome by using a different environment for data analysis, the latter required a number of assumptions to be made, for example about the decompression parameters of Landsat MSS.
Furthermore, a lack of a standardized terminology and units in the literature for radiometric and atmospheric corrections had to be experienced. This and transcript errors in the published literature strongly suggests that pre-processing procedures and routines should be documented and made available more easily.
In detail, the following conclusions from pre-processing Landsat MSS and NOAA AVHRR can be drawn:

- *Image Processing System*
  File format and data compatibility of the image processing system should be examined *a priori* by practical tests. Routines of the system must be documented.

- *Cloud Detection*
  For calibrations of VI data whole images should be rejected, if the presence of sub-pixel clouds is suspected over some ground data sites.

- *Local Variation*
  Sample sites with a C.V. of 10% or more should be excluded from VI calibrations (inhomogeneous area).

■ *Geometric Correction Procedure*

For an operational system a combination of orbital model and GCPs is recommended.

■ *Illumination Conditions*

A cosine correction and ratio VIs cannot correct for all variations introduced by changes in the solar elevation and may be omitted.

■ *Scan Angel*

The image from NOAA AVHRR should be restricted to the central 500 pixels. The variations in ratio VIs at larger scan angles are variable and are not fully understood.

■ *Landsat MSS Radiometric Correction*

Pre-processing of tapes should be more widely documented and standardized.

■ *Geometric Simulation of NOAA AVHRR LAC Data*

For bare soil areas of the Sahel NOAA AVHRR LAC pixels can be simulated by averaging Landsat MSS pixels without significant loss in spectral information.

■ *Radiometric Simulation of NOAA AVHRR Channel 2*

For bare soil areas of the Sahel the average of Landsat MSS bands 3 and 4 is not more closely related to NOAA AVHRR channel 2 than band 4 alone.

■ *Atmospheric Correction*

Image standardization to bare soil spectral reflectance values was found an acceptable method to reduce variations in atmospheric conditions between images. It cannot be directly employed to account for variations between different areas and additional work is required.

The implication of these unexpected difficulties for a satellite VI calibration to ground data is that quantitative results from independent investigations cannot be compared directly, since pre-processing procedures are likely to be different.

Generally, with respect to an operational system for monitoring

rangeland vegetation in the Sahel, an investigation into the capabilities of the image processing system is strongly recommended. Negligence of these considerations in the planning process could leave the provision of almost real-time quantitative rangeland estimates but a theoretical concept.

5. RELATIONSHIP BETWEEN GROUND AND SATELLITE DATA

In this chapter field survey and satellite data are combined and their relationships investigated. Concepts and feasibility of establishing a statistical correlation between the two data sets were introduced in Chapter 2.

Firstly, the various practices used for locating sample sites in terms of image co-ordinates are compared. Next, different approaches to establishing image values representing the satellite sensor response to reflected EM energy over the sample site are introduced. These are applied in order to assess the effects of spatial and radiometric simulations of NOAA AVHRR LAC data by Landsat MSS. Results from these investigations are utilized to interpret relationships between herbaceous vegetation estimates and satellite RVI, NDVI and PVI.

Linear and logarithmic relationships between herbaceous rangeland vegetation estimates and satellite VIs are assessed on the basis of the coefficient of determination (r^2) obtained from regression analyses. This represents the amount of variability in VIs, which is explained by the regression (Norusis, 1988). For relationships between field and satellite data to be considered useful for calibrating VIs a minimum of 50% for r^2 values was considered appropriate.

5.1 Transect Positions

The three data sets - ground survey data, Landsat MSS and NOAA AVHRR image data - were linked by the map co-ordinates of sample sites. Hence, a vital step in a successful correlation between data is the capability to determine survey site positions confidently and accurately in all three. Without positional congruence, the relationships established between satellite VIs and ground data are not representative, because

positional deviations, and not the sensitivity of VIs to vegetation quantities, will be the main source of variations between data sets. The degree of a tolerable error is determined by the variation of EM energy reflected from the ground at the scale of the IFOV and the radiometric sensitivity of the satellite sensor instrument.
For determining sample site positions a variety of methods were employed for different field surveys. They were presented in the appropriate sections of Chapter 3. In this chapter the influence of unavoidable differences between image and map positions of sample sites on the correspondence between ground and satellite data are estimated.

5.1.1 CIPEA Survey

The starting co-ordinates of transects during the 1985 CIPEA field survey were determined by standard instruments onboard a light aircraft (deLeuwe, 1986). An unknown amount of error associated with these positions can be expected. The transects were also recorded by aerial photographs. With the aid of these photographs transects were identified on a geometrically corrected Landsat MSS image with 50 m resampling (Taylor *et al*, 1986).
However, only eight transects, which were situated within the image acquired during the growing season of 1985 (31 August 1985, 194/49), could be re-positioned. For the majority of sites (17 sites) no high resolution satellite data acquired during a growing season was available (see Table A.20, Appendix II). It was found impossible to confidently determine any site locations on dry season images. Even a Landsat TM image did not display a sufficient amount of detail to allow transect positions to be fixed. The apparent uniformity on the ground was partly caused by a lack of photosynthetically active vegetation, but also by an uniform soil colour and dust in the atmosphere at the time of image acquisition. In those cases, positions recorded by the aircraft instruments had to be applied. In addition, no information on transect directions could be obtained for those sites and the starting point had to

be interpreted as the transect centre.
Table 5.1 summarizes map and image co-ordinates used during this survey. For sites, which could be identified on a Landsat MSS image discrepancies between positions recorded by the aircraft instrument and those established directly on images with the aid of aerial photographs are provided.

Table 5.1: Map and Image Co-ordinates of 1985 CIPEA Field Survey Sites

Site No.	Position from Aerial Photos UTM Co-Ordinates East (m)	North (m)	Direction (deg)	Difference to Aircraft Reading East (m)	North (m)
2	794827	1718593	300	167	-1737
3	794527	1738793	90	-2578	695
4	800877	1748043	270	-3474	718
5	802077	1775143	30	-1187	505
6	793977	1796693	60	-863	-475
7	791777	1822543	250	2793	353
11	288535	1845537	270		
12	368632	1863370			
13	348971	1854317			
14	307758	1812152	300		
15	300382	1788313	270		
16	218464	1722771	300		
17	804477	1685693	210	-1364	-583
18	816027	1750893	240	871	481
19	373499	1783124			
20	375973	1747153			
21	297460	1650887			
22	248719	1620908			
23	250729	1648561			
24	242401	1704000			
25	228161	1707817	0		
26	325910	1742836			
32	244997	1772278	300		
33	265102	1819989	270		
34	209930	1684121	180		

In some cases estimates for transect directions could be obtained without being in a position to locate the site accurately. These were mainly transects situated close to a road, which was visible on the Landsat TM image. The direction could be approximated, if the side of the road on which the transect was set could be determined. From the annual time when the photographs were taken, which was recorded by the camera, and the angle of shadows the transect direction was estimated. The central point of the transect could thus be estimated.

Since these sites were not relocated a change in sample site location could not be obtained.
On average, no systematic error in aircraft readings could be observed. Distances varied between 167 m and 3474 m in east-west and 475 m and 1737 m in north-south direction or up to 3 LAC pixels at nominal resolution. The rms difference was determined as being 1311 m in east-west and 806 m in north-south direction.

5.1.2 CAZS Survey

Site co-ordinates of the 1988 CAZS survey in Mali were established by identifying transect starting positions on 1:200000 maps and by a GPS (see Chapter 3.2.3).
Table 5.2 summarizes UTM co-ordinates established by map identification and differences to GPS positions.

Table 5.2: Map and Image Co-ordinates of 1988 CAZS Field Survey Sites

Site No.	Position from Maps (1:200000) UTM Co-Ordinates East (m)	North (m)	Direction (deg)	Difference to GPS Reading East (m)	North (m)
A	527549	1717173	330	-1512	200
B	525020	1715943	150	-1514	669
C	522791	1714713	135	-1337	586
D	522791	1714713	305	-1337	586
E	522191	1713639	220	-368	258
F	523066	1739446	275	-636	415
G	521877	1738681	250	-1165	241
H	521128	1738371	252	-1156	702
J	519638	1738370	252	-583	1048
K	518449	1738678	332	-829	1125
L	463842	1738855	200	-373	-970
M	467255	1735774	345	3388	-250
N	483185	1730989	232	76	-1310
P	484964	1730988	69	-137	-317

The rms difference between map and GPS co-ordinates in east-west direction was calculated as being 1311 m and 715 m in north-south direction. On average, readings provided by the GPS were further west and north than map co-ordinates.

5.1.3 ITE/Silsoe Surveys

The determination of site co-ordinates during the three ITE/Silsoe field surveys was based on maps, geometrically corrected Landsat MSS images from 1984, 1985 and 1988 and a GPS (see Chapters 3.3 and 3.4). Since the position of roads on the maps available was found to be unreliable, sites were mainly identified on images. For those 1985 and 1988 sites, which were revisited in 1989, GPS readings were obtained wherever possible. A comparison between image and GPS co-ordinated is presented in Table 5.3.

The rms difference between image and GPS co-ordinates was established as being 3234 m in east-west and 1451 m in north-south direction. The discrepancy of almost 8 km at Site 11 could not be explained. The GPS reading was recorded twice, rendering a transcription error unlikely. Also, the transect can be clearly identified on the image. Excluding site 11 from computing the rms difference values of 1978 m in east-west and 1538 m in north-south direction were calculated.

As was the case for CAZS sites the GPS provided positions further to the west and north for the majority of sites. This would indicate the presence of a systematic error of the instrument for site positions within the study areas.

5.2 Image Data Sampling Methods

Herbaceous rangeland vegetation measured along transects was averaged to provide an estimate of the yield over the sampling site. The spatial extent over which these estimates can be assumed to be valid is unknown. A single 1 km transect could be covered by three NOAA AVHRR LAC pixels, which contain the integrated reflected EM energy of surface features within the IFOV from approximately 3.6 km^2. In that case the value of a single pixel closest to the transect centre is not more representative for the whole site than any of the other two pixels. For that reason, several methods of sampling image data were employed.

Table 5.3: Map and Image Co-ordinates of 1985 and 1988 ITE/Silsoe Field Survey Sites

Site	Position from Image Hard-Copies UTM Co-Ordinates East (m)	North (m)	Direction (deg)	Difference to GPS Reading East (m)	North (m)
	1985 ITE/Silsoe Sites				
A	801727	1683343	212	-462	187
B	801127	1685193	233	-7962	-738
C	813877	1696693	230	-851	426
D	796127	1711493	80	*	
E	793677	1714543	256	*	
F	796027	1700843	180	*	
G	797377	1700043	160	*	
H	798527	1692793	160	*	
	1988 ITE/Silsoe Sites				
1	813877	1696693	230	-851	426
2	816027	1697993	327	*	
3	816077	1703993	325		
4	810977	1703743	186	-2429	2109
5	813227	1703593	230	*	
6	800177	1745243	220	-1011	11
7	793377	1733643	300	-1102	2875
8	793677	1718393	320	*	
9	797377	1700043	160	*	
10	799127	1690443	300	-844	1124
11	801127	1685193	233	-7962	-738
12	801727	1683343	212	-462	187

* No GPS readings available.

5.2.1 Image Data Sampling Methods for Landsat MSS

First, the following modifications were applied to Landsat MSS data to increase the correspondence with NOAA AVHRR data:

(a) **Spatial Degradation**

Geometrically corrected 50 m resolution images were degraded to simulate a 1.1 km image. Two methods were applied:

i. *Image Averaging*

For the whole image the average DNs over an area of 22 by 22 pixels was assigned to one new pixel.

These degraded images were also employed to geometrically match NOAA AVHRR data (see Chapter 4.3.4). Spatially simulated images were then radiometrically and atmospherically corrected.

ii. *Site Averaging*

For ground sampling sites only, geometrically corrected 50 m Landsat MSS data was degraded to 1 km resolution by computing the average spectral reflectance for an area of 20 by 20 pixels. The centre of the processing area corresponded to the centre of a transect. The procedure applied did not allow to average 22 by 22 pixels to simulate the nominal LAC pixel IFOV. The difference in size of 10% to the nominal size, however, was regarded as being not significant to the investigation.

For referencing data it should be considered that the programme used for image averaging (IM.REDUCE) introduces a shift of up to 21 50 m pixels. Some of the shift is systematic and can be accounted for, but there is also a random component introduced by geometrically correcting images. As a consequence, there is a limited suitability of the reduced Landsat MSS data to estimate the effect of spatial degradation on radiometric properties over specific sites. For this purpose site averaging was introduced. Here, the assumed transect position matches both 50 m and degraded data. This allows to estimate the effect of spatial degradation over a particular site. On the other hand, geometrically corrected NOAA AVHRR images could not be derived from spatially degraded Landsat MSS data.

(b) **Radiometric Simulation**

Nominal radiometric characteristics of NOAA AVHRR channel 2 deviate from those of Landsat MSS Band 4 (see Chapter 2.3.3). It was suggested to simulate channel 2 by using the average instrument response from bands 3 and 4 (Taylor *et al*, 1986; D'Souza & Hiederer, 1989). This was applied to all Landsat MSS data.

For investigations into the relationship between Landsat MSS and NOAA AVHRR LAC data image representations of sample sites were obtained from the following image data sampling methods:

(a) **Pixel Values Along Transects at 50 m Resolution**
Transects were located on geometrically corrected Landsat MSS images. The average values of pixel values along the transects within ± 1 pixel distance from the transects were obtained. A nearest neighbour algorithm was used to determine appropriate pixels. The programme employed is presented in more detail below.

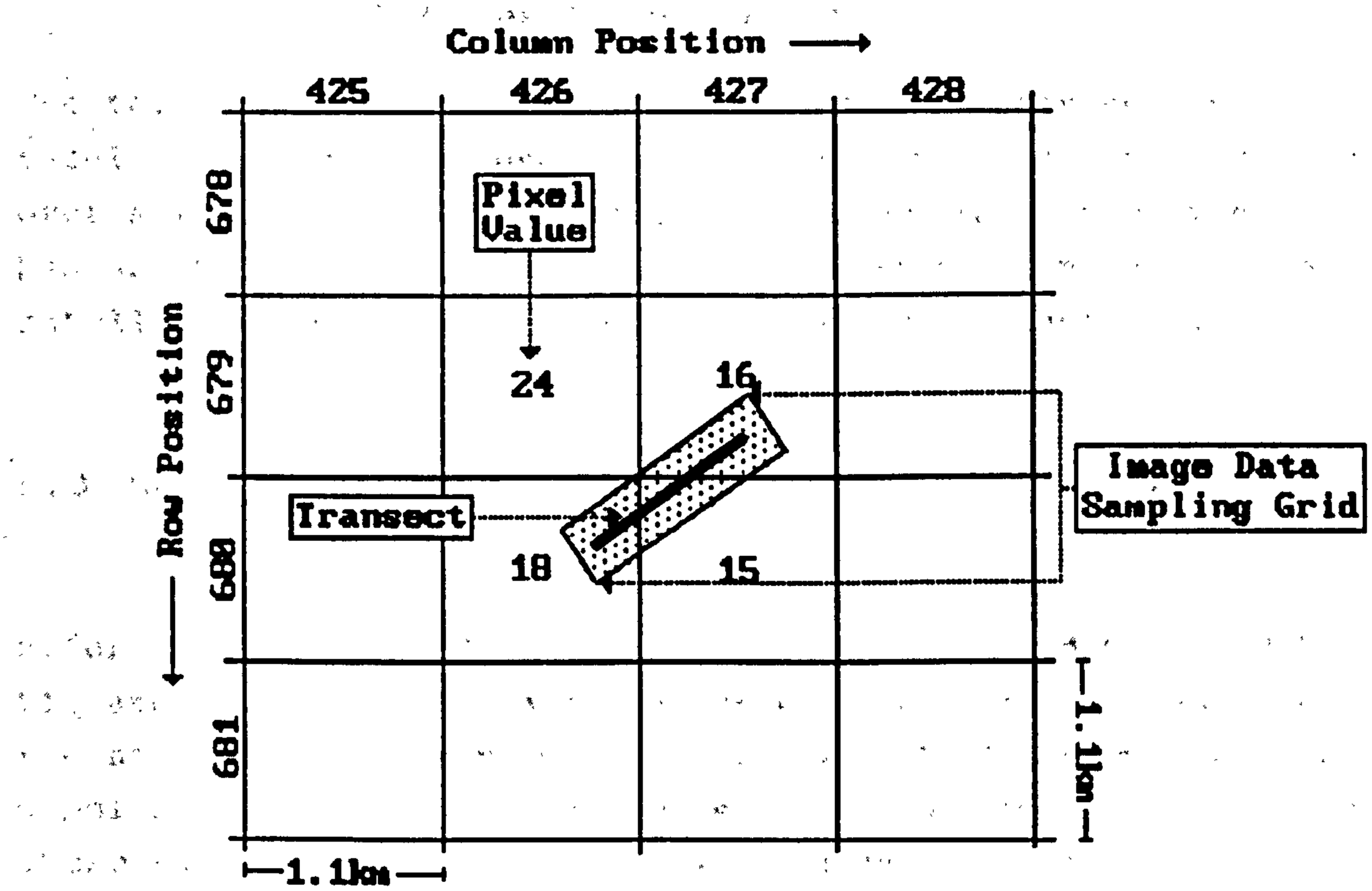
(b) **Site Averages 20 by 20 Pixels at 50 m Resolution**
The method of site averaging has been introduced in the previous section.

(c) **Central Pixel of Transect at 1.1 km Resolution**
The nearest pixel to the centre of a transect was determined.

(d) **3 by 3 Average Over Transect at 1.1 km Resolution**
The average value of the central pixel and the eight pixels surrounding it was established.

(e) **Pixel Values Along Transects at 1.1 km Resolution**
Transect directions were not aligned to columns or lines of the images, so a programme for resampling pixel values along the transects on the images was developed. A rectangular window was defined with sides of equal distance to the transect. Within the window pixel values are sampled at grid points. The size of the window and the spacing of grid points could be adjusted as required. Transect values were sampled either by selecting the value of the nearest pixel or by using a linear interpolation. The latter was found to be more useful for the small number of AVHRR pixels covering sample sites. A graphical description of the transect sampling method is given in Figure 5.1.

Figure 5.1: Schematic description of Transect Sampling Method for 1.1 km Resolution Landsat MSS and NOAA AVHRR Images



This method permits consistent results to be obtained and also provides a standard deviation of image data for the transect. Spectral reflectance values and the standard deviation were used to detect cloud covered and partially cloud covered sites.

5.2.2 Image Data Sampling Methods for NOAA AVHRR

Spectral albedos for survey sites were established by three different methods:

i. *Central Pixel of Transect*

ii. *3 by 3 Average Over Transect*

iii. *Pixel Values Along Transect*

The thus established data was interpreted as representing satellite sensor responses to EM energy reflected from surfaces over sample sites. It was employed for comparisons between Landsat MSS and NOAA AVHRR images and for relating ground to satellite data, as presented in the following sections.

5.3 Landsat MSS and NOAA AVHRR Data Comparison

Before the correspondence between Landsat MSS and NOAA AVHRR VIs and quantities of rangeland vegetation can be established the satellite sensor response to reflected EM energy over the sampling site has to be determined. Five methods of deriving at these values were investigated with respect to their suitability of representing satellite data.
Also investigated were the effects of differences in spatial resolution and radiometric sensitivity between the two sensors. The analysis was based on actual transect data and results are directly applicable to individual surveys.

5.3.1 Spatial Correspondence Between Satellite Data

NOAA AVHRR images were matched to the projection of Landsat MSS scenes by a second order polynomial to rms errors of 0.5 pixels or better (see Chapter 4.3.4). As stated before, the rms error is not necessarily representative of the average positional disparity between two images, because it is derived from the reference data, which was used to establish the transfer equation in the first place. In addition, completely excluded from it are GCPs, which are considered too far out of their calculated position by the software. A more characteristic rms error for the positional correspondence between images would

require an independent set of GCPs to be established and analysed. This was considered impractical for the amount of data involved. Also, a quantitative measurement of positional agreement between images was not needed. It is uneven across the image and would not provide a measurement of the discrepancy at a sampling site. Required was an indicator of how closely transects could be represented on NOAA AVHRR LAC images. For this purpose a linear regression analysis between results of five Landsat MSS and three NOAA AVHRR image data sampling methods for each of the four surveys (see Chapter 5.2) was carried out.

As a standard for comparisons Landsat MSS values at 50 m resampling were assigned. With transects being identified on geometrically corrected Landsat MSS scenes the corresponding spectral reflectances were assumed to be representative for the sites. The average spectral reflectance of 20 by 20 50 m Landsat MSS pixels over the centre of the transects (site averaging) simulated one NOAA AVHRR LAC pixel located exactly over the transect. Also employed were 1.1 km Landsat MSS data obtained from a routine on the host computer of the image processing system (IM.REDUCE), which introduces a shift of up to one pixel. The relationships between these data sets would be indicative of the spatial correspondence between images for the ground data sampling sites.

Results of the investigation are presented in this chapter for each of the surveys and sensor separately.

(a) **CIPEA Survey**

Linear relationships between Landsat MSS spectral reflectances from 31 August 1985 obtained from different image sampling methods are summarized in Tables 5.4.

Table 5.4: Relationships Between Image Data Sampling Methods for Landsat MSS Data for 1985 CIPEA Survey

Method Dependent	Method Independent Variable B1xB1	B2xB2	B3xB3	B4xB4	B1xB1	B2xB2	B3xB3	B4xB4
50 m	20x20 Average				Central Pixel			
Coeff.	1.00	1.02	1.02	1.03	0.93	0.93	0.79	0.86
Const.	-0.01	-0.42	-0.66	-0.87	1.93	1.95	5.57	3.84
r^2	0.99	0.99	0.99	0.99	0.61	0.57	0.48	0.59
50 m	3x3 average				Transect			
Coeff.	1.17	1.24	1.22	1.21	1.12	1.10	1.09	1.13
Const.	-3.73	-4.73	-5.35	-5.33	-2.42	-1.83	-1.87	-3.20
r^2	0.85	0.78	0.75	0.79	0.84	0.72	0.58	0.64
Central	3x3 average				Transect			
Coeff.	0.94	1.06	1.13	1.12	0.97	1.02	1.23	1.24
Const.	0.85	-1.62	-3.65	-3.31	0.33	-0.62	-5.81	-6.21
r^2	0.78	0.88	0.85	0.85	0.89	0.94	0.97	0.97

B1xB1: Band 1 spectral reflectance from method a vs. Band 1 spectral reflectance from method b

Landsat MSS data for CIPEA sites could only be established for eight transects (see previous paragraph). Due to the close similarity of Landsat MSS site averages to 50 m transects (r^2 of almost 1.0) only the 50 m transects were used for comparisons with NOAA AVHRR data. Apart from that, 50 m data only corresponds well ($r^2>0.75$) to 3 by 3 averages. The low correspondence ($r^2<0.5$) to central 1.1 km pixels indicated difficulties in covering actual transect positions by one NOAA AVHRR pixel. Results from the transect sampling method at 1.1 km resolution were in between those for single pixels and 3 by 3 averages. Values of coefficients of determination were mainly controlled by spectral reflectances attributed to Site No. 2. Local image data variations at that site also indicated that it was situated in a area of high diversity (C.V. of 26% for band 2, 50 m). Here, small positional changes produced largely different spectral reflectances.

Additional information on the effects of geometric correspondence on radiometric affinity was provided by

shifting the 1.1 km resolution data by 0.5 pixels in y-direction and excluding Site No. 2 from the analysis. The results are presented in Table A.22 in Appendix II. Practically no correlation between 50 m and the central 1.1 km pixel value could be observed. Also, central and 3 by 3 averages were not correlated. When excluding data from Site No. 2, relationships greatly improved to levels approximately comparable to those found when including Site No. 2 data for the original co-ordinates. These findings indicate that the resampling procedure employed on the image processing system did not match Landsat MSS data at 50 m and 1.1 km resolution accurately. The low correlation could not be attributed to the averaging process applied to spatially degrade the data, because 20 by 20 pixel averages were highly correlated to 50 m transect data. Furthermore, the findings suggest that in areas wiht spectrally different surfaces (C.V. more than 20% in case of Site No. 2) a spatial difference between images of even less than one pixel could result in low correspondences (see Chapter 5.6.1).

For NOAA AVHRR data results from linearly correlating channels 1 and 2 obtained from 3 by 3 averages and selecting a single pixel value (central position) are presented in Table 5.5.

For positions provided by aircraft instruments the correlation between the two methods for identical wavebands is generally very high ($r^2>0.88$). For image positions located from aerial photographs the correspondence drops to values of 0.61 for the coefficient of determination for 31 August 1985 image. A graphical presentation of the development of coefficients of determination over time is given in Figure 5.2.

Table 5.5: Relationships Between NOAA AVHRR Data from Different Image Sampling Methods for 1985 CIPEA Survey

Sampl. Method	Date of NOAA AVHRR Image Acquisition									
	21.08		22.08		30.08		31.08		10.09	
	1x1	2x2	1x1	2x2	1x1	2x2	1x1	2x2	1x1	2x2
Central	Aircraft Site Positioning, 3 x 3 Averages*									
Coeff.	1.01	0.94	1.21	1.14	0.87	0.83	0.93	0.93	1.14	1.15
Const.	-0.4	1.6	-4.4	-3.7	3.2	5.0	1.8	2.0	-3.9	-4.4
r^2	0.91	0.93	0.95	0.91	0.93	0.91	0.95	0.92	0.88	0.90
Central	Aerial Photograph Positions, 3 x 3 Averages**									
Coeff.	0.99	1.14	1.69	2.32	1.02	1.19	0.99	0.89	1.15	1.31
Const.	-0.1	-4.2	-14.3	-38.5	-0.8	-5.3	0.1	2.9	-3.8	-8.4
r^2	0.92	0.95	0.86	0.82	0.61	0.65	0.98	0.92	0.65	0.65
Central	Aerial Photograph Positioning, Transect Sampling**									
Coeff.							1.04	1.01		
Const.							-0.9	-0.2		
r^2							0.98	0.94		

1x1: Channel 1 spec. albedo vs. Channel 1 spec. albedo
*: Relates all CIPEA sites from aircraft positioning.
**: Relates 8 CIPEA sites from image positions.

The larger variation for sites identified by aerial photographs could be attributed to a general increase in scatter rather than just a single site as it was the case for Landsat MSS. Transect sampling was only applied to one image (31 August 1985), which corresponds to the date of the Landsat MSS image acquisition. It was found to provide almost identical coefficients of determination as were obtained from 3 by 3 or central pixel image sampling methods.

(b) 1985 ITE/Silsoe Survey

During the 1985 ITE/Silsoe survey rangeland vegetation along eight transects was estimated. The relationships between Landsat MSS from different image sampling methods are summarized in Table 5.6.

Figure 5.2: Development of Coefficients of Determination from Linear Regression Between Transect Sampling and a Single Pixel for Channels 1 and 2 over 1985 CIPEA Field Survey Sites

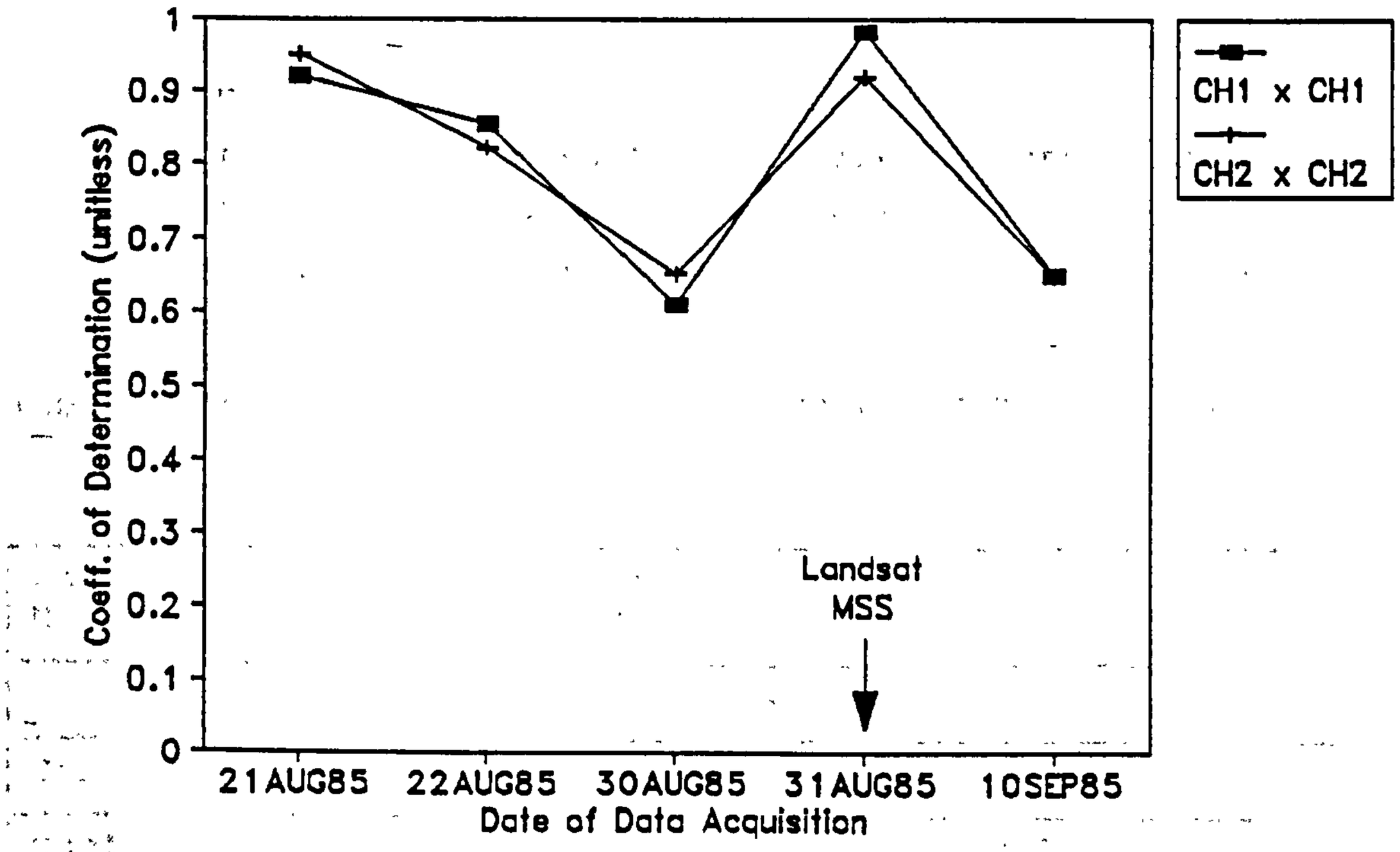


Table 5.6: Relationships Between Landsat MSS Data from Different Image Sampling Methods for 1985 ITE/Silsoe Survey

Method Dependent	Method Independent Variable B1xB1	B2xB2	B3xB3	B4xB4	B1xB1	B2xB2	B3xB3	B4xB4
50 m	20x20				Central			
Coeff.	1.10	1.10	1.00	1.00	1.19	1.14	1.08	1.11
Const.	-1.87	-1.98	-0.27	-0.21	-3.80	-2.83	-2.55	-3.27
r^2	0.98	0.96	0.97	0.97	0.79	0.81	0.88	0.88
50 m	3x3 average				Transect			
Coeff.	1.35	1.46	1.15	1.14	0.76	0.80	0.86	0.94
Const.	-6.57	-8.40	-3.73	-3.94	4.63	3.59	2.17	-0.08
r^2	0.81	0.88	0.83	0.84	0.41	0.41	0.52	0.60
Central	3x3 average				Transect			
Coeff.	1.09	1.11	1.01	0.98	0.71	0.57	0.71	0.75
Const.	-1.41	-1.66	0.02	0.51	5.66	8.25	6.34	5.35
r^2	0.94	0.81	0.87	0.87	0.64	0.32	0.47	0.53

Apart from transect sampling all other sample site representations were highly correlated. The deviation of a single site (Site G) proved to be sufficient to produce the comparatively low values for the coefficient of determination in Table 5.6 for the former image sampling method.

For NOAA AVHRR results of a linear regression analysis between the three methods of establishing sensor responses associated with the sample sites are provided in Table 5.7.

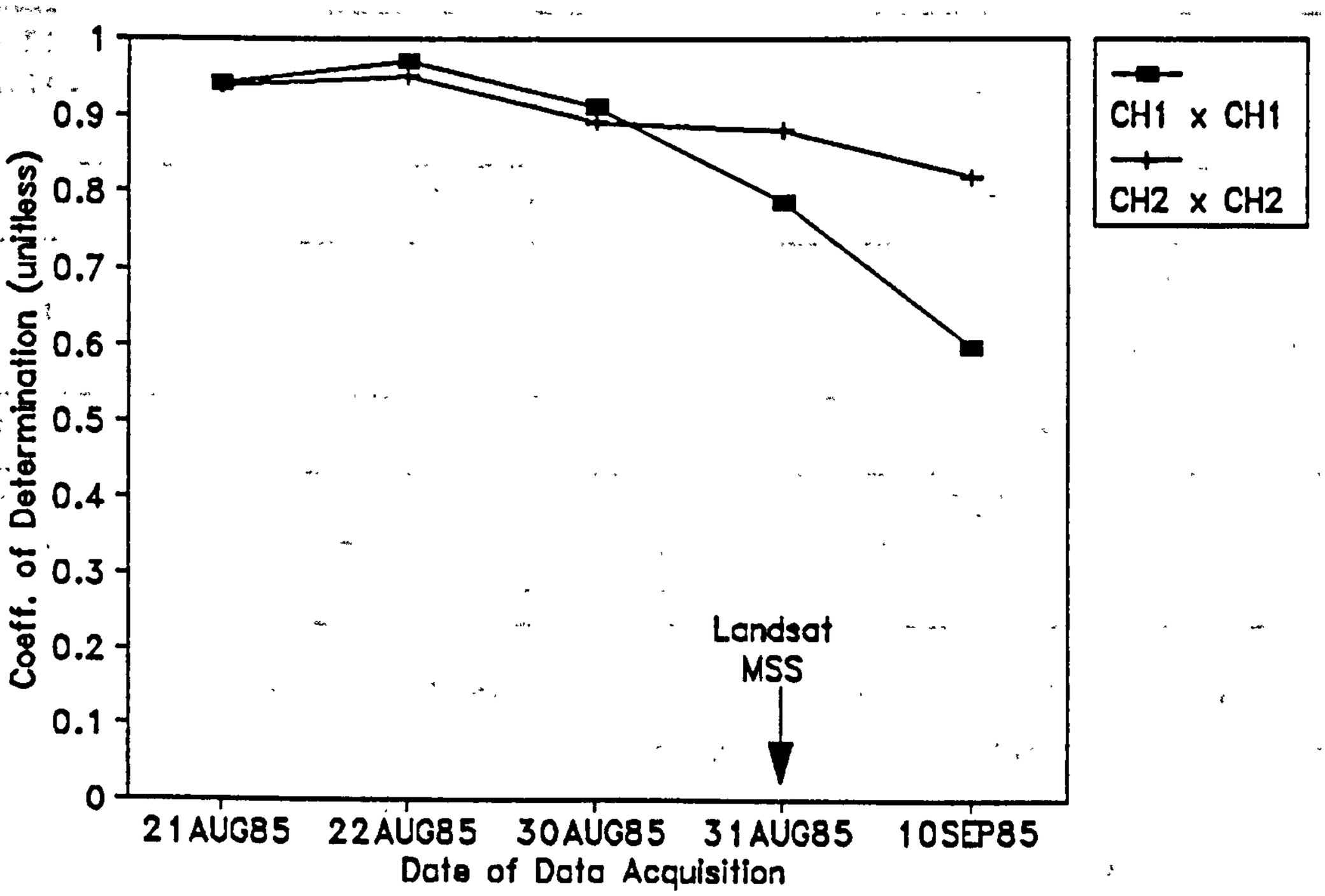
Table 5.7: Relationships Between NOAA AVHRR Data from Different Image Sampling Methods for 1985 ITE/Silsoe Survey

Sampl. Method	Date of NOAA AVHRR Image Acquisition									
	21.08		22.08		30.08		31.08		10.09	
	1x1	2x2	1x1	2x2	1x1	2x2	1x1	2x2	1x1	2x2
Central	3 x 3 Averages									
Coeff.	1.06	1.15	1.11	1.13	0.76	0.76	0.79	0.81	0.78	0.90
Const.	-1.9	-5.2	-3.4	-4.3	4.3	5.1	4.4	4.6	5.3	3.0
r^2	0.94	0.94	0.97	0.95	0.91	0.89	0.79	0.88	0.60	0.82
Central	Transect Sampling									
Coeff.							0.41	0.67		
Const.							11.99	7.63		
r^2							0.21	0.64		
3 x 3	Transect Sampling									
Coeff.							0.71	0.92		
Const.							5.95	1.42		
r^2							0.49	0.90		
1x1: Channel 1 spec. albedo vs. Channel 1 spec. albedo										

As with Landsat MSS the transect method produced a low linear relationship with central pixels and 3 by 3 averages for channel 1, but due to an increased variation at most sites. The slope decreased to 0.41 (channel 1), which indicates that the range of transect values was approximately twice as high as those from other image data sampling methods. A graphical representation of relationships between results from establishing NOAA AVHRR spectral albedos for sample

sites for the five dates of image acquisition is given in Figure 5.3.

Figure 5.3: Development of Coefficients of Determination from Linear Regression Between Transect Sampling and a Single Pixel for Channels 1 and 2 over 1985 ITE/Silsoe Field Survey Sites



As can be seen in Figure 5.3 the agreement within channels between 3 by 3 averages and single pixel values drops markedly for the last two images of that season and differ in that respect from CIPEA sites.

(c) CAZS Survey

During the 1988 CAZS survey in Mali 14 sample sites were visited repeatedly. Because the GPS provided apparently incorrect positions, transects were also located by their map co-ordinates.

Relationships of spectral reflectances obtained from different image sampling methods are given in Table 5.8 for a Landsat MSS image from 30 August 1988.

Table 5.8: Relationships Between Landsat MSS Spectral Reflectances Obtained from Five Different Image Sampling Methods for 1988 CAZS Field Survey and Map Positions

Method Dependent	Method Independent Variable B1xB1-B2xB2	B3xB3	B4xB4	B1xB1	B2xB2	B3xB3	B4xB4
50 m	20x20			Central			
Coeff.	1.00	1.00	1.01	1.02	0.79	0.82	0.83	0.83
Const.	-0.06	0.03	-0.39	-0.67	4.22	3.71	4.02	3.95
r^2	0.99	0.99	0.98	0.98	0.91	0.85	0.76	0.73
50 m	3x3 Average				Transect			
Coeff.	1.01	1.07	1.13	1.16	0.96	0.99	1.06	1.10
Const.	-0.49	-1.72	-3.62	-4.36	0.81	0.13	-1.71	-2.67
r^2	0.92	0.90	0.83	0.82	0.92	0.89	0.85	0.85
Central	3x3 Average				Transect			
Coeff.	1.26	1.25	1.26	1.27	1.19	1.16	1.15	1.16
Const.	-5.56	-5.33	-6.54	-6.89	-3.96	-3.30	-3.83	-4.12
r^2	0.98	0.96	0.94	0.93	0.97	0.94	0.91	0.92

Parameters for linear relationships for GPS positions are given in Table A.23 in Appendix II. Not included in the investigation were Sites L and M, since they were situated outside the Landsat image. The values for coefficients of determination in Table 5.8 display strong linear correlations between all image sampling methods employed.

A comparison between NOAA AVHRR spectral albedos obtained from averaging 3 by 3 pixels values and the central values is presented in Table 5.9.

Table 5.9: Relationships Between NOAA AVHRR Spectral Albedos Obtained from Different Image Sampling Methods for 1988 CAZS Field Survey

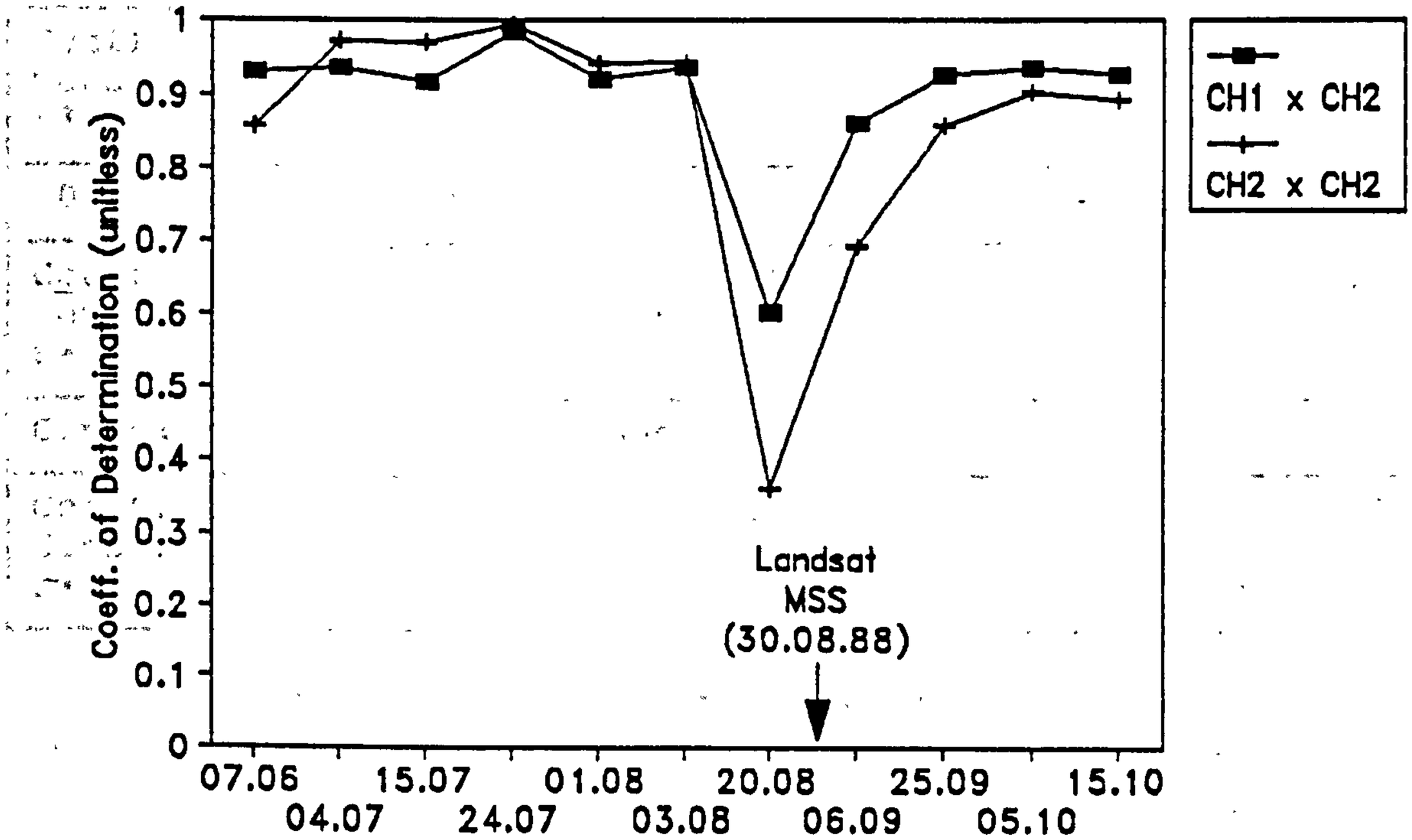
Sampl. Method	Date of NOAA AVHRR Image Acquisition							
	07.06.88		04.07.88		15.07.99		24.07.88	
	1x1	2x2	1x1	2x2	1x1	2x2	1x1	2x2
Central	3 x 3 Averages							
Coeff.	1.07	1.07	0.95	1.01	0.98	0.99	1.00	1.01
Cons.	-1.8	-2.3	1.0	-0.3	0.3	0.0	-0.4	-0.6
r^2	0.93	0.86	0.94	0.97	0.92	0.97	0.98	0.99
	01.08.88		03.08.88		20.08.88		06.09.88	
Coeff.	1.04	1.12	0.99	0.99	0.95	1.36	1.21	1.06
Const.	-1.3	-3.6	-0.1	0.2	-0.6	-10.5	-4.5	-1.4
r^2	0.92	0.94	0.94	0.94	0.60	0.36	0.86	0.69
	25.09.88		05.10.88		15.10.88			
Coeff.	1.37	1.55	1.12	1.09	1.04	1.08		
Const.	-8.0	-13.8	-3.0	-2.6	-1.1	-2.4		
r^2	0.93	0.86	0.93	0.90	0.93	0.89		
Central	Transect							
	20.08.88		06.09.88		25.09.88		05.10.88	
Coeff.	0.96	1.42	1.12	1.11	1.24	1.41	1.07	1.06
Const.	-0.1	-11.2	-2.5	-2.6	-4.7	-9.7	-1.7	-1.4
r^2	0.71	0.79	0.96	0.93	0.93	0.86	0.95	0.93
3 x 3	Transect							
Coeff.	0.89	0.59	0.83	0.83	0.86	0.83	0.93	0.92
Const.	2.5	10.4	3.7	4.6	3.5	4.7	1.9	2.4
r^2	0.94	0.69	0.90	0.83	0.92	0.85	0.96	0.93

Transect image sampling was found to be more closely related to both central and 3 by 3 averages than they were to each other. This could be expected, since the method constitutes basically a local average. Comparatively low values for the coefficient of determination were found for images from 20 August and 6 September. The former image was strongly cloud contaminated and only a few sites remain after cloud screening. On the September image the study area was partially covered by haze.

A graphical presentation of the development of

coefficients of determination over time is provided in Figure 5.4.

Figure 5.4: Development of Coefficients of Determination from Linear Regression Between Transect and a Single Pixel Image Sampling Methods for Channels 1 and 2 over 1988 CAZS Field Survey Sites



The time of the decrease in agreement between the two methods in August and September coincides with the date of the Landsat MSS image for CAZS field survey sites. A low correlation between comparable wavebands of the two sensors can, therefore, be expected.

(d) 1988 ITE/Silsoe Survey

During the 1988 ITE/Silsoe survey herbaceous rangeland vegetation was estimated at 12 sites. Image co-ordinates of the transects were deduced from image hard-copies available in the field. Since GPS positions were found to be unreliable, site so-ordinates were not based them. A summary of linearly relating Landsat MSS spectral reflectances obtained from the image sampling methods applied is given in Table 5.10.

Table 5.10: Relationships Between Landsat MSS Spectral Reflectances Obtained from Five Different Image Sampling Methods for 1988 ITE/Silsoe Field Survey and Image Positions

Method Dependent	Method Independent Variable B1xB1	B2xB2	B3xB3	B4xB4	B1xB1	B2xB2	B3xB3	B4xB4
50 m	20x20				Central			
Coeff.	1.19	1.19	1.19	1.19	0.23	0.55	0.74	0.81
Const.	-3.3	-3.3	-4.4	-4.8	11.4	6.3	4.2	3.0
r^2	0.88	0.92	0.90	0.90	0.05	0.21	0.29	0.33
50 m	3x3 Average				Transect			
Coeff.	0.77	0.80	1.03	1.06	0.78	0.89	1.04	1.11
Const.	2.9	2.6	-1.6	-2.5	2.8	1.1	-1.8	-3.5
r^2	0.43	0.46	0.50	0.44	0.34	0.44	0.50	0.52
Central	3x3 Average				Transect			
Coeff.	0.85	0.86	0.95	0.96	1.10	1.02	1.00	1.02
Const.	2.5	2.2	1.2	1.0	-1.3	-0.3	0.2	-0.3
r^2	0.60	0.76	0.82	0.72	0.77	0.84	0.89	0.89

The low correlation found between 50 m and 1.1 km resolution images indicates that one or more transects were close to areas of variable surface cover types. The coefficient of variation identified Site No. 2 as being responsible for the low agreement between image sampling methods (not related to Site No. 2 from CIPEA survey). Results of a linear regression analysis obtained when excluding Site No. 2 are presented in Table A.24 in Appendix II. The effect of a lateritic surface close to Site No. 2 (less than 500 m distance), which was almost bare of vegetation, and high vegetation quantities in a depression caused the discrepancy between the 50 m and 1.1 km Landsat MSS data.

Results from comparing 3 by 3 averages with the central pixel value for NOAA AVHRR spectral albedos are given in Table 5.11.

Table 5.11: Relationships Between NOAA AVHRR Spectral Albedos Obtained from Different Image Sampling Methods for 1988 ITE/Silsoe Field Survey

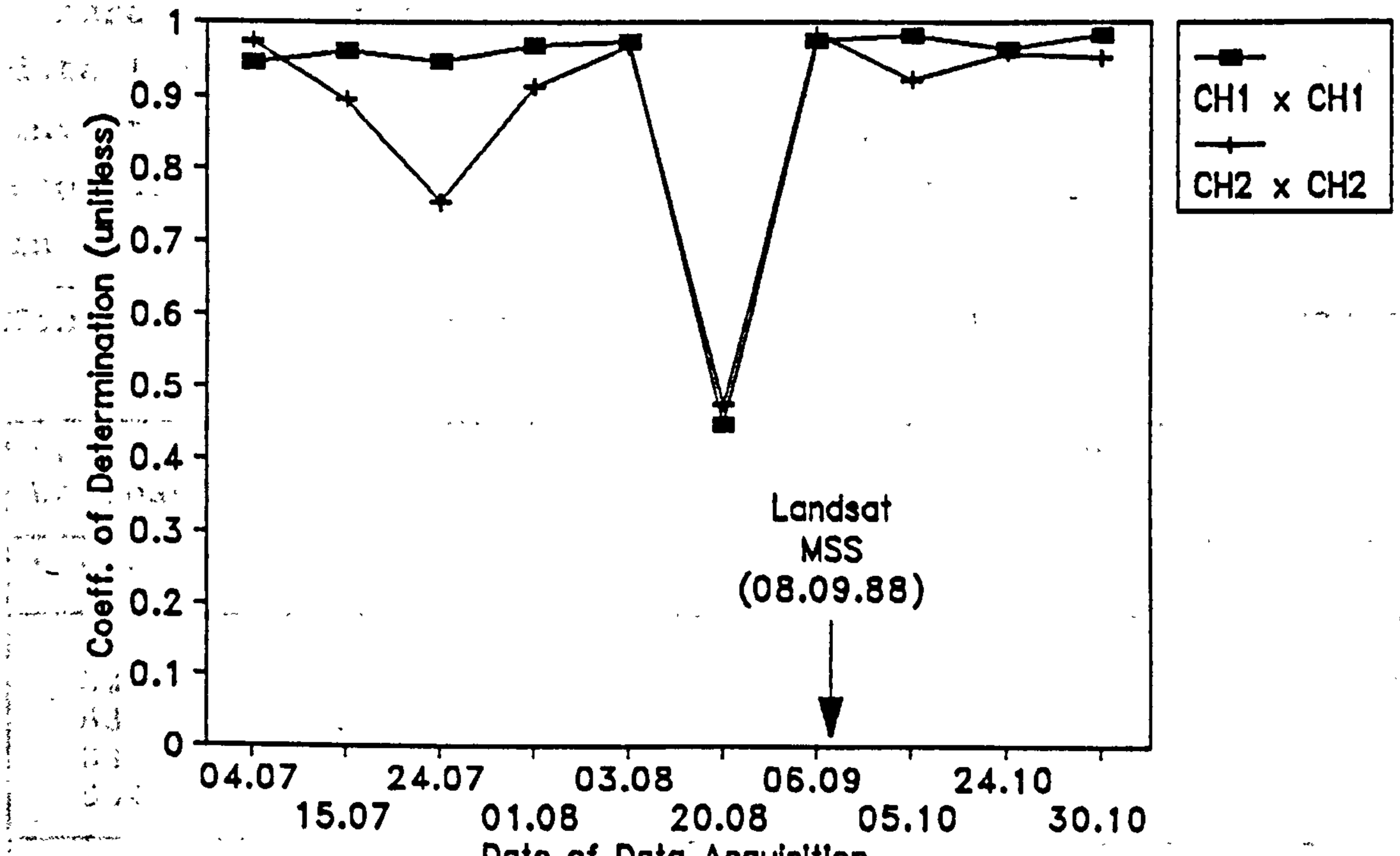
Sampl. Method	Date of NOAA AVHRR Image Acquisition							
	04.07.88		15.07.88		24.07.88		01.08.88	
	1x1	2x2	1x1	2x2	1x1	2x2	1x1	2x2
Central	3 x 3 Average							
Coeff.	1.18	1.20	1.09	1.01	1.07	1.12	1.07	0.89
Const.	-3.9	-5.3	-1.5	-0.4	-1.2	-3.0	-1.3	3.0
r^2	0.94	0.97	0.96	0.89	0.95	0.75	0.97	0.91
	03.08.88		20.08.88		06.09.88		05.10.88	
Coeff.	0.98	1.09	0.89	1.07	1.14	1.03	0.96	1.00
Const.	0.0	-2.4	1.5	-2.0	-2.3	-0.9	0.6	0.0
r^2	0.97	0.97	0.45	0.47	0.98	0.98	0.98	0.92
	24.10.88		30.10.88					
Coeff.	1.01	0.99	1.15	1.08				
Const.	-0.1	0.2	-2.5	-1.7				
r^2	0.96	0.96	0.98	0.95				
Central	Transect							
	20.08.88		06.09.88					
Coeff.	1.08	1.31	1.04	0.94				
Const.	-1.4	-7.4	-0.8	1.5				
r^2	0.71	0.77	0.98	0.99				
3 x 3	Transect							
Coeff.	0.89	0.89	0.91	0.91				
Const.	1.5	2.3	1.5	2.5				
r^2	0.87	0.86	0.99	0.99				

A low correspondence between 3 by 3 average and central position spectral albedos could be observed for the image acquired 20 August 1988. It was a consequence of an increase in variation on the whole rather than at a single site. The relationship improved markedly when using transect sampling instead of nine pixel averages. These findings suggest that Landsat MSS data from 8 September and NOAA AVHRR data from 20 August are unlikely to be closely correlated.

The development of coefficients of determination for channel 1 and 2 spectral albedos obtained from 3 by 3

averages and central pixel positions is graphically presented in Figure 5.5.

Figure 5.5: Development of Coefficients of Determination from Linear Regression Between Transect and a Single Pixel Image Sampling Methods for Channels 1 and 2 over 1988 ITE/Silsoe Field Survey Sites



The drop in agreement for 24 July and 20 August images coincides with the presence of clouds. For the latter data image spectral albedos from five sites (No. 2, 3, 4, 5 and 8) had to be removed, leaving only seven samples for the correlation. The image was, however, included to allow a comparison to the CAZS survey investigation.

5.3.2 Radiometric Correspondence Between Satellite Data

The plausibility of simulating NOAA AVHRR LAC data by Landsat MSS was investigated by relating Landsat MSS spectral reflectances to NOAA AVHRR spectral albedos acquired at dates closest to those of Landsat MSS images. For CIPEA and 1985 ITE/Silsoe survey dates images were acquired at the same day

(31 August 1985). Images from 1988 were found less useful for the purpose, because clear NOAA AVHRR images were acquired approximately four weeks before and after Landsat MSS. Widespread cloud cover and haze rendered images closer to the date of a Landsat MSS scene less suitable. In order to examine if a relationship between Landsat MSS and NOAA AVHRR could generally be expected, central pixel values of pre-processed data from the two satellites were compared *a priori* to detailed investigations for individual surveys. Results of a linear regression investigation of more than 250 points are summarized in Table 5.12.

Table 5.12: Relationship Between NOAA AVHRR and Landsat MSS DNs for 31 August 1985 Images

Dependent Waveband	Independent Waveband (NOAA AVHRR) Channel 1			Channel 2		
Landsat	Coeff.	Const.	r^2	Coeff.	Const.	r^2
B1	0.272	3.658	0.66	0.101	38.511	0.27
B2	0.592	-38.381	0.78	0.238	103.337	0.38
B3	0.809	-60.146	0.60	0.560	-17.659	0.87
B4	0.796	-69.037	0.47	0.644	-49.123	0.92
B34	0.802	-64.592	0.54	0.602	-33.391	0.91
B34: Average DNs from bands 3 and 4.						

Noticeable is a markedly higher coefficient of determination for the NIR wavebands than for red ones. This was unexpected, since it was assumed that channel 1 and band 2 are radiometrically more alike than channel 2 and band 4.
Furthermore, averaging band 3 and 4 information did not yield any higher degree of waveband correspondnece for DNs.
For 1985 the radiometric range of 1.1 km resolution Landsat MSS spectral reflectances appeared to be approximately 60% of the range of NOAA AVHRR spectral albedos. It was, therefore, concluded that NOAA AVHRR sensor detectors resolve more detail of the incident EM energy than those of Landsat MSS for the study area. Possible advantages in correlating ground to image data will be investigated in the following section.
After having established the feasibility of the assumption for DNs of 1985 in general, the radiometric affinity between atmospherically standardized Landsat MSS and NOAA AVHRR

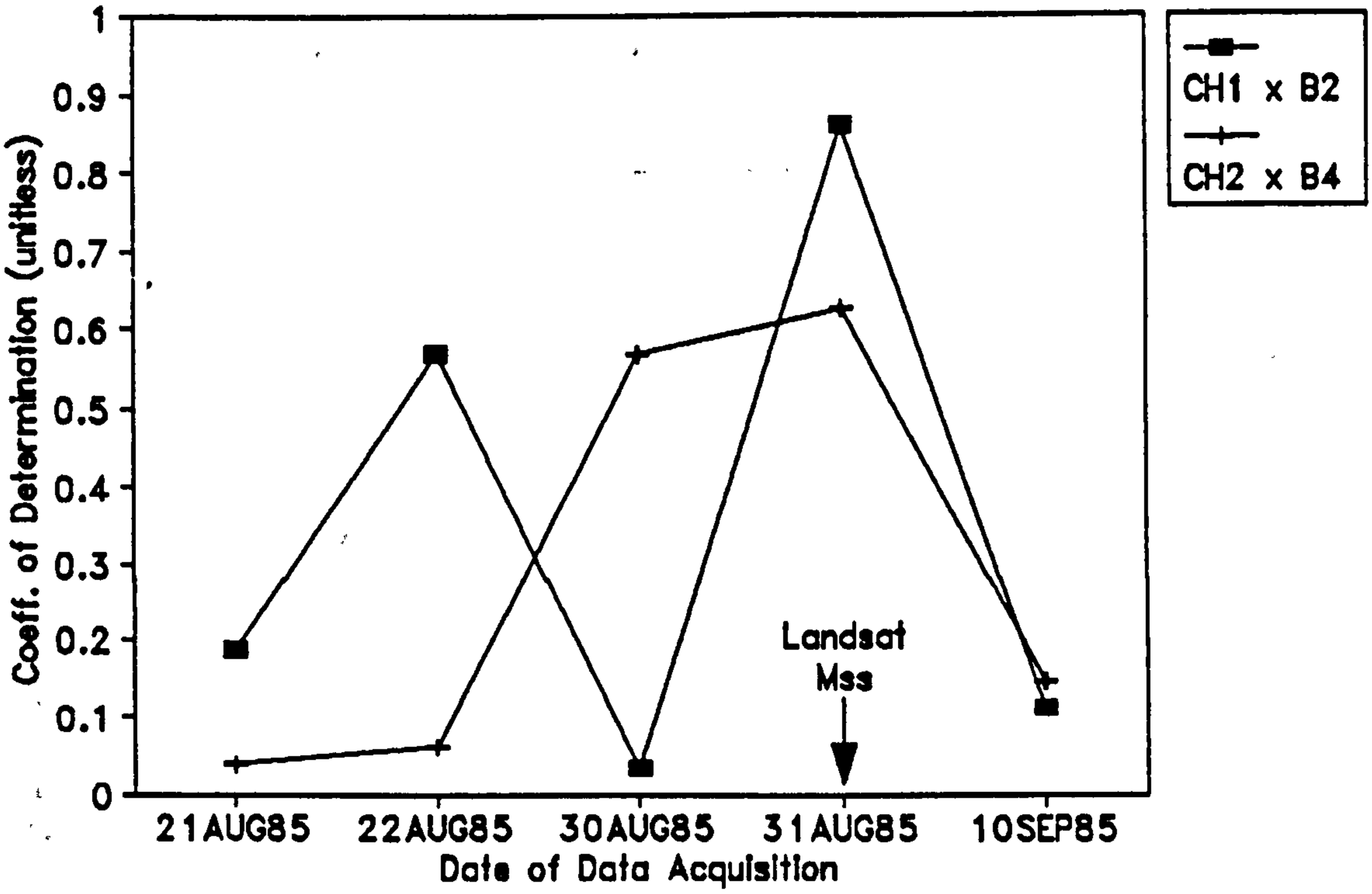
wavebands was established over sampling sites of the four field surveys. Landsat MSS spectral reflectances obtained from 3 by 3 averages were related to spectral albedos from all NOAA AVHRR images available, using the same method. The 3 by 3 pixel image sampling method was used in order to reduce the influence of positional variations introduced by geometrically matching images. When testing the positional agreement between images (see previous chapter) it provided the most constant results, although hardly ever the best fit. NOAA AVHRR channel 1 and 2 were compared to all four Landsat MSS bands.

For one or two NOAA AVHRR images, which corresponded best to the acquisition date of a Landsat MSS scene, data from all image sampling methods were related. The potential of simulating NOAA AVHRR LAC data by Landsat MSS could thus be evaluated. For that purpose channel 1 was compared with bands 1, 2 and 3 and channel 2 with bands 3, 4 and the average of Bands 3 and 4.

(a) CIPEA Survey

Eight sites within the ITE/Silsoe study area were covered by a Landsat MSS image from 31 August 1985. A suitable NOAA AVHRR image was acquired at the same day. The agreement between NOAA AVHRR channel 1 spectral albedos and Landsat MSS band 2 spectral reflectances on the one hand and channel 2 and band 4 on the other is graphically presented in Figure 5.6. More detailed information on all waveband correlations are given in Tables A.25 to A.27 in Appendix II.

Figure 5.6: Radiometric Affinity Between Spectral Albedos of NOAA AVHRR Channels 1 and 2 and Spectral Reflectances of Landsat MSS Bands 2 and 4 for 8 CIPEA Field Survey Sites (3 by 3 Average Image Sampling Method)



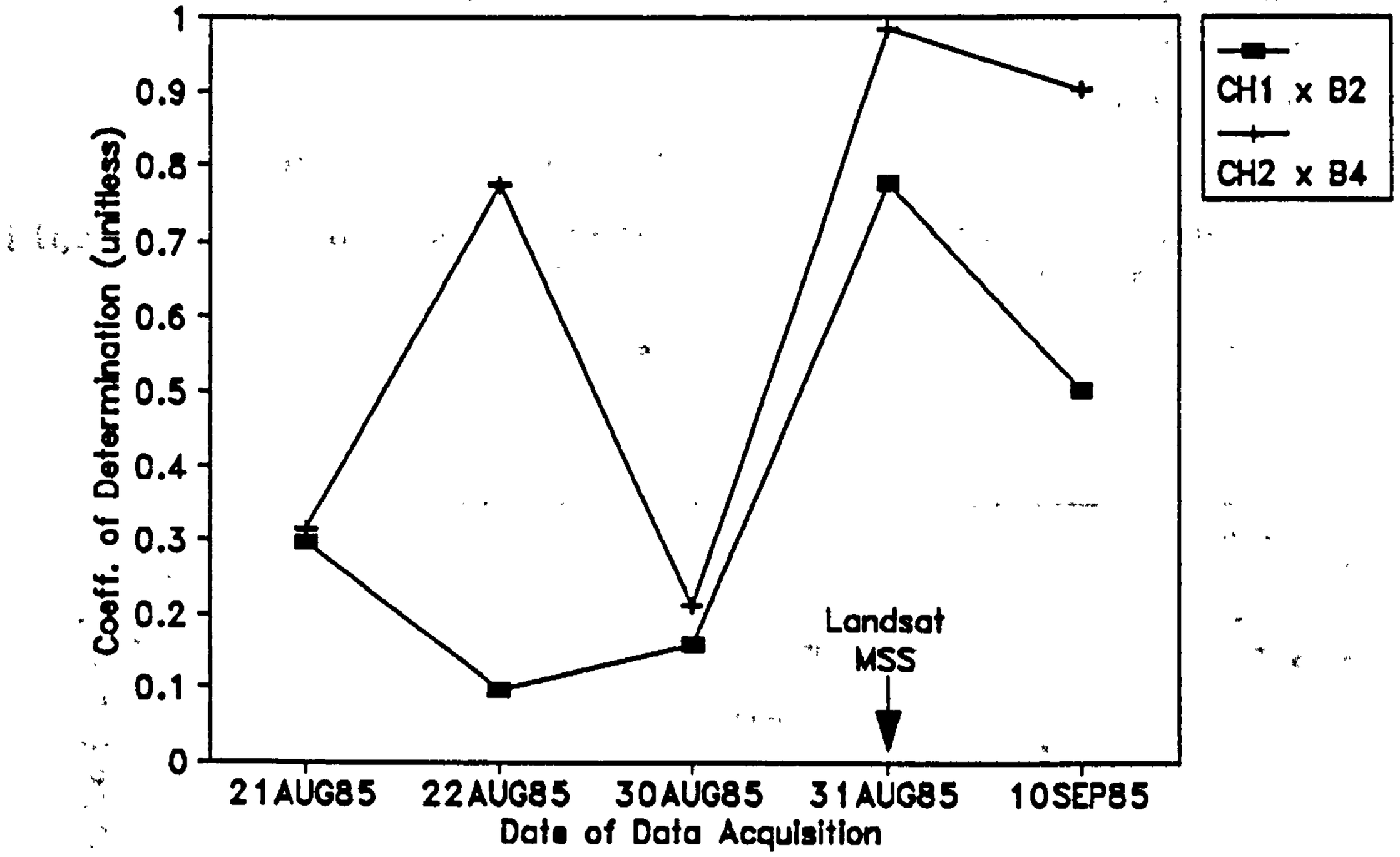
Only for one date (31 August 1985) could a close relationship between data from the two sensors be observed for both, red and NIR wavebands. When correlating channel 2 to Landsat MSS bands, neither band 3 or 4, nor their average yielded significantly different coefficients of determination.
Tables A.26 and A.27 in Appendix II contain the results of a linear regression analysis between Landsat MSS and NOAA AVHRR over those sites for 31 August. Highest correlations ($r^2 \geq 0.8$) for channel 1 vs. band 2 and channel 2 vs. band 4 were obtained for 50 m resolution Landsat MSS data. Much lower values, particularly for the NIR wavebands, were obtained when using other methods.

(b) **1985 ITE/Silsoe Survey**

Coefficients of determination derived from linear regressions of red and NIR wavebands of NOAA AVHRR and

Landsat MSS for eight sites of the 1985 ITE/Silsoe field survey are graphically presented in Figure 5.7.

Figure 5.7: Radiometric Affinity Between Spectral Albedos of NOAA AVHRR Channels 1 and 2 and Spectral Reflectances of Landsat MSS Bands 2 and 4 for 1985 ITE/Silsoe Field Survey Sites (3 by 3 Average Image Sampling Method)



The highest overall correlation was achieved for the date of the Landsat MSS image acquisition (31 August 1985). For the NOAA AVHRR image from 30 August 1985 no correlation with the Landsat MSS data, acquired just one day later, could be observed. Surface features themselves are not expected to have changed markedly. Hence, residual effects of the presence of clouds or a larger positional error may have been responsible for the drop in correspondence.

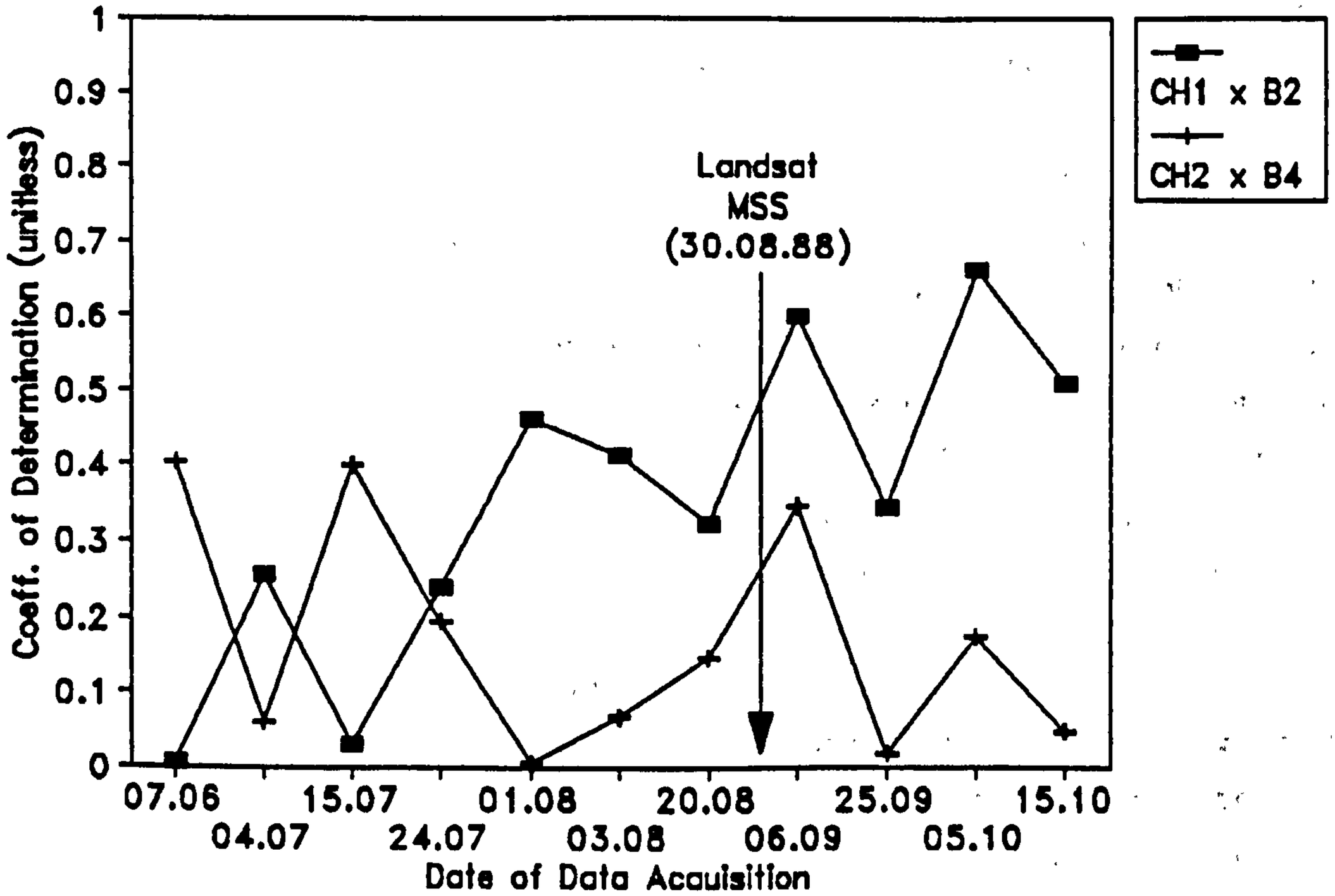
For NOAA AVHRR and Landsat MSS images from 31 August 1985 slopes, offsets and coefficients of determination of a linear regression analysis are summarized in Table A.29 in Appendix II. The highest level of agreement ($r^2 \geq 0.89$) for channel 1 vs. band 2 and channel 2 vs. band 4 was achieved for transect sampling of both,

Landsat MSS at 1.1 km resolution and NOAA AVHRR. For other image sampling methods the agreement was significantly lower. A more even performance was found for site averages of 50 m resolution Landsat MSS data and 3 by 3 averages.

(c) CAZS Survey

The correlation between 11 dates of NOAA AVHRR channels 1 and 2 spectral albedos and Landsat MSS bands 2 and 4 spectral albedos from 30 August 1988 is graphically displayed in Figure 5.8.

Figure 5.8: Radiometric Affinity Between Spectral Albedos of NOAA AVHRR Channels 1 and 2 and Spectral Reflectances of Landsat MSS Bands 2 and 4 for 1988 CAZS Field Survey Sites (3 by 3 Average Image Sampling Method)



While the correspondence between Landsat MSS and NOAA AVHRR increases for the NIR waveband with progressing growing season it remains low for the red waveband. For two dates (20 August and 6 September) NOAA AVHRR and Landsat MSS data were compared with respect to all image sampling techniques applied. Results from all regressions are given in Tables A.31 and A.32 in

Appendix II. For the earlier date low correlations ($r^2 \geq 0.37$) were obtained when using 50 m resolution Landsat MSS data and 3 by 3 averaging for NOAA AVHRR. As mentioned above, the differences in spectral responses between the two sensors are likely to be the consequence of widespread cloud cover across the Mali study area. For the September image no correlation between wavebands was found, regardless of the image sampling method used. The image was affected by haze, which resulted in comparatively low values for scene contrast. It was considered most likely that a larger than average positional error existed for that date, caused by difficulties in identifying GCPs during geometric correction.

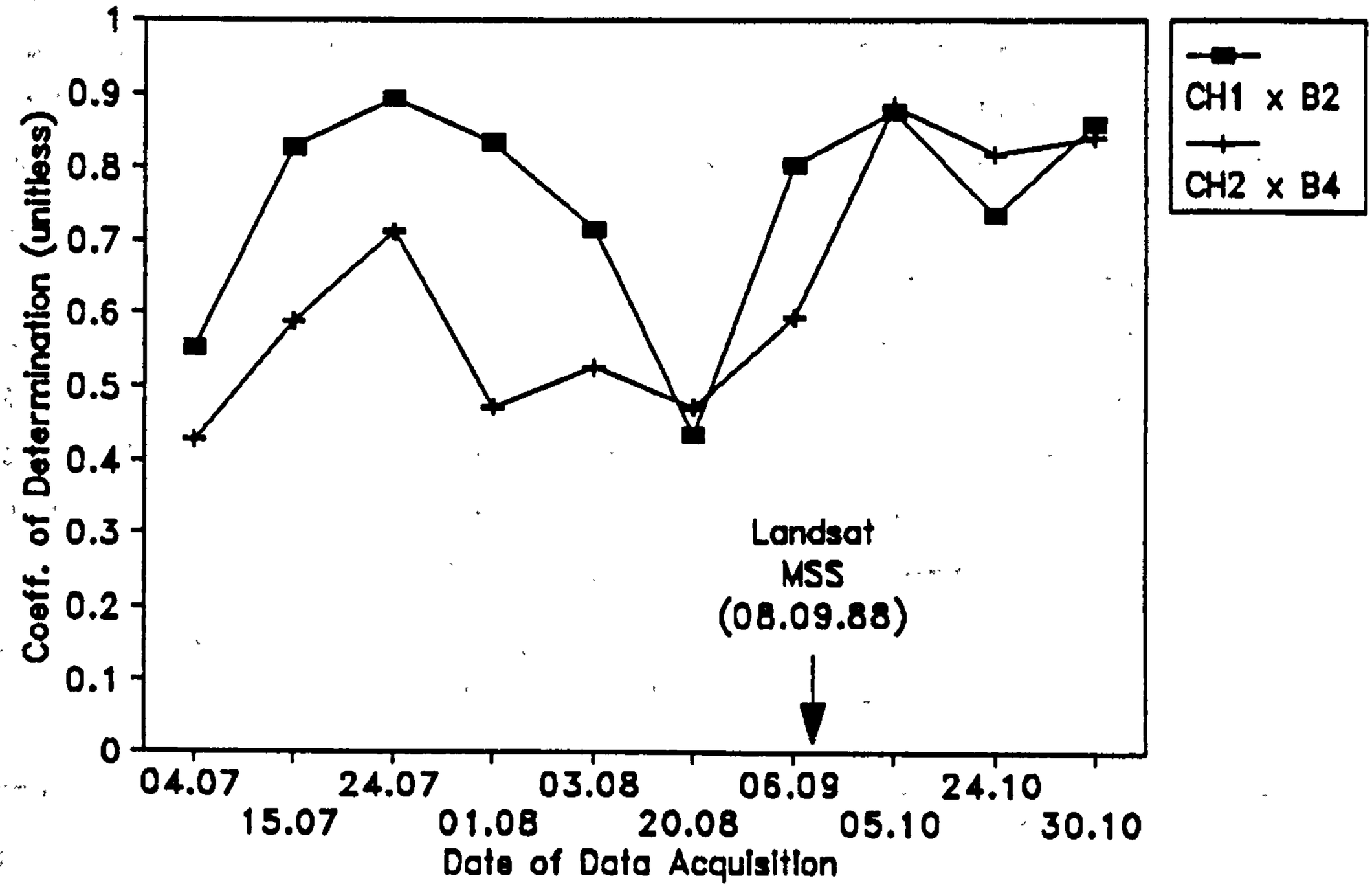
(d) 1988 ITE/Silsoe Survey

NOAA AVHRR spectral albedos from 10 dates were compared to a Landsat MSS image acquired at 8 September 1988. A graphical display of the coefficients of determination from linear regressions between channel 1 vs. band 2 and channel 2 vs. band 4 is given in Figure 5.9.

The absence of any correlation between Landsat MSS and the 20 August NOAA AVHRR image stands in strong contrast to correlations found at other, even earlier, dates. For NOAA AVHRR images from 20 August and 5 October channel 2 produced higher coefficients of determination, although not significantly so, when related to band 2 instead of band 4. No explanation could be given for the observed inversions of expected relationships.

Results of a linear regression analysis between two NOAA AVHRR images (20 August and 6 September) closest to the Landsat MSS scene from 8 September are presented in Tables A.34 and A.35 in Appendix II. After cloud screening r^2 values of 0.88 and higher were obtained for the coefficients of determination from relating wavebands from of the two sensors. For both dates 3 by 3 image sampling gave the best values of association between NOAA AVHRR and Landsat MSS wavebands.

Figure 5.9: Radiometric Affinity Between Spectral Albedos of NOAA AVHRR Channels 1 and 2 and Spectral Reflectances of Landsat MSS Bands 2 and 4 for 1988 ITE/Silsoe Field Survey Sites (3 by 3 Average Image Sampling Method)



5.4 Relationships Between Ground Data and VIs

Estimates of herbaceous rangeland vegetation derived from the field surveys of 1985 and 1988 were related to Landsat MSS and NOAA AVHRR VIs of pre-processed data. Image representations over transects were obtained by the image data sampling methods introduced in Chapter 5.2. For each combination of survey date and sampling method RVIs, NDVIs and PVIs were computed. In order to investigate, if an average of Landsat MSS bands 3 and 4 would be more closely related to NOAA AVHRR channel 2 information, RVIs, NDVIs and PVIs based on the means of the two bands were established for atmospherically standardized Landsat MSS spectral reflectances. These are denoted as RVI34, NDVI34 and PVI34. From NOAA AVHRR VIs maximum values were established for the period preceding ground surveys. They are referred to as RVImax, NDVImax and PVImax. Single date and maximum value VI

were commented upon separately to allow a direct comparison between Landsat MSS and NOAA AVHRR VI performances.
Since the theoretical relationship between vegetation quantities and VIs is logarithmic, a linear and a logarithmic regression was applied. The latter, based on a linear regression of the natural logarithm of dry matter estimates with VIs, will be referred to simply as logarithmic. Due to the volume of data analysed, most of results are presented in Tables A.36 to A.64 in Appendix II.
Before examining individual field survey data, the general viability of simulating NOAA AVHRR VIs from Landsat MSS data was tested. Analogous to the comparison of single wavebands of Landsat MSS and NOAA AVHRR (Chapter 5.3) more than 250 VIs drawn from DNs of the two sensors for images of 31 August 1985 were linearly related. The results are presented in Table 5.13.

Table 5.13: Relationship Between NOAA AVHRR and Landsat MSS Vegetation Indices from DNs for 31 August 1985 Images

NOAA AVHRR VI	Landsat MSS Vegetation Index								
	RVI			NDVI			PVI		
	Coeff.	Const.	r^2	Coeff.	Const.	r^2	Coeff.	Const.	r^2
RVI	0.532	0.48	0.90						
NDVI				0.561	0.01	0.91			
PVI							1.395	-7.89	0.90

In all cases VIs from Landsat MSS are highly correlated to those from NOAA AVHRR. It is, therefore, not unreasonable to expect similar performances of VIs from the two sensor when comparing VIs from field survey sites.

5.4.1 CIPEA Survey

The effect of the two methods of determining sample site positions, aircraft instruments and image identification of aerial photographs, on the correlation between ground and image data could only be assessed for the eight CIPEA sites, which were within the Landsat MSS scene from 31 August 1985. For all other sites only NOAA AVHRR VIs from aircraft positions were available. A summary of the results of the investigation is

given in Table 5.14. The best three types of image sampling and VIs are stated, but only if a coefficient of correlation of 0.5 or more was achieved. Row combinations within the table are not permissible, since entries are ordered separately within columns.

(a) **Landsat MSS Data**

Table A.36 in Appendix II summarizes the results of linear and logarithmic regressions between herbaceous vegetation estimates of eight CIPEA transects. Site co-ordinates were established from aerial photographs.

i. *Image Data Sampling Method*

The highest association (r^2 of 0.78 for PVI34) was achieved for VIs based on the 3 by 3 image data sampling method. The lowest values (r^2 of 0.62) was provided by central 1.1 km resolution data.

ii. *Vegetation Index*

The PVI attained the highest coefficients of determination for all image sampling methods. Furthermore, averages of bands 3 and 4 produced consistently higher values than band 2 and 4 VIs.

iii. *Regression Type*

In no case did the logarithmic relationship achieve medium values ($r^2 \geq 0.5$) for coefficients of correlation. The main cause could be identified in the position of Site No. 17, which favoured exponential relationships.

(b) **NOAA AVHRR LAC Data**

NOAA AVHRR VIs were computed for 25 CIPEA field survey sites. Their image co-ordinates were derived from aircraft instrument readings. Relationships from the analysis are summarized in Table A.37 in Appendix II. Estimates of herbaceous rangeland vegetation from the second sampling period (26.08.85 - 03.09.85) were used as the independent variable, because a closer temporal correspondence to the dates of satellite data acquisitions than other survey periods.

Correlation coefficients of eight sites within the Landsat MSS scene (see previous paragraph) were extracted and investigated separately (Table A.38, Appendix II). For the 31 August image the coefficient of determination increases from 0.61 to 0.73. Better results were achieved for the image from 10 September (r^2 of 0.88 for PVI).

i. *Image Data Sampling Method*

Image data sampling methods were compared for one scene (31 August), which coincided with the date of the Landsat MSS image. The average from 3 by 3 pixels around the transect provided the highest values (r^2 of 0.77 for PVI), while the transect method gave the worst results (r^2 of 0.71 for PVI).

ii. *Vegetation Index*

Although a PVI produced the highest overall value for the coefficient of determination for 31 August image, there was no significant difference at all between VIs of that date or for any other. VIs were, therefore, rated as equally applicable. Maximum value VIs achieved higher r^2 values in all cases tested than single dates. Again, no preference could be attributed to any VI.

iii. *Regression Type*

A linear relationship seemed to represent the relationship between herbaceous vegetation and VI more appropriately then a logarithmic one. The latter failed to produce coefficients of determination of 0.5 or more in all cases of comparisons for 31 August image.

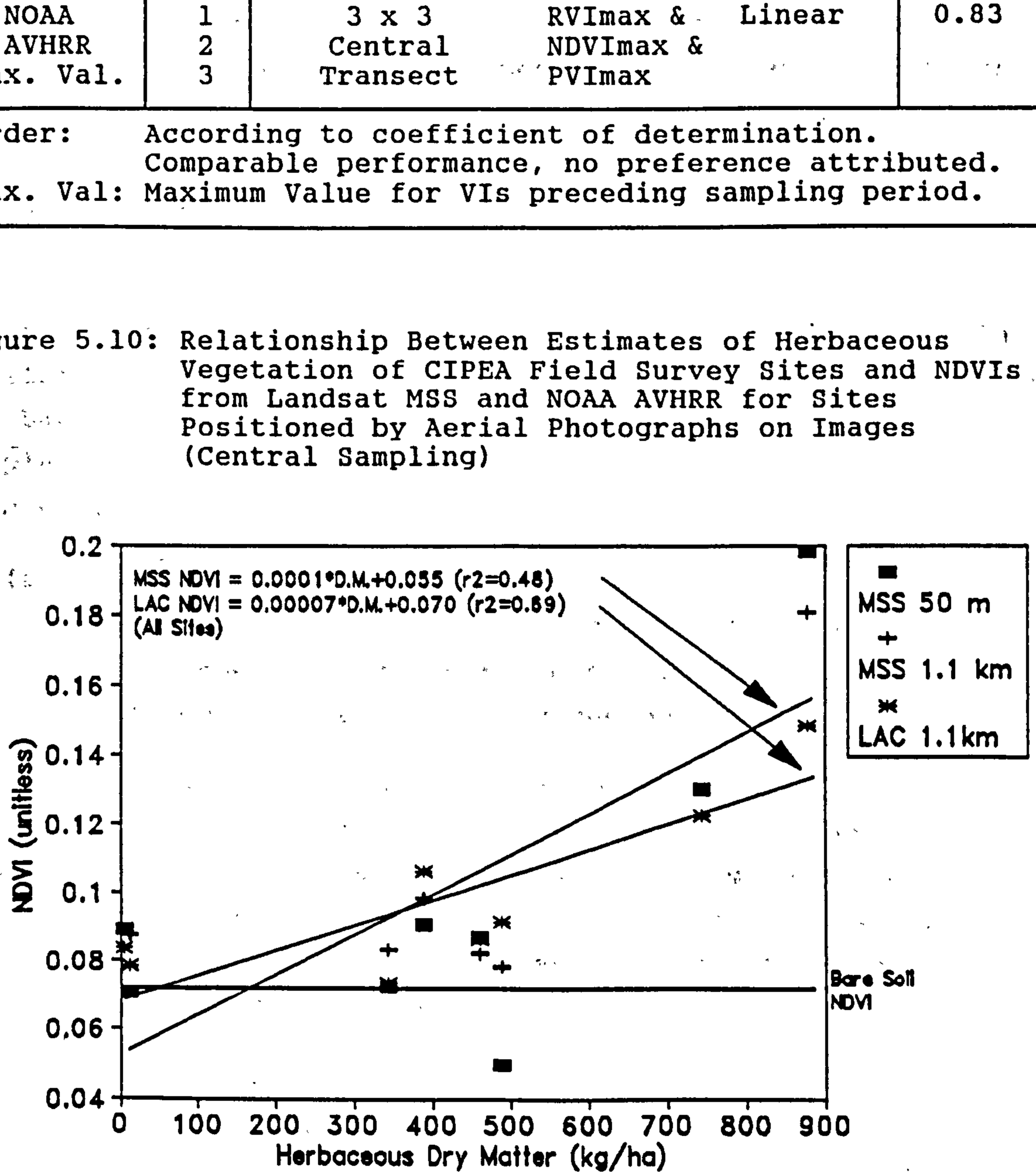
A graphical presentation of the relationship between estimated quantities of herbaceous vegetation and Landsat MSS and NOAA AVHRR NDVIs is given in Figure 5.10.

Table 5.14: Summary of Results of Vegetation Index Calibration of CIPEA Field Survey

Satellite Data	Order *	Image Data Sampl. Method ($r^2 \geq 0.5$)	VI Type	Regression Type	Coeff. Determ.
Landsat MSS	1 2 3	3 x 3 20 x 20 Transect	PVI34 NDVI34 RVI34	Linear	0.78
NOAA AVHRR 31.08.85	1 2 3	3 x 3 Central Transect	RVI & NDVI & PVI	Linear	0.77
NOAA AVHRR Max. Val.	1 2 3	3 x 3 Central Transect	RVImax & NDVImax & PVImax	Linear	0.83

Order: According to coefficient of determination.
&: Comparable performance, no preference attributed.
Max. Val: Maximum Value for VIs preceding sampling period.

Figure 5.10: Relationship Between Estimates of Herbaceous Vegetation of CIPEA Field Survey Sites and NDVIs from Landsat MSS and NOAA AVHRR for Sites Positioned by Aerial Photographs on Images (Central Sampling)



(c) **Association Between Landsat MSS and NOAA AVHRR VIs**

Landsat MSS VIs from 50 m and central pixel image data sampling were linearly related to central pixel NOAA AVHRR VIs (Table A.40, Appendix II).

VIs from central pixel sampling for both satellite data (r^2 of 0.89, NDVI) seemed to be better correlated than 50 m Landsat MSS and central pixel NOAA AVHRR VIs (r^2 of 0.82 NDVI). This is hardly surprising, since the NOAA AVHRR scene was geometrically matched to the Landsat MSS image, from which central pixel VIs were derived.

High correlations were found for both, orthodox VIs and those based on average spectral reflectances of bands 3 and 4 and no advantage of either could be verified.

5.4.2 1985 ITE/Silsoe Survey

A summary of the results from correlating herbaceous rangeland vegetation estimates obtained during the 1985 ITE/Silsoe survey and Landsat MSS and NOAA AVHRR VIs is given in Table 5.15. All sample site co-ordinates were determined by identifying transects directly on images.

(a) **Landsat MSS Data**

Compared to CIPEA sites findings for the eight 1985 ITE/Silsoe sites are more complex. Annotations for individual parameters are given below.

i. *Image Data Sampling Method*

The highest degree of similarity between ground and image data was attained with 50 m resampled data (r^2 of 0.93 for PVI). Comparable results were also produced by 20 by 20 averages and the central 1.1 km pixel value.

ii. *Vegetation Index*

The order of the performance of VIs depended on type of regression applied. For a logarithmic relationship the PVI gave higher and the RVI lower r^2 values than the NDVI in four out of five cases.

Applying a linear regression the order is reversed with the RVI producing the better results in five out of five cases. This trend of the PVI being apparently better suited for logarithmic correlations was also present for CIPEA sites, although for low r^2 values.

On the whole, averaging band 3 and 4 information did not alter the correlation of logarithmic relationships, but deteriorated those established from linear regressions in 12 out of 15 cases.

(b) NOAA AVHRR LAC Data

For the purpose of comparing Landsat MSS and NOAA AVHRR VIs the interpretation of the regression analysis concentrated on the image acquired on 31 August 1985.

i. *Image Data Sampling Method*

The central pixel position produced the highest r^2 values (r^2 of 0.85 for RVI), followed by 3 by 3 pixel averages. Decidedly inferior results were found for VIs derived from transect sampling.

ii. *Vegetation Index*

Although the PVI provided the leading value for the r^2 (0.85), no distinct difference between the three VIs for 31 August data could be identified. For 21, 22 August and 10 September images, however, RVI and NDVI exhibit comparable r^2 values, which are consistently better than those obtained for the PVI for linear regressions. For logarithmic regression no priority could be assigned to a single VI. Maximum value VIs improved on r^2 values for central and 3 by 3 image sampling, but not for transect sampling.

iii. *Regression Type*

Despite the fact that a logarithmic regression produced the best absolute figure for the fit of a VI to ground data, it was not significantly better than linear regressions (r^2 of 0.85 vs. 0.84). Taking into account results from other dates, a

linear regression seemed to attain more advantageous results in 8 out of 12 cases, where r^2 values of 0.5 or more were found.

Table 5.15 summarizes the results of the regression analysis between field data and satellite VIs for the 1985 ITE/Silsoe field survey.

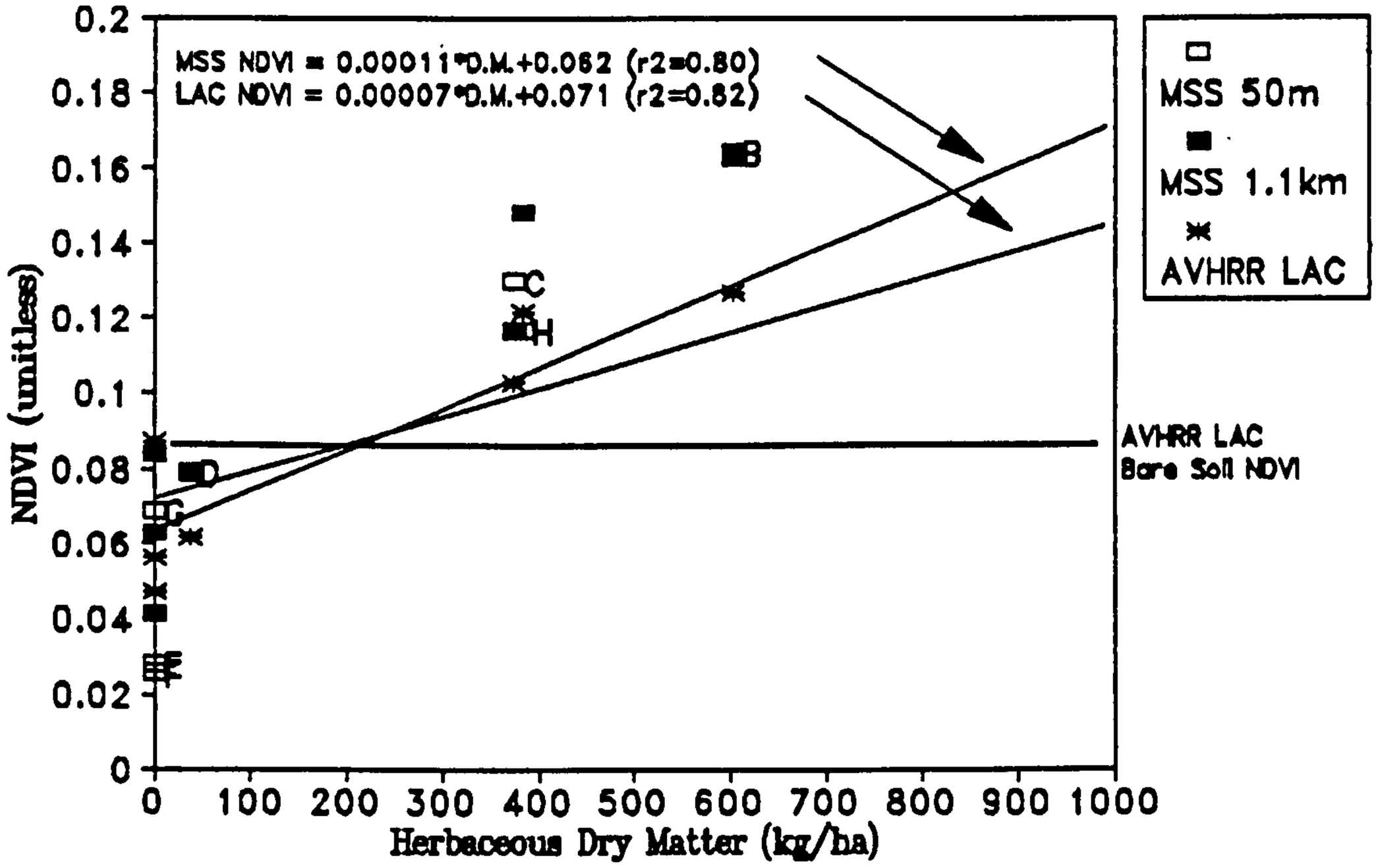
A graphical description of the correlation between herbaceous vegetation and Landsat MSS and NOAA AVHRR NDVIs is presented in Figure 5.11.

Table 5.15: Summary of Results of Vegetation Index Calibration of 1985 ITE/Silsoe Field Survey

Satellite Data	Order *	Image Data Sampl. Method ($r^2 \geq 0.5$)	VI Type	Regression Type	Coeff. Determ.
Landsat MSS	1 2 3	50 m 20 x 20 Central	PVI34 NDVI34 RVI34	Logarithmic	0.93
NOAA AVHRR 31.08.85	1 2 3	Central 3 x 3 Transect	RVI NDVI & PVI	Linear	0.85
NOAA AVHRR Max. Val.	1 2 3	Central 3 x 3 Transect	RVImax & NDVImax & PVImax	Linear	0.89

Order: According to coefficient of determination.
&: Comparable performance, no preference attributed.
Max. Val: Maximum Value for VI preceding sampling period.

Figure 5.11: Relationship Between Estimates of Herbaceous Vegetation of 1985 ITE/Silsoe Field Survey Sites and NDVIs from Landsat MSS and NOAA AVHRR (Central Sampling)



Calibrated Landsat MSS and NOAA AVHRR NDVI images over the ITE/Silsoe study area are provided in Figures 5.12 and 5.13. The zone displayed covers approximately 22 km by 22 km. Despite the loss in spatial resolution some features, which are smaller than a nominal LAC pixels, are visible on the NOAA AVHRR image, if they are spectrally different from surrounding areas. For example, the high vegetation along a river at the bottom right remains clearly distinguishable from areas with lower biomass quantities.

Figure 5.12: Image Representation of Landsat MSS NDVI (50 m Resampling, NN) from 31 August 1985

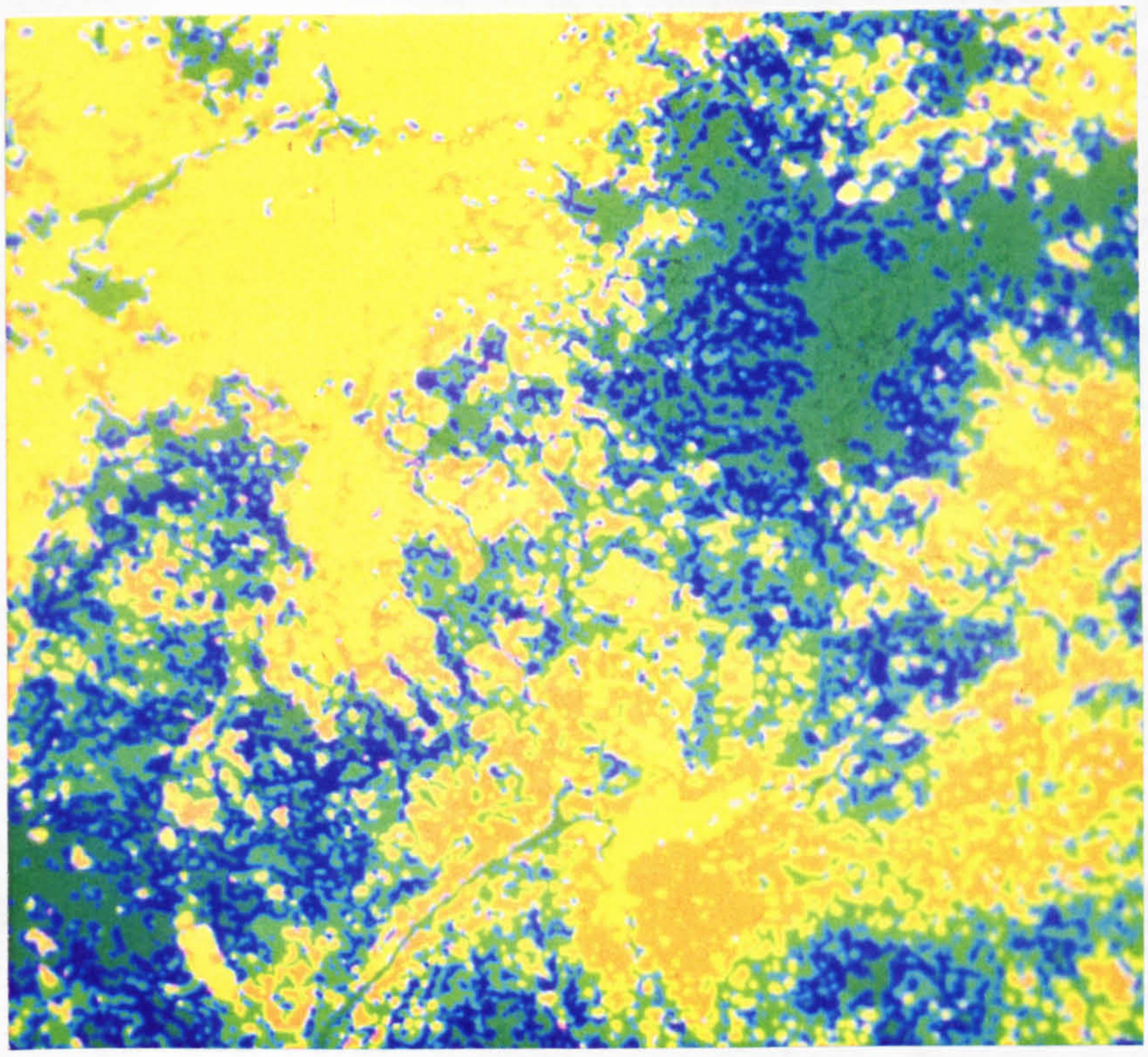
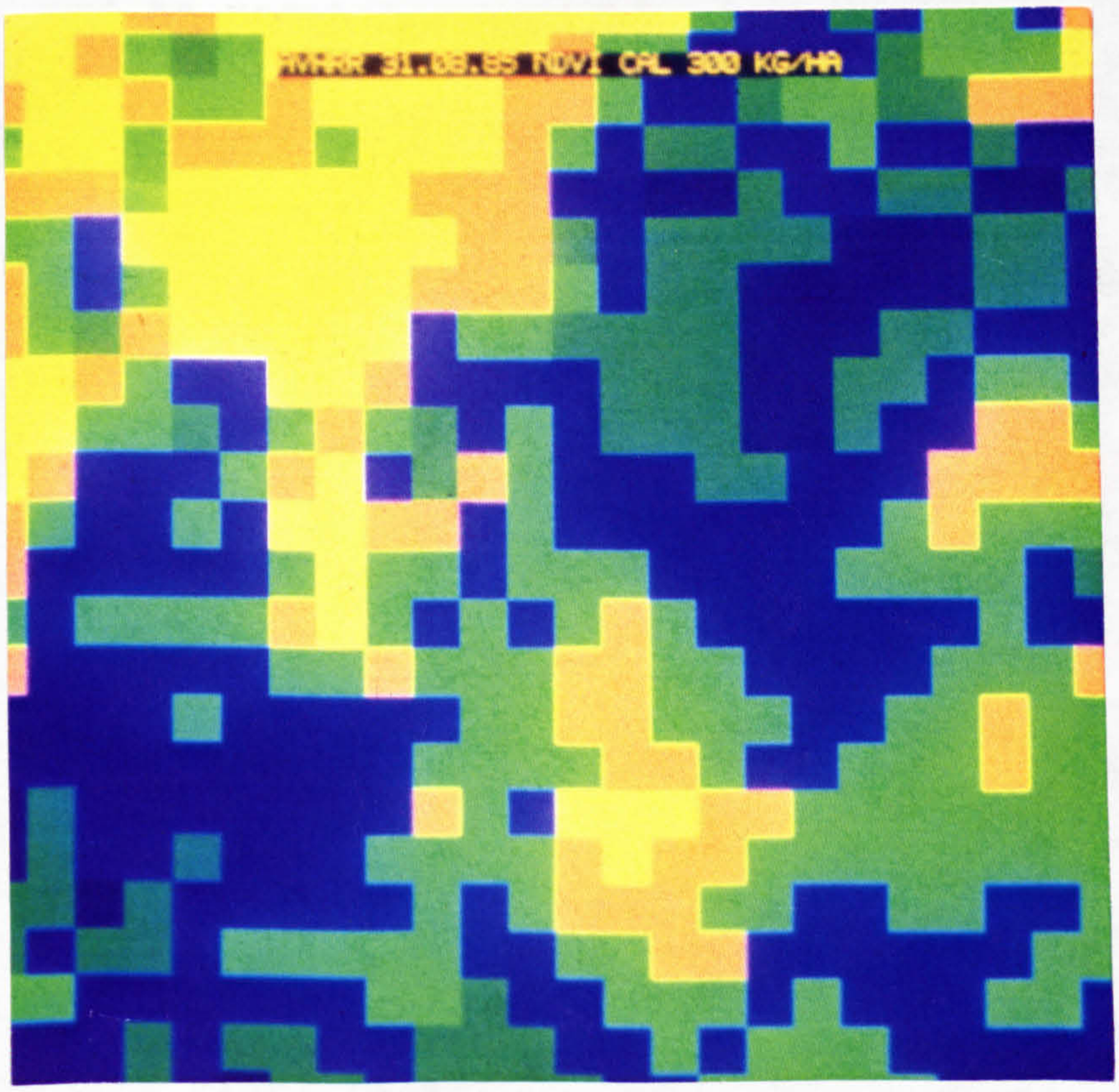


Figure 5.13: Image Representation of NOAA AVHRR NDVI (1.1 km, NN) from 31 August 1985



(c) **Association Between Landsat MSS and NOAA AVHRR VIs**

Correlating 50 m Landsat MSS and central pixel NOAA AVHRR VIs produced r^2 values of 0.90 (NDVI) (Table A.46, Appendix II). Applying central pixel image sampling to data from both satellites, the value increases to 0.97 (NDVI). VIs from spectral reflectance averages of bands 3 and 4 performed almost identically to band 2 and 4 VIs.

5.4.3 CAZS Survey

For the CAZS survey image data could be related to multi-temporal ground data. This allowed to monitor the development of NOAA AVHRR VIs throughout the 1988 growing season for the Mali sites. A summary of the regression analysis for Landsat MSS form 30 August and NOAA AVHRR VIs is given in Table 5.16.

(a) **Landsat MSS Data**

The date of acquisition of the Landsat MSS image was in between the 5th and 6th sampling period and it was correlated to vegetation estimates from both surveys. As a first step, transect co-ordinates derived from GPS positions were relates to the NDVI. For samples from the 5th period the variation in VIs, which could be explained by the ground data, was less than 50% in all cases. For estimates from the 6th period only the NDVI from the central pixel reached a coefficient of determination of 0.5 (see Tables A.47 to A.49, Appendix II). Subsequent analysis was then based on samples located by map positions.

i. *Image Data Sampling Method*

The method of obtaining spectral reflectances for VI computations had little effect on coefficients of determinations found. The highest r^2 value (0.58) was achieved for 50 m resampled transect VIs. It was followed by 20 by 20 averages and the central pixel value.

ii. *Vegetation Index*

For transect co-ordinates based on site positions identified on maps all VIs were computed (Tables A.48 and A.49, Appendix II). Again it was distinguished between field data of the 5th and 6th sampling period. The earlier estimates of herbaceous vegetation did not indicate any relationship to VIs, for neither a linear nor a logarithmic regression. For the 6th sampling period ratio VIs achieved the highest values.
There was practically no preference for orthodox VIs or those employing averages of bands 3 and 4. However, the order of VIs depended on the spatial resolution of the image data sampled. For 1.1 km resolution VIs (central, 3 by 3 and transect sampling) the PVI proved to be more closely correlated to ground data than ratio VIs. This trend could not be observed for 1985 field surveys and may be specific to the data set used.

iii. *Regression Type*

Applying a linear regression provided marginally higher r^2 values than a logarithmic correlation in all cases. On the other hand, the differences were not significant for individual cases.

(b) NOAA AVHRR LAC Data

NOAA AVHRR VIs were related to ground data from the nearest sampling period. For GPS co-ordinates of sample sites only NDVIs were computed, which were derived from central pixel positions (Table A.50, Appendix II). Contrary to Landsat MSS VIs, a comparison between NDVIs from GPS and map positions (Table A.51, Appendix II) produced no evidence for a preference of either method. All subsequent analysis was based on sample sites from map positions to allow direct comparisons to Landsat MSS VIs.

i. *Image Data Sampling Method*

No difference between methods of sampling image

data for VIs could be substantiated. The highest r^2 value (0.78 for 25.09.88) was attained from a central pixel value VI, but comparable values were also obtained from 3 by 3 pixel averages.

ii. *Vegetation Index*

VIs produced very similar coefficients of determinations for all dates. For linear and logarithmic regressions, where r^2 values of 0.5 or larger were found, the PVI achieved the highest value in 12 out of 18 cases. It has to be stressed, however, that no meaningful dominance of the PVI over the ratio VIs could be observed for any single date.

Maximum value VIs were computed for the whole season until the 5 October image. They were correlated to the maximum estimate of dry matter for all seven sampling periods (Table A.53, Appendix II). Only PVIs from linear and logarithmic regressions produced r^2 values above 0.5 (0.58 for logarithmic relationship).

iii. *Regression Type*

A summary of the results obtained from relating field survey data to NOAA AVHRR VIs is provided in Table 5.16. Over the first half of the growing season (until mid-August) a logarithmic relationship between ground data and NOAA AVHRR VIs produced higher r^2 values than a linear one. This tendency was present for central and 3 by 3 average VIs. During the second half both linear and logarithmic regressions provided equivalent results. This occurrence could be interpreted as a logarithmic relationship being more representative for low or photosynthetically active vegetation quantities (<800 kg/ha). For higher quantities or drier vegetation (<65% m.c.) the relationship becomes more linear. With data from only one season available, the general applicability of the observation could not be verified.

Table 5.16: Summary of Results of Vegetation Index Calibration of CAZS Field Survey

Satellite Data	Order *	Image Data Sampl. Method ($r^2 \geq 0.5$)	VI Type	Regression Type	Coeff. Determ.
Landsat MSS	1 2 3	50 m 20 x 20 Central	RVI34 & NDVI34 & RVI	Linear	0.58
NOAA AVHRR 25.09.88	1 2 3	3 x 3 & Central	RVI & NDVI & PVI	Linear & Logarithmic	0.78
NOAA AVHRR Max. Val.	1 2 3	3 x 3 & Central	PVI	Linear & Logarithmic	0.58

Order: according to coefficient of determination.
&: Comparable performance, no preference attributed.
Max. Val: Maximum Value for VI preceding sampling period.

A graphical description of the relationship between herbaceous vegetation quantities from the 5th sampling period and Landsat MSS NDVIs from 30 August 1988 and NOAA AVHRR NDVIs from 6 September 1988 is provided in Figure 5.14. The low correlations found for the two NDVIs could be attributed to values from Site A. Since the study area was not familiar, the source of the deviation of this site could not be established with certainty.

For CAZS sample sites the progression of VIs relative to herbaceous vegetation growth throughout the growing season could be monitored. This was done for the NDVI and a graphical demonstration of the development is provided in Figure 5.15.

Figure 5.14: Relationship Between Estimates of Herbaceous Vegetation of CAZS Field Survey Sites and NDVIs from Landsat MSS and NOAA AVHRR (Central Sampling)

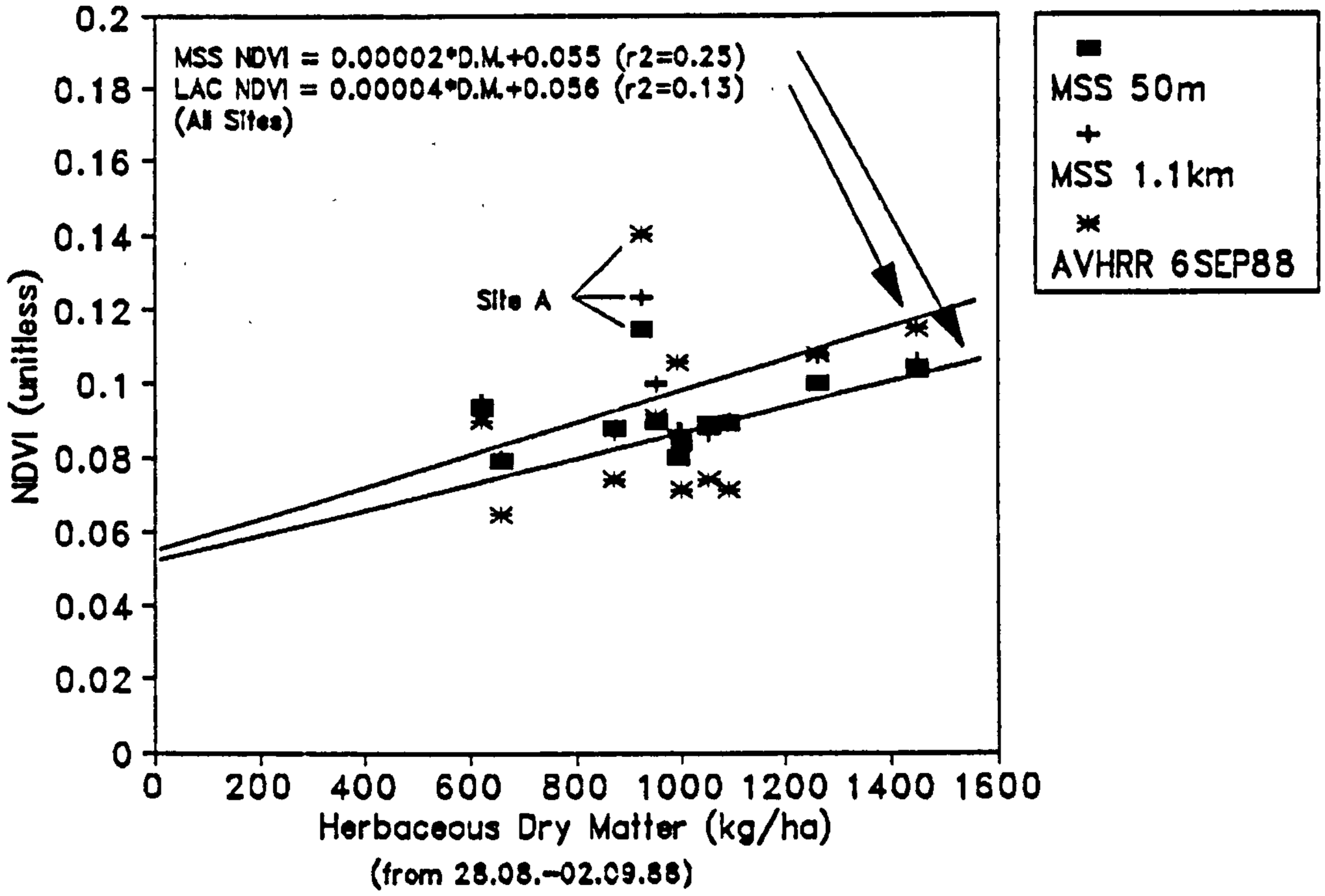
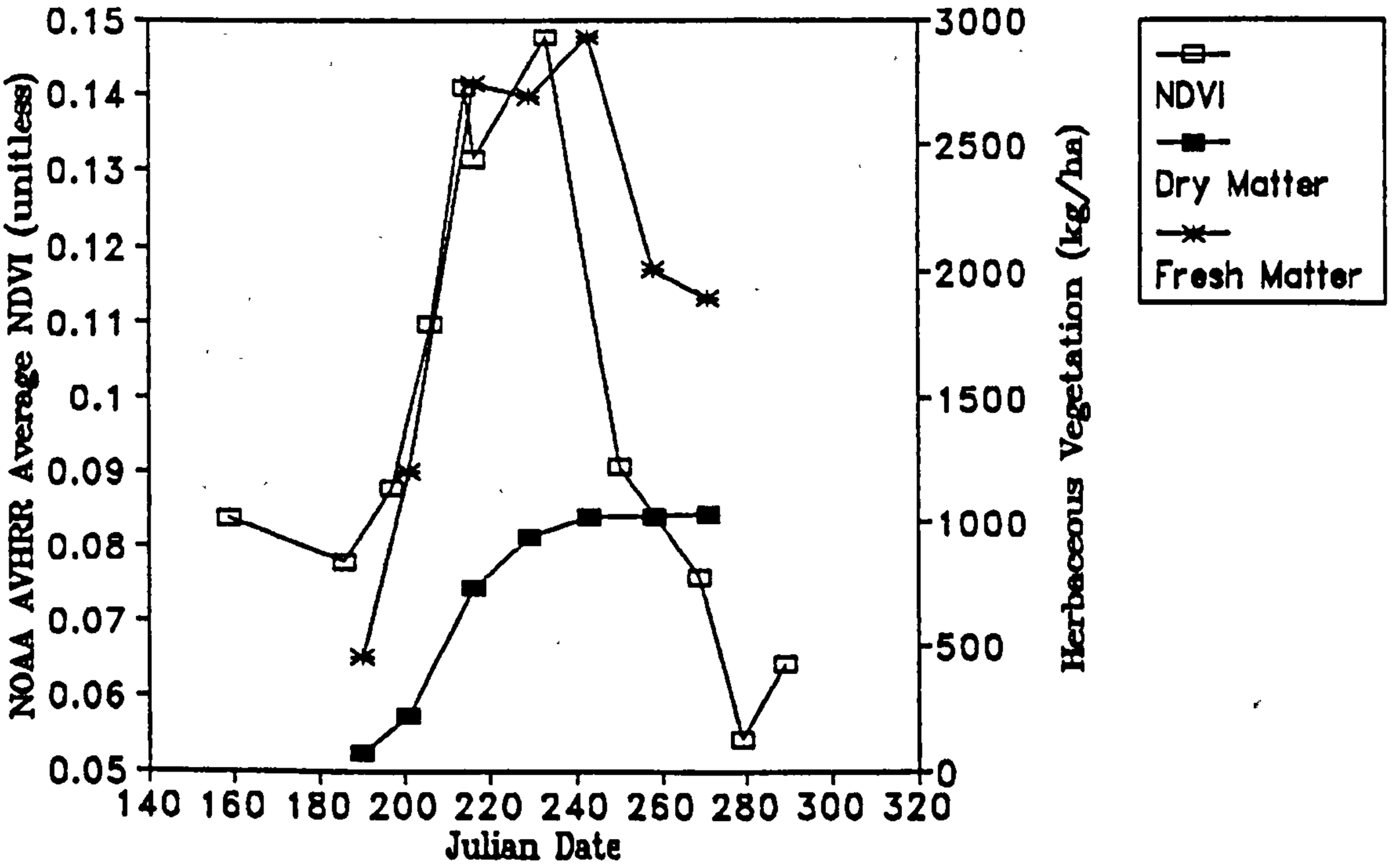


Figure 5.15: Development of NOAA AVHRR Average NDVIs Throughout 1988 Growing Season for CAZS Sample Sites



NOAA AVHRR average NDVIs were obtained from computing the mean NDVI from all sites for a date. The values are not comparable to other surveys, since the distribution of sites is not necessarily representative for the study area (no randomization of sample site positions). NDVIs were set against estimates of fresh weight and dry matter quantities of herbaceous vegetation. Until mid-August all three parameters increase more or less in parallel. The abrupt drop in NDVIs and fresh weight occurs in the vicinity of the point, where the vegetation m.c. drops below approximately 65% (see Chapter 3.2.3). While dry matter quantities stabilize until October, NDVIs and fresh weight values decrease. This may imply a stronger relationship between VIs and fresh weights in the second half of the growing season than between VIs and dry matter. Be that as it may, without a known relationship between fresh weight and dry matter at the time of image acquisition, even a high correlation between fresh weight and NOAA AVHRR NDVIs is of little use for estimating actual herbaceous vegetation quantities. For that reason no further investigations into the matter were performed.

(c) **Association Between Landsat MSS and NOAA AVHRR VIs**

For linear correlations between Landsat MSS and NOAA AVHRR VIs r^2 values of 0.92 (NDVI for 50 m sampling) and 0.97 for central pixel sampling were determined (Table A.55, Appendix II). No noteworthy differences between individual VIs could be substantiated.

5.4.4 1988 ITE/Silsoe Survey

Image co-ordinates for 1988 ITE/Silsoe field sample sites were based on positions on image hard-copies and maps. GPS readings, acquired during the 1989 field survey, were disregarded as a consequence of obvious deficiencies in accuracy. Sites No. 6 and 7 co-ordinates were originally established from maps. They were situated along the road between Kaou and Tchin Tabaraden. The positions along the road were estimated from the milage

meter of the vehicle. It was later discovered that the road was marked incorrectly on the map. The co-ordinates were determined on a Landsat MSS image, where the road was visible for most of its length. However, the position along the road could not be fixed with confidence. Furthermore, Site No. 8 co-ordinates could not be firmly established.
A summary of the results obtained from a regression analysis is given in Table 5.17.

(a) **Landsat MSS Data**

A Landsat MSS image from 8 September 1988 was available for VI correlation. The date was more than three weeks before the period of the field survey. Results of the analysis are presented in Tables A.56 and A.57 in Appendix II. As demonstrated (see Chapter 3.3), this temporal separation is more than sufficient to significantly change quantities of herbaceous vegetation. In none of the 60 cases assessed did the coefficient of determination reach a value of 0.5 or more. In addition to the temporal gap between ground and image data, seven of the 12 transects were situated in areas with C.V.s of more than 10%. Hence, small spatial changes could influence the results profoundly.
It was thus decided to remove vegetation estimates from sites with questionable co-ordinates (Sites 6, 7 and 8) from the regression and to compare the effect on the relationship between ground and satellite data to the complete number of samples (Table A.57, Appnedix II). Comments below generally relate to the reduced size of field data.

i. *Image Data Sampling Method*

The best results for r^2 values (0.77) were produced by central pixel VIs of 1.1 km resolution data for the reduced set of sample sites. When rating sampling methods according to their coefficients of determination, 50 m and 20 by 20 pixel averages came second.

ii. *Vegetation Index*

A distinction between VIs derived directly from 50 m resampled spectral reflectances (50 m and 20 by 20 averages) and those produces by the routine on the host computer (IM.REDUCE, central, 3 by 3 and transect) could be observed. For the former there was little to choose between VIs, while the latter favoured PVIs in six out of six cases.

VIs computed from average spectral reflectances of bands 3 and 4 achieved lower r^2 values in 27 out of 30 cases. In three cases, identical values were obtained.

iii. *Regression Type*

For all regressions conducted, both with all sample sites and when excluding Sites 6, 7 and 8, a logarithmic regression produced decidedly higher r^2 values than a linear one.

(b) NOAA AVHRR LAC Data

Although 10 NOAA AVHRR images for the 1988 growing season were available, estimates of herbaceous vegetation of only a single field survey at the end of September were available for comparison. Thus, VIs of the two images (06.09.88 and 05.10.88) were correlated to field data (Table A.58, Appendix II). The September image was included to allow comparisons to the CAZS survey investigation.

As it was the case for Landsat MSS, in addition to employing all sample sites regressions were also performed for data excluding Sites 6, 7 and 8 (Table A.60, Appendix II). Findings are summarized in Table 5.17.

When including all sample sites, for none of the VIs of the two satellite images could the variation in VIs be explained by more than 50% by estimates of herbaceous vegetation. Furthermore, maximum value VIs from eight scenes prior to the field survey did not exhibit any statistical association to vegetation estimates

(Table A.59, Appendix II). The VI of Site No. 9 at 6 September was identified as the cause of the poor correlation. Exceptionally high values for all VIs for that date, which were not repeated at any other date, induced the break-down of the relationship between vegetation quantities and VIs. More likely than a sudden and short lived surge in photosynthetically active vegetation is an inaccurate position of the site. A shift of one pixel to the west would have positioned it to include a depression with high amounts of photosynthetically active vegetation.

The following comments on regression results are, therefore, related to correlations of field data to VIs from the 5 October image, omitting Sites 6, 7 and 8.

i. *Image Data Sampling Method*

Only VIs from central pixel spectral albedos achieved r^2 values of 0.5 or more. VIs from 3 by 3 sampling stayed below that value in all six instances. Transect sampling was not investigated.

ii. *Vegetation Indices*

There was little discrepancy between VIs, but the PVI achieved higher r^2 values in 12 out of 12 cases. However, all individual differences were inconsequential for a rating of VIs in individual cases.

iii. *Regression Type*

In parallel with Landsat MSS findings a logarithmic regression apparently represented the relationship between ground data and VIs more favourably than a linear one.

Table 5.17: Summary of Results of Vegetation Index Calibration of 1988 ITE/Silsoe Field Survey

Satellite Data	Order *	Image Data Sampl. Method ($r^2 \geq 0.5$)	VI Type	Regression Type	Coeff. Determ.
Landsat MSS	1 2 3	none	-	-	-
Landsat MSS reduced*	1 2 3	Central 50 m & 20x20	PVI NDVI RVI	Logarithmic	0.77
NOAA AVHRR all sites	1 2 3	none	-	-	-
NOAA AVHRR Max. Val.	1 2 3	none	-	-	-
NOAA AVHRR reduced	1 2 3	Central	RVI NDVI RVI	Logarithmic	0.66

Order: According to coefficient of determination.
&: Comparable performance, no preference attributed.
Max. Val: Maximum Value for VI preceding sampling period.
*: Excluding Sites 6, 7 and 8.

A graphical presentation of relationships between herbaceous vegetation estimates and Landsat MSS, NOAA AVHRR 6 September and 5 October NDVIs is given in Figures 5.16 and 5.17.

Figure 5.16: Relationship Between Estimates of Herbaceous Vegetation of 1988 ITE/Silsoe Field Survey Sites and NDVIs from Landsat MSS and NOAA AVHRR from 6 September 1988(Central Sampling)

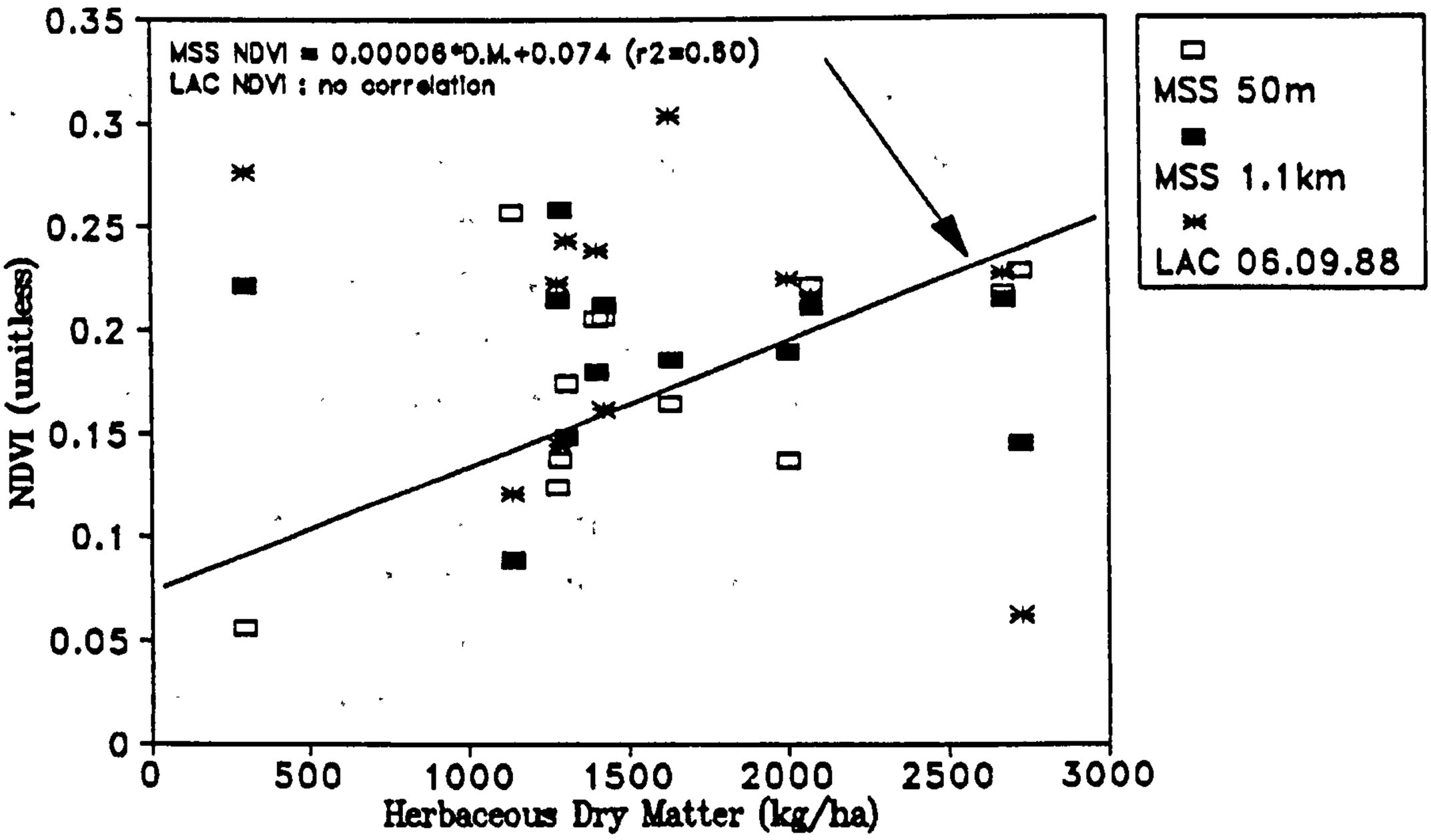
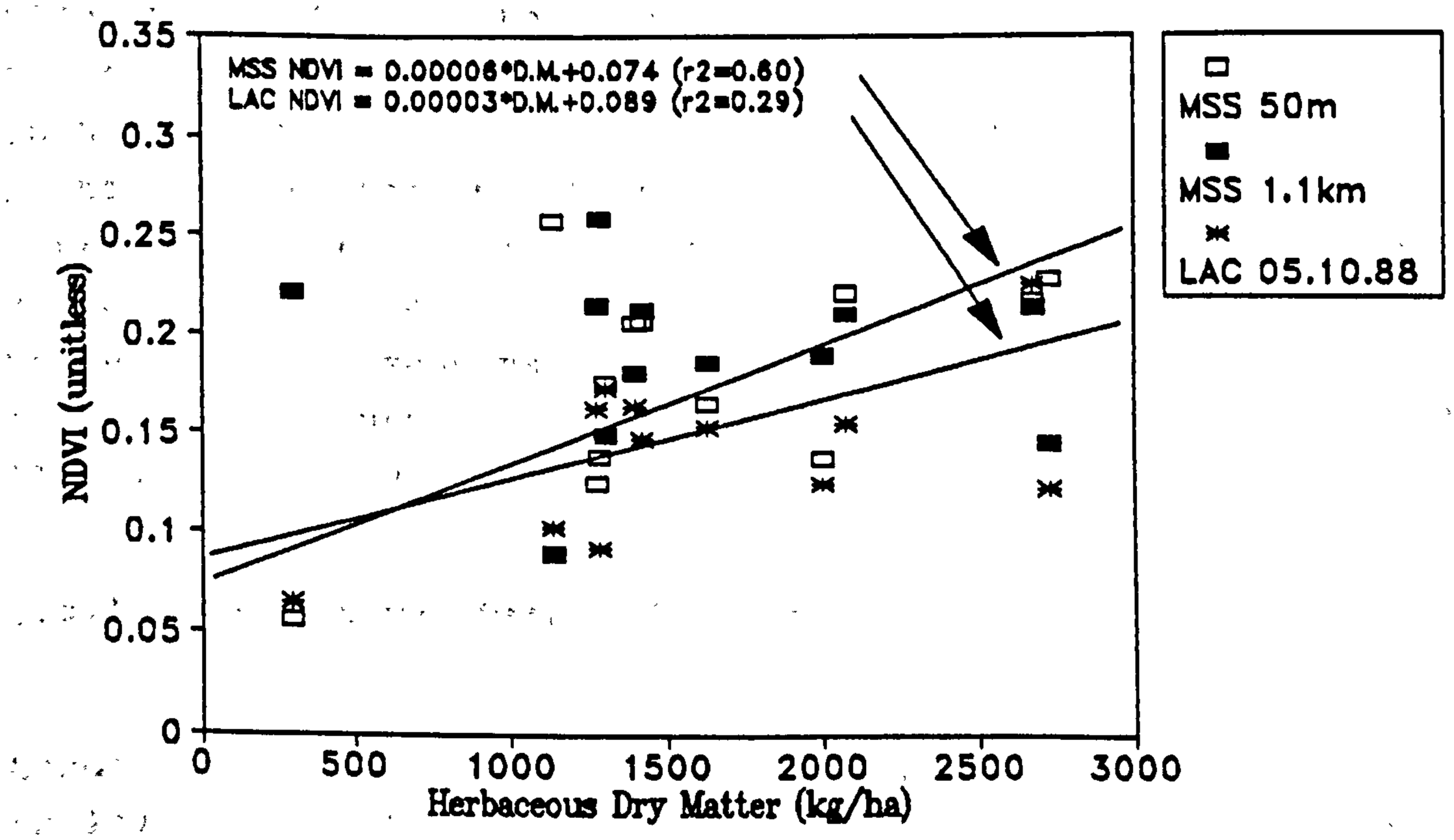


Figure 5.17: Relationship Between Estimates of Herbaceous Vegetation of 1988 ITE/Silsoe Field Survey Sites and NDVIs from Landsat MSS and NOAA AVHRR from 5 October 1988 (Central Sampling)



(c) Association Between Landsat MSS and NOAA AVHRR VIs

For 50 m VIs from the 8 September Landsat MSS and central pixel VIs of a NOAA AVHRR image from 6 September coefficients of determination of 0.47 were established from applying a linear regression (Table A.60, Appendix II). The low correlation was attributed to disparate geometric properties between the two images and inaccuracies in determining transect co-ordinates. In particular Site No. 8 on Landsat MSS and Site No. 9 on the NOAA AVHRR image contributed to the variation. That high correlations between Landsat MSS and NOAA - AVHRR VIs did exist for the sites could be demonstrated by relating the former to the 5 October data. Although the NOAA AVHRR image was acquired almost four weeks after the Landsat MSS scene, r^2 values of 0.81 (NDVI) were achieved.

5.5 Integration of Field Survey Data

Combinations of VIs from all surveys were investigated to evaluate, if a single calibration curve of herbaceous vegetation estimates to satellite data could be assumed. For the three different field survey regions (CIPEA and ITE/Silsoe in Niger and CAZS in Mali). A repetition of estimating herbaceous vegetation within another growing season was only carried out for ITE/Silsoe sites. Thus, the spatial influences cannot be separated from differences induced by variations between growing seasons. But it would be possible to compare 1985 and 1988 surveys to each other for spatial deviations and ITE/Silsoe surveys for temporal changes.

5.5.1 Field Survey Data and Landsat MSS VIs

Landsat MSS data was available from three dates. The image employed for CIPEA and 1985 ITE/Silsoe sites was identical. Only atmospherically adjusted data was investigated, which

would be related to NOAA AVHRR VIs (see following section). A graphical presentation of distribution of sample site NDVIs is given in Figure 5.18 for 50 m resolution data and in Figure 5.19 for 1.1 km resolution data from central pixel positions.

Figure 5.18: Comparison of Landsat MSS NDVIs Derived from 50 m Resolution Atmospherically Standardized Data for All Field Survey Sites

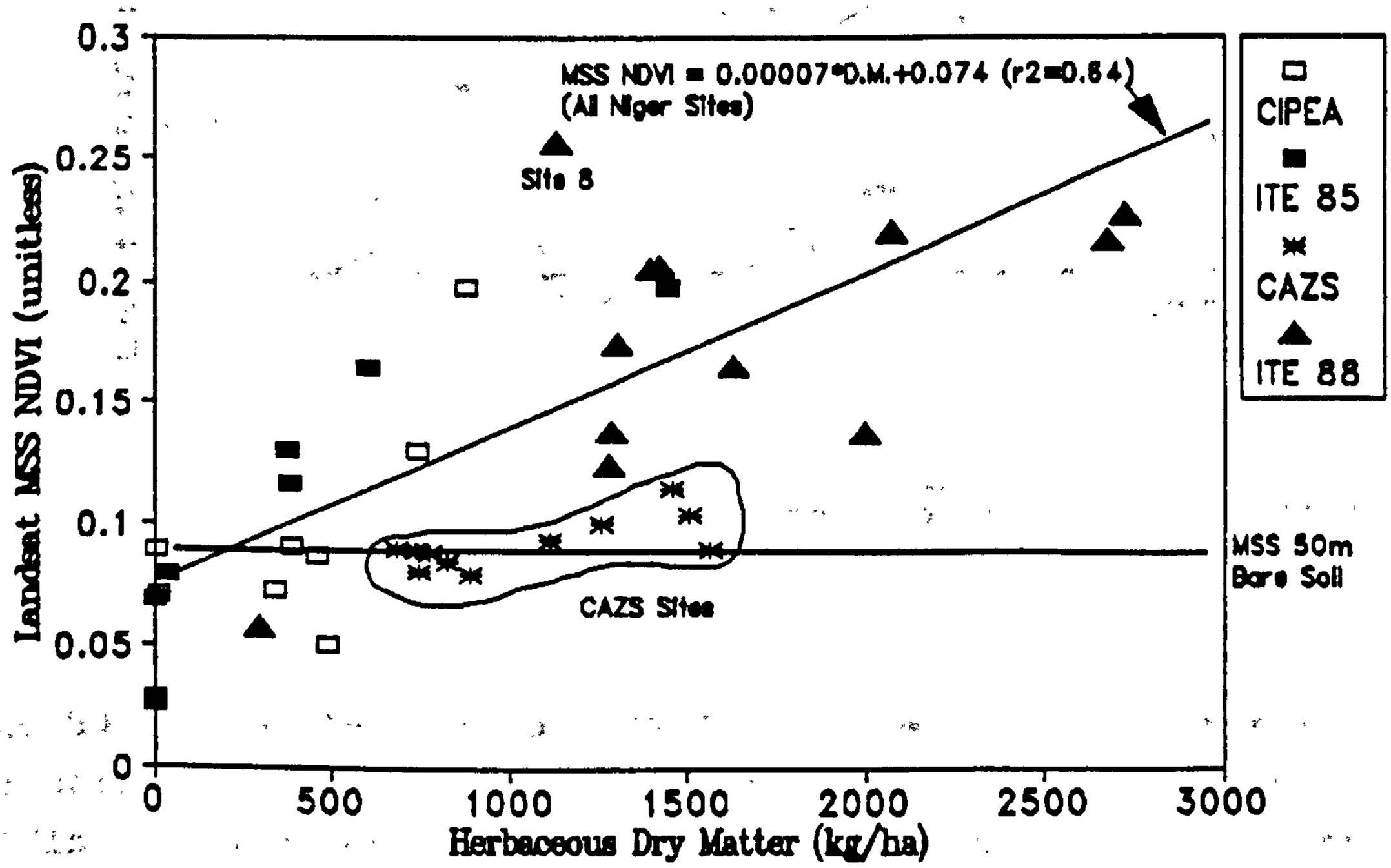
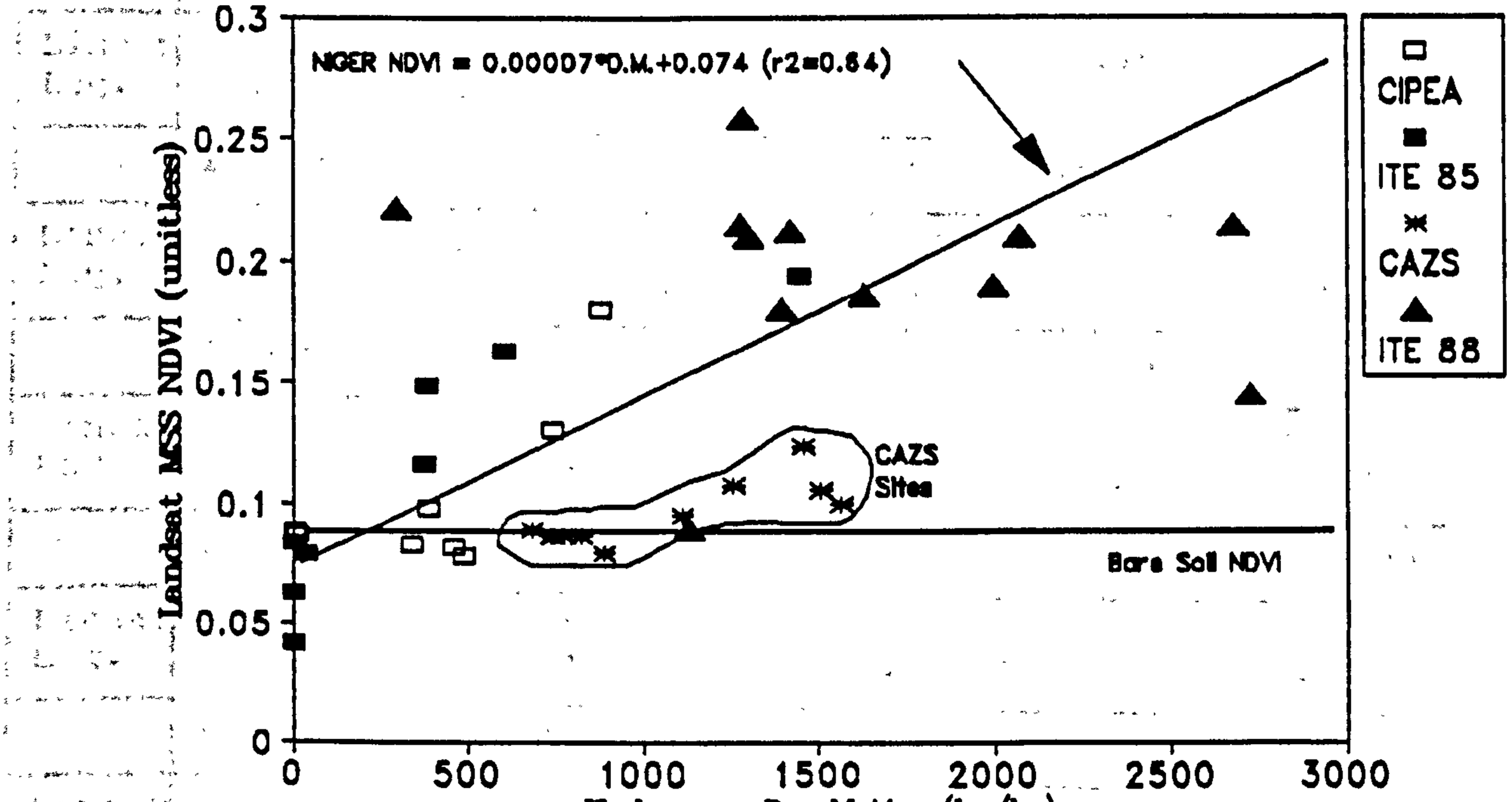


Figure 5.19: Comparison of Landsat MSS NDVIs Derived from 1.1 km Resolution Atmospherically Standardized Data for All Field Survey Sites



The 50 m resampled Landsat MSS NDVIs seem to be better related to herbaceous dry matter estimates than 1.1 km resolution NDVIs. For the former, CAZS sites are not in line with other surveys, while for the latter 1988 ITE/Silsoe sites reveal hardly any change with increasing quantities of vegetation. Coefficients of correlation from a regression analysis of linear and logarithmic herbaceous vegetation estimates are summarized in Table 5.18.

Table 5.18: Coefficients of Correlation from Linear and Logarithmic Regressions Between Herbaceous Vegetation Estimates and Landsat MSS VIs Derived from Atmospherically Standardized Data

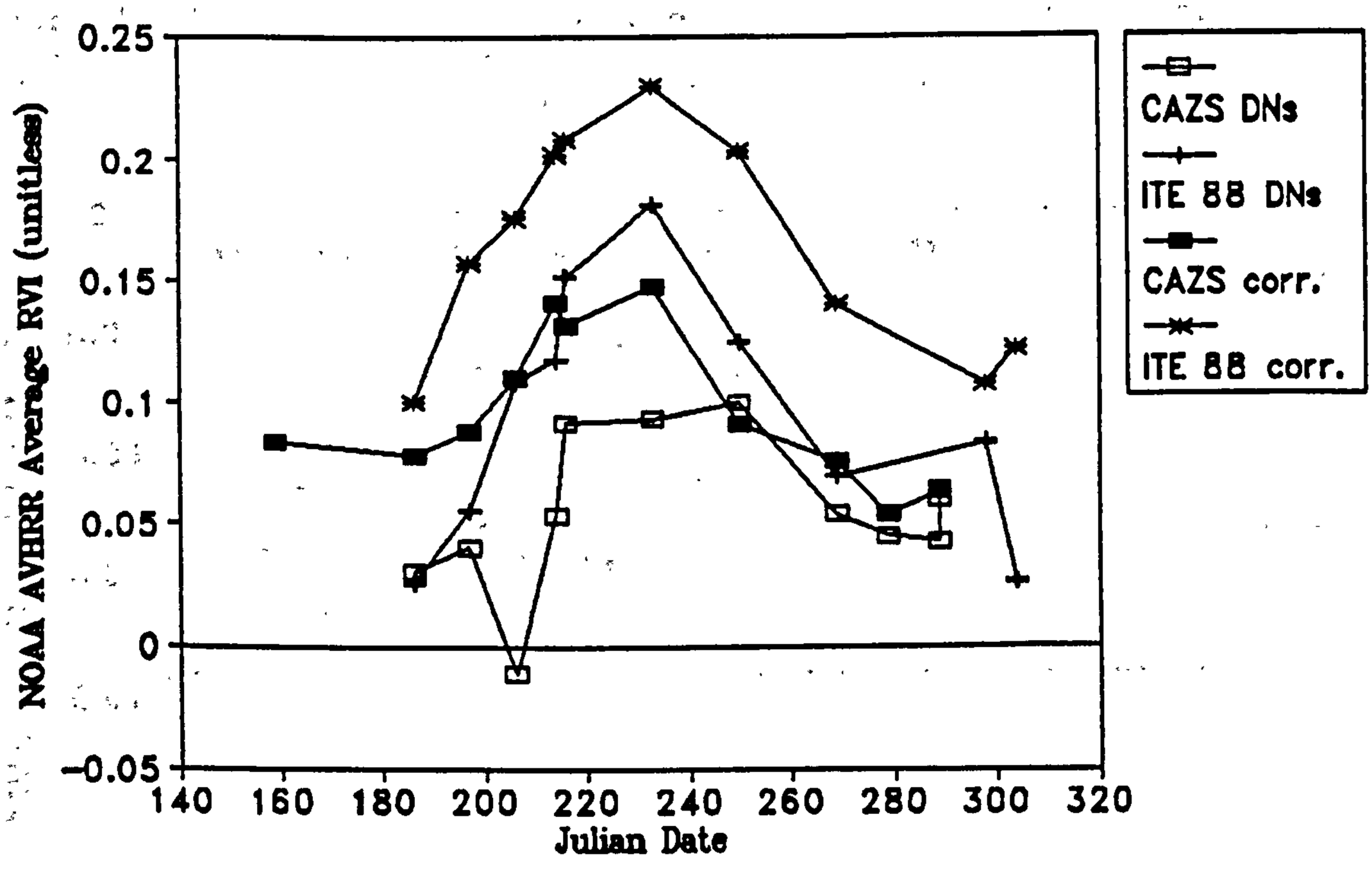
Regr. Type	50 m Resolution VIs RVI	NDVI	PVI	1.1 km Resolution VIs RVI	NDVI	PVI
	Integration of CIPEA and 1985 ITE/Silsoe Surveys					
Linear	0.849 *	0.840 *	0.693 *	0.769 *	0.765 *	0.693 *
Log.	0.711 *	0.728 *	0.802 *	0.675 *	0.688 *	0.802 *
	Integration of CAZS and 1988 ITE/Silsoe Surveys					
Linear	0.763 *	0.773 *	0.745 *	-0.383	-0.381	0.745 *
Log.	0.712 *	0.730 *	0.664 *	-0.215	-0.207	0.664 *
	Integration of 1985 and 1988 ITE/Silsoe Surveys					
Linear	0.840 *	0.835 *	0.413	0.203	0.216	0.413
Log	0.822 *	0.842 *	0.582 *	0.494	0.522	0.582 *
	Integration of CIPEA, 1985 and 1988 ITE/Silsoe Surveys					
Linear	0.828 *	0.823 *	0.344	0.268	0.276	0.344
Log.	0.726 *	0.743 *	0.560 *	0.479 *	0.501 *	0.560 *
	Integration of All Surveys					
Linear	0.711 *	0.715 *	0.123	0.253	0.268	0.123
Log.	0.565 *	0.590 *	0.151	0.470 *	0.494 *	0.151
* Significance of no relationship <0.01						

In general, 50 m resampled VIs are more closely related to herbaceous vegetation estimates than VIs from the simulated LAC resolution. For RVIs and NDVIs all survey integrations are significant at a 99% confidence level. The PVI is only significantly related to vegetation estimates for logarithmic regressions. It is the sole VI, which is repeatedly and significantly related to ground data for LAC resolution images. Differences in seasons did not influence the established relationships for ratio VIs, but the Mali sites (CAZS) were unrelated to 1985 Niger sample sites. This may have been caused by the inability to standardize data sets to similar atmospheric conditions.

5.5.2 Field Survey Data and NOAA AVHRR VIs

A comparison of VIs derived directly from DNs, from radiometrically corrected and from atmospherically adjusted data would allow a comparison of the pre-processing procedures applied for reducing temporal variations.
The general feasibility of reducing variations between images by standardizing atmospheric conditions is demonstrated in Figure 5.20.

Figure 5.20: Comparison of NOAA AVHRR NDVIs Derived from DNs and Atmospherically Standardized Data for CAZS and 1988 ITE/Silsoe Field Survey Sites



For ground and satellite data mean values for each date of data acquisition were established. Although the differences between adjacent dates were reduced by the method, NDVIs at the end of the growing season were found to be below those in June. A reasonable assumption for the findings is an increase of shadowed areas due to low solar angles, which becomes increasingly dominant as vegetation m.c.s drop. Still, the cause of the lower NDVI values at the end of the season could not be established with certainty.

The plausibility of integrating NOAA AVHRR VIs from different field surveys was investigated at each step of pre-processing procedures, where radiometric properties were altered. Graphical presentations of relationships are provided for NDVIs, since they are most widely used for NOAA AVHRR.

(a) Combining Survey Data Using VIs Derived from DNs

VIs were derived from DNs at 10 bit radiometric resolution and correlated to herbaceous vegetation estimates for each survey. A graphical arrangement of relationships is presented in Figure 5.21.

Figure 5.21: Relationship Between Herbaceous Vegetation Estimates of CIPEA, CAZS and ITE/Silsoe Field Surveys and NOAA AVHRR NDVIs Derived from DNs

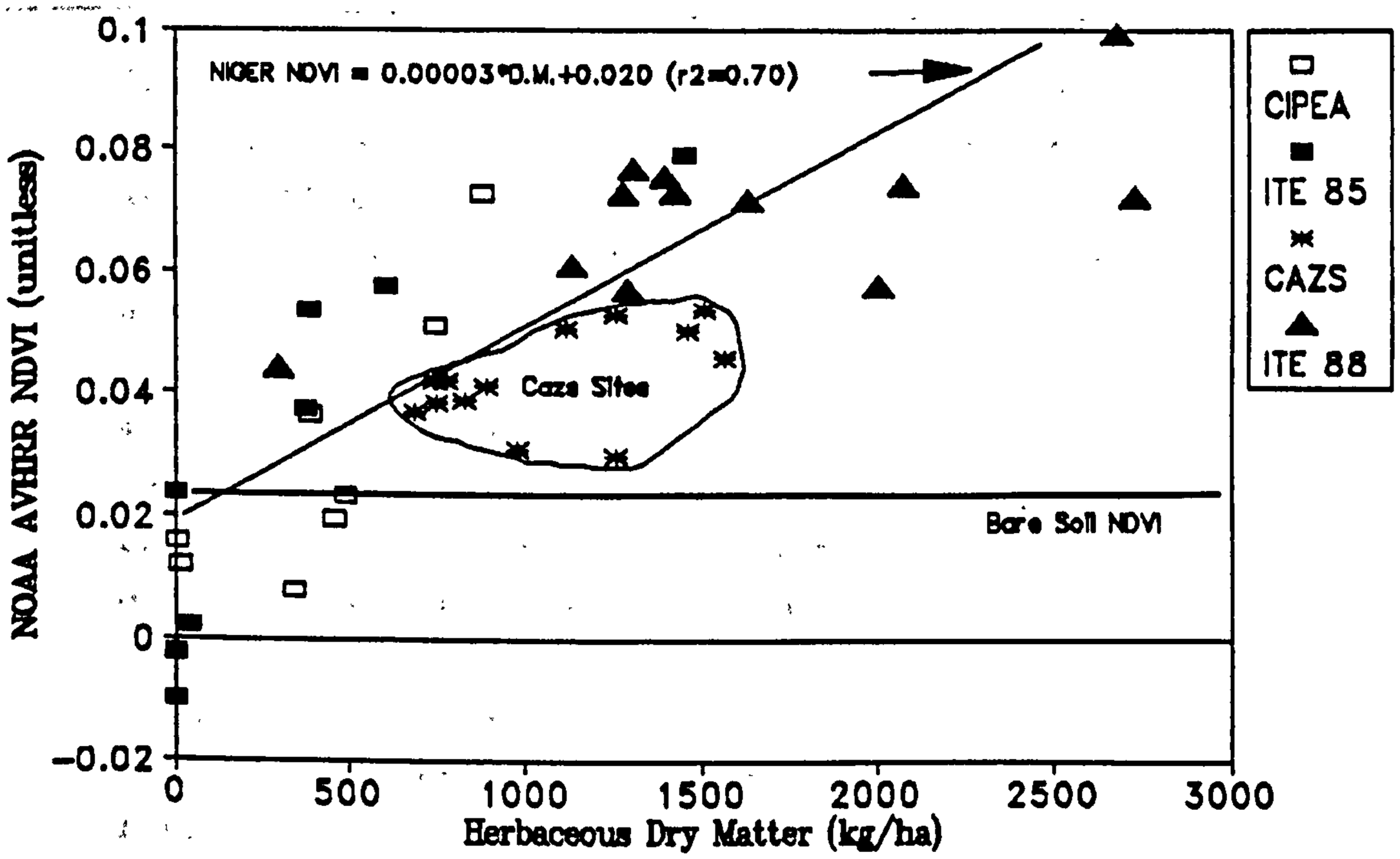


Table 5.19 summarizes coefficients of correlation (r) for linear and logarithmic regressions between herbaceous vegetation estimates and VIs derived from DNs. Also indicated is, if the relationship is significant at a 99% confidence level.

Table 5.19: Coefficients of Correlation from Linear and Logarithmic Regressions Between Herbaceous Vegetation Estimates and NOAA AVHRR VIs Derived from DNs

Surveys Combination	Regression Type	RVI	Sig.	NDVI	Sig.	PVI	Sig.
CIPEA & 1985 ITE	Linear	0.86	*	0.86	*	0.76	*
	Logarithmic	0.72	*	0.73	*	0.54	
CAZS & 1988 ITE	Linear	0.72	*	0.72	*	0.63	*
	Logarithmic	0.66	*	0.66	*	0.65	*
1985 ITE & 1988 ITE	Linear	0.83	*	0.82	*	-0.06	
	Logarithmic	0.89	*	0.89	*	0.15	
Niger Surveys	Linear	0.84	*	0.83	*	0.09	
	Logarithmic	0.81	*	0.81	*	0.24	
All Surveys	Linear	0.80	*	0.80	*	0.07	
	Logarithmic	0.74	*	0.75	*	0.14	
* Significance for no relationship <0.01.							

The highest correlation coefficients were achieved when combining survey results from the same area. Differences in growth pattern and quantities between the vastly disparate seasons of 1985 and 1988 apparently still allowed an integration of survey data to calibrate satellite VIs. CIPEA and ITE/Silsoe sites could be merged (denoted as Niger surveys) to base the calibration on a larger number of samples. Including CAZS site decreases the strength of the relationships, even if the same years are compared.

For integrated data the PVI only provided significant relationships for identical years. Despite the fact that ITE/Silsoe surveys covered the same area soil lines were found to be quite dissimilar. As a consequence, no relationship between herbaceous vegetation estimates and PVIs derived from DNs was found.

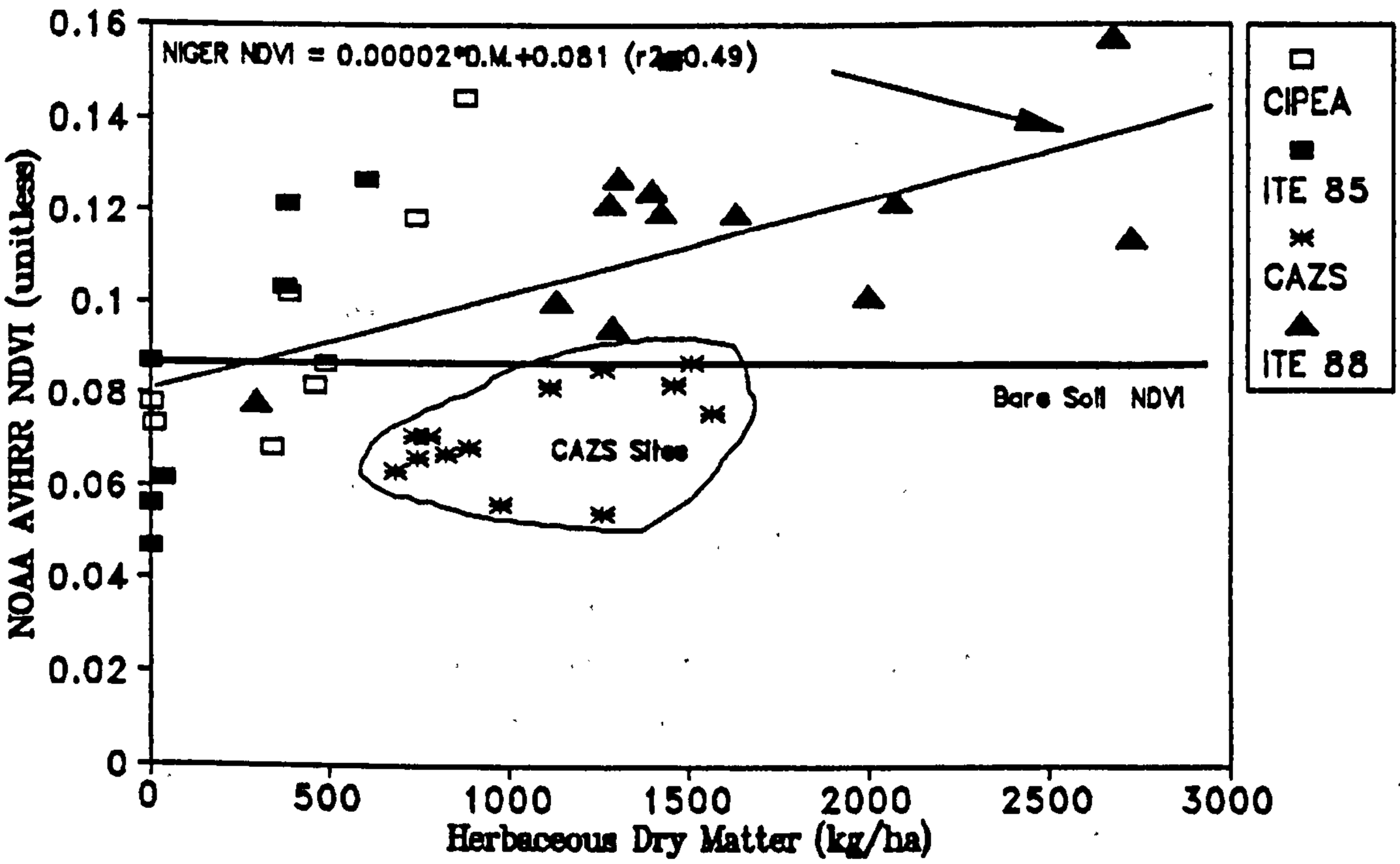
For different survey areas linear regressions seemed to be better representative of the relationship between ground and satellite data. For comparable sample sites (ITE/Silsoe surveys) logarithmic regressions achieved higher coefficients of correlation. The type of the relationship was determined by 1988 samples, for which a

stronger logarithmic association between herbaceous vegetation estimates and VIs was observed (Chapter 5.4.4).

(b) **Combining Radiometrically Corrected Data**

A graphical description of the distribution of VIs derived from radiometrically corrected data in relationship to herbaceous vegetation estimates is presented in Figure 5.22.

Figure 5.22: Relationship Between Herbaceous Vegetation Estimates of CIPEA, CAZS and ITE/Silsoe Field Surveys and NOAA AVHRR NDVIs Derived from Radiometrically Corrected Spectral Albedos



Compared with VIs based on DNs there seems to be more variation between different surveys (see Figure 5.21). The increase originates from two steps within the radiometric correction procedure, which affected channels 1 and 2 non-proportionally:

i. *Conversion of Solar Irradiance to Neckel and Labs*
Channel 1 values are relatively more reduced than those of channel 2. This amplifies ratio VIs, but independently of the date of data acquisition.

ii. *Compensation for Sensor Degradation*

Channel 1 detector elements degrade at a faster rate than channel 2 elements. However, the initial sensitivity for channel 1 is 95.3% as compared to 86.6% for channel 2 (see Chapter 4.2.5). For the 1988 growing season the relative sensitivity in both channels was approximately equal (75% to 77%). A compensation favours ratio VIs from earlier dates over those acquired at later stages. Accordingly, ratio VIs from 1985 are 8% higher than those from 1988.

The solar irradiance conversion from values based on Thekaekara to those from Neckel and Labs does not influence correlation coefficients for data from different dates, as does the sensor degradation compensation. Under the assumption that NOAA AVHRR detector elements deteriorate at the given rates then coefficients of correlation between herbaceous vegetation estimates and ratio VIs derived from DNs provide an unrealistically close similarity. Using radiometrically corrected spectral albedos for comparing relationships between field surveys would thus be preferable to DN-based VIs.

As a consequence of radiometrically correcting NOAA AVHRR data, coefficients of correlation are generally lower for VIs from radiometrically corrected data than for those derived directly from DNs. This is specific to the survey data employed and a generalization is only permissible for similar relationships between surveys VIs. A summary of survey combinations is given in Table 5.20.

Table 5.20: Coefficients of Correlation from Linear and Logarithmic Regressions Between Herbaceous Vegetation Estimates and NOAA AVHRR VIs Derived from Radiometrically Corrected Spectral Albedos

Surveys Combination	Regression Type	RVI	Sig.	NDVI	Sig.	PVI	Sig.
CIPEA & 1985 ITE	Linear	0.87	*	0.86	*	0.72	*
	Logarithmic	0.72	*	0.73	*	0.49	
CAZS & 1988 ITE	Linear	0.70	*	0.70	*	0.66	*
	Logarithmic	0.64	*	0.64	*	0.66	*
1985 ITE & 1988 ITE	Linear	0.69	*	0.69	*	0.33	
	Logarithmic	0.76	*	0.78	*	0.48	
Niger Surveys	Linear	0.69	*	0.69	*	0.48	*
	Logarithmic	0.72	*	0.73	*	0.49	*
All Surveys	Linear	0.52	*	0.52	*	0.46	*
	Logarithmic	0.43	*	0.44	*	0.41	*

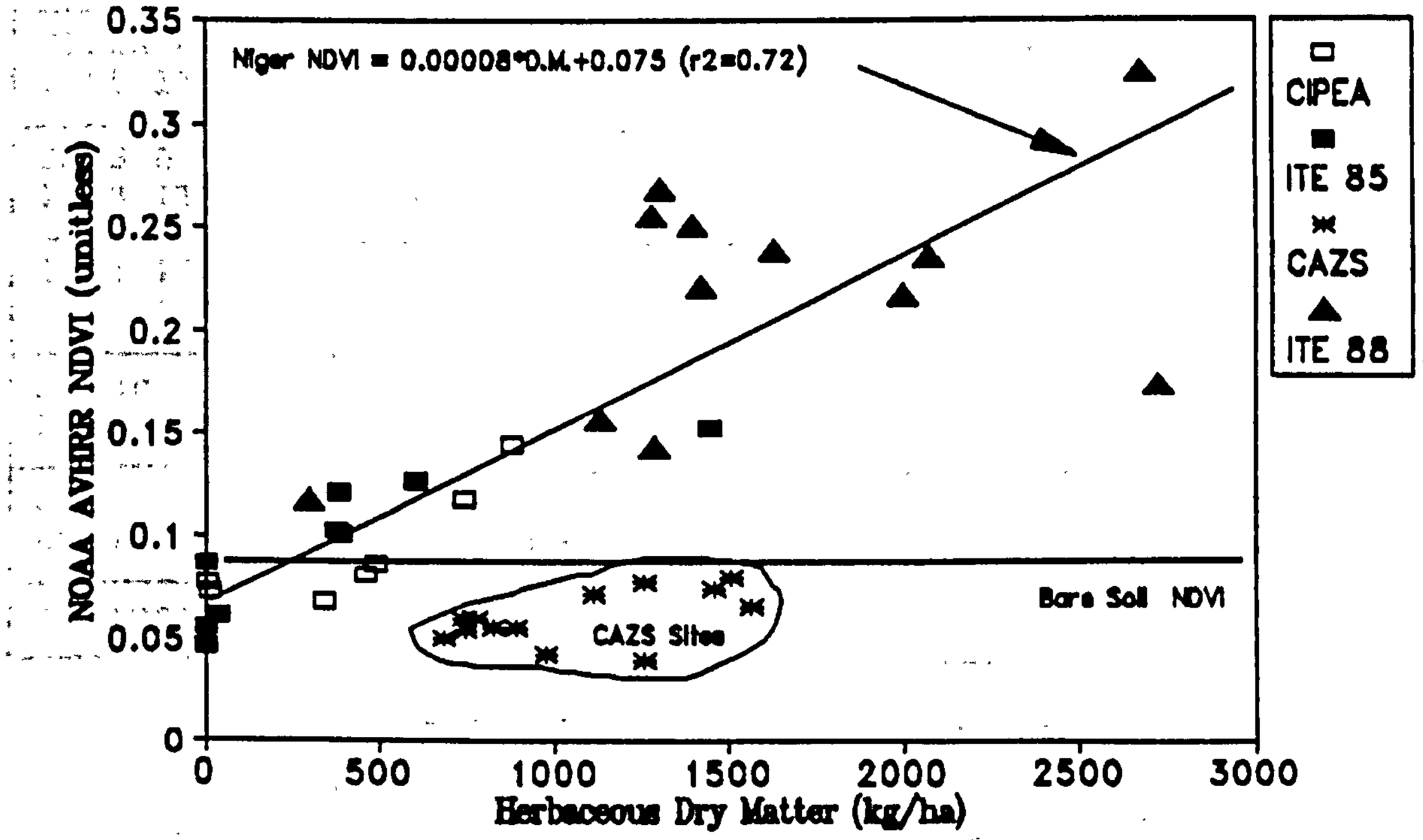
* Significance for no relationship <0.01.

Combined survey results from identical years score higher coefficients of correlation than comparable areas (ITE/Silsoe sites). Ratio VIs perform very similarly to each other, while PVIs are again restricted to identical seasons. On the other hand, radiometrically corrected PVIs achieve a 99% significance level for possibilities of a relationship to ground data in most instances. As in the case of DN-based VIs logarithmic regressions provide higher values than linear ones for ITE/Silsoe sites.

(c) Combining Atmospherically Standardized Data

The placement of VIs derived from atmospherically standardized data in relation to herbaceous vegetation quantities is graphically presented in Figure 5.23.

Figure 5.23: Relationship Between Herbaceous Vegetation Estimates of CIPEA, CAZS and ITE/Silsoe Field Surveys and NOAA AVHRR NDVIs Derived from Atmospherically Standardized



Compared with VIs derived from radiometrically corrected data coefficients of correlation increased for all combinations except when merging CAZS and 1988 ITE/Silsoe surveys. A summary of correlation coefficients and their significance for atmospherically standardized VIs is given in Table 5.21.
For Niger field survey sites high values for coefficients of correlation were achieved for all combinations and linear regressions. When combining CAZS sites relationships decline noticeably. This might indicate that conditions over the Mali study area were sufficiently different to affect ratio VIs. As before, ratio VIs perform almost identically with respect to their coefficients of correlation. From all 10 cases investigated the highest r value was achieved by the RVI once, by the NDVI four times and by the PVI five times. In most individual cases, however, were the differences insignificant.

Table 5.21: Coefficients of Correlation from Linear and Logarithmic Regressions Between Herbaceous Vegetation Estimates and NOAA AVHRR VIs Derived from Atmospherically Standardized Spectral Albedos

Surveys Combination	Regression Type	RVI	Sig.	NDVI	Sig.	PVI	Sig.
CIPEA & 1985 ITE	Linear	0.87	*	0.86	*	0.72	*
	Logarithmic	0.72	*	0.73	*	0.49	
CAZS & 1988 ITE	Linear	0.62	*	0.62	*	0.70	*
	Logarithmic	0.56	*	0.56	*	0.64	*
1985 ITE & 1988 ITE	Linear	0.80	*	0.82	*	0.81	*
	Logarithmic	0.71	*	0.75	*	0.80	*
Niger Surveys	Linear	0.83	*	0.85	*	0.82	*
	Logarithmic	0.65	*	0.69	*	0.67	*
All Surveys	Linear	0.64	*	0.63	*	0.72	*
	Logarithmic	0.39	*	0.40	*	0.51	*
* Significance for no relationship <0.01.							

Generally, ratio VIs seemed to be better suited to represent relationships between herbaceous vegetation estimates and satellite VIs for identical years or comparable sites, while PVIs scored higher when comparing different areas or growing seasons. But with only four surveys available, these findings cannot be considered conclusive.

5.5.3 Estimating NOAA AVHRR VIs from Landsat MSS VIs

The feasibility of estimating NOAA AVHRR VIs from Landsat MSS VIs was investigated for integrated survey data in order to evaluate the temporal stability of the relationship between NOAA AVHRR and Landsat MSS data. As demonstrated, Landsat MSS 50 m resampled VIs can be correlated to herbaceous vegetation estimates with more confidence than can NOAA AVHRR. This was mainly attributed to problems of geometrically matching images. For image-to-image calibrations the importance of matching data geometrically is of less prominence on the relationship, since much more data could be used for correlations. However, the investigation of the feasibility of using Landsat MSS VIs as an

intermediate step to calibrating NOAA AVHRR VIs to herbaceous vegetation quantities was based on survey sites and, therefore, includes locational errors. Thus, a more conservative estimate of the relationships of VIs derived from the two sensors can be expected.

Table 5.22 summarizes coefficients of correlation for regressions of linear and logarithmic Landsat MSS VIs with NOAA AVHRR VIs. Landsat MSS VIs based on average spectral reflectances from bands 3 and 4 were omitted, since no widely applicable improvement over orthodox VIs could be established. Furthermore, image data sampling methods were restricted to 50 m resampled and central pixel value data for Landsat MSS and just central pixel values for NOAA AVHRR.

A graphical presentation of the relationships between NDVIs of the two sensors is provided by Figure 5.24 for 50 m resampled data and in Figure 5.25 for 1.1 km resolution data.

Specifically marked on the figures are VIs from CAZS sites. For 50 m Landsat MSS data they were found to be situated at higher NDVI values than Niger sites for comparable NOAA AVHRR NDVIs. This condition was not as distinct for 1.1 km VIs, which suggests that data of comparable resolution should be employed for image-to-image calibrations.

Table 5.22: Coefficients of Correlation from Linear and Logarithmic Regressions Between Landsat MSS and NOAA AVHRR VIs Derived from Atmospherically Standardized Image Data

Image Sampl. VIs Method	Landsat MSS	NOAA AVHRR Linear Landsat VIs RVI	NDVI	PVI	Logarithmic Landsat VIs RVI	NDVI	PVI
	Integration of CIPEA and 1985 ITE/Silsoe Survey						
50 m Cent.	RVI	0.893*	0.885*	0.797*	0.890*	0.882*	0.792*
	NDVI	0.886*	0.879*	0.786*	0.882*	0.876*	0.779*
	PVI	0.928*	0.930*	0.714*	0.863*	0.870*	0.608
	RVI	0.969*	0.963*	0.892*	0.970*	0.966*	0.890*
	NDVI	0.971*	0.967*	0.888*	0.971*	0.968*	0.885*
	PVI	0.964*	0.962*	0.864*	0.908*	0.913*	0.761*
	Integration of CAZS and 1988 ITE/Silsoe Surveys						
50 m Centr.	RVI	0.714*	0.733*	0.771*	0.725*	0.744*	0.782*
	NDVI	0.736*	0.755*	0.792*	0.742*	0.761*	0.799*
	PVI	0.364	0.383	0.771*	0.472	0.495	0.834*
	RVI	0.822*	0.840*	0.837*	0.830*	0.849*	0.845*
	NDVI	0.835*	0.855*	0.852*	0.840*	0.860*	0.857*
	PVI	0.536*	0.559*	0.845*	0.611*	0.636*	0.875*
	Integration of 1985 and 1988 ITE/Silsoe Surveys						
50 m Centr.	RVI	0.628*	0.660*	0.751*	0.638*	0.670*	0.763*
	NDVI	0.647*	0.680*	0.774*	0.652*	0.6860	0.781*
	PVI	0.328	0.341	0.603*	0.464	0.478	0.655*
	RVI	0.747*	0.779*	0.827*	0.753*	0.787*	0.838*
	NDVI	0.757*	0.793*	0.848*	0.760*	0.796*	0.854*
	PVI	0.349	0.391	0.822*	0.418	0.462	0.841*
	Integration of CIPEA, 1985 and 1988 ITE/Silsoe Surveys						
50 m Cent.	RVI	0.684*	0.714*	0.785*	0.690*	0.721*	0.792*
	NDVI	0.700*	0.727*	0.797*	0.699*	0.730*	0.799*
	PVI	0.354	0.371	0.553*	0.420	0.437	0.506*
	RVI	0.795*	0.824*	0.858*	0.799*	0.829*	0.866*
	NDVI	0.801*	0.837*	0.871*	0.802*	0.835*	0.875*
	PVI	0.461	0.499*	0.832*	0.491*	0.531*	0.804*
	Integration of all Surveys						
50 m Cent.	RVI	0.726*	0.749*	0.800*	0.730*	0.753*	0.807*
	NDVI	0.733*	0.757*	0.812*	0.733*	0.757*	0.814*
	PVI	0.449*	0.466*	0.598*	0.497*	0.515*	0.555*
	RVI	0.829*	0.852*	0.863*	0.832*	0.855*	0.870*
	NDVI	0.833*	0.857*	0.875*	0.833*	0.858*	0.879*
	PVI	0.569*	0.602*	0.810*	0.596*	0.630*	0.783*

* Significance for no relationship <0.01.

Figure 5.24: Relationship Between Landsat MSS NDVIs of 50 m Resampled Image Data and NOAA AVHRR NDVIs Derived from Atmospherically Standardized for All Field Surveys

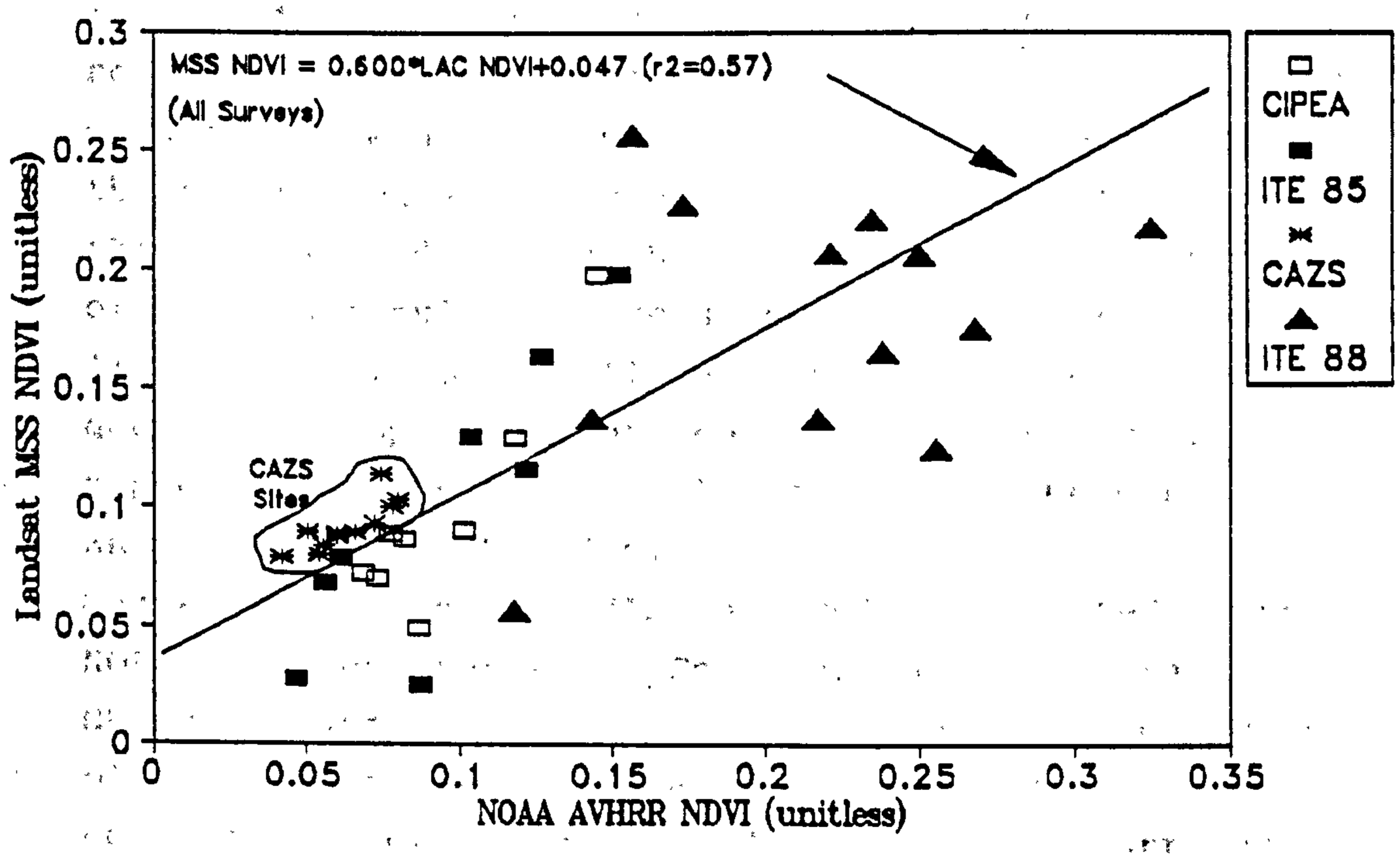
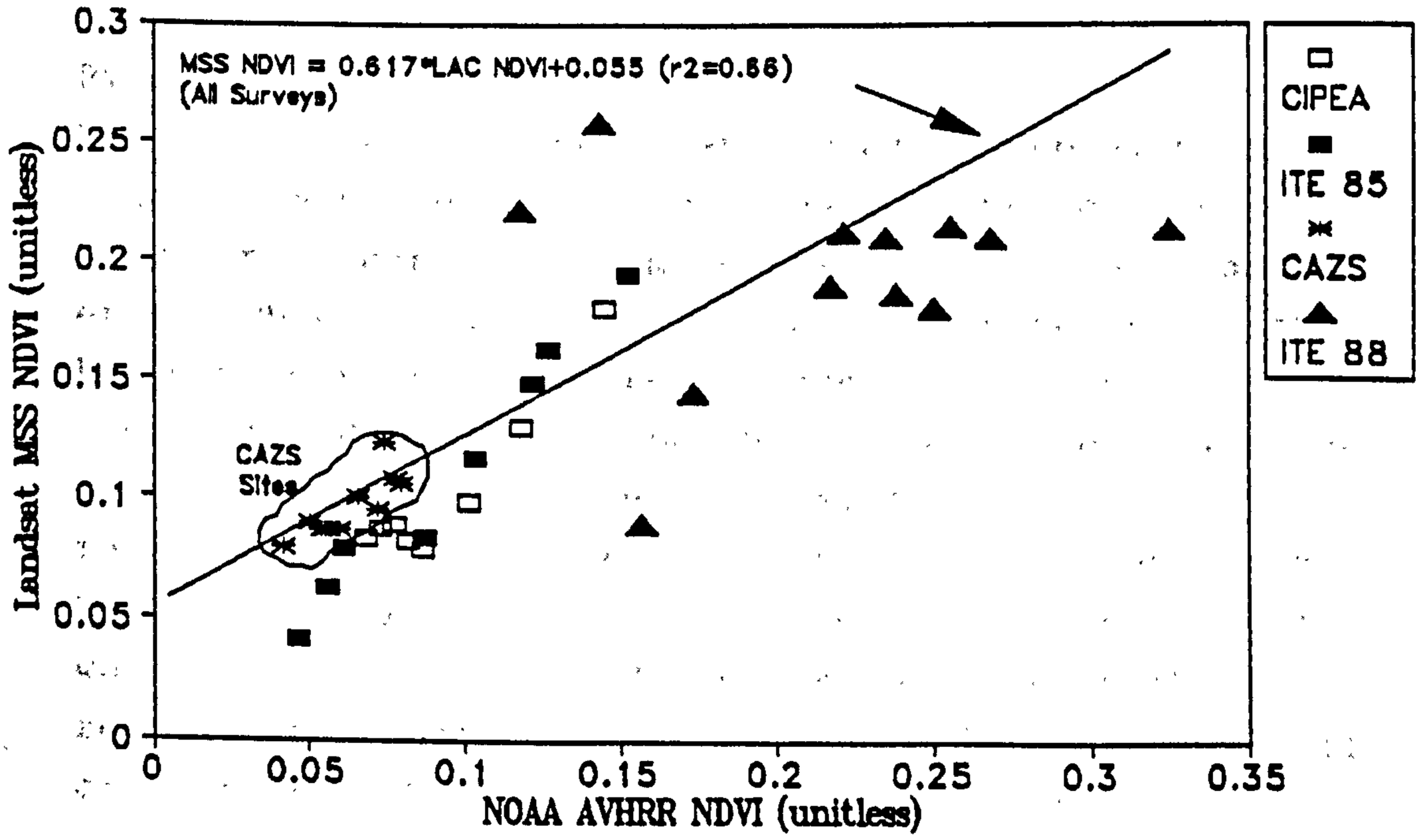


Figure 5.25: Relationship Between Landsat MSS NDVIs of 1.1 km Resolution Image Data and NOAA AVHRR NDVIs Derived from Atmospherically Standardized for All Field Surveys



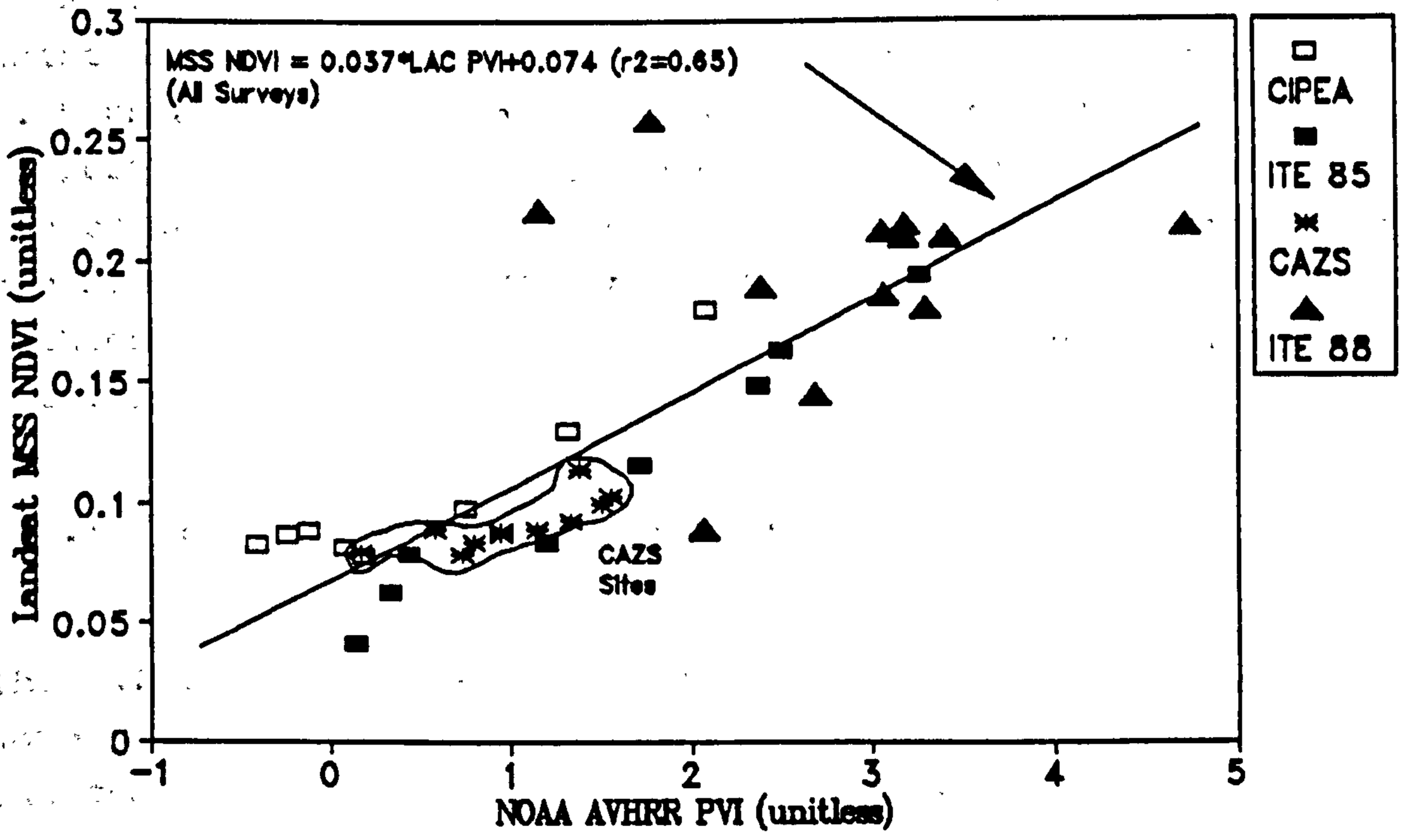
In most cases NOAA AVHRR VIs were found to be more closely related to Landsat MSS 1.1 km VIs than to those of 50 m resampled images. The coarser resolution of simulated and actual NOAA AVHRR LAC data can be interpreted as representing averages of higher resolution data over the IFOV. Since variations in data sets are generally reduced by averaging, the results of the regression analyses are in agreement with theoretical models. On the other hand, an interpretation of results should also consider that the discrepancy was likely to have been influenced by differences in geometric properties between images. This assumption is supported by the high similarities found between 50 m and 1 km Landsat MSS VIs.

Genrally, Landsat MSS VIs were well correlated to their NOAA AVHRR counterparts. For temporally integrated data NDVIs produced marginally better values of coefficients of correlation than RVIs and PVIs. In addition, for most combinations of ratio VIs and the PVI high correlations were achieved. An exception is formed by Landsat MSS PVIs and NOAA AVHRR ratio VIs. When integrating 1988 ITE/Silsoe sites the significance of no relationships between Landsat MSS and NOAA AVHRR PVIs and was more than 1% in most cases. The reason for these comparatively low relationships, particularly for 50 m PVIs, is yet unrecognized.

For ratio VIs identical years usually display higher relationships than similar sites. The performance of PVIs, in comparison, is more even between years and areas. When integrating different areas and years the highest correlations were achieved for Landsat MSS NDVIs and NOAA AVHRR PVIs, although the improvements were not significant for individual cases. A graphical representation of the relationship between Landsat MSS NDVIs and NOAA AVHRR PVIs is given in Figure 5.26. Also, when including 1988 ITE/Silsoe sites a logarithmic relationship performed better than a linear one in all cases tested. Yet, this may be caused by peculiarities

of the data set from that survey rather than a general trend.

Figure 5.26: Relationship Between Landsat MSS NDVIs of 1.1 km Resolution Image Data and NOAA AVHRR PVIs Derived from Atmospherically Standardized for All Field Surveys



5.6 Discussion of Ground to Satellite Data Relationships

Before commenting on the observations made, some general remarks on interpreting the outcome seem to be required. For individual surveys the most suitable VI or regression type differed considerably. As demonstrated, relationships also depend on the method applied for extracting the data. At this point two approaches to treating and interpreting regression products can be distinguished:

- *Investigating Procedures*
- *Investigation Potentials*

When investigating procedures, for example for establishing sample site co-ordinates, the method employed for obtaining data for comparisons is of concern. This implies that all samples are included in a regression analysis. The result depends thus on the procedures applied. In contrast, the potential, for example of estimating herbaceous vegetation from NOAA AVHRR, can be masked by specific circumstances which existed when acquiring the data. For that reason sample sites with unreliable positions or images with disputable geometric properties were excluded in some cases. By employing both approaches it could be demonstrated that herbaceous vegetation can be estimated from NOAA AVHRR VIs, but is restricted by the methods implemented to attain and relate both ground and satellite data.

5.6.1 Field Survey Sampling Layout

The calibration of satellite VIs to ground data also allows some conclusions about the feasibility of the survey designs. The comparison between 1985 and 1988 surveys indicated a lower correlation between ground and image data for the latter. However, not only were the two growing seasons completely different, but the sampling methods were disparate, too.
CAZS samples were collected over a comparatively small area and covered a narrow range of vegetation quantities. The auto-correlation of site conditions was most likely to contribute to the low statistical correlations found.
For the 1988 ITE/Silsoe sites the number of sample points per transect was too small to provide estimates for rangeland vegetation quantities at the desired degree of accuracy. The term "ground truth" is hardly applicable for the data. Therefore, the observed low correlations are not necessarily an indication of the inability of VIs to monitor rangeland vegetation at the quantities found. From the data available alone drawing a conclusive statement on the feasibility of using Landsat MSS and NOAA AVHRR VIs to estimate quantities of rangeland vegetation is not valid. For an interpretation of the

results the incorporation of the experience of survey team members is still required.

5.6.2 Transect Positions

Positioning sample sites in terms of map co-ordinates was found to be a very demanding task. Errors at this level had pre-eminent effects on VI calibrations. With a small number of samples (eight for 1985 surveys and Landsat MSS) positional changes of one LAC pixel were found to be sufficient to alter the nature of the relationship between field and satellite data. All four methods employed were found to lack in some area for the purpose of locating sample sites.

(a) **Aircraft Navigation (CIPEA Survey)**

The rms error in site positioning by aircraft instruments was 1311 m in east-west and 806 m in north-south direction. Some site were clearly incorrectly recorded, but in other cases the accuracy was below the nominal AVHRR LAC pixel size. In addition, information on transect directions were not available and the centres of sample sites were unknown. This was considered as being obstructive for precise image positioning of sites.

Even for 2 km transects aircraft readings may not be sufficiently accurate for VI calibrations. However, in combination with aerial photographs from the sites and high resolution imagery acquired at approximately the same time sample sites could be determined more accurately.

(b) **Map Identification (CAZS and ITE/Silsoe Surveys)**

Sample site established on maps were employed for CAZS sites, since the GPS was found to provide incorrect readings. An improvement in VI calibrations from map positions over GPS co-ordiantes was hampered by the small range of herbaceous vegetation estimates encountered.

Using roads to establish transect co-ordinates can be

misleading, because the positions of roads is unreliable.

(c) **Image Identification (ITE/Silsoe Surveys)**
The use of image hard-copies provides a practical confirmation of site position in the field. In particular, distances to spectrally different surfaces can be identified. On the other hand, sites can only be recognized, if they are close to these features. It was demonstrated that sample sites for NOAA AVHRR should be situated at least two LAC pixels away from markedly different surfaces. Again, the method of image identification would be more useful in combination with other systems allowing a wider choice in selecting sample sites on the ground.

(d) **Positioning by GPS (CAZS and 1988 ITE/Silsoe Survey)**
The system used provided inaccurate readings in a number of cases. The rms error of 3 LAC pixels in east-west direction is unacceptable for calibrating VIs. Should a more reliable system be available, it would be most useful in combination with image hard-copies.

5.6.3 Image Data Sampling Method

The performance of the image data sampling methods applied was found to be strongly related to the accuracy of identifying sample site positions and the distance of the site to spectrally different surfaces. Best results were obtained for central pixel values in cases, where image and map projections differed by less than one pixel. The method of resampling image data at intervals smaller than one pixel (transect method) performed less satisfactory, as did 3 by 3 pixel sampling. It also became obvious that the software used to process satellite data (IM.REDUCE) can alter pixel positions.

5.6.4 Landsat MSS vs. NOAA AVHRR Wavebands

It was demonstrated that NOAA AVHRR channel 1 and 2 spectral albedos are strongly related to Landsat MSS band 2 and 4 spectral reflectances. This was the case for both original Landsat MSS and spatially simulated NOAA AVHRR data.

(a) Spatial Correspondence

The loss in spatial resolution from 50 m resampled to 1 km data was found to be generally insignificant for correlating field to image data. This, however, was not always the case. In areas where values for the C.V. of 10% or more were present at 1.1 km resolution data a shift of 0.5 pixels in transect locations, which amounts to either none or a 1 pixel shift in image co-ordinates, was found to be sufficient to significantly alter intra-waveband relationships between different image resolutions.

Of importance were also positional shifts introduced by the software. The results suggest that in principal Landsat MSS data could be directly related to NOAA AVHRR data for transect averages (not to be confused with individual pixels).

(b) Radiometric Correspondence

Establishing the radiometric similarity between Landsat MSS and NOAA AVHRR for Sahelian rangelands was restricted by unstable sample site positions on images and small sample sizes. Yet, it can be concluded that NOAA AVHRR channel 1 is most closely related to Landsat MSS band 2 and channel 2 to band 4. An advantage of using the average of bands 3 and 4 to simulate channel 2, attained for 1985 field survey sites, could not be verified for all surveys.

5.6.5 Performance of VIs

Examining the performances of VIs was affected by ambiguous image co-ordinates of sample sites. In some cases, sites with unreliable locations had to be omitted before meaningful results could be obtained (1988 ITE/Silsoe survey).
Ratio VIs revealed very similar performances under most conditions. Results for the PVI differed from ratio VIs for a number of survey and sensor combinations. A dependable and reproducible ranking of VIs could not be deducted from the regression analyses.
For individual sensors preferences of VIs are give below:

(a) **Landsat MSS VIs**

For Niger sites of 1985 and 1988 the PVI seemed to be better suited to predict quantities of herbaceous vegetation than ratio VIs. For those, the NDVI achieved better results than the RVI. For CAZS sample sites no preference for any VI could be attributed. Also, linear and logarithmic regressions appeared to be alike.

(b) **NOAA AVHRR VIs**

For single date NOAA AVHRR images ratio VIs seemed to be more closely related to field data than the PVI. No preference could be assigned to either ratio VI.
For 1985 maximum value VIs RVI and NDVI achieved almost identical coefficients of determination. As it was the case for single dates, the PVI attained lower r^2 values. On the other hand, for CAZS sample sites the PVI was the only maximum value VI, which achieved r^2 values of more than 0.5.
A disadvantage of using maximum value VIs, which became obvious for 1988 surveys, is that VIs from inaccurately registered images are carried through. It is, therefore, not necessarily the maximum VI for a site, but only for pixel values, which have been attributed to that site.

5.6.6 Simulation of NOAA AVHRR VIs by Landsat MSS VIs

For individual surveys it was demonstrated that NOAA AVHRR and Landsat MSS VIs were strongly related (r^2 of 0.90). The integration of surveys revealed that the stability of a single calibration equation depends on the steps applied during pre-processing satellite data. CAZS survey sites VIs were found to be separate from those of Niger surveys. This could have been caused either by the inability to standardize atmospheric conditions or surface features (vegetation species and soil types) for the Mali study area were markedly different from those in Niger.

Landsat MSS VIs from simulated 1.1 km resolution data was found to be more closely related to NOAA AVHRR LAC VIs than 50 m VIs. NDVIs and PVIs were better correlated than RVIs and the highest similarity for integrated surveys were found to exist between Landsat MSS NDVI and NOAA AVHRR PVI. A reverse of the relationship was not applicable.

5.7 Conclusions for Relating Satellite to Ground Data

Of central concern for calibrating NOAA AVHRR VIs to estimates of herbaceous vegetation quantities is the geometric affinity between ground data positions and image co-ordinates. This was found to be an essential prerequisite in order to allow comparisons between conditions examined in the field and the sensor response of reflected EM to those conditions. Additional deductions from the investigation are:

- ***Field Survey Design of CAZS Survey***
  For the CAZS survey the small spatial spread of sample sites and the limited range of vegetation quantities collected very likely contributed to the low correlations found.

- *Field Survey Design of 1988 ITE/Silsoe Survey*
  The small number of sample points along a transect (five) contributed to the low correlations observed.

- *Site Positioning*
  Sites can be positioned from aerial photographs on Landsat MSS images, but only if comparable vegetation developments are present. The locational correspondence can then be improved by using aerial photographs. Also, the use of high resolution hard-copies in the field in combination with a GPS could provide very accurate sample site positions.

- *GPS and Map Agreement*
  A systematic difference in positioning between the GPS and maps of approximately 1600 m in east-west and 1000 m in north-south direction was found for Mali and Niger study areas.

- *Image Resampling*
  Image processing routines introduced an error of up to 2 pixel positions between Landsat MSS and NOAA AVHRR scenes. Processing routines must be documented.

- *Cloud Cover*
  Images with a high probability of sub-pixel cloud cover were found to provide low correlations between ground data and VIs and should be excluded from any calibration.

- *Image Data Sampling Method*
  The image sampling method for representing ground data sites significantly influenced the VI calibration.

- *Regression Type*
  A tendency of a linear relationship between DM and ratio VIs and of a logarithmic one between DM and the PVI was observed, but could not be verified sufficiently for generalizations.

- *Spatial Correspondence Between Landsat MSS and NOAA AVHRR*

Spatially degraded Landsat MSS data was found to be more closely related to NOAA AVHRR LAC data than 50 m resolution data.

- *Radiometric Correspondence Between Landsat MSS and NOAA AVHRR*
  No general advantage of simulating NOAA AVHRR Channel 2 by the average of Landsat MSS bands 2 and 4 for vegetated sites could be observed and the process is considered unnecessary.

- *Atmospheric Effects*
  Variations in atmospheric conditions very much influenced the relationship between Landsat MSS and NOAA AVHRR VIs. A method of standardizing imaging conditions (sensor and atmosphere) has to be applied in order to permit multi-temporal data integration.

- *Herbaceous Vegetation and VIs*
  The development of VIs over the growing period is more closely related to fresh weight than to dry matter.

- *Simulation of NOAA AVHRR VIs by Landsat MSS VIs*
  Landsat MSS ratio VIs are more closely related to NOAA AVHRR PVIs than VIs of the same type. For high correlations images should be acquired at the same day.

- *Calibrating NOAA AVHRR VIs via Landsat MSS VIs*
  An advantage of inter-calibrating NOAA AVHRR VIs by Landsat MSS VIs could not be observed.

6.1 CONCLUSIONS AND IMPLICATIONS

This project offered a unique opportunity for investigating new approaches of correlating data collected on the ground to digital data acquired from Landsat MSS and NOAA AVHRR satellites in term of advances in the three major sub-divisions:

i. *Field Surveys*

The availability of multi-temporal data sets allowed the implementation of an iterative course for assessing methods of processing satellite data. Thus, a ground data sampling scheme for Sahelian rangeland conditions was established, which was designed and tested in the field with some success.

ii. *Pre-Processing*

New refined and more appropriate techniques for geometrically correcting NOAA AVHRR images were designed and employed successfully. New radiometric correction procedures were derived to allow a close comparison of data from the two sensors employed. In addition, the spatial and radiometric simulation of NOAA AVHRR LAC data by Landsat MSS provided valuable insight nto the information content of that data. An adjusted atmospheric standardization method was tested and validated for the first time for Sahelian rangelands.

iii. *VI Calibration*

RVIs, NDVIs and PVIs derived from Landsat MSS, NOAA AVHRR LAC and simulated NOAA AVHRR LAC images were linearly and logarithmically related to herbaceous vegetation estimates with some success. The feasibility of using Landsat MSS VIs to calibrate NOAA AVHRR VIs to quantities of herbaceous rangeland vegetation was demonstrated.

Conclusions for the three main components of the project (field survey, pre-processing and VI calibration) were presented at the end of each corresponding chapter. In the first of the following sections overall conclusions with respect to the project as a whole are presented. This is followed by a section summarizing the implications that arise, should an operational rangeland monitoring system be established in the Sahel. The final section is concerned with suggestions for further research which could improve the relationship between NOAA AVHRR LAC VIs and quantities of herbaceous vegetation in the Sahel.

6.1 Calibration of NOAA AVHRR LAC VIs to Herbaceous Vegetation

In general, NOAA AVHRR VIs were successfully related to quantities of herbaceous rangeland vegetation over the study areas. Data from three very different growing seasons were analysed and integrated. This allowed the preparation of maps which indicated the actual amount of rangeland vegetation rather than qualitative maps produced so far.
In most cases the variations observed could be attributed to changes in the field data sampling technique rather than the satellite data. Systematic changes in satellite data could be accounted for, but further investigations are required to reduce the influence of atmospheric conditions in order to allow the integration of data over areas larger than the suggested central 500 pixels of a NOAA AVHRR image swath width.
The conclusions of the procedures applied to calibrate NOAA AVHRR VIs to Sahelian rangeland vegetation are:

- *Field Survey Team Composition*
  A strong recommendation can be given for including the person analysing satellite data directly in the field survey. This is of particular importance as long as sample site positions cannot be accurately determined on the ground other than by high resolution image hard-copies.

- *Selection of Sample Sites*
  Sample sites in the field should be situated well clear (2 pixels or more) of surfaces with very atypical spectral reflectance characteristics which contrast strongly with those to be measured. In the Sahel examples of such contrasting areas are lateritic rocks and depressions.

- *Identification of Sample Sites*
  Under the above condition that sample sites are situated at least 2 pixels away from surface features mentioned above, images have to be matched to each other to within ± 1 pixel of actual pixel positions.

- *Selection of Satellite Data*
  Satellite data with cloud or strong haze effects over the study area should be strictly excluded. Also, extracts should be restricted to the central ± 20° of the swath of NOAA AVHRR.

- *Satellite Data Processing*
  Geometric and atmospheric corrections were confirmed as factors of prime importance for analysing multi-temporal data of the Sahel. The implementation of an integration of an orbital model together with well defined GCPs is recommended in order to allow a close spatial correlation between images.

6.2 Structure of Operational Rangeland Monitoring System

Within the scope of this project an operational rangeland monitoring system could not be implemented and tested. Some conclusions and implications with respect to the possible structure of an operational rangeland monitoring system can be made in the light of the findings:

- *Data Availability*
  Satellite data should be readily available in order to

allow a timely evaluation of field conditions. Local receiving station within the country and central processing would greatly simplify and enhance the timely availability of quantitative vegetation estimates.

- *Data Processing System*
  Digital data format, hardware and software should be compatible and adjusted to user requirements. Preferably, all software should originate from just one source. Again, for routine processing, but not for investigations into VI calibrations, the system would be better located at the place where the derived products are used.

- *Data Adjustments*
  Any adjustments to processing satellite data should, wherever possible, be based on information provided by the image itself and the need to integrate additional information, for example for an atmospheric correction, should be kept to a minimum.

- *Automation of Data Processing*
  The interaction of a system operator should be reduced to a necessary minimum.

- *Use of Data Analysis*
  The distribution of the final product to users should be secured.

The implications for an operational rangeland monitoring system are mainly of a technical nature. It could be shown that principal obstacles in relating ground to image data can be overcome. From the experience obtained during this project it was concluded that the introduction of a monitoring system in the Sahel would to a large extend depend on technical procedures rather than principal processing methods.

6.3 Areas for Additional Research

The potential of applying NOAA AVHRR LAC VIs to estimate quantities of herbaceous rangeland vegetation in the Sahel could be established for extreme conditions. However, in order to extend the results over larger areas of the Sahel and to improve on the relationships, areas requiring further research could be identified.

- *Length of Transect*
  The length of the transect could only be established empirically from field experience. An investigation into the influence of the transect length on NOAA AVHRR LAC VI calibrations to rangeland vegetation quantities could provide information about an appropriate distance. This is closely linked to the accuracy of the geometric correction and could be integrated with a corresponding project.

- *Size of Sample Area*
  The size of the sampling area (1 m^2) was also found empirically. An optimum size of the sampling area may exist, but requires a dedicated investigation.

- *Herbaceous Cover*
  Procedures for obtain reliable and comparable in-field estimates over time of herbaceous vegetation cover should be examined.

- *Geometric Correction*
  The performance of a geometric correction procedure based on an orbital model in combination with a few GCPs on VI calibrations should be assessed.

- *Resampling Method*
  The influence of the resampling method (Nearest Neighbour, bilinear interpolation and cubic convolution) on VI calibrations could be examined to provide a recommendation for an operational monitoring system.

- *Atmospheric Correction*
  A method of atmospherically correcting images should be established in order to allow the comparison of quantitative results derived over different areas.

- *Performance of VIs*
  A definite preference for any of the VIs or regression types employed could not be given. Additional data is required to establish, if a generally superior VI exists for Sahelian rangelands. Furthermore, information from thermal channels could be included, for example for estimating tree cover.

- *Multi-Variate Analysis of Site Conditions*
  The calibration of VIs may be improved by including additional information on site conditions, in particular m.c., the number of trees and bushes and soil colour, into the relationship between herbaceous vegetation estimates and satellite VIs. The stratification of the study area according to local conditions should be investigated. This could be supported by using a spatial analysis system.

Improving and extending the calibration coefficients for quantitative estimates of herbaceous rangeland vegetation in the Sahel by NOAA AVHRR VIs relies on additional ground surveys over previous study areas (temporal stability) and at various distances from the ITE/Silsoe area (spatial stability). In this respect and for future investigations the exchange of data between organizations, as in the case of CIPEA and CAZS surveys, can be strongly recommended.

APPENDICES

APPENDIX I: CONCEPTS OF DATA ANALYSIS

A1. CONCEPT OF ESTIMATING GROUND DATA VALIDITY

A1.1 Confidence Limits of Rangeland Estimates

Ground measurements of phytomass and satellite VIs represent data of disparant characteristic and spatial extend. Phytomass measurements are commonly restricted to a small area, 0.25m^2 for 1985 and 1988, and utilized to estimate production levels over a larger area. Satellite VIs on the other hand are based on the integral response of all surface features to incident EM energy over 0.656 ha for Landsat MSS and 121 ha for NOAA AVHRR LAC data.

During the course of this project measurements of a site were averaged over the length of the transect to provide a phytomass production estimate for subsequent relation to VIs. Since the reference data for the calibration is based on the arithmetic mean of samples, it contains an element of variation when estimating rangeland production over the IFOV of a satellite sensor. An assessment of the degree of uncertainty in the ground data can be used to

- determine confidence limits for the calibration of classes of rangeland production levels when producing maps of phytomass quantities and
- decide on the number of samples required to achieve a certain confidence limit for a given class width of phytomass production estimates.

Confidence limits for the mean rangeland production along a transect depend on the variability of vegetation quantities present within the site. For the sampling schemes two forms of variations can be distinguished, corresponding to the scale of the measurements:

- Variations over the Length of the Transect
  These may be variations in vegetation growth from one sampling point to the next or gradual changes over the length of the transect. The impact on the data of these variations can be reduced by carefully selecting homogeneous sites.

- Variations over the Measurement Area
  Vegetation densities may change abruptly within the measurement area, even over 50 cm, as has been discussed in Chapter 3.3.4. The error introduced to rangeland production estimates by these changes can be reduced by increasing the number of sample points and the measurement area (see following pargraph).

For the purpose of assessing the validity of the average rangeland production level from sample points of a transect as being representative for the production level of a site, an analysis of the combined effect of these variations on the average was considered sufficients.
The first step to confidence limits is an analysis of variance. For each transect the standard deviation in dry matter quantities was computed. Bessel's correction factor was applied to accomodate for small sample sizes:

$$s_B = s * \left[\frac{n}{n - 1} \right]^{1/2} \qquad (A.1)$$

Next, a regression between rangeland production and standard deviation is computed. Non-linear relationships were analysed by taking the log of either the dependent or independent data set.
To provide an estimate of strength of the relation, a t-test of the coefficient of determination (Bravais - Pearson's coefficient of correlation) was performed. The following equation was used:

$$t = \frac{|r_{pop} - r_{samp}|}{\frac{1}{\sqrt{(n-1)}}} \qquad (A.2)$$

(After: Ebdon, 1985)

It was based on the assumption that there was no relationship between rangeland production level and the corresponding standard deviation (null-hypothesis). The substitution of the standard deviation by the expression $1/\sqrt{(n-1)}$ is a consequence of the assumption made in the null-hypothesis ($r = 0$). It is the expected value for the sum of mean square deviation of r for the sample (Florentz, 1979).
Confidence limits for the regression curve were then obtained by the following equation:

$$\hat{y}_0 \pm t * \left[M_{res} * \left[\frac{1}{n} + \frac{(x_0 - x)^2}{\Sigma x_i^2 - n*x^2} \right] \right]^{1/2} \qquad (A.3)$$

The standard error of the y-estimate (M_{res}) is computed as the sum of squares of residuals divided by the degrees of freedom:

$$M_{res} = \frac{\Sigma(Y_i - \hat{Y}_0)^2}{n - 2} \qquad (A.4)$$

Using the standard deviation for comparing variations preserves the original unit of the measured values. This may be desirable, but it also includes a dependency of the values to be compared on the magnitude of the figures. A standardization can be achieved by using the coefficient of variation (C.V.). It represents the standard deviation per unit and is independent of the production level. It therefore allows direct comparison of vegetation uniformities between different levels. They were computed according to

$$C.V. = \frac{s}{x} * 100 \quad (\%) \qquad (A.5)$$

Calibrated VI images require a division of vegetation quantities into classes for a visual interpretation. The accuracy of assigning a pixel to a class depends on the increment of codification system: the smaller the increment the lower the accuracy. The class size was set to the range of the true mean for a given confidence level. This range was found by

$$\bar{x} - t * \frac{\hat{s}}{\sqrt{n}} * \sqrt{c} \leq \mu \leq \bar{x} + t * \frac{\hat{s}}{\sqrt{n}} * \sqrt{c} \qquad (A.6)$$

where:

$$c = \left[\frac{N-n}{n-1}\right]$$

The correction factor c can be omitted, since less than 5% of the elements of the total population has been sampled. It can therefore be regarded as being 1.
Due to the small size in number of samples available, 10 points at maximum, the best estimate of the standard deviation was employed (Florentz, 1979).
In order to estimate the number of samples needed for a given calibration class width, the confidence level for the increment has to be computed. It can be found by rearranging Equation A.6 to

$$t = \frac{w_c * \sqrt{n}}{2 * s} \qquad (A.7)$$

Having calculated t, the corresponding confidence level can be found in tables for Student's t-test for a two-tailed test with n-1 degrees of freedom.
The computation of the number of samples is an iterative process between the t-value for the confidence level and the sample size.

A1.2 Required Sample Size for Desired Confidence Limit

The number of samples was determined by the following equation:

$$n = \left[t * \frac{C.V.}{e} \right]^2 \qquad (A.8)$$

(After: Curran & Williamson, 1985;
Curran & Williamson, 1986)

When using Equation A.8 for estimating the number of samples required for a specific confidence level it should be noted that the C.V. and the admissible error are expressed in the same unit.
For the purpose of producing a calibration for fixed intervals of production levels, the estimate of the number of samples is based on the standard error of the mean and not the C.V. The number of samples at a specified confidence level for a given standard error can be calculated by

$$n = \left[\frac{t * s}{w_c} \right]^2 \qquad (A.9)$$

A1.3 Duration for Sampling Period

Estimations of the required length of a sampling period were based on an extrapolation of results from the survey. Since the variations of rangeland production at the sites were unknown, they were estimated by the variation of samples. As the number of samples per site the number actually collected was used. For the first period, the expected range of vegetation quantities could then be estimated at an 80% confidence level by the following equation:

$$\bar{x}_1 - t_{80} * \frac{sx_1}{\sqrt{n}} \leq \mu_1 \leq \bar{x}_1 + t_{80} * \frac{sx_1}{\sqrt{n}} \quad (kgha^{-1}) \qquad (A.10)$$

In a second step the possible duration of a mission is estimated. The duration is determined by the vegetation growth dynamic, variability and sampling size. It comprises the number of days when the probability of observing a difference between the means of the acquired and a hypothetical sample before or after the sampling date is 10% or less. The Null-hypothesis is that there is no difference between the two means and the likelihood of the difference is assessed.
The computions are based on the mean, standard deviation and sample size of each survey. The steps involved are:

1. *Difference between means*:

$$d\bar{x} = |\bar{x}_2 - \bar{x}_1| \qquad (A.11)$$

2. *Standard error of difference*:

$$s_{ed} = \sqrt{\left(\frac{s_{x1}^2}{n_1} + \frac{s_{x2}^2}{n_2}\right)} \qquad (A.12)$$

3. Standardized difference (or score):

$$s_{dd} = \frac{d\bar{x}}{s_{ed}} \qquad (A.13)$$

The standardized difference or score represents the t-value in a t-distribution. The t-distribution is used instead of the normal distribution, because the standard deviation of the population mean is not known. The two-tailed probability, or observed significance level, for a difference as large as the one presumed can be obtained from a t-table.
A pooled-variance t-test is not appliccable for Sahelian rangeland vegetation, since the variance changes with quantities of herbaceous dry matter. Hence, a separate-variance t-test is required (Norusis, 1988).

A2. STATISTICAL CONCEPT OF REGRESSION ANALYSIS

Throughout the data analysis of this project relationships between different sets of dependend and independend variables were established. Amongst them were moisture content and Wile 35 instrument readings and dry matter production and VIs. All relationships were based on linear regressions using a least squares fit. Strength and significance were established by employing the Pearson's correlation coefficient r and a t-test. However, it was intended to use the information from samples to derive at estimates of the relationship for the whole population, for example an image. This would allow to establish areal estimates of rangeland phytomass levels.
To avoid repetition in the main text the procedures applied for regression analyses are summarized in this chapter. The example used to illustrate the method applied is the relationship between phytomass measurements and VIs from satellite data.
For a more detailed discussion of linear regression analyses it may be refered to the literature. The main textbook used was Norusis (1988), pp 298 - 382. Data analysis was based on statistical programmes, in particular SPSS/PC+ Studentware^{tm} with data transfered from and to a spreadsheet (Quattro^{tm}) for additional investigation and graphical presentation.

A2.1 Assumptions for Hypothesis Testing with Linear Regression

The objective of relating for example phytomass to a VI is to determine a linear regression line between the independend variable phytomass and the dependend variable VI, which would be representative for the whole population, an area covered by an image. Although a linear regression is used, non-linear relationships were analysed by transforming one or both variables and applying the same testing procedure on the transformed data sets.
The Pearson correlation coefficient alone only indicates the strength between two variables from samples taken. However, the null hypothesis for the population correlation coefficient that there is no relationship between the two variables phytomass and VI over an image is to be tested. Testing the hypothesis about the population regression line and correlation coefficient requires the sampling distribution of the slope and intercept to be normal. The distributions are normal, if a number of assumptions about the population, an image, are met.

(a) **Linearity of Sample Means**
The means of all VIs for each production level in the image can be connected by a straight line.

(b) **Normality of Observations**
For each rangeland production level there is a most frequent value of a VI. But there are also lower and

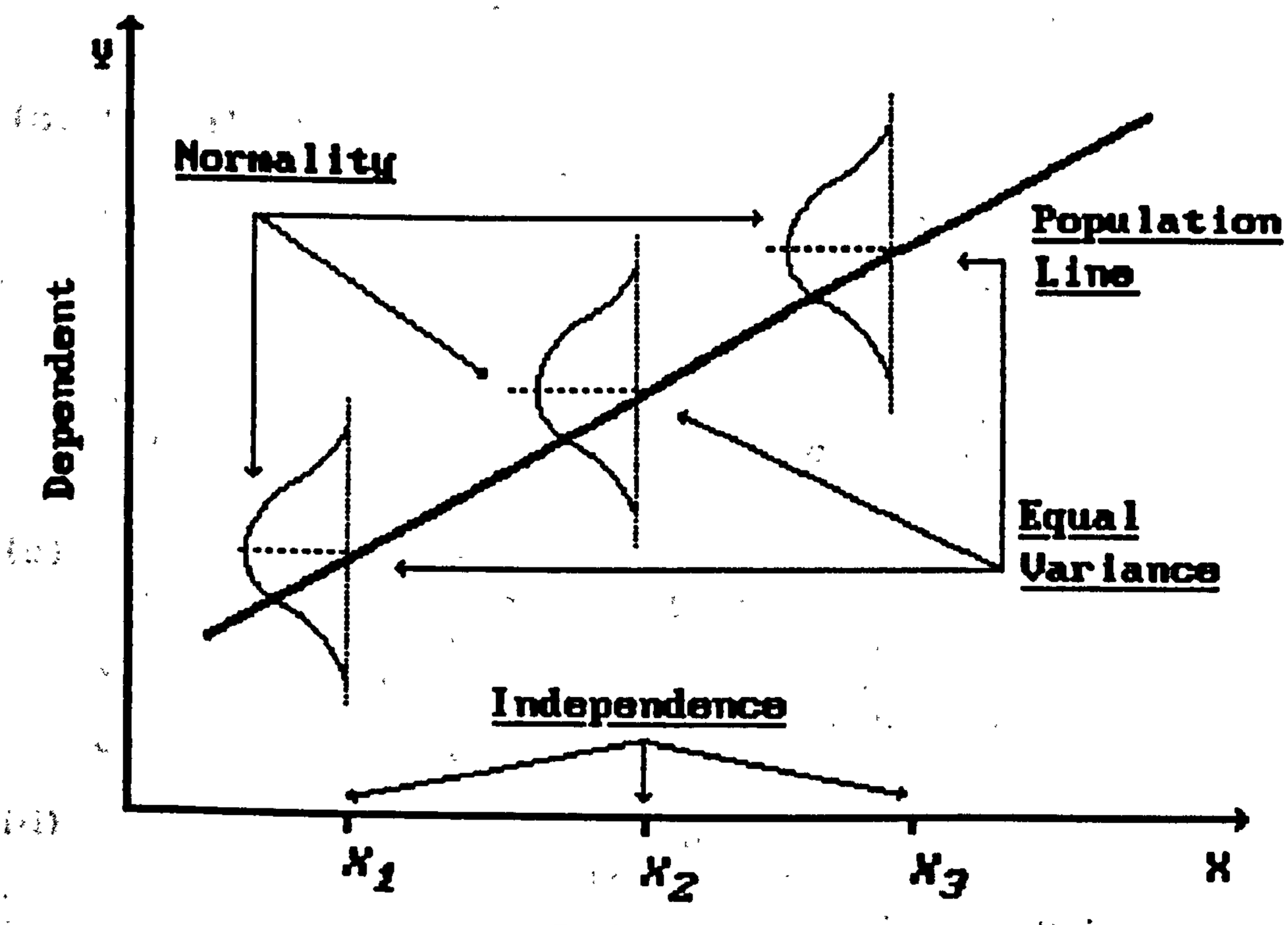
higher VI. The distribution of the VIs for each rangeland production level is normal.

(c) **Equal Variance of Observations**
The variation of VIs from the mean VI for each rangeland production level is constant. This means that VIs vary for low production levels as much as for high production levels.

(d) **Independence of Observations**
The data should be a random sample from the population. The selection of one sample does not influence any other sample to be selected.

The assumptions about the population distribution are graphically displayed in Figure A.1. It shows a normal distribution of dependend values for each independend value with a constant variance. The distribution means are connected by a straight line.

Figure A.1: Assumption About Data Characteristics for Regression Analysis



(After: Norusis, 1988)

In case these assumptions are not appropriate nonparametric procedures should be applied.

A2.2 Procedure for Hypothesis Testing

The following assumptions about the data for testing the Null-hypothesis are made:

(a) **Linearity**
The Pearson regression coefficient requires a linear relationship between dependent and independent variables. A visual examination of the assumption can be obtained by plotting the two variables in a scatter polt.
A non-linear relation could also be detected in scatterplots of residuals against predicted values or against values of the independent variable. The latter plots would also reveal variations in the distribution of variances.
The residuals from a linear regression are analysed to identify suspicious outliers. In order to obtain comparable values the residuals are standardized by dividing the residuals by their estimated standard deviation. With a normal distribution of residuals 95% of all cases occure within ± 2 standard deviations from the mean. Larger values for standardized residual indicate a need for further investigation of those points.

(b) **Normality**
Normality of the distribution of VIs for rangeland production levels over the whole image can be tested by relating the residuals to the sample values. The distribution of the residuals should be normal.
An asymetric distribution of the residuals can be caused by for example a non-constant variance of VIs for different rangeland production levels. With a small number of samples an estimate of normality is also problematic.

(c) **Constant Variance**
A constant variance of VIs for each rangeland production level can be tested by relating residuals to predicted values and production levels in a scatterplot. There should be no change in the distribution of residuals with varying predicted or independent values.

(d) **Independence of Observations**
As stated above a regression analysis relies on observations being selected without influence of other observations taken. This implies a random sampling procedure for obtaining observations. For non-random procedures, like stratified random sampling, a separate regression analysis for each group will have to be implemented. The standarized residuals should be evenly distributed over the sampling period. With a sequential selection of observations a plot of standardized residuals against the sequential number could identify a dependence between observations.

For each linear regression computed during the project these four steps for testing the null hypothesis for the population were carried out. In some cases, like establishing a relationship between ITE/Silsoe ground measurements and VIs for 1985, the number of observations and, consequently, residuals was too small to derive at cogent conclusions about the validity of the assumptions. The assumptions were considered met, if the opposite could not be verified.

A3. GEOMERIC CORRECTION

The repositioning of image elements to a desired geometry depends on sensor and platform errors. These must be either predictable or measurable (Bernstein, 1985).
The sources of geometric distortions and methods for estimating their extent for Landsat MSS and NOAA AVHRR images will be presented below.

A3.1 Sources of Deviations of Images from Map Projections

Sources of distortions of satellite images from a plane geometric representation can be separated into two groups:

(a) **Systematic Sources**
This group contains deviations, which can be predicted from sensor, spacecraft orbital and ephemeris data and knowledge of internal sensor distortions. They can be corrected for by computations based on orbital geometry models.

i. *Instrument Properties*
Distortions may be introduced by the optical system, non-linearity of the scanning mechanism or non-uniform sampling rates. Landsat MSS images, for example, are over-sampled by 40% in the across-track direction.

ii. *Scan Skew*
While scanning one line perpendicular to the flight direction, the sensor platform moves along the ground track. Therefore, the ground swath scanned is slightly skewed to the perpendicular of the ground track.

iii. *Flight Path Inclination*
The flight paths of orbiting satellites are inclined at an angle with the longitudinal direction of a map projection.

iv. *Earth Rotation*
While scanning the surface, the earth rotates beneath the satellite. Therefore, each scan line starts at a different longitude.

v. *Panoramic Distortions*
With the IFOV being constant the area covered on the ground increases with distance from the nadir. NOAA AVHRR images are particularly distorted due to their wide FOV.

vi. *Perspective Distortions*
The geometric properties of satellite data do not represent a projection of points on a plane geometric surface, which is tangent to the surface at the nadir. Since projection lines are not normal to the plane, along-scan distortions are introduced to the image.

(b) Non-systematic Sources
Geometric distortions caused by non-systematic errors are variable and non-predictable in their magnitude. They are caused by platform pertubations and scene characteristics. Their computation depends on knowledge of accurate satellite position data and conditions on the ground. In most cases such data is not available.

i. *Altitude Variation*
The satellite height above the earth surface is not constant but varies considerably, since neither earth nor the orbit are spherical. For example the flying height of the NOAA platform varies between 833 km and 870 km.

ii. *Velocity Variation*
With the altitude the velocity of the platform over ground changes. Thus, variations in along-track pixel sizes are introduced.

iii. *Attitude Variation*
Satellites rotate around three axes:

- pitch: movement around the across-track axis;
- roll : rotation around the vertical axis;
- yaw : movement around the along-track axis.

(After: Harris, 1987)

The TIROS-N platform of NOAA AVHRR satellites is controlled to values better than 0.1 deg in each of the attitude movements. The tolerance should be sufficient to achieve locational errors of 1km when neglecting a correction for attitude variations (Emmery, 1989). A graphical representation of the effect of systematic and non-systematic distortions is frequently given in the literature, for example in Bernstein (1983).

A3.2 Image Referencing

Two main approaches, direct and inverse image referencing, were distinguished (Ho & Asem, 1986). With direct image referencing longitude and latitude for each pixel position are calculated. A unique image is being produced, rendering the method unsuitable for data comparisons. Inverse image referencing uses longitudes and latitudes as the independent variables to calculate the corresponding pixel position. This allows the

formation of a linear relationship between images and images and maps.
Relating ground to image information, which is one of the main purposes of this investigation, demands the spatial representation of the two to concur. For the ground sampling procedure it is convenient to use maps for identifying site locations. By using the same projection for the satellite data, images can be linearly related to maps. Thus, sample sites to be readily identified on an image. Therefore, only methods of inverse image referencing will be considered in this section. The second step in geometrically correcting satellite data by inverse image referencing consists of resampling the input data. Since the transformation equation provides non-integer pixel positions, the sensor response at the map position has to be interpolated from surrounding values.
The main techniques of image referencing and resampling are presented and discussed below.

(a) **Image Referencing**
For the conversion of image positions to agree with a reference projection a transform equation has to be established to compute the position of image points in reference to a map. The main approaches are:

i. *Orbital Models Without GCPs*
The simplest approach is to assume a spherical earth and circular orbits. For NOAA AVHRR positional accuracies of 4 to 5 km were reported (Emmery *et al*, 1986). Using an oblate earth and ephemeris data position accuracies of 1 to 1.5 km can be achieved (ibid). One source providing ephemeris data is NOAA TBUS information, which is publicised on a daily basis by NOAA.

ii. *Orbital Models With GCPs*
Part of the positional error in orbital models can be attributed to the drift of the clock onboard TIROS-N satellites (see Appendix 3). By using one GCP the image can be accurately positioned along the flight path. In addition, platform altitude and inclination at the time of data acquisition can be determined. Using this method, errors of 2 pixel positions for NOAA AVHRR LAC data were reported (Ho & Asem, 1986).
Locational errors of less than 3 pixels were also reported from another correction with one GCP (Tozawa, 1983). The procedure allowed for the effect of earth rotation and proposed compact transformation equations for faster calculations. For Landsat MSS a routine of using the centre image co-ordinates as a GCP and an elliptical orbit was developed (Forrest, 1981).

iii. *Image Referencing to Map*
The positional accuracy of pixels in a geometrically corrected image using a polynomial equation very much depends on the quality of the data involved. It is a function of the number of

GCPs identified, their position on the image, altitude variations across the scene, the order of the polynomial, accuracy of maps and more. Under favourable conditions rms errors of less than 1 pixel positions are obtainable.

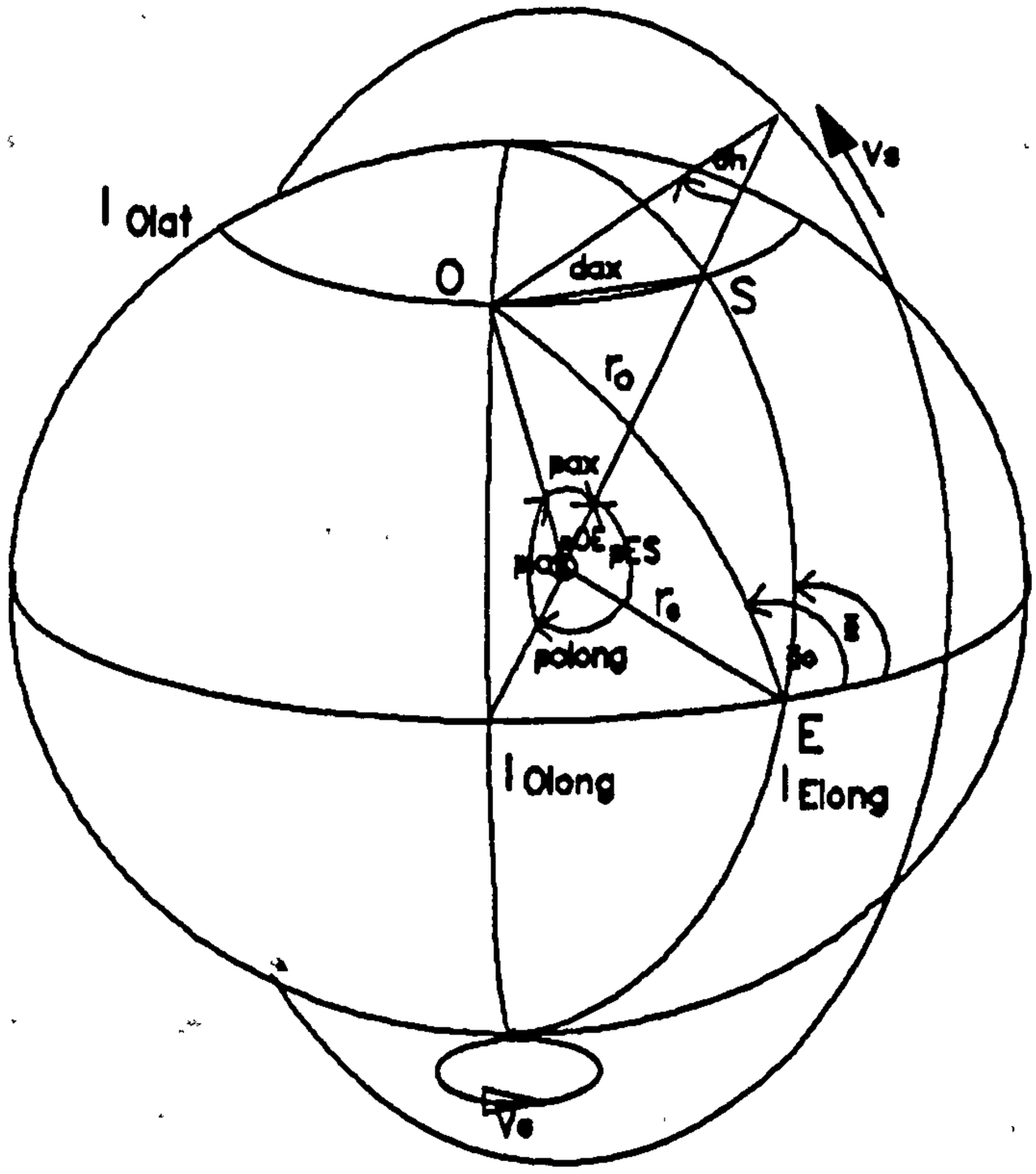
iv. *Image to Image Referencing*
A special case of referencing an image to a map is to substituted the map reference by a geometrically corrected image. Manual and automated methods can be distinguished. With a manual system the whole reference image is used. As GCPs those pixels are employed, which can be identified on both images by the operator. As far the algorithm is concerned, there are only minor differences between using a map or an image as a reference. Yet, the saving in time needed to identify GCPs is considerable.
An automated system relies on a pattern recognition algorithm. The areas for GCPs can be restricted to small extracts of the whole reference image. These sub-scenes are referred to as chips (Cracknell & Paithoonwattanakij, 1989).

(b) Resampling Methods
In inverse image referencing the original satellite image forms the input data set. The reference image constitutes the co-ordinate system of the map projection. The output image comprises the sensor response to incident EM energy at the defined map co-ordinates of the reference image. Data are considered to be arranged in form of a regular two-dimensional lattice. For each output pixel position the corresponding row and column value in the input image is computed. The values are likely to be non-integers and the DN at that point has to be interpolated from DNs of surrounding pixels.
The choice of a resampling method and the position of its implementation within the processing operation is determined by the intention of the data analysis. For routine operations the fastest method (NN) seems to be suited best. An additional advantage is that the original sensor response is retained. Disadvantages when identifying surface features seem to be of minor importance.

A3.3 Estimation of Geometric Errors

This section introduces the mathematical representation of geometric image distortions. With known values of the sensor systematic and non-systematic variations geometric image distortions can be computed and corrected for. A graphical description of the parameters envolved is given in Figure A.2.

Figure A.2: Orbital Model for Geometric Image Referencing



(After: Ho & Asem, 1986)

(a) **Introduction to Sensor Geometry Description**

The approximate image position is taken from the time t, which constitutes the difference between the time of the equator crossing and data acquisition. Every scan line is associated with a specific time of acquisition from the internal clock. However, the internal clock on TIROS-N satellites varies by 70 ms per day, making it an unreliable reference for accurate geometric correction (Emery *et al*, 1989). It is, therefore, necessary to use at least one GCP to move the image along its flight path to the correct position.

Conveniently, subsequent computations are based on angular velocities (polar co-ordinates (r_e, V)). The earth angular velocity L_e is given by

$$V_e = \frac{2 * \pi}{d_s} \text{ (rad s}^{-1}\text{)} \qquad \text{(A.14)}$$

(After: Duck & King, 1985)

The angular velocity of the satellite can be found by

$$V_s = \left[\frac{g_c}{(r_e+H)3} \right]^{1/2} \text{ (rad s}^{-1}\text{)} \qquad \text{(A.15)}$$

Thus, the orbital period of the satellite is given by

$$T = \frac{2 * \pi}{V_S} \text{ (s)} \qquad \text{(A.16)}$$

The orbit plane rotates about the polar axis due to earth oblateness. This precession can be expressed as a change in longitude (Duck & King, 1985). An approximate value can be found by

$$P_e = -\frac{3}{2} * O_e * r_e^2 * (g_c)^{1/2} * (r_e+H)^{-7/2} * \cos(\Phi) \text{ (rad s}^{-1}) \qquad \text{(A.17)}$$

(After: Duck & King, 1985)

The rotation rate of the earth relative to the satellite orbit plane or node comprises the difference between the inertial earth rotation rate V_e and the precession P_e:

$$V_n = V_e - P_e \text{ (rad s}^{-1}) \qquad \text{(A.18)}$$

(After: Duck & King, 1985)

(b) Estimating Image Errors

i. *Correction for Instrument Properties*

■ Mirror Velocity Variations

Landsat MSS sensors sample data at equal angular intervals. However, the mirror velocity varies while scanning. The magnitude of the error can reach 370 m (Bernstein, 1983).
With information on the actual mirror angle at the nth scan line element, the across-track displacement due to mirror velocity variations can be found by:

$$d_{nax} = H * \left[\frac{2*\phi}{N_X} * n_x - \phi_v(n_x) \right] \text{ (m)} \qquad \text{(A.19)}$$

For Landsat MSS a third order polynomial is used to describe scan rate non-lineatities of the instrument (Forrest, 1981). The AVHRR sensor uses a rotating mirror system and avoids velocity variations of the oscillating mirror of Landsat MSS.
Because of the close relationship between mirror velocity variations and panoramic distortions a combined correction equation was presented by Bernstein (1983).

■ Detector Array Sample Delay
Landsat MSS scans six lines simultaneously by an array of six detector elements. Data sampling within the array occurs sequentially at a fixed temporal lag between elements. The shear effect between the first and the sixth line is 22 m,

independent of the satellite position (Bernstein, 1983).

- Across-Track Over-Sampling
  Contrary to NOAA AVHRR Landsat MSS sensors oversample in across-track direction by 25%. Therefore, the spatial representation of a pixel differs in x- and y-direction. A simple method of squaring Landsat MSS images is to insert 900 new lines between original lines. This is achieved by inserting five new lines between 13 original lines. The DNs of the newly formed pixels are commonly derived by averaging the DNs of pixels values from the neighbouring lines (Hord, 1983). More accurate is the use of an orbital transform equation or a polynomial allows for a continuous adjustmant along- and across- scan pixel sizes (see below). For NOAA AVHRR images no correction for over-sampling is required.

ii. *Skan Skew Correction*
The scan lines of Landsat MSS and NOAA AVHRR sensors are both perpendicular to the line of flight of the platform. The movement of the platform during scanning introduces a change in the angle between the orbital path and the direction of the scan line on the surface, which is non-perpendicular. The angle can be found by

$$\Phi_s = \tan^{-1}\left[\frac{t_l * V_s}{2 * \phi_{max}} \right] \text{ (rad)} \qquad \text{(A.20)}$$

For Landsat MSS and NOAA AVHRR the movement in flight direction during data acquisition along a scan line is compensated for by scanning lines in a non-orthogonal angle to the line of flight. Therefore, this movement may be disregared when correcting images.

iii. *Flight Inclination Correction*
The orbit inclination (98.2° for Landsat MSS and 98.8° for NOAA AVHRR) introduces an angle to the longitude, which increases with latitude. For any longitude it can be calculated by

$$\Phi_l = -\cos^{-1}\left[\frac{\sin(\Phi)}{\cos(l_{lat})} \right] \text{ (deg)} \qquad \text{(A.21)}$$

The rotation angle Φ_l changes in latitudal direction across the image. In order to simplify procedures, the value l_{lat} for the latitude in Equation A.21 is taken from the position of the central pixel of an image line. With distance from the centre, the thus computed skew angle will

increasingly differ from the normal value at the equator.

iv. *Earth Rotation Correction*
The correction for earth rotation in the longitudal direction during image acquisition is caused by the time it takes to scan the area represented in the image. This delay results in a non-orthogonal angle between the north-south and the east-west lines in the image.
Approximate deskewing of Landsat MSS images can be achived by off-setting groups of lines. For this purpose, the 3240 lines of squared Landsat MSS images are divided into 270 groups of 12 lines each. The groups are off-set by one column position to the left with respect to the group above. The output image consists of 3509 columns per line (Hord, 1983).
A more accurate and generally applicable correction can be achieved by computing the distance the earth rotates in latitudal direction during the time of image acquisition. The displacement caused by the earth rotation from one line to the next can be found as the distance the earth rotates during the time required to scan one line and the satellite orbit precession:

$$ß_r = V_n * t_l \text{ (rad)} \qquad \text{(A.22)}$$

The actual longitude of the pixel position can be found by adding the earth rotation displacement $ß_r$ to the longitude of a non-rotating orbit.

v. *Panoramic Distortion Correction*
With a constant scan angle the IFOV increases with distance from the flight line. Affected are both across-track and along-track pixel dimensions. The variation of the surface area covered requires stretching the image in across-scan direction. The degree of stretching lines corresponds to the ground distance covered by the sensor element and can be found by using plane trigonometry.
Assuming a plane surface, the information required are flying height of the platform and the sensor FOV.
An approximation of the area covered by the FOV can be obtained by multiplying the nadir pixel size by the number of pixels in across-track direction. For small scan angles this yields a close approximation to the actual ground cover. The larger the scan angle, however, the disagreement between the estimated image size and the area actually covered by the sensor increases over-proportionally. The calculation of the latter and individual off-nadir pixel sizes when considering a spherical Earth are presented below.

■ Ground Distance in Across-Track Direction
The arc $ß_{ax}$ between the nadir to the pixel of interest at scan angle ø can be calculated according to

$$ß_{ax} = \arcsin\left[\frac{r_e + h}{r_e} * \sin(ø)\right] - ø \text{ (rad)} \quad \text{(A.23)}$$

(After: Emery *et al*, 1989)

The corresponding ground distance d_{ax} is thus given by

$$d_{ax} = r_e * ß_{ax} \text{ (m)} \quad \text{(A.24)}$$

Using the arc between the nadir and the area viewed by the scanning instrument instead of pixel or scan angle intervals accounts for the increase in pixel size with distance from the nadir. This method has been described as linearization (Brush, 1988; Emery *et al*, 1989). It is used for an inverse image referencing (Ho & Asem, 1986; see Chapter 4.1.2). There, the transformation is based on geographic co-ordinates to apply the corresponding pixel position in an image.
Landsat MSS and NOAA AVHRR instruments use fixed angular incremets $ø_i$ for scanning a line. For Landsat MSS the scan step angle is 7.46/180*π/1620 rad. For NOAA AVHRR it is 55.3849*π/180/1024 ($0.955*10^{-3}$ rad, Emery *et al*, 1989). For inverse referencing the image pixel position with respect to an angle of $ß_{ax}$ from the nadir can be found by rearranging Equation A.23 to solve for the off-nadir scan angle ø.

$$ø = \arctan\left[\frac{\sin(ß_{ax})*r_e}{h+re*[1-\cos(ß_{ax})]}\right] \text{ (rad)} \quad \text{(A.25)}$$

Then, the corresponding pixel position is given by

$$P_x = \frac{ø_{max} - ø}{ø_i} \quad \text{(A.26)}$$

■ Pixel Size in Along- and Across-Track Direction
For a geometric correction procedure spatial distortions have to be dealt with on a pixel by pixel basis rather than the total area covered by the sensor as introduced in Equations A.25 and A.26. The pixel size parallel to the direction of flight increases with the reciprocal value of the cosine of the viewing angle ø. The pixel along

the scan direction, however, increases at a larger pace, with the reciprocal value of the square of the cosine of the viewing angle ø. For computing the pixel size in along-track direction, the following equation can be applied:

$$P_{al} = 2 * ß_s * r_e \text{ (m)} \qquad \text{(A.27)}$$

where

$$ß_s = \arcsin\left[\frac{r_e+S}{r_e} * \sin(0.5*ø_{IFOV})\right] - 0.5*ø_{IFOV} \qquad \text{(A.28)}$$

and

$$S = \frac{\sin(ß_{ax})}{\sin(ø)} * r_e \text{ (rad)} \qquad \text{(A.29)}$$

The pixel size P_{ax} in across-scan direction can be calculated according to

$$P_{ax} = r_e*[\tan(ß_{ax}+ß_i) - \tan(ß_{ax})] \text{ (m)} \qquad \text{(A.30)}$$

The values for the geocentric arc $ß_{ax}$ and $ß_i$ can be obtained from the scan angles ø and $ø_i$ and Equation A.31.

vi. *Geocentric to Geodetic Reference Conversion*
Inverse image referencing is mainly based on the geocentric angle $ß_{ax}$ and the corresponding scan view angle ø to compute the pixel position within an image. The transformation for a geocentric to a geographic latitude can be found by

$$l_{latgeographic} = \arctan\left[\frac{r_e^2}{r_p^2} * \tan(l_{latgeocentric})\right] \qquad \text{(A.31)}$$

(After: Emery *et al*, 1989)

The earth radius r_{lat} at latitude l_{lat} is given by

$$r_{lat} = r_e - 21.26663 * \sin^2(l_{lat}) \qquad \text{(A.32)}$$

(After: Brush, 1988)

A3.4 General Approach to Orbital Models

In this section the general procedure for applying an orbital model to image geometric correction is presented. A spherical

earth and a circular orbit are assumed. The steps loosely follow procedures provided by Emmery *et al* (1989) and Ho and Asem (1986). Additional relevant papers are mentioned at the end of this section and it is recommended to obtain further details from the original papers. An introduction to the abbreviations used and their derivation has been given in Chapter A3.3, Appendix I.

Inverse image referencing is based on the relationship between the geocentric arc $ß_{ax}$ and the sensor scan angle ø. For a desired size of pixels in a geometrically corrected image the increment $ß_i$ is determined as the step size. The corresponding sensor view angle is given by

$$ø = \arctan\left[\frac{\sin(ß_{max}-(n_x-1)*ß_i)*r_e}{h+re*[1-\cos(ß_{max}-(n_x-1)*ß_i))]}\right] \text{ (rad)} \qquad \text{(A.33)}$$

The view angle ø depends on the variations in platform altitude. If only nominal orbital data is available, the height at the time of data acquisition can be estimated by an iterative process (Ho & Asem, 1986). A transformation between geocentric and geographic co-ordinates can be achieved by using Equation A.31.

The computations for the scan angle ø start with the time t, which represents the time span between the crossing of the ascending node (usually the equator) and the time of data acquisition. Nodal longitude and crossing time of the ascending nide are given in the tape header. The longitude $ß_{long}$ of the observed point O can be found from

$$ß_{long} = ß_{Olong} - ß_r + l_{Elong}*\frac{\pi}{180} \text{ (rad)} \qquad \text{(A.34)}$$

The geocentric arc $ß_{OE}$ between the equator crossing point E and the observed point O is given by

$$ß_{OE} = \arccos[\cos(ß_{ax})*\cos(ß_{long})] \text{ (rad)} \qquad \text{(A.35)}$$

Next, the arc Φ_O between the equator and the line EO can be found according to

$$\Phi_O = \arcsin\left[\frac{\sin(ß_{lat})}{\sin(ß_{OE})}\right] \text{ (rad)} \qquad \text{(A.36)}$$

Subsequently, the geocentric arc $ß_{ax}$ between the point of observation and the nadir can be obtained:

$$ß_{ax} = \arcsin\left[\frac{\sin(ß_{OE})*\sin(\Phi-\Phi_O)}{\sin(\Phi_S)}\right] \text{ (rad)} \qquad \text{(A.37)}$$

The arc $ß_{ES}$ from the ascending node E to the sub-satellite point S is the found by

$$\cos(ß_{OE}) = \cos(ß_{ax})*\cos(ß_{ES})+\sin(ß_{ax})*\sin(ß_{ES})*\cos(\Phi_S) \qquad \text{(A.38)}$$

The latitude S_{lat} of the sub-satellite point S could be directly established from the time t as:

$$S_{lat} = \arcsin[\sin(t*V_s)*\sin(\Phi)] \quad (A.39)$$

(After: Tozawa, 1981)

The longitude S_{long} of the sub-satellite point S can be found by

$$S_{long} = \arctan[\cos(\Phi)*\tan(t*V_s)] + t*V_n \quad (A.40)$$

(After: Duck & King, 1983)

The longitude S_{long} in Equation A.40 is corrected for earth rotation during time t since the crossing of the ascending node.
The sub-satellite point S can then be used to recalculate the time t, which was initially derived from the on-board clock. The new time t is estiamted by

$$t = \frac{\beta_{OE}}{V_s} \text{ (s)} \quad (A.41)$$

An iterative procedure between t and β_{OE} can be employed to obtain a more accurate estimate for t.
The off-nadir scan angle ϕ for the arc β_{ax} is given by

$$\phi = \arctan\left[\frac{\sin(\beta_{ax})*r_e}{h+re*[1-\cos(\beta_{ax})]}\right] \text{ (rad)} \quad (A.42)$$

This in return provides the pixel number in the image by using Equation A.26. The line number can be found by

$$L_n = \frac{t - t_f}{t_l} + 1 \text{ (unitless)} \quad (A.43)$$

The simplifying assumptions of a spherical earth and a circular orbit can lead to positional errors of 10 km for each of these effects (Emmery *et al*, 1989). Positional accuracies achievable with these models are 4 to 5 km. For higher accuracies factors such as an elliptic orbit, earth oblateness and rotation have to be considered. For NOAA AVHRR images satellite ephemeris information can be obtained from NOAA in form of TBUS data. Using a model based on this data locational errors of 1 pixel position could be achieved (Emmery *et al*, 1989).
Without accurate ephemeris data non-systematic platform variations require at least one GCP to account for altitude variations and three GCPs for its attitude.
Additional details on geometric correction procedures based on orbital models of varying degrees of complexities, direct and indirect image referencing and their geometric realization can be found in the literature and are, therefore, not repeated here (for example Forrest, 1981; Tozawa, 1983; Hayes & Cracknell, 1984; Bernstein, 1985; Duck & King, 1985;

Astronomical Almanach, 1986; Ho & Asem, 1986; Brush, 1988; Emery *et al*, 1989).

A3.5 General Approach to Polynomial Correction

The method of employing GCPs comprises a direct comparison between image and map co-ordinates. GCPs have to be well defined features, which are accurately and reliably recognizable on both the image and the corresponding map (Mather, 1987). The accuracy of the output image is mainly determined by:

- *number*,
- *distribution* and
- *positional accuracy*

of the GCPs.
The minimum number of GCPs to be selected has to correspond to the number of coefficients of the polynomial. The statistical requirements for a reliable result suggest 10 to 15 GCPs for a first order fit (Mather, 1987). For this number to suffice, GCPs will have to be located to $^1/_3$ pixel accuracy or better. For cases of lower positional accuracy 20 to 25 GCPs are recommended (Bernstein, 1975).
A transform equation between image co-ordinates and map positions of the GCPs is established by the method of least squares. The transform equation can be of first order or higher. A first order polynomial least squares function can compensate for distortions in scaling, rotation and shearing. In order to correct for panoramic distortions introduced by wide scan angles, a second order polynomial has to be applied (Mather, 1987). Orders higher than three can introduce new distortions and require longer computations. For Landsat MSS and NOAA AVHRR images second order polynomials are recommended (Hayes & Cracknell, 1984). For the input image column number X it has the form of

$$X = a_1 + a_2*M_x + a_3*M_y + a_4*M_x^2 + a_5*M_{xy} + a_6*M_y^2 \qquad (A.44)$$

and for the row number Y

$$Y = b_1 + b_2*M_x + b_3*M_y + b_4*M_x^2 + b5*M_{xy} + b_6*M_y^2 \qquad (A.45)$$

Compared to a orbital model rectification the use of GCPs often results in a higher correspondence between image and reference data set. The accuracy of positioning GCPs on the image can be 0.5 pixel positions. Typically, the RMS error is below one pixel.

A3.6 Resampling

After having established a transform equation, the next step in geometrically relating an image to a map projection is to determine the number of pixels and their size in the corrected image. The DNs for the new pixels are determined by computing from each pixel position of the corrected image the corresponding co-ordinates in the original image.
The input data values (original image data) can be assumed to be arranged as points on a regular lattice pattern. The output pixel positions (corrected image) are then used to compute the co-ordinates of the corresponding input pixel in the original image. Since image co-ordinates are determined by integers, the computed position generally does not coincide exactly with the original pixel position. Hence, DNs of pixels in the corrected image have to be interpolated from DNs of surrounding pixels in the original image. Resampling methods are designed to estimate the continuum of the scene reflectance pattern. It is assumed that the DNs of the discrete pixels represent one sample point of the continous surface (Billingsley, 1983).
The method of interpolation is largely determined by the objectives of subsequent processing and the time required for corresponding computations.
The three major interpolation methods are presented below.

(a) **Nearest Neighbour (NN)**
The DN assigned to the pixel in the corrected image is given by the value of the pixel in the original image closest to the computed position. It can be expressed as:

$$DN_{c,r} = DN_{x',y'} \qquad (A.46)$$

where

x'= integer part of (X + 0.5)
y'= integer part of (Y + 0.5)

(After: Billingsley, 1983)

Advantages of using NN are the speed of the computations involved and the preservation of original DNs. Only pixel positions are computed and DNs are assigned. On the other hand, the corrected pixel positions can be off-set of up to $\sqrt{2}$ of the pixel size. In addition, images resampled using NN appear to be blocky, which can render more difficult the identification of ground features.

(b) **Bilinear Interpolation (BI)**
When using BI the new DN of a pixel is determined by the values of the four pixels closest to the computed position of the pixel in the original image.
Interpolations are performed in x- and y-direction in

the original image. A mathematical expression of the following form can be used to describe BI resampling:

$$DNc,r = (X-x')*(Y-y')*(DN_{x'+1,y'}+DN_{x',y'+1}-DN_{x',y'} - DN_{x'+1,y'+1}) \quad (A.47)$$

(After: Billingsley, 1983)

BI constitutes essentially a averaging process between DNs of neighbouring pixels weighted by the distance. The consequence of applying it to resampling is a loss of high frequency variation in the data and a blurred output image. The time for performing the computations are about 10 times longer than for NN (Bernstein, 1983). Disadvantageous may also be the alteration of original DNs to interpolated values.

(c) Cubic Convolution (CC)
With CC the nearest 16 pixels in the input image around the computed position are employed. The method is based on fitting a two-dimensional third order polynomial surface over 4 x 4 pixels in the input image, thus adjusting the relative combinations of pixels over the sampling area.
An advantage of using CC over NN or BI is an image, which looks less blocky or blurred. This may improve the identification of ground features on the image. However, the time required for resampling the image increases approximately 20 times when compared to using NN (Bernstein, 1975). This significantly restricts the use of CC for operational applications. Moreover, grey level overshoots occur on either side of sharp edges and the original DNs are altered.

Other methods of resampling images are less widely applied than those mentioned above and generally require longer computations.
The effect of the method chosen for resampling is not restricted to image appearance and computing time. Particularly classification and filtering processes are affected by the resampling method. But these are not procedures applied in this project. However, when comparing NOAA AVHRR single bands and VIs with Landsat MSS data, which were averaged over 15 x 15 pixels to simulate AVHRR LAC resolution, continuously higher values for correlation coefficients between the to sensor data sets were obtained from resampling with a linear interpolation as compared to nearest neighbour (Hayes & Cracknell, 1984).
The correction function applied after establishing a mathematical description of the image transformation and selecting a resampling method are guided by processing efficiency. Rather than applying the transformation function to each pixel of an image a block of pixels is used, whose position is defined by computing the position of a single pixel within that block. The position of the points between computed pixels may be obtained from an interpolation (Billingsley, 1983) or a block size may be defined by an acceptable change in pixel position, usually 0.5 pixels (Emmery *et al*, 1989).

A4. RADIOMETRIC CORRECTIONS

A comparison of satellite data acquired at different dates or from different instruments requires a transformation of the relative DNs to standardized units. This is achieved by adjusting for internal and external sources of variations of instrument properties and scene conditions.

A4.1 Sensor Response Characteristic

Variations in satellite sensor responses to incident EM energy may be divided into the relative sensitivity of detector elements within a band, which cause line-dependent variations, and temporal changes, which affect the whole scene. Correction procedures can be either relative, compensating for differences relative to other deviations from the norm, or absolute, which comprises a conversion to physical units (Teillet, 1986). The latter calibration of DNs constitutes calibrating data to known values of energy emitted from a calibration source. Sources of almost constant output of EM energy are the sun or on-board calibration instruments. For on-board calibration instruments pre-flight measurements are performed and the spectral radiant energy emitted is assumed to be constant over time. Calibration coefficients for Landsat MSS are derived from internal calibration lamps and deep space viewing. For NOAA AVHRR Channels 1 and 2 merely deep space viewing is available (Planet, 1988). Thus, for a linear transformation of adjusting the AVHRR sensor response to changes in sensitivity only the off-set value is known.

A4.1.1 In-scene Differences in Detector Sensitivity

Multiple detectors, such as Landsat MSS, have slight physical variations between detector elements. The radiance recorded by these detectors for identical scenes varies accordingly. With Landsat MSS the effect is a six-line banding visible as a striping effect repeated every six lines.
The calibration differences within the detector of each band can be reduced on a scene to scene basis (Price, 1987) by using in-scene statistics. The methods are based on the assumption that each detector element scans an almost identical distribution of surfaces over the scene. Accordingly, the radiometric probability density function (histogram) of each detector response to the incident EM energy should be very similar. Any differences between the histograms of the detector element data can be attributed to the instrument response rather than to actual differences within the scene (Ahern *et al*, 1987). Compensation procedures involve a linear transfer of

original to adjusted sensor data (Mather, 1987; Sabins, 1987; Lillesand & Kiefer, 1987). For destriping images these relative procedures were found to be preferable to using on-board calibration lamps (Ahern *et al*, 1987).

A4.1.2 Temporal Changes in Sensor Sensitivity

Detectors on board satellite sensors can have slow changes of sensitivity over time. For an accurate correction of temporal changes in sensor sensitivity an absolute calibration to surface features of known reflectance, usually desert sand, is needed. Internal calibration lamps, like used for Landsat MSS, are less suitable, since these lamps are themselves prone to changes in the energy emmitted.
Landsat MSS calibration coefficients are frequently updated and published (Price, 1987; Price, 1988). As mentioned above, NOAA AVHRR calibrations coefficients originate from pre-launch investigations (Kidwell, 1988). For NOAA AVHRR-9 a deterioration in sensor sensitivity of 8% in Channel 1 and 15% in Channel 2 shortly after launch has been observed (Holben & Kaufman, 1988; Holben *et al*, 1990). The decline was found to be almost linear with time in both channels. The following relationships between sensor degradation and time were established:

$$Chl_{deg} = -0.42 * (\text{months after launch}) + 95.30$$

and

$$Ch2_{deg} = -0.22 * (\text{Months after launch}) + 86.63$$

(Holben *et al*, 1990)

These changes in sensor sensitivity modify VI values of temporal sequences. For long-term investigations they will have to be taken into account.

A4.1.3 Digitization Errors

Another source of error, which is caused by the sensor electronics, will only be briefly introduced. The analog signals from sensor elements have to be represented in a finite number of bits by an analog-to-digital converter, which causes errors in quantization. The converter may also introduce bias and gain errors from non-linear transformations (Bernstein, 1983).

A4.2 Scene Illumination

The amount of EM energy incident upon a satellite sensor is also a result of changing sensor-target geometry, for example the solar zenith angle, azimuth and distance and surface aspect. Subsequently, the bidirectional reflectance characteristics of surfaces are a function of the diurnal time and date of data acquisition. Even for single-date images, the influence of these variations on the radiance reflected towards the satellite sensor have to be considered (Ashley & Rea, 1975).

A4.2.1 Solar Elevation

The effect of increasing radiance with solar elevation angle is reduced by normalizing the data to a standard solar zenith angle. Thus, the correction accounts for the seasonal changes of the position of the sun relative to the earth. The constant reference angle of the solar altitude can be the zenith angle of 0° or an angle more likely to be present for the area of observation, for example the 39° solar zenith angle used by ERIM (Nelson, 1985a).
A normalization is accomplished by multiplying original DNs with only one correction factor, which contains the solar zenith angle for the particular time and location of image acquisition:

$$DN_C = DN_u * \frac{\cos(\alpha_Z)}{\cos(\alpha_X)} \quad \text{(count)} \qquad \text{(A.48)}$$

The solar zenith angle at the time of data acquisition can be calculated by the following equation:

$$\cos(\alpha_Z) = \sin(\delta_S)*\sin(\phi_O) + \cos(\delta_S)*\cos(\phi_O)*\cos(15)*(T_h + \frac{T_m}{60} - SLN) \qquad \text{(A.49)}$$

(After: Astronomical Almanach, 1986; Duggin, 1985b; Kowalik *et al*, 1982)

The solar azimuth Θ_S can be found by

$$\cos(\Theta_S) = \frac{\sin(\delta_S)*\cos(\phi_O) - \cos(\delta_S)*\sin(\phi_O)*\cos(h)}{\sin(\alpha_Z)} \qquad \text{(A.50)}$$

(After: Astronomical Almanach, 1986)

The cosine correction assumes a Lambertian behaviour of earth surface features and the atmosphere, which does not correspond

to the real situation (Dave, 1981). Completely ignored are for example non-Lambertian topographic and atmospheric effects, changes in proportion of shadowed areas of partially covered surfaces and leaf orientation. Consequently, although differences in scene illumination conditions can be normalized, the effect of varying solar angles go beyond changes in incident EM energy on a canopy and are not fully compensated for by the cosine correction (Jackson *et al*, 1979; see Chapter 2.2). Some of the main factors causing variations in scene illumination, which are not corrected for by a cosine standardisation, are presented below.

(a) **Surface Cover**
The influence of the solar zenith angle on the NDVI was found to be dependent on the percentage canopy cover and to decrease with decreasing cover values (Singh, 1988). For the simulated data it would appear feasible to omit the solar elevation correction for data acquired at solar zenith angles of up to 30°. The PVI was also found to increase with an increasing solar zenith angle, but the change was not related to soil reflectance characteristics (Huete, 1987).

(b) **Soil Reflectance Characteristics**
The influence of the solar zenith angle on the NDVI was found to be smallest over dark soils and increasingly expressed with higher reflecting soils. The RVI behaved similar to the NDVI, but was more sensitive to changes in the soil background. The PVI increases with soil brightness and at an almost constant slope (Huete, 1987).

(c) **Geometric Structure of Canopy**
A planophile canopy has a low response with a changing solar angle in the red waveband. An erectophile canopy cover increases in response in the red with decreasing solar zenith angles. For both canopies NIR reflectance increases with smaller solar zenith angles. As a consequence, NDVI and RVI values will vary for planophile and erectophile plant communities with the same amount of phytomass (Pinter *et al*, 1985; Jackson *et al*, 1979). An interaction between angular anisotropy and solar zenith angle was also observed for the PVI (Gross *et al*, 1988).

(d) **Time of Data Acquisition**
The dependence of VIs on the solar zenith angle is not symmetric around the minimum zenith angle. Generally, afternoon scenes are less affected than images acquired during a morning over-pass (ibid).

Therefore, a meaningful scan angle correction for ration VIs would have to include a physical description of the plant canopy geometry and a relation between the sunlit to shaded soil component (Huete, 1987).

A4.2.2 Solar Distance Adjustment

The distance between the sun and the earth varies throughout the year. With it varies the amount of solar irradiation incident upon a surface on the earth. The difference in solar irradiation is ± 3.4% from the nominal value for the solar constant. Since alterations of the EM energy incident upon a surface are directly proportional to the square of the distance a standardization can be employed using a single correction factor. A factor c_{sd} correcting for divergences can be found by

$$c_{sd} = \left[1 + e_o * \cos\left(2 * \pi * \frac{d-3}{365}\right)\right]^2 \text{ (unitless)} \qquad \text{(A.51)}$$

When using ratio VIs, solar distance and elevation correction factors can be omitted from computations. Since they are constants they cancel during calculations.
Contrary to ratio VIs, the PVI values are affected by a cosine correction for changing solar elevations. The soil line slope remains unaltered, but the intercept changes with the correction factor applied. This amounts to a parallel shift of the soil line depending on the cosine correction factor. The parrallel shift only applies to points on the soil line, not to signatures of vegetated areas at a distance from the line. The further away from the soil line these points are located the greater the change introduced by the cosine correction. Subsequently, the PVI increases for correction factors larger than one and decreases for one smaller than one. The PVI, defined as the perpendicular distance from the soil line, can be found by:

$$PVI = \sin(m_s) * \left[\frac{NIR - b_s}{m_s} - R\right] \text{ (unitless)} \qquad \text{(A.52)}$$

Applying a cosine correction factor c_{cos}, Equation A.52 can be written as

$$PVI_{cos} = \sin(m_s) * \left[\frac{NIR * c_{cos} - b_s * c_{cos}}{m_s} - R * c_{cos}\right] \text{ (unitless)} \qquad \text{(A.53)}$$

or simplified

$$PVI_{cos} = PVI * c_{cos} \qquad \text{(A.54)}$$

As a consequence, correction factors for variations in the solar distance and elevation cannot necessarily be omitted when computing SLIs and PVIs.

A4.3 Viewing Geometry

The comparatively large scan angle of ± 55.4° of the NOAA AVHRR instrument causes variations in the spectral response detected, which can be attributed to changes in the viewing geometry across a scene. The relative increase between the minimum and the maximum detected spectral response, which occurred within the scan angle range, is called the scan angle contrast (Royer *et al*, 1985).
With increasing solar altitude the scan angle contrast decreases due to the reduced difference between backward and forward scattering. The radiance variations induced by off-nadir viewing are maximized when the scan direction is nearly parallel to the incoming solar radiation.
The off-nadir viewing effects are systematic variations of digital data with viewing angle. Three causes for the effect were identified (Singh & Cracknell, 1985):

(a) **Non-Lambertian Nature of Surface Cover**
Earth surfaces are non-Lambertian reflectors. For most vegetated canopies there is a non-linear increase in reflected radiance values with increasing off-nadir viewing angle away from the sun (Royer *et al*, 1985). However, the off-nadir effects are asymmetric about the nadir and different for most canopies.

i. *Angular Scattering of Vegetation*
Antispecular (hot spot) reflection which results from back-scatter. The radiance increases when viewing away from the sun (forward scattering direction).

ii. *Angular Scattering of Soil*
Forward or specular reflection mode. The radiance increases with viewing towards the sun (backward scattering direction).

Typically, rangelands are partially covered by vegetation and a mixture of vegetation and soil is present within the IFOV of a sensor. Using simulated AVHRR data it was demonstrated that NDVI values generally increase with an increasing view angle (Holben & Fraser, 1984). Areas of sparse vegetation were found to be less affected by a wide viewing angle than areas with high quantities of green vegetation. In addition, a smaller solar zenith angle diminished the influence of the viewing angle on the NDVI.

(b) **Atmospheric Contribution**
A large portion of the influence of the viewing geometry on the total spectral response of a canopy can be attributed to atmospheric effects.
The variation caused by Rayleigh scattering increases with view angle without directional preference. The scattering of aerosols takes place predominatly in the

forward scattering direction. The influence of the viewing angle on VIs was linked to the extent of atmospheric turbidity. An increase in atmospheric particles was found to pronounce the effect of the viewing angle on VIs (Holben & Fraser, 1984).

(c) Non-uniform Illumination

Shadows cast by vertical protrusions cause non-uniform illumination as seen by the sensor. When scanning in the backward scattering direction (illuminated side) the surface appears to have a larger fraction of illuminated areas and less shadow than the surface viewed in the forward scattering direction (Singh & Cracknell, 1985). The effect of the scan angle on the detected spectral response varies with wavelength. It is lowest at wavelengths in the red portion of the EM energy spectrum and increases with wavelength (Royer *et al*, 1985; Tucker, 1977). Although the scan angle contrast is much smaller in the red waveband than in the NIR, the influence of the sun-scanner look angle on the total spectral response of a surface is much larger. In the red waveband the sun-scanner look angle accounts for approximately 24% of the total spectral response variation, compared to 6.4% in the NIR (Stohr & West, 1985). While the actual values vary over different terrain, the general trend remains constant for most surfaces.

A correction for variations in recorded radiance caused by changes in the viewing geometry encounters severe limitations (Royer *et al*, 1985; Barnsley, 1983; Morris & Barnsley, 1989). The main obstacles are:

- Atmosphere and surface form an interactive system In order to calculate correction factors all surface and atmospheric parameters should be known.
- *A priori* knowledge of the conditions is required A bidirectional reflectance distribution model should be established with knowledge of the values of the parameters.

For routine monitoring of vegetation by NOAA AVHRR data in an operational environment a correction of individual bands for the effects of viewing geometry on satellite data may be considered as being too demanding in terms of requirements for investigating surface conditions and processing time.

Under the assumption of a view angle, which is independent of directional reflectance properties of the surface, a number of correction procedures were suggested and tested (Royer *et al*, 1985; Morris and Barnsley, 1989). They are based on fitting a second order polynomial to the means of all pixels in along-track direction. Although improvements for classifications could be achieved, normalization procedures could not rectify the decrease in variation in radiance values with increasing off-nadir viewing (Kay & Barnsley, 1989).

At the Canadian Centre for Remote Sensing a method based on scene contrast has been adopted to compensate for off-nadir viewing effects in satellite data. An image is divided into

stripes of 50 km in across-track and 500 km in along-track direction. Average radiance values from these extracts are related to the distance from the nadir. A low order polynomial is then fitted to the averages and the data is adjusted accordingly (Ahern *et al*, 1987). The method requires a cloud free image or a procedure for scanning first for clouds. Further procedures are band ratios and restrictions of the image size. These methods are identical to some of the procedures applied for atmospheric corrections of recorded radiance values and will be discussed in Chapter A5.4 in Appendix I.

A4.4 Conversion of DNs to Spectral Reflectance

The EM energy incident upon the detector elements of a sensor causes an analog electrical signal, which is transformed into digital values (DNs) representing the signal strength. The relation between recorded DNs and exoatmospheric spectral reflectance is assumed to be of first order.

A4.1.1 Conversion of Landsat MSS DNs to Spectral Radiance

Aided by sensor calibration sources (sun or on-board calibration lamps) the sensor response is linearly related to the incident spectral radiance by using calibration coefficients:

$$L(i) = a_i * DN_i + b_i \quad (Wm^{-2}\Omega_i^{-1}sr^{-1}) \qquad (A.55)$$

Slope and intercept parameters a_i and b_i were derived from in-band spectral radiance threshold and saturation values (Markham & Barker, 1987). Their transformation to values of spectral radiance has caused some inconsistence in the use of the term spectral radiance. When applying the values for threshold and saturation radiance to Equation A.55, the spectral band radiance for the waveband L(i) is determined. The magnitude of this value depends on the bandwidth of the waveband. This form of spectral radiance will be referred to as *spectral band radiance* to avoid confusion with the spectral radiance L(*l*,i) from Equation A.56. The latter is based on one µm and independent of the bandwidth. Threshold and saturation radiance values were usually given as in-band values in $mWcm^{-2}sr^{-1}$ (Markham & Barker, 1987). In order to compare Landsat MSS spectral radiances with those from other sensors a conversion to the spectral radiance L(*l*,i) of band i should be performed. This can be achieved by normalizing the spectral band radiances of the four MSS bands to their bandwidths. The mathematical formulation can be written as:

$$L(\lambda,i) = \frac{L(i)}{\Omega_i} \quad (Wm^{-2}\mu m^{-1}sr^{-1}) \qquad (A.56)$$

The bandwidth Ω_i quoted for Landsat MSS corresponds to the difference between the upper and lower band edges. However, the sensor response function to incident EM radiation is not rectangular. Therefore, several methods of deriving at an integrated bandwidth, which takes the sensor response characteristic into account, were designed (Markham & Barker, 1987; Price, 1987). When comparing spectral radiance values from different instruments the measurements of the bandwidths should take different response characteristics into account.

A4.1.2 Conversion of Landsat MSS Spectral Radiance to Spectral Reflectance

Spectral radiance values $L(\lambda,i)$ of Landsat MSS band i are converted to exoatmospheric spectral reflectance by assuming a Lambertian surface and specifying the solar irradiance $E(\lambda,i)$ for the central wavelength of a spectral interval. The transformation equation can be written as

$$p(\lambda,i) = \frac{\pi}{E(\lambda,i)} * L(\lambda,i) \quad \text{(dimensionless)} \qquad (A.57)$$

The solar exoatmospheric irradiance $E(\lambda,i)$ is based on the central wavelength of a waveband. It is thus independent of the bandwidth. The central wavelength λ depends on the method of determining the bandwidth, since the sensor response function is not symmetrical. Therefore, slight differences exist between the values provided in the literature for the solar exoatmospheric irradiance $E(\lambda,i)$ (Markham & Barker, 1987; Price, 1987).
The value of the solar irradiance at the top of the atmosphere changes with the variation of the sun-earth distance. For a specific day of the year it is given by

$$E(\lambda i,d) = E(\lambda,i) * c_{sd} \quad (Wm^{-2}\mu m^{-1}) \qquad (A.58)$$

The annual variation in the sun-earth distance account for a change of 6.7% in the solar constant. Performed on its own, a correction for this variation has been shown to be of no practical use (Nelson, 1985). For the sun-earth distance correction to be useful, satellite data has also to be corrected for response variability and atmospheric changes. As shown above, the solar irradiance further varies with the solar zenith angle. Both effects can be accounted for by re-writing Equation A.58 for spectral reflectance to:

$$p(\lambda i,d,\Theta) = \frac{\pi}{E(\lambda i,d)*\cos(\Theta)*c_{sd}} * L(\lambda,i) \quad \text{(unitless)} \qquad (A.59)$$

The reflectance $p(l_i,d,\Theta)$ constitutes the apparent at-satellite reflectance and not the reflectance of surface features. Yet, the method of radiometric normalization allows a reduction in scene variability for data acquired under divergent conditions (Hill & Sturm, 1988).

A4.1.3 Conversion of NOAA AVHRR DNs to Spectral Albedo

Spectral albedo $a(l_i)$ for channel i is defined as

$$a(l_i) = \frac{L(l,i)}{S(l,i)} * 100 \quad (\% \text{ albedo}) \tag{A.60}$$

The link between spectral reflectance measurements from Landsat MSS and equivalent solar albedo measurements from NOAA AVHRR data is given by the *equivalent solar radiance* S(*l*,i). It is defined as the solar irradiance E(*l*,i) converted to the radiance resulting from the Sun at normal incidence on a perfectly reflecting diffuse surface (Price, 1987):

$$S(l,i) = \frac{E(l,i)}{\pi} \quad (Wm^{-2}\mu m^{-1}sr^{-1}) \tag{A.61}$$

The solar irradiance $E(l,_i)$ is based on the integrated solar spectral band irradiance E(i), which is weighted by the spectral response function of the channel. The solar irradiance $E(l_i)$ for channel i can be obtained from the integrated solar spectral band irradiance by:

$$E(l,i) = \frac{E(i)}{Q_{ai}} \ (Wm^{-2}\mu m^{-1}) \tag{A.62}$$

The bandwidth Q_{ai} denotes the equivalent width of the spectral response function in channel i (Planet, 1988).
The relationship between percent equivalent spectral albedo and spectral radiance is given by Equation A.63. Using solar spectral irradiance instead of equivalent solar irradiance, the relation can be more generally expressed as

$$a(l_i) = \frac{\pi}{E(l,i)} * L(l,i) * 100 \quad (\% \text{ albedo}) \tag{A.63}$$

Equation A.63 reveals the identical nature of equivalent spectral albedo and spectral reflectance as defined in Equation A.57.
For direct comparisons of spectral reflectances from different satellites or VIs based on them it has to be considered that the equivalent solar albedo for NOAA AVHRR (*a*(i)) is based on Thekaekara's values for the solar constant. Spectral reflectance for Landsat MSS and TM are calculated by using values of the solar constant from Neckel and Labs, which are

slightly different. The conversion of spectral albedo values from Thekaekara's mean solar constants to those based on Neckel and Labs is performed by dividing Channel 1 of NOAA AVHRR by a factor of 1.052 and Channel 2 by 1.017 (Price, 1988). If not mentioned differently, the values stated for the equivalent solar radiance are based on Neckel and Labs. From these values the slope coefficient for linearly relating raw DNs to spectral radiances can be calculated by:

$$a(i) = \frac{g(i)}{100} * S(\lambda,i) \quad (Wm^{-2}\mu m^{-1}sr^{-1}count^{-1}) \qquad (A.64)$$

and the off-set coefficient by

$$b(i) = \frac{d(i)}{100} * S(\lambda,i) \quad (Wm^{-2}\mu m^{-1}sr^{-1}) \qquad (A.65)$$

Combining Equations A.64 and A.65 provides the relationship for converting NOAA AVHRR Channel 1 and Channel 2 DNs to values of spectral radiance $L(\lambda,i)$:

$$L(\lambda,i) = \left[g(i)*DN(i)+d(i)\right] * \frac{S(\lambda,i)}{100} \quad (Wm^{-2}\mu m^{-1}sr^{-1}) \qquad (A.66)$$

A conversion of spectral albedo to spectral radiance can be achieved by:

$$L(\lambda,i) = \frac{E(i) * a(\lambda_i)}{\Omega_{ai} * \pi * 100} \quad (Wm^{-2}\mu m^{-1}sr^{-1}) \qquad (A.67)$$

(After: Planet, 1988)

A5. ATMOSPHERIC CORRECTION

A5.1 Forms of Atmospheric Scattering and Absorption

The composition of the atmosphere can be divided into three groups of constituents. Associated with a group of constituents is a specific form of atmospheric absorption or scattering of EM energy. Distinguished are:

(a) **Rayleigh Scattering by Permanent Gases**
Rayleigh scattering, which is also called molecular scattering for the visible and NIR wavebands (Fraser & Kaufman, 1985) occurs for particles, whose circumference is less than the interacting wavelength (Swain & Davis, 1978). It is caused solely by density fluctuations in the atmosphere (Slater, 1980). The scattered flux is inversely related to the wavelength by the fourth power. Rayleigh scattering causes a flux to be symmetrically scattered about the scattering centre. There is no preference in the forward or backward scattering direction.

(b) **Mie Scattering by Aerosol Particles**
The Mie scattering theory is mainly applied to particles, whose circumference is larger than the interacting wavelength, but can also be smaller (Fraser & Kaufman, 1985). The distribution of the scattered flux from aerosols is a complex function depending on the wavelength, the particle size, the refractive index of the molecules and the viewing azimuth angle. It is strongly expressed in the forward scattering direction. For semi-arid areas gross differences in the number, size and distribution of aerosols occur. Particularly changing rates of humidity and dust particles cause spatial and temporal variations.

(c) **Scattering by Ozone, Water Vapour and Carbon Dioxide**
The influence of H_20 and CO_2 is often incorporated as part of the aerosol and Rayleigh optical thickness. The contribution of Ozone to the atmospheric radiance is small compared with the effects caused by the permanent gases and aerosols. For this reason the ozone path radiance is commonly ignored (Sing *et al*, 1985).

For particle sizes, which fall between Rayleigh and Mie scattering a mixture of both scattering theories is applied. Atmospheric absorption of EM energy causes bright objects to appear darker by reason of atmospheric attenuation. Dark objects appear brighter due to atmospheric scattering. Scattering of incident EM energy by atmospheric components constitutes an additive component to the radiance reflected by surface features towards the sensor, while the effect of

absorption is multiplicative (Chaves, 1988). As a consequence, atmospheric influences reduce the scene contrast. The spatial variation of a non-uniform surface is lowered by the diffusion of upward radiance (Fraser & Kaufman, 1985; Kaufman & Sendra, 1988). Both effects influence VIs, which are based on a low reflectance in the red and a high reflectance of EM over vegetated areas in the NIR.
Molecular scattering causes an increase of at-satellite radiance values, which is particularly noticeable over dark, low reflecting cover types. The molecular composition of the atmosphere is generally uniform and well known. Its variation over time and for different areas is minimal. Molecular scattering of EM energy for the visible and near IR portions only depends on atmospheric pressure. Hence, Rayleigh optical thickness $t_r(\lambda)$ can be calculated with sufficient accuracy for many remote sensing applications (Robinson, 1985).
Aerosol absorption and scattering are the main sources of a variable influence of the atmosphere on reflected energy detected by satellite sensors (Kaufman & Sendra, 1988). The contribution to the signal depends not only on the amount of aerosols, but also on their composition. Aerosol absorption increases continuously as a function of surface reflectance, while scattering increases radiance for dark surfaces and decreases it for bright ones through scattering. In addition, both distribution and quantity of aerosol particles are much more susceptible to fluctuate than those of molecules. In addition, estimating the effect of Mie scattering requires knowledge or assumptions about environmental conditions.
As a consequence of the complexity of the interaction between atmospheric constituents and EM energy it has been concluded that an atmospheric correction of the red and NIR waveband data from fundamental physical models alone does not appear to be possible for a routine data analysis (Robinson, 1985).

A5.2 Influence of Atmospheric Conditions on VIs

The reflected energy detected by a sensor may be attenuated or increased by the atmosphere. Even with both effects in balance the signal is deteriorated in its quality by a reduced contrast. The effects of absorption and scattering and their magnitude depend on the wavelength of the EM energy. The relative magnitude of atmospheric path radiance decreases with increasing wavelength. Additionally, reflectance of vegetation is low in the red waveband, which gives the influence of the path radiance a higher proportion than in the NIR (lower signal/noise level), where reflectance of vegetation is higher and the scattering of energy in the atmosphere lower (Jackson *et al*, 1983). Consequently, the influence of the atmosphere on the incident radiance detected by satellite sensors over vegetated areas in the red portion of the EM spectrum is likely to be an increase. The higher reflectance of vegetation in the NIR causes an attenuation in incident radiance due to aerosol

and gaseous absorption (Fraser & Kaufman, 1985). The combined effect of the atmosphere on the upward radiance from vegetated areas on VIs is generally a reduction in VI values with an increase in atmospheric signal modification.

A5.3 Atmospheric Modell

The spectral radiance at the top of the atmosphere $L(\lambda)$ incident on the satellite sensor represents a mixture of reflected energy from the surface and the interaction of the atmosphere with this signal. The atmospheric contribution is commonly referred to as the path radiance $L_p(\lambda)$. It may be considered as a noise component in a linear transfer model between surface leaving radiance and at-sensor radiance (Teillet, 1986). The relationship is presented in the following equation:

$$L(\lambda) = L_s(\lambda) * t_{dir}(\lambda,\phi) + L_p(\lambda) \quad (Wm^{-2}\mu m^{-1}sr^{-1}) \qquad (A.68)$$

The direct atmospheric transmittance $t_{dir}(\lambda)$ constitutes the atmospheric influence of a straight beam from the surface to the sensor and is sometimes refered to as beam transmittance (Deschamps *et al*, 1983). It can be separated into Rayleigh ($\tau_r(\lambda)$), aerosol ($\tau_a(\lambda)$) and gaseous ($\tau_g(\lambda)$) optical depths. The atmospheric transmittance from surface to satellite can be rewritten as being

$$t_{dir}(\lambda) = e^{-[\tau_r(\lambda)+\tau_a(\lambda)+\tau_g(\lambda)]/\cos(\phi)} \quad (unitless) \qquad (A.69)$$

(After: Saunders, 1990)

Due to inappropriate use of the term path radiance and the restriction of the formula to cases, where the IFOV is small relative to the scale of the scattering effect, the term path radiance has been suggested to be replaced by atmospheric radiance $L_a(\lambda)$ and background radiance $L_b(\lambda)$ (Deschamps *et al*, 1983). Hence, the path radiance $L_p(\lambda)$ from Equations A.68 can be written as:

$$L(\lambda) = L_s(\lambda)*t_{dir}(\lambda,\phi)+L_a(\lambda)+L_b(\lambda) \quad (Wm^{-2}\mu m^{-1}sr^{-1}) \qquad (A.70)$$

The term of atmospheric radiance $L_a(l)$ applies to the EM energy scattered by the atmosphere alone. It contains no information about the nature of the earth surface. It is found by observations of visibility or derived from radiance values of presumably black surfaces.
Background radiance $L_b(l)$ contains both the influence of the surface and atmospheric properties. It is reflected by the background surface and then scattered by the atmosphere towards the sensor. It can be expressed as a function of the diffuse transmittance $t_{dif}(\lambda,\phi)$ as:

$$L_b(\lambda) = L_e(\lambda) * t_{dif}(\lambda,\phi) \qquad (A.71)$$

For a uniform surface larger than the IFOV and for pixel sizes greater than 500 m the environmental radiance $L_e(\lambda)$ corresponds to the surface radiance of the target $L_s(\lambda)$. The background radiance causes a change in the effective point spread function. Due to scattering a pixel contains information of a larger area than the IFOV suggests. The effect is a reduced spatial variation (blurring) for data from sensors with less than 500m pixel size (Kaufman & Sendra, 1988).
The sum of diffuse transmittance $t_{dif}(\lambda,\phi)$ and direct transmittance $t_{dir}(\lambda,\phi)$ forms the total transmittance $t(\lambda,\phi)$. Thus, for a homogeneous area surface leaving radiance is linearly related to incident at-satellite radiance by:

$$L(\lambda) = L_s(\lambda)* t_{dir}(\lambda,\phi) + L_e(\lambda)* t_{dif}(\lambda,\phi) + L_a(\lambda) \quad (Wm^{-2}\mu m^{-1}sr^{-1}) \qquad (A.72)$$

The total atmospheric transmittance $t(\lambda,\phi)$ can be approximated by the following relationship:

$$t(\lambda,\phi) \approx \left[1 + \frac{b_r*\tau_r(\lambda)+b_a*\tau_a(\lambda)}{\cos(\phi)}\right]^{-1} \qquad (A.73)$$

(After: Deschamps *et al*, 1983)

The coefficients b_r and b_a for the optical thicknesses of molecular and aerosol scattering ($\tau_r(\lambda)$ and $\tau_a(\lambda)$) were determined for main types of atmospheric conditions (Tanre *et al*, 1979, in: Deschamps *et al*, 1983).
Molecular and aerosol optical thicknesses are given by

$$\tau_r(\lambda) = \left[\frac{84.35}{\lambda^4} - \frac{1.225}{\lambda^5} + \frac{1.41}{\lambda^6}\right]10^{-6} \qquad (A.74)$$

and the aerosol optical depth as

$$\tau_a(\lambda) = \left[\frac{1.0317}{\lambda} - \frac{0.0317}{\lambda^2}\right] * \tau_r(\lambda) \qquad (A.75)$$

(λ in μm)

Aerosol optical transmittance has been defined more generally as:

$$t_a(\lambda,\Theta) = e^{-\left[\frac{\tau_{H2O}/2+\tau_g+\tau_{oz}+\tau_r}{\cos(\Theta_s)}\right]} \qquad (A.76)$$

(After: Saunders, 1990)

For multi-temporal data and investigations into the nature of the earth surface cover types, the spectral radiance is

conveniently normalized to spectral reflectance.
Under the assumption that the surrounding pixels have the same average reflectance as the target pixel the surface reflectance $L_s(\lambda)$ can be expressed as

$$L_s(\lambda) = \frac{E_s(\lambda)}{\pi} * p_s(\lambda) \ (Wm^{-2}\mu m^{-1}sr^{-1}) \qquad (A.77)$$

The total irradiance at the surface $E_s(\lambda)$ is related to the solar irradiance at the top of the atmosphere $E(\lambda,d)$ by

$$E_s(\lambda) = \frac{E(1,d)*\cos(\Theta_s)*t(\lambda,\Theta_s)}{1-p_s(\lambda)*a_s(\lambda)} \ (Wm^{-2}\mu m^{-1}sr^{-1}) \qquad (A.78)$$

The fraction of upward radiation backscattered by the atmosphere to the surface $a_s(\lambda)$ can be approximated by

$$a_s(\lambda) \approx \frac{2*[b_r*\tau_r(\lambda)+b_a*\tau_a(\lambda)]}{1+2*[b_r*\tau_r(\lambda)+b_a*\tau_a(\lambda)]} \qquad (A.79)$$

The normalization of at-sensor spectral radiance $L(\lambda)$ and the atmospheric radiance $L_a(\lambda)$ provides the total reflectance $p(\lambda)$ and atmospheric reflectance $p_a(\lambda)$ by

$$p(\lambda) = \frac{\pi}{E(\lambda,d)*\cos(\alpha_z)} * L(\lambda) \ (unitless) \qquad (A.80)$$

and

$$p_a(\lambda) = \frac{\pi}{E(\lambda,d)*\cos(\alpha_z)} * L_a(\lambda) \ (unitless) \qquad (A.81)$$

(After: Fraser & Kaufman, 1985)

The normalized at-satellite radiance $p(\lambda)$ can then be expressed as a function of the viewing geometry, atmospheric conditions and surface reflectance as:

$$p(\lambda) = \frac{t(\lambda,\Theta_s)}{1-p_s(\lambda)*a_s(\lambda)} * [p_s(\lambda)*t_{dir}(\lambda,\phi) + p_e(\lambda)*t_{dif}(\lambda,\phi)] + p_a(\lambda) \qquad (A.82)$$

Under simplified conditions, for an area, where the target and the average of the surrounding pixel have the same, or negligible different, reflectance it becomes:

$$p(1) = p_s(1) * \frac{t(1,\Theta_s)*t(1,\phi)}{1-p_s(1)*a_s(1)} + p_a(1) \qquad (A.83)$$

The atmospheric reflectance $p_a(1)$ can be found by the sum of the aerosol reflectance $p_a(1,\varepsilon)$ and molecular reflectance $p_r(1,\varepsilon)$. The molecular reflectance is approximated by

$$p_r(1,\varepsilon) = \frac{p_r(\varepsilon)*\left[1-e^{-\left[\tau_r(1)*\left[\frac{1}{\cos(\Theta_s)}+\frac{1}{\cos(\phi)}\right]\right]}\right]*t_{oz}(\Theta_s)*t_{oz}(\phi)}{4*[\cos(\Theta_s)+\cos(\phi)]} \qquad (A.84)$$

(After: Phulpin *et al*, 1989)

Similarly, aerosol reflectance can be approximated by

$$p_a(1,\varepsilon) = \frac{p_a(\varepsilon)*w*\left[1-e^{-\left[\tau_a(1)*\left[\frac{1}{\cos(\Theta_s)}+\frac{1}{\cos(\phi)}\right]\right]}\right]*t_{oz}(\Theta)*t_{oz}(\phi)}{4*[\cos(\Theta_s)+\cos(\phi)]} \qquad (A.85)$$

(After: Phulpin *et al*, 1989)

The aerosol single scattering albedo w accounts for reflectance characteristics of aerosol particles.
The phase function for atmospheric scattering $p_r(\varepsilon)$ can be found by

$$p_r(\varepsilon) = 0.75 + 0.75 * \cos^2(\varepsilon) \qquad (A.86)$$

(After: Hill & Sturm, 1988)

The backscattering angle ε is given by

$$\cos(\varepsilon)=\cos(\Theta_s)*\cos(\phi) + \sqrt{[1-\cos^2(\Theta_s)]}\sqrt{[1-\cos^2(\phi)]}*\cos(\Theta_s-\Theta_{rel}) \qquad (A.87)$$

(After: Phulpin *et al*, 1989)

or

$$\varepsilon = 180-\cos^{-1}[\cos(\Theta_{rel})*\sin(\Theta_s*\sin(\phi)+\cos(\phi)*\sin(\Theta_s)$$

(After: Saunders, 1990)

The relationship between reflectance of surface features and the one computed from satellite sensors are still approximately linearly related.

A5.4 Atmospheric Correction Techniques

A5.4.1 Image Processing Side Products

Some image processing methods reduce the effect of atmospheric conditions on satellite data, although they were not particularly intended for that purpose. Yet, in combination with specifically designed correction procedures discussed later in this section, they may support further reduction of atmospheric influences on satellite data and, therefore, deserve to be considered.

(a) **Restriction of Image Size**
This approach is relevant to sensors with a wide scan angle, like NOAA AVHRR. Atmospheric effects increase with scan angle since the energy reflected has to travel through a longer path length. With NOAA AVHRR the atmospheric optical path length between the satellite and the earth surface increases by a factor of 2.2 from the nadir to the extreme off-nadir viewing angles (Holben & Fraser, 1984). The distance which energy travels to the sensor from an object at the edge of the scan line through the atmosphere is greater than the distance between sensor and an object at the nadir. Beside the loss of contrast in radiance at the edges the wide FOV of ± 55.4° of AVHRR, non-Lambertian reflectance of the vegetation targets is introduced. The magnitude depends on the nature of the vegetation present and on the sun-target-sensor geometry. When using uncorrected AVHRR data at scan angles beyond 20°, an uncertainty of approximately 10 to 15% for radiant energy detected by the sensor exists (Holben & Fraser, 1983). Therefore, it has been suggested to restrict the data analysis to an area within ± 20° from the nadir (Duggin *et al*, 1982; Tucker *et al*, 1983; Harris, 1987)).

(b) **Band Ratios**
Band ratios are widely applied for vegetation monitoring. Ratios can compensate for those factors that are similar in magnitude and equal in phase in the spectral bands (Maxwell, 1976b). These conditions comply with the general influence of the atmosphere on the surface leaving radiance since, contrary to vegetation, changes in atmospheric conditions affect both wavebands in the same direction, although with different amplitude. Thus, alterations in atmospheric condition from one image to the next and rapid atmospheric propagation variations along the scan line will be reduced by band ratios (Maxwell, 1976b).
The contribution of the atmospheric radiance $L_a(\lambda)$ to the spectral radiance at the top of the atmosphere $L(\lambda)$ is interpreted as being an additive rather than a

multiplicative constant. The relationship may be expressed by

$$R_{a/b} = \frac{c_a * s(a) + n(a)}{c_b * s(b) + n(b)} \quad \text{(unitless)} \qquad \text{(A.88)}$$

The more c_a agrees with c_b, and the larger s(a,b) is compared to $c_{(a,b)}$ and n(a,b) the more advantageous are ratios in reducing the influence of the constants ca and cb on the spectral response in a band. This is the case when wavebands a and b are close to each other and the variations expressed in ca and cb are positively related.
As a consequence, ratios can only lower the influence of atmospheric conditions but not fully compensate for them. Generally, ratios moderate the influence of topographic effects significantly, decrease the scan angle contrast and lower variations caused by viewing angle effects. The effectiveness of ratios in reducing the contribution of the atmosphere to the surface leaving radiance varies and depends on scene conditions. Influencing factors are:

i. *Magnitude of Atmospheric Turbidity*
An increase in atmospheric path radiance decreases RVI and NDVI values. For interpretable results an additional atmospheric reflectance adjustment is recommended when employing ratios as vegetation indices.

ii. *Surface Reflectance*
As long as the additive effects n(a,b) are small compared to the multiplicative effects $c_{(a,b)}$ ratios can effectively lower between-scene variations. These conditions exist over areas with a high reflectance. Over areas of low reflectance ratios are less effective and atmospheric conditions show a significant influence on band ratios (Nelson, 1985a; Tueller, 1987; Kimes *et al*, 1985).

iii. *Sensor Characteristic*
Small widths and close affinity of the spectral bands give better results than widely spaced broad bands. The utilization of spectral ratios for AVHRR images, compared to for example Landsat MSS data, is reduced in its effectiveness by the comparatively large bandwidth of the red and NIR wavebands (Barnsley, 1983).

iv. *Scan Angle*
When restricting the off-nadir viewing angle to less than 30° the NDVI transformation greatly reduces directional variation in the signal as compared to single bands (Holben & Fraser, 1984).

Due to the number of variables influencing the efficiency of ratios for reducing scene variations they can only act as an approximation for a complete correction (Lillesand & Kiefer, 1987). But the performance of band ratios can be significantly improved by data adjustments for atmospheric path radiance and sensor calibration offsets prior to band rationing (Crippen, 1988).

A5.4.2 Empirical Methods

Empirical methods were developed to correct for the influence of the atmosphere on radiance without knowing exact atmospheric conditions. Most of the methods assume that the variability in spectral radiance received by the sensor is due to the additive effect of molecular scattering to the atmospheric radiance $L_a(\lambda)$. To determine the spectral atmospheric radiance, most empirical methods employ the spectral radiance recoded by the sensor over dark areas on the surface. Dark ground features may consist of large water bodies, dense vegetation in the red waveband or shadow (Slater, 1980). The spectral reflectance of these targets is taken as homogeneous with a Lambertian behaviour and a linear sensor response function.

(a) ***Histogram Minimum Method (Dark Pixel Subtraction)***
The histogram minimum or dark pixel subtraction method requires low reflecting surfaces or steep slopes to be present in the scene and employs DNs from these areas in the NIR waveband, which should be zero. Histograms are off-set towards higher values due to atmospheric scattering effects, particularly in the visible wavebands. The point of a distinct increase in the frequency of DNs found is interpreted as the atmospheric contribution to the signal from the surface. The amount is then subtracted from all pixel values (Sabins, 1987). The regression method has been improved by incorporating assumption from a relative atmospheric scattering model. Depending on the amount of atmospheric turbidity suspected within a scene a relationship between haze components of different wavebands is selected. A basic haze value is determined in one band and haze values for other bands are then estimated on the basis of the scattering model (Chavez, 1988).

(b) **Regression Method**
The regression method employs radiance values from shadowed areas or dark surface covers in the red waveband, which are plotted against those from the NIR. A linear regression is performed on the cluster and the radiance at the intercept with the red waveband axis is established (Chavez, 1975).
The regression method assumes that the amount of off-set is caused by the additive effect of atmospheric scattering of the atmospheric radiance $L_a(\lambda)$. The calibration is based on the a priori specified

atmospheric path radiance for the NIR waveband, which is defined as being zero. The correction is accomplished by subtracting the value of the intercept from the measured radiance value of each pixel (Mather, 1987). For more than two wavebands the method has been extended to the covariance matrix method (Switzer *et al*, 1981).

(c) **Regression Intersection Method**
The regression intersection method is based on the simple regression method presented above (Crippen, 1987). Instead of using one regression line to estimate the amount of atmospheric scattering, two or more regression lines are employed. Each line is based on at-sensor radiance values in two wavebands of one surface cover type under different illumination conditions. The intersection of two regression lines should correspond to zero ground radiance. The displacement of the intersection from the origin corresponds to the atmospheric radiance $L_a(\lambda)$. Compared to the one-line regression method the regression intersection method provides absolute correction values without knowledge of surface reflectance characteristics. A disadvantage of the method is that the regression lines of two homogeneous surface cover types can be very similar and that the point of intersection depends on pixels chosen to represent a cover type.

(d) **Shadow-Illumination Regression**
Estimates of the irradiation over partly illuminated and partly shadowed areas for the same surface cover are plotted as pairs for various cover types. By fitting a straight line through the cluster of points the amount of scattering within a waveband can be estimated. The method was originally developed for aerial colour photographs, but was suggested to be used with satellite data (Piech & Walker, 1974).

The first two methods were suggested as atmospheric correction procedures for Landsat MSS images (Sabins, 1987) but could in principle be applied to NOAA AVHRR data. The IFOV of the sensor restricts the use, however.
A major disadvantage of these empirical methods is that in some cases the adjustment may lead to incorrect results (Switzer *et al*, 1981). The regression method was found to be superior to the histogram minimum method, which assigns abnormally large ratio values for poorly illuminated sites. This can be attributed to an environmental scattering effect $L_b(\lambda)$, which influences reference areas of small spatial extent and becomes increasingly relevant with decreasing IFOV (Royer *et al*, 1987).

A5.4.3 Atmospheric Correction Based on Physical Models

Most of the procedures in this group are based on the presence of dark surface features with known reflectance values in the image and use assumptions from generalized meteorological data

for the area of interest.
The reflected radiance from dark surfaces is employed to estimate the atmospheric radiance $L_a(\lambda)$. It is interpreted as the sum of the radiance caused by molecular and aerosol scattering. Since the molecular optical depth $\tau_r(\lambda)$ can be computed for a standard Rayleigh atmosphere and the Rayleigh scattering phase function $p_r(\lambda,\varepsilon)$ only depends on the backscattering angle ε and the wavelength the extent of molecular scattering can be obtained. Consequently, the amount of aerosol scattering is found. From here onwards the models vary with respect to the degree of atmospheric conditions taken into account.

(a) **Clear Water Reflectance in NIR**
One surface feature of known spectral reflectance, which is dark in the visible and NIR portion of the EM spectrum are deep clear water bodies. The diffuse spectral reflectance $p_s(\lambda)$ of these surfaces is assumed to be zero in the NIR.
An atmospheric correction procedure based on clear water reflection is used by the Canadian Centre of Remote Sensing for Landsat MSS (Royer *et al*, 1988).
An automatic method for Landsat TM was developed by Hill & Sturm (1988). There, molecular scattering of water bodies is obtained from the histogram minimum. The model also takes into account ozone absorption and differences in the average reflectance of areas surrounding the target pixel.
A fast atmospheric correction procedure was developed for TM under a more simplistic approach (Richter, 1990). Assumed is nadir viewing and a fixed ground reflectance to approximate the global irradiance $E_g(\lambda)$. The algorithm does not necessarily require the presence of clear water, but dark surfaces with known reflectances should be visible on the image. The atmospheric radiance is computed by another programme for atmospheric correction (LOWTRAN-7).
However, large clear water bodies can hardly be found in the Sahel.

(b) **Shadow Radiance Subtraction**
Shadows caused by an irregular topography can be employed for a haze correction technique. Without the influence of the atmosphere shadowed areas do not possess any surface leaving spectral radiance $L_s(\lambda)$. With an assumption about diffuse spectral reflectance $p_s(\lambda)$ the atmospheric radiance $L_a(\lambda)$ can be estimated in the above described way. Some knowledge, however, about the terrain and its diffuse spectral reflectance is required, since the spectral radiance $L(\lambda)$ received from shadowed areas is not directly proportional to the atmospheric radiance $L_a(\lambda)$. An additional problem with AVHRR data arises from the size of the IFOV. Pixels are unlikely to consist of completely shadowed areas but contain cloud or illuminated canopies on the ground.

(c) **Dense Vegetation**
Dense, dark vegetation larger than the size of one pixel

was suggested to be used to estimate atmospheric reflectance (Ahern *et al*, 1987). Coniferous forest was found to be very stable with respect to its reflectance properties over different areas and seasons. For Canada and similar areas it was proposed as a standard reflectance target to adjust AVHRR images for varying atmospheric conditions (Ahern *et al*, 1987). Forest reflectance was employed for an automatic atmospheric correction of Landsat TM data (Kaufman & Sendra, 1988). The model did not consider gaseous absorption or a background radiance, which is different than the target radiance.

A5.4.4 Analysis of Multi-temporal Sequences

A high temporal frequency of data acquisition during the growing season may result in images with larger differences between data caused by atmospheric disturbances and view angle than by vegetation growth. The methods are based on the assumption that the recorded sensor response over time constitutes a signal of low frequency and a noise component with a high frequency. With a widely spaced dates of data acquisition the atmospheric disturbances are usually smaller than the observable differences in vegetation development. With a high temporal repeat rate of image data acquisitions, which is possible with NOAA AVHRR, the influence of changing atmospheric conditions can be taken into account by looking at the temporal sequence of data.

(a) **Averaging**
For daily images of terrain with low spatial variability the average VI over adjacent pixels for a week could be calculated to produce a composite image.
For weekly images this method would be inapplicable because vegetation would be at very different stages of development.

(b) **Curve Fitting**
By fitting a curve through the sequence of images the amount of noise is reduced and the signal becomes the main component. The curves are based on second or third order polynomials or a Fourrier analysis (vanDijk *et al*, 1987).

(c) **Filtering Profiles**
Fluctuations can be eliminated by filtering VI profiles, for example, with a high filter or moving averages (vanDijk *et al*, 1987).

(d) **Standardization to One Image**
For multi-temporal images the standardization to one image of the sequence is proposed to normalize atmospheric effects (Goetz, 1973; Slater, 1980). The lowest values found over a number of dates could be used to identify a reference image, to which all other images

are corrected. Required is the presence of pseudo-invariant cover types in the scenes, like urban features or water (Schott *et al*, 1988). This would not constitute an atmospheric correction in the true sense, but relative variations between images would be taken into account.

(e) Maximum-Value Composite (MVC) Images

For reducing the influence of varying conditions like differences in the atmosphere, off-nadir viewing or cloud cover, maximum-value composite images (MVC) of the NDVI have been employed (Holben, 1986). MVC images reduce the varying effects of directional reflectance behaviour, off-nadir viewing, sun angle, shadow and aerosol and water vapour.

MVC were first proposed by NOAA in 1983 to reduce cloud and atmospheric effects for global vegetation index (GVI) images. Originally, an interval of 7 days was used. A series of GAC data is spatially matched to a geometric reference projection. The composite image derived from the series consists of the highest NDVI value for each pixel of the series. With the increase in NDVI values at scan angles beyond 30° from the nadir, the area for MCVs is restricted to about a strip 700 km wide (Gutman, 1987).

NOAA-9 satellites cover an area once a day during local day-time. At one out of three days an area can be expected to be within ± 20° of the nadir. Hence, MVC images based on a 10-day basis would consist of data from at least three dates.

Although variations in recorded sensor response caused by changing atmospheric conditions can be reduced by MVC images, some disadvantages of the method remain. For example, the effect of cloud may not be totally removed, dates of image acquisition should be closely spaced and off-nadir viewing effects are still present (Gutman, 1987). In addition, primary production may be over-estimated, if growth is spatially very variable and short in comparison to the period for the maximum-value composites. Also, instead of choosing a "clearer" atmosphere, the darkest soil surface conditions, wether due to shading or rainfall, may be selected (Huete & Jackson, 1988).

APPENDIX II: TABLES

Table A.1: Map Coordinates of 1985 CIPEA Sampling Sites in Niger

Site No.	CIPEA Position Long. (deg)	Lat. (deg)	Image Position Long. (deg)	Lat. (deg)	Difference East (m)	North (m)
2	5.742	15.517	5.748	15.528	-698	-1237
3	5.733	15.717	5.748	15.710	-1578	695
4	5.767	15.800	5.808	15.793	-4474	718
5	5.817	16.050	5.823	16.038	-687	1371
6	5.750	16.233	5.750	16.233	2	24
7	5.750	16.467	5.733	16.467	1853	11
11	7.017	16.683	7.017	16.683	-34	36
12	7.767	16.850	7.767	16.850	-25	0
13	7.583	16.767	7.583	16.767	35	-36
14	7.200	16.383	7.200	16.383	0	36
15	7.133	16.167	7.133	16.167	35	-36
16	6.375	15.567	6.375	15.567	-0	-36
17	5.817	15.217	5.834	15.229	-1864	-1449
18	5.950	15.817	5.950	15.817	5	-18
19	7.817	16.125	7.817	16.125	-35	0
20	7.842	15.800	7.842	15.800	-35	0
21	7.117	14.925	7.117	14.925	-35	0
22	6.667	14.650	6.667	14.650	-35	0
23	6.683	14.900	6.683	14.900	35	-0
24	6.600	15.400	6.600	15.400	0	0
25	6.467	15.433	6.467	15.433	-35	37
26	7.375	15.758	7.375	15.758	0	36
T2	6.617	16.017	6.617	16.017	-135	-36
T3	6.800	16.450	6.800	16.450	0	0
T4	6.300	15.217	6.300	15.217	-0	-36

Table A.2: Average Rangeland Production and Cover Values for 1985 CIPEA Survey

Site	1. Period			2. Period			3. Period	
No.	D.M. ($kgha^{-1}$)	S.D.	Cover (%)	D.M. ($kgha^{-1}$)	S.D.	Cover (%)	D.M. ($kgha^{-1}$)	Cover (%)
2	0.2	1.4	0.0	5.5	30.4	0.1	96.0	1.9
3	320.5	205.7	20.2	744.2	764.9	26.5	666.2	27.3
4	32.7	58.4	2.2	387.9	471.4	9.6	792.4	18.0
5	7.1	19.4	0.4	342.5	540.9	15.1	85.8	3.5
6	10.5	23.8	0.4	12.5	38.2	0.5	332.5	10.0
7	23.1	74.1	1.1	488.4	747.9	10.9	437.6	8.8
11	65.9	363.6	1.4	383.8	660.2	16.5	301.1	10.5
12	28.1	34.3	1.4	326.2	401.4	8.9	264.8	9.8
13	16.2	38.8	1.0	165.2	268.3	8.3	135.4	5.3
14	2.6	4.1	0.2	96.6	156.2	2.9	111.2	3.8
15	5.4	19.0	0.5	67.3	256.0	1.3	23.1	0.7
16	270.8	326.6	17.8	2355.9	2014.6	32.2	*	*
17	106.8	54.8	1.4	877.5	454.3	34.9	339.7	31.5
18	21.8	66.2	0.8	459.9	1268.7	7.1	201.9	6.2
19	199.1	144.5	18.8	336.3	300.6	18.4	408.7	16.0
20	34.1	71.2	2.6	549.0	835.4	20.1	956.4	25.2
21	2.3	9.8	0.3	847.8	856.9	19.0	1760.0	21.0
22	10.5	17.9	1.2	914.3	705.2	22.9	1065.9	23.4
23	287.2	477.7	14.3	1616.5	2581.4	27.3	1149.9	20.1
24	106.2	268.9	4.9	223.2	250.0	6.6	343.3	9.0
25	225.8	358.3	13.0	1549.2	2477.9	23.2	1151.2	24.3
26	503.1	476.9	33.0	1212.6	1158.4	40.1	1090.6	35.2
32	36.7	99.5	3.0	559.7	734.1	23.2	262.4	8.4
33	8.9	22.0	0.4	72.9	178.4	3.4	373.6	6.9
34	42.2	38.2	2.3	376.6	537.8	17.4	455.8	18.2

* No data available
D.M. Dry Matter
S.D. Standard deviation

Table A.3: Map Coordinates of 1985 and 1988 ITE/Silsoe Sampling Sites in Niger

Site No. 1985	Site No. 1988	Position from Hard-copy Latitude (deg)	Longitude (deg)	Easting (m)	Northing (m)	Direction (deg)
A	12/88	15.205	5.813	802427	1683993	212
B	11/88	15.217	5.793	801477	1685893	233
C	1/88	15.318	5.912	814427	1697243	230
D		15.458	5.750	796577	1711943	80
E		15.490	5.730	794427	1664793	256
F		15.360	5.772	796727	1700843	180
G	9/88	15.350	5.763	797977	1699993	160
H		15.292	5.767	798377	1693393	160
	2/88	15.338	5.928	816027	1697993	327
	3/88	15.372	5.907	816077	1703993	325
	4/88	15.385	5.895	810977	1703743	186
	5/88	15.375	5.918	813227	1703593	230
	6/88	15.790	5.812	800177	1745243	220
	7/88	15.528	5.677	793377	1733643	300
	8/88	15.350	5.763	793677	1718393	320
	10/88	15.262	5.773	799127	1690443	300

Table A.4: Position of CAZS Sampling Sites

Site No. 1988	Position from GPS Latitude (deg)	Longitude (deg)	Easting (m)	Northing (m)	Direction (deg)
A	3.243	15.530	526037	1716973	330
B	3.219	15.515	523506	1715274	150
C	3.209	15.504	521454	1714127	135
D	3.209	15.504	521454	1714127	305
E	3.203	15.498	521823	1713381	220
F	3.209	15.730	522430	1739031	275
G	3.193	15.724	520712	1738440	250
H	3.186	15.717	519972	1737669	252
J	3.178	15.714	519055	1737322	252
K	3.164	15.716	517620	1737553	332
L	2.659	15.737	463469	1739825	200
M	2.726	15.702	470643	1736024	345
N	2.844	15.669	483261	1732299	232
P	2.858	15.660	484827	1731305	69

Table A.5: Standard Deviation, Coefficient of Variation and Standard Error of Mean for Herbaceous Rangland Vegetation Qunatities of CAZS Field Survey

Site No.	Dry Matter (kg ha^{-1})	Std. dev. of D.M. (kg ha^{-1})	C.V. of D.M. (%)	Range of mean D.M. Confidence Level * 95%	80%	60%
	First Sampling Period					
A	49.1	66.4	135.3	31.1	19.7	12.8
B	52.1	113.9	218.5	53.3	33.9	21.9
C	95.7	98.2	102.6	46.0	29.2	18.9
D	36.3	65.9	181.5	30.8	19.6	12.7
E	89.8	89.1	99.2	41.7	26.5	17.2
F	88.1	54.2	61.6	25.4	16.1	10.4
G	67.1	40.8	60.9	19.1	12.1	7.9
H	51.1	68.4	133.7	32.0	20.3	13.2
J	64.2	44.1	68.7	20.6	13.1	8.5
K	126.9	70.0	55.2	32.8	20.8	13.5
L	106.8	130.7	122.4	61.2	38.9	25.2
M	107.8	94.9	88.0	44.4	28.2	18.3
N	30.9	19.9	64.4	9.3	5.9	3.8
P	36.3	25.2	69.4	11.8	7.5	4.9
	Second Sampling Period					
A	233.9	326.4	139.5	152.8	97.1	62.8
B	161.5	221.7	137.3	103.8	65.9	42.7
C	527.7	280.5	53.1	131.3	83.4	54.0
D	396.6	396.0	99.8	185.3	117.8	76.2
E	141.6	143.9	101.6	67.3	42.8	27.7
F	144.9	84.3	58.2	39.5	25.1	16.2
G	201.6	88.5	43.9	41.4	26.3	17.0
H	323.6	205.7	63.6	96.3	61.2	39.6
J	173.4	113.4	65.4	53.1	33.7	21.8
K	186.0	119.7	64.3	56.0	35.6	23.0
L	295.8	262.4	88.7	122.8	78.0	50.5
M	131.2	83.0	63.3	38.9	24.7	16.0
N	63.4	39.6	62.4	18.5	11.8	7.6
P	49.4	36.4	73.6	17.0	10.8	7.0
	Third Sampling Period					
A	955.0	755.0	79.1	353.4	224.5	145.4
B	602.0	433.4	72.0	202.9	128.9	83.4
C	900.4	310.6	34.5	145.4	92.4	59.8
D	639.0	271.0	42.4	126.9	80.6	52.2
E	604.7	320.1	52.9	149.8	95.2	61.6
F	633.0	300.6	47.5	140.7	89.4	57.9
G	1212.7	421.3	34.7	197.2	125.3	81.1
H	922.2	305.6	33.1	143.0	90.9	58.8
J	915.8	323.4	35.3	151.4	96.2	62.3
K	650.0	343.7	52.9	160.9	102.2	66.2
L	736.8	586.2	79.6	274.4	174.3	112.9
M	989.9	675.2	68.2	316.0	200.8	130.0
N	250.6	113.8	45.4	53.3	33.9	21.9
P	187.9	209.1	111.3	97.8	62.2	40.3

Table A.5: continued

Site No.	Dry Matter (kg ha^{-1})	Std. dev. of D.M. (kg ha^{-1})	C.V. of D.M. (%)	Dry Matter Range at Confidence Level * ±125	±150	±200
	Fourth Sampling Period					
A	1372.7	660.4	48.1	57.0	67.0	82.0
B	487.1	385.1	79.1	84.0	89.0	98.0
C	999.3	166.5	16.7	100.0	100.0	100.0
D	624.1	226.4	36.3	98.0	100.0	100.0
E	1040.4	421.1	40.5	79.0	87.0	95.0
F	608.3	196.0	32.2	100.0	100.0	100.0
G	754.0	217.9	28.9	99.0	100.0	100.0
H	740.1	272.1	36.8	95.0	97.0	100.0
J	843.0	226.2	26.8	98.0	100.0	100.0
K	757.6	374.4	49.4	84.0	91.0	94.0
L	1816.7	333.4	18.3	89.0	94.0	99.0
M	1604.4	724.4	45.2	87.0	62.0	75.0
N	445.4	130.7	29.3	100.0	100.0	100.0
P	989.9	840.0	84.8	51.0	57.0	71.0
	Fifth Sampling Period					
A	926.5	720.6	77.8	57.0	62.0	75.0
B	1259.6	613.2	48.7	62.0	71.0	84.0
C	1450.1	562.5	38.8	67.0	75.0	87.0
D	953.9	525.4	55.1	71.0	79.0	89.0
E	622.7	611.4	98.2	62.0	71.0	84.0
F	1093.1	282.1	25.8	94.0	97.0	100.0
G	873.4	138.6	15.9	100.0	100.0	100.0
H	1054.4	684.6	64.9	57.0	67.0	79.0
J	1000.9	141.8	14.2	100.0	100.0	100.0
K	995.1	492.1	49.5	71.0	82.0	91.0
L	1203.8	296.3	24.6	92.0	96.0	100.0
M	1314.8	589.5	44.8	62.0	71.0	84.0
N	656.9	153.0	23.3	100.0	100.0	100.0
P	890.6	245.3	27.5	94.0	99.0	100.0
	Sixth Sampling Period					
A	1354.8	405.8	30.0	82.0	89.0	96.0
B	852.5	169.9	19.9	100.0	100.0	100.0
C	1286.2	304.1	23.6	91.0	96.0	99.0
D	1012.0	277.5	27.4	94.0	100.0	100.0
E	1061.1	426.8	40.2	79.0	87.0	95.0
F	644.6	122.9	19.1	100.0	100.0	100.0
G	797.6	91.4	11.5	100.0	100.0	100.0
H	1193.7	333.3	27.9	89.0	94.0	99.0
J	652.2	100.9	15.5	100.0	100.0	100.0
K	483.2	84.1	17.4	100.0	100.0	100.0
L	1306.5	235.7	18.0	98.0	99.0	100.0
M	1705.1	389.6	22.8	82.0	89.0	96.0
N	813.8	99.8	12.3	100.0	100.0	100.0
P	1146.2	1004.1	87.6	44.0	51.0	62.0

Table A.5: continued

Site No.	Dry Matter (kg ha^{-1})	Std. dev. of D.M. (kg ha^{-1})	C.V. of D.M. (%)	Dry Matter Range at Confidence Level * ±125	±150	±200
	Seventh Sampling Period					
A	1462.7	652.3	44.6	62.0	67.0	82.0
B	1259.1	559.1	44.4	67.0	75.0	87.0
C	1511.4	413.6	27.4	82.0	87.0	96.0
D	1567.5	786.1	50.2	51.0	62.0	72.0
E	1116.1	597.6	92.3	62.0	72.0	84.0
F	685.1	67.1	9.8	100.0	100.0	100.0
G	776.7	98.6	12.7	100.0	100.0	100.0
H	740.7	299.7	40.5	92.0	96.0	100.0
J	827.4	87.2	10.5	100.0	100.0	100.0
K	749.4	245.2	32.7	96.0	99.0	100.0
L	976.1	151.2	15.5	100.0	100.0	100.0
M	1258.7	354.8	28.2	87.0	92.0	98.0
N	890.6	144.7	16.3	100.0	100.0	100.0
P	589.9	127.1	21.5	100.0	100.0	100.0

* 1-sided range for 2-sided t

Table A.6: Average Rangeland Production Values for 1988 CAZS Survey

Site	Dry Matter of Herbaceous Vegetation (kgha^{-1}) Sampling Period						
No.	1	2	3	4	5	6	7
A	49.1	233.9	955.0	1372.7	926.5	1354.8	1462.7
B	52.1	161.5	602.0	487.1	1259.6	852.5	1259.1
C	95.7	527.7	900.4	999.3	1450.1	1286.2	1511.4
D	36.3	396.6	639.0	624.1	953.9	1012.0	1567.5
E	89.8	141.6	604.7	1040.4	622.7	1061.1	647.8*
F	88.1	144.9	633.0	608.3	1093.1	644.6	685.1
G	67.1	201.6	1212.7	754.0	873.4	797.6	776.7
H	51.1	323.6	922.2	740.1	1054.4*	1193.7	740.7
J	64.2	173.4	915.8	843.0	1000.9	652.2	827.4
K	126.9	186.0	650.0	757.6	995.1	483.2	749.4
L	106.8	295.8	736.8	1816.7	1203.8	1306.5	976.1
M	107.8	131.2	989.9	1604.4	1314.8	1705.1	1258.7
N	30.9	63.4*	250.6	445.4	656.9	813.8	890.6
P	36.3	49.4	187.9	989.9	890.6	1146.2	589.9

Table A.7: Average Herbaceous Cover and Trees and Shrubs Counts for 1988 CAZS Survey

Site	Herbaceous Ground Cover (%) Sampling Period							Trees Shrubs (ha^{-1})	
No.	1	2	3	4	5	6	7	≤ 2m	> 2m
A	20	25	40	35	30	40	30	139	0
B	20	20	45	35	40	30	30	<1	0
C	30	55	50	50	50	45	45	11	<1
D	20	40	50	35	35	35	35	11	1
E	25	25	30	35	20	30	25	21	2
F	30	30	45	45	40	30	35	5	5
G	25	40	50	50	40	50	35	<1	<1
H	20	40	40	35	40	40	30	2	2
J	25	25	40	45	40	30	40	4	2
K	25	30	40	45	30	30	30	2	0
L	25	50	40	55	45	40	35	6	3
M	20	25	40	50	40	45	35	5	<1
N	10	15	35	35	30	45	35	10	0
P	10	15	25	35	40	30	25	10	<1

Table A.8: Estimated Herbaceous Production Levels for Transects of 1988 Field Survey

Site No.	Sample No.	Original Weight * (g)	Instrument Reading (average) (unitless)	M.C. of Sample ** (%)	Dry Matter Weight of Sample (g)	Dry Matter Production (average) (kg ha^{-1})
1	1	85	4.0	78.7	18.1	
	2	39	9.8	56.5	17.0	
	3	124	4.3	77.2	28.3	
	4	79	8.0	62.5	29.7	
	5***	152	11.3	54.4	69.3	
	6	87	8.0	62.5	32.7	
	7	93	15.7	40.1	55.8	
	8	33	17.0	37.2	20.7	
	9	30	23.2	26.0	22.2	1305
2	1	89	14.2	43.7	50.1	
	2	30	24.0	24.8	22.6	
	3***	101.5	12.0	66.5	34.0	
	4	28	22.3	27.4	20.3	
	5	40.5	29.0	18.6	33.0	1280
3	1	51	24.0	24.8	38.3	
	2	27	28.0	19.7	21.7	
	3***	85	23.7	45.5	46.3	
	4	33	33.8	14.1	28.3	
	5	91	10.0	55.7	40.4	1400
4	1	79	20.8	29.8	55.4	
	2	84	18.0	35.1	54.5	
	3***	37	30.3	36.8	23.4	
	4	93	18.7	33.4	61.9	
	5	84	18.3	34.6	55.0	2002
5	1	43	23.0	26.3	31.7	
	2	77	14.3	43.4	43.6	
	3***	43.5	27.0	23.6	33.2	
	4	39	26.0	22.1	30.4	
	5	76	34.0	13.9	65.4	1634
6	1	146	7.5	64.3	52.1	
	2	142	2.8	84.6	21.9	
	3***	226	3.8	58.3	94.3	
	4	96	9.3	58.1	40.2	
	5	173	25.0	23.4	132.5	2728

Table A.8: continued

Site No.	Sample No.	Original Weight * (g)	Instrument Reading (average) (unitless)	M.C. of Sample ** (%)	Dry Matter Weight of Sample (g)	Dry Matter Production (average) (kg ha^{-1})
7	1	32	17.5	36.1	20.4	
	2	89	14.0	44.2	49.7	
	3***	25	-	17.6	20.6	
	4	51	15.3	41.1	30.0	
	5	103	8.5	60.7	40.5	1290
8	1	20	31.0	16.6	16.7	
	2	97	8.5	60.7	38.1	
	3***	13	-	32.3	8.8	
	4	59	16.7	37.8	36.7	
	5	48	34.8	13.3	41.6	1135
9	1***	7	-	57.1	3.0	
	2***	4.5	-	22.2	3.5	
	3***	7.5	-	53.3	3.5	
	4***	13	-	50.9	6.4	
	5***	22.5	-	8.6	20.6	296
10	1	315	9.3	58.1	131.9	
	2	299	4.0	78.7	63.7	
	3***	181	4.3	63.0	66.9	
	4	116	4.5	76.4	27.3	
	5	174	5.0	74.3	44.8	2677
11	1	64	8.5	60.7	25.2	
	2	52	12.3	48.7	26.7	
	3***	133	31.5	13.1	115.6	
	4	58	17.5	36.1	37.1	
	5	76	22.0	27.8	54.8	2,075
12	1	52	16.5	38.2	32.1	
	2	55	15.8	39.9	33.0	
	3***	77	13.0	43.8	43.3	
	4	54	16.3	38.8	33.0	
	5	47	26.3	21.8	36.8	1426

Drying a 105° C for 24 hours

M.C. = 99.123 * $e^{-0.058*\text{nstrument rading}}$ (%)

* Weight of clipped off grass over 50cm by 50cm square.
Sample weight >10g: 100g spring balance (0.5g accuracy)
Sample weight <10g: 10g spring balance (0.1g accuracy)

** Moisture content determined by
M.C. = 99.123 * $\exp^{(-0.058 * \text{reading})}$ (%)

*** Moisture content determined by oven-drying samples.

\- Sample size too small for insrument reading.

Table A.9: Results of In-Field WILE 35 Moisture Meter Readings During 1988 ITE/Silsoe Field Survey

Transect No.	Sample No.	Original Weight * (g)	M.C. of Original Sample (%)	Instrument Reading in Field (unitless)
1/88	5	152.0	54.4	11.3
2/88	3	101.5	66.5	12.0
3/88	3	85.0	45.5	23.7
4/88	3	37.0	36.8	30.3
4/88	4	93.0	33.4	18.7
5/88	3	43.5	23.6	27.0
6/88	3	226.0	58.3	3.8
10/88	3	181.0	63.0	4.3
11/88	3	133.0	13.1	31.5
12/88	3	77.0	43.8	13.0

Drying a 105° C for 24 hours
* Weight of clipped off grass over 50cm by 50cm square.
Sample weight >10g: 100g spring balance (0.5g accuracy)
Sample weight <10g: 10g spring balance (0.1g accuracy)

Table A.10: Results of Laboratory WILE 35 Moisture Meter Readings During 1988 ITE/Silsoe Field Survey of Air-dired Samples

Transect No.	Sample No.	Original Weight * (g)	M.C. of Original Sample (%)	Instrument Reading at Laboratory (unitless)
1/88	5	41.3	10.5	33.3
2/88	3	37.9	10.4	36.8
3/88	3	28.3	9.2	39.3
4/88	3	13.3	9.7	37.5
4/88	4	44.9	9.6	41.7
5/88	3	27.9	9.7	40.0
6/88	3	39.8	9.8	40.5
7/88	3	22.9	10.1	40.5
8/88	3	9.8	10.2	39.5
9/88	1	3.4	11.8	38.0
9/88	2	3.9	10.3	35.5
9/88	3	3.9	10.3	**
9/88	4	7.2	11.3	33.0
9/88	5	22.5	8.6	39.8
10/88	3	26.2	11.1	39.0
11/88	3	56.7	9.6	41.5
12/88	3	32.8	9.2	41.5

* Weight of clipped off grass over 50cm by 50cm square.
Sample weight >10g: 100g spring balance (0.5g accuracy)
Sample weight <10g: 10g spring balance (0.1g accuracy)
** No instrument reading, material too brittly (herbs).

Table A.11: Calibration of WILE 35 to Moisture Content (Non-linear regression)

Transect No.	Sample No.	Weight of Sample (g)	M.C. of Sample (%)	Instrument Reading (unitless)	Calibrated M.C. ($e^{4.59} * e^{-0.058x}$)
6/88	3	226.0	58.3	3.8	79.6
10/88	3	181.0	63.0	4.3	77.3
1/88	5	152.0	54.4	11.3	51.6
2/88	3	101.5	66.5	12.0	49.6
12/88	3	77.0	43.8	13.0	46.8
4/88	4	93.0	33.4	18.7	33.7
3/88	3	85.0	45.5	23.7	25.2
5/88	3	43.5	23.6	27.0	20.9
4/88	3	37.0	36.8	30.3	17.2
11/88	3	133.0	13.1	31.5	16.1
9/88	4	7.2	11.3	33.0	14.8
1/88	5	41.3	10.5	33.3	14.5
9/88	2	3.9	10.3	35.5	12.8
2/88	3	37.9	10.4	36.8	11.8
4/88	3	13.3	9.7	37.5	11.4
9/88	1	3.4	11.8	38.0	11.1
10/88	3	26.2	11.1	39.0	10.4
3/88	3	28.3	9.2	39.3	10.3
8/88	3	9.8	10.2	39.5	10.1
9/88	5	22.5	8.6	39.8	10.0
5/88	3	27.9	9.7	40.0	9.9
6/88	3	39.8	9.8	40.5	9.6
7/88	3	22.9	10.1	40.5	9.6
12/88	3	32.8	9.2	41.5	9.0
11/88	3	56.7	9.6	41.5	9.0
4/88	4	44.9	9.6	41.7	8.9

Regression Output:

$\ln(y) = a * x + b$, $y = 99.123 * \exp^{-0.058*x}$

a = 4.5963

b = -0.0577

r^2 = 0.8913

Table A.12: Estimated Herbaceous Cover and Moisture Content of 1988 ITE/Silsoe Field Visit to Niger

Transect No.	Sample No.	Dry Matter Weight of Sample (g)	M.C. of Sample ** (%)	Vegetation Cover grass herbs (%)	bushes & trees < 2m No.	2-8m No.	Total No.
1	1	18.1	78.7	85	0	28	28
	2	17.0	56.5	50	5	13	18
	3	28.3	77.2	30	7	11	18
	4	29.7	62.5	70	18	2	20
	5***	69.3	54.4	80	5	10	15
	6	32.7	62.5	50	15	11	26
	7	55.8	40.1	85	7	4	11
	8	20.7	37.2	50	15	19	34
	9	22.2	26.0	70	27	0	27
2	1	50.1	43.7	90	22	3	25
	2	22.6	24.8	50	3	10	13
	3***	34.0	66.5	50	4	9	13
	4	20.3	27.4	30	16	12	28
	5	33.0	18.6	75	20	8	28
3	1	38.3	24.8	40	0	1	1
	2	21.7	19.7	25	0	0	0
	3***	46.3	45.5	20	0	0	0
	4	28.3	14.1	20	0	2	2
	5	40.4	55.7	45	10	25	35
4	1	55.4	29.8	50	5	5	10
	2	54.5	35.1	35	3	2	5
	3***	23.4	36.8	15	1	1	2
	4	61.9	33.4	50	5	9	14
	5	55.0	34.6	50	3	4	7
5	1	31.7	26.3	45	1	1	2
	2	43.6	43.4	25	3	0	3
	3	33.2	23.6	10	4	0	4
	4	30.4	22.1	40	12	8	20
	5	65.4	13.9	20	0	20	20
6	1	52.1	64.3	40	6	7	13
	2	21.9	84.6	50	0	5	5
	3	94.3	58.3	30	14	7	21
	4	40.2	58.1	40	2	3	5
	5	132.5	23.4	70	2	1	3
7	1	20.4	36.1	10	7	0	0
	2	49.7	44.2	10	13	9	22
	3	20.6	17.6	10	7	12	19
	4	30.0	41.1	10	4	7	11
	5	40.5	60.7	10	22	7	29

Table A.12: continued

Transect No.	Sample No.	Dry Matter Weight of Sample (g)	M.C. of Sample ** (%)	Vegetation Cover grass herbs (%)	bushes & trees < 2m No.	2-8m No.	Total No.
8	1	16.7	16.6	1	1	6	7
	2	38.1	60.7	1	6	9	15
	3	8.8	32.3	1	14	7	21
	4	36.7	37.8	1	3	4	7
	5	41.6	13.3	1	11	8	19
9	1	3.0	57.1	1	8	2	10
	2	3.5	22.2	1	7	0	7
	3	3.5	53.3	1	12	4	16
	4	6.4	50.9	1	6	9	15
	5	20.6	8.6	10	4	8	12
10	1	131.9	58.1	35	0	6	6
	2	63.7	78.7	25	0	0	0
	3	66.9	63.0	40	15	1	16
	4	27.3	76.4	40	2	2	4
	5	44.8	74.3	40	2	0	2
11	1	25.2	60.7	45	11	11	22
	2	26.7	48.7	50	15	14	29
	3	115.6	13.1	40	33	11	44
	4	37.1	36.1	50	7	15	22
	5	54.8	27.8	55	15	26	41
12	1	32.1	38.2	65	24	8	32
	2	33.0	39.9	50	16	13	29
	3	43.3	43.8	40	16	15	31
	4	33.0	38.8	35	8	15	23
	5	36.8	21.8	40	21	12	33

Drying a 105° C for 24 h
* Weight of clipped off grass over 50cm by 50cm square.
  Sample weight >10g: 100g spring balance (0.5g accuracy)
  Sample weight <10g: 10g spring balance (0.1g accuracy)
** Moisture content determined by
  $M.C. = 99.123 * \exp^{-0.058*reading}$ (%)
*** Moisture content determined by oven-drying samples.
- Sample size too small for insrument reading.

Table A.13: Variations in Dry Matter Production for Samples of 1985 and 1988 ITE/Silsoe Field Survey in Niger

Site No.	No. of Sample Points	Dry Matter Production ($kgha^{-1}$)	Standard Deviation ($kgha^{-1}$)	Range of Mean at 95% conf. level	Coeff. of Variat. (%)
A/85	9	1452	414.1	338	28.5
B/85	10	604	314.4	237	52.0
C/85	9	374	369.5	302	98.7
D/85	10	38	60.7	46	161.5
H/85	8	383	553.0	493	144.4
1/88	9	1306	723.2	591	55.4
2/88	5	1280	472.4	657	36.9
3/88	5	1400	394.7	549	28.2
4/88	5	2002	607.8	845	30.4
5/88	5	1634	587.1	816	35.9
6/88	5	2728	1789.1	2487	65.6
7/88	5	1290	511.4	711	39.7
8/88	5	1135	585.9	814	51.6
9/88	5	296	300.0	417	101.4
10/88	5	2677	1586.4	2205	59.3
11/88	5	2075	1501.1	2086	72.3
12/88	5	1426	186.0	259	13

Table A.14: Relation Between Dry Matter Production and Class Width for 1985 and 1988 ITE/Silsoe Field Surveys

Site	D.M. Prod.	No. of Samples for Class Width: 200$kgha^{-1}$ | 250$kgha^{-1}$ | 300 $kgha^{-1}$ — Reliability of Sample for Confidence Level (%)								
No.	$kgha^{-1}$	80%	70%	60%	80%	70%	60%	80%	70%	60%
A/85	1452	29	20	13	20	13	9	14	10	7
B/85	604	18	12	8	12	8	6	9	6	4
C/85	374	24	16	11	16	118	8	12	8	6
D/85	38	2	2	1	6	2	1	2	2	1
H/85	383	52	34	23	34	23	15	24	16	11
1/88	1306	88	58	38	57	37	24	40	27	18
2/88	1280	38	25	17	25	17	12	18	12	8
3/88	1400	27	18	12	18	12	8	13	9	6
4/88	2002	62	41	27	41	27	18	29	19	13
5/88	1634	58	38	26	38	25	17	27	18	12
6/88	2728	>100	>100	>100	>100	>100	>100	>100	>100	>100
7/88	1290	55	30	20	29	19	13	21	14	10
8/88	1135	59	38	26	38	25	17	27	18	12
9/88	296	16	11	8	11	8	6	8	6	4
10/88	2677	>100	>100	>100	>100	>100	>100	>100	80	
11/88	2075	>100	>100	>100	>100>	100	>100	>100	72	
12/88	1426	7	5	4	5	4	3	4	3	19

Table A.15: Image and GPS Co-ordinates of 1988/89 ITE/Silsoe Sample Sites (Starting Points)

Survey 1988 Site	Survey 1989 Site	From Image UTM E	From Image UTM N	From GPS UTM E	From GPS UTM N	Distance (m)
1/88	1/89	812.7	1695.6	813.0	1696.3	738
2/88	2/89	814.4	1697.8			*
3/88	3/89	812.1	1701.6			*
4/88		809.8	1707.0			*
	4/89			808.5	1701.6	*
5/88	5/89	813.3	1701.9			*
6/88	6/89	801.3	1747.7	799.2	1745.3	3246
7/88	7/89	795.3	1734.1	792.3	1730.8	4551
8/88		794.6	1718.9			*
9/88		796.7	1698.9			*
10/88	10/89	797.9	1689.2	798.3	1689.3	444
11/88	11/89	800.1	1684.2	793.2	1685.9	7105
12/88	12/89	802.2	1682.9	801.3	1683.2	993
	13/89			792.2	1734.5	*
	14/89			793.1	1737.4	*
	15/89			794.1	1696.1	*
	16/89			810.8	1692.1	*
	17/89			810.2	1694.0	*
	18/89			811.4	1703.2	*

* No difference could be computed.

Table A.16: Relationship Between Fresh Weight and Oven-dried M.C. for Individual Sites of Both Sampling Periods of 1989 CASTE/ITE/Silsoe Field Survey

Site No.	Oven-Dried M. C. Avg. M.C. (%)	Std. Dev. (%)	Std. Error	Fresh Weight Avg. Weight (gm^{-2})	Std. Dev. (gm^{-2})	Linear Regression Coeff. corr. r	Slope ($\%m^2g^{-1}$)	Const.	Sig. T (%)
	First Sampling Period								
1	68.5	4.36	4.11	237.3	28.2	0.41	0.099	45.1	0.36
2	66.5	2.35	2.49	333.8	269.2	0.15	0.003	65.4	0.51
3	58.8	8.46	9.41	185.0	82.8	0.17	-0.043	66.7	0.58
4	64.7	5.28	5.56	264.5	275.6	0.11	0.006	63.0	0.52
5	64.3	8.38	2.43	103.5	23.6	0.94	-0.346	100.1	0.03
6	76.2	2.57	2.78	464.0	118.8	0.12	0.007	72.8	0.57
7	73.6	3.17	3.34	187.6	65.3	0.17	0.020	69.9	0.50
10	70.2	3.59	3.76	180.1	63.8	0.18	0.024	65.9	0.48
11	72.8	4.31	4.97	99.4	21.1	0.00	0.012	71.6	0.92
12	58.5	2.65	2.99	159.3	68.8	0.04	-0.008	59.8	0.73
	Second Sampling Period								
1	59.4	6.29	7.54	344.3	170.8	0.04	-0.007	61.9	0.80
2	58.5	5.72	5.33	318.3	143.0	0.42	0.026	50.2	0.35
3	57.7	7.28	7.59	193.6	74.4	-0.28	-0.048	67.0	0.47
4	61.0	9.13	6.80	243.1	175.9	0.58	-0.040	70.6	0.83
5	58.4	3.90	4.77	163.8	27.8	0.01	-0.010	60.0	0.93
6	75.0	3.57	4.85	299.0	308.4	0.08	0.003	74.0	0.82
7	68.4	6.39	6.81	175.6	78.0	0.15	0.032	59.3	0.52
10	61.1	2.86	3.29	241.0	57.8	0.01	-0.005	62.3	0.88
11	69.5	1.85	1.85	148.1	25.2	0.33	0.042	59.0	0.42
12	54.2	4.65	4.97	160.8	64.0	0.14	0.027	49.8	0.53
13	66.5	1.63	1.55	186.6	87.0	0.33	-0.011	68.5	0.31
14	73.6	2.51	2.70	252.3	148.7	0.13	0.006	72.1	0.55
15	53.7	6.32	7.03	83.4	35.3	0.07	-0.048	57.7	0.66
16	52.2	5.30	5.68	222.8	54.4	0.14	-0.036	60.3	0.54
17	56.0	10.13	9.82	264.9	226.8	0.29	-0.024	62.4	0.34
18	53.0	7.83	5.14	180.9	107.5	0.71	0.061	41.9	0.16

Sig. T: Probability to observe a larger/smaller correlation coefficient when assuming that there is no linear relation in the population (reject null hypothesis).

Table A.17: Results of 1989 CASTE/ITE/Silsoe Field Survey (Averages from all Sites)

Site No.	Cover (%)	Height (cm)	Soil Colour	Oven M.C.	D.M. $kgha^{-1}$	Bushes & Trees <2m	>2m
	First Sampling Period						
1	17.6	23.5	10/7/6	68.5	741	263	84
2	16.7	24.7	10/7/6	66.6	858	107	62
3	15.0	17.5	75/6/8	56.0	785	52	39
4	19.1	26.9	10/7/8	64.7	894	100	79
5	9.3	15.7	10/7/6	61.3	500	0	0
6	8.7	22.0	75/6/6	75.7	976	338	17
7	10.0	21.5	10/7/6	73.7	515	128	107
10	6.0	17.5	10/7/6	70.2	529	39	9
11	7.5	13.0	10/8/4	72.8	269	161	255
12	5.7	20.0	75/6/4	58.5	664	27	150
	Second Sampling Period						
1	10.0	19.4	75/6/6	59.4	1414	97	36
2	7.5	36.9	75/6/6	58.4	1283	38	47
3	5.6	20.0	75/6/6	65.6	673	19	15
4	10.1	27.5	10/7/6	61.0	1046	19	15
5	9.2	19.2	75/6/6	58.4	682	20	0
6	2.6	17.8	75/7/6	75.0	726	93	30
7	7.5	25.3	10/7/6	64.9	601	105	67
10	9.3	20.8	10/7/6	61.2	937	-	-
11	12.0	17.3	10/7/4	69.5	755	337	287
12	7.3	33.0	10/7/6	54.2	727	52	126
13	5.8	17.5	75/7/6	66.6	630	58	30
14	6.3	30.3	10/7/6	73.6	655	148	190
15	6.7	19.4	75/7/8	53.6	391	70	2
16	6.5	29.5	10/7/6	52.2	1073	761	15
17	4.3	28.5	10/7/8	56.0	1266	154	7
18	8.9	24.2	10/6/6	53.0	797	34	10

Soil Colour Class: according to Munsell Soil Colour Chart
Order: Hue YR / Value / Chroma
- : not counted

Table A.18: Standard Deviation, Coefficient of Variation and Standard Error of the Mean for Herbaceous Rangeland Vegetation of 1989 CASTE/ITE/Silsoe Field Survey

Site No.	Samples No.	D.M. estim. $kgha^{-1}$	Std. dev. $kgha^{-1}$	C.V. (%)	Std. Error of Mean 95% $kgha^{-1}$	80% $kgha^{-1}$	60% $kgha^{-1}$
	First Sampling Period						
1	17	768	558	72	301	185	119
2	15	880	818	92	470	289	185
3	8	667	343	51	260	163	105
4	16	1036	980	94	546	336	215
5	14	687	400	58	238	146	94
6	10	757	504	66	332	211	137
7	20	565	301	53	155	94	59
10	10	522	115	22	77	49	31
11	10	415	198	47	132	83	54
12	10	642	229	35	154	97	62
	Second Sampling Period						
1	17	999	497	49	254	160	104
2	8	1300	457	35	342	216	139
3	20	558	299	53	139	88	57
4	10	1239	1280	103	844	536	348
5	11	750	384	51	242	153	99
6	15	386	481	124	262	165	107
7	20	666	332	49	158	99	64
10	20	799	201	25	94	59	38
11	19	689	396	57	189	120	78
12	19	736	252	34	120	76	49
13	20	649	766	118	377	232	150
14	20	603	483	80	241	148	95
15	17	554	220	39	123	74	47
16	20	895	239	26	111	70	46
17	20	996	655	65	305	194	126
18	16	1051	399	38	208	132	85

Table A.19: Classes of Soil Colour and Average Rangeland Production for 1989 CASTE/ITE/Silsoe Field Survey

Soil Colour	Average Rangeland Production						
Class	Period 1	Std.	Cases	Period 2	Std.	Cases	Avg. 1&2
10/5/8	1414	633.6	6	768	140.0	4	983
10/6/6	919	698.2	12	988	771.4	22	963
10/6/8	508	142.7	3	1105	970.2	8	942
10/6/4	486	258.2	3	963	501.8	13	874
7.5/6/6	849	714.1	17	876	544.6	38	868
7.5/6/4	681	254.0	11	1720	-.-	1	768
10/7/6	676	466.5	32	573	386.2	86	733
10/7/8	416	283.6	7	824	327.9	23	729
10/7/4	798	984.4	6	568	398.2	10	654
7.5/7/6	1133	1100.2	6	560	622.2	38	638
7.5/7/8	745	72.1	2	543	235.0	7	588
7.5/6/8	531	71.0	4	637	441.9	3	576
10/8/6	283	213.5	2	682	480.3	3	522
10/8/4	408	137.8	5	-	-.-	0	408

Soil Colour Class: according to Munsell Soil Colour Chart
Order: Hue YR / Value / Chroma
Std.: Standard deviation
Total No. samples: 368

Table A.20: Landsat MSS and NOAA AVHRR LAC Data Used for Geometric Correction and Image to Ground Data Correlation

Survey	Satellite	Comments
CIPEA	Landsat TM Path Row Date 190 49 11.06.84	Driest season in 1980s. No features apart from rocks.
	Landsat MSS 190 49 20.05.85	Dry season image, blurred by atmospheric particles from Harmattan. Used as reference for geometric correction.
	NOAA AVHRR LAC Position* Date	
	+ 450 21.08.85	many small clouds
	+ 250 22.08.85	no clouds
	+ 600 30.08.85	partial cloud cover
	+ 350 31.08.85	almost cloud free
	+ 350 10.09.85	very hazy
ITE/Silsoe	Landsat MSS Path Row Date 191 49 07.10.84	Used as reference image for geometric corrections.
	191 49 11.05.85	Dry season, featureless.
	191 49 31.08.85	Corresponds to field survey.
	191 49 08.09.88	Corresponds to field survey.
1985	NOAA AVHRR LAC Position* Date	
	26.06.85	not used (cloud cover)
	06.07.85	not used (too far off-nadir)
	14.07.85	not used (wrong area(
	+ 350 21.08.85	many small clouds
	+ 100 22.08.85	partial cloud cover
	+ 500 30.08.85	partial cloud cover
	+ 200 31.08.85	Corresponds to Landsat MSS. almost cloud free
	03.09.85	not used (wrong area)
	09.09.05	not used (tape error)
	+ 200 10.09.85	hazy, partial cloud cover
	17.09.85	not used (too far off-nadir)
	18.09.85	not used (too far off-nadir)

Table A.20: continued

Survey	Satellite		Comments
ITE/Silsoe		06.07.88	not used (cloud cover)
1988	+ 550	04.07.88	almost cloud free
	- 50	15.07.88	clear image
	+ 50	24.07.88	clear image
	+ 400	01.08.88	partial cloud cover
	- 250	03.08.88	partial cloud cover
	- 50	20.08.88	small clouds, hazy
	+ 550	06.09.88	hazy, massive cloud cover
		25.09.88	not used (cloud cover)
	+ 300	05.10.88	hazy, cloud free
	- 250	15.10.88	clear image
	- 280	24.10.88	cloud free, haze
	+ 650	30.10.88	very hazy
CAZS	Landsat MSS Path Row Date 192 49 20.09.84		Used as reference image for geometric corrections.
	NOAA AVHRR LAC Position* Date		
	+ 100	07.06.88	cloud free
	+ 300	04.07.88	almost cloud free
	- 400	15.07.88	clear image
	- 300	24.07.88	largely cloud covered
	+ 50	01.08.88	partial cloud cover
	- 550	03.08.88	almost cloud free
	- 200	20.08.88	small clouds, hazy
	+ 200	06.09.88	partial cloud cover
		25.09.88	not used (cloud cover)
	- 200	05.10.88	hazy, cloud free
		15.10.88	not used (cloud cover)
	- 600	24.10.88	cloud free, haze
		30.10.88	not used (too late)

* -: Survey Centre located No. of pixels West of nadir
+: Survey Centre located No. of pixels East of nadir

Table A.21: Ratio Between Bright and Dark Soil Surfaces for NOAA AVHRR Images for CIPEA, 1985 ITE/Silsoe, CAZS and 1988 ITE/Silsoe Field Surveys

Date	Quar-tile	Average Spectral Albedo Date Ch 1	Date Ch 2	Reference Ch 1	Reference Ch 2	Relative Scene Contrast Date	Reference
	CIPEA 1985 (31 August 1985)						
21.08.85	High	29.6	32.9	28.8	32.8	1.29	1.32
	Low	23.0	25.6	21.8	25.4		
22.08.85	High	29.6	32.9	28.8	32.8	1.27	1.32
	Low	23.2	25.9	21.8	25.4		
30.08.85	High	32.1	35.6	27.4	31.9	1.25	1.29
	Low	25.8	28.9	21.2	25.8		
10.09.85	High	30.0	35.5	28.0	32.4	1.20	1.29
	Low	25.0	29.3	21.8	25.6		
	ITE/Silsoe 1985 (31 August 1985)						
21.08.85	High	28.6	31.7	26.4	29.8	2.15	2.23
	Low	13.3	13.1	11.8	11.9		
22.08.85	High	26.1	29.6	28.5	32.4	1.50	1.58
	Low	17.4	19.4	18.1	20.4		
30.08.85	High	27.7	30.3	25.4	29.0	1.57	1.81
	Low	17.7	18.4	14.0	15.0		
10.09.85	High	25.1	29.1	25.8	29.3	1.69	1.84
	Low	14.8	16.1	14.0	15.1		
	CAZS 1988 (3 August 1988)						
06.07.88	High	24.5	27.1	24.0	25.1	1.40	1.80
	Low	13.6	13.9	17.2	19.7		
04.07.88	High	26.3	29.1	24.0	26.3	1.55	1.93
	Low	13.6	14.0	15.5	16.3		
15.07.88	High	26.4	29.2	28.5	31.5	1.41	1.90
	Low	13.9	14.4	20.3	21.1		
01.08.88	High	26.6	29.5	24.0	26.5	1.80	1.94
	Low	13.7	14.0	13.4	13.8		
20.08.88	High	27.0	29.7	24.6	27.8	1.88	1.96
	Low	13.8	14.2	13.1	13.5	CLOUD!	
06.09.88	High	28.0	30.9	23.4	26.2	1.46	1.90
	Low	14.7	15.5	16.0	16.8		
25.09.88	High	27.1	30.0	20.3	23.4	1.40	1.83
	Low	14.9	15.7	14.5	14.9		
05.10.88	High	25.9	28.4	26.1	29.9	1.49	1.86
	Low	13.9	14.2	17.4	18.0		
15.10.88	High	23.6	25.5	22.4	25.5	1.74	1.81
	Low	13.0	13.2	12.9	13.2		

Table A.21: continued

Date	Quar-tile	Average Spectral Albedo Date Ch 1	Ch 2	Reference Ch 1	Ch 2	Relative Scene Contrast Date	Reference
ITE/Silsoe 1988 (3 August 1988)							
04.07.88	High	18.4	21.8	21.7	23.1	1.55	1.83
	Low	10.1	11.1	14.0	13.9		
15.07.88	High	18.6	21.5	22.6	25.1	1.29	1.85
	Low	10.1	11.1	17.6	17.8		
01.08.88	High	18.3	21.4	20.2	22.7	1.48	1.81
	Low	10.1	11.7	13.6	16.4		
*20.08.88	High	22.9	27.6	23.1	27.4	1.84	2.02
	Low	11.3	12.2	12.6	15.5		
06.09.88	High	19.4	22.7	16.9	20.7	1.29	1.85
	Low	10.5	11.5	13.1	15.7		
05.10.88	High	18.7	22.0	18.8	22.0	1.33	1.82
	Low	10.3	11.9	14.2	16.7		
24.10.88	High	18.7	22.0	15.5	19.2	1.64	1.82
	Low	10.3	11.9	9.5	11.8		
30.10.88	High	19.5	22.9	14.0	15.1	1.27	1.84
	Low	10.6	12.1	11.1	11.7		

* Only 4 values to compare!

Table A.22: Relationships Between Landsat MSS Spectral Reflectances Obtained from Five Different Image Sampling Methods for 1985 CIPEA Survey for Shifted Image and Without Site No. 2

Method Dependent	Method Independent Variable							
	Including Site No. 2				Without Site No. 2			
	B1xB1	B2xB2	B3xB3	B4xB4	B1xB1	B2xB2	B3xB3	B4xB4
50m	Site Average							
Coeff.	1.00	1.02	1.02	1.03				
Const.	-0.01	-0.42	-0.66	-0.87				
r^2	0.99	0.99	1.00	1.00				
50m	Central Central							
Coeff.	0.85	0.72	0.43	0.63	0.91	0.90	0.52	0.64
Const.	3.37	6.23	14.41	9.68	2.58	3.01	12.86	9.96
r^2	0.44	0.26	0.09	0.22	0.60	0.57	0.31	0.49
50m	3x3 Average							
Coeff.	1.09	1.16	1.15	1.10				
Const.	-2.00	-3.20	-3.61	-2.52				
r^2	0.85	0.78	0.77	0.79				
50m	Transect				Transect			
Coeff.	0.77	0.62	0.55	0.61	0.81	0.72	0.58	0.62
Const.	4.96	7.65	11.08	10.00	4.05	5.45	10.15	9.71
r^2	0.88	0.76	0.69	0.76	0.88	0.78	0.52	0.60
Central	3x3 Average				3x3 Average			
Coeff.	0.82	4.89	0.58	0.60	0.90	0.99	1.33	1.53
Const.	4.07	0.77	10.44	10.19	1.73	-0.18	-8.80	-14.4
r^2	0.57	0.52	0.28	0.31	0.78	0.89	0.86	0.94
Central	Transect				Transect			
Coeff.	0.86	0.84	0.68	0.72	0.89	0.93	0.73	0.72
Const.	3.13	3.36	7.92	7.21	2.62	1.69	7.06	7.38
r^2	0.66	0.69	0.51	0.58	0.78	0.91	0.91	0.98

Table A.23: Relationships Between Landsat MSS Spectral Reflectances Obtained from Five Different Image Sampling Methods for 1988 CAZS Field Survey for GPS Transect Positions

Method Dependent	Method Independent Variable B1xB1	B2xB2	B3xB3	B4xB4	B1xB1	B2xB2	B3xB3	B4xB4
50m	20x20				Central			
Coeff.	1.04	1.07	1.06	1.05	0.79	0.77	0.79	0.78
Const.	-0.76	-1.59	-1.47	-1.38	4.38	5.01	5.22	5.43
r^2	0.99	0.97	0.97	0.97	0.83	0.70	0.61	0.59
50m	3x3 Average				*			
Coeff.	0.79	1.01	0.96	1.05				
Const.	5.26	-0.25	0.80	-1.38				
r^2	0.60	0.90	0.78	0.72				
Central	3x3 Average				*			
Coeff.	1.25	1.26	1.26	1.26				
Const.	-5.39	-5.61	-6.57	-6.75				
r^2	0.97	0.94	0.91	0.91				

* Transect Sampling Method not applied.

Table A.24: Relationships Between Landsat MSS Spectral Reflectances Obtained from Five Different Image Sampling Methods for 1988 ITE/Silsoe Field Survey for Shifted Image and Without Site No. 2

Method Dependent	Method Independent Variable B1xB1	B2xB2	B3xB3	B4xB4	B1xB1	B2xB2	B3xB3	B4xB4
50m	20x20				Central			
Coeff.	1.02	1.04	0.98	0.97	0.82	0.82	0.89	0.92
Const.	-0.4	-0.7	0.3	0.5	2.7	2.8	2.0	1.6
r^2	0.95	0.95	0.96	0.97	0.76	0.76	0.88	0.92
50m	3x3 Average				Transect			
Coeff.	0.71	0.69	0.89	0.93	0.85	0.82	0.92	0.98
Const.	4.3	4.6	2.0	1.3	2.1	2.6	1.4	0.2
r^2	0.64	0.59	0.79	0.73	0.71	0.65	0.84	0.89
Central	3x3 Average				Transect			
Coeff.	0.91	0.92	0.99	0.99	1.05	1.06	1.03	1.05
Const.	1.3	1.0	0.1	0.2	-0.9	-1.1	-0.7	-1.1
r^2	0.93	0.93	0.89	0.76	0.97	0.96	0.96	0.93

Table A.25: Relationships Between Landsat MSS Spectral Reflectances and NOAA AVHRR Spectral Albedos for 1985 CIPEA Field Survey Sites (3 by 3 Averages)

AVHRR	CH 1				CH 2				
MSS	B 1	B 2	B 3	B 4	B 1	B 2	B 3	B 4	B3,4
	21 August 1985								
Coeff.	0.31	0.26	0.02	-0.11	-0.19	-0.23	-0.03	0.09	0.03
Const.	15.5	15.7	25.0	28.6	27.5	27.8	26.4	23.9	25.1
r^2	0.21	0.19	0.00	0.05	0.09	0.15	0.00	0.04	0.00
	22 August 1985								
Coeff.	0.18	0.22	0.08	0.01	0.21	0.34	0.19	0.11	0.15
Const.	17.7	16.1	23.4	26.2	15.6	11.0	19.6	23.0	21.3
r^2	0.34	0.57	0.14	0.00	0.11	0.33	0.18	0.06	0.12
	30 August 1985								
Coeff.	-0.08	0.31	-0.16	0.11	-1.02	-0.57	2.19	2.08	2.14
Const.	24.2	14.4	28.6	23.7	50.9	37.2	-35.3	-31.5	-33.4
r^2	0.00	0.03	0.01	0.02	0.42	0.15	0.60	0.57	0.59
	31 August 1985								
Coeff.	1.21	1.17	0.96	0.08	1.58	0.90	0.88	0.90	0.89
Const.	-4.6	-4.7	3.9	24.6	-20.6	-3.2	1.7	2.0	1.8
r^2	0.81	0.86	0.55	0.00	0.33	0.13	0.62	0.62	0.64
	10 September 1985								
Coeff.	0.08	0.16	0.15	-0.13	-0.09	0.04	0.20	0.19	0.20
Const.	20.2	17.9	22.1	29.0	24.4	20.4	20.3	21.3	20.8
r^2	0.03	0.11	0.09	0.11	0.02	0.00	0.16	0.15	0.16

Table A.26: Relationships Between Landsat MSS Spectral Reflectances (31.08.85) and NOAA AVHRR Spectral Albedos (31.08.85) Obtained from Five Different Image Sampling Methods for 1985 CIPEA Field Survey Sites

Sensor	AVHRR	CH 1			CH 2		
	MSS	B 1	B 2	B 3	B 3	B 4	B 3,4
Method	Landsat MSS 50m Transect Sampling						
Central	Coeff.	1.45	1.66	1.45	1.50	1.59	1.55
	Const.	-10.0	-15.1	-6.7	-14.9	-16.5	-15.8
	r^2	0.74	0.88	0.63	0.80	0.92	0.89
3x3 Average	Coeff.	1.45	1.65	1.47	1.40	1.36	1.38
	Const.	-9.9	-15.0	-7.2	-12.0	-10.2	-11.1
	r^2	0.73	0.87	0.65	0.80	0.77	0.81
Transect	Coeff.	1.41	1.61	1.41	1.25	1.33	1.30
	Const.	-8.9	-13.9	-5.6	-8.2	-9.6	-9.0
	r^2	0.76	0.91	0.65	0.69	0.80	0.77
	Landsat MSS 20 x 20 Averages						
Central	Coeff.	1.46	1.66	1.43	1.47	1.55	1.51
	Const.	-10.1	-15.1	-6.2	-14.1	-15.3	-14.7
	r^2	0.75	0.92	0.65	0.81	0.93	0.90
3x3 Average	Coeff.	1.45	1.64	1.45	1.35	1.33	1.34
	Const.	-9.8	-14.7	-6.5	-10.7	-9.4	-10.1
	r^2	0.73	0.90	0.66	0.79	0.79	0.81
Transect	Coeff.	1.41	1.59	1.39	1.23	1.31	1.27
	Const.	-8.8	-13.5	-5.0	-7.5	-8.8	-8.2
	r^2	0.76	0.93	0.66	0.70	0.82	0.78
	Landsat MSS 1.1km Central Pixels						
Central	Coeff.	1.24	1.19	0.96	0.98	1.03	1.00
	Const.	-5.7	-5.4	3.7	-1.4	-1.9	-1.7
	r^2	0.76	0.70	0.36	0.44	0.49	0.48
3x3 Average	Coeff.	1.17	1.11	0.89	0.72	0.71	0.71
	Const.	-4.1	-3.6	5.1	5.7	6.7	6.2
	r^2	0.66	0.60	0.31	0.28	0.27	0.28
Transect	Coeff.	1.13	1.09	0.87	0.73	0.80	0.77
	Const.	-3.1	-3.0	5.8	5.2	4.2	4.7
	r^2	0.68	0.64	0.32	0.31	0.36	0.34

Table A.26: continued

Sensor	AVHRR	CH 1			CH 2		
	MSS	B 1	B 2	B 3	B 3	B 4	B 3,4
	Landsat MSS 1.1km, 3 x 3 Averages						
Central	Coeff.	1.22	1.21	0.96	1.03	1.08	1.06
	Const.	-4.9	-5.5	4.0	-2.5	-3.1	-2.8
	r^2	0.84	0.92	0.55	0.75	0.80	0.79
3x3 Average	Coeff.	1.21	1.17	0.96	0.88	0.90	0.89
	Const.	-4.6	-4.7	3.9	1.7	2.0	1.8
	r^2	0.81	0.86	0.55	0.62	0.62	0.64
Transect	Coeff.	1.14	1.12	0.89	0.85	0.92	0.89
	Const.	-2.9	-3.4	5.6	2.5	1.2	1.9
	r^2	0.79	0.86	0.51	0.62	0.71	0.69
	Landsat MSS 1.1km, Transect Sampling						
Central	Coeff.	1.24	1.21	0.91	0.80	0.88	0.84
	Const.	-5.5	-5.5	4.9	3.5	2.2	2.8
	r^2	0.80	0.79	0.51	0.46	0.57	0.53
3x3 Average	Coeff.	1.19	1.13	0.86	0.63	0.67	0.65
	Const.	-4.4	-3.9	5.9	8.1	8.0	8.0
	r^2	0.73	0.69	0.46	0.33	0.37	0.37
Transect	Coeff.	1.16	1.12	0.84	0.61	0.72	0.67
	Const.	-3.4	-3.5	6.6	8.6	6.7	7.6
	r^2	0.76	0.75	0.47	0.33	0.46	0.41

Table A.27: Relationships Between Landsat MSS Spectral Reflectances (31.08.85) and NOAA AVHRR Spectral Albedos (31.08.85) Obtained from Five Different Image Sampling Methods for 1985 CIPEA Field Survey Sites for Shifted Image and Without Site No. 2

Sensor	AVHRR	CH 1			CH 2		
	MSS	B 1	B 2	B 3	B 3	B 4	B 3,4
Method	Landsat MSS 50m Transect Sampling						
Central	Coeff.	1.54	1.62	0.98	1.49	2.05	1.77
	Const.	-11.9	-14.3	4.00	-14.6	-29.0	-21.9
	r^2	0.69	0.83	0.47	0.49	0.86	0.72
3 x 3	Coeff.	1.67	1.74	0.99	2.01	2.13	2.07
	Const.	-14.9	-16.8	3.80	-28.8	-31-1	-30-0
	r^2	0.70	0.82	0.41	0.56	0.58	0.62
	Landsat MSS 50m resolution, 20 x 20 Averages						
Central	Coeff.	1.58	1.69	0.98	1.49	1.87	1.68
	Const.	-12.9	-15.7	4.1	-14.6	-24.1	-19.3
	r^2	0.72	0.90	0.49	0.52	0.84	0.72
3 x 3	Coeff.	1.72	1.80	0.98	1.89	1.90	1.89
	Const.	-16.0	-18.4	4.0	-25.4	-24.8	-25.1
	r^2	0.72	0.88	0.42	0.52	0.54	0.57
	Landsat MSS 1.1km resolution, central pixel						
Central	Coeff.	1.43	1.27	0.65	1.07	1.39	1.23
	Const.	-10.2	-7.3	10.6	-3.9	-11.7	-7.9
	r^2	0.83	0.73	0.18	0.22	0.33	0.29
3 x 3	Coeff.	1.48	1.49	0.55	0.41	0.49	0.45
	Const.	-11.3	-7.6	12.8	13.9	12.6	13.2
	r^2	0.76	0.64	0.11	0.02	0.03	0.02
	Landsat MSS 1.1km resolution, 3 x 3 average						
Central	Coeff.	1.44	1.36	0.62	0.97	1.02	1.00
	Const.	-9.7	-8.8	11.7	-0.7	-1.4	-1.1
	r^2	0.86	0.91	0.34	0.37	0.45	0.44
3 x 3	Coeff.	1.56	1.43	0.60	0.79	0.61	0.70
	Const.	-12.6	-10.4	12.2	3.9	9.9	6.9
	r^2	0.87	0.86	0.27	0.16	0.10	0.14

Table A.28: Relationships Between Landsat MSS Spectral Reflectances (31.08.85) and NOAA AVHRR Spectral Albedos for 1985 ITE/Silsoe Field Survey Sites (3 by 3 Averages)

AVHRR	CH 1				CH 2				
MSS	B 1	B 2	B 3	B 4	B 1	B 2	B 3	B 4	B3,4
	21 August 1985								
Coeff.	-0.09	-0.10	-0.29	-0.36	-0.16	-0.16	-0.31	-0.34	-0.32
Const.	21.2	20.9	29.1	31.8	23.7	23.2	31.2	33.3	32.3
r^2	0.23	0.30	0.62	0.66	0.40	0.40	0.37	0.32	0.34
	22 August 1985								
Coeff.	-0.01	-0.03	-0.13	-0.18	-0.02	-0.04	-0.17	-0.23	-0.20
Const.	19.6	19.4	26.9	29.5	20.1	20.0	29.0	32.1	30.6
r^2	0.03	0.10	0.62	0.76	0.05	0.13	0.66	0.77	0.73
	30 August 1985								
Coeff.	-0.07	-0.05	0.03	0.09	-0.06	-0.04	0.09	0.16	0.13
Const.	21.1	20.0	21.6	21.2	20.9	19.7	19.6	18.5	19.0
r^2	0.29	0.16	0.02	0.08	0.14	0.06	0.10	0.21	0.16
	31 August 1985								
Coeff.	0.90	1.02	2.01	2.24	0.24	0.31	0.92	1.14	1.04
Const.	1.0	-1.9	-17.9	-21.5	13.2	10.8	-0.4	-4.8	-2.7
r^2	0.63	0.78	0.79	0.68	0.24	0.41	0.93	0.98	0.97
	10 September 1985								
Coeff.	0.30	0.33	0.82	1.00	0.16	0.20	0.51	0.62	0.57
Const.	13.1	11.9	5.7	3.3	15.1	13.8	9.9	8.4	9.2
r^2	0.43	0.50	0.84	0.85	0.36	0.50	0.89	0.90	0.91

Table A.29: Relationships Between Landsat MSS (31.08.85) Spectral Reflectances and NOAA AVHRR (31.08.85) Spectral Albedos Obtained from Five Different Image Sampling Methods for 1985 ITE/Silsoe Field Survey Sites (3 by 3 Averages)

Sensor	AVHRR	CH 1			CH 2		
	MSS	B 1	B 2	B 3	B 3	B 4	B 3,4
Method	Landsat MSS 50m Transect Sampling						
Central	Coeff.	1.71	1.73	2.01	1.22	1.48	1.35
	Const.	-15.2	-16.3	-18.5	-7.8	-13.3	-10.6
	r^2	0.78	0.73	0.40	0.76	0.78	0.78
3x3 Average	Coeff.	1.56	1.59	2.28	1.03	1.26	1.15
	Const.	-12.1	-13.3	-23.7	-3.5	-8.2	-5.9
	r^2	0.83	0.79	0.65	0.74	0.77	0.76
Transect	Coeff.	1.22	1.42	1.88	0.95	1.16	1.06
	Const.	-5.1	-9.7	-15.4	-2.0	-6.3	-4.2
	r^2	0.50	0.61	0.43	0.66	0.68	0.68
	Landsat MSS 20 x 20 Averages						
Central	Coeff.	1.50	1.57	2.04	1.26	1.54	1.41
	Const.	-11.0	-13.0	-19.1	-8.8	-14.7	-11.9
	r^2	0.74	0.76	0.43	0.85	0.88	0.87
3x3 Average	Coeff.	1.44	1.51	2.35	1.09	1.32	1.21
	Const.	-9.8	-11.7	-25.1	-4.8	-9.7	-7.3
	r^2	0.87	0.90	0.72	0.86	0.88	0.88
Transect	Coeff.	1.11	1.24	1.74	0.99	1.18	1.09
	Const.	-2.9	-6.1	-12.4	-2.9	-6.9	-5.0
	r^2	0.50	0.59	0.38	0.75	0.74	0.75
	Landsat MSS Central Pixel						
Central	Coeff.	0.95	1.28	2.01	1.09	1.35	1.22
	Const.	0.2	-7.1	-17.9	-4.1	-9.3	-6.8
	r^2	0.44	0.65	0.53	0.82	0.91	0.87
3x3 Average	Coeff.	0.92	1.11	2.09	0.92	1.11	1.02
	Const.	0.9	-3.5	-19.3	-0.1	-3.8	-2.0
	r^2	0.52	0.62	0.73	0.78	0.84	0.82
Transect	Coeff.	1.01	0.96	1.39	0.79	0.93	0.86
	Const.	-0.8	-0.3	-5.1	2.8	0.0	1.4
	r^2	0.61	0.45	0.31	0.61	0.63	0.62

Table A.29: continued

Sensor	AVHRR	CH 1			CH 2		
	MSS	B 1	B 2	B 3	B 3	B 4	B 3,4
	Landsat MSS 3 x 3 Average						
Central	Coeff.	0.88	1.00	1.63	0.99	1.25	1.12
	Const.	1.3	-1.7	-10.5	-1.9	-7.1	-4.6
	r^2	0.47	0.59	0.41	0.80	0.86	0.84
3x3 Average	Coeff.	0.90	1.02	2.01	0.92	1.14	1.04
	Const.	1.0	-1.9	-17.9	-0.4	-4.8	-2.7
	r^2	0.63	0.78	0.79	0.93	0.98	0.97
Transect	Coeff.	1.02	1.03	1.56	0.88	1.07	0.98
	Const.	-1.2	-2.1	-8.7	0.1	-3.5	-1.7
	r^2	0.78	0.78	0.47	0.90	0.90	0.91
	Landsat MSS Transect Sampling						
Central	Coeff.	0.62	0.58	1.28	0.70	0.98	0.85
	Const.	6.6	7.0	-2.6	6.0	0.3	3.1
	r^2	0.15	0.13	0.23	0.36	0.52	0.45
3x3	Coeff.	0.71	0.80	1.94	0.82	1.06	0.94
	Const.	4.9	2.7	-15.8	2.9	-1.9	0.5
	r^2	0.25	0.31	0.67	0.66	0.82	0.75
Transect	Coeff.	1.30	1.36	2.08	0.92	1.13	1.03
	Const.	-6.7	-8.5	-18.3	-0.2	-4.2	-2.3
	r^2	0.80	0.89	0.75	0.89	0.98	0.95

Table A.30: Relationships Between Landsat MSS Spectral Reflectances and NOAA AVHRR Spectral Albedos for 1988 CAZS Field Survey Sites (3 by 3 Averages)

AVHRR	CH 1				CH 2				
MSS	B 1	B 2	B 3	B 4	B 1	B 2	B 3	B 4	B3,4
	7 JUNE 1988								
Coeff.	0.04	-0.01	0.08	0.08	0.04	0.01	0.06	0.07	0.07
Const.	19.6	21.1	22.6	22.8	19.6	20.5	22.7	23.0	22.8
r^2	0.12	0.01	0.27	0.27	0.20	0.00	0.43	0.40	0.42
	4 July 1988								
Coeff.	0.48	0.54	0.54	0.55	0.48	0.81	0.32	0.24	0.28
Const.	9.7	8.2	12.1	12.4	7.6	-1.5	16.0	18.5	17.2
r^2	0.38	0.26	0.35	0.31	0.40	0.59	0.12	0.06	0.09

Table A.30: continued

	15 July 1988								
Coeff.	0.07	-0.08	0.22	0.27	0.10	-0.03	0.23	0.25	0.24
Const.	19.2	22.5	19.7	18.9	18.0	21.6	18.6	18.2	18.4
r^2	0.04	0.03	0.33	0.43	0.11	0.01	0.36	0.40	0.38
	24 July 1988								
Coeff.	0.01	0.04	-0.02	-0.03	0.00	0.02	-0.02	-0.02	-0.02
Const.	20.6	19.9	25.1	25.6	20.8	20.1	25.1	25.6	25.4
r^2	0.01	0.24	0.08	0.14	0.00	0.16	0.13	0.19	0.16
	1 August 1988								
Coeff.	0.35	0.48	0.38	0.35	-0.06	0.10	-0.01	0.04	0.02
Const.	13.4	10.7	16.8	17.7	22.5	17.9	24.8	23.8	24.3
r^2	0.47	0.46	0.39	0.30	0.02	0.03	0.00	0.01	0.00
	3 August 1988								
Coeff.	0.17	0.35	0.11	0.09	-0.03	0.13	0.10	0.19	0.15
Const.	17.4	13.7	22.4	23.2	21.5	17.2	22.0	20.0	21.0
r^2	0.18	0.41	0.06	0.03	0.00	0.03	0.02	0.07	0.04
	20 August 1988								
Coeff.	0.14	0.14	0.09	0.07	0.20	0.27	0.17	0.14	0.16
Const.	18.2	18.0	23.0	23.7	15.9	14.2	20.7	21.5	21.1
r^2	0.58	0.32	0.18	0.09	0.46	0.43	0.22	0.15	0.18
	6 September 1988								
Coeff.	0.14	0.30	0.03	-0.02	0.28	0.42	0.31	0.33	0.32
Const.	17.7	14.3	24.1	25.4	13.8	10.1	16.8	16.8	16.8
r^2	0.26	0.60	0.01	0.00	0.39	0.48	0.36	0.35	0.36
	25 September 1988								
Coeff.	0.05	0.17	-0.04	-0.08	0.20	0.43	0.13	0.07	0.10
Const.	19.8	17.1	25.6	26.7	15.9	10.2	21.6	23.2	22.4
r^2	0.04	0.34	0.03	0.09	0.21	0.50	0.06	0.02	0.04
	5 October 1988								
Coeff.	0.24	0.44	0.10	0.04	0.32	0.45	0.26	0.23	0.24
Const.	15.1	10.5	22.3	24.0	12.3	8.9	17.9	19.1	18.5
r^2	0.38	0.66	0.05	0.01	0.57	0.59	0.27	0.17	0.22
	15 October 1988								
Coeff.	0.11	0.25	0.03	0.00	0.16	0.29	0.11	0.08	0.09
Const.	18.3	15.4	24.0	25.1	16.7	13.5	22.1	23.0	22.5
r^2	0.21	0.51	0.01	0.00	0.31	0.51	0.09	0.05	0.07

Table A.31: Relationships Between Landsat MSS (30.08.88) Spectral Reflectances and NOAA AVHRR (20.08.88) Spectral Albedos Obtained from Five Different Image Sampling Methods for 1988 CAZS Field Survey Sites, Map Positions

Sensor	AVHRR	CH 1			CH 2		
	MSS	B 1	B 2	B 3	B 3	B 4	B 3,4
Method	Landsat MSS 50m Transect Sampling						
Central	Coeff.	0.27	0.33	0.23	0.17	0.15	0.16
	Const.	16.1	15.0	20.4	20.9	21.5	21.2
	r^2	0.32	0.39	0.27	0.16	0.13	0.14
3x3 Average	Coeff.	0.37	0.40	0.32	0.59	0.57	0.58
	Const.	13.8	13.1	18.4	10.2	11.1	10.6
	r^2	0.40	0.39	0.34	0.39	0.35	0.37
Transect	Coeff.	0.36	0.40	0.31	0.39	0.36	0.37
	Const.	14.2	13.4	18.7	15.4	16.3	15.9
	r^2	0.45	0.45	0.37	0.33	0.28	0.31
	Landsat MSS 50m resolution, 20 x 20 Average						
Central	Coeff.	0.26	0.31	0.22	0.15	0.14	0.14
	Const.	16.3	15.3	20.8	21.3	21.8	21.5
	r^2	0.30	0.36	0.24	0.14	0.12	0.13
3x3 Average	Coeff.	0.37	0.40	0.31	0.58	0.56	0.57
	Const.	13.9	13.2	18.7	10.7	11.3	11.0
	r^2	0.40	0.39	0.33	0.39	0.37	0.38
Transect	Coeff.	0.35	0.39	0.30	0.37	0.35	0.36
	Const.	14.3	13.5	19.0	15.8	16.5	16.1
	r^2	0.44	0.44	0.37	0.33	0.30	0.31
	Landsat MSS 1.1km Resolution, Central Pixel						
Central	Coeff.	0.31	0.36	0.22	0.14	0.12	0.13
	Const.	15.6	14.5	20.8	21.6	22.3	21.9
	r^2	0.29	0.36	0.22	0.10	0.08	0.09
3x3 Average	Coeff.	0.46	0.48	0.36	0.63	0.61	0.62
	Const.	12.3	11.8	17.9	9.5	10.4	9.9
	r^2	0.43	0.42	0.39	0.41	0.41	0.41
Transect	Coeff.	0.40	0.43	0.30	0.37	0.33	0.35
	Const.	13.6	12.8	19.1	15.9	17.1	16.5
	r^2	0.38	0.41	0.32	0.28	0.23	0.26

Table A.31: continued

Sensor	AVHRR	CH 1			CH 2		
	MSS	B 1	B 2	B 3	B 3	B 4	B 3,4
	Landsat MSS 1.1km resolution, 3x3 average						
Central	Coeff.	0.26	0.28	0.16	0.08	0.06	0.07
	Const.	16.5	16.0	22.1	23.2	23.9	23.5
	r^2	0.32	0.37	0.18	0.05	0.03	0.04
3x3 Average	Coeff.	0.36	0.36	0.25	0.42	0.38	0.40
	Const.	14.2	14.1	20.2	14.7	16.1	15.4
	r^2	0.43	0.41	0.33	0.32	0.27	0.30
Transect	Coeff.	0.35	0.36	0.24	0.26	0.21	0.23
	Const.	14.5	14.2	20.4	18.8	20.2	19.5
	r^2	0.47	0.48	0.33	0.22	0.16	0.19
	Landsat MSS 1.1km, Transect Sampling						
Central	Coeff.	0.26	0.29	0.17	0.10	0.08	0.09
	Const.	16.3	15.7	21.7	22.6	23.2	22.9
	r^2	0.31	0.34	0.20	0.07	0.06	0.06
3x3 Average	Coeff.	0.38	0.38	0.28	0.51	0.48	0.49
	Const.	13.8	13.5	19.4	12.4	13.5	12.9
	r^2	0.41	0.40	0.34	0.38	0.35	0.37
Transect	Coeff.	0.35	0.37	0.25	0.28	0.25	0.27
	Const.	14.4	14.0	20.0	18.0	19.0	18.5
	r^2	0.43	0.43	0.33	0.24	0.20	0.22

Table A.32: Relationships Between Landsat MSS (30.08.88) Spectral Reflectances and NOAA AVHRR (06.09.88) Spectral Albedos Obtained from Five Different Image Sampling Methods for 1988 CAZS Field Survey Sites, Image Positions

Sensor	AVHRR	CH 1			CH 2		
	MSS	B 1	B 2	B 3	B 3	B 4	B 3,4
Method	Landsat MSS 50m Transect Sampling						
Central	Coeff.	0.13	0.28	0.10	0.13	0.06	0.10
	Const.	18.1	14.7	22.4	21.3	23.2	22.3
	r^2	0.03	0.13	0.02	0.02	0.00	0.01
3x3 Average	Coeff.	0.24	0.41	0.20	0.36	0.34	0.35
	Const.	15.9	12.0	20.3	15.3	16.1	15.7
	r^2	0.07	0.17	0.05	0.09	0.07	0.08
Transect	Coeff.	0.10	0.26	0.07	0.16	0.09	0.12
	Const.	18.8	15.2	23.0	20.6	22.5	21.5
	r^2	0.02	0.09	0.01	0.02	0.01	0.01

Table A.32: continued

	Landsat MSS 50m resolution, 20 x 20 Average						
Central	Coeff.	0.16	0.29	0.13	0.15	0.10	0.13
	Const.	17.5	14.6	21.9	20.8	22.4	21.6
	r^2	0.05	0.14	0.04	0.02	0.01	0.02
3x3 Average	Coeff.	0.26	0.42	0.22	0.37	0.35	0.36
	Const.	15.3	11.7	19.9	15.2	16.0	15.6
	r^2	0.09	0.18	0.07	0.09	0.08	0.09
Transect	Coeff.	0.14	0.28	0.11	0.20	0.15	0.18
	Const.	18.0	14.8	22.3	19.5	21.2	20.3
	r^2	0.03	0.10	0.02	0.03	0.02	0.02
	Landsat MSS 1.1km resolution, Central Pixel						
Central	Coeff.	0.25	0.38	0.15	0.19	0.12	0.16
	Const.	15.6	12.6	21.6	19.8	22.1	20.9
	r^2	0.09	0.19	0.04	0.03	0.01	0.02
3x3 Average	Coeff.	0.38	0.55	0.26	0.48	0.43	0.46
	Const.	13.0	9.0	19.1	12.4	14.0	13.2
	r^2	0.12	0.24	0.08	0.14	0.11	0.13
Transect	Coeff.	0.24	0.40	0.14	0.29	0.20	0.25
	Const.	15.9	12.3	21.7	17.4	20.0	18.7
	r^2	0.06	0.16	0.03	0.05	0.03	0.04
	Landsat MSS 1.1km resolution, 3x3 average						
Central	Coeff.	0.20	0.30	0.09	0.13	0.06	0.10
	Const.	16.7	14.7	23.0	21.6	23.6	22.6
	r^2	0.09	0.18	0.03	0.03	0.01	0.01
3x3 Average	Coeff.	0.30	0.41	0.15	0.29	0.23	0.26
	Const.	14.6	12.3	21.8	17.4	19.2	18.3
	r^2	0.12	0.21	0.04	0.08	0.06	0.07
Transect	Coeff.	0.19	0.29	0.07	0.17	0.10	0.13
	Const.	17.1	14.8	23.4	20.6	22.7	21.6
	r^2	0.06	0.14	0.01	0.03	0.01	0.02
	Landsat MSS 1.1km, Transect Sampling						
Central	Coeff.	0.23	0.35	0.14	0.20	0.12	0.16
	Const.	16.0	13.3	21.8	19.8	22.0	20.9
	r^2	0.11	0.23	0.06	0.05	0.02	0.03
3x3 Average	Coeff.	0.35	0.50	0.24	0.44	0.39	0.41
	Const.	13.4	10.1	19.7	13.6	15.2	14.4
	r^2	0.15	0.28	0.10	0.17	0.13	0.15
Transect	Coeff.	0.24	0.38	0.15	0.30	0.22	0.26
	Const.	16.0	12.7	21.6	17.1	19.6	18.3
	r^2	0.09	0.21	0.05	0.09	0.05	0.07

Table A.33: Relationships Between Landsat MSS Spectral Reflectances and NOAA AVHRR Spectral Albedos for 1988 ITE/Silsoe Field Survey Sites (3 by 3 Averages)

AVHRR	CH 1				CH 2				
MSS	B 1	B 2	B 3	B 4	B 1	B 2	B 3	B 4	B3,4
	4 July 1988								
Coeff.	1.40	1.50	1.90	1.81	0.78	0.82	1.14	1.17	1.16
Const.	-13.0	-15.5	-18.4	-14.7	-3.9	-5.1	-8.0	-6.9	-7.5
r^2	0.55	0.55	0.65	0.67	0.26	0.25	0.36	0.43	0.39
	15 July 1988								
Coeff.	0.92	1.01	1.25	1.18	0.57	0.59	0.86	0.89	0.87
Const.	0.5	-1.3	0.0	3.0	3.0	2.0	1.3	2.3	1.8
r^2	0.80	0.83	0.93	0.94	0.33	0.31	0.48	0.59	0.53
	24 July 1988								
Coeff.	0.70	0.76	0.90	0.82	0.73	0.77	1.04	1.05	1.05
Const.	3.5	2.1	4.8	8.0	-2.4	-3.7	-5.2	-3.6	-4.4
r^2	0.88	0.89	0.93	0.88	0.48	0.46	0.62	0.71	0.67
	1 August 1988								
Coeff.	0.71	0.76	0.90	0.82	0.69	0.73	0.97	0.99	0.99
Const.	4.1	2.9	5.8	8.8	-1.2	-2.4	-3.1	-1.9	-2.5
r^2	0.84	0.83	0.87	0.83	0.32	0.30	0.40	0.47	0.44
	3 August 1988								
Coeff.	0.58	0.64	0.76	0.71	0.52	0.58	0.78	0.80	0.79
Const.	6.0	4.7	7.8	10.5	2.7	1.0	1.3	2.5	1.9
r^2	0.70	0.72	0.76	0.75	0.31	0.33	0.44	0.53	0.48
	20 August 1988								
Coeff.	0.60	0.65	0.64	0.52	0.56	0.59	0.68	0.62	0.65
Const.	7.2	6.1	11.4	15.0	3.6	2.5	5.8	8.8	7.3
r^2	0.43	0.44	0.32	0.23	0.52	0.51	0.49	0.47	0.48
	6 September 1988								
Coeff.	0.62	0.66	0.82	0.77	0.59	0.65	0.87	0.86	0.86
Const.	5.2	4.1	6.6	9.2	0.3	-1.5	-1.9	0.2	-0.8
r^2	0.81	0.80	0.91	0.93	0.40	0.41	0.53	0.59	0.57
	5 October 1988								
Coeff.	0.71	0.76	0.85	0.74	0.74	0.80	0.97	0.89	0.93
Const.	5.8	4.6	8.7	11.9	1.9	0.4	2.6	5.8	4.2
r^2	0.88	0.88	0.79	0.70	0.84	0.85	0.91	0.88	0.90

Table A.33: continued

AVHRR	CH 1				CH 2				
MSS	B 1	B 2	B 3	B 4	B 1	B 2	B 3	B 4	B3,4
	24 October 1988								
Coeff.	1.30	1.36	1.59	1.45	1.01	1.06	1.36	1.30	1.33
Const.	-5.3	-6.6	-5.1	-1.1	-4.5	-6.0	-6.7	-3.8	-5.2
r^2	0.78	0.73	0.74	0.71	0.67	0.65	0.78	0.82	0.80
	30 October 1988								
Coeff.	1.17	1.25	1.48	1.37	0.89	0.97	1.22	1.17	1.19
Const.	-3.5	-5.2	-3.7	0.0	-3.0	-5.1	-5.0	-2.2	-3.6
r^2	0.87	0.86	0.88	0.86	0.67	0.69	0.80	0.84	0.82

Table A.34: Relationships Between Landsat MSS (08.09.88) Spectral Reflectances and NOAA AVHRR (20.08.88) Spectral Albedos Obtained from Five Different Image Sampling Methods for 1988 ITE/Silsoe Field Survey Sites

Sensor	AVHRR	CH 1			CH 2		
	MSS	B 1	B 2	B 3	B 3	B 4	B 3,4
Method	Landsat MSS 50m Transect Sampling						
Central	Coeff.	0.54	0.57	0.96	0.55	0.64	0.60
	Const.	8.5	7.8	7.6	9.0	8.8	8.9
	r^2	0.27	0.25	0.55	0.28	0.40	0.34
3x3 Average	Coeff.	0.85	0.89	1.26	0.71	0.73	0.72
	Const.	3.9	3.2	3.2	5.2	6.5	5.9
	r^2	0.59	0.54	0.83	0.60	0.67	0.65
Transect	Coeff.	0.70	0.73	1.13	0.73	0.79	0.76
	Const.	6.2	5.6	5.2	5.0	5.4	5.2
	r^2	0.41	0.37	0.69	0.52	0.64	0.59
	Landsat MSS 50m resolution, 20 x 20 Averages						
Central	Coeff.	0.57	0.58	0.92	0.58	0.65	0.62
	Const.	8.2	7.9	8.4	8.6	8.8	8.7
	r^2	0.36	0.31	0.55	0.33	0.42	0.38
3x3 Average	Coeff.	0.88	0.90	1.22	0.73	0.74	0.73
	Const.	3.8	3.1	4.1	5.1	6.7	5.9
	r^2	0.73	0.67	0.82	0.68	0.69	0.70
Transect	Coeff.	0.74	0.75	1.10	0.77	0.81	0.78
	Const.	5.8	5.4	5.9	4.5	5.4	5.0
	r^2	0.53	0.47	0.70	0.61	0.67	0.65

Table A.34: continued

Sensor	AVHRR	CH 1			CH 2		
	MSS	B 1	B 2	B 3	B 3	B 4	B 3,4
Method		Landsat MSS 1.1km resolution, central pixel					
Central	Coeff.	0.93	0.96	1.21	0.86	0.86	0.86
	Const.	3.2	2.4	4.4	2.5	4.2	3.4
	r^2	0.70	0.63	0.69	0.54	0.55	0.55
3x3	Coeff.	1.17	1.24	1.46	0.94	0.92	0.93
Average	Const.	-0.5	-1.8	0.5	0.4	2.6	1.5
	r^2	0.96	0.92	0.87	0.83	0.81	0.83
Transect	Coeff.	1.09	1.14	1.39	1.03	1.01	1.02
	Const.	0.8	-0.2	1.7	-1.3	0.7	-0.3
	r^2	0.86	0.81	0.82	0.81	0.81	0.82
	Landsat MSS 1.1km resolution, 3 x 3 average						
Central	Coeff.	0.91	0.96	1.14	0.82	0.79	0.81
	Const.	3.8	2.8	5.8	3.9	6.3	5.1
	r^2	0.66	0.64	0.70	0.55	0.61	0.58
3x3	Coeff.	1.18	1.24	1.39	0.91	0.85	0.88
Average	Const.	-0.3	-1.5	1.9	1.7	4.7	3.2
	r^2	0.96	0.94	0.91	0.88	0.90	0.89
Transect	Coeff.	1.10	1.15	1.33	0.98	0.93	0.96
	Const.	1.1	0.0	3.0	0.2	3.1	1.7
	r^2	0.86	0.83	0.87	0.84	0.89	0.87
	Landsat MSS 1.1km, transect sampling						
Central	Coeff.	0.82	0.85	1.10	0.81	0.81	0.82
	Const.	4.8	4.2	6.1	3.8	5.6	4.7
	r^2	0.67	0.62	0.70	0.59	0.63	0.61
3x3	Coeff.	1.06	1.11	1.32	0.87	0.83	0.85
Average	Const.	1.3	0.3	2.7	2.3	4.8	3.6
	r^2	0.96	0.93	0.88	0.86	0.85	0.86
Transect	Coeff.	0.99	1.03	1.28	0.96	0.93	0.95
	Const.	2.5	1.6	3.6	0.5	2.8	1.7
	r^2	0.86	0.82	0.85	0.86	0.88	0.87

Table A.35: Relationships Between Landsat MSS (08.09.88) Spectral Reflectances and NOAA AVHRR (06.09.88) Spectral Albedos Obtained from Five Different Image Sampling Methods for 1988 ITE/Silsoe Field Survey Sites

Sensor	AVHRR	CH 1			CH 2		
	MSS	B 1	B 2	B 3	B 3	B 4	B 3,4
Method	Landsat MSS 50m Transect Sampling						
Central	Coeff.	0.33	0.34	0.66	0.73	0.66	0.69
	Const.	9.3	8.9	8.2	0.8	4.4	2.6
	r^2	0.23	0.21	0.38	0.19	0.15	0.17
3x3 Average	Coeff.	0.42	0.43	0.77	0.72	0.66	0.69
	Const.	7.9	7.4	6.5	1.0	4.3	2.7
	r^2	0.27	0.25	0.38	0.17	0.14	0.15
Transect	Coeff.	0.38	0.39	0.71	0.65	0.60	0.63
	Const.	8.4	8.0	7.3	2.8	5.9	4.4
	r^2	0.27	0.25	0.39	0.17	0.14	0.15
	Landsat MSS 50m resolution, 20 x 20 Averages						
Central	Coeff.	0.36	0.36	0.66	0.69	0.60	0.94
	Const.	9.3	8.9	8.8	2.3	6.3	16.9
	r^2	0.42	0.36	0.59	0.27	0.20	0.06
3x3 Average	Coeff.	0.44	0.45	0.76	0.68	0.61	0.84
	Const.	7.9	7.5	7.1	2.4	6.1	19.4
	r^2	0.49	0.41	0.59	0.25	0.18	0.05
Transect	Coeff.	0.39	0.40	0.69	0.64	0.57	0.79
	Const.	8.6	8.3	8.2	3.6	7.2	20.9
	r^2	0.46	0.40	0.58	0.26	0.19	0.05
	Landsat MSS 1.1km resolution, central pixel						
Central	Coeff.	0.43	0.48	0.68	0.69	0.55	0.61
	Const.	8.5	7.1	9.0	3.1	8.5	5.9
	r^2	0.43	0.60	0.77	0.33	0.20	0.26
3x3 Average	Coeff.	0.52	0.58	0.78	0.69	0.55	0.62
	Const.	7.0	5.5	7.4	2.8	8.2	5.6
	r^2	0.48	0.65	0.75	0.31	0.19	0.25
Transect	Coeff.	0.46	0.52	0.70	0.64	0.52	0.58
	Const.	8.1	6.5	8.6	4.2	9.3	6.8
	r^2	0.44	0.61	0.74	0.32	0.20	0.26

Table A.35: continued

Sensor	AVHRR	CH 1			CH 2		
	MSS	B 1	B 2	B 3	B 3	B 4	B 3,4
	Landsat MSS 1.1km, 3 x 3 average						
Central	Coeff.	0.52	0.55	0.69	0.84	0.82	0.83
	Const.	6.9	5.8	8.7	-1.1	1.2	0.1
	r^2	0.76	0.75	0.86	0.54	0.59	0.57
3x3 Average	Coeff.	0.62	0.66	0.82	0.87	0.86	0.86
	Const.	5.2	4.1	6.6	-1.9	0.2	-0.8
	r^2	0.81	0.80	0.91	0.53	0.59	0.57
Transect	Coeff.	0.56	0.60	0.74	0.80	0.79	0.79
	Const.	6.2	5.1	7.9	0.1	2.1	1.1
	r^2	0.79	0.79	0.89	0.54	0.60	0.57
	Landsat MSS 1.1km, transect sampling						
Central	Coeff.	0.44	0.47	0.68	0.73	0.65	0.69
	Const.	8.2	7.2	8.9	1.8	5.5	3.7
	r^2	0.71	0.72	0.85	0.42	0.34	0.38
3x3 Average	Coeff.	0.53	0.57	0.79	0.75	0.68	0.71
	Const.	6.7	5.6	7.1	1.2	4.8	3.1
	r^2	0.78	0.78	0.86	0.40	0.34	0.37
Transect	Coeff.	0.48	0.51	0.71	0.70	0.63	0.67
	Const.	7.6	6.5	8.3	2.6	6.0	4.4
	r^2	0.75	0.76	0.85	0.42	0.36	0.39

Table A.36: Results of Regression Analysis Between CIPEA Ground Data and Landsat MSS VIs for Sites Positioned by Aerial Photographs on Images

Image Sampl.	VI Type	Regression Type Linear			Logarithmic		
Method		Coeff.	Const.	r^2	Coeff.	Const.	r^2
		For Sampling Period 26.08.85 - 03.09.85					
50m	RVI	0.00028	1.108	0.49	0.02302	1.104	0.13
	RVI34	0.00024	1.106	0.55	0.02144	1.093	0.18
	NDVI	0.00010	0.055	0.48	0.00855	0.054	0.13
	NDVI34	0.00009	0.053	0.55	0.00833	0.048	0.17
	PVI	0.00352	0.522	0.56	0.32868	0.267	0.20
	PVI34	0.00314	2.144	0.66	0.34617	1.639	0.32
20x20	RVI	0.00029	1.108	0.55	0.02479	1.098	0.16
	RVI34	0.00025	1.105	0.60	0.02262	1.090	0.20
	NDVI	0.00011	0.055	0.56	0.00929	0.052	0.16
	NDVI34	0.00010	0.053	0.61	0.00882	0.047	0.20
	PVI	0.00362	0.543	0.63	0.34631	0.236	0.23
	PVI34	0.00320	2.163	0.72	0.35348	1.645	0.35
Central	RVI	0.00022	1.143	0.54	0.01893	1.136	0.16
	RVI34	0.00019	1.134	0.58	0.01718	1.123	0.19
	NDVI	0.00008	0.069	0.54	0.00715	0.066	0.16
	NDVI34	0.00007	0.064	0.58	0.00671	0.060	0.19
	PVI	0.00285	0.944	0.58	0.25775	0.780	0.19
	PVI34	0.00253	2.459	0.62	0.25122	2.198	0.25
3x3	RVI	0.00023	1.136	0.63	0.02200	1.117	0.23
	RVI34	0.00020	1.129	0.67	0.01971	1.109	0.26
	NDVI	0.00009	0.066	0.64	0.00850	0.058	0.24
	NDVI34	0.00008	0.062	0.68	0.00783	0.054	0.27
	PVI	0.00302	0.866	0.71	0.30951	0.503	0.30
	PVI34	0.00268	2.427	0.78	0.30302	1.957	0.40
Transect	RVI	0.00025	1.129	0.58	0.02337	1.112	0.20
	RVI34	0.00022	1.123	0.60	0.02031	1.107	0.21
	NDVI	0.00010	0.063	0.59	0.00888	0.057	0.20
	NDVI34	0.00008	0.060	0.61	0.00795	0.054	0.22
	PVI	0.00314	0.812	0.64	0.30423	0.527	0.24
	PVI34	0.00268	2.404	0.68	0.27791	2.066	0.29

Table A.37: Results of Regression Analysis Between CIPEA Ground Data and NOAA AVHRR VIs for Sites Positioned by Aircraft Instrument (Central Sampling)

Date	VI Type	Regression Type Linear			Logarithmic		
		Coeff.	Const.	r^2	Coeff.	Const.	r^2
		For Sampling Period 03.08.85 - 10.08.85					
21.08.85	RVI	0.00076	1.212	0.34	0.07372	1.021	0.41
	NDVI	0.00028	0.094	0.38	0.02669	0.025	0.45
	PVI	0.00990	0.796	0.42	0.07112	1.020	0.30
		For Sampling Period 26.08.85 - 03.09.85					
21.08.85	RVI	0.00014	1.208	0.24	0.07436	0.856	0.27
	NDVI	0.00005	0.092	0.28	0.02716	-0.036	0.31
	PVI	0.00186	0.750	0.30	0.95839	-3.785	0.33
22.08.85	RVI	1.13300	0.000	0.55	0.16764	0.326	0.48
	NDVI	0.00013	0.067	0.58	0.05841	-0.214	0.52
	PVI	0.00419	-0.318	0.63	1.93720	-9.681	0.58
30.08.85	RVI	0.00005	1.179	0.14	0.02598	1.054	0.20
	NDVI	0.00002	0.081	0.14	0.01070	0.030	0.19
	PVI	0.00078	0.007	0.19	0.42568	-2.021	0.24
31.08.85	RVI	0.00012	1.137	0.44	0.03812	0.988	0.28
	NDVI	0.00005	0.064	0.45	0.01526	0.004	0.28
	PVI	0.00178	-0.658	0.43	0.55731	-2.814	0.26
10.09.85	RVI	0.00005	1.145	0.19	0.01455	1.091	0.10
	NDVI	0.00002	0.067	0.18	0.00600	0.045	0.10
	PVI	0.00081	-0.415	0.21	0.24154	-1.323	0.11
		Sites on Landsat MSS 191/49 only For Sampling Period 26.08 - 03.09					
31.08.85	RVI	0.00022	1.116	0.60	0.02030	1.103	0.20
	NDVI	0.00009	0.057	0.60	0.00794	0.052	0.20
	PVI	0.00293	-0.790	0.61	0.26820	-0.972	0.20

Table A.38: Results of Regression Analysis Between CIPEA Ground Data and NOAA AVHRR VIs for Sites Positioned by Aerial Photographs on Images (Central Sampling)

Date	VI Type	Regression Type Linear			Logarithmic		
		Coeff.	Const.	r^2	Coeff.	Const.	r^2
		For Sampling Period 03.08.85 - 10.08.85					
21.08.85	RVI	0.00114	1.236	0.37	0.12957	0.869	0.64
	NDVI	0.00041	0.102	0.40	0.04603	-0.028	0.67
	PVI	0.01424	1.043	0.40	1.58990	-3.450	0.69
		For Sampling Period 26.08 - 03.09					
21.08.85	RVI	0.00063	1.025	0.68	0.07770	0.877	0.28
	NDVI	0.00022	0.029	0.68	0.02774	-0.026	0.29
	PVI	0.00741	-1.401	0.67	0.95017	-3.328	0.29
22.08.85	RVI	0.00076	0.961	0.75	0.10689	0.711	0.39
	NDVI	0.00027	0.002	0.73	0.03987	-0.097	0.42
	PVI	0.00892	-2.517	0.71	1.34703	-6.000	0.43
30.08.85	RVI	0.00014	1.162	0.57	0.02610	1.133	0.60
	NDVI	0.00006	0.075	0.56	0.01055	0.064	0.60
	PVI	0.00184	-0.179	0.59	0.33832	-0.546	0.63
31.08.85	RVI	0.00021	1.129	0.73	0.02575	1.079	0.30
	NDVI	0.00008	0.062	0.73	0.01027	0.042	0.31
	PVI	0.00274	-0.587	0.73	0.34932	-1.287	0.32
10.09.85	RVI	0.00016	1.138	0.76	0.03015	1.042	0.70
	NDVI	0.00007	0.065	0.76	0.01259	0.024	0.72
	PVI	0.00222	-0.469	0.88	0.40722	-1.747	0.79
		3 x 3 Image Data Sampling Method For Sampling Period 26.08 - 03.09					
31.08.85	RVI	0.00016	1.147	0.76	0.01870	1.116	0.42
	NDVI	0.00006	0.069	0.76	0.00759	0.056	0.42
	PVI	0.00219	-0.377	0.77	0.26300	-0.840	0.44
		Transect Image Data Sampling Method					
31.08.85	RVI	0.00020	1.141	0.69	0.02164	1.111	0.33
	NDVI	0.00008	0.067	0.69	0.00860	0.055	0.34
	PVI	0.00266	-0.445	0.71	0.29795	-0.898	0.36

Table A.39: Results of Regression Analysis Between CIPEA Ground Data and Maximum Value VIs of NOAA AVHRR for Sites Positioned by Aerial Photographs on Images

Image Sampl.	VI Type	Regression Type Linear			Logarithmic		
Method		Coeff.	Const.	r^2	Coeff.	Const.	r^2
		For Sampling Period 03.08 - 10.08					
Central	RVImax	0.00057	1.113	0.80	0.06397	1.015	0.41
	NDVImax	0.00020	0.063	0.83	0.02268	0.025	0.45
	PVImax	0.00672	-0.555	0.82	0.80322	-1.958	0.47
3x3	RVImax	0.00054	1.102	0.76	0.05976	1.016	0.37
	NDVImax	0.00019	0.058	0.78	0.02141	0.024	0.41
	PVImax	0.00638	-0.658	0.79	0.75326	-1.943	0.44

Table A.40: Results of Regression Analysis Between Landsat MSS and NOAA AVHRR VIs for CIPEA Field Survey Site, Positioned by Image Identification

VI Type		Bands 2 and 4			Bands 2, 3 and 4		
AVHRR	MSS	Coeff.	Const.	r^2	Coeff.	Const.	r^2
		50m Landsat MSS vs. Central NOAA AVHRR					
RVI	RVI	0.48121	0.632	0.84	0.60069	0.497	0.87
NDVI	NDVI	0.49711	0.050	0.82	0.60566	0.043	0.85
PVI	PVI	0.54151	-0.444	0.82	0.65534	-1.629	0.81
		Central Landsat MSS vs. Central NOAA AVHRR					
RVI	RVI	0.65867	0.408	0.89	0.78689	0.266	0.90
NDVI	NDVI	0.68498	0.028	0.89	0.79652	0.023	0.89
PVI	PVI	0.68890	-0.834	0.84	0.75897	-2.034	0.75

Table A.41: Results of Regression Analysis Between 1985 ITE/Silsoe Ground Data and Landsat MSS VIs for Sites Positioned by Image Identification

Image Sampl.	VI Type	Regression Type					
		Linear			Logarithmic		
Method		Coeff.	Const.	r^2	Coeff.	Const.	r^2
50m	RVI	0.00029	1.132	0.84	0.04519	1.070	0.84
	RVI34	0.00024	1.123	0.84	0.03810	1.070	0.86
	NDVI	0.00011	0.062	0.80	0.01807	0.035	0.86
	NDVI34	0.00010	0.058	0.81	0.01560	0.035	0.88
	PVI	0.00343	0.699	0.76	0.58394	-0.209	0.90
	PVI34	0.00299	2.029	0.70	0.53912	1.128	0.93
20x20	RVI	0.00026	1.142	0.83	0.04231	1.081	0.88
	RVI34	0.00022	1.133	0.82	0.03569	1.081	0.89
	NDVI	0.00010	0.066	0.80	0.01693	0.040	0.90
	NDVI34	0.00009	0.062	0.79	0.01462	0.040	0.90
	PVI	0.00323	0.809	0.75	0.56035	-0.083	0.92
	PVI34	0.00284	2.141	0.68	0.51887	1.261	0.92
Central	RVI	0.00025	1.167	0.83	0.03871	1.116	0.80
	RVI34	0.00021	1.155	0.80	0.03291	1.110	0.80
	NDVI	0.00010	0.077	0.80	0.01511	0.056	0.81
	NDVI34	0.00008	0.072	0.77	0.01319	0.053	0.81
	PVI	0.00301	1.158	0.74	0.50466	0.389	0.85
	PVI34	0.00259	2.492	0.64	0.46604	1.715	0.85
3 x 3	RVI	0.00024	1.188	0.76	0.03521	1.143	0.69
	RVI34	0.00020	1.172	0.73	0.02979	1.133	0.68
	NDVI	0.00009	0.085	0.72	0.01355	0.067	0.68
	NDVI34	0.00008	0.078	0.70	0.01180	0.063	0.68
	PVI	0.00283	1.367	0.68	0.45381	0.718	0.71
	PVI34	0.00246	2.639	0.60	0.41454	2.002	0.70
Transect	RVI	0.00023	1.228	0.62	0.03467	1.185	0.55
	RVI34	0.00020	1.207	0.60	0.02919	1.171	0.54
	NDVI	0.00009	0.101	0.59	0.01294	0.084	0.54
	NDVI34	0.00008	0.092	0.57	0.01125	0.078	0.52
	PVI	0.00262	1.945	0.52	0.41200	1.375	0.53
	PVI34	0.00221	3.207	0.44	0.35963	2.683	0.48

Table A.42: Results of Regression Analysis Between 1985 ITE/Silsoe Ground Data and NOAA AVHRR VIs for Sites Positioned by Image Identification (Central Value)

Date	VI Type	Regression Type: Linear			Logarithmic		
		Coeff.	Const.	r^2	Coeff.	Const.	r^2
21.08.85	RVI	0.00047	1.145	0.87	0.06264	1.082	0.64
	NDVI	0.00016	0.069	0.83	0.02265	0.044	0.67
	PVI	0.00550	-0.265	0.69	0.83623	-1.355	0.65
22.08.85	RVI	0.00049	1.052	0.88	0.07155	0.966	0.77
	NDVI	0.00018	0.026	0.84	0.02828	-0.012	0.80
	PVI	0.00779	-3.556	0.73	1.27581	-5.436	0.80
30.08.85	RVI	0.00052	1.118	0.78	0.02518	1.123	0.43
	NDVI	0.00021	0.055	0.75	0.01007	0.058	0.40
	PVI	0.00747	-0.044	0.78	0.35413	0.031	0.42
31.08.85	RVI	0.00018	1.153	0.84	0.02763	1.115	0.84
	NDVI	0.00007	0.071	0.82	0.01120	0.055	0.85
	PVI	0.00221	0.742	0.82	0.35189	0.246	0.85
10.09.85	RVI	0.00011	1.135	0.38	0.02092	1.097	0.58
	NDVI	0.00005	0.062	0.39	0.00883	0.046	0.57
	PVI	0.00134	0.292	0.34	0.25104	-0.147	0.49

21.08.85: excluding Site D
30.08.85: excluding Site A and B

Table A.43: Results of Regression Analysis Between 1985 ITE/Silsoe Ground Data and NOAA AVHRR VIs for Sites Positioned by Image Identification (3 by 3 Image Data Sampling)

Date	VI Type	Regression Type: Linear			Logarithmic		
		Coeff.	Const.	r^2	Coeff.	Const.	r^2
21.08.85	RVI	0.00041	1.159	0.81	0.05710	1.095	0.65
	NDVI	0.00014	0.073	0.77	0.02105	0.048	0.66
	PVI	0.00511	-0.185	0.65	0.79038	-1.247	0.63
22.08.85	RVI	0.00042	1.051	0.90	0.06211	0.976	0.79
	NDVI	0.00016	0.025	0.86	0.02517	-0.008	0.82
	PVI	0.00711	-3.367	0.74	1.15095	-5.032	0.79
30.08.85	RVI	0.00048	1.130	0.57	0.02267	1.134	0.31
	NDVI	0.00019	0.060	0.56	0.00909	0.062	0.29
	PVI	0.00704	-0.010	0.57	0.33030	0.069	0.30
31.08.85	RVI	0.00016	1.176	0.73	0.02423	1.143	0.71
	NDVI	0.00006	0.080	0.71	0.00969	0.067	0.70
	PVI	0.00197	1.056	0.72	0.30787	0.633	0.72
10.09.85	RVI	0.00008	1.166	0.25	0.01627	1.135	0.41
	NDVI	0.00003	0.075	0.26	0.00675	0.063	0.41
	PVI	0.00090	0.764	0.22	0.19047	0.389	0.41

Table A.44: Results of Regression Analysis Between 1985 ITE/Silsoe Ground Data and NOAA AVHRR VIs for Sites Positioned by Image Identification (Transect Image Data Sampling)

Date	VI Type	Regression Type: Linear			Logarithmic		
		Coeff.	Const.	r^2	Coeff.	Const.	r^2
21.08.85	RVI	0.00036	1.210	0.61	0.05703	1.130	0.63
	NDVI	0.00013	0.092	0.60	0.02060	0.062	0.63
	PVI	0.00445	0.631	0.54	0.75356	-0.534	0.63
22.08.85	RVI	0.00039	1.116	0.63	0.06576	1.016	0.72
	NDVI	0.00015	0.050	0.64	0.02550	0.011	0.74
	PVI	0.00620	-2.133	0.57	1.01427	-3.624	0.62
30.08.85	RVI	0.00016	1.208	0.06	-0.00058	1.232	0.00
	NDVI	0.00007	0.091	0.07	0.00001	0.101	0.00
	PVI	0.00278	1.080	0.09	0.01346	1.413	0.00
31.08.85	RVI	0.00016	1.211	0.55	0.02407	1.182	0.48
	NDVI	0.00006	0.094	0.52	0.00936	0.083	0.46
	PVI	0.00202	1.512	0.54	0.29799	1.145	0.48
10.09.85	RVI	0.00005	1.199	0.09	0.00843	1.187	0.09
	NDVI	0.00002	0.089	0.10	0.00353	0.084	0.09
	PVI	0.00053	1.162	0.07	0.08611	1.038	0.07

Table A.45: Results of Regression Analysis Between 1985 ITE/Silsoe Ground Data and NOAA AVHRR Maximum Value VIs for Sites Positioned by Image Identification (Transect Image Data Sampling)

Image Sampl.	VI Type	Regression Type Linear			Logarithmic		
Method		Coeff.	Const.	r^2	Coeff.	Const.	r^2
Central	RVImax	0.00045	1.169	0.89	0.05906	1.113	0.64
	NDVImax	0.00015	0.080	0.87	0.02090	0.058	0.67
	PVImx	0.00450	0.893	0.88	0.64150	0.157	0.73
3 x 3	RVImax	0.00037	1.194	0.81	0.05129	1.140	0.63
	NDVImax	0.00013	0.088	0.79	0.01840	0.068	0.64
	PVImax	0.00377	1.255	0.79	0.53562	0.643	0.65
Transect	RVImax	0.00031	1.265	0.53	0.04404	1.214	0.45
	NDVImax	0.00011	0.114	0.51	0.01541	0.096	0.43
	PVImax	0.00311	2.014	0.51	0.44248	1.506	0.42

Table A.46: Results of Regression Analysis Between Landsat MSS and NOAA AVHRR VIs for 1985 ITE/Silsoe Field Survey Site, Positioned by Image Identification

VI Type		Bands 2 and 4			Bands 2, 3 and 4		
AVHRR	MSS	Coeff.	Const.	r^2	Coeff.	Const.	r^2
		50m Landsat MSS vs. Central NOAA AVHRR					
RVI	RVI	0.58074	0.499	0.90	0.70017	0.369	0.92
NDVI	NDVI	0.58913	0.036	0.90	0.69276	0.032	0.91
PVI	PVI	0.59189	0.393	0.90	0.64833	-0.477	0.89
		Central Landsat MSS vs. Central NOAA AVHRR					
RVI	RVI	0.68432	0.356	0.97	0.80493	0.226	0.97
NDVI	NDVI	0.71078	0.017	0.97	0.80990	0.014	0.97
PVI	PVI	0.68421	0.004	0.96	0.72286	-0.938	0.92

Table A.47: Results of Regression Analysis Between CAZS Field Survey Data from 5th and 6th Sampling Period and Landsat MSS NDVI for Sites Positioned by GPS

Image Sampl.	VI Type	Regression Type Linear			Logarithmic		
Method		Coeff.	Const.	r^2	Coeff.	Const.	r^2
		Field Survey Period 26.08.88 - 31.08.88					
50m	NDVI	0.00000	0.085	0.02	0.00409	0.061	0.02
20x20	NDVI	0.00001	0.077	0.19	0.01224	0.005	0.21
Central	NDVI	0.00002	0.075	0.12	0.01772	-0.027	0.11
3x3	NDVI	0.00002	0.075	0.15	0.01670	-0.022	0.15
		Field Survey Period 10.09.88 - 15.09.88					
50m	NDVI	0.00001	0.084	0.06	0.00509	0.055	0.05
20x20	NDVI	0.00001	0.083	0.06	0.00475	0.056	0.05
Central	NDVI	0.00003	0.064	0.50	0.02797	-0.095	0.46
3x3	NDVI	0.00002	0.072	0.33	0.01791	-0.029	0.28
Site P not included.							

Table A.48: Results of Regression Analysis Between CAZS Field Survey Data from 5th Sampling Period and Landsat MSS NDVI for Sites Positioned by Map Identification

Image Sampl.	VI Type	Regression Type Linear			Logarithmic		
Method		Coeff.	Const.	r^2	Coeff.	Const.	r^2
50m	RVI	0.00004	1.161	0.15	0.03733	0.946	0.13
	RVI34	0.00004	1.160	0.15	0.03170	0.978	0.13
	NDVI	0.00002	0.075	0.15	0.01540	-0.014	0.13
	NDVI34	0.00001	0.074	0.15	0.01313	-0.001	0.13
	PVI	0.00034	0.368	0.05	0.30302	-1.377	0.04
	PVI34	0.00026	0.330	0.04	0.22144	-0.938	0.03
20x20	RVI	0.00004	1.163	0.17	0.03582	0.957	0.15
	RVI34	0.00004	1.161	0.18	0.03152	0.979	0.15
	NDVI	0.00002	0.076	0.18	0.01475	-0.009	0.16
	NDVI34	0.00001	0.075	0.18	0.01304	0.000	0.15
	PVI	0.00028	0.437	0.05	0.25154	-1.009	0.04
	PVI34	0.00022	0.374	0.04	0.19048	-0.714	0.03
Central	RVI	0.00005	1.163	0.13	0.04480	0.903	0.12
	RVI34	0.00004	1.161	0.12	0.03857	0.938	0.11
	NDVI	0.00002	0.076	0.14	0.01839	-0.031	0.13
	NDVI34	0.00002	0.075	0.13	0.01591	-0.017	0.11
	PVI	0.00044	0.388	0.07	0.41453	-2.020	0.06
	PVI34	0.00036	0.330	0.06	0.32477	-1.549	0.05
3 x 3	RVI	0.00005	1.157	0.17	0.04577	0.889	0.17
	RVI34	0.00004	1.156	0.16	0.03924	0.927	0.16
	NDVI	0.00002	0.073	0.17	0.01891	-0.038	0.17
	NDVI34	0.00002	0.072	0.16	0.01629	-0.023	0.16
	PVI	0.00047	0.311	0.10	0.45706	-2.360	0.10
	PVI34	0.00038	0.273	0.08	0.36007	-1.823	0.08
Transect	RVI	0.00005	1.156	0.18	0.05080	0.859	0.19
	RVI34	0.00005	1.154	0.18	0.04393	0.898	0.17
	NDVI	0.00002	0.072	0.19	0.02095	-0.050	0.19
	NDVI34	0.00002	0.072	0.18	0.01820	-0.034	0.18
	PVI	0.00047	0.344	0.09	0.45105	-2.293	0.09
	PVI34	0.00037	0.300	0.08	0.35031	-1.739	0.07

Site P not included.

Table A.49: Results of Regression Analysis Between CAZS Field Survey Data from 6th Sampling Period and Landsat MSS NDVI for Sites Positioned by Map Identification

Image Sampl.	VI Type	Regression Type Linear			Logarithmic		
Method		Coeff.	Const.	r^2	Coeff.	Const.	r^2
50m	RVI	0.00007	1.139	0.57	0.05741	0.813	0.52
	RVI34	0.00006	1.141	0.58	0.04959	0.860	0.53
	NDVI	0.00003	0.066	0.57	0.02351	-0.068	0.52
	NDVI34	0.00002	0.066	0.58	0.02044	-0.050	0.53
	PVI	0.00088	-0.109	0.48	0.72677	-4.224	0.43
	PVI34	0.00075	-0.104	0.48	0.61299	-3.574	0.43
20x20	RVI	0.00006	1.151	0.49	0.04714	0.883	0.45
	RVI34	0.00005	1.151	0.48	0.04097	0.918	0.43
	NDVI	0.00002	0.071	0.50	0.01930	-0.039	0.45
	NDVI34	0.00002	0.070	0.48	0.01689	-0.025	0.44
	PVI	0.00073	0.043	0.48	0.60419	-3.379	0.43
	PVI34	0.00063	0.015	0.48	0.51408	-2.892	0.42
Central	RVI	0.00007	1.143	0.42	0.05981	0.805	0.37
	RVI34	0.00006	1.143	0.41	0.05272	0.845	0.35
	NDVI	0.00003	0.068	0.42	0.02414	-0.069	0.37
	NDVI34	0.00003	0.068	0.41	0.02146	-0.054	0.35
	PVI	0.00105	-0.140	0.52	0.86975	-5.071	0.47
	PVI34	0.00092	-0.170	0.53	0.76805	-4.527	0.48
3 x 3	RVI	0.00006	1.148	0.38	0.04871	0.873	0.32
	RVI34	0.00005	1.147	0.38	0.04388	0.899	0.33
	NDVI	0.00002	0.070	0.38	0.01982	-0.042	0.32
	NDVI34	0.00002	0.069	0.38	0.01800	-0.033	0.33
	PVI	0.00085	-0.001	0.44	0.68932	-3.895	0.38
	PVI34	0.00076	-0.048	0.45	0.61924	-3.549	0.40
Transect	RVI	0.00007	1.145	0.44	0.05685	0.822	0.40
	RVI34	0.00006	1.144	0.44	0.05075	0.856	0.39
	NDVI	0.00003	0.068	0.44	0.02312	-0.063	0.40
	NDVI34	0.00002	0.068	0.44	0.02080	-0.050	0.40
	PVI	0.00089	-0.013	0.47	0.73452	-4.176	0.42
	PVI34	0.00078	-0.053	0.48	0.64648	-3.717	0.43

Site P not included.

Table A.50: Results of Regression Analysis Between CAZS Field Survey Data and NOAA AVHRR NDVI for Sites Positioned by GPS (Central Image Data Sampling)

Date	VI Type	Regression Type: Linear			Logarithmic		
		Coeff.	Const.	r^2	Coeff.	Const.	r^2
07.06.88	NDVI	0.00006	0.069	0.00	0.00617	0.048	0.00
04.07.88	NDVI	0.00011	0.075	0.05	0.01048	0.039	0.09
15.07.88	NDVI	0.00009	0.074	0.34	0.02163	-0.020	0.51
24.07.88	NDVI	0.00006	0.088	0.02	0.02992	-0.053	0.13
01.08.88	NDVI	0.00007	0.089	0.25	0.03801	-0.110	0.28
03.08.88	NDVI	0.00008	0.077	0.50	0.04366	-0.151	0.56
20.08.88	NDVI	0.00003	0.094	0.02	0.02650	-0.061	0.04
06.09.88	NDVI	0.00003	0.053	0.46	0.02999	-0.122	0.48
25.09.88	NDVI	0.00005	0.021	0.58	0.05128	-0.280	0.57
05.10.88	NDVI	0.00002	0.036	0.33	0.01741	-0.066	0.31
15.10.88	NDVI	0.00003	0.038	0.66	0.02589	-0.114	0.67

Site P not included.

Table A.51: Results of Regression Analysis Between CAZS Field Survey Data and NOAA AVHRR NDVI for Sites Positioned by Map Identification (Central Image Data Sampling)

Date	VI Type	Regression Type: Linear			Logarithmic		
		Coeff.	Const.	r^2	Coeff.	Const.	r^2
07.06.88	RVI	0.00010	1.155	0.00	0.01142	1.115	0.00
	NDVI	0.00006	0.069	0.00	0.00617	0.048	0.00
	PVI	0.00426	1.092	0.01	0.34594	-0.049	0.01
04.07.88	RVI	0.00026	1.164	0.04	0.02429	1.080	0.08
	NDVI	0.00011	0.075	0.05	0.01048	0.039	0.09
	PVI	0.00394	0.633	0.04	0.37243	-0.641	0.09
15.07.88	RVI	0.00021	1.160	0.33	0.05147	0.938	0.50
	NDVI	0.00009	0.074	0.34	0.02163	-0.020	0.51
	PVI	0.00317	1.012	0.35	0.78166	-2.366	0.51
24.07.88	RVI	0.00015	1.203	0.02	0.07257	0.858	0.12
	NDVI	0.00006	0.088	0.02	0.02992	-0.053	0.13
	PVI	0.00290	1.456	0.03	1.19544	-4.132	0.14
01.08.88	RVI	0.00018	1.193	0.24	0.10137	0.664	0.27
	NDVI	0.00007	0.089	0.25	0.03801	-0.110	0.28
	PVI	0.00222	1.517	0.24	1.27514	-5.140	0.27
03.08.88	RVI	0.00020	1.162	0.48	0.11315	0.572	0.54
	NDVI	0.00008	0.077	0.50	0.04366	-0.151	0.56
	PVI	0.00251	1.173	0.51	1.44234	-6.361	0.58
20.08.88	RVI	0.00015	1.164	0.16	0.13396	0.396	0.19
	NDVI	0.00006	0.078	0.15	0.05045	-0.212	0.19
	PVI	0.00129	1.443	0.11	1.22184	-5.625	0.15
06.09.88	RVI	0.00007	1.110	0.45	0.07097	0.696	0.47
	NDVI	0.00003	0.053	0.46	0.02999	-0.122	0.48
	PVI	0.00108	0.381	0.51	1.05566	-5.777	0.52
25.09.88	RVI	0.00019	0.970	0.77	0.19903	-0.209	0.76
	NDVI	0.00008	-0.007	0.76	0.08393	-0.504	0.76
	PVI	0.00251	-1.419	0.78	2.68498	-17.34	0.77
05.10.88	RVI	0.00004	1.073	0.33	0.03904	0.845	0.31
	NDVI	0.00002	0.036	0.33	0.01741	-0.066	0.31
	PVI	0.00060	0.049	0.30	0.59946	-3.461	0.28
15.10.88	RVI	0.00006	1.078	0.66	0.05925	0.729	0.67
	NDVI	0.00003	0.038	0.66	0.02589	-0.114	0.67
	PVI	0.00085	0.158	0.64	0.88672	-5.072	0.65

Site P not included.

Table A.52: Results of Regression Analysis Between CAZS Field Survey Data and NOAA AVHRR NDVI for Sites Positioned by Map Identification (3 by 3 Pixel Image Data Sampling)

Date	VI Type	Regression Type: Linear			Logarithmic		
		Coeff.	Const.	r^2	Coeff.	Const.	r^2
07.06.88	RVI	0.00039	1.148	0.07	0.02596	1.068	0.07
	NDVI	0.00017	0.069	0.08	0.01131	0.034	0.07
	PVI	0.00691	1.158	0.07	0.46262	-0.280	0.07
04.07.88	RVI	0.00015	1.151	0.02	0.01658	1.093	0.06
	NDVI	0.00007	0.070	0.02	0.00730	0.044	0.06
	PVI	0.00234	0.436	0.02	0.26628	-0.509	0.05
15.07.88	RVI	0.00018	1.145	0.40	0.04653	0.943	0.64
	NDVI	0.00008	0.067	0.40	0.01990	-0.019	0.64
	PVI	0.00288	0.774	0.40	0.73927	-2.447	0.65
24.07.88	RVI	0.00022	1.157	0.08	0.07491	0.815	0.24
	NDVI	0.00010	0.070	0.09	0.03219	-0.076	0.25
	PVI	0.00439	0.626	0.11	1.38434	-5.622	0.26
01.08.88	RVI	0.00022	1.144	0.58	0.12312	0.503	0.64
	NDVI	0.00008	0.069	0.60	0.04812	-0.182	0.67
	PVI	0.00300	0.730	0.59	1.70333	-8.138	0.65
03.08.88	RVI	0.00020	1.142	0.55	0.12135	0.502	0.67
	NDVI	0.00008	0.067	0.56	0.04843	-0.189	0.70
	PVI	0.00282	0.742	0.57	1.67952	-8.105	0.70
20.08.88	RVI	0.00015	1.165	0.19	0.12306	0.468	0.20
	NDVI	0.00005	0.079	0.18	0.04562	-0.180	0.19
	PVI	0.00150	1.304	0.17	1.27002	-5.918	0.18
06.09.88	RVI	0.00008	1.114	0.15	0.07407	0.684	0.13
	NDVI	0.00003	0.054	0.16	0.03097	-0.125	0.14
	PVI	0.00109	0.510	0.16	0.99649	-5.259	0.15
25.09.88	RVI	0.00016	0.995	0.74	0.16962	-0.011	0.74
	NDVI	0.00007	0.004	0.74	0.07186	-0.423	0.74
	PVI	0.00217	-1.121	0.76	2.34451	-15.038	0.76
05.10.88	RVI	0.00004	1.067	0.36	0.04372	0.812	0.33
	NDVI	0.00002	0.033	0.35	0.01936	-0.080	0.32
	PVI	0.00072	-0.090	0.33	0.70645	-4.220	0.31
15.10.88	RVI	0.00007	1.064	0.65	0.07167	0.642	0.64
	NDVI	0.00003	0.032	0.65	0.03126	-0.152	0.64
	PVI	0.00106	-0.085	0.63	1.08996	-6.507	0.63

Site P not included.

Table A.53: Results of Regression Analysis Between CAZS Field Survey Data and NOAA AVHRR Maximum Value VIs for Sites Positioned by Map Identification

Image Sampl.	VI Type	Regression Type Linear			Logarithmic		
Method		Coeff.	Const.	r^2	Coeff.	Const.	r^2
Central	RVI	0.00019	1.116	0.47	0.25200	-0.433	0.46
	NDVI	0.00007	0.064	0.46	0.09071	-0.494	0.45
	PVI	0.00275	0.327	0.57	3.63999	-22.11	0.58
3 x 3	RVI	0.00015	1.148	0.34	0.19879	-0.079	0.35
	NDVI	0.00006	0.073	0.33	0.07454	-0.388	0.35
	PVI	0.00200	0.802	0.42	2.67724	-15.73	0.44
Site P not included.							

Table A.54: Results of Regression Analysis Between CAZS Field Survey Data and NOAA AVHRR Moving Average VIs for Sites Positioned by Map Identification (Central Data Image Sampling)

Date	VI Type	Regression Type Linear			Logarithmic		
		Coeff.	Const.	r^2	Coeff.	Const.	r^2
04.07.88	RVI	-0.00007	1.188	0.00	-0.00188	1.191	0.00
	NDVI	-0.00001	0.084	0.00	0.00025	0.082	0.00
	PVI	-0.00086	1.416	0.00	-0.02261	1.447	0.00
15.07.88	RVI	0.00012	1.169	0.08	0.04305	0.968	0.20
	NDVI	0.00005	0.077	0.09	0.01823	-0.008	0.21
	PVI	0.00205	0.916	0.09	0.70974	-2.375	0.20
24.07.88	RVI	0.00012	1.223	0.09	0.04910	0.990	0.28
	NDVI	0.00005	0.098	0.10	0.02026	0.002	0.30
	PVI	0.00187	1.809	0.10	0.74568	-1.714	0.29
01.08.88	RVI	0.00022	1.121	0.71	0.14160	0.355	0.78
	NDVI	0.00008	0.059	0.71	0.05558	-0.242	0.79
	PVI	0.00299	0.419	0.72	1.97621	-10.29	0.81
03.08.88	RVI	0.00023	1.136	0.50	0.14914	0.332	0.54
	NDVI	0.00009	0.066	0.53	0.05745	-0.244	0.57
	PVI	0.00290	0.791	0.47	1.88746	-9.411	0.52

Table A.54: continued

Date	VI Type	Regression Type Linear			Logarithmic		
		Coeff.	Const.	r^2	Coeff.	Const.	r^2
20.08.88	RVI	0.00013	1.157	0.38	0.10309	0.575	0.38
	NDVI	0.00005	0.074	0.38	0.04042	-0.155	0.39
	PVI	0.00142	1.160	0.36	1.17347	-5.490	0.37
06.09.88	RVI	0.00007	1.148	0.26	0.06173	0.793	0.23
	NDVI	0.00003	0.067	0.29	0.02660	-0.086	0.26
	PVI	0.00107	0.745	0.44	0.97580	-4.874	0.39
25.09.88	RVI	0.00012	1.030	0.76	0.13419	0.234	0.76
	NDVI	0.00005	0.019	0.76	0.05632	-0.315	0.76
	PVI	0.00166	-0.543	0.76	1.78586	-11.14	0.77
05.10.88	RVI	0.00009	1.041	0.54	0.09320	0.490	0.51
	NDVI	0.00004	0.022	0.53	0.03983	-0.213	0.50
	PVI	0.00126	-0.397	0.53	1.30633	-8.112	0.50

Site P not included.

Table A.55: Results of Regression Analysis Between Landsat MSS and NOAA AVHRR VIs for CAZS Field Survey Site, Positioned by Image Identification

VI Type		Bands 2 and 4			Bands 2, 3 and 4		
AVHRR	MSS	Coeff.	Const.	r^2	Coeff.	Const.	r^2
		50m Landsat MSS vs. Central NOAA AVHRR					
RVI	RVI	2.16811	-1.412	0.92	2.56933	-1.877	0.95
NDVI	NDVI	2.14036	-0.108	0.92	2.52218	-0.136	0.95
PVI	PVI	1.73735	0.353	0.80	2.09020	0.357	0.83
		Central Landsat MSS vs. Central NOAA AVHRR					
RVI	RVI	1.79648	-0.980	0.97	1.99981	-1.210	0.97
NDVI	NDVI	1.79738	-0.083	0.97	1.98394	-0.094	0.97
PVI	PVI	1.63799	0.222	0.92	1.88407	0.292	0.94

Table A.56: Results of Regression Analysis Between 1988 ITE/Silsoe Field Survey Data and Landsat MSS VIs for Sites Positioned by Image Identification

Image Sampl.	VI Type	Regression Type: Linear			Logarithmic		
Method		Coeff.	Const.	r^2	Coeff.	Const.	r^2
50m	RVI	0.00013	1.233	0.30	0.17610	0.163	0.40
	RVI34	0.00011	1.210	0.28	0.14442	0.336	0.35
	NDVI	0.00005	0.101	0.33	0.06553	-0.298	0.45
	NDVI34	0.00004	0.093	0.30	0.05506	-0.241	0.39
	PVI	0.00133	1.582	0.32	1.76702	-9.116	0.41
	PVI34	0.00112	1.411	0.30	1.45734	-7.384	0.36
20x20	RVI	0.00011	1.266	0.31	0.15946	0.291	0.44
	RVI34	0.00010	1.235	0.31	0.13229	0.429	0.41
	NDVI	0.00004	0.114	0.34	0.05882	-0.247	0.49
	NDVI34	0.00004	0.103	0.32	0.05014	-0.203	0.45
	PVI	0.00119	1.917	0.34	1.60578	-7.837	0.44
	PVI34	0.00103	0.296	0.31	1.34905	-7.854	0.38
Central	RVI	0.00008	1.348	0.16	0.12833	0.541	0.32
	RVI34	0.00007	1.305	0.18	0.10983	0.618	0.33
	NDVI	0.00003	0.143	0.20	0.04713	-0.153	0.37
	NDVI34	0.00003	0.128	0.21	0.04149	-0.131	0.38
	PVI	0.00085	2.707	0.24	1.29137	-5.305	0.39
	PVI34	0.00076	2.306	0.25	1.11585	-4.584	0.39
3 x 3	RVI	0.00004	1.391	0.13	0.06531	0.988	0.20
	RVI34	0.00004	1.343	0.16	0.05506	1.006	0.22
	NDVI	0.00002	0.162	0.14	0.02228	0.025	0.21
	NDVI34	0.00001	0.146	0.17	0.01954	0.026	0.23
	PVI	0.00057	3.066	0.38	0.68498	-1.003	0.40
	PVI34	0.00049	2.645	0.42	0.58247	-0.798	0.42
Transect	RVI	0.00006	1.359	0.19	0.09582	0.761	0.34
	RVI34	0.00005	1.314	0.21	0.08152	0.809	0.34
	NDVI	0.00002	0.150	0.21	0.03416	-0.063	0.37
	NDVI34	0.00002	0.134	0.22	0.02998	-0.052	0.37
	PVI	0.00073	2.779	0.32	1.00906	-3.379	0.44
	PVI34	0.00064	2.377	0.32	0.86526	-2.876	0.42

Table A.57: Results of Regression Analysis Between 1988 ITE/Silsoe Field Survey Data and Landsat MSS VIs for Sites Positioned by Image Identification, Excluding Sites No. 6, 7 and 8

Image Sampl.	VI Type	Regression Type					
		Linear			Logarithmic		
Method		Coeff.	Const.	r^2	Coeff.	Const.	r^2
50m	RVI	0.00016	1.159	0.51	0.18448	0.078	0.61
	RVI34	0.00013	1.146	0.47	0.14792	0.284	0.53
	NDVI	0.00006	0.075	0.53	0.06899	-0.331	0.64
	NDVI34	0.00005	0.070	0.48	0.05677	-0.262	0.56
	PVI	0.00154	0.896	0.51	1.75665	-9.393	0.60
	PVI34	0.00126	0.843	0.48	1.41785	-7.439	0.55
20x20	RVI	0.00014	1.212	0.49	0.16652	0.225	0.64
	RVI34	0.00011	1.191	0.46	0.13484	0.394	0.59
	NDVI	0.00005	0.095	0.50	0.06181	-0.273	0.67
	NDVI34	0.00004	0.087	0.47	0.05154	-0.219	0.62
	PVI	0.00133	1.419	0.50	1.58168	-7.932	0.64
	PVI34	0.00109	-0.126	0.45	1.27462	-7.628	0.55
Central	RVI	0.00014	1.251	0.54	0.16307	0.286	0.70
	RVI34	0.00011	1.227	0.54	0.13575	0.425	0.68
	NDVI	0.00005	0.111	0.55	0.05858	-0.237	0.73
	NDVI34	0.00004	0.101	0.55	0.05044	-0.197	0.71
	PVI	0.00127	1.873	0.61	1.49188	-6.929	0.77
	PVI34	0.00107	1.644	0.60	1.25204	-5.737	0.74
3 x 3	RVI	0.00006	1.406	0.28	0.07535	0.949	0.47
	RVI34	0.00005	1.357	0.28	0.06125	0.986	0.44
	NDVI	0.00002	0.168	0.30	0.02550	0.013	0.49
	NDVI34	0.00002	0.151	0.29	0.02160	0.020	0.46
	PVI	0.00055	3.263	0.43	0.65947	-0.637	0.55
	PVI34	0.00046	2.821	0.41	0.54029	-0.364	0.51
Transect	RVI	0.00009	1.326	0.36	0.11113	0.657	0.53
	RVI34	0.00007	1.289	0.34	0.09138	0.740	0.50
	NDVI	0.00003	0.139	0.37	0.03934	-0.098	0.56
	NDVI34	0.00003	0.125	0.35	0.03349	-0.076	0.52
	PVI	0.00085	2.521	0.42	1.03697	-3.643	0.57
	PVI34	0.00071	2.187	0.40	0.85937	-2.911	0.53

Table A.58: Results of Regression Analysis Between 1988 ITE/Silsoe Field Survey Data and NOAA AVHRR VIs for Sites Positioned by Image Identification

Image Sampl.	VI Type	Regression Type Linear			Logarithmic		
Method		Coeff.	Const.	r^2	Coeff.	Const.	r^2
		Image from 06.09.88					
Central	RVI	-0.00010	1.690	0.11	-0.12641	2.446	0.12
	NDVI	-0.00003	0.258	0.11	-0.04072	0.499	0.12
	PVI	-0.00065	9.317	0.05	-1.06238	15.994	0.09
3 x 3	RVI	-0.00005	1.624	0.05	-0.05694	1.950	0.04
	NDVI	-0.00002	0.239	0.06	-0.01967	0.351	0.04
	PVI	-0.00008	8.628	0.00	-0.31334	10.782	0.01
Transect	RVI	-0.00008	1.642	0.09	-0.08122	2.106	0.07
	NDVI	-0.00003	0.245	0.10	-0.02780	0.403	0.07
	PVI	-0.00163	8.150	0.12	-1.64743	17.507	0.09
		Image from 05.10.88					
Central	RVI	0.00010	1.178	0.32	0.12243	0.443	0.37
	NDVI	0.00004	0.084	0.32	0.04631	-0.196	0.40
	PVI	0.00136	1.091	0.38	1.73402	-9.331	0.44
3 x 3	RVI	0.00006	1.236	0.15	0.07643	0.780	0.16
	NDVI	0.00002	0.106	0.14	0.02801	-0.062	0.16
	PVI	0.00087	1.895	0.17	1.02851	-4.183	0.17

Table A.59: Results of Regression Analysis Between 1988 ITE/Silsoe Field Survey Data and NOAA AVHRR Maximum Value VIs for Sites Positioned by Image Identification

Image Sampl.	VI Type	Regression Type Linear			Logarithmic		
Method		Coeff.	Const.	r^2	Coeff.	Const.	r^2
Central	RVI	-0.00005	1.697	0.03	-0.06348	2.078	0.04
	NDVI	-0.00002	0.258	0.04	-0.02007	0.377	0.04
	PVI	-0.00051	9.364	0.03	-0.85918	14.785	0.06
3 x 3	RVI	0.00005	1.558	0.06	0.04414	1.315	0.03
	NDVI	0.00001	0.216	0.06	0.01283	0.146	0.03
	PVI	0.00019	8.331	0.01	-0.08401	9.245	0.00

Table A.60: Results of Regression Analysis Between 1988 ITE/Silsoe Field Survey Data and NOAA AVHRR VIs for Sites Positioned by Image Identification, Excluding Sites No. 6, 7 and 8

Image Sampl.	VI Type	Regression Type Linear			Logarithmic		
Method		Coeff.	Const.	r^2	Coeff.	Const.	r^2
		Image from 05.10.88					
Central	RVI	0.00013	1.153	0.58	0.14423	0.321	0.61
	NDVI	0.00005	0.075	0.59	0.05421	-0.240	0.65
	PVI	0.00180	0.836	0.61	1.97076	-10.59	0.66
3 x 3	RVI	0.00009	1.242	0.42	0.09351	0.702	0.43
	NDVI	0.00003	0.110	0.42	0.03394	-0.087	0.46
	PVI	0.00113	2.094	0.47	1.20410	-4.843	0.48

Table A.61: Results of Regression Analysis Between Landsat MSS and NOAA AVHRR VIs for 1988 ITE/Silsoe Field Survey Site, Positioned by Image Identification

VI Type		Bands 2 and 4			Bands 2, 3 and 4		
AVHRR	MSS	Coeff.	Const.	r^2	Coeff.	Const.	r^2
		50m Landsat MSS vs. Central NOAA AVHRR					
RVI	RVI	-0.70387	2.543	0.29	-0.84903	2.703	0.33
NDVI	NDVI	-0.64047	0.317	0.28	-0.75501	0.323	0.31
PVI	PVI	-0.87339	11.525	0.47	-1.02178	11.549	0.49
06.09.88		Central Landsat MSS vs. Central NOAA AVHRR					
RVI	RVI	-0.45242	2.194	0.08	-0.60379	2.382	0.10
NDVI	NDVI	-0.40790	0.281	0.07	-0.53220	0.294	0.09
PVI	PVI	-1.06739	12.627	0.39	-1.25825	12.708	0.40
05.10.88		Central Landsat MSS vs. 3 x 3 NOAA AVHRR					
RVI	RVI	1.22411	-0.458	0.79	1.55236	-0.851	0.81
NDVI	NDVI	1.36021	-0.114	0.81	1.64972	-0.137	0.83
PVI	PVI	2.26101	-5.717	0.88	2.67784	-5.928	0.85

Table A.62: Results of Regression Analysis Between Combined CIPEA and 1985 ITE/Silsoe Ground Data for Landsat MSS VIs for Sites Positioned by Image Identification

Image Sampl.	VI Type	Regression Type Linear			Logarithmic		
Method		Coeff.	Const.	r^2	Coeff.	Const.	r^2
50m	RVI	0.00028	1.120	0.70	0.03492	1.075	0.47
	RVI34	0.00024	1.115	0.73	0.03026	1.073	0.52
	NDVI	0.00011	0.058	0.68	0.01390	0.038	0.49
	NDVI34	0.00009	0.055	0.71	0.01235	0.037	0.54
	PVI	0.00344	0.624	0.69	0.47083	-0.135	0.57
	PVI34	0.00305	2.095	0.69	0.46244	1.221	0.71
20x20	RVI	0.00027	1.129	0.71	0.03366	1.082	0.50
	RVI34	0.00022	1.123	0.72	0.02902	1.081	0.53
	NDVI	0.00010	0.061	0.70	0.01338	0.042	0.53
	NDVI34	0.00009	0.059	0.71	0.01182	0.040	0.56
	PVI	0.00333	0.719	0.71	0.46086	-0.041	0.60
	PVI34	0.00296	2.182	0.69	0.45002	1.327	0.71
Central	RVI	0.00024	1.153	0.71	0.02894	1.118	0.46
	RVI34	0.00020	1.144	0.71	0.02501	1.111	0.48
	NDVI	0.00009	0.072	0.70	0.01132	0.057	0.48
	NDVI34	0.00008	0.068	0.70	0.01005	0.054	0.50
	PVI	0.00294	1.045	0.68	0.39119	0.443	0.54
	PVI34	0.00257	2.472	0.63	0.37567	1.796	0.60
3 x 3	RVI	0.00023	1.163	0.67	0.02638	1.135	0.39
	RVI34	0.00019	1.152	0.67	0.02279	1.126	0.41
	NDVI	0.00009	0.076	0.66	0.01022	0.064	0.40
	NDVI34	0.00008	0.071	0.66	0.00909	0.060	0.42
	PVI	0.00284	1.152	0.66	0.36166	0.643	0.48
	PVI34	0.00250	2.560	0.64	0.35037	1.973	0.56
Transect	RVI	0.00023	1.184	0.51	0.02418	1.165	0.25
	RVI34	0.00019	1.170	0.51	0.02057	1.154	0.25
	NDVI	0.00009	0.084	0.50	0.00909	0.077	0.25
	NDVI34	0.00007	0.078	0.50	0.00799	0.072	0.25
	PVI	0.00267	1.465	0.49	0.30311	1.153	0.28
	PVI34	0.00228	2.876	0.46	0.27853	2.521	0.31

Table A.63: Results of Regression Analysis Between Combined CIPEA and 1985 ITE/Silsoe Ground Data for NOAA AVHRR for Sites Positioned by Image Identification

Image Sampl.	VI Type	Regression Type Linear			Logarithmic		
Method		Coeff.	Const.	r^2	Coeff.	Const.	r^2
Central	RVI	0.00018	1.151	0.79	0.02299	1.117	0.61
	NDVI	0.00007	0.071	0.78	0.00933	0.056	0.62
	PVI	0.00224	0.695	0.77	0.29519	0.249	0.60
3 x 3	RVI	0.00016	1.163	0.71	0.01958	1.136	0.50
	NDVI	0.00006	0.075	0.69	0.00790	0.064	0.50
	PVI	0.00198	0.859	0.69	0.24989	0.515	0.49
Transect	RVI	0.00027	1.193	0.51	0.03405	1.148	0.35
	NDVI	0.00010	0.088	0.53	0.01259	0.071	0.38
	PVI	0.00318	0.883	0.51	0.36923	0.473	0.31

Table A.64: Results of Regression Analysis Between Combined CIPEA and 1985 ITE/Silsoe Ground Data for NOAA AVHRR Maximum Value VIs for Sites Positioned by Image Identification

Image Sampl.	VI Type	Regression Type Linear			Logarithmic		
Method		Coeff.	Const.	r^2	Coeff.	Const.	r^2
Central	RVImax	0.00048	1.154	0.84	0.05606	1.090	0.51
	NDVImax	0.00016	0.076	0.85	0.02001	0.050	0.56
	PVImx	0.00506	0.414	0.80	0.60749	-0.328	0.52
3 x 3	RVImax	0.00042	1.166	0.76	0.04869	1.112	0.46
	NDVImax	0.00015	0.079	0.76	0.01752	0.058	0.49
	PVImax	0.00440	0.594	0.70	0.50496	0.054	0.41
Transect	RVImax	0.00026	1.198	0.38	0.02568	1.185	0.16
	NDVImax	0.00009	0.090	0.38	0.00927	0.085	0.17
	PVImax	0.00273	0.838	0.28	0.22264	0.902	0.08

Table A.65: Cloud Cover Over Field Survey Samples of 1985 ITE/Silsoe Field Survey Single Band Threshold and Local Variation Methods

Site	NOAA AVHRR Image Date 2108	2208	3008	3108	1009	Landsat MSS Band 2
A			*++			
B		+	*++			
C		+				
D	++	*			+	
E	*+	*+	+			
F		*+	+			
G		*+				+
H		+				

* NOAA AVHRR CH 2 >= 30% apparent spectral albedo
Landsat MSS B 2 >= 25% apparent spectral reflectance
\+ NOAA AVHRR CH 2 >= 10% coefficient of variation (DN)
Landsat MSS B 2 >= 10% coefficient of variation (DN)
++ NOAA AVHRR CH 2 >= 20% coefficient of variation (DN)
Landsat MSS B 2 >= 20% coefficient of variation (DN)
NOAA AVHRR and Landsat MSS from 3 x 3 1.1km pixel area
Landsat MSS2 from 20 x 20 50m pixel area

Table A.66: Cloud Cover Over Field Survey Samples of 1985 CIPEA Field Survey Single Band Threshold and Local Variation Methods

Site	Positions from aircraft NOAA AVHRR Image Date 2108 2208 3008 3108 1009	Site	Positions from image NOAA AVHRR Image Date 2108 2208 3008 3108 1009
2	++ + +	2	++ ++ ++ ++ ++
3	++	3	+
4	+	4	
5		5	
6	+ *+	6	+ *+
7	+	7	+
11	* +		
12	*+ *++ *+		
13	* *+		
14	*		
15	*+ *		
16	+		
17	*++	17	*++
18	+	18	
19	*		
20	*		
22	* * * ++		
23	+ *+ * *		
24	*		
25	*		
26			
32			
33	*		
34	+ +		

* NOAA AVHRR CH 2 >= 30 % apparent spectral albedo
\+ NOAA AVHRR CH 2 >= 10 % coefficient of variation (DN)
++ NOAA AVHRR CH 2 >= 20 % coefficient of variation (DN)
All data from 3 x 3 1.1km pixel area

Table A.67: Cloud Cover Over Field Survey Samples of CAZS and 1988 ITE/Silsoe/CASTE Field Survey Single Band Threshold and Local Variation Methods

	Position from Map Identification NOAA AVHRR Image Date	Land-sat
CAZS Field Survey		
Site	1507 2407 0108 0308 2008 3008 0609 2509 0510 1510	Band 2
A		+
B		
C		+
D		+
E		+
F		
G		+
H		
J		
K		
L	*	
M	*	
N		+
P	*	*
1988 ITE/Silsoe/CASTE Field Survey		
Site	0407 1507 2407 0108 0308 2008 0609 0510 2410 3010	Band 2
1		
2		++
3	+	
4	+	
5	++	+
6		
7		
8	++	+
9		+
10		+
11		+
12	+	+

* NOAA AVHRR CH 2 >= 30% apparent spectral albedo
Landsat MSS B 2 >= 25% apparent spectral reflectance
\+ NOAA AVHRR CH 2 >= 10% coefficient of variation (DN)
Landsat MSS B 2 >= 10% coefficient of variation (DN)
++ NOAA AVHRR CH 2 >= 20% coefficient of variation (DN)
Landsat MSS B 2 >= 20% coefficient of variation (DN)
NOAA AVHRR and Landsat MSS1 from 3 x 3 1.1km pixel area
Landsat MSS2 from 20 x 20 50m pixel area

Table A.68: Correction Factors of Variations in Solar Illumination Conditions for Landsat MSS

Date	Solar Distance (AU)	Solar Zenith α_z (deg)	Solar Distance Correction c_{sd} (unitless)	Solar Elevation Correction c_{cos} * (unitless)
31.08.85	1.00908	31.96	1.018	0.916
30.08.88	1.00930	31.82	1.019	0.915
08.09.88	1.00703	32.97	1.014	0.927

* For 39° reference angle.

Table A.69: Correction Factors of Variations in Solar Illumination Conditions for NOAA AVHRR LAC Data

Date	Sensor Degradation Correction Ch 1 (unitless)	Sensor Degradation Correction Ch 2 (unitless)	Solar Distance (AU)	Solar Zenith α_z (deg)	Solar Distance Correction c_{sd} (unitless)	Solar Elevation Correction c_{cos} * (unitless)
			1985 CIPEA Field Survey			
21.08.85	91.77	84.78	1.0113	39.51	1.0228	1.007
22.08.85	91.76	84.77	1.0111	39.57	1.0224	1.008
30.08.85	91.65	84.72	1.0093	40.20	1.0187	1.017
31.08.85	91.63	84.71	1.0091	40.29	1.0182	1.019
10.09.85	91.49	84.64	1.0066	41.38	1.0132	1.036
			1985 ITE/Silsoe Field Survey			
21.08.85	91.77	84.78	1.0113	39.40	1.0228	1.006
22.08.85	91.76	84.77	1.0111	39.47	1.0224	1.007
30.08.85	91.65	84.72	1.0093	40.09	1.0187	1.016
31.08.85	91.63	84.71	1.0091	40.19	1.0182	1.017
10.09.85	91.49	84.64	1.0066	41.28	1.0132	1.034
			1988 CAZS Field Survey			
07.06.88	77.48	77.29	1.0151	52.33	1.0305	1.272
04.07.88	77.10	77.10	1.0167	52.34	1.0337	1.272
15.07.88	76.95	77.02	1.0164	52.43	1.0330	1.275
24.07.88	76.82	76.95	1.0157	52.57	1.0316	1.279
01.08.88	76.10	76.89	1.0147	52.78	1.0297	1.285
03.08.88	79.68	76.61	1.0145	52.84	1.0292	1.287
20.08.88	76.44	76.75	1.0115	53.67	1.0231	1.312
06.09.88	76.20	76.63	1.0075	55.05	1.0151	1.357
25.09.88	75.94	76.49	1.0024	57.15	1.0048	1.433
05.10.88	75.80	76.38	0.9995	58.67	0.9990	1.495
24.10.88	75.53	76.28	0.9942	61.52	0.9884	1.678
			1988 ITE/Silsoe Field Survey			
04.07.88	77.10	77.10	1.0167	52.44	1.0337	1.275
15.07.88	76.95	77.02	1.0164	52.53	1.0330	1.277
24.07.88	76.82	76.95	1.0157	52.68	1.0316	1.282
01.08.88	76.10	76.89	1.0147	52.89	1.0297	1.288
03.08.88	79.68	76.61	1.0145	52.95	1.0292	1.290
20.08.88	76.44	76.75	1.0115	53.77	1.0231	1.315
06.09.88	76.20	76.63	1.0075	55.16	1.0151	1.360
05.10.88	75.80	76.38	0.9995	58.78	0.9990	1.499
24.10.88	75.53	76.28	0.9942	61.62	0.9884	1.635
30.10.88	75.45	76.23	0.9926	62.50	0.9852	1.683

* Standardized to 39° solar zenith angle.

Table A.70: Linear Coefficients for Direct Conversion of NOAA AVHRR DNs into Exoatmospheric Spectral Albedo, Including Correction for Earth-Sun Constellation

Date	Channel 1 Slope $\alpha(i)$ (% DN^{-1})	Channel 1 Intercept $\beta(i)$ (%)	Channel 2 Slope $\alpha(i)$ (% DN^{-1})	Channel 2 Intercept $\beta(i)$ (%)
CIPEA 1985				
21.08.85	0.1082	-3.5926	0.1217	-3.7216
22.08.85	0.1084	-3.5976	0.1219	-3.7268
30.08.85	0.1099	-3.6429	0.1235	-3.7737
31.08.85	0.1102	-3.6518	0.1238	-3.7830
10.09.85	0.1127	-3.7311	0.1266	-3.8651
ITE/Silsoe 1985				
21.08.85	0.1081	-3.5890	0.1216	-3.7179
22.08.85	0.1083	-3.5940	0.1218	-3.7231
31.08.85	0.1099	-3.6447	0.1236	-3.7755
30.08.85	0.1098	-3.6393	0.1234	-3.7700
10.09.85	0.1125	-3.7239	0.1264	-3.8576
CAZS Mali 1988				
07.06.88	0.1607	-4.5038	0.1674	-4.6655
04.07.88	0.1610	-4.4902	0.1673	-4.6514
15.07.88	0.1618	-4.5038	0.1680	-4.6655
24.07.88	0.1628	-4.5241	0.1689	-4.6865
01.08.88	0.1641	-4.5537	0.1701	-4.7172
03.08.88	0.1645	-4.5630	0.1711	-4.7268
20.08.88	0.1692	-4.6794	0.1751	-4.8474
06.09.88	0.1769	-4.8780	0.1828	-5.0532
25.09.88	0.1894	-5.2028	0.1954	-5.3896
05.10.88	0.1991	-5.4607	0.2054	-5.6568
15.10.88	0.2084	-5.7057	0.2147	-5.9106
CASTE/ITE/Silsoe 1988				
04.07.88	0.1613	-4.5008	0.1677	-4.6624
15.07.88	0.1620	-4.5109	0.1682	-4.6729
24.07.88	0.1632	-4.5347	0.1693	-4.6975
01.08.88	0.1645	-4.5643	0.1705	-4.7282
03.08.88	0.1649	-4.5736	0.1715	-4.7379
20.08.88	0.1696	-4.6901	0.1755	-4.8585
06.09.88	0.1773	-4.8888	0.1832	-5.0643
05.10.88	0.1996	-5.4753	0.2059	-5.6719
24.10.88	0.2209	-6.0361	0.2273	-6.2528
30.10.88	0.2283	-6.2335	0.2349	-6.4573

Table A.71: Ratio Between Bright and Dark Soil Surfaces for NOAA AVHRR Images for CIPEA, 1985 ITE/Silsoe, CAZS and 1988 ITE/Silsoe Field Surveys

Date	Relative Scene Contrast			
	Date		Reference	
	Ch 1 (unitless)	Ch 2 (unitless)	Ch 1 (unitless)	Ch 2 (unitless)
CIPEA 1985				
21.08.85	1.29	1.29	1.32	1.29
22.08.85	1.27	1.27	1.32	1.29
30.08.85	1.25	1.23	1.29	1.24
10.09.85	1.20	1.21	1.29	1.27
ITE/Silsoe 1985				
21.08.85	2.15	2.42	2.23	2.50
22.08.85	1.50	1.53	1.58	1.59
30.08.85	1.57	1.65	1.81	1.93
10.09.85	1.69	1.81	1.84	1.94
CAZS 1988				
06.07.88	1.40	1.27	1.80	1.95
04.07.88	1.55	1.61	1.93	2.08
15.07.88	1.41	1.49	1.90	2.03
01.08.88	1.79	1.92	1.94	2.11
20.08.88	1.88	2.06	1.96	2.09
06.09.88	1.46	1.56	1.90	1.99
25.09.88	1.40	1.57	1.82	1.91
05.10.88	1.50	1.66	1.86	2.00
15.10.88	1.74	1.93	1.82	1.93
ITE/Silsoe 1988				
04.07.88	1.55	1.66	1.82	1.96
15.07.88	1.28	1.41	1.84	1.94
01.08.88	1.49	1.38	1.81	1.83
*20.08.88	1.83	1.77	2.03	2.26
06.09.88	1.29	1.32	1.85	1.97
05.10.88	1.32	1.32	1.82	1.85
24.10.88	1.63	1.63	1.82	1.85
30.10.88	1.26	1.29	1.84	1.89
**31.08.85	1.71	1.75	1.73	1.72

* Only 4 values to compare.
** Only 7 values to compare.

APPENDIX: FIGURES

Figure A.1: Relationship Between Fresh Sample Weight and Oven-Dried Moisture Content for 1988 ITE/Silsoe Survey

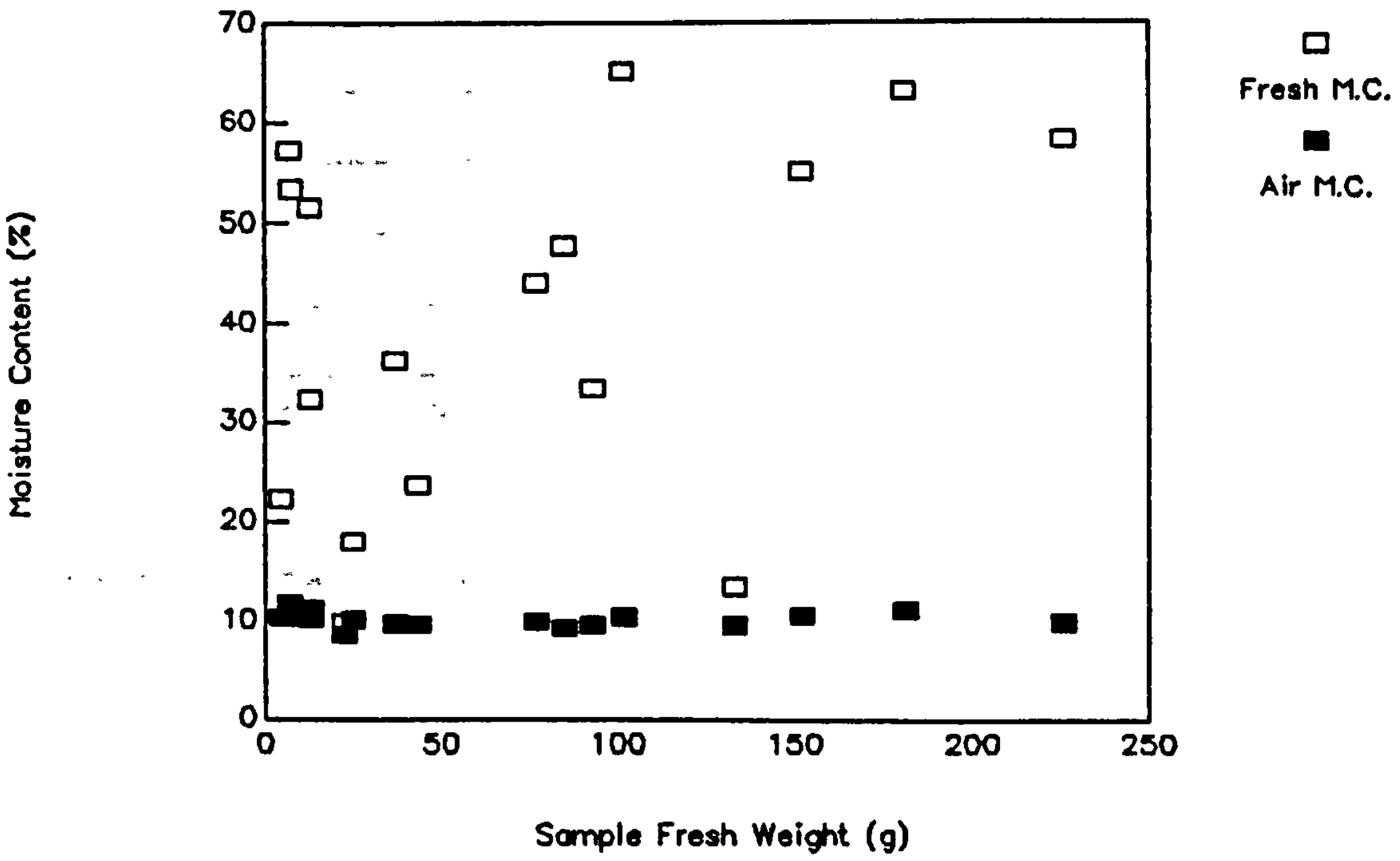


Figure A.2: Relationship Between View Angle and NOAA AVHRR Channel 1 Sensor Response of 1985

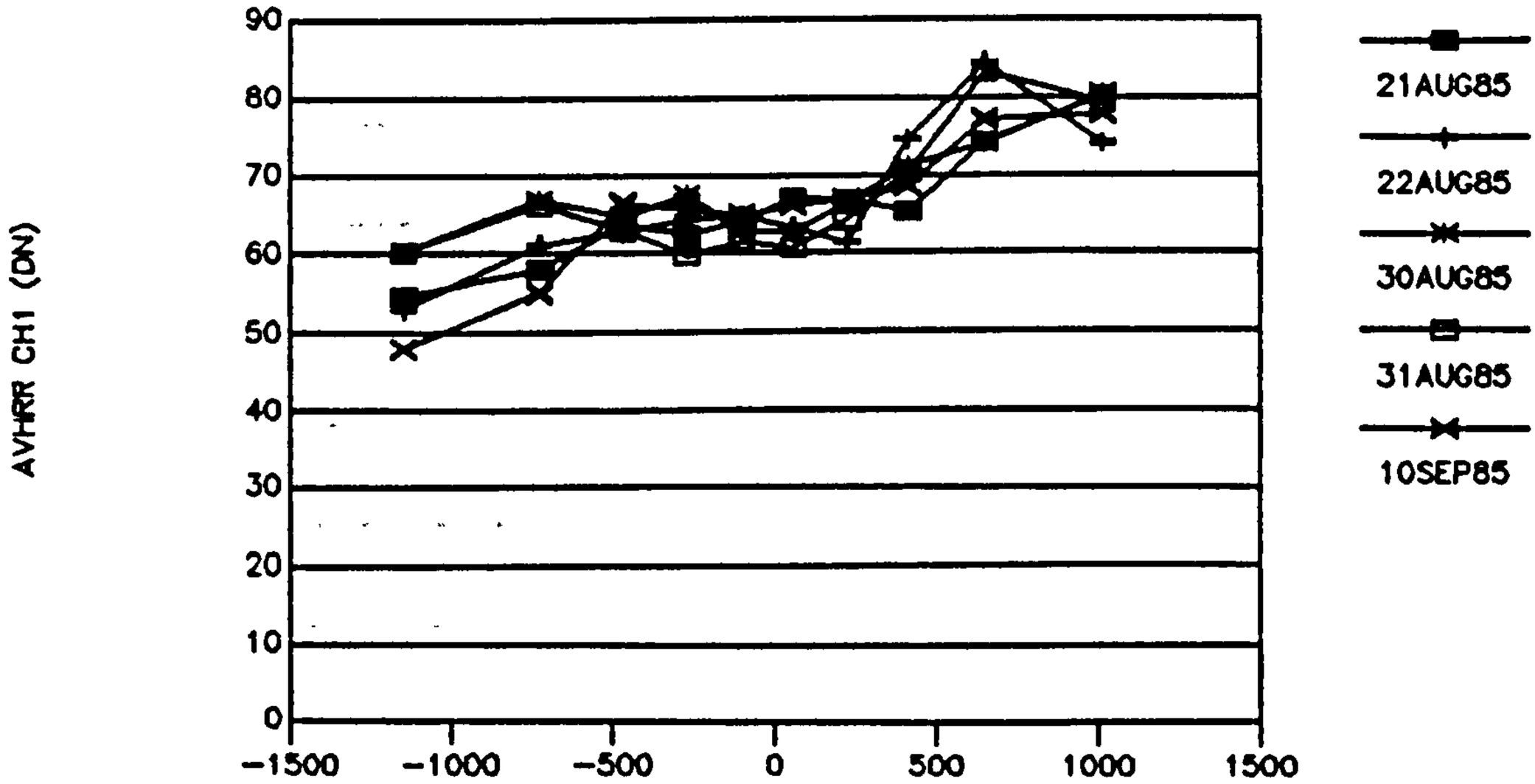


Figure A.3: Relationship Between View Angle and NOAA AVHRR Channel 2 Sensor Response of 1985

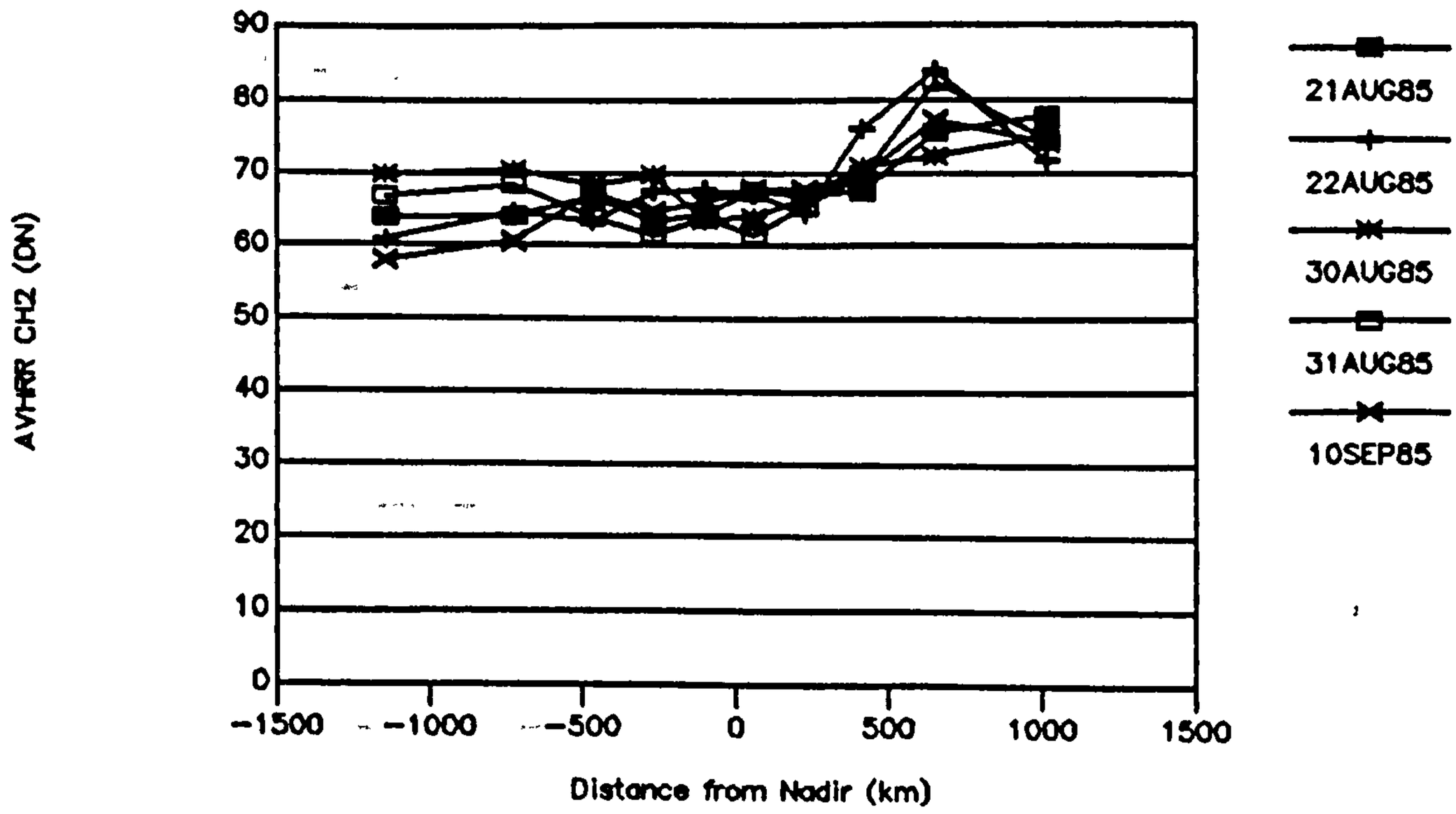


Figure A.4: Relationship Between View Angle and NOAA AVHRR RVI of 1985

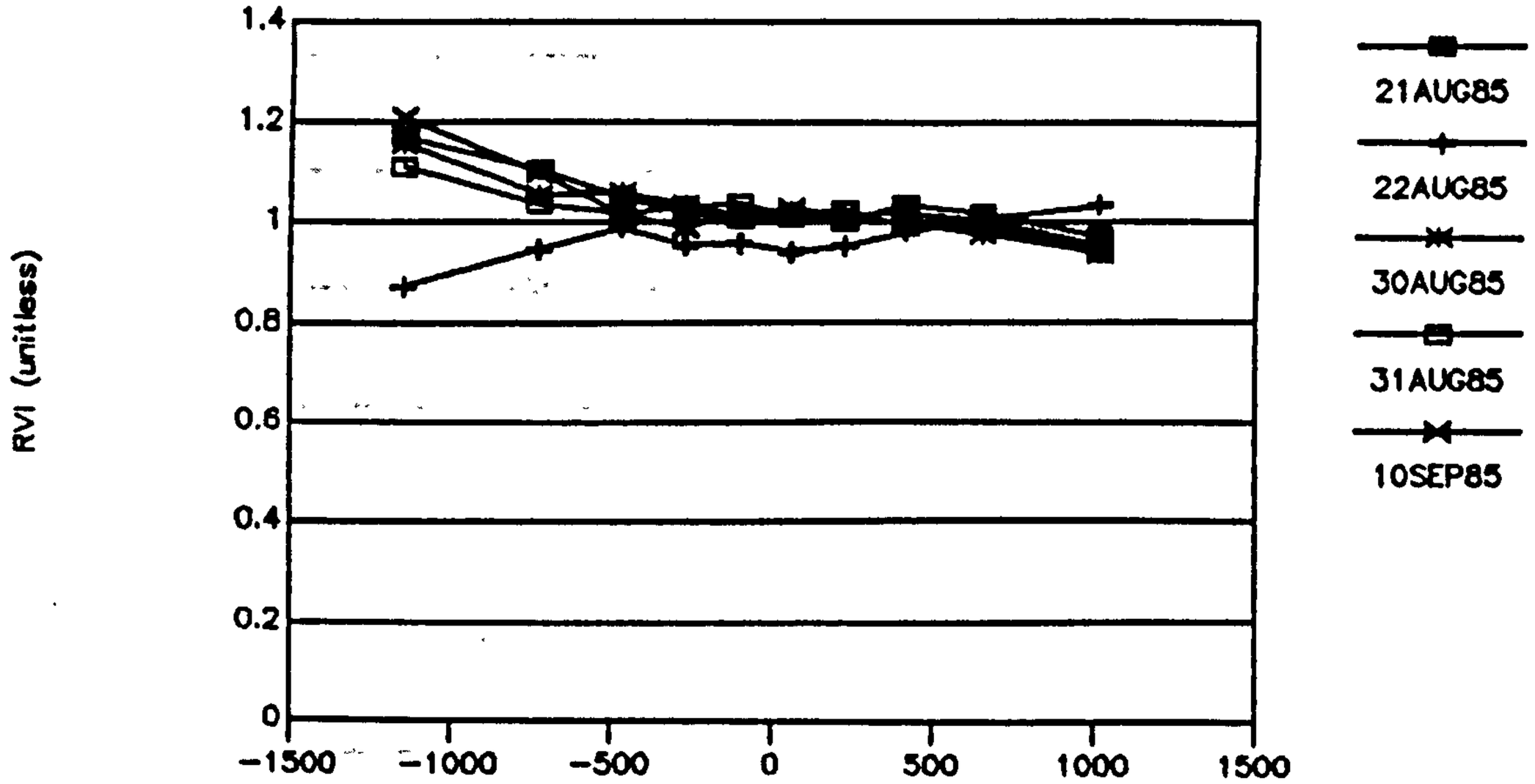


Figure A.5: Relationship Between View Angle and NOAA AVHRR Channel 1 Sensor Response of 1988, First Half of Growing Season

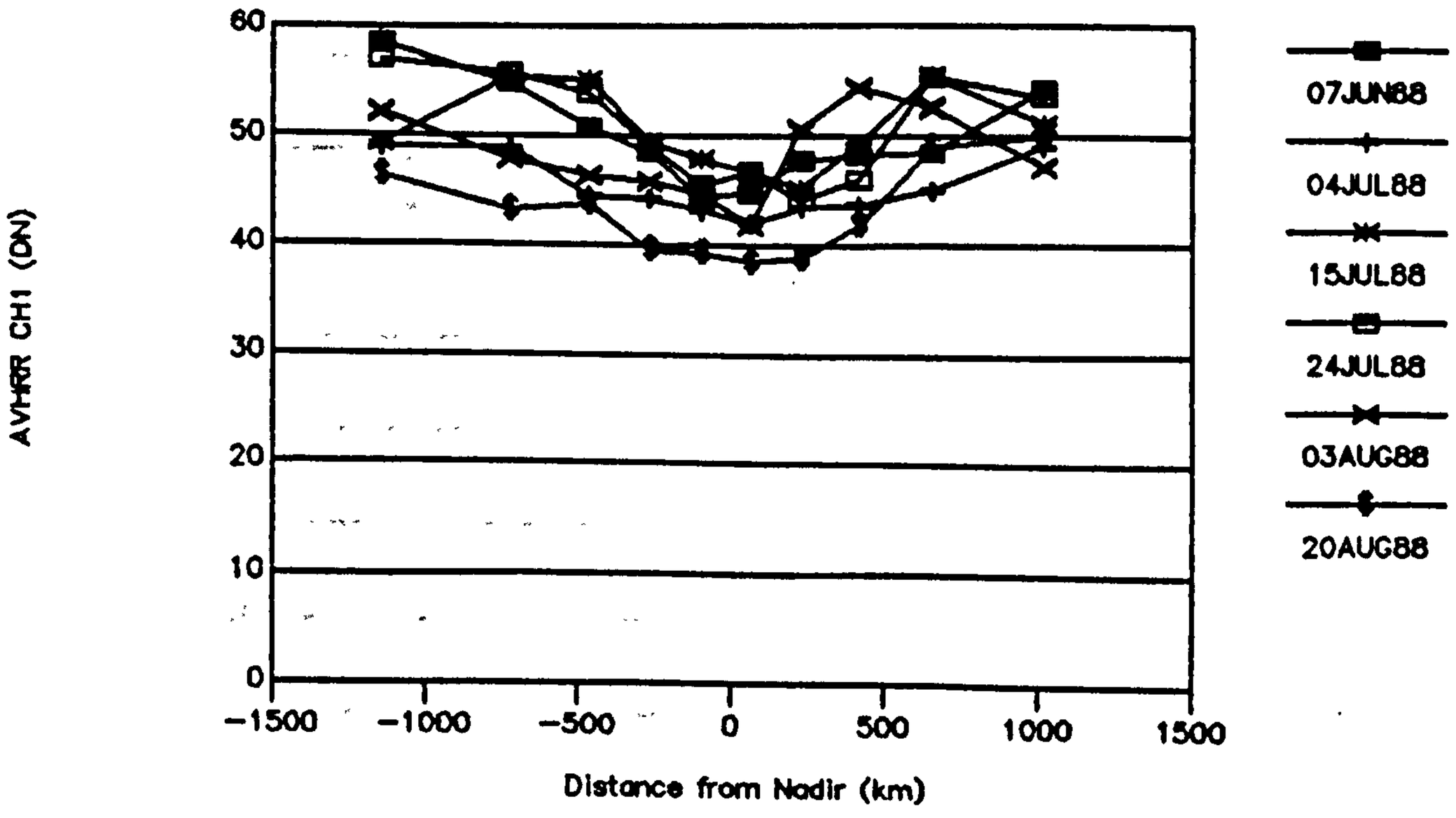


Figure A.6: Relationship Between View Angle and NOAA AVHRR Channel 1 Sensor Response of 1988, Second Half of Growing Season

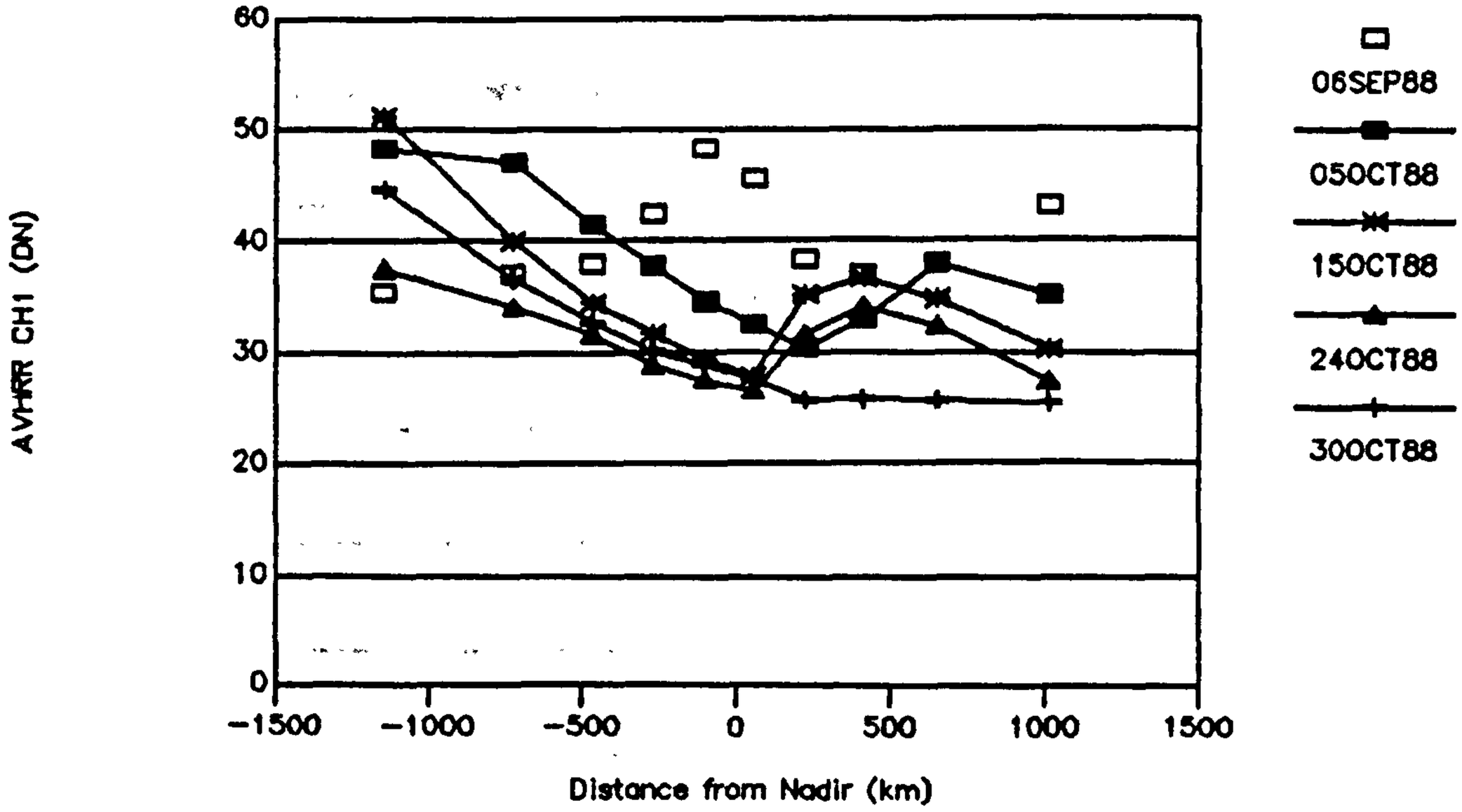


Figure A.7: Relationship Between View Angle and NOAA AVHRR Channel 2 Sensor Response of 1988, First Half of Growing Season

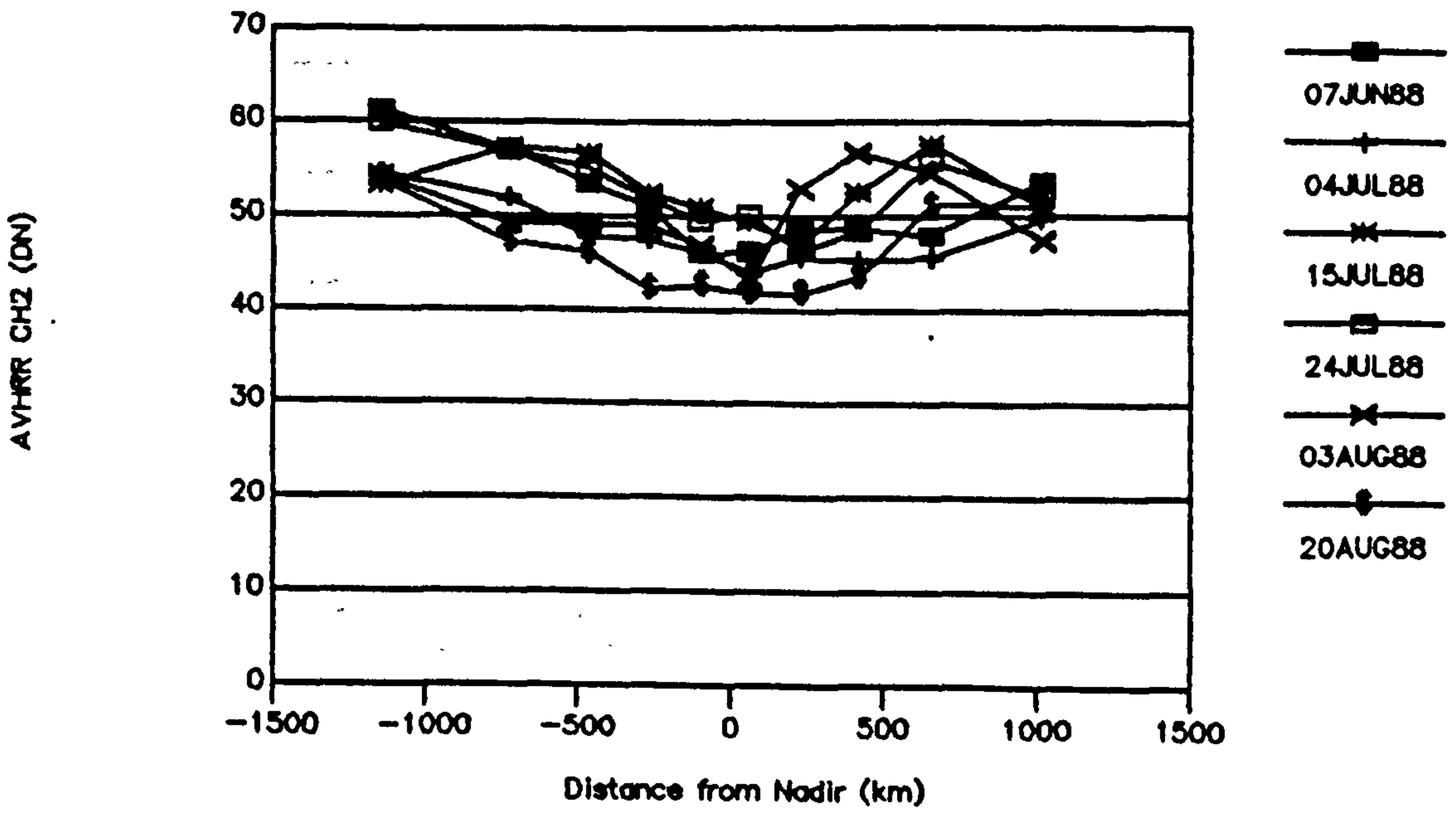


Figure A.8: Relationship Between View Angle and NOAA AVHRR Channel 2 Sensor Response of 1988, Second Half of Growing Season

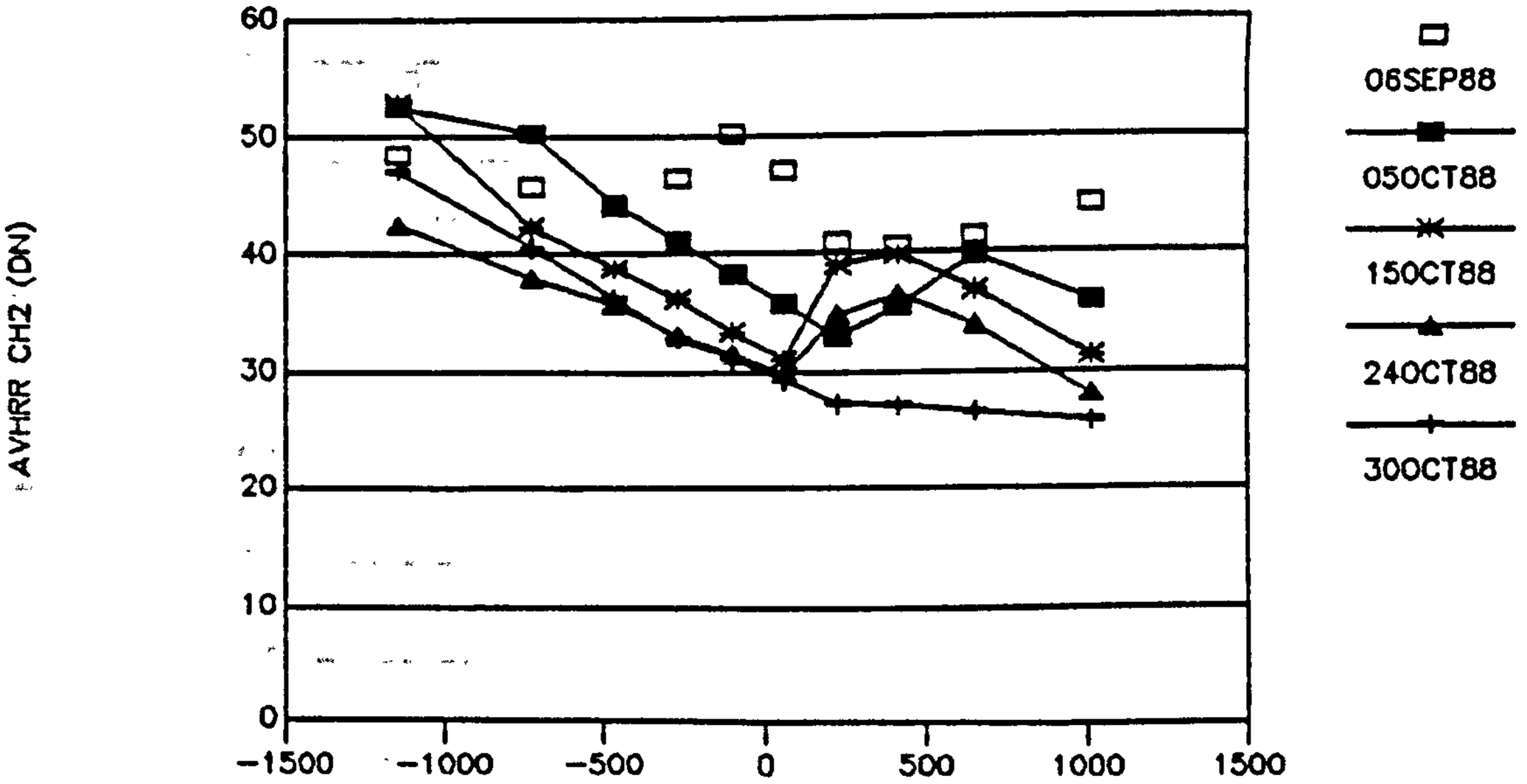


Figure A.9: Relationship Between View Angle and RVI for NOAA AVHRR Images of 1988, First Half of Growing Season

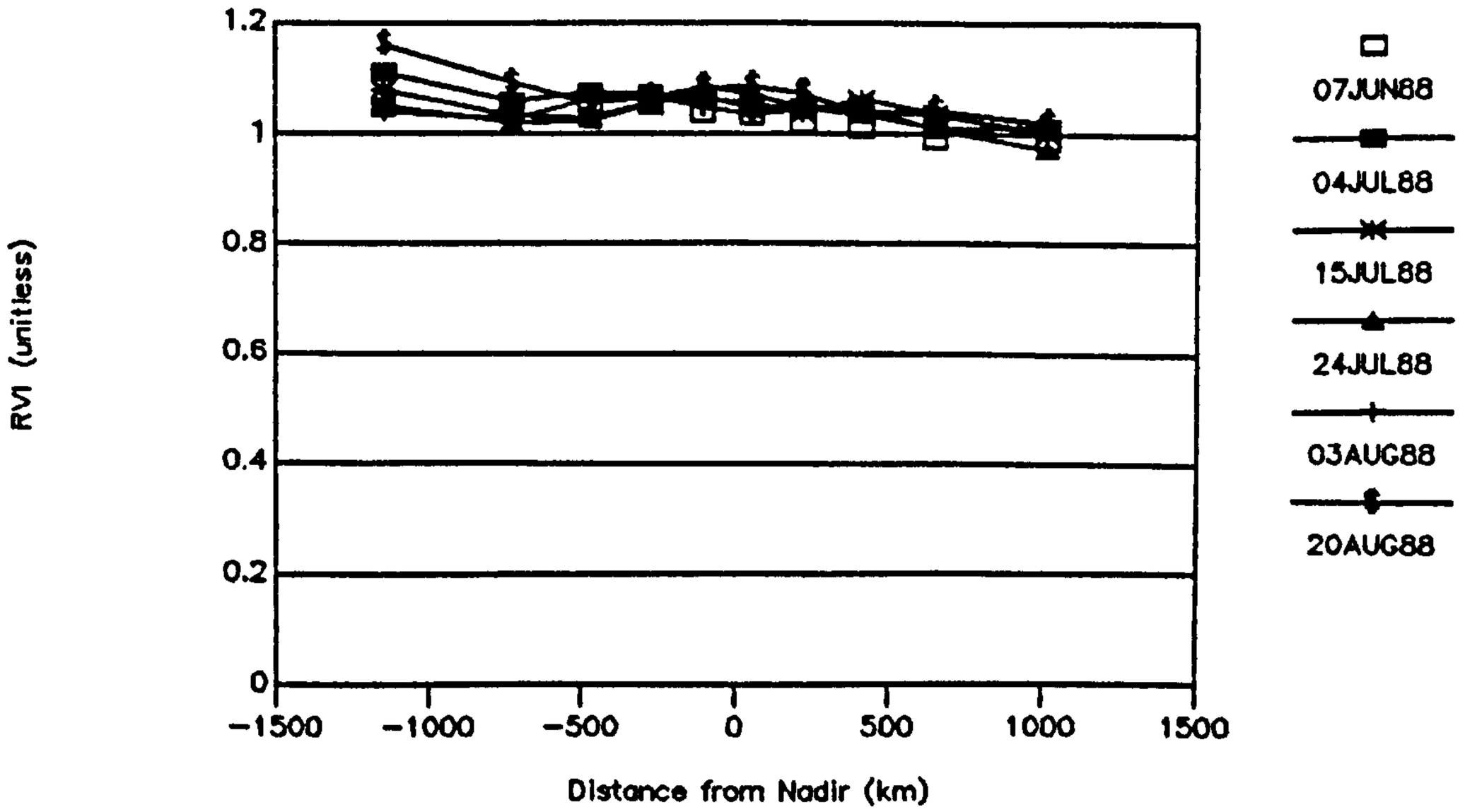
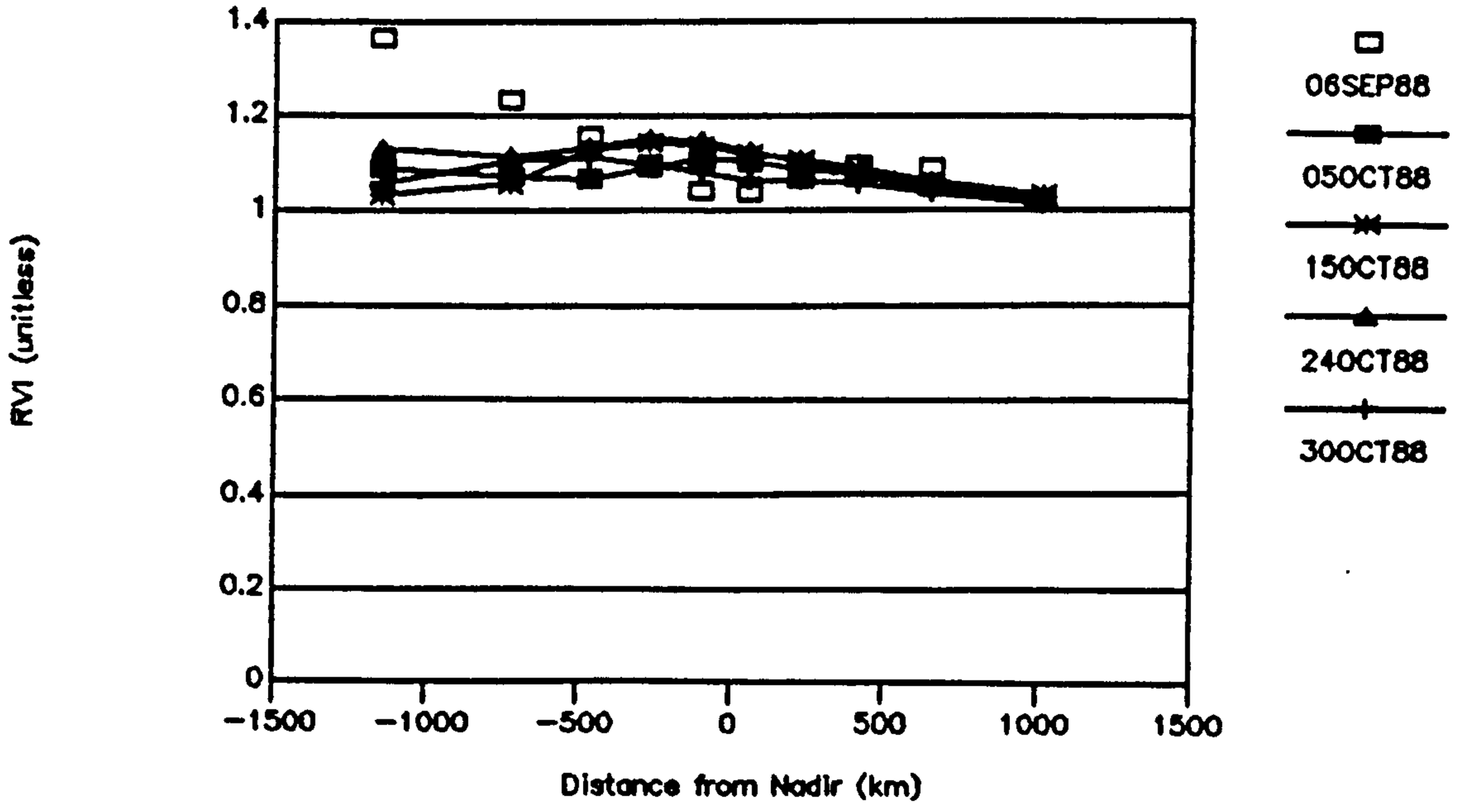


Figure A.10: Relationship Between View Angle and RVI for NOAA AVHRR Images of 1988, Second Half of Growing Season



BIBLIOGRAPHY

BIBLIOGRAPHY

AARONSON, A.C. and L.L.Davis (1979) *An Evaluation of the Relationship Between Vegetation Indices, Soil Moisture and Wheat Yields.* AgRISTARS, Crop Condition Assessment Division, Foreign Agricultural Service, Technical Memorandum No. 9, USDA/FAS, Houston, Texas.

AHERN, F.J., R.J. Brown, J. Cihlar, R. Gauthier, J. Murphy, R.A. Neville and P.M. Teillet (1987) Radiometric Correction of Visible and Infrared Remote Sensing Data at the Canada Centre for Remote Sensing. *International Journal of Remote Sensing*, Vol 8. No. 9 pp. 1349-1376.

AHLCRONA, E. (1988) *The Impact of Climate and Man on Land Transformation in Central Sudan - Applications of Remote Sensing.* Doctoral Dissertation at the Department of Physical Geography, Lund, Sweden, 140 pp.

AHN, P.M. (1970) *West African Soils, Vol. 1.* Oxford University Press, Oxford.

ALLAN, J.A. and T.S. Richards (1983) Remote Sensing for Identifying Low Density Vegetation Cover in Semi-arid and Coastal North-west Egypt. *Application of Remote Sensing for Rangeland Monitoring and Management, Proc. of an International Conference*, Silsoe 1983, pp. 69-79.

ANTROP, M. (1983) Inventorying and Monitoring of Landscape as a Natural and Cultural Resource. *Proc. of a EARSeL/ESA Symp. on Remote Sensing, Applications for Environmental Studies*, Brussels, 26-29 April 1983, ESA SP-188, pp. 105-113.

ASHBURN, P. (1979) The Vegetation Index Number and Crop Identification. *Proc. LACIE Symposium*, July 1979, JSC-16015, NASA, Johnson Space Centre, Houston, Texas, pp. 843-855.

ASHLEY, M.D. and J. Rea (1975) Seasonal Vegetation Differences form ERTS Imagery. *Photogrammetric Engineering and Remote Sensing*, Vol. 41, pp. 713-719.

ASRAR, G.H., E.T. Kanemasu, R.D. Jackson and P.J. Pinter (1984) Estimation of Total Above Ground Phytomass Production Using Remotely Sensed Data. *Remote Sensing of Environment*, Vol. 17, pp. 211-220.

ASRAR, G., R.B. Mgneni, Y. Li and E.T. Kaufman (1989) Measuring and Modelling Spectral Characteristics of Tall-Grass Prairie. *Remote Sensing of Environment*, Vol. 27, pp. 143-155.

ASTRONOMICAL ALMANACH (1986) *Astronomical Almanach for 1987.* Issued by: Her Majesty's Nautical Almanach Office, London.

BARNSLEY, M.J. (1983) The Implications of View Angle Effects on the Use of Multi-Spectral Data for Vegetation Studies. *Remote Sensing for Rangeland Monitoring and Management, Proc. of an International Conf.*, Silsoe, UK, Sept. 1983, pp. 166-177.

BARTHOLOME, E. (1989) Calibration of Vegetation Indices for APAR Measurements Using Intrinsic Satellite Image Information. *Remote Sensing for Operational Appositions, Technical Contents of the 15th Annual Conference of the Remote Sensing Society*, University of Bristol, 13-15 September 1989, pp. 47-52.

BAUER, M.E. (1978) Spectral Characteristics of Remote Sensing of Corn and Soybean. *Proc. 1978 LACIE Corn-Soybean Seminar, JSC-13744*, NASA, Johnson Space Centre, Houston, Texas, pp. 3-24.

BECKER, F., F. Nerry, P. Ramanantsizehena and J. Fisher (1988) Towards a Quantitative Use of Aerial Colour Infrared Films. *Photogrammetric Engineering and Remote Sensing*, Vol. 54, No. 6, pp. 743-750.

BERGES, J.C. (1989) *Introduction a l'Application des Techniques de Teledection au Suivi Pastoral.* Atelier sur le Suivi des Ressources Pastorales au Sahel, Pay du CILS, Centre Agrhyment, Niamey, Niger, pp. 27-38.

BERNSTEIN, R. (1975) Digital Image Processing. *Photogrammetric Engineering and Remote Sensing*, Vol. 41, pp. 1465-1476.

BERNSTEIN, R. (1983) *Image Geometry and Rectification.* *Manual of Remote Sensing*, 2nd ed., Colwell, R.N. (ed.), American Society of Photogrammetry, Falls Church, Virginia, Ch. 21.

BILLINGLEY, F.C. (1983) *Data Processing and Reprocessing.* Manual of Remote Sensing, 2nd ed., Colwell, R.N. (ed.), American Society of Photogrammetry, Falls Church, Virginia, Ch. 17, pp. 719-792.

BOLLE, H.-J. (1986) Vegetation Identification and Variability in the Tahoua Area, Niger. *Proc. ISLSCP Conference*, Rome 2-6 Dec. 1985, ESA SP-248. pp. 461-466.

BOUTTON, J.E. and L.L. Tieszen (1983) Estimation of Plant Biomass by Spectral Reflectance in an East African Grassland. *Journal of Range Management*, Vol. 36, No. 2, pp. 213-221.

BRADBURY, P.A. and E.M. Rollin. (ed.) (1986) Ground Truth for Remote Sensing. *Proc. of a Remote Sensing Workshop, University of Nottingham*, Remote Sensing Group, pp. 152-161.

BREMAN. H. and C.T. DeWit (1983) Rangeland Production and Exploitation on the Sahel. *Science*, Vol. 221, pp. 1341-1347.

BROWN, R. (1988) *Report on EMDUP Field Work, Mali 1988.* Centre of Arid Zone Studies, University College of North Wales, 7 pp.

BRUSH, R.J.H. (1988) The Navigation of AVHRR Imagery. *International Journal of Remote Sensing*, Vol. 9, No. 9, pp. 1491-1502.

CASELLES, V. and M.J. Lopez Garcia (1989) An alternative Approach to Estimate Atmospheric Correction in Multitemporal Studies. *International Journal of Remote Sensing*, Vol. 10, No. 6, pp. 1127-1134.

CHAHINE, M.T. (1983) *Interaction Mechanisms with the Atmosphere.* Manual of Remote Sensing, Cowell, R.N. (ed.), American Society of Photogrammetry, Fall Church, Virginia, 2nd ed., pp. 165-230.

CHAVEZ, P.S. (1975) Atmospheric, Solar and MTF Corrections for ERTS Digital Imagery. *Proceedings of the American Society of Photogrammetry*, Fall Technical Meeting, Phoenix, AZ, p. 69.

CHAVEZ, P.S. (1988) An Improved Dark-Object Subtraction Technique for Atmospheric Scattering Correction of Multispectral Data. *Remote Sensing of Environment*, Vol. 24, pp. 459-479.

CHOUDHURY, B.J. (1987) Monitoring Global Vegetation Using NIMBUS 7 37 GHz Data - Some empirical Relations. *International Journal of Remote Sensing* Vol. 8, No. 7, pp. 1085-1090.

CHOUDHURY, B.J. and C.J. Tucker (1987) Satellite Observed Seasonal and Interannual Variation over the Kalahari, the Great Victoria Desert and the Great Sandy Desert: 1979 - 1984. *Remote Sensing of Environment*, Vol. 23, pp. 233-241.

CICONE, R.C. and M.D. Metzler (1984) Comparison of Landsat MSS, Nimbus-7 CZCS and NOAA-7 AVHRR Features for Land-Use Analysis. *Remote Sensing of Environment*, Vol. 14, pp. 257-265.

CLEVERS, J.G.P.W. (1988) The Derivation of a Simplified Reflectance Model for Estimation of Leaf Area Index. *Remote Sensing of Environment*, Vol. 25, pp. 53-69.

COINER, J.C. (1980) Using Landsat to Monitor Changes in Vegetation Cover Induced by Desertification Processes. *Proc. of 14th International Symp. on Remote Sensing of Environment*, 23-30 April 1980, ERIM, Ann Arbor, Michigan, pp. 1341-1351.

COLE, M. M. (1986) *The Savannas*. Academic Press, London, 438 pp.

COLWELL, J.E. (1974) Vegetation Canopy Reflectance. *Remote Sensing of Environment*, Vol. 3, pp. 175-183.

COLWELL, R.N. (ed.) (1983) *Manual of Remote Sensing* (2nd ed.), Vol. I, Ch. 16, American Society of Photogrammetry, Falls Church, Virginia, pp. 699-717.

CRACKNELL, A.P. and K. Paithoonwattanakij (1989) Pixel and Sub-pixel Accuracy in Geometrical Correction of AVHRR Imagery. *International Journal of Remote Sensing*, Vol. 10, No. 4, pp. 661-667.

CRIPPEN, R.E. (1987) The Regression Intersection Method of Adjusting Image Data for Band Rationing. *International Journal of Remote Sensing*, Vol. 8, No. 2, pp. 137-155.

CRIPPEN, R.E. (1988) The Dangers of Underestimating the Importance of Data Adjustments in Band Rationing. *International Journal of Remote Sensing*, Vol. 9, No. 4, pp. 767-776.

CRIPPEN, R.E. (1990) Calculating the Vegetation Index Faster. *Remote Sensing of Environment*, Vol. 34, pp. 71-73.

CURRAN, P.J. and H.D. Williamson (1985) How Many Ground Data Samples? A Question for Remote Sensing. *Remote Sensing: Data Acquisition, Management and Applications, Proc. of the Poster Session at the International Conference of the Remote Sensing Society and the Centre for Earth Resource Management*, London, 9 - 12 Sept. 1985, Remote Sensing Society, pp. 163-169.

CURRAN, P.J. and H.D. Williamson (1986) Sample Size for Ground and Remotely Sensed Data. *Remote Sensing of Environment*, Vol. 20, No. 1, pp. 31-41.

DAUBENMIRE, R. (1959) A Canopy-Coverage Method of Vegetation Analysis. *Northwest Science*, Vol. 33, No. 1 , pp. 43-64.

DAUGHTRY, C.S.T. (1988) Estimating Absorbed Radiation and Phytomass from Multispectral Reflectance of Corn and Soybeans. *Proc. of Conference on Monitoring towards the 21st Century*, 12-16 Sept. 1988, Edinburgh, ESA SP-284, pp. 821-824.

DAVE, J.V. (1980) Effect of Atmospheric Conditions on Remote Sensing of Vegetation Parameters. *Remote Sensing of Environment*, Vol. 10, pp. 87-99.

DAVE, J.V. (1981) Influence on Illumination and Viewing Geometry and Atmospheric Composition on the "Tasselled Cap" Transformation of Landsat MSS Data. *Remote Sensing of Environment*, Vol. 11, pp. 37-55.

DAVISON, G.J. (1986) Ground Control Pointing and Geometric Transformation of Satellite Imagery. *International Journal of Remote Sensing*, Vol. 7, No. 1, pp. 65-74.

DEFOURNY, P. (1989) Étude Dynamique de la Végétation Lingeuse en Région Soudano-Sahélienne (Burkina Faso) à Partier de Données Landsat MSS. *Photo Interprétation*, No.2, fascicule 4, pp. 37-48.

DESCHAMPS, P.Y., M. Herman and D. Tandre (1983) Definitions of Atmospheric Radiance and Transmittance in Remote Sensing. *Remote Sensing of Environment*, Vol. 13, pp. 89-92.

DeWISPELAERE, G. and B. Peyre de Fabregues (1988) *Evalution des Ressources Fourrageres par Teledection SPOT Dans la Region du Sud-Tamesna (Niger)*. Etude Thematique, Campagne 1986-87, Ministere d'Elevage, Niamey, 73 pp.

D'HOORE, J.L. (1964) *Soil Map of Africa Scale 1 to 5000000 Explanatory Monograph*. Commission of Technical Cooperation in Africa, Lagos, 250 pp.

vanDIJK, A., S.L. Callis, C.M. Sakamoto and W.L. Decker (1987) Smoothing Vegetation Index Profiles: An Alternative Method for Reducing Radiometric Disturbance in NOAA/AVHRR Data. *Photogrammetric Engineering and Remote Sensing*, Vol. 53, No. 8, pp. 1059-1067.

DREGNE, H.E. and C.J. Tucker (1988) Green Biomass and Rainfall in Semi-Arid Sub-Saharan Africa. *Journal of Arid Environments*, No. 15, pp. 245-252.

D'SOUZA, G. and R. Hiederer (1989) Monitoring Rangeland Vegetation in the Sahel Using NOAA AVHRR Data. *Proc. 4th AVHRR Users' Meeting*, 5-8 September, 1989, Rothenburg, Germany, pp. 111-116.

DUCK, K.I. and J.C. King (1983) Orbital Mechanics for Remote Sensing. *Manual of Remote Sensing*, Colwell, R.N. (ed.), American Society of Photogrammetry, Falls Church, Virginia, Ch. 16., pp. 873-922.

DUGGIN, M.J. (1981) Intercalibration of Landsat 1 - 3 and NOAA 6 and 7 Scanner Data. *Applied Optics*, Vol. 20, pp. 3815-3816.

DUGGIN, M.J., D. Piwinski, V. Whitehead and G. Ryland (1982) Evaluation of NOAA AVHRR Data for Crop Assessment. *Applied Optics*, Vol. 21, pp. 1873-1875.

DUGGIN, M.J. (1985a) Factors Limiting the Discrimination and Quantification of Terrestrial Features Using Remotely Sensed Radiance. *International Journal of Remote Sensing*, Vol. 6, No. 1, pp. 3-27.

DUGGIN, M.J. (1985b) Comments on the Intercalibration of Multisensor, Multitemporal, Multichannel Digital Radiance Data. *Applied Optics*, Vol. 24, pp. 2292-2294.

DUGGIN, M. J. (1987) Impact of Radiance Variations on Satellite Sensor Calibration. *Applied Optics*, Vol. 26, pp. 1264-1271.

EBDON, D. (1985) *Statistics in Geography*. (2nd ed.), Basil Blackwell Inc., New York, 232 pp.

ELVIDGE, C.D. and R.J. Lyon (1985) Influence of Rock-Soil Spectral Variation on the Assessment of Green Biomass. *Remote Sensing of Environment*, Vol. 17, pp. 265-279.

EMERY, W.J., J. Brown and P. Nowak (1989) AVHRR Image Navigation: Summary and Review. *Photogrammetric Engineering and Remote Sensing*, Vol. 555, No. 8, pp. 1175-1183.

ESCADAFAL, R., M.-C. Girard and D. Courault (1989) Munsell Soil Colour and Soil Reflectance in the Visible Spectral Bands of Landsat MSS and TM Data. *Remote Sensing of Environment*, Vol. 27, pp. 27-37.

EYRE, J.R. (1986) Estimating Sea-Surface temperature from AVHRR Data; Comments on a Paper by Singh et al (1985). *International Journal of Remote Sensing*, Vol. 7, No. 3, pp. 465-469.

EZRA, C.E., R.L. Tinney and R.D. Jackson (1984) Effect of soil Background on Vegetation Discrimination Using Landsat Data. *Remote Sensing of Environment*, Vol. 16, pp. 232-242.

FORAN, B.D. (1987) Detection of Yearly Cover Change with LANDSAT MSS on Pastoral Landscape in Central Australia. *Remote Sensing of Environment*, Vol. 23, pp. 233 - 350.

FORREST, R.B. (1981) Simulation of Orbital Image-Sensor Geometry. *Photogrammetric Engineering and Remote Sensing*, Vol. 47, No. 8, pp. 1187-1193.

FRASER, R.S., Y.J. Kaufman and R.C. Mahoney (1984) Satellite Measurements of Aerosol Mass and Transport. *Atmospheric Environment*, Vol. 18, pp. 2577-2584.

FRASER, R.S. and Y.J. Kaufman (1985) The Relative Importance of Aerosol Scattering and Absorption in Remote Sensing. *Transactions on Geoscience and Remote Sensing*, Vol. GE-23, No. 5, pp. 625-633.

FRASER, S.J. and A.A. Green (1987) A Software Defoliant for Geological Analysis of Band Ratios. *International Journal of Remote Sensing*, Vol. 8, No. 3, pp. 525-535.

FROUIN, R. and C. Gautier (1987) Calibration of NOAA-7 AVHRR, GEOS-5 and GEOS-6 VISS/VAS Solar Channels. *Remote Sensing of Environment*, Vol. 22, pp. 73-101.

GALLO, K.P. and C.S.T. Daughtry (1987) Differences in Vegetation Indices for Simulated Landsat-5 MSS and TM, NOAA-9 AVHRR and SPOT-1 Sensor Systems. *Remote Sensing of Environment*, Vol. 23, pp. 439-452.

GALLO, K.P. and J.C. Eidenshink (1988) Differences in Visible and Near-IR Responses, and Derived Vegetation Indices, for the NOAA-9 and NOAA-10 AVHRRs: A Close Study. *Photogrammetric Engineering and Remote Sensing*, Vol. 54, No. 4, pp. 485-490.

GATES, D.M., H.J. Keegan, J.C. Schleter and V.R. Weidner (1965) Spectral Properties of Plants. *Applied Optics*, Vol. 4, pp. 11-20.

GERVIN, J.C., A.G. Kerber, R.G. Witt, Y.C. Lu and R. Sekkon (1985) Comparison of Level 1 Classification Accuracy for Landsat MSS and AVHRR Data. *International Journal of Remote Sensing*, Vol. 6, No. 1, pp. 47-58.

GRAETZ, R.D. and M.R. Gentle (1982) The Relationship Between Reflectance and Landsat Wavebands and the Composition of an Australian Semi-Arid Shrubs Rangeland. *Photogrammetric Engineering and Remote Sensing*, Vol. 48, No. 11, pp. 1721-1730.

GRAETZ, R.D. (1987) Satellite Remote Sensing of Australian Rangelands. *Remote Sensing of Environment*, Vol. 23, pp. 313-331.

GRAY, T.I. and D.G. McCrary (1981) *The Environmental Vegetation Index, a Tool Potentially Useful for Arid Land Management.* AgRISTARS Report No. EW-N1-04076; JSC-17132, pp. 1-7.

GRIFFITH, G.H. and W.G. Collins (1981) Landsat Imagery for Mapping and Monitoring Vegetation in Northern Kenya. *Proc. of Matching Remote Sensing Technologies and Their Applications, Remote Sensing Society,* London, pp. 53-64.

GRIFFITH, G.H. and W.G. Collins (1983) Mapping the Greenness of Semi-arid Rangeland Vegetation in Northern Kenya from Landsat Digital Data. *Remote Sensing for Rangeland Monitoring and Management, Proc. of an International Conference,* Silsoe, U.K., Sept. 1983, pp. 108-121.

GRIFFITH, G.H. and T.G. Tekie (1990) An Evaluation of Multi-Sensor Satellite Data for Monitoring Semi-Arid Rangeland Vegetation in Northern Kenya. *Proc. of 16th Annual Conference of the Remote Sensing Society,* 19-21 Sept. 1990, Swansea, U.K., pp. 250-262.

GROSS, M.F., M.A. Hardisky and V. Klemas (1988) Effects of Solar Angle Reflectance from Wetland Vegetation. *Remote Sensing of Environment,* Vol. 26, pp. 195-212.

GUTMAN, G. (1987) The Derivation of Vegetation Indices from AVHRR Data. *International Journal of Remote Sensing,* Vol. 8, No. 8, pp. 1235-1243.

GUTMAN, G., D. Tarpley and G. Ohring (1987) Cloud Screening for Determination of Land Surface Characteristics in a Reduced Resolution Satellite Data Set. *International Journal of Remote Sensing,* Vol. 8, No. 6, pp. 859-870.

GUTMAN, G. (1989) On the Relationship Between Monthly Mean and Maximum-Value Composite Normalized Vegetation Index. *International Journal of Remote Sensing,* Vol. 10, No. 8, pp. 1327-1337.

HALLUM, C. R. and C.R. Perry (1984) Estimating Optimal Sampling Unit Size for Satellite Surveys. *Remote Sensing of Environment,* Vol. 14, pp. 183-196.

HARRIS, R. (1987) *Satellite Remote Sensing - An Introduction.* Rontledge & Kegan Paul, London. 220 pp.

HASTINGS, D., M. Matson and A.H. Horvitz (1988) Using AVHRR for Early Warning of Famine in Africa. *Photogrammetric Engineering and Remote Sensing,* Vol. 54, No. 1, pp. 103-105.

HAY, A. M. (1979) Sampling Designs to Test Land-use Map Accuracy. *Photogrammetric Engineering and Remote Sensing,* Vol. 45, No. 4, pp. 529-533.

HAYES, L. and A.P. Cracknell (1984) A Comparison of TIROS-N Series Satellite Data and Landsat Data Over Scotland. *Proc. of Conference on Integrated Approaches in Remote Sensing*, Guildford, U.K., 8-11 April, 1984, pp. 63-74.

HAYES, L. (1985) The Current use of TIROS-N Series of Meteorological Satellites for Land Cover Studies. *International Journal of Remote Sensing*, Vol. 6, No. 1, pp. 35-45.

HAYES, L. and A.P. Cracknell (1985) An Investigation of NOAA-7 LAC Data for the Provision of Land Cover Information Over Large Areas. *Remote Sensing: Data Acquisition, Management and Applications, Proceedings of the Poster Session*, 9-12 Sept. 1985, London, pp. 81-88.

HENLEY, J.P. and M.B. Satterwhite (1987) Spectral Characteristics of Selected Soils and Vegetation in Northern Nevada and their Discrimination Using Band Ration Techniques. *Remote Sensing of Environment*, Vol. 23, pp. 155-175.

HENRICKSEN, B.L. and J.W. Durkin (1986) Growing Period and Drought Early Waring in Africa Using Satellite Data. *International Journal of Remote Sensing*, Vol. 7, No. 11, pp. 1583-1601.

HIEDERER, R. and A. Maidoukia (1988) Report on Field Work - 1988 Wet Season. Unpublished report, Cranfield Institute of Technology, Silsoe Campus, Silsoe, U.K. 51 pp.

HIEDERER, R. and A. Maidoukia (1989) Report on Field Work - 1989 Wet Season. Unpublished report, Cranfield Institute of Technology, Silsoe Campus, Silsoe, U.K. 69 pp.

HIEDERER, R. and B.K. Wyatt (1990) Sampling Vegetation in Sahel Rangelands for Calibrating NOAA AVHRR Vegetation Indices. *Proc. 16th Annual Conference of the Remote Sensing Society*, 19-21 Sept. 1990, Swansea, pp. 263-275.

HIELKEMA, A., S.D. Prince and W.L. Astle (1986) Rainfall and Vegetation Monitoring in the Savanna zone of the Democratic Republic of Sudan Using the NOAA AVHRR. *International Journal of Remote Sensing*, Vol. 7, No. 11, pp. 1499-1513.

HIERNAUX P.H.Y. and C.O. Justice (1986) Suive du Development Vegetal au Cours de L'ete 1984 dans le Sahel Malien. *International Journal of Remote Sensing*, Vol. 7, No. 11, pp. 1515-1532.

HIERNAUX P.H.Y. (1989) *Le Suivi des Ressources Pastorales et de Leur Gestion en Regard des Production Animales qu'ellles Engredrent au Sahel - Approche Methodologique*. Document de Travail, Atelier sur le Suivi des Ressources Pastorales au Sahel, Niamey; CIPEA, BP 60, Bamako, Mali.

HILL, J. and B. Sturm (1988) Radiometric Correction of Multi-Temporal Thematic Mapper Data for the Use in Agricultural Land-Cover Classification and Vegetation Monitoring. *Proc. of 8th EARSeL Symposium*, Capri, 17-20 May 1988, Director General for Science, Research and Development, Joint Research Centre, Ispra Establishment (EUR-11851 EN), pp. 21-40.

HO, D. and A. Asem (1986) NOAA AVHRR Image Referencing. *International Journal of Remote Sensing*, Vol. 7, No. 7, pp. 895-904.

HOCK, J.C. (1984) Monitoring Environmental Resources Through NOAA's Polar Orbiting Satellites. *International Institute for Aerospace Survey and Earth Sciences*, ITC Journal 1984/4, pp. 263-268.

HOLBEN B.N. and R.S. Fraser (1984) Red and NIR Sensor Response to Off-nadir Viewing. *International Journal of Remote Sensing*, Vol. 5, No. 1, pp. 145-160.

HOLBEN B.N. (1986) Characteristics of Maximum-value Composite Images from Temporal AVHRR Data. *International Journal of Remote Sensing*, Vol. 7, No. 11, pp. 1417-1434.

HOLBEN B.N., D. Kimes and R.S. Fraser (1986) Directional Reflectance Response in AVHRR Red and NIR Bands for Three Cover Types and Varying Atmospheric Conditions. *Remote Sensing of Environment*, Vol. 19, pp. 213-236.

HOLBEN B. N. and Y.J. Kaufman (1989) Calibration of the AVHRR Visible and Near-IR Bands by Atmospheric Scattering, Ocean Glint and Desert Reflection. *Paper Submitted to Journal of Applied Meteorology*.

HOLBEN B. N., Y.J. Kaufman and J.D. Kendall (1990) NOAA-11 AVHRR Visible and Near-IR Inflight Calibration. *International Journal of Remote Sensing*, Vol. 11, No. 8, pp. 1511-1519.

HORD, R.M. (1982) *Digital Image Processing of Remotely Sensed Data*. Academic Press, New York, 256 pp.

HUETE, A.R., D.F. Post and R.D. Jackson (1984) Soil Spectral Effects on 4-Space Vegetation Discrimination. *Remote Sensing of Environment*, Vol. 15, pp. 155-165.

HUETE, A.R., R.D. Jackson and D.F. Post (1985) Spectral Response of Plant Canopy with Different Soil Backgrounds. *Remote Sensing of Environment*, Vol. 17, pp. 37-53

HUETE, A.R. (1987) Soil and Sun Angle Interaction on Partial Canopy Spectra. *International Journal of Remote Sensing*, Vol. 8, No. 9, pp. 13071317.

HUETE, A.R. and R.D. Jackson (1987) Suitability of Spectral Indices for Evaluating Vegetation Characteristics of Arid Rangelands. *Remote Sensing of Environment*, Vol. 23, pp. 213-232.

HUETE, A.R. (1988) A Soil-Adjusted Vegetation Index (SAVI). *Remote Sensing of Environment*, Vol. 25, pp. 295-309.

HUETE, A.R. and R.D. Jackson (1988) Soil and Atmosphere Influence on the Spectra of Partial Canopies. *Remote Sensing of Environment*, Vol. 25, No. 1, pp. 89105.

JACKSON, R.D., P.J. Pinter, R.J. Reginato and S.B. Idso (1979a) Wheat Spectral Reflectance: Interactions Between Crop Configuration and Azimuth Angle. *Applied Optics*, Vol. 18, pp. 3730-3732.

JACKSON, R.D., R.J. Reginato, P.J. Pinter and S.B. Idso (1979b) Plant Canopy Information Extraction from Composite Scene Reflectance of Row Crops. *Applied Optics*, Vol. 18, pp. 3775-3782.

JACKSON, R.D. (1983) Spectral Indices in n-Space. *Remote Sensing of Environment*, Vol. 13, pp. 409-421.

JACKSON, R. D., P.N. Slater and P.J. Pinter (1983) Discrimination of Growth and Water Stress in Wheat by Various Vegetation Indices Through Clear and Turbid Atmospheres. *Remote Sensing of Environment*, Vol. 13, pp. 187-208.

JUSTICE, C.O, J.R.G. Townshed, B.N. Holben and J.C. Tucker (1985) Analysis of Phenology of Global Vegetation Using Meteorological Satellite Data. *International Journal of Remote Sensing*, Vol. 6, No. 8, pp. 1271-1318.

JUSTICE, C.O. (ed.) (1986) Monitoring Grasslands of Semi-Arid Africa using NOAA-AVHRR Data. Special Issue: *International Journal of Remote Sensing*, Vol. 7, No. 11, pp. 1383-1622.

JUSTICE, C.O and P.H.Y. Hiernaux (1986) Monitoring the Grass Lands of the Sahel using NOAA AVHRR Data: Niger 1983. *International Journal of Remote Sensing*, Vol. 7, No. 11, pp. 1475-1497.

JUSTICE, C.O., B.N. Holben and M.D. Gwynne (1986) Monitoring East African Vegetation Using AVHRR Data. *International Journal of Remote Sensing*, Vol. 7, No. 11, pp. 1453-1474.

JUSTICE, C.O., B.L. Markham, J.R.G. Townshed and R.L. Kennard (1989) Spatial Degradation of Satellite Data. *International Journal of Remote Sensing*, Vol. 10, No. 9, pp. 1539-1561.

JUSTICE, C.O., J.R.G. Townshend and V.L. Kalb (1991) Representation of Vegetation by Continental Data Sets Derived from NOAA-AVHRR Data. *International Journal of Remote Sensing*, Vol. 12, No. 5, pp. 999-1021.

KAUFMAN, Y.J. and R.S. Fraser (1984) The Effect of Finite Field Size on Classification and Atmospheric Correction. *Remote Sensing of Environment*, Vol. 15, pp. 95-118.

KAUFMAN, Y.J. (1987) The Effect of Sub-pixel Clouds on Remote Sensing. *International Journal of Remote Sensing*, Vol. 8, No. 6, pp. 839-857.

KAUFMAN, Y.J. and C. Sendra (1988) Algorithm for Automatic Atmospheric Correction to Visible and Near IR Satellite Imagery. *International Journal of Remote Sensing*, Vol. 9, No. 8, pp. 1357-1381.

KAUFMAN, Y.J. and B.N. Holben (1989) Calibration of the AVHRR Visible and Near-IR Bands by Atmospheric Scattering, Ocean Glint and Desert Reflection. *Paper Submitted to International Journal Applied Meteorology*, 25 pp.

KAUTH, R.G. and G.S. Thomas (1976) The Tasselled Cap, A Graphic Description of the Spectral-Temporal Development of Agricultural Crops as Seen by Landsat. *Proc. of the Symp. on Machine Processing of Remote Sensing Data*, Purdue, Indiana, pp. 6.23-7.20.

KAY, S.A.W. (1989) A Holistic Methodology for Processing of Multiple View Angle Image Data. *Remote Sensing for Operational Applications, Technical Contents of the 15th Annual Conference of the Remote Sensing Society*, University of Bristol, 13 - 15 September 1989, pp. 201-206.

KAY, S.A.W. and M.J. Barnsley (1989) The Relationship Between Vegetation Canopy Geometry and Image Statistics in an Multiple View Angle Data Set. *Proc. of 15th Annual Conference of Remote Sensing Society*, 13-15 Sept. 1989, University of Bristol, pp. 207-213.

KENNEDY, P.J. (1989) Monitoring the Phenology of Tunisian Grazing Lands. *International Journal of Remote Sensing*, Vol. 10, No. 4, pp. 835-845.

KERBER, A.G. (1986) Utility of AVHRR Channels 3 and 4 in Land Cover Mapping. *Photogrammetric Engineering and Remote Sensing*, Vol. 52 No. 12, pp. 1877-1883.

KIDWELL. K.B. (1988) *NOAA Polar Orbiter Data Users Guide.* National Oceanic and Atmospheric Administration, U.S. Dept. Commerce, Washington D.C., Satellite Data Services Division.

KIM, H.H. and G.C. Elman (1990) Normalization of Satellite Imagery. *International Journal of Remote Sensing*, Vol. 11, No. 8, pp. 1331-1347.

KIMES, D.S., J.A. Smith and K.J. Ranson (1980) Vegetation Reflectance Measurements as a Function of Solar Zenith Angle. *Photogrammetric Engineering and Remote Sensing*, Vol. 46, No. 12, pp. 1563-1573.

KIMES, D.S., W.W. Newcomb and J.B. Schutt (1984) Directional Factor Distributions of Cotton Row Crop. *International Journal of Remote Sensing*, Vol. 5, No. 2, pp. 263-277.

KIMES, D.S. (1985) Dynamics of Directional Reflectance Factor Distribution for Vegetation Canopies. *Remote Sensing of Environment*, Vol. 18, pp. 1-19.

KIMES, D.S. (1985) Directional Reflectance Factor Distribution for Cover Types of Northern Africa. *Applied Optics*, Vol. 22, pp. 1364-1372.

KNEPPER, D.H. and G.L. Raines (1985) Determining Stretch Parameters for Lithologic Discrimination on Landsat MSS Band Ratio Images. *Photogrammetric Engineering and Remote Sensing*, Vol. 51, No. 1, pp. 63-70.

KOFFLER, R. and W.M. Callicot (1985) *NOAA's Environmental Satellite Data Processing and Derived Products.* Schnapf, A. (ed), Monitoring Earth's Ocean, Land and Atmosphere from Space - Sensors, Systems and Applications. Progress in Astronautics and Aeronautics, New York, Vol. 97, pp. 198-215.

KOWALIK, W.S., R.J.P. Lyon and P. Switzer (1983) The Effects of Additive Radiance Terms on Ratios of Landsat Data. *Photogrammetric Engineering and Remote Sensing*, Vol. 49, No. 5, pp. 659-669.

LAMBECK, P.F. (1977) *Signature Extension Processing for Landsat MSS Data.* Report No. ERIM 122700-32-F, Environmental Research Institute of Michigan, Ann Arbor.

LAMPREY, R.H. and P.N. DeLeeuw (1987) *Monitoring East African Vegetation with the Use of NOAA AVHRR Imagery.* 2nd Year Report to International Livestock Centre of Africa, Nairobi, 41 pp.

LAWRENCE, V.V. and R.A. Vaughan (1989) An Investigation of the Vegetation, Soil, Topographic and Solar Variables which Contribute to the Reflectance of a Grassland Area Using two Different Methods of Radiometric Data Collection. *Remote Sensing for Operational Applications, Technical Contents of the 15th Annual Conference of the Remote Sensing Society*, University of Bristol, 13 - 15th September 1989, pp. 229-236.

LeCOMPTE, D. (1989) Using AVHRR for Early Warning of Famine in Africa. *Photogrammetric Engineering and Remote Sensing*, Vol 55, No. 2, pp. 168-169.

LeHOUREOU, H.N. and C.H. Hoste (1977) Rangeland Production and Annual Rainfall Relations in the Mediterranean Basin and in the African Sahelo-Sudanian Zone. *Journal of Range Management*, Vol. 30, No. 3, pp. 181-189.

LeHOUREOU, H. N. (1984) Rain Use Efficiency: A Unifying Concept in Arid-Land Ecology. *Journal of Arid of Environment*, Vol. 7, pp. 1-35.

LILLESAND, T.M. and R.W. Kiefer (1987) *Remote Sensing and Image Interpretation*. John Wiley & Sons, New York, 721 pp.

LO, T.H.C., F.L. Scarpace and T.M. Lillesand (1986) Use of Multitemporal Spectral Profiles in Agricultural Land Cover Classification. *Photogrammetric Engineering and Remote Sensing*, Vol. 52, No. 4, pp. 535-544.

MACE, R. (1991) Overgrazing Overstated. *Nature*, Vol. 349, pp. 280-281.

MAGNAVOX ADVANCED PRODUCTS AND SYSTEM COMPANY (ed.) (1982) *MX 1502 - Satellite Surveyor Operation and Service Manual*. Magnavox Report R-6245A, Torrance, California.

MAJOR, D.J., F. Barret and G. Guyot. (1990) A Ratio Vegetation Index Adjusted for Soil Brightness. *International Journal of Remote Sensing*, Vol. 11, No. 5, pp. 727-740.

MARKHAM, B.L. and J.L. Barker (1987) Radiometric Properties of U.S. Processed Landsat MSS Data. *Remote Sensing of Environment*, Vol. 22, pp. 39-71.

MATHER, P.M. (1987) *Computer Processing of Remotely Sensed Images*. John Wiley & Sons, Chichester, 352 pp.

MATHESON, W. and S. Ringrose (1987) Spectral Assessment of Indicators of Range Degradation in the Botswana Hardveld Environment. *Remote Sensing of Environment*, Vol. 23, pp. 376-396.

MAXWELL, E.L. (1976a) A Remote Rangeland Analysis System. *Journal of Range Management*, Vol. 29, No. 1, pp. 6673.

MAXWELL, E.L. (1976b) Multivariate System Analysis of Multispectral Imagery. *Photogrammetric Engineering and Remote Sensing*, Vol. 42, No. 9, pp. 1173-1186.

McGRAW, J.F. and P.T. Teuller (1983) Landsat Computer-aided Analysis Techniques for Range Vegetation Mapping. *Journal of Range Management*, Vol. 36, No. 5, pp. 627631.

MILLER, L.D. and R.L. Pearsons (1978) Remote Mapping of Standing Crop Biomass for Estimation of the Productivity of Short Grass Prairie, Pawnee National Grasslands, Colorado. *Proc. of the 8th International Symposium on Remote Sensing of the Environment*, University of Michigan, Ann Arbor, pp. 1355-1381.

MILLER, W.A. (1987) Land Science Applications Utilizing AVHRR Data. *1st North American Polar Orbiter Users' Group Meeting*, 14-16 July 1987, Boulder, Colorado, pp. 94-95.

MILLINGTON, A.C., R.J. Saull, P. Kennedy, J.R.G. Townshed, R. Madams and S.D. Prince (1987) Biomass Energy Appraisal in Southern Africa - The Role of Remote Sensing. *Advanced in Digital Image Processing: Proc. of Annual Conference of the Remote Sensing Society*, 7-11 Sept. 1987, Nottingham, pp. 134-144.

MILNE, G. (1935) Some Suggested Units of Classification and Mapping, Particularly for East African Soils. *Soil Research*, Vol. 4, pp. 183-198.

MINISTERE DU COMMERCE ET DES TRANSPORTS (ed.) (1984) *Annual Meteorologique du Niger, 1984.* Direction de la Meteorologie Nationale, Niamey, Republique du Niger.

MORRIS, K.P. and M.J. BARNSLEY (1989) An Assessment of Various Procedures for the Radiometric Correction of the Sensor View Angle Effect. *Remote Sensing for Operational Applications, Technical Contents of the 15th Annual Conference of the Remote Sensing Society*, University of Bristol, 13-15 September 1989, pp. 283-290.

MUEGGLER, W.F. (1976) *Number of Plots Required for Measuring Productivity on Mountain Grasslands in Montana.* USDA Forest Service, Research Note INT-207, Intermountain Forest and Range Experiment Station, Ogden, Utah, 6 pp.

MUNSELL COLOR COMPANY (ed) (1954) *Munsell Soil Color Charts.* Munsell Color Company, Inc., Baltimore.

NAGLE, F.W. (1987) Satellite Navigation and De-Navigation. *1st North American Polar Orbiter Users' Group Meeting*, 14-16 July 1987, Boulder, Colorado, pp. 79-88.

NELSON, R.F. (1985a) Reducing Landsat MSS Scene Variability. *Photogrammetric Engineering and Remote Sensing*, Vol. 51, No. 5 pp. 583-593.

NELSON, R.F. (1985b) Sensor-Induced Variability of Landsat MSS Data. *Remote Sensing of Environment* Vol. 18, pp. 35-48.

NATURAL ENVIRONMENT RESEARCH COUNCIL (1986) *Monitoring of Pastureland Ecosystems in the Sahel and Mapping of Cloud Cover and Rainfall.* Final Report to the Commission of the European Communities, Development Directorate DGVIII, Swindon: NERC.

NORWINE, J. and D.H. Gregor (1983) Vegetation Classification Based on Advanced Very High Resolution Radiometer (AVHRR) Satellite Imagery. *Remote Sensing of Environment*, Vol. 13, pp. 69-87.

OJO, O. (1977) *The Climate of West Africa.* Heinemann, New York, 216 pp.

ORMSBY, J.P. (1982) Classification of Simulated and Actual NOAA-6 AVHRR Data for Hydrological Land Surface Feature Definition. *Institute of Electric and Electronic Engineers, Transitions on Geoscience and Remote Sensing*, VOL. 20, No. 3, pp. 262-268.

ORMSBY, J.P., B.J. Choudhury and M. Owe (1987) Vegetation Spatial Variability and its Effect on Vegetation Indices. *International Journal of Remote Sensing*, Vol. 8, No. 9, pp. 1301-1306.

OTTERMAN, J. and R.S. Fraser (1976) Earth-Atmosphere System and Surface Reflectivities in Arid Regions from Landsat MSS Data. *Remote Sensing of Environment*, Vol. 5, pp. 247-266.

PEARSON, R.L. and L.D. Miller, (1973) Remote Mapping of Standing Crop Biomass for Estimation of the Productivity of Short Grass Prairie. *8th International Symp. on Remote Sensing of Environment*, University of Michigan, Ann Arbor, pp. 1355-1379.

PERRY, C.R. and L.R. Lautenschlager (1984) Functional Equivalence of Spectral Vegetation Indices. *Remote Sensing of Environment*, Vol. 14, pp. 169-182.

PHILIPSON, W.R. and W.L. Teng (1988) Operational Interpretation of AVHRR Vegetation Indices for World Crop Information. *Photogrammetric Engineering and Remote Sensing*, Vol. 54, No. 1, pp. 55-59.

PHULPIN, T., J.P. Jullien and D. Lasselin (1989) AVHRR Data Processing to Study the Surface Canopies in Temperate Regions - First Results of HAPEX-MOBILHY. *International Journal of Remote Sensing*, Vol. 10, No. 4, pp. 869-884.

PIECH, K.R. and J.E. Walker (1974) Interpretation of Soils. *Photogrammetric Engineering and Remote Sensing*, Vol. 40, No. 2, pp. 87-94.

PINTER, P.J., G. Zipoli, G. Maracchi and R.J. Reginato (1987) Influence of Topography and Sensor View angles on NIR/Red Ratio and Greenness Vegetation Indices of Wheat. *International Journal of Remote Sensing*, Vol. 8, No. 6, pp. 953-957.

PLANET, W.G. (ed.) (1988) *Data Extraction and Calibration of TIROS-N/NOAA Radiometers*. United States Department of Commerce, National Oceanic and Atmospheric Administration, National Environmental Satellite Data and Information Service, NOAA Technical Memorandum, NESS 107, Rev.1.

POPHAM, R.W. (1988) *Appendix B to NOAA TM107 for NOAA-H/11*. United States Department of Commerce, National Oceanic and Atmospheric Administration, 23 pp.

POTTER, J.F. (1977) The Correction of Landsat Data for the Effects of Haze, Sun Angle and Background Reflectance. *Proc. 4th Annual Symp. on Machine Processing on Remotely Sensed Data*, 21-23 July, 1977, IEEE Catalogue No. 77 CH 1218-7 MPRSD, pp. 24-32.

POWER, C.H. and E.C. Barrett (1989) Remote Sensing Applied to Food Production and Food Security: The Development of Integrated Operations. *Remote Sensing for Operational Applications, Technical Contents of the 15th Annual Conference of the Remote Sensing Society*, University of Bristol, 13-15 September 1989, pp. 337-344.

PRICE, J.C. (1987) Calibration of Satellite Radiometers and the Comparison of Vegetation Indices. *Remote Sensing of Environment*, Vol. 21, pp. 15-27.

PRICE, J.C. (1988a) An Update on Visible and Near Infrared Calibration of Satellite Instruments. *Remote Sensing of Environment*, Vol. 24, pp. 419-422.

PRICE, J.C. (1988b) Scene Location Overpass Dates for Landsat and SPOT Scenes. *International Journal of Remote Sensing*, Vol. 9, No. 12, pp. 1951-1958.

PRINCE, S.D. and W.L. Astle (1986) Satellite Remote Sensing of Rangelands in Botswana, I. Landsat MSS and Herbaceous Vegetation. *International Journal of Remote Sensing*, Vol. 7, No. 11, pp. 1533-1553.

PRINCE, S.D. and C.J. Tucker (1986) Satellite Remote Sensing of Rangelands in Botswana, II. NOAA AVHRR and Herbaceous Vegetation. *International Journal of Remote Sensing*, Vol. 7, No. 11, pp. 1555-1570.

RICHARDSON, A.J. and C.L. Wiegand (1977) Distinguishing Vegetation from Soil Background Information. *Photogrammetric Engineering and Remote Sensing*, Vol. 43, No. 12, pp. 1541-1552.

RICHTER, R. (1990) A Fast Atmospheric Correction Algorithm Applied to Landsat TM Images. *International Journal of Remote Sensing*, Vol. 11, No. 1, pp. 159-166.

RINGROSE, S. (1985) Consideration of Effective Indicators for Monitoring Desertification in Botswana using Satellite Systems. *Remote Sensing: Data Acquisition, Management and Applications, Proc. of the Poster Session at the International Conference of Remote Sensing Societies and the Centre for Earth Resource Management*, London, 9-12 Sept. 1985. pp. 101-111.

RINGROSE S. and W. Matheson (1986a) Monitoring Desertification on Botswana Using Landsat MSS Data with Consideration as to the Nature of the Infrared Paradox. *African Resources Symposium*, Reading, U.K. pp. 13-26.

RINGROSE S. and W. Matheson (1986b) Spectral Assessment of Range Degradation in the Botswana Hardveld Environment. *Remote Sensing of Environment*, Vol. 23, pp. 379-396.

RINGROSE S. and W. Matheson (1991) A Landsat Analysis of Rangeland Conditions in the Botswana Kalahari Drought. *International Journal of Remote Sensing*, Vol. 12, No. 5, pp. 1023-1051.

RIPPLE, W.J. (1985) Asymptotic Reflectance Characteristics of Grass Vegetation. *Photogrammetric Engineering and Remote Sensing*, Vol. 51, No. 12, pp. 1915-1921.

ROBINOVE, C.J., P.S. Chavez, D. Gehring and R. Holmgren (1981) Arid Land Monitoring Using Landsat Albedo Difference Images. *Remote Sensing of Environment*, Vol. 11, pp. 133-156.

ROBINOVE, C.J. (1982) Computation with Physical Values from Landsat MSS Digital Data. *Photogrammetric Engineering and Remote Sensing*, Vol. 48, No. 5, pp. 781-784.

ROBINSON, I.S. (1985) *Satellite Oceanography.* John Wiley & Sons, Chichester, 455 pp.

ROSENFIELD, G.H., K. Fitzpatrick-Lins, K. Lins and H.S. Ling (1982) Sampling for Thematic Map Accuracy Testing. *Photogrammetric Engineering and Remote Sensing*, Vol. 48, No. 1, pp. 131-137.

ROYER, A., P. Vincent and F. Bonn (1985) Evaluation and Correction of Viewing Angle Effects on Satellite Measurements of Bidirectional Reflectance. *Photogrammetric Engineering and Remote Sensing*, Vol. 51, No. 12, pp. 1899-1914.

ROYER, A., L. Charbonneau, R. Brochu, J.M. Murphy and P.M. Teillet (1987) Radiometric Comparison of the Landsat-5 TM and MSS Sensors. *International Journal of Remote Sensing*, Vol. 8, No. 4, pp. 579-591.

ROYER, A., L. Charbonneau and P.M. Teillet (1988) Interannual Landsat MSS Reflectance Variation in an Urbanized Temperate Zone. *Remote Sensing of Environment*, Vol. 24, pp. 423-446.

SABINS, F.F. (1987) *Remote Sensing - Principles and Interpretation*. W.H. Freeman Co., San Francisco, 2nd ed., 449 pp.

SAKAMOTO, C., G. Johnson, A. van Dijk and S. Leduc (1987) Application of NOAA Polar Orbiter Data for Operational Agricultural Assessment. *1st North American Polar Orbiter Users' Group Meeting*, 14-16 July 1987, Boulder, Colorado, pp. 134-160.

SALAMONOVICZ, P.H. (1986) Satellite Orientation and Position for Geometric Correction of Scanner Imagery. *Photogrammetric Engineering and Remote Sensing*, Vol. 52. No. 4, pp. 491-499.

SATTERWHITE, M.B. and J.P. Henley (1982) Effects of Ground Cover and Leaf Area on Spectral Reflectance of Vegetation-Soil Targets. *Proc. American Society of Photogrammetry, Technical Paper*, pp. 352-361.

SAULL, R. (1985) Land Applications of the Advanced Very High Resolution Radiometer (AVHRR): A U.K. Example. *Remote Sensing, Data Acquisition, Management and Applications; Proc. of the Poster Session at the International Conference of the Remote Sensing Society and the Centre of Earth Resources Management*, 9-12 Sept. 1985, pp. 57-66.

SAUNDERS, R.W. (1986) An Automated Scheme for the Removal of Cloud Contamination from AVHRR Radians Over Western Europe. *International Journal of Remote Sensing*, Vol. 7, No. 7, pp. 867-886.

SAUNDERS, R.W. (1990) The Determination of Broad Band Surface Albedo from AVHRR Visible and Near-Infrared Radiances. *International Journal of Remote Sensing*, Vol. 11, No. 1, pp. 49-67.

SCHNAPF, A. (ed.) (1985) *Monitoring Earth's Ocean, Land and Atmosphere from Space - Sensors, Systems and Applications*. Progress in Astronautics and Aeronautics, American Institute of Aeronautics and Astronautics (pub.), Vol. 97, 830 pp.

SCHNEIDER, S.R., D.F. McGinnis and G. Stephens (1985) Monitoring Africa's Lake Chad Basin with Landsat and NOAA Satellite Data. *International Journal of Remote Sensing*, Vol. 6, No. 1, pp. 59-73.

SCHOTT, J.R., C. Salvaggio and W.J. Volchok (1988) Radiometric Scene Normalization Using Pseudo-invariant Features. *Remote Sensing of Environment*, Vol. 26, No. 1, pp. 1-16.

SELLERS, W.D. (1965) *Physical Climatology*. The University of Chicago Press, Chicago, 272 pp.

SELLERS, P.J. (1985) Canopy Reflectance, Photosynthesis and Transpiration. *International Journal of Remote Sensing*, Vol. 6, No. 8, pp. 1335-1372.

SEZE, G. and W.B. Rossow (1991) Time Cumulated Visible and Infrared Radiance Histograms Used as Descriptors of Surface and Cloud Variation. *International Journal of Remote Sensing*, Vol. 12, No. 5, pp. 877-920.

SHIBAYAMA, M. and C.L. Wiegand (1985) View Azimuth and Zenith, and Solar Angle Effects on Wheat Canopy Reflectance. *Remote Sensing of Environment*, Vol. 18, pp. 91-103.

SIEGAL, B.S. and A.R.H. Goetz (1977) Effect of Vegetation on Rock and Soil Type Discrimination. *Photogrammetric Engineering and Remote Sensing*, Vol. 43, No. 2, pp. 191-196.

SINGH, S.M. (1984) Removal of Atmospheric Effects on a Pixel by Pixel Basis from the Thermal Infrared Data from Instruments on Satellites - The Advanced Very High Resolution Radiometer (AVHRR). *International Journal of Remote Sensing*, Vol. 5, No. 1, pp. 161-184.

SINGH, S.M. and A.P. Cracknell (1985) Effect of Shadow Cast by Vertical Protrusions on AVHRR Data. *International Journal of Remote Sensing*, Vol. 6, No. 11, pp. 1767-1771.

SINGH, S.M., A.P. Cracknell and A.F.G. Fiuza (1985a) The Estimation of Atmospheric Corrections to One-Channel Data from AVHRR Simulation Using AVHRR/2. *International Journal of Remote Sensing*, Vol. 6, No. 6, pp. 927-945.

SINGH, S.M., A.P. Cracknell and D. Spitzer (1985b) Evaluation of Sensitivity Decay of Coastal Zone Colour Scanner (CZCS) Detectors by Comparison with in situ Near-Surface Radiance Measurements. *International Journal of Remote Sensing*, Vol. 6, No. 5, pp. 749-758.

SINGH, S.M. and A.P. Cracknell (1986) The Estimation of Atmospheric Effects for SPOT Using AVHRR Channel 1 Data. *International Journal of Remote Sensing*, Vol. 7, No. 3, pp. 361-377.

SINGH, S.M. (1988) Simulation of Solar Zenith Angle Effect on Global Vegetation Index (GVI) Data. *International Journal of Remote Sensing*, Vol. 9, No. 2, pp. 237-248.

SINGH, S.M. and R.J. Saull (1988) The Effect of Atmospheric Correction on the Interpretation of Multitemporal AVHRR-Derived Vegetation Index Dynamics. *Remote Sensing of Environment*, Vol. 25, pp. 37-51.

SINGH, S.M. (1989) Comparison of TM, HRV and AVHRR-derived Vegetation Indices: A Simulation Study for Sensor Intercalibration. *Remote Sensing for Operational Applications, Technical Contents of the 15th Annual Conference of the Remote Sensing Society*, University of Bristol, 13-15 September 1989, pp. 381-387.

SLATER, P.N. (1980) *Remote Sensing - Optics and Optical Systems*. Addison-Wesley Publishing Company, Reading, 575 pp.

SLATER, P.N. and R.D. Jackson (1982) Atmospheric Effect on Radiation Reflected from Soil and Vegetation as Measured by Orbiting Sensors Using Various Scanning Directions. *Applied Optics*, Vol. 21, pp. 3923-3931.

SMITH, J.A. (1983) Matter-Energy Interaction in the Optical Region. *Manual of Remote Sensing*, Cowell, R.N. (ed.), American Society of Photogrammetry, Falls Church, Virginia, Ch. 3, pp. 61-113.

SPIEGEL, M.R. (1972) *Theory and Problems of Statistics*. McGraw-Hill, New York, 359 pp.

STEEL, G.D. and J.H. Torrie (1980) *Principles and Procedures of Statistics*. (2nd ed.) McGraw-Hill Kogakuska, Tokyo, 633 pp.

STOHR, C.J. and T.R. West (1985) Terrain and Look Angel Effects upon Multispectral Scanner Response. *Photogrammetric Engineering and Remote Sensing*, Vol. 51, No. 2, pp. 229-235.

SUITS, G., W. Malila and T. Weller (1988) The Prospects for Detecting Spectral Shifts Due to Satellite Sensor Aging. *Remote Sensing of Environment*, Vol. 26, pp. 17-29.

SWAIN, P.H. and S.M. Davis (1978) Remote Sensing: The Quantitative Approach. McGraw-Hill, New York, 396 pp.

SWITZER, P., W.S. Kowalik and R.J.P. Lyon (1981) Estimation of Atmospheric Path Radiance by the Covariance Matrix Method. *Photogrammetric Engineering and Remote Sensing*, Vol. 47, No. 10, pp. 1469-1476.

TANRE, D., C. Deroo, P. Duhaut, M. Herman, J.J. Morcrette, J. Perbos and P.Y. Deschamps (1990) Technical Note: Description of a Computer Code to Simulate Satellite Signal in the Solar Spectrum: the 5S Code. *International Journal of Remote Sensing*, Vol. 11, No. 4, pp. 659-668.

TARPLEY, J.D., S.R. Schneider and R.L. Money (1984) Global Vegetation Indices from NOAA-7 Meteorological Satellite. *Journal of Climate and Applied Meteorology*, Vol. 23, No. 4, pp. 491-493.

TAYLOR, J.C., A.S. Belward, D.G. Hewett and B.K. Wyatt (1986) *Mapping of Vegetation and Soils - An Estimation of Biomass in the Sahel, Appendix III.* Monitoring of Pastureland Ecosystem in the Sahel and Mapping of Cloud Cover and Rainfall, Final report to the Commission of European Communities Development Directorate (DG VIII), NERC, Swindon, 41 pp.

TEILLET, P.M. (1986) Image Correction for Radiometric Effects in Remote Sensing. *International Journal of Remote Sensing*, Vol. 7, No. 12, pp. 1637-1651.

THOMAS, I.L., V.M. Benning and N.P. Ching (1987) *Classification of Remotely Sensed Images.* Adam Hilger, Bristol, 268 pp.

TOWNSHEND, J.R.G. and C.J. Tucker (1981) Utility of AVHRR of NOAA-6 and 7 for Vegetation Mapping. *Proceedings of Matching Remote Sensing Technologies and their Applications, Remote Sensing Society*, London, pp. 97-109.

TOWNSHEND, J.R.G., C.O. Justice, B. Holben and C. Tucker (1984) Monitoring and Mapping Vegetation Cover Using Data from meteorological Satellites. *Proc. of Conference on Integrated Approaches in Remote Sensing*, Guilford, U.K., 8-11 April 1984, ESA SP-214, pp. 75-79.

TOWNSHEND, J.R.G. and C.J. Tucker (1984) Objective Assessment of Advanced Very High Resolution Radiometer Data for Land Cover Mapping. *International Journal of Remote Sensing*, Vol. 5, No. 2, pp. 497-504.

TOWNSHEND, J.R.G. and C.O. Justice (1986) Analysis of the Dynamics of African Vegetation Using the Normalized difference Vegetation Index. *International Journal of Remote Sensing*, Vol. 7, No. 11, pp. 1435-1445.

TOWNSHEND, J.R.G. and C.O. Justice (1987) Selecting the Spatial Resolution of Satellite Sensor Required for Global Monitoring of Land Transformations. *International Journal of Remote Sensing*, Vol. 9, No. 2, pp. 187-236.

TOWNSHEND, J.R.G. and C.O. Justice (1989) The Spatial Variation of Land Cover at Very Coarse Scales. *Remote Sensing for Operational Applications, Technical Contents of the 15th Annual Conference of the Remote Sensing Society*, University of Bristol, 13-15 September 1989, pp. 415-420.

TOZAWA, Y. (1983) Fast Geometric Correction for NOAA AVHRR. *Proc. of 1983 Machine Processing of Remotely Sensed Data Symposium, LARS*, Purdue University, West Lafayette, Indiana, pp. 46-53.

TUCKER, C.J. (1977) Asymptotic Nature of Grass Canopy Reflectance. *Applied Optics*, Vol. 6, pp. 1151-1156.

TUCKER, C.J. and L.D. Miller (1979) Soil Spectra Contribution to Grass Canopy Spectral Reflectance. *Photogrammetric Engineering and Remote Sensing*, Vol. 43, No. 6, pp. 721-726.

TUCKER, C.J. (1979) Red and Photographic Infrared Linear Combinations for Monitoring Vegetation. *Remote Sensing of Environment*, Vol. 8, pp. 127-150.

TUCKER, C.J., C.L. VanPraet, C. Boerwinkel and A. Gaston (1983) Satellite Remote Sensing of Total Dry Matter Production in the Senegalese Sahel. *Remote Sensing of Environment*, Vol. 13, pp. 461-474.

TUCKER, C.J., J.A. Gatlin and S.R. Schneider (1984) Monitoring Vegetation in the Nile Delta with NOAA-6 and NOAA-7 AVHRR Imagery. *Photogrammetric Engineering and Remote Sensing*, Vol. 50, No. 1, pp. 53-61.

TUCKER, C.J., C.L. VanPraet, M.J. Sharman and G. VanIttersum (1985) Satellite Remote Sensing of Total Herbaceous Biomass Production in the Senegalese Sahel: 1980-1984. *Remote Sensing of Environment*, Vol. 17, pp. 233-249.

TUCKER, C.J., J.R.G. Townshend and T.E. Goff (1985) African Land-Cover Classification using Satellite Data. *Science*, Vol. 227, pp. 369-375.

TUCKER, C.J. and P.J. Sellers (1986) Satellite Remote Sensing of Primary Production. *International Journal of Remote Sensing*, Vol. 7, No. 11, pp. 1395-1416.

TUELLER, P.T. (1987) Remote Sensing Applications in Arid Environments. *Remote Sensing of Environment*, Vol. 23, pp. 143-154.

TUELLER, P.T. and R.D. Wilson (1987) Aerial and Ground Spectral Characteristics of Rangeland Plant Communities in Nevada. *Remote Sensing of Environment*, Vol. 23, pp. 177-191.

TUELLER, P.T. and S.G. Olsen (1989) Diurnal Radiance and Shadow Fluctuations in a Cold Desert Shrub Plant Community. *Remote Sensing of Environment*, Vol. 29, pp. 1-13.

VERDIN, J.P. (1985) Monitoring Water Quality Conditions in a Large Western Reservoir with Landsat Imagery. *Photogrammetric Engineering and Remote Sensing*, Vol. 51, No. 3, pp. 343-353.

WAGENAAR, K.T. and N. deRidder (1986) *Estimations de la Production et de la Distribution de la Biomasse dans la Zone du Projet d'Elevage Integre (PEI) en 1985 d'apres les Valeurs NDVI Obtenues par Satellite.* Document de Travail RSU/86001, Group de Recherche sur les Zones Pastorales (Accord No. 520440-3111), préparé pour le Ministèr des Ressources Animales, Niamey, Niger, Tufts University, North Grafton, U.S.A., pp. 32.

WARREN, S.D., M.O. Johson, W.D. Goran and V.E. Diering (1990) An Automated, Objective Procedure for Selecting Representative Field Sample Sites. *Photogrammetric Engineering and Remote Sensing*, Vol. 56, No. 3, pp. 333-335.

WALSH, S.J. (1987) Comparison of NOAA AVHRR Data to Meteorological Draught Indices. *Photogrammetric Engineering and Remote Sensing*, Vol. 53, No. 8, pp. 1069-1074.

WARDLEY, N.W. (1984) Vegetation Index Variability as a Function of Viewing Geometry. *International Journal of Remote Sensing*, Vol. 5, No. 5, pp. 861-870.

WARDLEY, N.W., E.J. Milton and C.T. Hill (1987) Remote Sensing of Structurally Complex Semi-Natural Vegetation - An Example from Heathland. *International Journal of Remote Sensing*, Vol. 8, No. 1, pp. 31-42.

WARREN, P.L. and C.F. Hutchinson (1984) Indicators of Rangeland Change and Their Potential for Remote Sensing. *Journal of Arid Environments*, Vol. 7, No. 1, pp. 107-126.

WARREN, P.L., M.O. Johnson, W.D. Goran and V.E. Diersing (1990) An Automated, Objective Procedure for Selecting Representative Field Sample Sites. *Photogrammetric Engineering and Remote Sensing*, Vol. 56, No. 3, pp. 333-335.

WATSON, R.D. (1972) Spectral Reflectance and Photometric Properties of Selected Rocks. *Remote Sensing of Environment*, Vol. 2, pp. 95-100.

WHITE, F. (1983) *The Vegetation of Africa*. UNESCO, Natural Resources Research, Vol. XX, Paris, 358 pp.

WIEGAND C.L. and A.J. Richardson (1982) Comparison Among a New Soil Index and Other Two- and Four-Dimensional Vegetation Indices. *American Society of Photogrammetry, Proc. of the 48th Annual Meeting*, pp. 210-227.

WILLIAMSON, H.D. (1988) Soil Influences on Vegetation Reflectance of a Semi-Arid Shrubland. *Monitoring towards the 21st Century, 12-16 Sept., Edinburgh, 1988 International Geoscience and Remote Sensing Symposium*, Vol. II, ESA SP-284, pp. 837-840.

WILLIAMSON, H. D. (1988) Vegetation Sampling for Studies Using Remotely Sensed Data. *Monitoring towards the 21st Century*, 12-16 Sept., Edinburgh, 1988 International Geoscience and Remote Sensing Symposium, ESA SP-284, pp. 849-852.

WILLIAMSON, H.D. (1989) Reflectance from Shrubs and Under-Shrub Soil in an Semi-arid Environment. *Remote Sensing of Environment*, Vol. 29. pp. 263-271.

WILSON, R.O. and P.T. Tueller (1987) Aerial and Ground Spectral Characteristics of Rangeland Plant Communities in Nevada. *Remote Sensing of Environment*, Vol. 23, pp. 177-191.

WYLIE, B., J. Harrington, R. Piper, A. Maman and I. Denda (1988a) *1987 Pasture Assessment Early Warning System - Research on Satellite Based Pasture Assessment Implementation Techniques*. Ministry of Animal and Water Resources, Niamey, Republic of Niger, 32 pp.

WYLIE, B., J. Harrington, A. Nabada, B. Maidaji and D. Issa (1988b) *La Production de Biomass dans la Zone Pastorale du Niger*. Systeme d'Alerte Precoce, Rapport 1988, New Mexico State University, Las Cruces, 16 pp.

WYLIE, B. (1989) personal communication.

XIANG NING KONG and D. Vidal-Madjar (1988) Effect de la Resolution Spatiale sur des Proprietes Statistique des Images Satellites - une Etude de Cas. *International Journal of Remote Sensing*, Vol. 9, No. 8, pp. 1315-1328.

YATES, H., A. Strong, D. McGinnis and D. Tarpley (1986) Terrestrial Observations from NOAA Operational Satellites. *Science*, Vol. 231, pp. 463-470.